Advancing Low-Valent Germanium Chemistry

Synthesis, Characterization and Reactivity Studies

Dissertation

zur

Erlangung des Doktorgrades

(*Dr. rer. nat.*)

der
Mathematisch-Naturwissenschaftlichen Fakultät

der

Rheinischen Friedrich-Wilhelms-Universität Bonn

vorgelegt von

Avnish Singh

aus

Kanpur, Uttar Pradesh, Indien

Bonn, 2025

Angefertigt mit Genehmigung der Mathematisch-Naturwissenschaftlichen Fakultät der Rheinischen Friedrich-Wilhelms-Universität Bonn

Betreuer und Gutachter: Prof. Dr. Alexander C. Filippou

Gutachter: Jun. Prof. Dr. Alessandro Bismuto

Tag der Promotion: 16.03.2026

Erscheinungsjahr: 2026

Acknowledgements

First and foremost, I would like to extend my deepest gratitude to my esteemed supervisor, **Prof. Dr. Alexander C. Filippou**, for his invaluable guidance, unwavering support, and insightful feedback throughout this research. His scholarly expertise and discerning critiques have not only shaped the direction of this dissertation but also significantly elevated its intellectual rigour and coherence. I am incredibly grateful for his meticulous attention to detail and astute recommendations, which have been instrumental in refining the precision, depth, and clarity of this work. The privilege of learning under his mentorship has been truly transformative, and for this, I consider myself profoundly fortunate.

I extend my deepest gratitude to Dr. Ujjal Das for his exceptional supervision and unwavering guidance throughout the experimental phase of this research. His profound expertise and insightful feedback were instrumental in shaping the success of this work. I am equally indebted to Dr. Gregor Schnakenburg for meticulous proofreading and constructive revisions of the initial manuscript, which greatly enhanced its clarity and precision.

I would also like to express my sincere appreciation to Dr. Jürgen Tirrée for his indispensable role in maintaining the seamless operation of the laboratory. His diligent oversight of technical and safety protocols ensured an efficient and secure research environment, for which I am profoundly grateful. A special note of thanks goes to the exceptional technical staff, Kerstin Kühnel-Lysek, Katrin Werthmann, Dietmar Kühlmorgen, and Charlotte Rödde, for their indispensable support in daily laboratory operations. Their expertise and willingness to assist were vital to the progress of this work.

I am deeply thankful to my fellow researcher's Dr. Prasenjit Palui, Dr. Sandeep Kumar, Dr. Kanishk Tomer, Dr. Fabian Gstrein, Dr. Tobias Deckstein, Marcel Krumpholz, Dr. Leonard Maurer and Jens Rump for their stimulating discussions and the collaborative spirit they fostered in the lab. Their intellectual contributions and moral support created an inspiring and productive research atmosphere.

I would like to express my deepest gratitude to the individuals whose unwavering support, invaluable insights, and generous contributions were indispensable to the completion of this work:

- The staff members of the NMR department for their invaluable support, particularly Dipl.-Ing. Karin Prochnicki, Hannelore Spitz, Ulrike Weynand, and

Dr. Senada Nozinovic. A special thanks goes to Frau Prochnicki for her patience and dedication in recording numerous full characterization and variable-temperature NMR measurements.

- Dr. Gregor Schnakenburg and Charlotte Rödde for the X-ray crystallographic measurements and molecular structure solutions.
- Kerstin Kühnel-Lysek, Hannelore Spitz, Anna Martens, Charlotte Rödde and Dr. Sabine Rings for the preparation and measurement of the elemental analysis samples.
- Dr. Gregor Schnakenburg for quantum chemical calculations that enabled an enhanced understanding of my molecules. A special thanks also to Jens Rump and Dr. Gregor Schnakenburg for their technical IT support, particularly with the server.
- Kerstin Kühnel-Lysek for the UV-Vis measurements.
- Dr. Jürgen Tirrée and Katrin Werthmann for ensuring the proper functioning of the instruments and the seamless operation of the lab.
- Frau Denise Dupont, Frau Maryam Toliati, Dr. Sabine Rings and Frau Christine Dolf for their support in administrative matters.
- The University of Bonn for providing infrastructure and financial support of this work.

Words can scarcely capture the depth of my heartfelt gratitude to my beloved parents, Mr. Rakesh Kumar and Mrs. Susheela Devi, whose unconditional love and values have been my guiding light; their blessings, sacrifices, and encouragement have been the true foundation of my academic journey, and without them, this doctoral achievement would not have been possible. To my dear sisters, Asst. Er. Priyanka Gautam and Asst. Manager Babita Baraik, and my brothers, Mr. Manish Kumar, Mr. Vivek Kumar, and Mr. Abhinav Singh, I owe an endless debt of gratitude for their unwavering encouragement, constant motivation, and unshakable faith in me. To my love, Akansha Gautam, your unwavering belief in me, your endless patience, and your boundless love have been the anchor of my journey. You stood by me in moments of doubt, uplifted me with your faith, and inspired me with your strength. I am eternally grateful to have you by my side.

Finally, with profound humility, I bow in reverence to the Almighty God, whose boundless grace, mercy, and blessings have sustained me throughout. It is by His divine strength, wisdom, and protection that I was able to overcome challenges and bring this work to fruition.

For my Mother and Father

Whose sacrifices and encouragement have shaped my path.

Every brilliant experiment, like every great work of art, starts with an act of imagination.

— Jonah Lehrer

Table of Contents

Overview

This thesis summarizes the key research themes explored during my doctoral studies, integrating both experimental and theoretical investigations in the field of inorganic molecular chemistry. It is divided into five main sections, illustrated in ***Figure 1***.

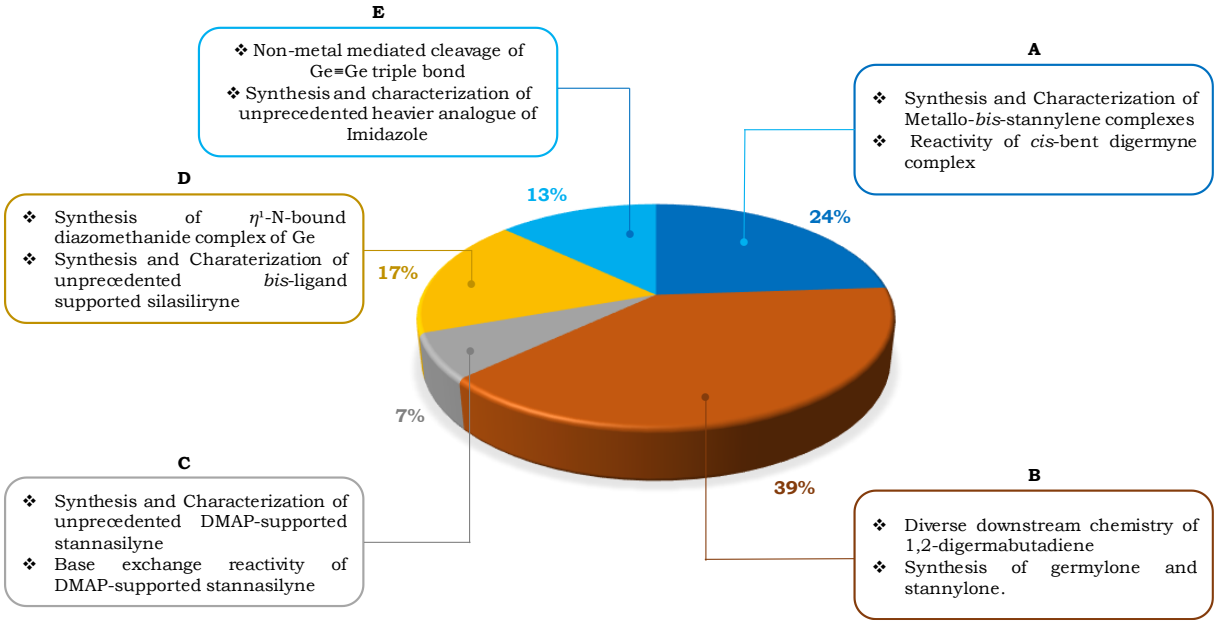

Figure 1. Illustration of the main topics studied in the presented work (the percentage was determined based on the relative numbers of compounds presented in this work).

Section **A** focuses on the isolation of novel metallo-*bis*-stannylene complexes of Co/Rh and the reactivity of *cis*-bent digermyne complex with polar unsaturated molecules. Their structural characterization and experimental properties were explored and rationalized. Section **B** places particular emphasis on the downstream chemistry of the 1,2-digermabutadiene, leading to the successful isolation of low-valent Ge/Sn compounds, germylone and stannylone.

Following this, Section **C** delves into the isolation and characterization of novel DMAP-supported stannasilyne and its reactivity study. Section **D** is pivotal in the quest for base-free germyne/silyne species and the development of new methods or approaches for the successful isolation of these *in silico* compounds. This section includes the successful synthesis of a rarely observed η^1-N-bound diazomethanide complex of Ge and an unprecedented bis-ligand supported silasiliryne.

The last portion of the dissertation is presented in Section **E**, which explores the non-metal-mediated cleavage of the Ge≡Ge triple bond, highlighting its intriguing electronic and structural characteristics. Additionally, this section includes the synthesis and characterization of NHC-supported germyne and an unprecedented heavier analogue of imidazole derivative under standard laboratory conditions.

1. Introduction

Considering the complete pantheon of known elements, Carbon, often hailed as the "element of life", forms the very foundation of biology and organic chemistry. Its remarkable ability to make strong, diverse bonds single, double, and even triple through efficient orbital hybridisation (sp^3, sp^2, sp) allows for the intricate molecular architectures of DNA, proteins, and synthetic polymers. With a compact atomic radius (77 pm) and moderate electronegativity (2.55), carbon excels at forming stable covalent networks, enabling everything from the methane in natural gas to the complex structures of pharmaceuticals. Silicon, carbon's more substantial congener reigns supreme within the inorganic domain, comprising 26% of the terrestrial crust in the form of silicates and silica.[1] Though it mirrors carbon's tetravalent propensity, silicon's expanded atomic radius (117 pm) and diminished electronegativity (1.90) engender profound divergences in its chemical behaviour. Endowed with unparalleled terrestrial abundance, silicon serves as the cornerstone of industrial modernity, fulfilling quintessential functions that traverse disciplines from the precision-driven realm of microelectronics (transistors, diodes and photovoltaics)[2] to its geochemical omnipresence in quartz, granite, and constructional matrices.[3,4] Unlike carbon, which weaves intricate organic tapestries, silicon exhibits an innate predisposition toward robust crystalline frameworks, thereby manifesting a dualistic identity: as both an elemental geological substrate and the ultra-purified medium essential to avant-garde semiconductor technology. Contemporary industrial praxis utilises silicon-derived materials on a staggering scale of 28.6 gigatons annually deploying them across a wide range of applications, from infrastructure engineering and semiconductor fabrication to silicone-based elastomers. These versatile polymers, in turn, permeate specialized fields, including biomedical prosthetics, aeronautical sealing systems, and a wide range of other high-performance applications.

The striking divergence in the physical properties of carbon and silicon—despite their shared group in the Periodic Table—and their respective compounds (e.g., CO_2 vs. SiO_2) arises from fundamental differences in their electronic and structural characteristics. Most notably, silicon's substantially lower electronegativity and larger atomic radius as metioned above significantly influence the bonding behaviour. Furthermore, the pronounced disparity in the size and overlap efficiency of their s- and p-valence orbitals (***Figure 2***) significantly reduces silicon's ability to form stable hybrid orbitals, thereby limiting its capacity for the diverse bonding modes characteristic of carbon.[1,5,6] Additionally, the significantly lower electronegativity of

the heavier group 14 elements compared to carbon further destabilizes multiply bonded compounds containing these elements. The reduced electronegativity decreases the polarity and strength of π-bonds, rendering such compounds highly reactive and thermodynamically less stable than their carbon analogues.[7]

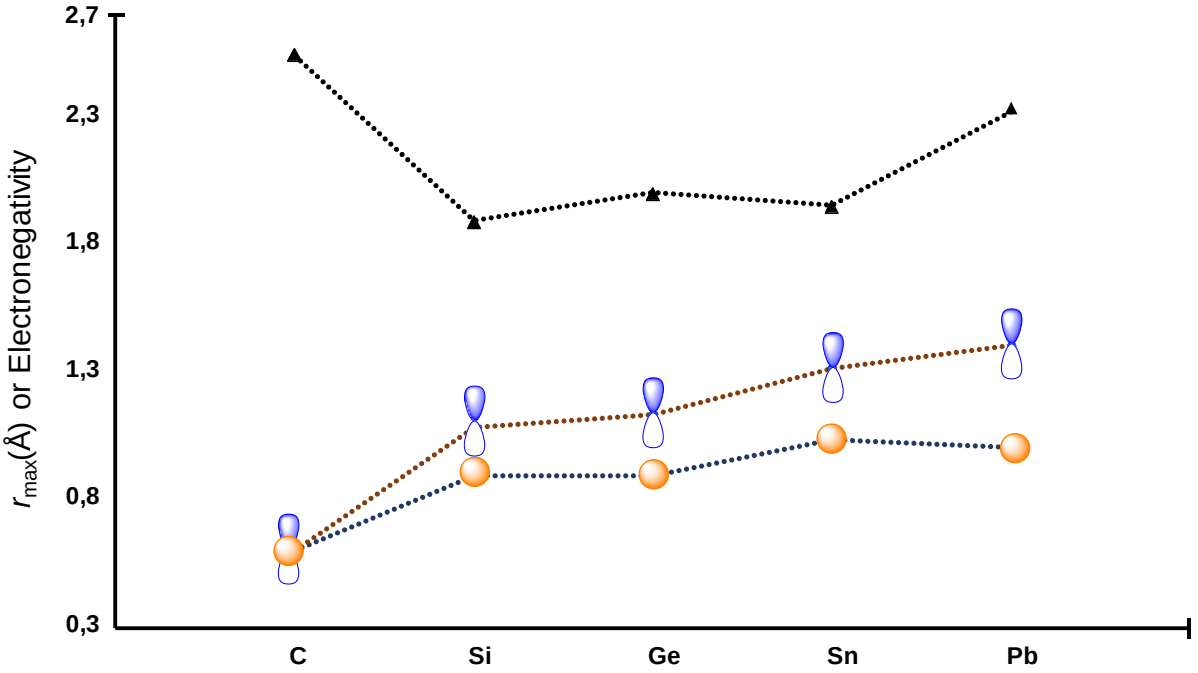

Figure 2. Expected radii (Å) of maximum radial density r_{max} of the respective s- and p-valence orbitals or electronegativity of group 14 elements. The values were taken from the literature.[6,7]

In the valence bond framework, a C=C double bond is formed between two sp^2-hybridized carbon atoms through the overlap of their sp^2 hybrid orbitals, resulting in a σ bond, and the lateral overlap of their remaining unhybridised 2p orbitals, forming a π bond. Silicon, however, exhibits a pronounced reluctance to adopt such hybridisation, historically impeding the formation of classical multiple bonds and leading to the empirical "multiple bond rule." This rule posited that stable (np−(n+1)p)π bonds (where n ≥ 2) between main group elements beyond the second period were inherently unattainable.[8] This paradigm was first challenged in the 1970s by Lappert, who isolated the distannene $(Dsi)_2Sn=Sn(Dsi)_2$ (Dsi = $CH(SiMe_3)_2$). While this compound dissociates in solution, the crystallographic analysis revealed a weak but discernible Sn=Sn double bond in the solid state,[9,10] marking a pivotal departure from the previously assumed limitations. Subsequent research has demonstrated that nonclassical stabilising interactions often involving sterically demanding substituents play a crucial role in the bonding of heavier group 14 dimers (E_2R_4 and E_2R_2, where E = Sn or Pb and R = bulky ligand).[11] These findings have

since redefined the understanding of multiple bonding in heavier main group elements.

1.1. Bonding in the heavier main-group elements

1.1.1. Multiple bonds to tetrels

The first significant milestones of the contemporary low-coordinate molecular tetrel chemistry occurred in 1973, marked by the isolation of a Sn analogue and then in 1976, a Ge analogue of an alkene, $(Dsi)_2E{=}E(Dsi)_2$ (E = Sn (**I-1**), Ge (**I-2**) and Dsi = $CH(TMS)_2$; TMS = $SiMe_3$)[9,10] by Lappert and coworkers Noteworthy, they aimed to synthesize monomeric bottleable dialkyl tetrylenes $:E(Dsi)_2$ (E = Ge, Sn) , but the solid-state structure of the aforementioned low-coordinate tetrels revealed dimeric structure with an E=E bond and considerable pyramidalization of the core tetrel centres, which is counterintuitive to the analogous carbon compounds. The same research group also reported the comprehensive structural characterization of the monomeric Pb compound $Pb(Dsi)_2$ (**I-3**),[9] and it's solid state structure revealed no considerable Pb···Pb interaction (*d*(Pb···Pb) = 4.129 Å) with the second independent molecule in the crystal lattice. The successful instalment of the double bond between the missing link of the carbon immediate heavier analogue (Si), was accomplished by West and coworkers in 1981. Irradiation of a hydrocarbon solution of predesigned silane $(Mes)_2Si(TMS)_2$ with UV light (λ = 254 nm) affords $Mes_2Si{=}SiMes_2$ (Mes = C_6H_2-2,4,6-Me_3) (**I-4**) [12] with the concomitant formation of disilane as sole byproduct. Interestingly, **I-4** exhibits a short Si=Si bond (2.16 Å) and nearly planar silicon center (356°), in good agreement with its lighter analogue but showing stark contrast to its heavier analogues.

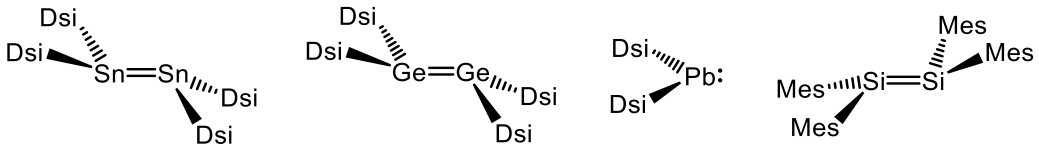

Lappert, 1973 — **I-1** | Lappert, 1976 — **I-2** | Lappert, 1973 — **I-3** | West, 1981 — **I-4**

Figure 3. First examples of a distanene (**I-1**), digermene (**I-2**), dialkylplumbylene (**I-3**), and disilene (**I-4**).

Since then, the chemistry of low-valent main group compounds, primarily silicon, has advanced rapidly, resulting in numerous review articles on the subject.[8,13,14,15] Disproving the typical "double-bond rule" also leads to open questions to discuss, like disilenes generally exhibit the expected planar geometry typical of alkenes; however, heavier ditetrylenes tend to show pyramidalization of the tetrel atoms,

resulting in trans-bending of the substituents (ranging from θ ≈ 15° for Si to 70° for Pb).[8,13,16,17]

As we descend the group of tetrylenes (heavy carbene analogues, E = Si, Ge, Sn, Pb) in the periodic table, the lone pair character of the divalent center becomes more pronounced due to the increasing energy gap between the ns^2 lone pair and the np orbitals. This enhanced s-character in the non-bonded electron pair results in greater pyramidalization at the central atom and significant bending of the substituents, which correlates with the observed weakening of E=E multiple bonds down the group. Furthermore, ditetrylenes ($R_2E{=}ER_2$) exhibit a notable propensity to undergo dissociation into their monomeric tetrylene forms ($:ER_2$) in solution,[13] establishing a dynamic equilibrium that is highly sensitive to steric and electronic effects. This equilibrium is particularly prevalent for heavier group 14 elements (E = Si, Ge, Sn, Pb), where the diminished π-bond strength and increased lone pair nucleophilicity favor monomer formation.

In the Carter-Goddard-Malrieu-Trinquier (CGMT) model, the E=E double bonding is essentially described as a double donor-acceptor interaction (akin to Lewis acid/base adduct formation) between two amphiphilic tetrylenes in their electronic singlet ground state due to the aforementioned insufficient hybridisation of the heavier tetrel atoms (***Figure 4***). The greater the hybridisation (corresponding to a minor energy difference between the singlet and triplet states $\Delta E_{S\rightarrow T}$), the less the trans-bending with E=E bond cleavage energy and singlet-triplet energy gaps of the tetrylene fragments. Once the value of the bond cleavage energy (total intrinsic interaction energy, BCE) is higher than the double of energy difference between the singlet and triplet states of the tetrylene fragments ($BCE > 2{\cdot}\Delta E_{S\rightarrow T}$), no trans-bending is expected.[5,18,19]

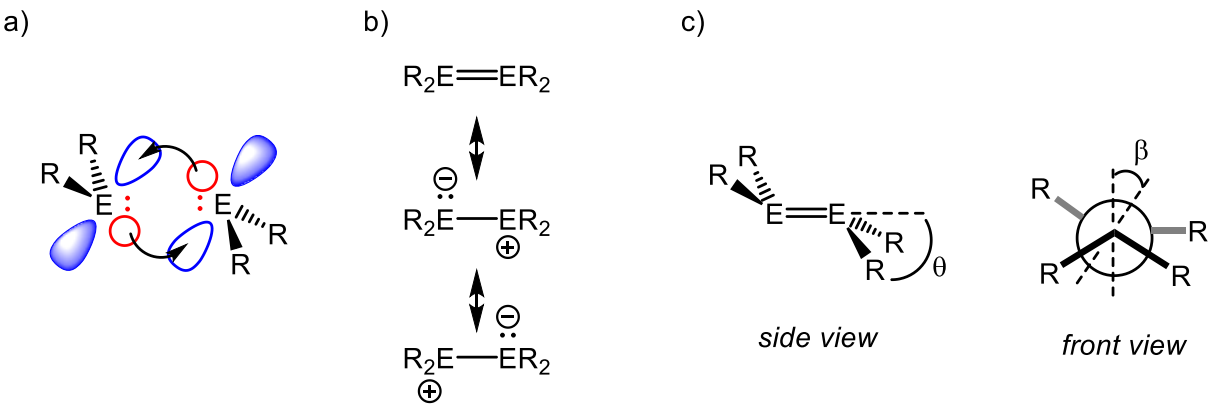

Figure 4. (a) Double donor-acceptor bonding model; (b) valence-bond description of heavy ditetrylenes;[13],[20],[21] (c) the trans-bent angle θ is measured between the E=E bond vector and the plane defined by the substituents; the twisting angle (β) highly depends on the E=E distance, steric bulk and nonclassical

interactions between the individual substituents.[22] For example $Mes_2Si=SiMes_2$: d = 2.160 Å, θ = 18° and β = 5°,[23] $Mes_2Ge=GeMes_2$: d = 2.2856(8) Å, θ = 33° and β = 3°.[24]

A fundamental theoretical framework connected to molecular orbital (MO) theory is the second-order Jahn-Teller (SOJT) distortion model. This formalism describes how symmetry-allowed interactions between bonding (σ and π, of a_g and b_{2u} symmetry) and antibonding (b_{1g} and b_{3u}) orbitals induce a substantial stabilization energy, concomitant with a symmetry reduction from D_{2h} (planar E_2R_4) to C_{2h} (trans-bent E_2R_4) (***Figure 5***). The SOJT framework provides a rigorous quantum mechanical rationale for the observed structural distortion, particularly the trans-bending of substituents, while also accounting for the concomitant weakening of the E-E σ-bond a phenomenon well-documented experimentally in heavier homologues (Sn, Pb).[13,20,21]

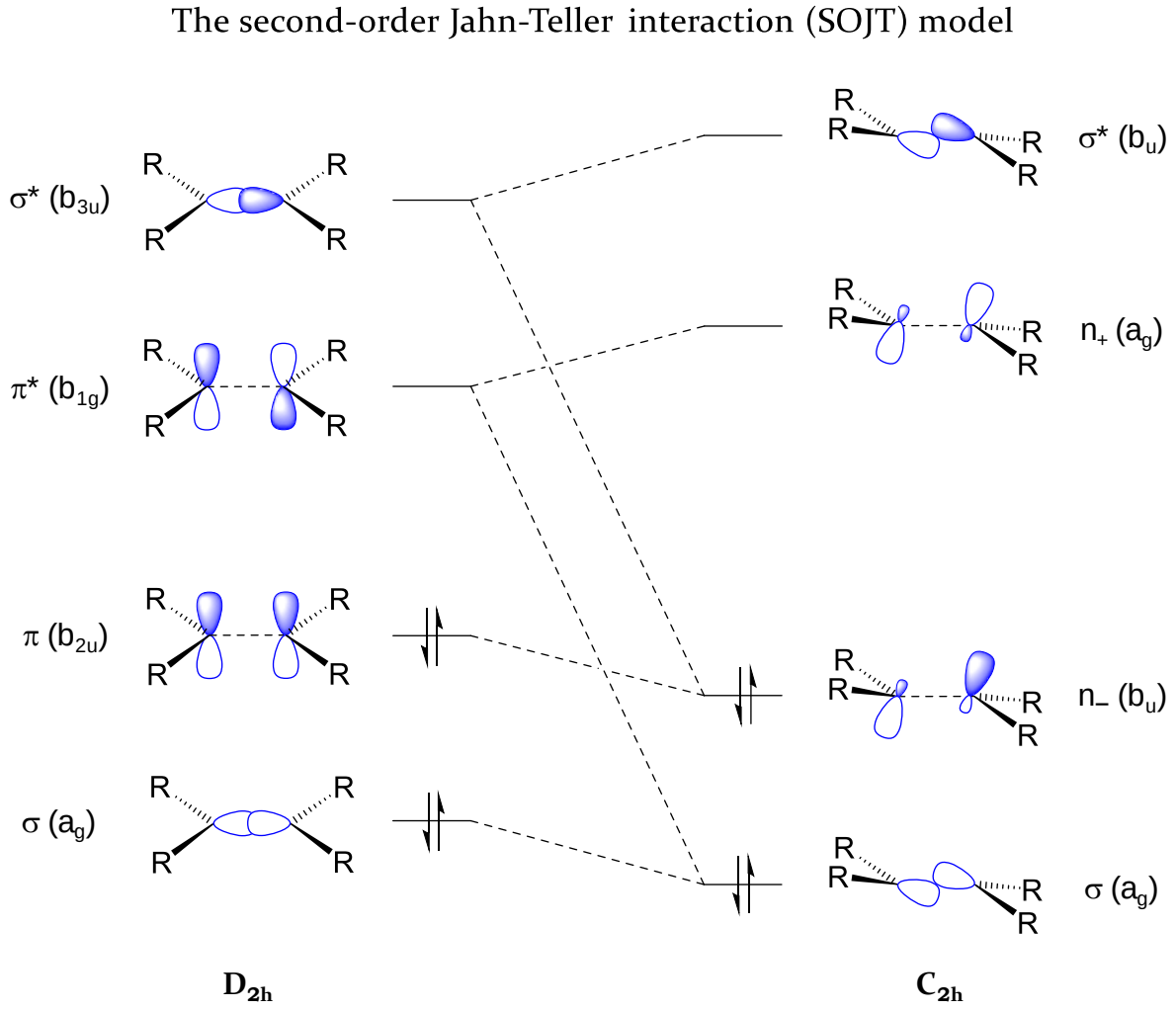

Figure 5. Second-order John-Teller distortion (SOJT) in heavier ditetrylenes.[13,20,21]

1.1.2. Multiple bonds to tetrelynes

Alkynes, compounds featuring a C≡C triple bond, are highly valued in modern chemistry for their versatility and reactivity across various industries. The simplest alkyne, acetylene (C_2H_2), is widely used in welding torches [25] and serves as a precursor in the production of PVC.[26] In pharmaceuticals, alkynes serves as key intermediates in drugs such as Taxol [27] and facilitate click chemistry for efficient drug discovery.[28] They are also crucial in organic synthesis, participating in reactions such as hydrogenation and Sonogashira coupling.[29] Beyond this, their π-conjugated systems make them essential in advanced materials, including conductive polymers (e.g., polyacetylene),[30] carbon nanotubes,[31] and organic light-emitting diodes (OLEDs) for display technologies.[32] Additionally, alkynes find applications in agrochemicals, fragrances, and biochemical labelling, underscoring their broad utility in science and industry.

In contrast to the well-developed chemistry of alkynes, synthesizing their heavier Group 14 analogues (ditetrelynes, E≡E, where E = Si, Ge, Sn and Pb) has proven significantly more challenging. The primary obstacle stems from the kinetic instability of the E≡E triple bond, which necessitates the use of bulky substituents to prevent decomposition or polymerization. Remarkably, these heavier alkyne analogues remained elusive until 2000, when Power and coworkers made a serendipitous breakthrough. While attempting to prepare $PbH(C_6H_3\text{-}2,6\text{-}Trip_2)$ by reacting $PbBr(C_6H_3\text{-}2,6\text{-}Tip_2)$ with $LiAlH_4$, they unexpectedly isolated the diplumbylene $Ar^{Tip}PbPbAr^{Tip}$ (where Tip = C_6H_2-2,4,6-^{i}Pr$_3$) (**I-5**)[33], marking the first synthesis of such a compound. This was quickly followed in 2002 by reports from the same group on digermyne $Ar^{Dipp}GeGeAr^{Dipp}$ (Dipp = C_6H_3-2,6-^{i}Pr$_2$) (**I-6**)[34] and the distannyne $Ar^{Dipp}SnSnAr^{Dipp}$ (**I-7**)[35] (***Figure 6***). In 2004, Sekiguchi and co-workers achieved a $R_2(^i\text{Pr})Si{\equiv}Si(^i\text{Pr})R_2$ (where R = $CH(SiMe_3)_2$) (**I-8**),[36] through the reduction of the

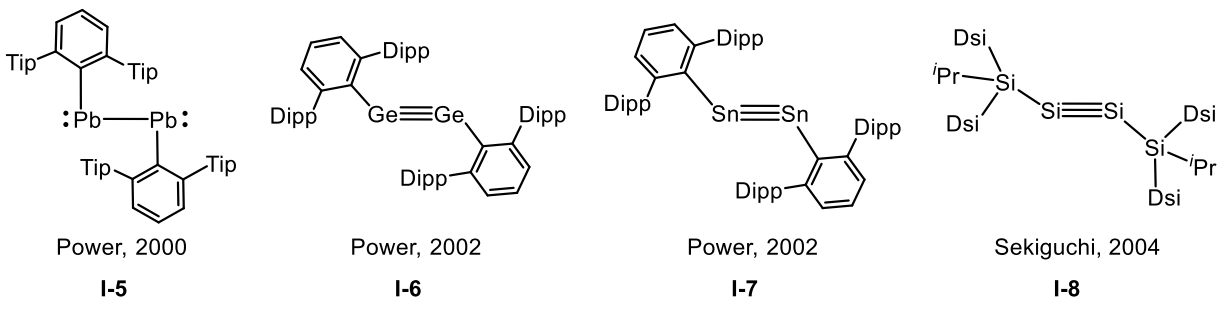

Dsi = $CH(SiMe_3)_2$, Dipp = C_6H_3-2,6-^{i}Pr$_2$, Tip = C_6H_2-2,4,6-^{i}Pr$_3$

Figure 6. First examples of the structurally characterized ditetrylines.

corresponding tetrabromodisilane with KC_8 (***Figure 6***). Notably, Wiberg and co-workers had already proposed the existence of such a species (RSi≡SiR, where R = Si{Si(^{t}Bu)$_3$}$_2$Me) in 2002.[37,38] However, at the time, no structural evidence was obtained to confirm its formation.

The pronounced structural divergence between alkynes and their heavier group 14 analogues can be rationalized within the framework of the Carter-Goddard-Malrieu-Trinquier (CGMT) model (***Figure 7***).[19,39,40] This model posits that the coupling of two E–R (E = C) fragments in a quartet state yields a linear geometry featuring a formal triple bond, whereas their combination in a doublet state (E = Si – Pb) results in a trans-bent configuration.[41] Crucially, since E–R fragments inherently exhibit a doublet ground state, the equilibrium geometry of R–E≡E–R species is governed by a delicate balance between two competing energetic factors: the promotion energy required to excite two doublet E–R fragments to the quartet state ($2\Delta E_{D\rightarrow Q}$) and the stabilization energy derived from the formation of two π-bonds ($E_{2\pi}$). For the case of carbon (C–R fragments), the substantial π-bonding energy ($E_{2\pi}$) dominates over the relatively compensate for the significantly larger promotion energy, resulting in the small excitation penalty ($2\Delta E_{D\rightarrow Q}$), thereby favouring the linear alkyne motif. In contrast, for heavier congeners (E = Si–Pb), the diminished π-bond strength fails to

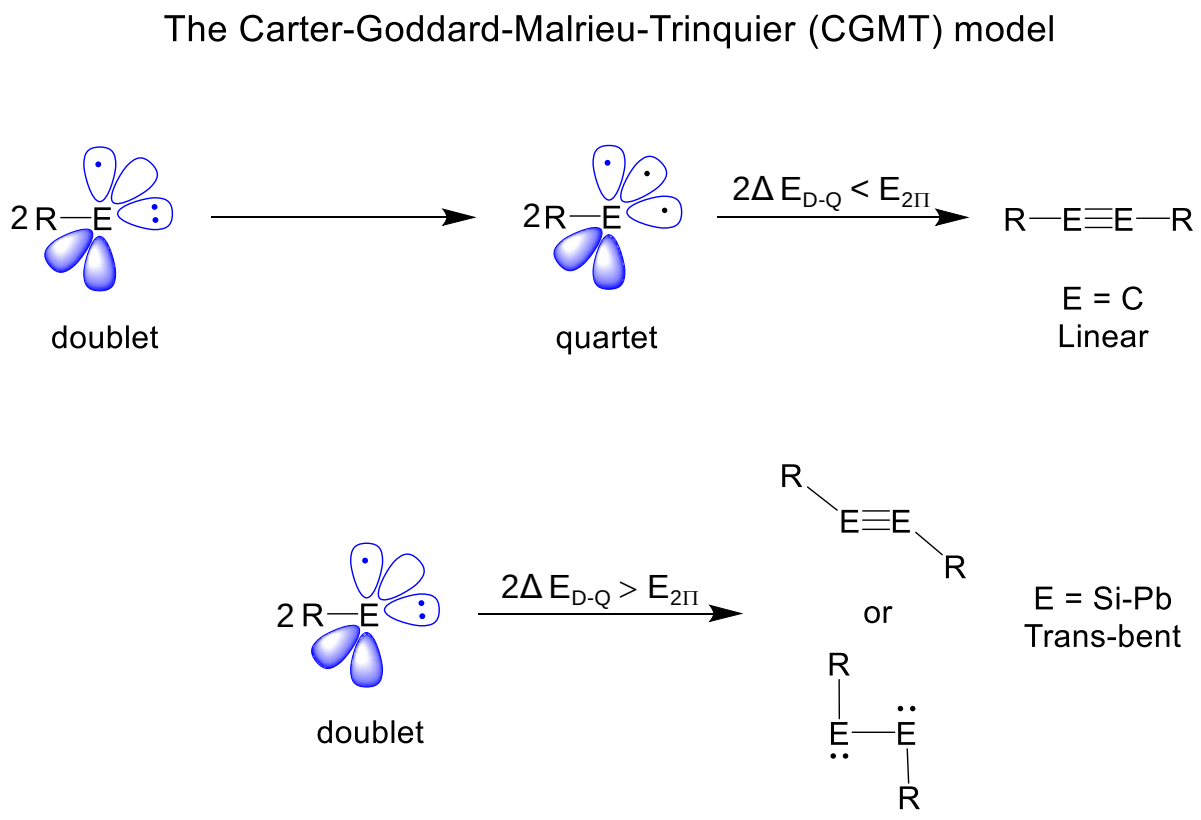

Figure 7. Representation of the contrast between the linear and trans-bent geometries of alkynes and their heavier group 14 element counterparts as per the CGMT model.

preferential adoption of a trans-bent geometry. This fundamental dichotomy arises from the progressive weakening of π-bonding interactions and increasing excitation energies down the group 14 series.

The observed geometric deviations from linear to bent configurations in multiply bonded heavy primary group analogues of alkynes can be rationalised through a second-order Jahn-Teller (SOJT)[42] distortion framework (***Figure 8***). These structural perturbations arise from vibronic coupling between the highest occupied molecular orbital (HOMO) and a low-lying unoccupied orbital (LUMO+1), facilitated by a symmetry-allowed interaction. The SOJT effect manifests as a stabilization of the HOMO and concomitant destabilisation of the LUMO+1, generating nonbonding electron density localised on the heavy main group centers. This electron density redistribution induces geometric distortions driven by increased interelectronic

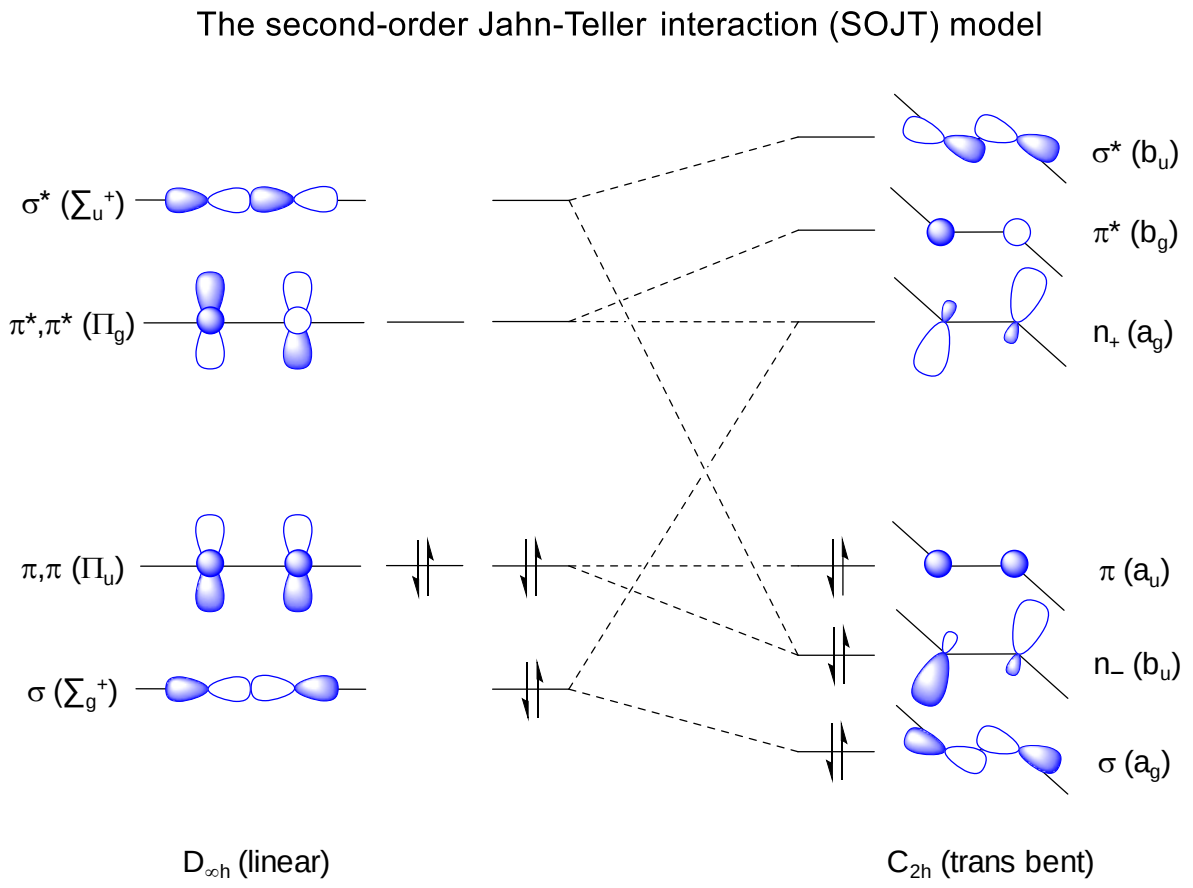

Figure 8. Second-order Jahn–Teller mixing of σ* and π as well as σ and π* levels (n_+ and n_- signify non-bonding orbital which is symmetric or unsymmetric with respect to inversion) leads to non-bonded electron pair character (as in the b_u (n_-) orbital, right) at the heavier group 14 elements.

repulsion, which is further amplified by the relatively weaker bond strengths and reduced orbital overlap in heavier congeners. The magnitude of this distortion is inversely proportional to the HOMO – LUMO+1 energy gap and is modulated by the

electronegativity of the substituents,[42] which influences orbital hybridisation and charge polarisation.

In subsequent years, the successful synthesis of compounds featuring analogous structural motifs expanded to encompass a diverse array of disilynes (***Figure 9***),[36,43,44–47] digermynes,[48–54] and distannynes.[49,53,55,56,57] Further reactivity studies unveiled remarkable chemical transformations, including small-molecule activation,[58] C–C coupling reactions,[47] and even a notable example of a digermyne catalysing the regioselective cyclotrimerisation of terminal alkynes.[59]

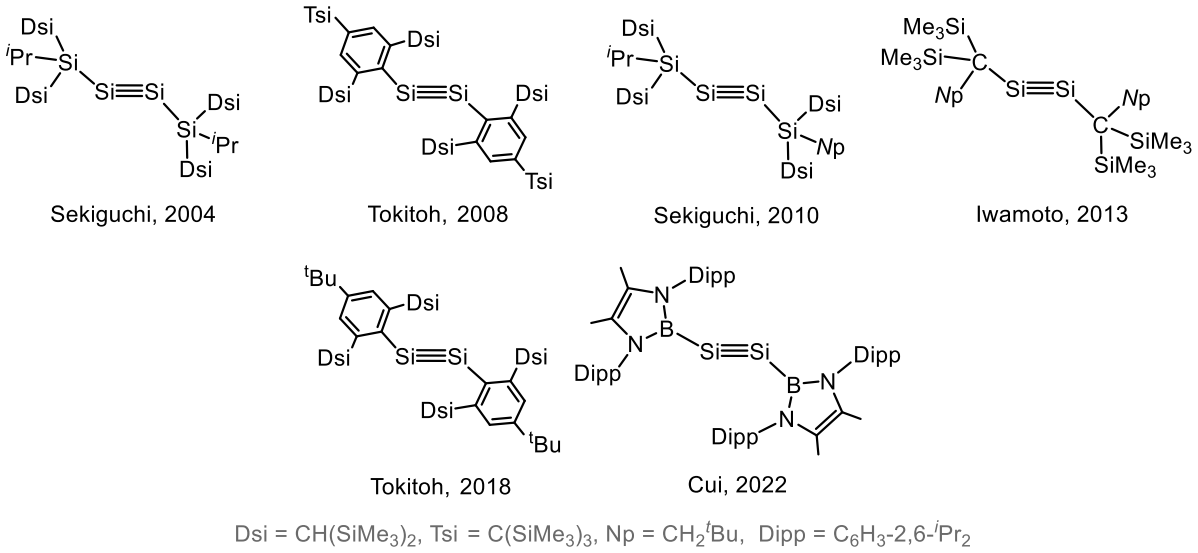

Figure 9. Chronological order of evolution of disilynes over the years.

1.2. Unsaturated metallacycles in heavier group-14 chemistry

In carbon chemistry, unsaturated metallacycles and metallacyclopolyenes are recognized as pivotal reactive intermediates in a wide array of transition metal-mediated stoichiometric and catalytic transformations involving alkynes. These include alkyne hydrofunctionalization, C–C coupling reactions, cyclotrimerization, alkyne metathesis, and polymerization processes.[60–63,64] Characterized by their unsaturated MC_n ring frameworks (M = transition metal and n = 2 – 5), these metallacycles adopt structures typified by motifs **I** – **IV**. Their distinctive electronic configurations, structural diversity, and mechanistic roles have been the subject of extensive experimental and theoretical investigations, culminating in comprehensive reviews that underscore their significance as a fundamental class of metallacyclic compounds in organometallic chemistry.

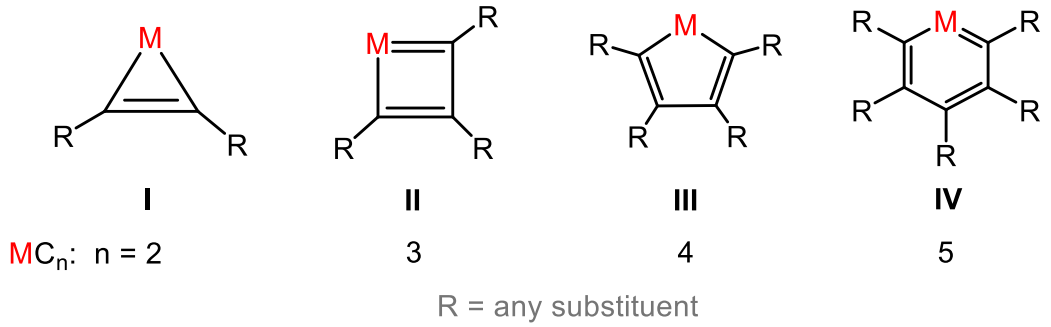

Figure 10. A general representation of metallacyclopolyenes (**I** – **IV**) containing unsaturated MC_n rings (M = any transition metal).

In comparison, the chemistry of metallacycles containing a transition metal (M) and heavier group 14 elements (E = Si–Pb) as the only heteroatoms in the ring is dominated by two common structures: (1) 1-metallacyclotetrelanes, the heavier analogues of metallacycloalkanes, and (2) 1-metalla-2,5-bistetrelacyclopent-3-enes, the heavier counterparts of metallacyclopent-3-enes.[65–73] These metallacycles feature R_2E–M–ER_2 linkages (R = ring substituent) with tetracoordinated tetrel centers, distinguishing them from metallacyclopolyenes.

Recent advances in the coordination chemistry of low-valent heavy tetrel elements have enabled the isolation of novel heavier metallacycles featuring three-coordinated tetrel centers stabilized in unconventional geometries and oxidation states. Initial breakthrough occurred in 2010, marked by the isolation of the first example of a heavier group 14 element alkyne analogue-transition-metal π-complex, Ag(I)-complex $[AgGe_2(Ar^{Dipp})_2][SbF_6]$ (Ar^{Dipp} = C_6H_3-2,6-(C_6H_3-2,6-$^iPr_2$)$_2$) (**I-9**) (***Figure 11***)[74] in the group of Power that features a significantly type-**I** metallacyclic character. Then three years later in 2013, Iwamoto and co-workers reported the seminal isolation of the

first η^2-disilyne complexes [$(PCy_3)M(Si_2(R_s)_2$, M = Pd (**I-10**), Pt (**I-11**)] (***Figure 11***).[75] showing a metallacycle character. This was accomplished through the reaction of a meticulously designed disilyne (R_s–Si≡Si–R_s, where R_s = – $C(TMS)_2(CH_2{}^tBu)$) with zero valent transition metal complex $M(Cy_3P)_2$ (M = Pd, Pt), yielding the corresponding η^2-coordinated disilyne-metal complexes through ligand substitution. Since then, research on heavier metallacycles has advanced significantlly, leading to report of numerous articles (**I-12** to **I-17**, ***Figure 11***).[46,76–80,81]

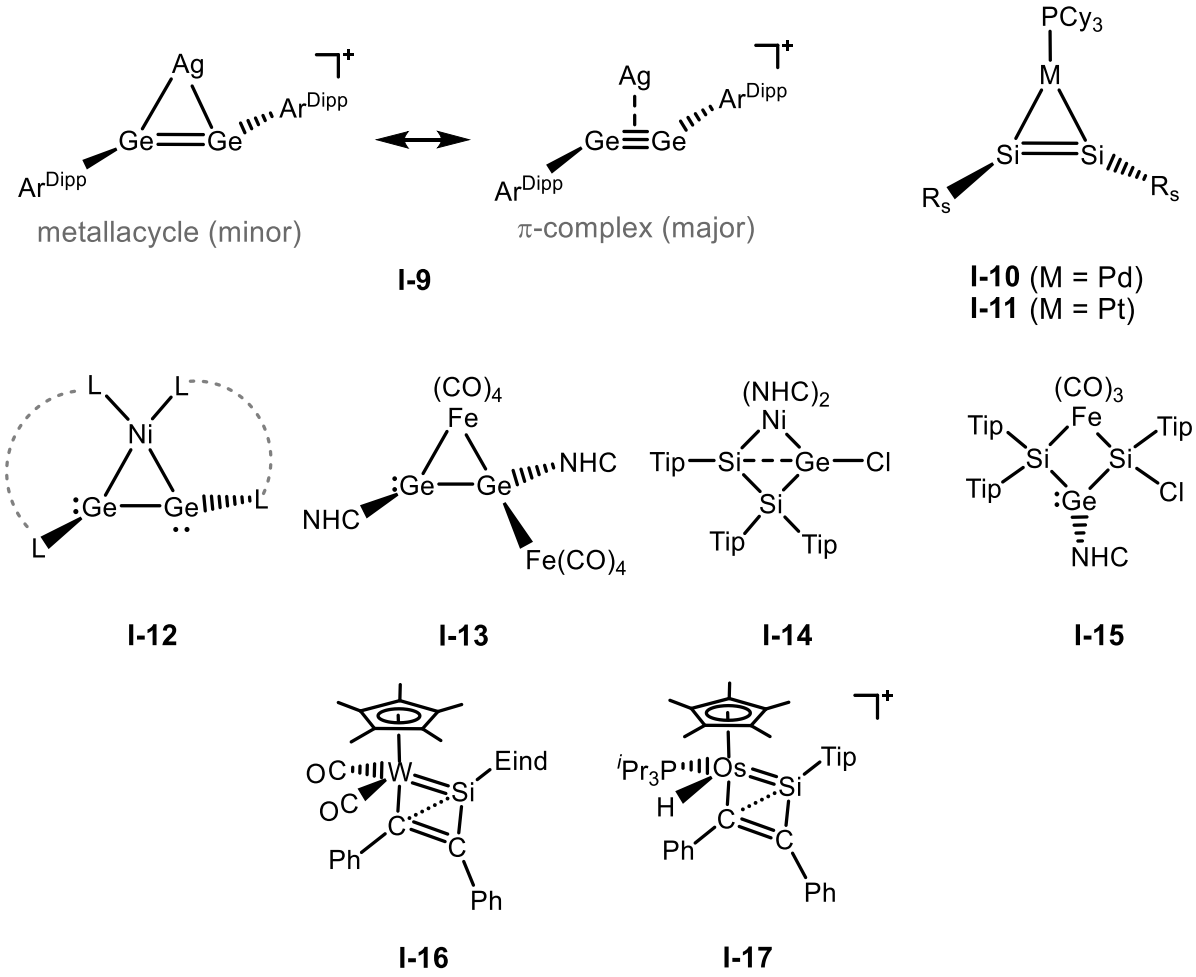

Ar^{Dipp} = C_6H_2-2,6-(C_6H_3-2,6-$^i pr_2)_2$; R_s = $C(SiMe_3)_2(CH_2CMe_3)$; L---L= bis(Si[($N^tBu)_2C(Ph)$])xanthene; NHC = $C[N(^iPr)C(Me)]_2$; Tip = C_6H_2-2,4,6-$^iPr_3$; Eind = 1,1,3,3,5,5,7,7-octaethyl-s-hydrindacene-4-yl.

Figure 11. Metallacycles (**I-9 – I-17**) containing low-valent heavier tetrels; formal charges are not included in the Lewis structures for simplicity; for all the cationic complexes, the corresponding counter anions are not depicted for clarity.

To date, the complex designated as **I-10** and **I-11** remain the only examples of a type-**I** metallacycles containing two low-valent silicon centers.[75] Additionally, the structurally analogous complexes **I-12**[81] and **I-13**[76] can be classified as closely related type-**I** metallacycles distinguished by their LGe–Ni–GeL (where L = imidinatosilylene ligand) and Ge–Fe–Ge bridging motifs. Within the category of type-

II metallacycles, apart from **I-14**[77,78] and **I-15**[82], all others (**I-16** and **I-17**)[79,80] (***Figure 11***) have been documented as products stemming from [2+2]-cycloaddition reactions involving silylidyne or germylidyne complexes with an alkyne. Notably, the majority of these advancements have been pioneered by Filippou and coworkers (**I-18** to **I-21**)(***Figure 12***).[1][83,84,85], underscoring their significant contributions to this field.

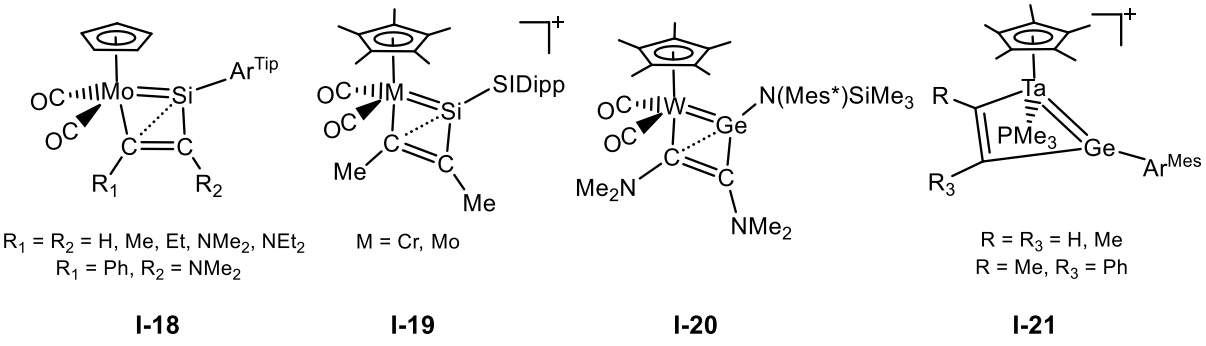

$R_1 = R_2$ = H, Me, Et, NMe_2, NEt_2
R_1 = Ph, R_2 = NMe_2

M = Cr, Mo

R = R_3 = H, Me
R = Me, R_3 = Ph

I-18 **I-19** **I-20** **I-21**

Ar^{Tip}=C_6H_2-2,6-(C_6H_2-2,4,6-$^{i}Pr_3$)$_2$;SIDipp = 1,3-bis-(2,6-diisopropylphenyl)imidazolidin-2-ylidene; Mes* = C_6H_2-2,4,6-^{t}Bu; Mes = C_6H_2-2,4,6-Me

Figure 12. Metallacycles (**I-18 – I-21**) represent the contribution from Filippou and coworkers.

[1] The metallacycles (**I-18**) were thoroughly characterized and reported in the following doctoral thesis; Oleg Chernov, "*Novel Molecular Si(II) Precursors for Synthesis of the First Compounds with Metal-Silicon Triple Bonds*", *Dissertation*, Rheinische Friedrich-Wilhelms-Universität Bonn, **2012**.

1.3. Zero-oxidation state heavier tetrel species E_nL_m($m \geq n$)

1.3.1. Base-supported mononuclear E_1(0) (E = Si – Pb)

While diamond and graphite, the two most common allotropes, possess remarkable industrial utility, the C(0) atom, the most straightforward building block of these stable carbon allotropes, is highly reactive. As a result, the study of complexes containing a carbon(0) core is intriguing. The first compound containing a carbon(0) core is traced to the carbodiphosphorane (CDP) $(PPh_3)_2C$, synthesized by Ramirez and coworkers in 1961.[86] Decades later, Frenking further clarified the "carbon(0) compound" essence of CDPs with theoretical and experimental data.[87] Theoretical evidence for the presence of a divalent carbon(0) core in $(NHC)_2C$ complexes (i.e., carbodicarbenes, CDCs) was also obtained.[88,89] Consistent with the molecular orbitals of CDPs, the HOMO and HOMO–1 of CDCs correspond to the π-type and σ-type lone pair orbitals, respectively.[88] For CDPs and CDCs, while the σ-type lone pair orbital is localized at the central carbon atom, the π-type lone pair orbital primarily resides at the central carbon, showing a measure of delocalization over the phosphine or carbene ligands.

a) Canonical Molecular Orbitals (MOs) of CDP $(PPh_3)_2C$

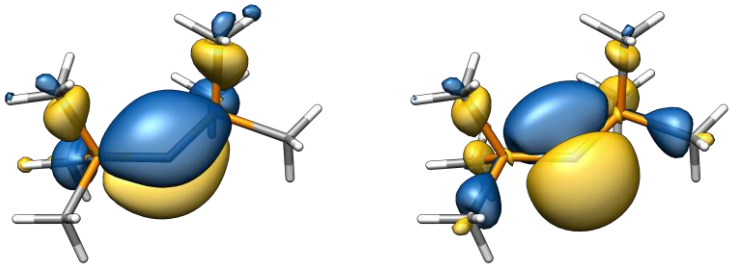

HOMO — $\pi_{oop}(P{-}C^{cent}{-}P)$ | HOMO−1 — $LP_{ip}(C^{cent})$

b) Resonance structures of CDP

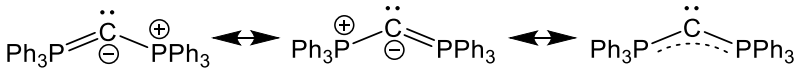

I-22-a **I-22-b** **I-22-c**

Figure 13. (a) Selected canonical molecular orbitals (MOs) of carbodiphosphorane $(PPh_3)_2C$ (CDP) (**I-22**) calculated by Dr. L. R. Maurer at B97-D3(BJ)-ATM/def2-TZVP level of theory; (b) Resonance structures (**I-22-a**, **I-22-b**, and the resonance hybrid form **I-22-c)** of CDP obtained from natural resonance theory.

The bonding between the central C(0) atom and the ligands in CDPs and CDCs, is thus most accurately described as donor–acceptor interactions (L→C←L). Singlet

carbenes (such as NHCs and CAACs) have a lone pair of electrons and an empty p orbital on the carbene carbon atom. Consequently, the most remarkable distinction between carbones and carbenes is the unique double donor capability of the former. Soon after the theoretical prediction by Frenking.[88] Bertrand and Fürstner experimentally validated this by synthesizing and structurally characterizing a benzoannulated derivative of $C(NHC)_2$ *via* X-ray crystallography.[90] This breakthrough marked the beginning of efforts to extend the carbone bonding concept to a broader range of donor ligands.[91,92,93,94] This leads to the conceptualization of a new class of complexes with the general structure $L:\rightarrow E^0\leftarrow:L$ (L=σ-donor, E=C, Si, Ge, Sn, Pb).

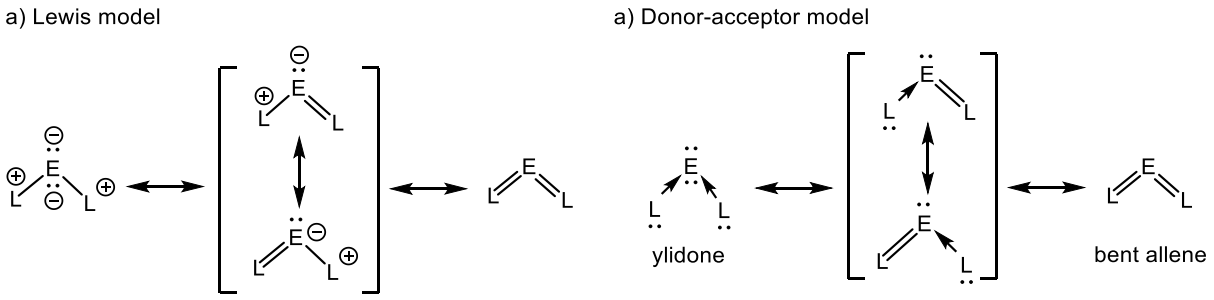

Figure 14. Resonance structures of ylidone E_1L_2 (E = C − Pb); L = 2e-donor neutral ligand.

The mononuclear E(0) complex (E = C, Si, Ge, Sn, Pb), formally classified as an ylidone,, is stabilized by two neutral 2e-donor ligands with subclassifications based on the central element: carbone (C)**,** silylone (Si)**,** germylone (Ge)**,** stannylone (Sn), and plumbylone (Pb).[95] The E^0 center retains four valence electrons, distributed as two distinct lone pairs: one occupies an in-plane molecular orbital, while the other, oriented perpendicularly, delocalizes into a π-type orbital across the supporting ligands.[96,97] (***Figure 14***).

Since the discovery of the first trisilaallene by Kira and coworkers in 2003,[98] later described as a silylone bearing two silylene ligands,[99] the number of known silylones expanded rapidly (***Figure 15***). Notable examples of this development include the bis(NHC)-supported silylone **I-23**,[100] the CAAC-supported silylones **I-24** ($Caac^{Me}$) [101] and **I-25** ($Caac^{Cy}$)[102], the germylene-supported silylone **I-27**,[103] and the cyclic bis(NHSi)-supported silylones **I-28**[104], **I-29**[105] and **I-30**[106] (***Figure 15***). Most recently, Iwamoto and coworkers reported the (CAASi)-supported silylone **I-31**, which is particularly intriguing due to its distinct electronic structures: a π-localized silenylidene structure in the solid-state **I-31** (Greenish-Black Solid) (***Figure 15***) and a π-delocalized silenylidene structure in solution **I-32** (Dark-Purple Solution).[107] Among these advancements, the first heteroleptic silylone **I-26** (***Figure 15***)[108],

reported by the So research group in 2016, is particularly noteworthy. The heteroleptic environment induces an asymmetric structure, where the silicon atom forms a double bond with the CAAC ligand while the $IMe_2{}^iPr_2$ ligand is oriented perpendicular to the C^{CAAC}–Si–$C^{IiPr2Me2}$ plane.

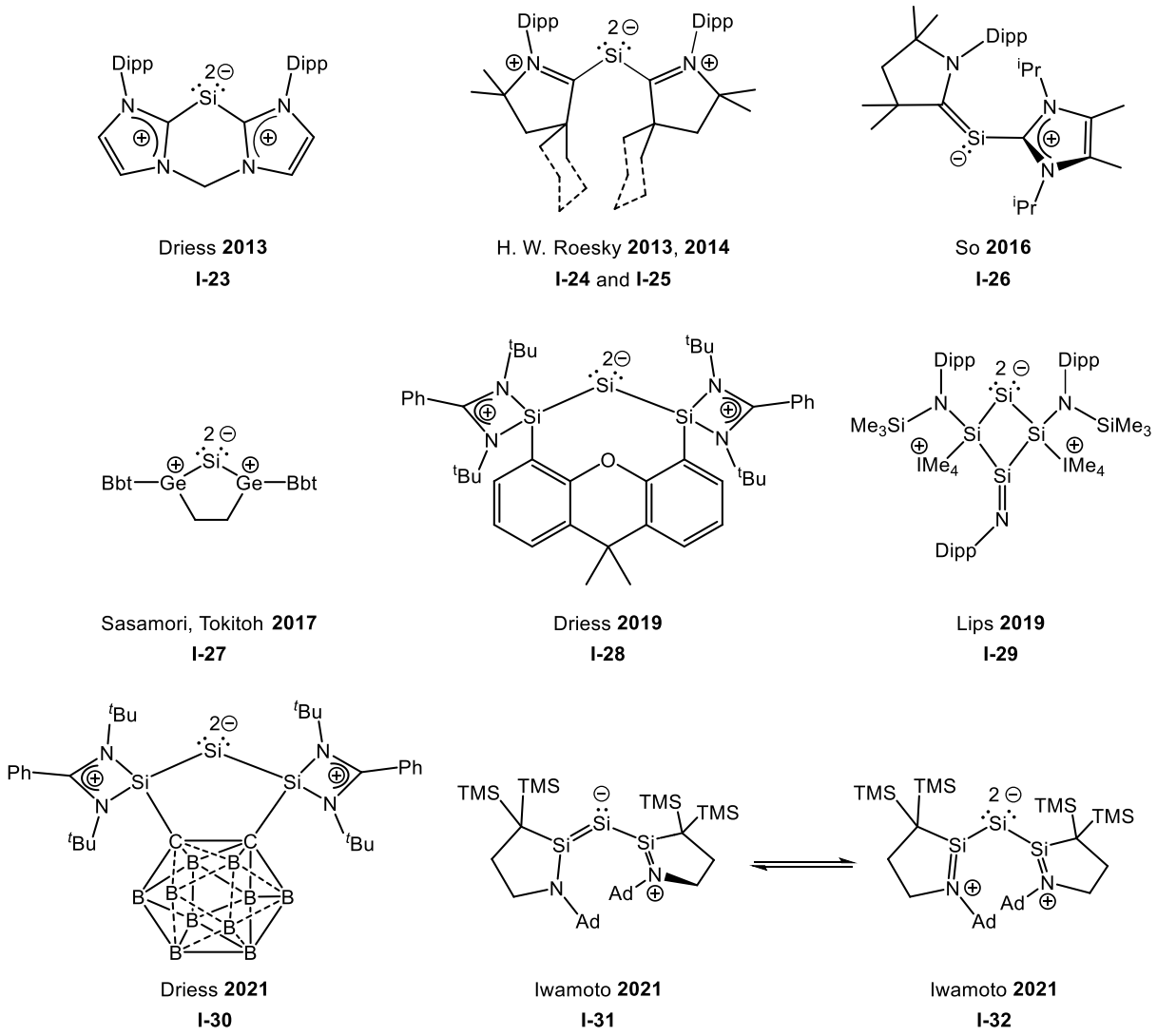

Figure 15. Litertaure known homoleptic and heteroleptic monoatomic Si(0) complexes **I-23** – **I-32**; In compound **I-30**, all B atoms contain H atom on boron and are not depicted due to clarity.

Over the past decade, the isolation of various silylones (**I-23** to **I-32**) has enabled extensive exploration of their chemistry (***Figure 15***). For instance, the reaction of the bis(NHC) silylone **I-23** with Lewis acids, such as $GaCl_3$ and $ZnCl_2$, resulted in mono- and bis-Lewis acid-base adducts, respectively.[97] Oxidation of silylones **I-23** and **I-29** with chalcogens (S, Se, Te) yielded base-supported SiX_2 compounds (X = S, Se, Te), which can be viewed as heavy homologues of CO_2.[100,112] The reaction of silylone **I-23** with CO_2 led to the formation of a dicarbonato complex (bis-NHC)$Si(CO_3)_2$.[110] However, the reaction of **I-23** with N_2O proved uncontrollable, yielding different dimeric silicon-oxo-species depending on the reaction conditions.[104] These findings

underscore the rapid progress in exploring silylone chemistry. Notably, despite the literature on homoleptic silylones like $(CAAC)_2Si$ and $(NHC)_2Si$, and heteroleptic silylone (CAAC)Si(NHC), a vital report on heteroleptic silylone featuring only N-heterocyclic carbenes ($(NHC)Si(IMe_2{}^iPr_2)$, NHC = SIDipp, IDipp) was achived by Filippou group and coworkers.[111]

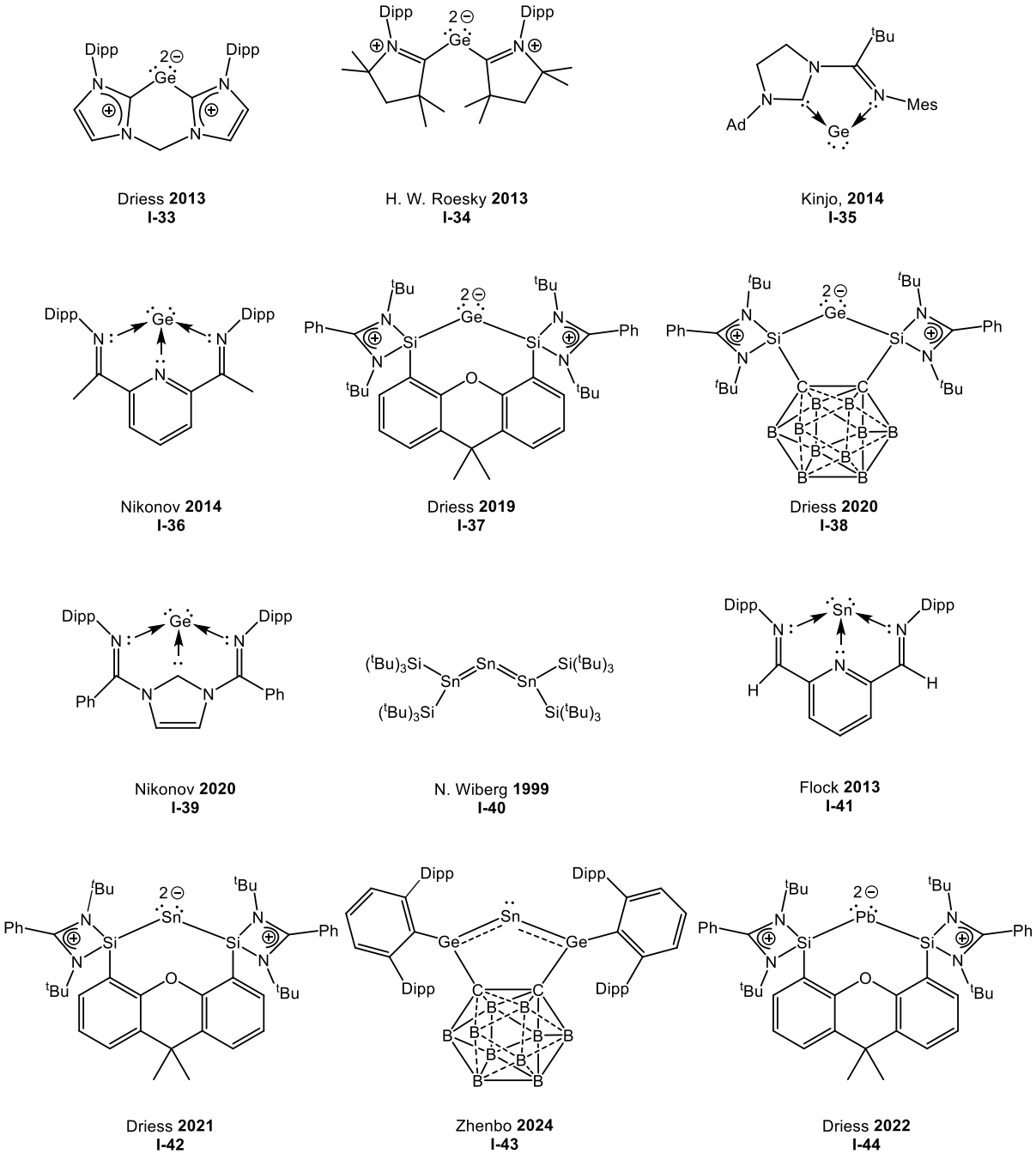

Figure 16. Literature known homoleptic and heteroleptic monoatomic Ge(0), Sn(0) and Pb(0) complexes **I-38** – **I-49**; In compound **I-38** and **I-43**, all B atoms contain H atom on boron and are not depicted due to clarity.

The isolation of several structurally similar motifs was extended to a broader range by employing different strong donor ligand systems, leading to experimentally

accessible germylones (**I-33**,[112] **I-34**,[113] **I-35**,[114] **I-36**,[115] **I-37**,[81] **I-38**[116] and **I-39**[117]) (***Figure 16***). However, moving to the heaviest Group 14 elements, tin and lead, the synthesis of such complexes becomes rather difficult due to their intrinsic lability, which readily leads to decomposition of the products as free ligands and elemental tin or lead. The first bent tristannaallene **I-40**[118] (***Figure 16***) was reported in year 1999. Subsequently, Flock and co-workers synthesized complex **I-41**[119] containing tin atom in the formal oxidation state of zero. In 2021, the synthesis of genuine stannylone **I-42**[120] (***Figure 16***) with a monoatomic two-coordinate tin(0) atom supported by a bis(silylene) ligand was reported by Dries group and the same group also reported the synthesis of a monoatomic, zero valent lead complex, Plumbylone **1-44**[121], the recently synthesized bisgermylene-stabilized stannylone **I-43**[122] (***Figure 16***) was also reported by Zhenbo et. al. undergoing catalytic reduction of nitrous oxide and nitro compounds *via* element-ligand cooperativity.

1.3.2. Base-supported Si°-Isocyanide compounds

Cyano-(Si(CN)H) and isocyanosilylenes (Si(NC)H) are highly reactive silicon(II) species that play a significant role in interstellar silicon chemistry. Given that silicon is the seventh most abundant element in the cosmos,[123–126] these compounds are of particular interest in astrochemical studies. Quantum chemical investigations of the [H,Si,C,N] potential energy surface reveal six low-energy isomers, each with corresponding triplet-state configurations. Among these, singlet cyanosilylene (**A**) is identified as the global minimum structure, while singlet isocyanosilylene (**B**) lies slightly higher in energy. The six isomers can be classified into three distinct structural classes (***Figure 17***)[127–129]:

i). Cyanosilylenes **A** and isocyanosilylenes **B**.

ii). 3-H-2-aza-1-silacyclopropenylidene **C** and silaisocyanocarbene **D** results from the side-on and end-on addition of hydrogen cyanide (HCN) to a ^{1}Si atom.

iii). the iminosilenylidene **E** and 2-H-2-aza-1-silacyclopropenylidene **F** are formal products of hydrogen isocyanide (HNC) addition to ^{1}Si.

The generation and spectroscopic identification of the aforementioned silicon species remains highly challenging, with only the isomers **A** – **D** being observed to date. Recent advances in silicon chemistry in unusually low oxidation states have demonstrated that N-heterocyclic carbenes (NHCs) serve as particularly effective Lewis bases for the thermodynamic stabilization of highly reactive, unsaturated silicon species. Building on this understanding, Prof. Filippou's research group

successfully isolated and fully characterized the first NHC-supported iminosilenylidene, (SIDipp)Si=C=N(Ar^{Mes}) (**I-45**)[130] (SIDipp = C[N(Dipp)CH$_2$]$_2$, Dipp =

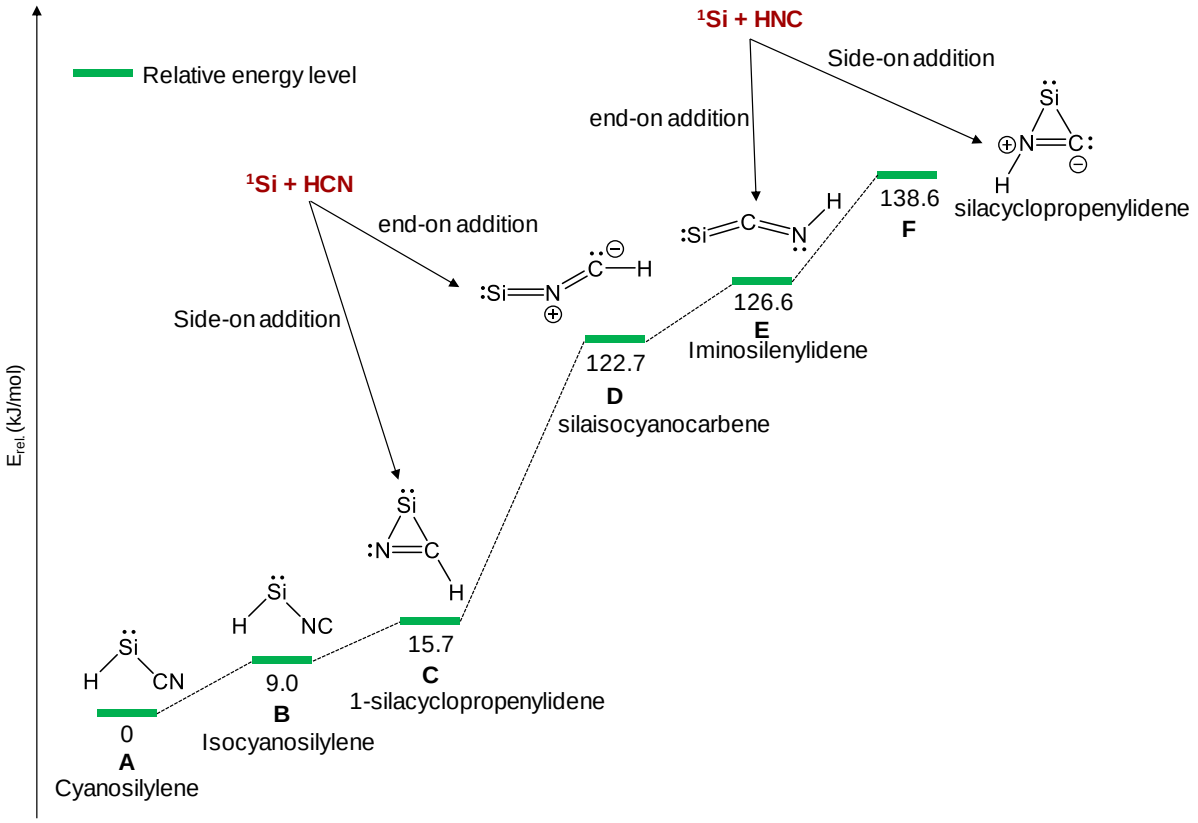

Figure 17. Six lowest-lying singlet isomers **A** – **F** of the [H,Si,C,N] potential energy hypersurface ordered with increasing energy (bottom to top). Relative energies are given in kJ·mol^{-1} at the RHF-UCCSD(∞) + E_T + E_{CC} + E_{BD} + E_{SO} + E_{CG} + E_{ZPE} level of theory.[127] Formal charges are encircled in the Lewis structures, and the two dots at the Si, C and N atoms represent a lone pair of electrons.

2,6-diisopropylphenyl; Ar^{Mes} = C$_6$H$_3$-2,6-Mes, Mes = 2,4,6-trimethylphenyl) (***Figure 18*** top). A silicon atom economic two-step synthesis of **I-46** involve a 2e-reduction of the isocyanide-supported silyliumylidene salt [SiBr(CNAr^{Mes})(SIDipp)][B(Ar^F)$_4$] (Ar^F = B(C$_6$H$_3$-3,5-(CF$_3$)$_2$)$_4$] (**I-45**) with KC$_8$. The silyliumylidene salt **I-45** was obtained from SiBr$_2$(SIDipp) after bromide abstraction with an equimolar mixture of Na[B(Ar^F)$_4$] and Ar^{Mes}NC.[130]

However, isocyanides are generally weaker σ-donors than NHCs, as evidenced by their lower proton affinities.[131,132] As a result, isocyanide compounds with low-coordinate silicon centers are relatively rare.[133–138] Only a limited number of isocyanide-silylene adducts of the general formula R$_2$Si(CNR) (R = univalent group) have been isolated. These features pyramidal, tricoordinate silicon centers. More recently, 1-silaketeniminyl lithium compounds of the type R$_2$B(Li)Si=C=NR´ (where BR$_2$ = diaminoboryl; R´ = 1-adamantyl, 2,6-diisopropylphenyl)[138] were also reported, and

the reductive coupling of two isocyanides was achieved using a bis(NHSi) scaffold (NHSi = N-heterocyclic silylene).[139]

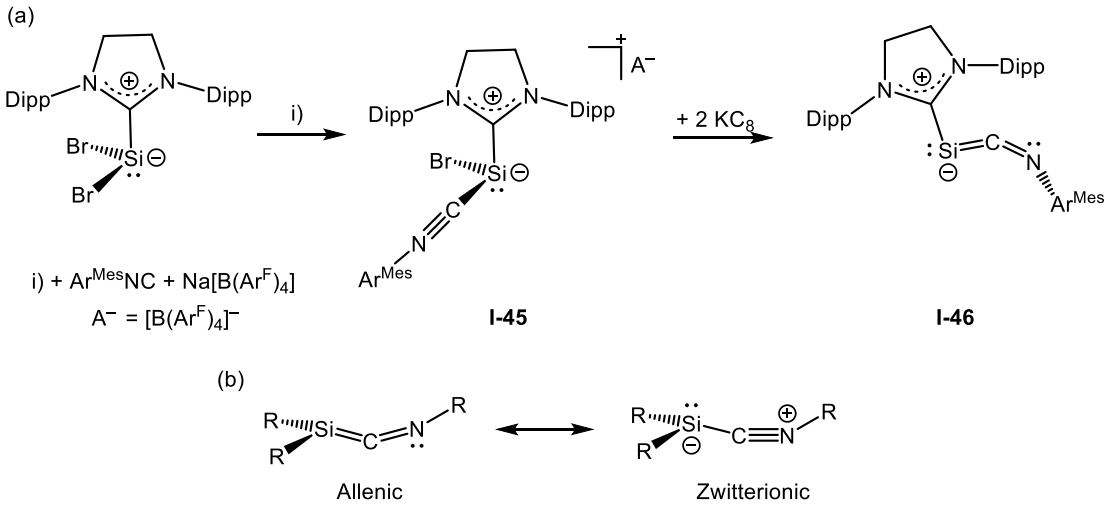

Figure 18. (a) Synthetic pathway for the unprecedented Si^0-isocyanide compound (SIDipp)Si=C=N(Ar^{Mes}) (**I-46**) reported in the literature; (b) Resonance structures of isocyanide-silylene adducts.

Structural, spectroscopic, and quantum chemical studies suggest that the bonding in $R_2Si(CNR)$ can be described by combining allenic and zwitterionic resonance structures (***Figure 18*** bottom). This insight helps explain the observed isocyanide dissociation and the silylene-like reactivity of these compounds,[133,134,140] which differs from the addition chemistry of Si=C bonds in silenes [141,142] and 1-silaallenes. [143,144] These studies also suggest that electropositive substituents on silicon, which are known to reduce the singlet-triplet gap in silylenes,[145–147] would increase the contribution of the allenic form, thereby strengthening the $Si–C_{isocyanide}$ bond. Furthermore, Si(NHC) fragments, which possess a triplet ground state [148] are expected to bind strongly to isocyanides. Capitalizing on this theoretical framework, Filippou and coworkers successfully isolated the unprecedented Si^0-isocyanide compound (SIDipp)Si=C=N(Ar^{Mes}) **I-46**.[130] They further demonstrated its utility as a Si(NHC) transfer reagent by achieving its quantitative conversion into the novel NHC-supported germasilyne (*Z*)-(SIDipp)(Cl)Si=GeAr^{Mes} **I-54** (***Scheme 1***).[130]

1.3.3. Carbene-supported dinuclear E_2L_2 (E = C – Sn) complexes

Seminal breakthroughs in low-oxidation-state silicon chemistry over the past four decades have been marked by two pivotal achievements: West's 1981 synthesis of the first disilene, $Mes_2Si=SiMes_2$ (**I-4**, ***Figure 3***) and Sekiguchi's 2004 isolation of the first disilyne, R-Si≡Si-R (R = $Si^iPr_2Dsi_2$), featuring silicon in +II and +I oxidation states, respectively.[36] These landmark discoveries not only expanded the frontiers of silicon multiple-bond chemistry but also spurred a compelling question in subsequent years:

Could the boundaries be pushed even further to isolate a compound containing a silicon(0) dimeric core?. This inquiry gains further significance in light of the highly reactive diatomic $Si_2(0)$ molecule, which exhibits a triplet ground state ($X^3\Sigma g^-$) and has been characterized in both gas-phase studies and low-temperature argon matrices.[149] A landmark achievement in this field was the carbene-stabilized disilicon(0) complex, $Si_2(0)$ (**I-47^{NHC}**), first reported by Robinson and coworkers in 2008 *via* the potassium graphite reduction of (IDipp)$SiCl_4$ (***Figure 19***).[150] Following this breakthrough, Roesky and coworkers isolated the CAAC^{Me}/^{Cy}-supported disilicon(0) analogue (**I-47^{CAAC}**), which exhibited pronounced donor-acceptor interactions between the silicon(0) centers and the carbene carbon.[151] More recently, Mo and coworkers expanded this chemistry by synthesizing an N-heterocyclic silylene (NHSi)-stabilized disilicon(0) complex (**I-47^{NHSi}**).[152] Despite these advancements, exploring new facets of disilicon(0) chemistry poses significant research challenges.

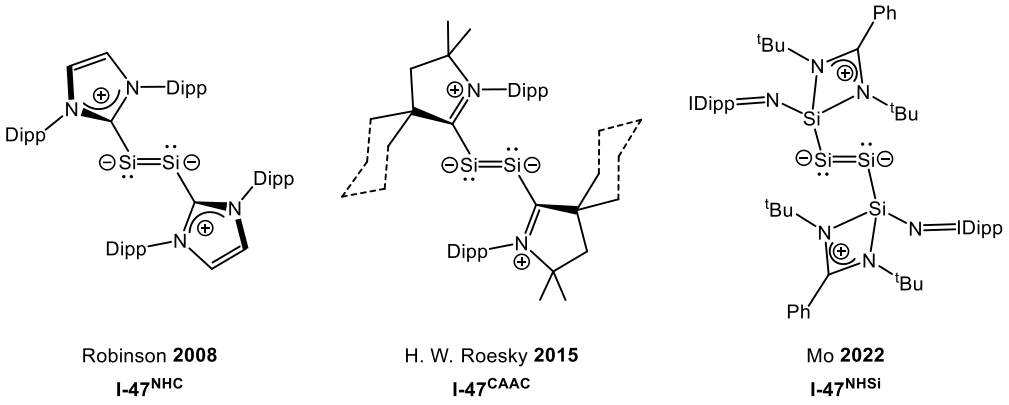

Figure 19. Chronological order of evolution of base-supported dinuclear Si(0) compounds.

Just one year after the discovery of the first $Si_2(0)$ complex stabilized by an N-heterocyclic carbene (**I-47^{NHC}**), Jones and coworkers synthesized the germanium analogue $Ge_2(0)$ (**I-48^{NHC}**)[153] (***Figure 20***) by reducing an NHC-supported germylene precursor with one equivalent of the magnesium(I) dimer $[\{Mg\{[N(Mes)CMe]_2CH\}\}_2]$. The same group extended this methodology to the heavier congener, successfully isolating the tin analogue $Sn_2(0)$ (**I-49^{NHC}**)[154] in 2012, albeit in a modest 5% yield. The carbon analogue of these group 14 element (0) complexes was initially only a theoretical prediction. However, in 2014, Roesky and coworkers achieved a breakthrough by reporting the first isolable $C_2(0)$ species (**I-50^{CAAC}**),[155] stabilized by a cyclic (alkyl)(amino)carbene (CAAC) ligand. In 2016, the same research group reported the synthesis of a cyclic triatomic centre, Si_3CAAC_3 (**I-51^{CAAC}**)[156], through the potassium graphite reduction of (CAAC)$SiCl_4$ (***Figure 20***).

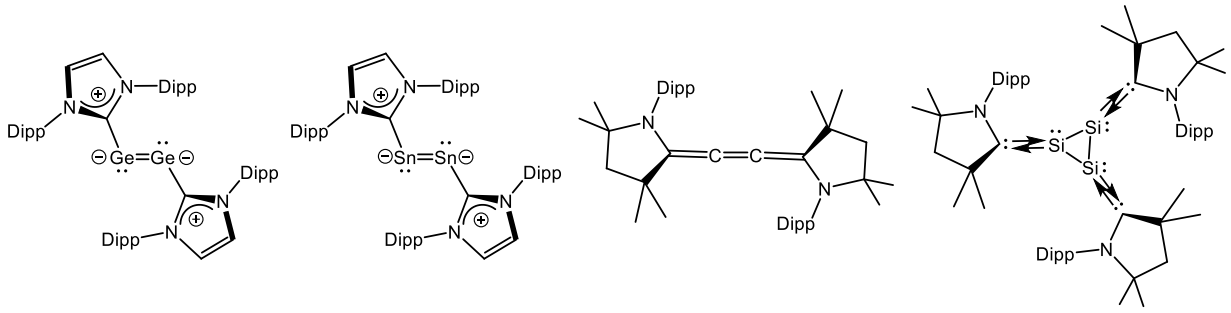

Figure 20. Chronological order of evolution of base-supported $Ge_2(0)$, $Sn_2(0)$, $C_2(0)$ and trinuclear $Si_3(0)$ compounds.

1.4. Base-supported heteroditetrelynes and their constitutional isomers

The heavier group 14 homologues of alkynes, RE≡ER (E = Si–Pb; R = monodentate substituent), along with their valence isomerization to vinylidene analogues (:E=ER_2), have garnered significant attention in both theoretical and experimental chemistry due to their unique electronic structures and reactivity profiles [13,157] Computational analyses of the potential energy hypersurface (PES) reveal a pronounced divergence between acetylene (C_2H_2) and its heavier congeners. For carbon systems, vinylidene (H_2C=C:) exists as the sole high-energy minimum on the PES, undergoing rapid isomerization to acetylene *via* a facile 1,2-hydrogen shift with a remarkably low activation barrier of 10.40 ± 0.04 kJ·mol^{-1}.[158,159]

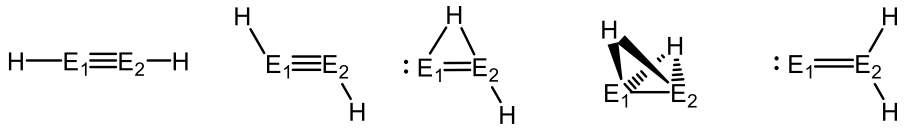

	A	**B**	**C**	**D**	**E**
E1 = E2 = Si	0.0	–79.5	–95.0	–157.7	–98.7
E1 = E2 = Ge	0.0	–107.9	–131.0	–192.5	–132.2
E1 = Ge; E2 = Si	0.0	–94.1	–142.5	–167.5	–132.3
E1 = Si; E2 = Ge	0.0	–94.1	–119.4	–167.5	–86.7

Figure 21. Calculated minimum structures of E_2H_2. Depicted are linear **A**, trans-bent **B**, monohydrid bridged **C**, bishydride bridged **D** and vinylidene **E** and calculated energies in kJ·mol^{-1} for Si and Ge from the literature.[160,161]

In contrast to carbon, the linear alkyne-like structure **A** for heavier analogues E_2H_2 (E = Si − Pb) lies relatively high in energy. This reflects the reduced E−E bond order in the heavier congeners, which can be attributed to mixing between the σ* and π-orbitals due to significantly increased core-core repulsion.[162] However, other isomers

are predicted to be energetically closer to the minimum: a trans-bent structure **B**, a structure bridged by one hydrogen **C** and two hydrogen atoms **D**, and the vinylidene isomer **E**.[157,163,164] Experimental evidence for the exotic structures **C** and **D** has been provided for Si_2H_2 through rotational spectroscopy conducted in low-temperature matrices.[165,166] Additionally, isomer **E**, like vinylidene $H_2C{=}C{:}$ and disilavinylidene $H_2Si{=}Si{:}$, has been experimentally observed as a transient species in the gas phase.

Over the past two decades, homonuclear ditetrelynes (RE≡ER) have emerged as a pivotal area in main group chemistry. However, the development of base-free heteroditetrelynes remains scarce, representing a critical challenge in the field. Conventionally, homonuclear ditetrelynes are synthesized *via* reductive dehalogenation of tetrel(II) or tetrel(IV) precursors,[58,167] however this approach has proven ineffective for accessing heteronuclear analogues.[168] To date, the only successful strategy reported by Filippou and coworkers relies on a "$SnAr^{Dipp}$" unit transfer reaction. Specifically, the distannyne $Sn_2Ar^{Dipp}_2$ reacts with germanium(II) halide ($Ar^{Dipp}GeCl$) at ambient temperature, yielding the isolable dark-purple stannagermyne $Ar^{Dipp}Sn{\equiv}GeAr^{Dipp}$ (**I-53**, ***Scheme 1***).[169]

The only base-free heteroditetrelyne

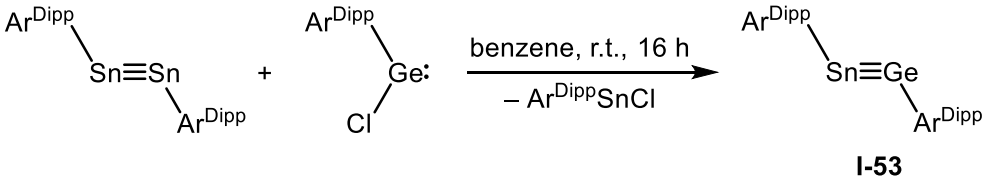

I-53

Way to the first base-supported heteroditetrelyne

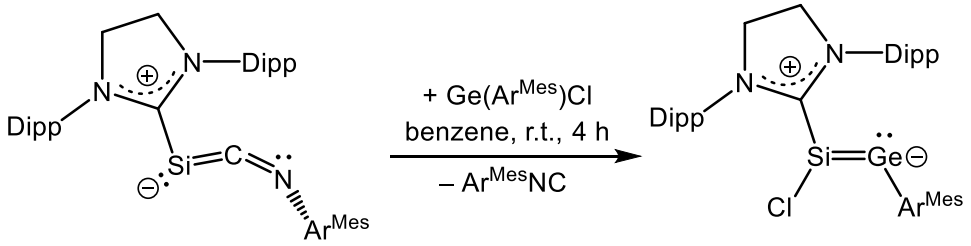

I-52 **I-54**

Scheme 1. (***top***) synthesis of a stannagermyne **I-53** following the cross coupling of a distannyne $Sn_2Ar^{Dipp}_2$ with Ge(II) precursor; (***bottom***) synthesis of an NHC-supported germasilyne **I-54**.

As mentioned earlier, the stabilization of highly reactive low-valent main-group species using *N*-heterocyclic carbenes (NHCs) cyclic (alkyl)(amino)carbenes (CAACs) as potent σ-donors has unlocked a wealth of novel compounds with remarkable

synthetic potential in recent years.[130,170–176] While base-free heteroditetrelynes remain exceedingly rare, even base-supported variants are scarcely represented in the literature, with a notable example recently reported by Filippou and coworkers.[130] Leveraging NHC stabilization, the first two-coordinate Si^0-isocyanide complex (**I-52**) was successfully isolated. Subsequent reaction with $Ar^{Mes}GeCl$ induced an unusual "Si(NHC)" transfer, enabling the isolation of the base-supported heteroditetrelyne (Z)-(NHC)(Cl)Si=GeAr^{Mes} (**I-54**) (***Scheme 1***).[130]

Notably, base-supported heteroditetrelynes remain exceptionally rare in the literature, in stark contrast to their constitutional isomers base-supported heteronuclear ditetrelavinylidenes which have been more extensively investigated (***Figure 22***).[177,178] The inaugural entry into this intriguing class of compounds was reported by D. Scheschkewitz and coworkers, who achieved the coreduction of $Tipp_2SiCl_2$ and ($I^iPr_2Me_2$)$GeCl_2$ using lithium naphthalenide (LiNp). This synthetic strategy afforded the $I^iPr_2Me_2$-supported silagermenylidene **I-55**, marking a significant milestone in the field.[179] Building upon this foundational work, the same research group later introduced a structurally related derivative, **I-56**, *via* an alternative synthetic route involving the reduction of ($I^iPr_2Me_2$)$GeCl_2$ with a disilenide reagent.[82] Further expanding the scope of these systems, L. Wesemann and coworkers successfully synthesized the phosphine-supported germasilenylidene **I-57**, exploiting an intramolecular germylene-phosphine Lewis pair as a key stabilizing motif.[180] The most recent advancement in this area was reported by Filippou and coworkers, who disclosed the synthesis of the first cyclic (alkyl)(amino)carbene (CAAC)-stabilized germasilenylidene, **I-58**, thereby broadening the structural and electronic diversity of this emerging class of compounds. [177]

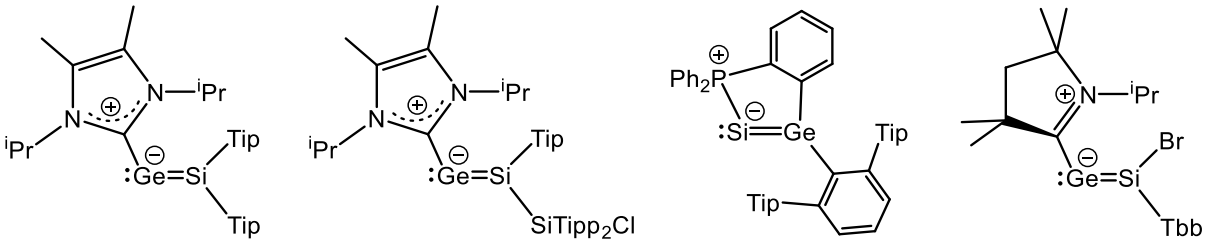

Figure 22. Literature known heavier congeners of hetero ditetrelavinylidenes.

It is rather intriguing that cyclic (alkyl)(amino)carbenes (CAACs) have not been extensively employed in stabilizing heavier group-14 vinylidenes despite their distinct electronic and steric properties compared to traditional N-heterocyclic carbenes

(NHCs).[179,181,182] Unlike conventional NHCs, CAACs exhibit significantly enhanced π-accepting capabilities due to their reduced σ-donating character and lower-lying vacant π*-orbitals, which should, in principle, facilitate the stabilization of low-valent group-14 species. [174,175,183]

1.5. Diradicaloids in heavier group-14 elements

Molecules harboring two unpaired electrons in degenerate or near-degenerate molecular orbitals are classified as diradicals.[184–186] Singlet diradicals (or diradicaloids) hold particular significance owing to their fascinating electronic configurations [187,188] and unique reactivity profiles.[189–191] These open-shell species, celebrated for their remarkable optical, magnetic, and electronic properties,[192,193] have attracted substantial interest as promising candidates for next-generation functional materials.[194] Based on the degree of coupling between the two radical centers, they can be bifurcated into two principal classes: disjoint diradicals (uncorrelated spins) or conjugated biradicals (spin-coupled systems) (***Figure 23***). [183]

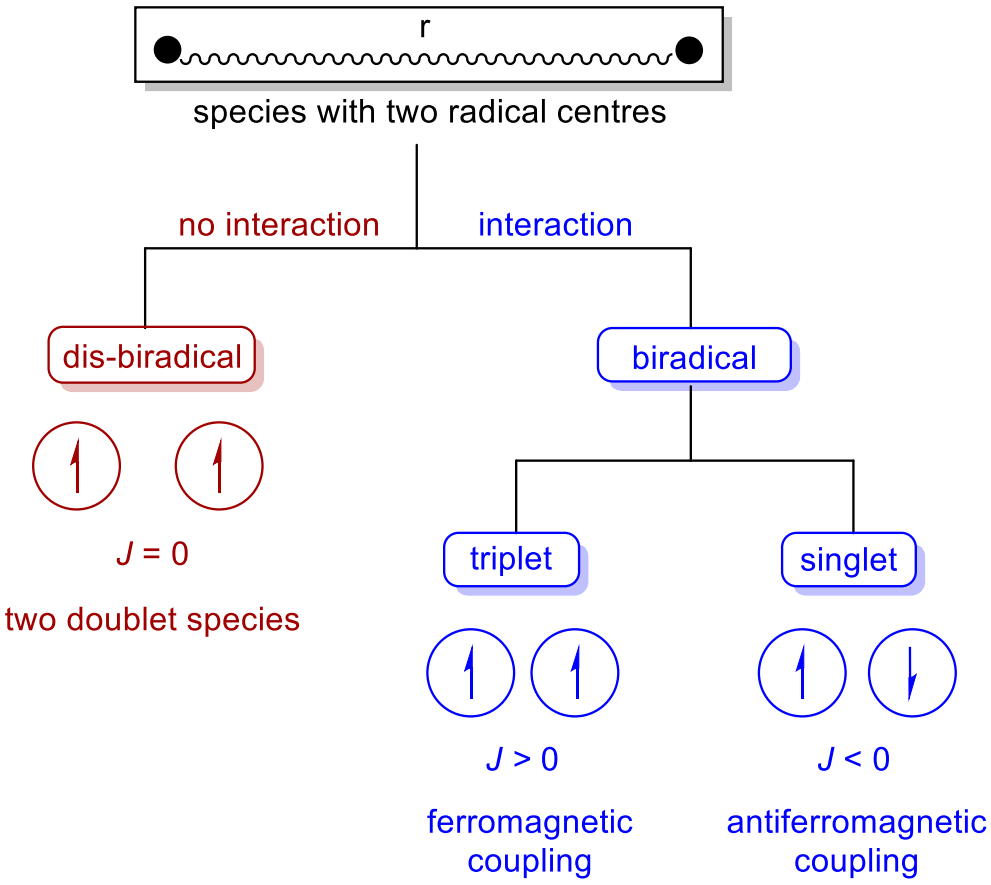

Figure 23. Definition of dis-biradicals and biradicals according to the reference [195].

In disjoint diradicals, where the unpaired electrons are either spatially segregated by a significant distance (r) or exhibit orthogonal spin alignment, exchange interactions

(J) are negligible, thereby categorizing them as non-interacting diradicals. These systems essentially function as two isolated spin doublets coexisting within a single molecular framework. Conversely, if substantial coupling exists between the radical sites, the species is designated as a conjugated biradical. This interaction manifests in two distinct scenarios: (a) ferromagnetic alignment of spins, yielding a positive exchange interaction and a triplet ground state, or (b) antiferromagnetic alignment, resulting in a negative exchange interaction and a singlet ground state.

Four-membered non-Kekulé ring systems, exemplified by the classic S_2N_2,[196] represent prominent examples of stable main-group diradicaloids. In the domain of heavier group 14 elements, Lappert and coworkers pioneered the field with the first reported Sn(I) diradicaloid **I-59** (***Figure 24***).[197] Subsequently, Power and coworkers achieved a landmark synthesis in 2004 by isolating the first stable germanium(II) diradicaloids, **I-60**.[198,199] In 2011, Sekiguchi and coworkers reported the first stable Si_2N_2 four-membered ring, exhibiting an intriguing non-Kekulé singlet diradical character **I-61**.[200] (***Figure 24***) Further expanding this chemistry, Sasamori and coworkers (2019) introduced the structurally unique 1,4-digermabenzene **(I-62)**,[201] a system exhibiting substantial diradical character capable of facile H_2 activation.[201] Most recently, Ghadwal and coworkers made significant advances by isolating cyclic tin(I) **(I-63)** [202] and germanium(I) **(I-64)** [203] diradicaloids, further enriching the landscape of low-valent group 14 radical species (***Figure 24***).

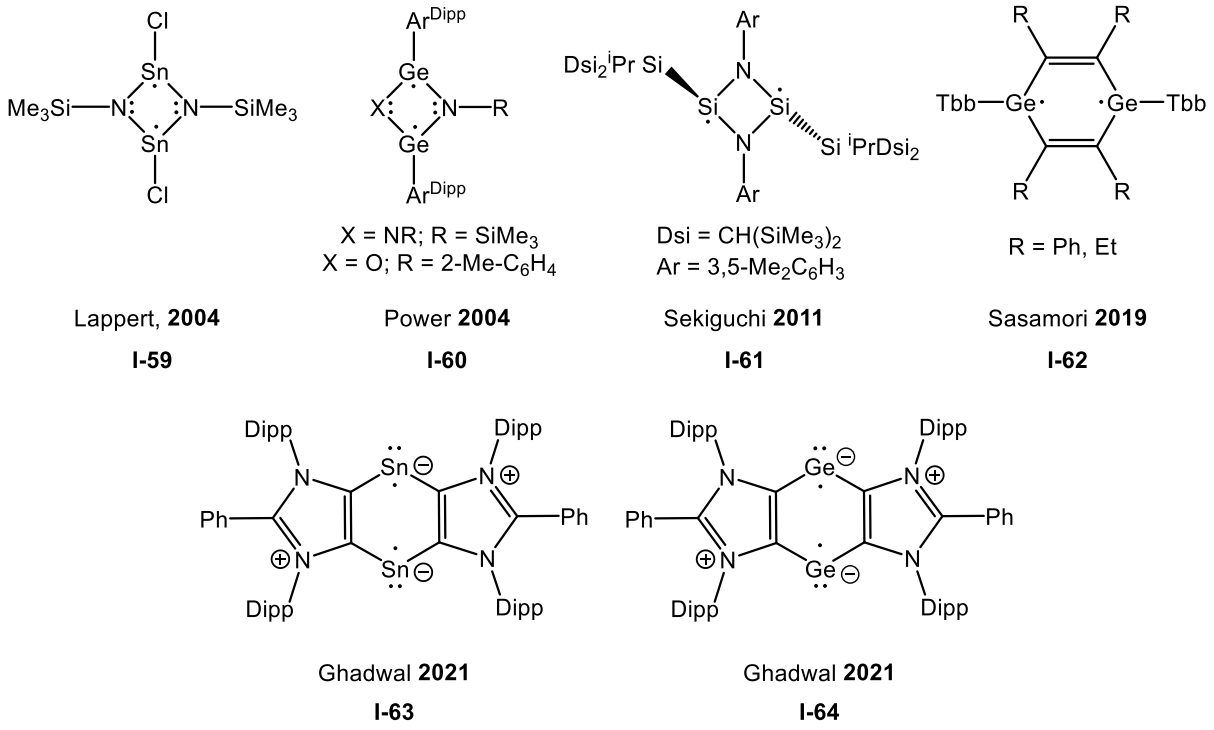

Figure 24. Chronological order of selected examples of literature known Group 14 diradicaloids.

1.6. Heteronuclear analogous of alkynes R–C≡E–R' (E = Si – Pb)

Alkynes are highly versatile organic compounds characterized by a C≡C triple bond, which enable them to participate in diverse reactions that yield a wide array of functional groups and structures.[204] Researchers have extensively explored the substitution of the triple-bonded carbon atoms with the next heavier group 14 element, such as silicon,[205–207] germanium,[34] tin [35] and lead [33] providing access to unique compounds known as heavier homonuclear alkyne analogues, namely disilyne, digermyne, distannyne and diplumyne. (R^1−E≡E−R^2, E = Si, Ge, Sn, Pb). These studies, conducted both experimentally and theoretically,[36,206,207] have revealed that heavier main-group analogues of alkyne exhibit distinctive reactivity due to their unique trans-bent geometry, which features two non-degenerate π-bonds.[13] Pioneering work by the research groups of Power,[34,35] Sekiguchi [36,205] and Wiberg [206] led to the successful isolation of the aforementioned compounds, opening new avenues for further investigation. Extending this approach, the replacement of one carbon atom in alkynes with silicon yields heteronuclear analogues known as silynes (R–C≡Si–R', whereas E = Ge (Germynes), Sn (Stannynes), Pb (Plumbynes)). Theoretical studies predict that R–C≡E–R' adopt a trans-bent molecular geometry similar to R^1−E≡E−R^2,[208–210] further highlighting the intriguing structural and chemical behaviour of these heavier group 14 analogues.

Quantum chemical investigations of the [E, C, 2H] potential energy surface (PES) (where E = Si, Ge) have demonstrated that 1-tetrelavinylidenes (E=CH_2, **A**) constitute the global energy minima. These are followed in stability by the *trans*-bent tetrelaacetylenes (H−E≡C−H, **B**) and 2-tetrelavinylidenes (C=EH_2, **C**) (Figure 22).[208,211–215] Notably, the least stable isomers, **C**, occupy shallow potential wells and undergo a two-step isomerization process *via* intermediate **B**, characterized by low activation barriers, ultimately converting into the thermodynamically favored **A** (***Figure 25***). Remarkably, the compounds that have been proven sufficiently stable for structural characterization of the aforementioned isomers are as follows:

i). 1-tetrelavinylidenes: The first synthetic realization of the global minimum isomer, a single donor-supported 1-silavinylidene (:Si=CR_2), occurred in 2016 by So's research group through the 2e⁻ reduction of NHC-CAAC-silyliumylidene iodide [($Caac^{Me}$)SiI($I^iPr_2Me_2$)]I.[108] This reaction yielded the first 1-silavinylidene [($Caac^{Me}$)Si($I^iPr_2Me_2$)] **I-65** (***Figure 26***a). Experimental and theoretical studies suggest that **I-65** can be described as a bent silaallene with a perturbed electronic structure. This unique electronic behaviour is attributed to the differing donor-acceptor

properties of Caac^{Me} and I^{i}Pr$_2$Me$_2$.[108] More recently, Sindlinger and coworkers reported the successful characterisation of another single-donor-supported 1-silavinylidene **I-66**[216] (***Figure 26***a).

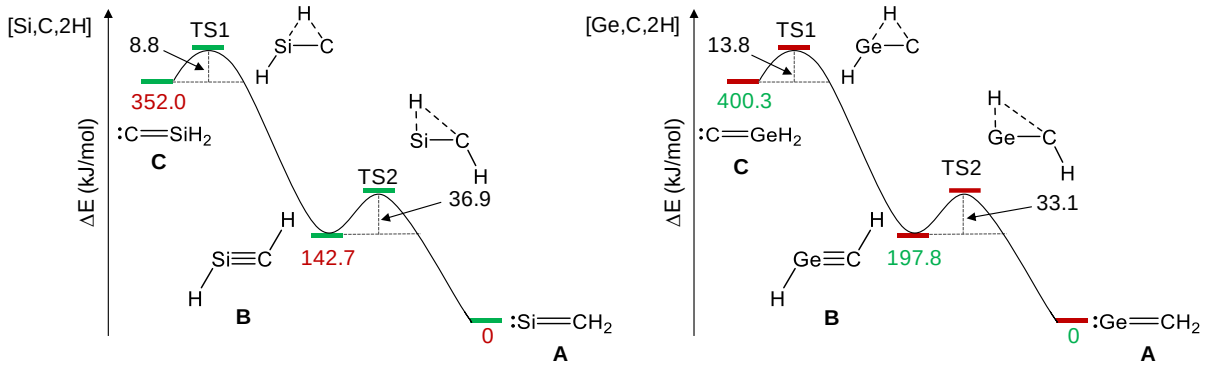

Figure 25. Isomers **A** – **C** of the [Si,C,2H] (***left***) and [Ge,C,2C] (***right***) potential energy hypersurfaces ordered with increasing energy relative to the global minimum **A**. Relative energies (kJ·mol^{-1}) are given for Si and Ge at the (CCSD(T)/TZ2P(fd)+ZPVE//CCSD(T)/TZ2P) [212] and (CCSD(T)/TZ(2df,2pd)//CCSD/TZ(2df,2pd) [213] level of theory, respectively.

ii). 2-tetrelavinylidenes: According to quantum chemical studies, 2-tetrelavinylidenes (C=EH$_2$; E = Si, Ge) are the least stable isomers on the [E,C,2H] potential energy hypersurface.[212,213] Experimental investigation of 2-tetrelavinylidenes (:C=ER$_2$) and their derivatives has been a long-standing objective. Remarkably, in 2024, Filippou and coworkers reported the first experimental studies of the first N-heterocyclic carbene (NHC)-supported 2-silavinylidene (NHC)C=SiBr(Tbb) **I-67** and 2-germavinylidenes (NHC)C=GeBr(R) (R = Tbb, Mind) **I-68** and **I-69** (***Figure 26***b).[217] They achieved this breakthrough by employing a chemically innovative approach, using diazoolefin (IDipp)CN$_2$ as a vinylidene surrogate and (*E*)-R(Br)E=E(Br)R (E = Si, Ge; R = Tbb, Mind) as a tetrel source.

iii). Silyne: Despite significant advancements in the chemistry of disilynes, the chemistry of their lighter analogue, silynes, remains relatively scarce in comparison. A significant challenge in synthesizing silynes is their tendency to undergo energetically favoured isomerization to 1-silavinylidenes R$_2$C=Si, mainly when R represents small substituents (***Figure 25***).[208–210] Theoretical predictions suggest that this isomerization could be reversed, making the silyne more stable by introducing more electronegative substituents on silicon [208] or using sterically more demanding substituents.[218,219] Another promising strategy is the use of Lewis base ligands, as low-coordinate silicon species, such as silenes,[220,221] disilynes,[222] or disilicon(0) compounds,[150] have been shown to form stable donor-acceptor complexes. As of now, the only neutral species proven to be sufficiently stable for –

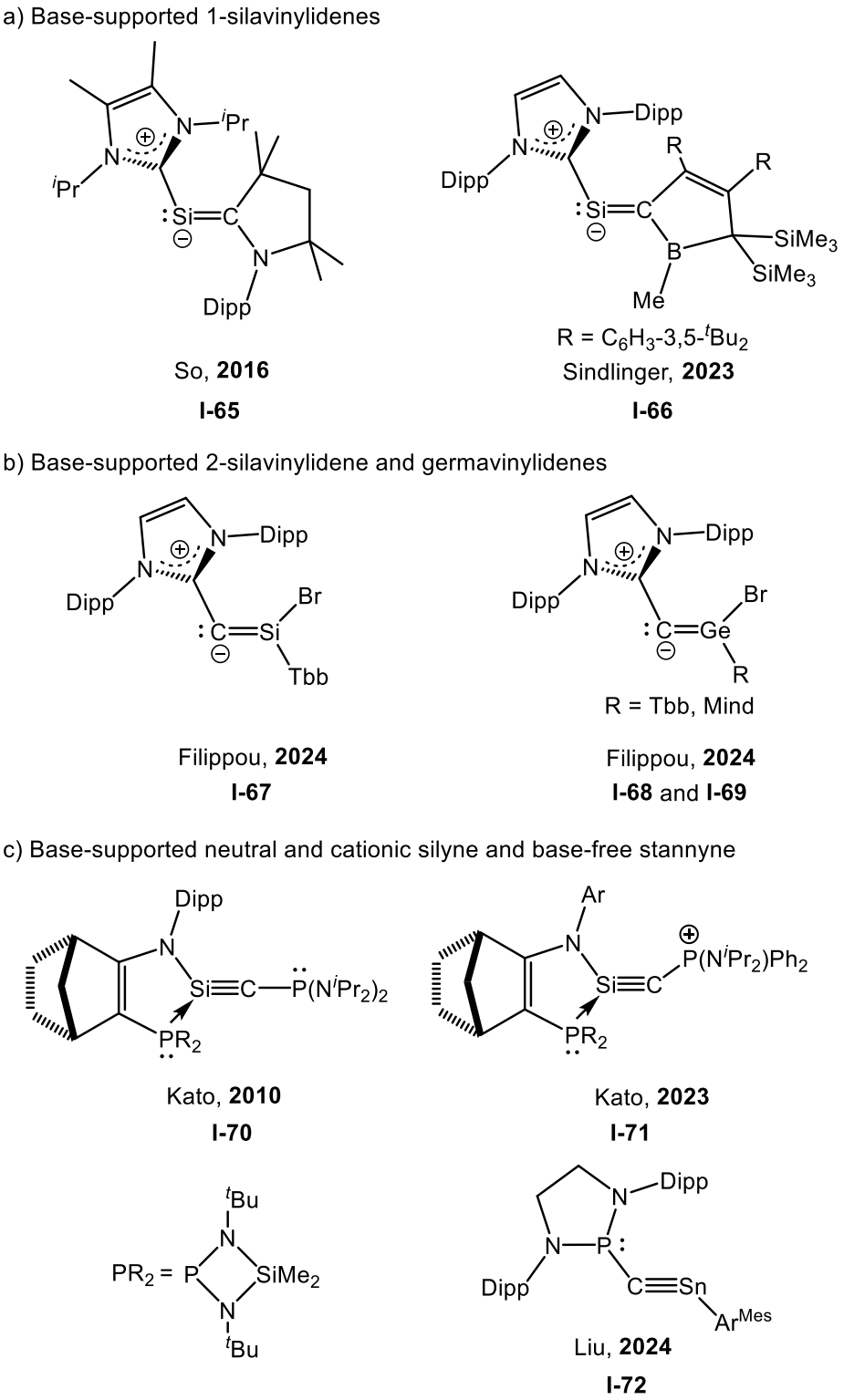

Figure 26. Literature known examples of (a) base-supported 1-silavinlidenes; (b) base-supported 2-silavinylidene and 2-germavinylidenes; (c) base-supported neutral and cationic silynes and base-free stannyne.

structural characterization below −30 °C is the base-supported *C*-phosphino-*Si*-amino silyne **I-70**[223] (***Figure 26***c), which was first reported over a decade ago by Kato and coworkers. However, it has been observed that **I-70** undergoes an intramolecular rearrangement reaction when the temperature exceeds this

threshold.[223] More recently, the same research group isolated a base-supported cationic silyne with a π-accepting phosphino substituent **I-71**[224] (***Figure 26***c), which exhibited moderate stability at room temperature, with a half-life time of $t_{1/2}$ = 7 days in THF. Remarkably, in 2024, Liu and coworkers demonstrated the isolation of a base-free crystalline stannyne **I-72**[225] (***Figure 26***c), which exhibits a pronounced allenic nature. This was achieved through a strategic combination of a bulky cyclic phosphino and a bulky terphenyl substituent.

1.7. Goals and Objectives

As outlined in the preceding discussion, a central aim of modern inorganic chemistry is the synthesis and comprehensive characterization of compounds that exhibit novel and previously unobserved bonding arrangements. The study of such compounds provides invaluable insights into the intrinsic nature of chemical bonding, thereby advancing our theoretical understanding of bonding paradigms. The successful isolation of these species necessitates the development of innovative synthetic methodologies, the design of tailored precursors, and the incorporation of sterically demanding substituents. These strategic substituents act as protective groups, offering kinetic stabilization to otherwise highly reactive intermediates, thus enabling their isolation, characterization, and subsequent study under controlled conditions.

This work primarily focuses on the development of novel synthetic strategies to access unprecedented metallo-*bis*-stannylene complexes and metalacyclic compounds featuring low-coordinate germanium and tin centers. In addition, it establishes a synthetic route for the stabilization of germanium(0) and tin(0) species exhibiting intriguing bonding motifs, enabled by a cyclic bis-germylene scaffold. A secondary emphasis is placed on attempting to access the base-free or base-supported unsaturated compound incorporating novel heterotetrel center motifs, as well as testing their reactivity to furnish compounds with novel bonding environments.

In this context, the primary objectives of this work are elegantly summarized as follows:

- To synthesize and characterize novel metallo-*bis*-stannylene complexes of Co and Rh, and the structural and electronic properties of *cis*-bent-digermyne complex was explored with non-polar unsaturated molecules to afford metallacycles compounds containing a low-valent Ge centre in intriguing bonding motifs, and to establish an efficient one-step synthetic route for accessing unprecedented tetraphosphadigerma dewar benzene complex.
- To conduct a comprehensive and systematic study of downstream chemistry of the 1,2-digermabutadiene, to access cyclic bis-germelene-supported germylone (Ge(0)) and stannylone (Sn(0)), elucidating their structural and electronic properties while investigating their reactivity with a broad spectrum of organic and main group reagents to give unprecedented η^5-Ge(0) half sandwich complex and other intriguing germanium cluster compounds.

- To develop a novel synthetic route for a bis-ligand-supported silasilyryne (L^1–C($SiMe_2$)Si-L^2; L = Lewis base) featuring an unprecedented CSi_2 silasilyryne core.
- To enable the successful isolation of the first examples of isocyanide coupling products mediated by Si(I) and Ge(I) tetrel centres to give novel 1,2-disile/digermetene.
- To develop a robust synthetic pathway for isolating the first DMAP-supported stannasilyne, revealing its distinctive bonding characteristics and reactivity, including facile ligand substitution reaction towards strong σ-donor and weak π-acceptor ligands like IMe_4 and Mes-NC.
- To synthesize and characterize unprecedented single donor-supported heavier analogue of an Imidazole derivative exhibiting novel structural features with extensive delocalization.

The synthesis of these novel compounds presents significant challenges due to their extreme sensitivity to air and moisture, as well as their inherent high reactivity. Isolable reaction products should undergo comprehensive characterization using standard analytical techniques, including elemental analysis, NMR spectroscopy, melting point determination, and X-ray diffraction (XRD). For unstable species, characterization should be primarily performed using appropriate spectroscopic methods. Depending on the nature of the compounds, additional techniques such as IR, Raman, and UV-Vis spectroscopy, as well as density functional theory (DFT) calculations, may be employed to provide detailed insights into their electronic structures, bonding characteristics, and structure–reactivity relationships, thereby advancing the fundamental understanding of low-valent tetrel chemistry.

2. Results and discussion

2.1. *Cis*-bent digermyne complex: Unlocking the reactivity

2.1.1. Synthesis and characterization of Metallo-bis-stannylene complexes

As highlighted in the introduction, the metal alkyne complexes are well studied both experimentally and theoretically[60–63],[64] However, research on metal-ditetrelyne complexes of type ($LnM(E_2R_2)$, where Ln = ligand sphere; E = Si–Pb; and R represents mono-coordinated sterically demanding bulky substituents remained largely underexplored and warrants comprehensive investigation. A significant milestone in this field was achieved by Dr. P. Palui in the research group of Prof. Filippou, enabling the structural characterization of the unprecedented mono-carbonyl digermyne complex [226] *rac*-[Cp(CO)M{η^2-*trans*-Ge_2Tbb_2}] (**1-Co** (M = Co), **1-Rh** (M = Rh); ***Scheme 2***). The selective facilitation of the metal-ditetrelyne complexes **1-Co** and **1-Rh** was achieved through the reaction of commercially accessible $CpM(CO)_2$ (M = Co, Rh) with Ge_2Tbb_2 (Tbb = C_6H_2-4-^{t}Bu-2,6-$(CH(SiMe_3)_2)_2$)[227] in aliphatic solvents at ambient conditions. Both complexes **1-Co** and **1-Rh** unveil the isotypic structural arrangement and spectroscopic perusals.

In our pursuit of integrating heavier tetrel centers into three-membered bis-tetrel metallacycles, we sought to investigate the reactivity of distannyne with $CpM(CO)_2$. (M = Co, Rh). Notably, the dropwise addition of an *n*-hexane stock solution of $CpM(CO)_2$ (M = Co, Rh) to the intensely green suspension of $Ar^{Dipp}{}_2Sn_2$ (where Ar^{Dipp} = C_6H_3-2,6-$Dipp_2$ and Dipp = 2,6-^{i}Pr$_2$-C_6H_3) in *n*-hexane was accompanied by a gradual colour transition to dark brown (M = Co) and dark green (M = Rh) over a 16-hour period. The progression of the reaction was meticulously monitored using *in-situ* solution IR and ^{1}H NMR spectroscopy, which revealed the complete consumption of the starting materials and the selective formation of the unprecedented acyclic mono-carbonyl metallo-bis-stannylene complexes **2-Co** and **2-Rh** (***Scheme 2***). Both complexes, **2-Co** and **2-Rh**, were obtained as highly coloured crystals: **2-Co** as intense brown and **2-Rh** as green, following workup and crystallization from Et_2O and *n*-hexane at −30 °C, with yields of 60 % for each. These complexes are highly sensitive to air but can be stored indefinitely under an argon atmosphere and exhibit good solubility in common organic solvents. Thermal decomposition studies, conducted in vacuum-sealed glass capillaries revealed that **2-Co** and **2-Rh** decompose upon melting at 207 °C and 169 °C, respectively. ^{1}H NMR analysis of the

soluble part of the melted residues in (D_6)benzene indicated that both complexes undergo unselective decomposition.

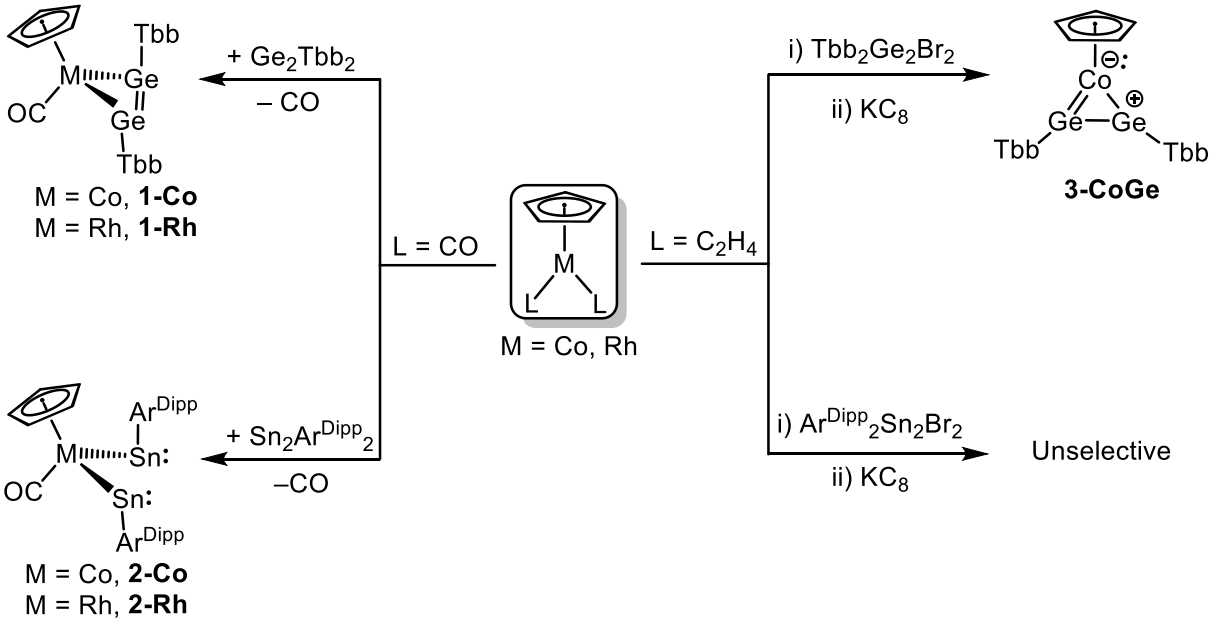

Scheme 2. Synthesis of trans bent-digermyne complex **1-Co** and **1-Rh** [226] and acyclic metallo-bis-stannylene complexes **2-Co** and **2-Rh** (**this work**) (***left***); Synthesis of cis-bent digermyne complex **3-CoGe** (***right***).[226]

Complexes **2-Co** and **2-Rh** represent the first reported 3d- and 4d-transition metal-coordinated bis-stannylene complexes, as confirmed by a search of the CCDC structural database. These complexes were comprehensively characterized using single-crystal X-ray diffraction (scXRD) analysis and multinuclear NMR spectroscopy. Suitable crystals (Needle-shaped dark-brown crystals of **2-Co·(Et₂O)** and plate-shaped dark-green crystals of **2-Rh·(Et₂O)** for scXRD analysis were obtained by slowly cooling their respective saturated Et_2O solutions at −30 °C. Both complexes, **2-Co** and **2-Rh**, crystallize in the monoclinic space group *C*2/c. Both complexes **2-Co** and **2-Rh** exhibits nearly identical skeleton arrangement and possess a *pseudo-C*$_1$-symmetric structure in the solid state. The primary structural characteristics of these complexes include:

i) Both complexes display a three-legged piano-stool geometry at the Co/Rh centers, along with the two di-coordinated V-shaped tin centers (∠C1−Sn1−M) = 110.95(16)° (**2-Co**) 108.84(4)° (**2-Rh**); (∠C2−Sn2−M) = 113.09(16)° (**2-Co**) and 111.91(5)° (**2-Rh**)). These angles indicate the presence of a lone pair of electrons at Sn centers, primarily in an *s*-hybrid orbital.

ii) The sterically demanding Ar^{Dipp} substituents are arranged in trans orientation with C1−Sn1−Sn2−C2 torsion angle of −174.0(3)° (**2-Co**) and −172.2(1)° (**2-Rh**) and bonded to the metal centers *via* a Co−Sn and Rh−Sn single bond (d(Co−Sn)$_{mean}$ =

2.575(1) Å; d(Rh−Sn)$_{mean}$ = 2.646(1) Å). These bond distances are consistent with the sum of the single bond covalent radii of Sn and Co/Rh, as reported in Pyykkö table (d(Co−Sn) = 2.51 Å; d(Rh−Sn) = 2.65 Å).[228] The Sn−C^{ipso} bond distances (d(Sn−C^{ipso})$_{mean}$ = 2.230 Å (**2-Co**), d(Sn−C^{ipso})$_{mean}$ = 2.228 Å (**2-Rh**)) are considerably shorter than those observed in the literature for bis-aryl stannylenes Sn(Ar^{Dipp})$_2$ (d(Sn−C^{ipso})$_{mean}$ = 2.272 Å)[229]. This shortening suggests a partial double bond character between C^{ipso} and Sn centers in both complexes.

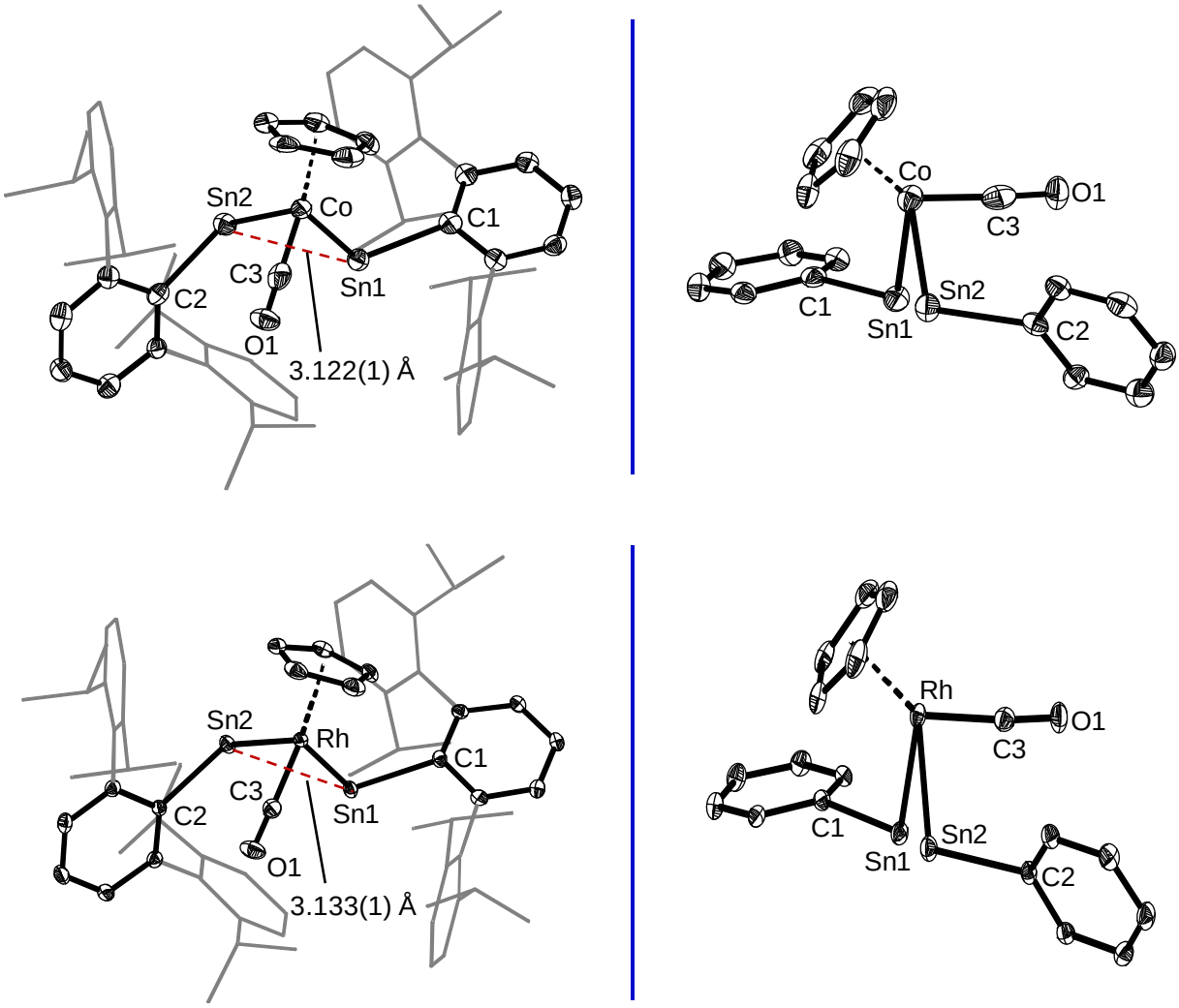

Figure 27. DIAMOND plots of the molecular structures of **2-Co** (***top, left***) and **2-Rh** (***bottom, left***) and their concentrated views **2-Co** (***top, right***) and **2-Rh** (***bottom, left***) along the Sn1···Sn2 bond vector. Thermal ellipsoids are set at 50 % probability level; Hydrogen atoms are omitted and the Dipp substituents of the Ar^{Dipp} ligand are presented in wire-frame for clarity. Selected bond lengths [Å], bond angles [°] and torsion angle [°]: (**2-Co**): Co−Sn1 2.5670(11), Co−Sn2 2.5849(11) Sn1−C1 2.233(6), Sn2−C2 2.227(7), Co−C3 1.741(8), C3−O1 1.147(8) Co−Sn1−C1 110.95(16), Co−Sn2−C2 113.09(16), Sn1−Co−Sn2 74.60(3), C1−Sn1−Sn2−C2 −174.0(3), Sn1···Sn2 3.122(1); (**2-Rh**): Rh−Sn1 2.6430(2), Rh−Sn2 2.6507(2) Sn1−C1 2.233(2), Sn2−C2 2.222(2), Rh−C3 1.8338(19), C3−O1 1.147(2) Rh−Sn1−C1 108.84(4), Rh−Sn2−C2 111.91(5), Sn1−Rh−Sn2 72.579(6), C1−Sn1−Sn2−C2 −172.2(1), Sn1···Sn2 3.133(1).

iii) The closest Sn1···Sn2 separation observed in the **2-Co** (3.122(1) Å) and **2-Rh** (3.133(1) Å) complexes significantly exceeds the covalent bond distance of Sn (d(Sn−Sn)$_{covalent}$ = 2.80 Å)[228] but is slightly less than the sum of the van der Waals radii of Sn (d(Sn−Sn)$_{van\ der\ Waals}$ = 4.34 Å). The Sn1···Sn2 distance shows an elongation (Δd) of 0.46 Å compared to the uncoordinated $Ar^{Dipp}Sn{\equiv}SnAr^{Dipp}$ (d(Sn−Sn) = 2.6675(4) Å) [35] representing a 15% shift in the bond length. This shift is significantly grater than the 5% change observed in Ge–Ge bond distance in the **1-Co** on comparing with uncoordinated Ge_2Tbb_2.[226] Interestingly, the distance is consistent with the reported Sn–Sn bond length of 3.1434(5) Å in the literature for an amido-distannyne complex ($L^{\dagger}SnSnL^{\dagger}$, $L^{\dagger}$ = N(Ar†)(Si^{i}Pr$_3$), Ar† = C_6H_2{C(H)Ph$_2$}$_2$^{i}Pr-2,6,4)).[57] These findings underscore the uncertainlity surrounding the existence of a genuine bond between Sn1 and Sn2 centers.

Further structural characterization of the complexes **2-Co** and **2-Rh** was accomplished through comprehensive multinuclear NMR and IR spectroscopic analyses. The ^{1}H and ^{13}C{^{1}H} NMR spectra of both the complexes, recorded in (D_8)THF at 253 K and 263 K respectively, revealing a similar time-averaged C_s-symmetric structure in solution (***Figure 28***) for both the complexes. In this structure, the symmetry plane bisects the ∠M-C3-O1 (where M = Co, Rh) and the centroid of the freely rotating Cp ring. This symmetry renders the two tin centers and Ar^{Dipp} groups enantiotopic, with hindered rotation of the sterically demanding Ar^{Dipp} substituents around the Sn−C^{ipso} bond axis. This dynamic behaviour results in a complex ^{1}H and ^{13}C{^{1}H} NMR spectrum. The assignment of these spectra was achieved through a combination of ^{13}C−^{1}H HSQC and HMBC correlation experiments. Notably, no ^{119}Sn{^{1}H} resonance was observed in a wide chemical shift range (-2000 ppm to +2000 ppm) for either **2-Co** or **2-Rh**, which can be attributed to the dynamic behaviour around the di-coordinate tin centers. This absence of ^{119}Sn{^{1}H} signals persisted across a range of temperatures, from low to high, further supporting the dynamic nature of the tin centers. The ^{13}C{^{1}H} NMR spectra of **2-Co** and **2-Rh** exhibit distinct resonances for the carbonyl carbon: a broad singlet ($\Delta\nu_{1/2}$ = 48 Hz) at δ_{CO}/ppm = 192.6 for **2-Co** and a doublet (^1J(^{103}Rh-^{13}C) = 88 Hz) at δ_{CO}/ppm = 198.5 for **2-Rh**. These carbonyl resonances are particularly noteworthy, as they align closely with those observed in the cyclic germanium analogues, CpMCO(Ge_2Tbb_2), which exhibit δ_{CO}/ppm = 203.1 (M = Co); 193.14 (M = Rh).[226]

The solution IR spectra of both complexes in *n*-hexane display a strong absorption band at 1936 cm^{-1} (**2-Co**) and 1957 cm^{-1} (**2-Rh**) (***Figure 29***). These bands appear at lower wavenumbers compared to their cyclic germanium analogues,

CpMCO(Ge$_2$Tbb$_2$), which exhibit absorption bands at 1987 cm^{-1} (M = Co) and 2003 cm^{-1} (M = Rh).[226] The observed red shift in the carbonyl stretching frequencies for the tin-based complexes suggests a subtle electronic difference between the germanium and tin centers, likely due to the weaker π-backdonation from the metal center to the carbonyl ligand in the tin complexes.

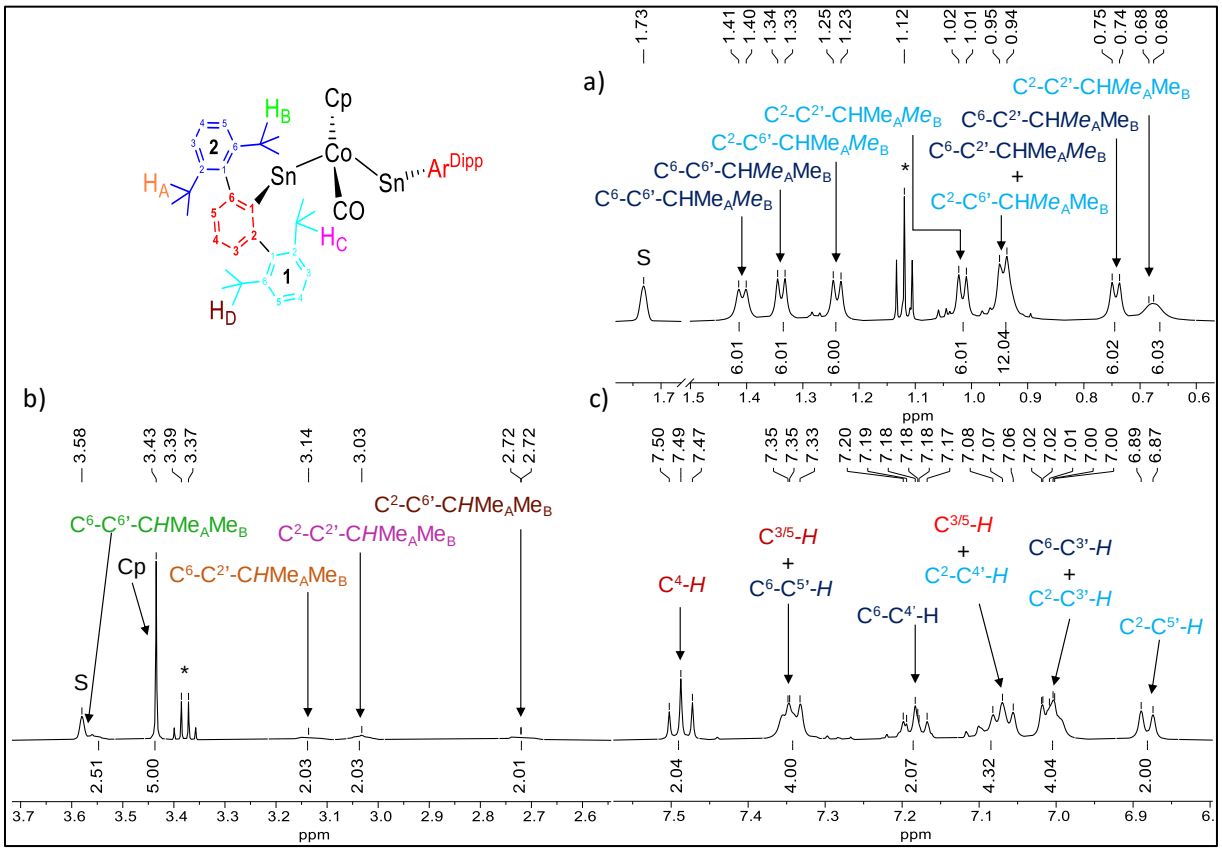

Figure 28. ^{1}H NMR spectrum excerpts of **2-Co** in (D$_8$)thf at 253 K; the residual proton signal of the deuterated solvent is marked with the character S.

Additionally, attempts to determine the rotational thermodynamic activation parameters for the hindered rotation of the sterically demanding Ar^{Dipp} substituents around the Sn–C^{ipso} bond axis were unsuccessful. This was due to the unresolved overlap of resonances in the ^{1}H NMR spectra recorded in (D$_8$)THF over the temperature range of 203 K to 333 K. The complexity of the spectra, arising from the dynamic behaviour of the Ar^{Dipp} groups, precluded accurate simulation and extraction of the activation parameters.

Notably, the liberation of CO from the complexes **2-Co** and **2-Rh** proved unattainable through prolonged reflux in *n*-heptane or irradiation using a broad-wavelength-range high-pressure Hg lamp. These efforts aimed to facilitate the synthesis of the unprecedented *cis*-bent distannyne complex, featuring a 14-VE "CpM" (M = Co, Rh) fragment. This observation aligns well with the behaviour of its germanium

analogues**,** CpMCO(Ge_2Tbb_2) (M = Co, Rh).[226] The conversion of a CO-coordinated trans-bent digermyne complex (**1-Co** and **1-Rh**) to a cis-bent digermyne complex (**3-CoGe**) can be efficiently accomplished using a two-step synthetic approach described in the literature.[226]

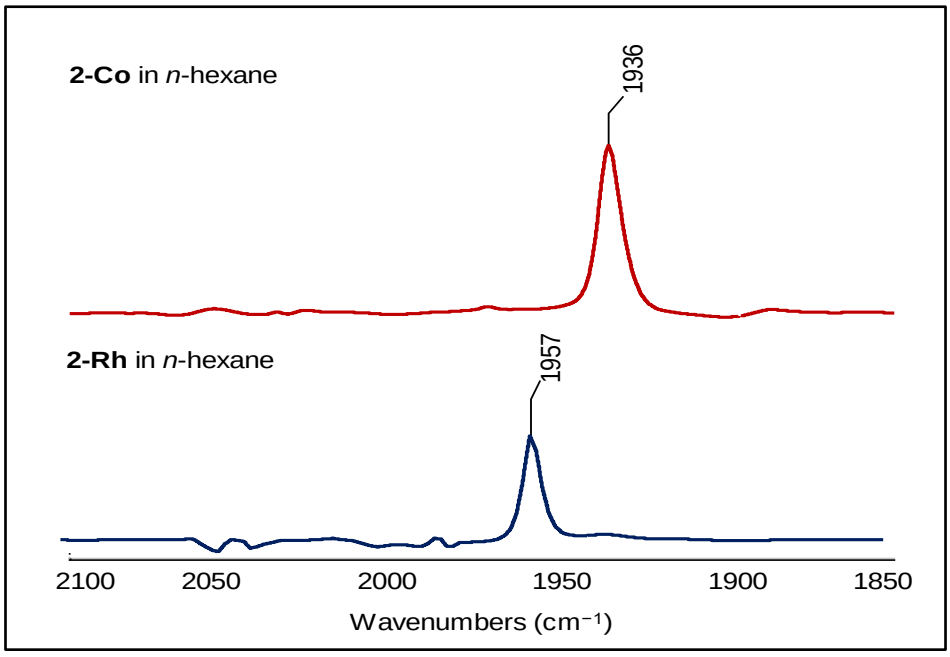

Figure 29. Exerpts of the solution state IR spectrum of the acyclic bis-stannylenes metal complexes **2- Co** (***top***) and **2-Rh** (***bottom***) recorded in *n*-hexane at 298 K.

The process begins with the selective synthesis of a bis-germylidene Co-complex and then subjected to a $2e^-$ reduction under ambient conditions, yielding the intensely brown-coloured **3-CoGe** complex in a consistent and reproducible manner (***Scheme 2***).[226] Despite employing the same synthesis methodology, it was not possible to replicate the process for the corresponding tin analogues, resulting in only non-selective outcomes (***Scheme 2***).

The three-membered *cis*-bent digermyne complex (**3-CoGe**) features multiple reactive sites, enabling further functionalization and offering access to novel, unprecedented, low-coordinate cyclic germanium compounds. Previous studies by P. Palui have extensively investigated the reactivity of **3-CoGe** with nonpolar unsaturated organic molecules (terminal/internal alkynes). However, the reactivity of **3-CoGe** with polar unsaturated organic molecules-such as alkyl/aryl isocyanides, isocyanates, ketones, and isothiocyanates as well as polar small molecules, remains largely unexplored. This presents a promising opportunity to synthesize a diverse array of unprecedented low-coordinate germanium compounds. In the following section, we will explore the reactivity of **3-CoGe** in greater detail.

2.1.2. Reactivity of *cis*-digermyne complex (3-CoGe)

2.1.2.1. Addition reaction

The aforementioned *cis*-digermyne complex (**3-CoGe**) demonstrates amphiphilic and dual-centered reactivity. Consequently, complex **3-CoGe** exhibits Ge-centered reactivity upon reacting with nonpolar unsaturated organic molecules (terminal/internal alkynes). Additionally, **3-CoGe** also demonstrates Co-centered reactivity when treated with small phosphane (for instance, PMe_3). The dropwise addition of an *n*-hexane stock solution of PMe_3 to an orange brown solution of **3-CoGe** was accompanied by an instant colour transition to green, and the progression of the reaction was meticulously monitored using ^1H NMR spectroscopy, which revealed the complete consumption of the starting materials and the selective formation of the isotypic PMe_3 adduct of *trans*-bent digermyne complex (**3-Co**). The intense green crystals of **3-Co** were isolated after careful workup and crystallization from Et_2O at −30 °C with a 73% yield. The **3-Co** complex is highly sensitive to air but can be stored indefinitely under an argon atmosphere and exhibits good solubility in common organic solvents. Thermal decomposition studies conducted in vacuum-sealed glass capillaries revealed that **3-Co** decomposes upon melting at 192 °C.

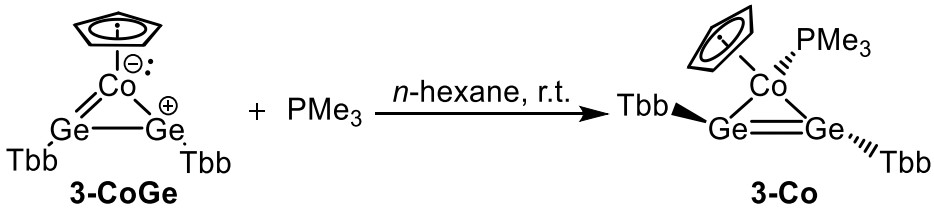

Scheme 3. Neutral nucleophile (PMe_3) mediated irreversible conversion of *cis*-bent digermyne complex (**3-CoGe**) to *trans*-bent digermyne complex (**3-Co**).

Suitable block-shaped brown single crystals for X-ray diffraction studies of **3-Co•(Et_2O)** were grown by the slow cooling of a saturated Et_2O solution at −30 °C. Complex **3-Co** was crystallized in asymmetric orthorhombic space group *P*bca space group with a unit cell composed of a racemate of structurally identical (***R,R***)**-3-Co** and (***S,S***)**-3-Co** enantiomers with two stereogenic Ge centers (***Figure 30***). Complex **3-Co** is isotypic to its CO analogues **1-Co**[226], and the bonding matrices are nearly identical; the selected bonding parameters are tabulated in ***Table 1***.

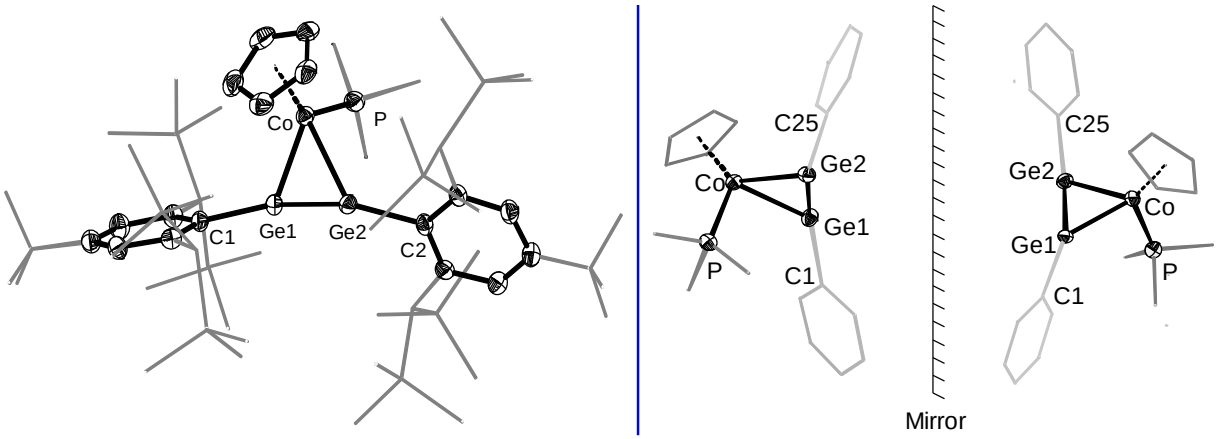

Figure 30. (***left***) DIAMOND plot of the molecular structure of (***R,R***)**-3-Co**. Thermal ellipsoids are set at 30 % probability level. Hydrogen atoms are omitted and the Dsi and ^{t}Bu substituents of the Tbb ligand are presented in wire-frame for clarity. Selected bond lengths [Å] and bond angles [°]: Co−P 2.1326(9), Co−Ge1 2.3616(16), Co−Ge2 2.4349(10), Ge1−Ge2 2.378(2), Ge1−C1 1.966(3), Ge2−C2 2.012(2), Co−Ge1−C1 119.97(9), Co−Ge1−Ge2 61.93(5), Co−Ge2−C2 128.99(6), Co−Ge2−Ge 1 58.71(4), C1−Ge1−Ge2−C2 140.6(6). (***right***) A side-on view of the truncated molecular structures of two enantiomers (***S,S***)-**3-Co** and (***R,R***)-**3-Co** present in the unit cell of **3-Co•(Et$_2$O)**.

Table 1. Selected structural parameters of *trans*-bent digermyne complexes (**1-Co**, **1-Rh**, and **3-Co**), acyclic bis-stannylene complexes (**2-Co** and **2-Rh**), and *cis*-bent digermyne complex **3-CoGe**.

Complex	d(E1−E2) /pm	d(M−E1) /pm	d(M−E2) /pm	∑∢(E1) /°	∑∢(E2) /°	C1−E1−E2−C2 /°	*Ref.*
1-Co	2.3456(3)	2.5010(4)	2.3675(4)	306.6	316.8	155.9(1)	[226]
1-Rh	2.3368(4)	2.5560(4)	2.4700(4)	228.6	191.8	157.6(1)	[226]
2-Co	3.122(1)	2.5670(11)	2.5849(11)	–	–	−174.0(3)	This work
2-Rh	3.133(1)	2.6430(2)	2.6507(2)	–	–	−172.2(1)	This work
3-CoGe	2.3137(4)	2.2268(4)	2.2223(4)	359.9	359.6	4.3(1)	[226]
3-Co	2.378(2)	2.3616(16)	2.4349(10)	321.7	326.3	140.6(6)	This work

Further structural characterization of the complex **3-Co** was accomplished through comprehensive multinuclear NMR spectroscopy. The ^{1}H spectra of the **3-Co** complex, recorded in (D_8)THF at 193 K, revealed two sets of signals for each Tbb substituent, indicating a time-averaged C_1−symmetry (Tbb groups are diastereotopic) with a frozen rotation of each Tbb substituents around Ge−C^{ipso} bond and resulting in two peaks for C3,5-*H* bonded proton in integral ratio of 1:1 for each Tbb. Interestingly, ^{1}H NMR spectra recorded in (D_8)THF at an elevated temperature of 333 K show highly symmetric spectra and exhibit only one set of signals for both Tbb, suggesting an

intriguing dynamic process within the temperature range of 193 K to 333 K, which is discussed in detail (*vide infra*).

Complex **3-Co** crystallizes as a racemate of ***(R,R)*-3-Co** and ***(S,S)*-3-Co** enantiomers, it exists in solution as a racemic mixture, which should render the Tbb substituents diastereotopic, one pointing toward Cp (Ge1 bonded Tbb) and the other away from Cp (Ge2 bonded Tbb) (***Figure 30***), and were arbitrarily assigned as Tbb_X and Tbb_Y, respectively. Therefore, a separate set of signals for Tbb_X and Tbb_Y was expected in the ^{1}H NMR spectrum of **3-Co**. Surprisingly, the ^{1}H NMR spectrum of **3-Co** at 298 K in (D_6)benzene displays two sets of broad signals for the two diastereotopic Tbb groups, suggesting fast dynamics in the NMR timescale, which was studied by variable temperature ^{1}H NMR spectroscopy. Indeed, a separate set of signals is observed for each Tbb substituent in the slow exchange limit spectrum at 213 K (***Figure 31***), e.g. one singlet for each of the ^{t}Bu methyl protons of Tbb_X and Tbb_Y at δ = 1.36 ppm and 1.41 ppm. Three distinct chemical exchange processes were resolved by remeasuring the NMR sample at different temperatures, as evidenced by the broadening, collapsing, and sharpening of the respective coalescence signals. The first process involves coalescence (T_{c1}) at 263 K for the aromatic $C^{3,5}$-*H* signals of the Tbb substituent, T_{c2} = 283 K for the ^{t}Bu signals of Tbb_x and Tbb_Y and the third one at T_{c3} = 303 K due to the coalescence of C^3-*H* and C^5-*H* of the second Tbb substituent. Finally, in the fast exchange limit spectrum at 333 K, a time-averaged local C_{2v}-symmetry of **3-Co** was observed, suggesting that all processes involve complicated stereodynamics. The barriers for these processes at the respective coalescence temperature calculated by plugging in the Gutowsky-Holm formula $k_{exch} = 2.22\,(\Delta\upsilon_{max})$ (k_{exch} = first order exchange rate constant in Hz, $\Delta\upsilon_{max}$ = peak-to-peak separation in Hz of the two exchanging signals in the low-temperature limit spectrum) in the Eyring-Polanyi equation (assuming the transmission coefficient κ = 1) were $\Delta G^{\ddagger}_1$ = 56.8 KJ/mol, $\Delta G^{\ddagger}_2$ = 60.5 KJ/mol and $\Delta G^{\ddagger}_3$ = 64.1 kJ/mol suggesting that these processes occur either non-synchronously or synchronously. Due to the close domain of calculated standard Gibbs (ΔG) free energy for each discussed process and does not provides a concrete outcome. Full line shape analysis using the gNMR programme for the second dynamic processes yielded the following activation parameters: $\Delta H^{\ddagger}_2$ = 89.5(±2) kJ/mol, $\Delta S^{\ddagger}_2$ = 106.5(±12) kJ/K. The remaining two dynamic processes could not be resolved due to the extensive overlap of the relevant signals with other signals in the ^{1}H NMR spectra.

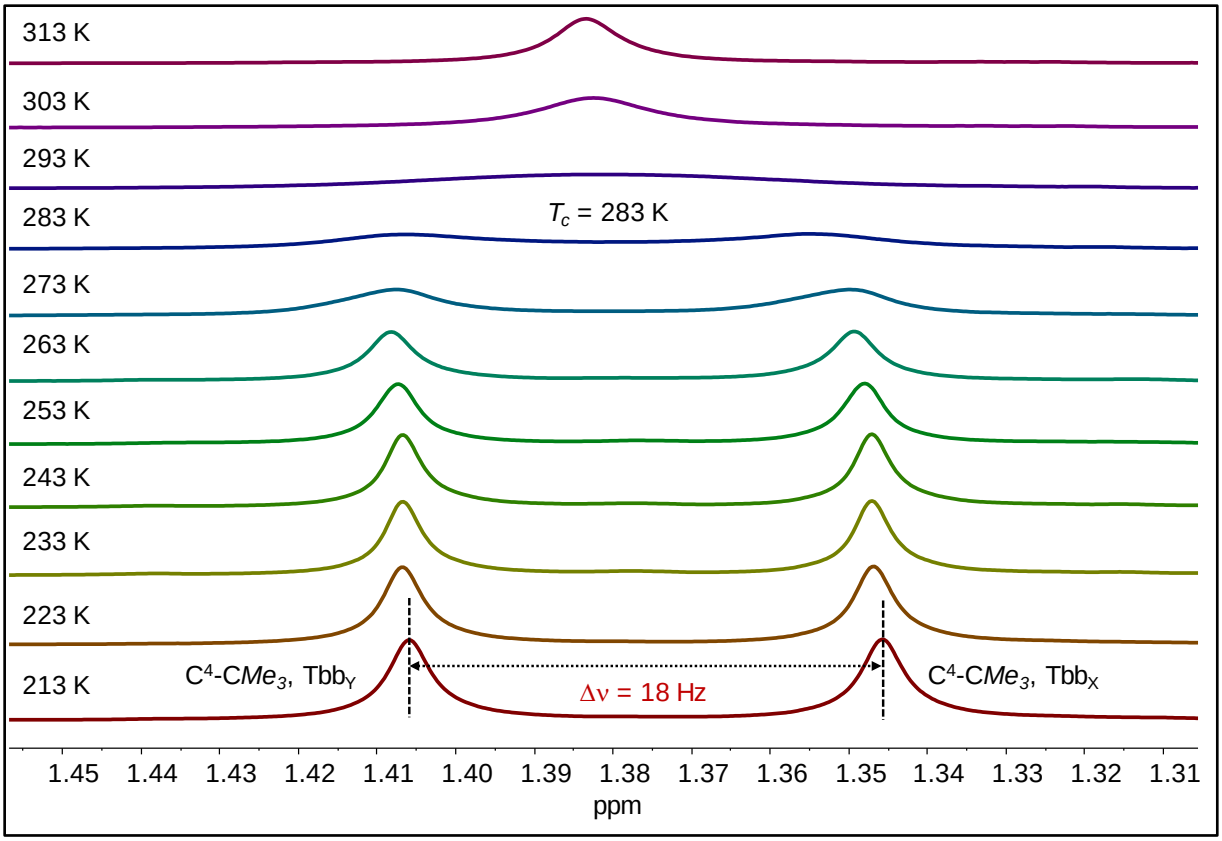

Figure 31. Excerpt of the VT ^{1}H NMR spectra (300.1 MHz) of **3-Co** in (D_8)THF (chemical shift range: 1.31 − 1.45 ppm) in temperature range 213 − 313 K showing the exchanging C^4-CMe_3 signals of the Tbb_X and Tbb_Y substituents.

2.1.2.2. Cycloaddition reaction

The exploration of the Ge-centered reactivity of complex **3-CoGe** towards polar, unsaturated organic molecules, such as nitriles, ketones, and isocyanates, presents a promising pathway for the synthesis of a diverse array of unprecedented, low-coordinate germanium compounds *via* a [2+2] cycloaddition mechanism. Initial investigations focused on the reactivity towards organic nitriles, where a colourless *n*-hexane solution of *p*-tolyl nitrile was added dropwise to a stirred orange-brown *n*-hexane solution of **3-CoGe** under ambient conditions. This addition resulted in an immediate colour transition to dark green, indicating the formation of a new species. The reaction progress was monitored using ^{1}H NMR spectroscopy, which confirmed the complete consumption of the starting materials and the selective formation of **4-Co** (***Scheme 4***) *via* a proposed [2+2] cycloaddition mechanistic pathway. Dark green crystals of **4-Co** were isolated following workup and crystallization from *n*-hexane at −30 °C as *n*-hexane hemi-solvate **4-Co**·(***n*-hexane**)$_{0.5}$, yielding 82% of the product which is highly sensitive to air and moisture but remains stable indefinitely when stored under an inert argon atmosphere. It demonstrates good solubility in aliphatic (*n*-hexane, *n*-pentane and petro ether), etherate (Et_2O and THF) and aromatic solvents

(benzene and toluene). Thermal decomposition analysis, conducted using vacuum-sealed glass capillaries, revealed that **4-Co** decomposes upon melting at 175 °C.

To investigate cycloaddition chemistry in a diverse manner of **3-CoGe**, the reactivity towards ketone (for instance (*p*-tol)$_2$CO) and CO_2 activation were studied. Where a solution of an (*p*-tol)$_2$CO) was treated with a solution of **3-CoGe** under ambient conditions to afford an orange-red colour reaction mixture, indicating the formation of a new product which turned out to be **5-Co** (***Scheme 4***) and was isolated in analytically pure form after crystallization from a solvent mixture of CH_3CN:Et_2O at ambient temperature in 70% yield. An attempt to isolate **6-Co** was made by reacting an orange-brown *n*-hexane solution of **3-CoGe** with excess CO_2 at −78 °C. This resulted in the formation of multiple products, suggesting the generation of reactive intermediates that further reacted with CO_2, rendering the reaction unselective. Subsequently, the same reaction was repeated using a stoichiometric amount of CO_2, which improved selectivity and led to the formation of **6-Co** (***Scheme 4***). The product was isolated in analytically pure form after careful workup and was crystallized from *n*-hexane at −30 °C, yielding **6-Co** in 59% yield. Both **5-Co** and **6-Co** are extremely air-sensitive and well soluble in dry, de-oxygenated *n*-hexane, benzene and THF. Their solutions in (D_6)benzene show no sign of decomposition for at least two days at ambient temperature. Remarkably, both displays very high thermal stability in the solid state with a decomposition temperature (T_{dec}) of 218 °C and 253 °C for **5-Co** and **6-Co**, respectively as compared to that of **3-CoGe** (T_{dec} = 160 °C).[226]

Finally, complex **3-CoGe** was reacted with isocyanate (Mes−NCO) at ambient temperature to afford a red-brown solution, instantly revealing the selective formation of **7-Co** (***Scheme 4***). Isolation of analytically pure red solid **7-Co** was carried out by workup and crystallization from *n*-pentane at −30 °C. The desired product was isolated with a 67 % yield. The compound **7-Co** exhibit good solubility in common organic solvents. Thermal decomposition (T_{dec}) analysis showed that **7-Co** decomposes upon melting at 221 °C.

It is worth noting that heavier tetrel elements (E = Si-Pb) in metallacyclopolyenes with the general formula [LnM{κ²(1,3)-(CR)n}] (where n = 3 for metallacyclobutadiene)[64], (n = 4 for metallacyclopentadiene or metallacyclopentatriene)[61], and (n = 5 for metallabenzene)[63] are rare. Only a few examples of monosila- and monogerma-metallacyclobutadienes involving metals such as Cr,[83] Mo[i] [83], W[79,84] Ta[85], and Os[230] have been reported so far. The complexes **4-Co**, **5-Co**, **6-Co**, and **7-Co** belong to the class of 2,5-digerma-cobaltacyclopentatriene, a novel category of metallacycles.

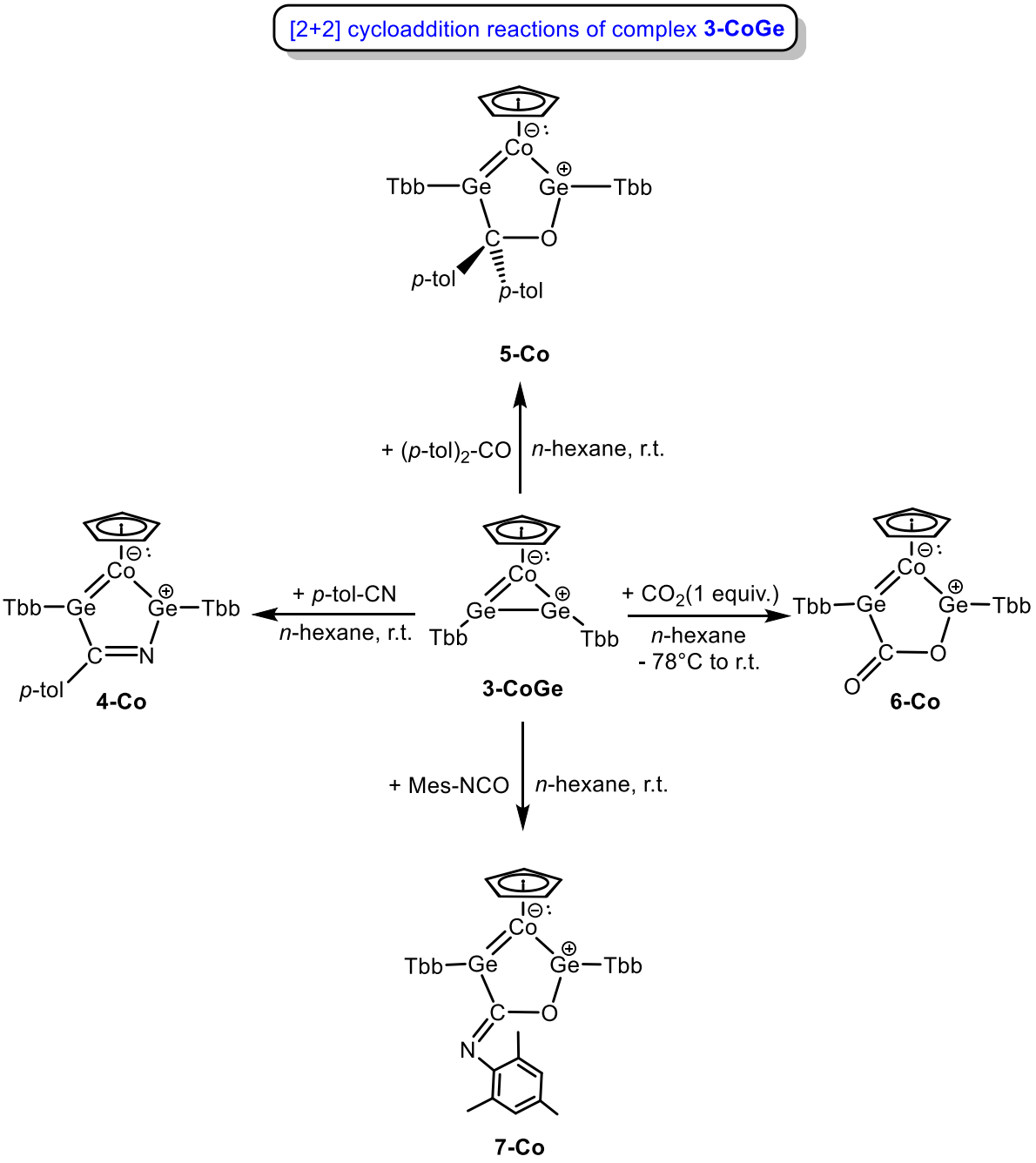

Scheme 4. Synthesis of [2+2] cycloaddition product of **3-CoGe** to afford **4-Co, 5-Co, 6-Co** and **7-Co**.

These were first isolated by Dr. P. Palui, with ($CpCoGe_2C_2Me_2Tbb_2$)[226] serving as an example of a heavier ditetrel congener within the metallacyclopolyene family. These complexes mark the first examples of reactivity between 3-CoGe and non-polar unsaturated organic molecules. They were comprehensively characterized using single-crystal X-ray diffraction (scXRD) analysis and multinuclear NMR spectroscopy.

The molecular structure of **4-Co** was determined by sc-XRD analysis of the block-shaped dark brown crystals, which were grown by slow cooling of its saturated *n*- hexane solution at −30 °C. Complex **4-Co** was crystallized in the triclinic space group *P*-1. The Ge1 and Ge2 atoms are trigonal planar coordinated ∑∠(Ge1) = 359.92°

and ∑∠(Ge2) = 359.99°, and the phenyl rings of Tbb are nearly orthogonally arranged with respect to the cobaltacycles (interplane angles of 117.7(4)° (Ge1−Tbb) and 122.9(4)° (Ge2−Tbb)), the metallacyclic ring plane (***Figure 32***) is nearly orthogonal to the Cp plane with a pyramidality angle α of 174.8(6)°. This spatial arrangement in the crystal lattice gives rise to C_s symmetry of **4-Co,** with the molecular plane passing through the five-membered metalacyclic along with the centroid of the Cp ring. The Co−Ge1 (2.1692(3) Å) and Co−Ge2 (2.156(3) Å) distances are quite similar as in reported bis-germylidene complex $CpCo(GeBrTbb)_2$[226] but far too short compared to the Co−Ge single bond lengths of the CSD reported Co(I)-germyl complexes (2.294 Å – 2.525 Å) and are in the range expected for a Co=Ge double bond. The C3−N bond length (1.273(3) Å) aligns with a typical localized C=N double bond, and the Ge1−N and Ge2−C3 distances (1.9221(3) Å, 2.062(2) Å) aligns with the single bond covalent radii of Ge−N and Ge−C.

The 2,5-trans-annular distance between the Ge1 and Ge2 atoms in **4-Co** is measured at 2.8671(3) Å, which is notably longer than typical Ge−Ge single bonds found in digermanes (average: 2.45 Å). However, this distance is well within the sum of the van der Waals radii of two Ge atoms (4.22 Å). A search of the Cambridge Structural Database (CSD) for structures with Ge···Ge separations ranging from 2.80 Å to 2.90 Å between two tri-coordinated Ge atoms (excluding the trans-annular Ge atom) revealed several examples featuring similarly long Ge···Ge distances. Quantum chemical calculations have interpreted these interactions in various ways, including as a π-single bond [231], an ultra-long σ-bond,[232] a component of a multi-centered bond ($\pi(3c\text{-}2e^-)$)[233], a stretched bond with singlet diradical character,[234] and even as a no-bond interaction.[235,236] As a result, the nature of the Ge···Ge bond in **4-Co** cannot be conclusively determined by merely comparing its molecular structure with the available structural data in the CSD database.

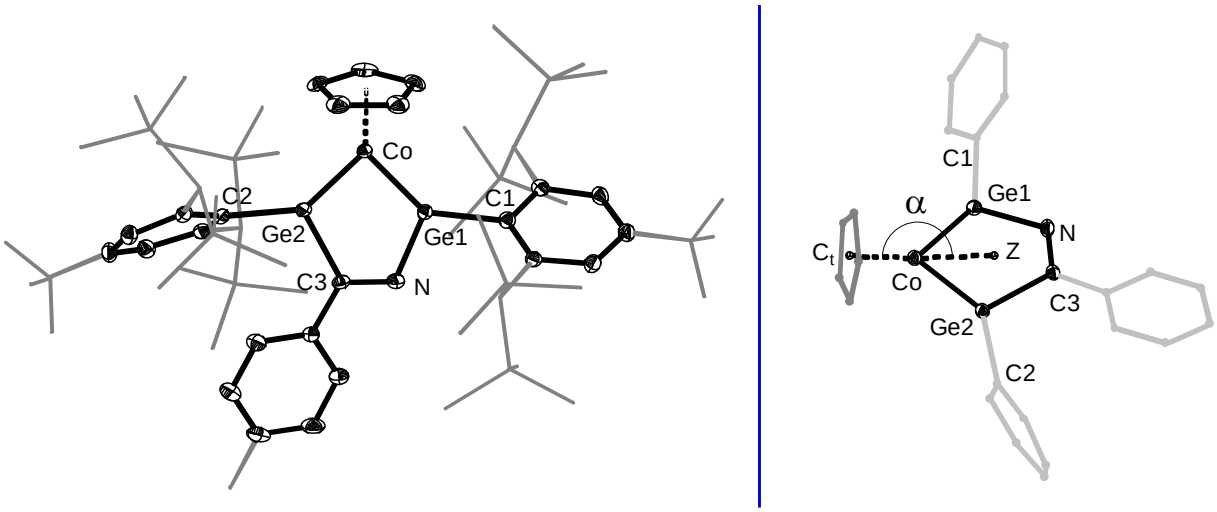

Figure 32. (***left***) DIAMOND plot of the molecular structure of **4-Co**. Thermal ellipsoids are set at 30 % probability level. Hydrogen atoms are omitted and the Dsi and ^{t}Bu substituents of the Tbb ligand are presented in wire-frame for clarity. Selected bond lengths [Å] and bond angles [°]: Co-Ge1 2.1692(3), Co-Ge2 2.1756(3), Ge1-N 1.9221(18), Ge1-C1 1.953(2), Ge2-C3 2.062(2), C3-N 1.273(3), Ge2-C2 1.9610(19), Co-Ge1-N 104.68(8), Co-Ge1-C1 137.37(6), C1-Ge1-N 104.68(8), C2-Ge2-C3 109.15(8), Co-Ge2-C2 139.52(7) Co-Ge2-C3 111.31(6). (***right***) A side-on view of the truncated molecular structure of **4-Co**; α = 174.8(6)°, C_t and Z is the centroid of the Cp and the cobaltacycle, respectively.

Further structural characterisation of the **4-Co** complex was achieved through comprehensive multinuclear NMR spectroscopy. The ^{1}H and ^{13}C{^{1}H} NMR spectra of **4-Co** in (D_6)benzene at 298 K. In solution, complex **4-Co** exhibits a time-averaged C_s-symmetric structure consisting a molecular symmetry plane that passes through the five-membered metallacycle and the centroid of the freely rotating Cp ring. Notably, here Ge centers are heterotopic as they are bonded with hetero atoms (for instance, Ge1−N and Ge2−C3), making the Tbb's also heterotopic, in which most likely, one sterically demanding Tbb substituent experiences hindered rotation (Ge1−Tbb) and other rotation is completely frozen (Ge2-Tbb) due to the presence of *p*-tol group in its vicinity making the $SiMe_3$ group of $C^{2,6}CH(SiMe_3)_A(SiMe_3)_B$ magnetically inequivalent as can be easily depicted by the broad and sharp sets of TMS signals in 18:18:18:18 due to dynamic behaviour around the Ge−C^{ipso} bond axis at ambient temperature. This dynamic behaviour is reflected in the ^{1}H and ^{13}C{^{1}H} NMR spectra. The assignment of these spectra was facilitated by a combination of ^{13}C−^{1}H HSQC and HMBC correlation experiments. The ^{13}C{^{1}H} NMR spectra of **4-Co** display distinct resonances for the nitrile at δ_{CN}/ppm = 192.1. This unsaturated carbon resonances are particularly significant, as they closely match those observed in the acyclic germanium isocyanide adduct (ArDippGe←CN-Mes)$_2$, which exhibits a δ_{CN}/ppm value of 196.[237].

Suitable single crystals for X-ray diffraction study of **5-Co** (clear red plate) were grown by slow evaporation of saturated Et_2O/CH_3CN (3:1, v/v) solutions at ambient temperature, **6-Co** (clear dark orange plank) and **7-Co** (clear dark yellow plate) were grown from a saturated *n*-hexane and *n*-pentane solution at −30 °C respectively.

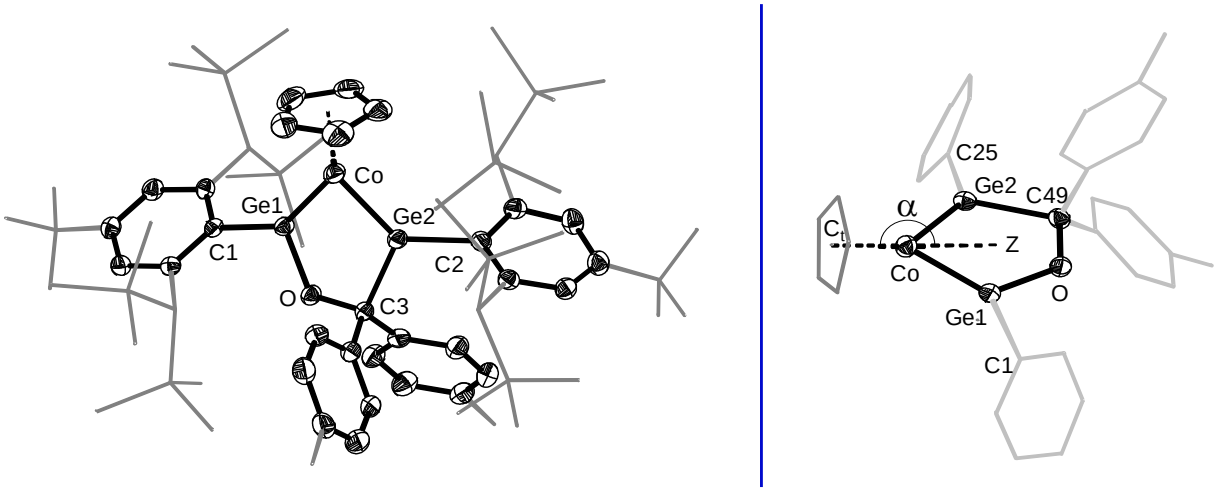

Figure 33. (***left***) DIAMOND plot of the molecular structure of **5-Co**. Thermal ellipsoids are set at 30 % probability level. Hydrogen atoms are omitted and the Dsi and ^{t}Bu substituents of the Tbb ligand are presented in wire-frame for clarity. Selected bond lengths [Å] and bond angles [°]: Co-Ge1 Co-Ge1 2.1684(4), Co-Ge2 2.1855(5), Ge1-O 1.8065(15), Ge1-C1 1.973(2), Ge2-C2 1.994(2), Ge2-C3 2.102(2), C3-O 1.434(3), Co-Ge1-C1 142.90(7), Co-Ge1-O 115.39(5), C1-Ge1-O 101.70(8), Co-Ge2-C2 133.68(7)), Co-Ge2-C3 111.42(6), C3-Ge2-C2 114.56(9). (***right***) A side-on view of the truncated molecular structure of **5-Co**; α = 176.0(7)°, C_t and Z is the centroid of the Cp and the cobaltacycle, respectively.

The complexes **5-Co** and **7-Co** crystallized in the triclinic crystal system, adopting the centrosymmetric space group $P\bar{1}$, whereas **6-Co** formed crystals in the monoclinic system, belonging to the chiral space group $P2_1$. Key solid-state structural characteristics of these metallacycles include:

i) All the complexes exhibit similar geometries around the cobalt (Co) center, forming five-membered metallacycles with bond angles around cobalt ∠(Ge1−Co−Ge2) = 85.321(17)° (**5-Co**), 84.09(7)° (**6-Co**), and 84.81(4)° (**7-Co**). Additionally, the two trigonal planar germanium centers in each complex show nearly ideal geometries, with Ge1 and Ge2 being ∑∢ (Ge1) and (Ge2) = 360° and 359.66° (**5- Co**); ∑∢ (Ge1) and (Ge2) =359.94° and 359.74°(**6-Co**); and ∑∢ (Ge1) and (Ge2) =359.78° and 359.92° (**7-Co**). These results indicate that the germanium centers adopt a nearly perfect trigonal planar configuration in all complexes.

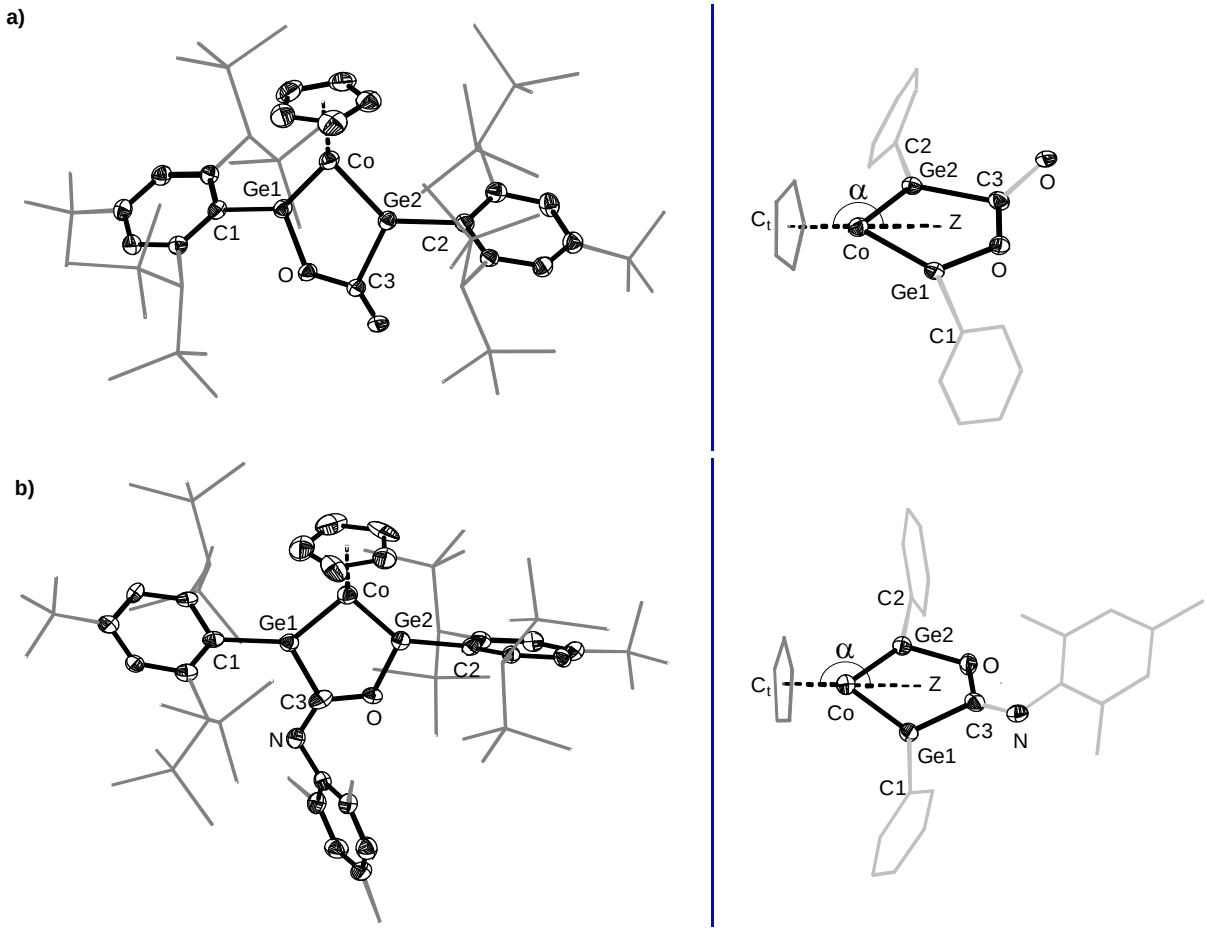

Figure 34. DIAMOND plot of the molecular structure of **6-Co** (***top, left***) and **7-Co** (***bottom, left***). Thermal ellipsoids are set at 30 % probability level. Hydrogen atoms are omitted and the Dsi and ^{t}Bu substituents of the Tbb ligand are presented in wire-frame for clarity. Selected bond lengths [Å] and bond angles [°]: **a)** Co-Ge1 2.183(2), Co-Ge2 2.176(2), Ge1-C1 1.959(11), Ge1-O1 1.866(8), Ge2-C2 1.969(11), Ge2-C3 2.027(11), C3-O 1.355(14), C3-O2 1.209(14), Co-Ge1-C1 141.6(3), Co-Ge1-O1 116.8(3), Co-Ge2-C2 142.2(3), Co-Ge2-C3 111.6(3); **b)** Co-Ge1 2.1742(10), Co-Ge2 2.1635(10), Ge1-C1 1.973(6), Ge1-C3 2.006(6), Ge2-C2 1.945(5), Ge2-O 1.859(4), C3-O 1.353(7), C3-N 1.277(7), Co-Ge1-C1 130.40(16), Co-Ge1-C3 110.70(19), C1-Ge1-C3 118.7(2), Co-Ge2-C2 144.11(17), Co-Ge2-O 115.43, C2-Ge2-O 100.4(2). A side-on view of the truncated molecular structure of **6-Co** (***top, right***) α = 177.4(3)° and **7-Co** (***bottom, right***) α = 175.5(4)°; C_t and Z is the centroid of the Cp and the cobaltacycle, respectively.

ii) The metallacyclic ring plane is nearly orthogonal to the Cp Plane with pyramidal angle (α): 176.0(7)° (**5-Co**)(***Figure 33***), 177.4(3)° (**6-Co**) and 175.5(4)° (**7- Co**)(***Figure 34***).

iii) The sterically demanding Tbb substituents are arranged nearly orthogonally with respect to the plane of the five-membered cobaltacycle. This spatial arrangement in the crystal lattice gives rise to a C_s symmetry for **5-Co, 6-Co** and **7-Co**. The Co−Ge double bond distances of all the complexes are discussed in a row, which are as follows: $d(\text{Co−Ge})_{mean}$ = 2.176(5) Å (**5-Co**), $d(\text{Co−Ge})_{mean}$ = 2.183(8) Å (**6-Co**), and $d(\text{Co−Ge})_{mean}$ = 2.168(5) Å (**7-Co**). Furthermore, they align well with the bond distance

observed in the reported bis-germylidene complex CpCo(GeBrTbb)$_2$ (d(Co−Ge)$_{mean}$ =2.17(5) Å.[226] and Ge-O single bond distance *d*(Ge−O) = 1.8065(15) Å for **5-Co**, *d*(Ge−O) = 1.866(8) for **6-Co** and *d*(Ge−O) = 1.859(4) for **7-Co** compares well with the typical Ge-O single bond (1.75−1.87 Å).

Further structural characterization of the complexes **5-Co**, **6-Co**, and **7-Co** was achieved through comprehensive multinuclear NMR spectroscopy. The ^{1}H and ^{13}C{^{1}H} NMR spectra of **6-Co** were recorded in (D_6)benzene at 298 K, while those of **5-Co** and **7-Co** were recorded in (D_8)toluene at 243 K and 236 K, respectively. The spectroscopic analysis of solution state samples of **5-Co** at low temperature exhibits a time-averaged C_s symmetry where the molecular plane bisects the five-membered metallacycle and the centroid of the freely rotating Cp ring. The two Ge centers are heterotopic because of the different chemical environments around them and make Tbb substituents also heterotopic where one of the sterically demanding Tbb substituent rotation is completely frozen, and other rotation is hindered around Ge−C^{ipso} as evident by sharp and broad Dsi (CH(SiMe$_3$)$_A$(SiMe$_3$)$_B$) signals with diastereotopic SiMe$_3$ groups labelled with subscripts A and B respectively. Whereas in the case of **7-Co**, the rotation of both the Tbb around Ge−C^{ipso} is freezed, denoted by the sharp TMS and Dsi (CH(SiMe$_3$)$_A$(SiMe$_3$)$_B$) signals at low temperature. This dynamic behaviour is reflected in the ^{1}H and ^{13}C{^{1}H} NMR spectra. The assignment of these spectra was facilitated by a combination of ^{13}C−^{1}H HSQC and HMBC correlation experiments. The ^{13}C{^{1}H} NMR spectra of **5-Co** and **7-Co** display distinct resonances for the functionalized ketonic and isocyanate carbon atoms, with δ_{CO}/ppm = 98.06 for **5-Co** and δ_{CO}/ppm = 176.50 for **7-Co**, respectively. In solution, **6-Co** adopts a time-averaged structure with Cs symmetry. In this configuration, the molecular symmetry plane bisects the five-membered metallacycle and passes through the centroid of the freely rotating Cp ring. The Ge centers and Tbb substituents are heterotopic, as the Ge centers are bonded to heteroatoms (e.g., C and O). One sterically demanding Tbb group rotates freely, while the other Tbb group experiences hindered rotation as evidenced by the broad signal of C^{2,6}(CH(SiMe$_3$)$_A$(SiMe$_3$)$_B$) group with diastereotopic SiMe$_3$ groups labelled with subscripts A and B respectively due to steric interactions around the Ge−C^{ipso} bond axis at ambient temperature. This dynamic behaviour is evident in the ^{1}H and ^{13}C{^{1}H} NMR spectra, where sharp and broad signals corresponding to the TMS groups are observed, reflecting the differing rotational freedom of the Tbb substituents. A combination of ^{13}C−^{1}H HSQC and HMBC correlation experiments facilitated the assignment of these spectra. The

$^{13}C\{^{1}H\}$ NMR spectra of **6-Co** shows distinct resonance for the *C*O carbons at δ_{CO}/ppm = 188.78.

The solution IR spectra of the **4-Co** and **6-Co** in *n*-hexane exhibit strong absorption bands at 1605 cm^{-1} (**4-Co**) and 1682 cm^{-1} (**6-Co**), as shown in (***Figure 35***). These bands fall within the characteristic frequency range for imine (C=N) and carbonyl (C=O) stretching vibrations.

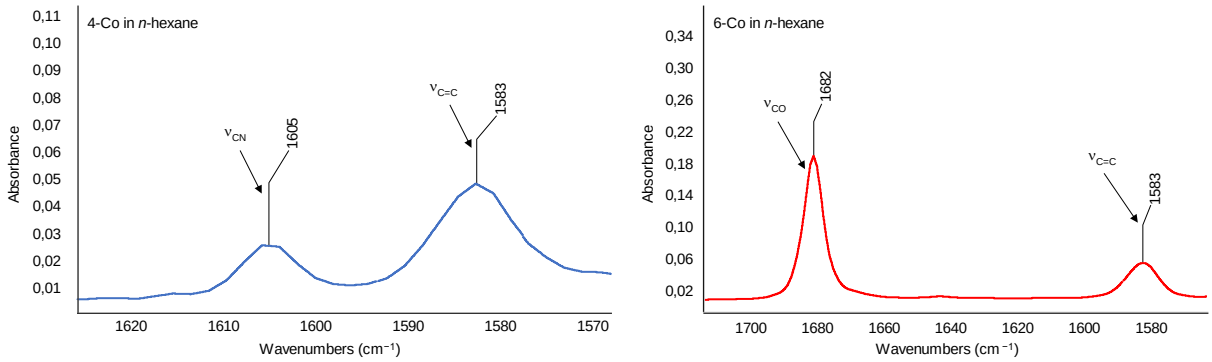

Figure 35. Solution state IR spectrum of the metallacycle complexes **4-Co** (*left*) and **6-Co** (*right*) recorded in *n*-hexane at 298 K.

2.1.2.3. Insertion reaction

To investigate the Ge-centered insertion reactivity of the complex **3-CoGe** with polar unsaturated organic substrates, such as azides, diazoalkanes, isothiocyanates, and elemental phosphorus, a series of systematic experiments were conducted, unveiling a novel and efficient synthetic pathway for accessing a diverse array of unprecedented low-coordinate germanium compounds *via* an insertion mechanism. Initial investigations focused on the reaction of a colourless *n*-hexane solution of *p*-tolyl isothiocyanate (*p*-tol-NCS) with an orange-brown *n*-hexane solution of **3-CoGe** under ambient conditions. Upon dropwise addition to **3-CoGe**, an immediate colour change to an intense black-brown solution was observed, indicative of a rapid chemical transformation. The reaction progress was meticulously monitored by ^{1}H NMR spectroscopy, which confirmed the complete consumption of the starting materials and the formation of multiple products, including **8-Co** in approximately 50% yield as per ^{1}H NMR. Dark purple crystals of Sulphur-inserted product **8-Co** (***Scheme 5***) were successfully isolated following workup and subsequent crystallization from *n*- hexane at −30 °C, yielding 30% of the product. Building on these findings, further exploration of **3-CoGe** reactivity was pursued, including its reaction with a purple *n*- hexane solution of diazomethane (*p*-tol)$_2$-CN_2. Unlike the rapid transformation

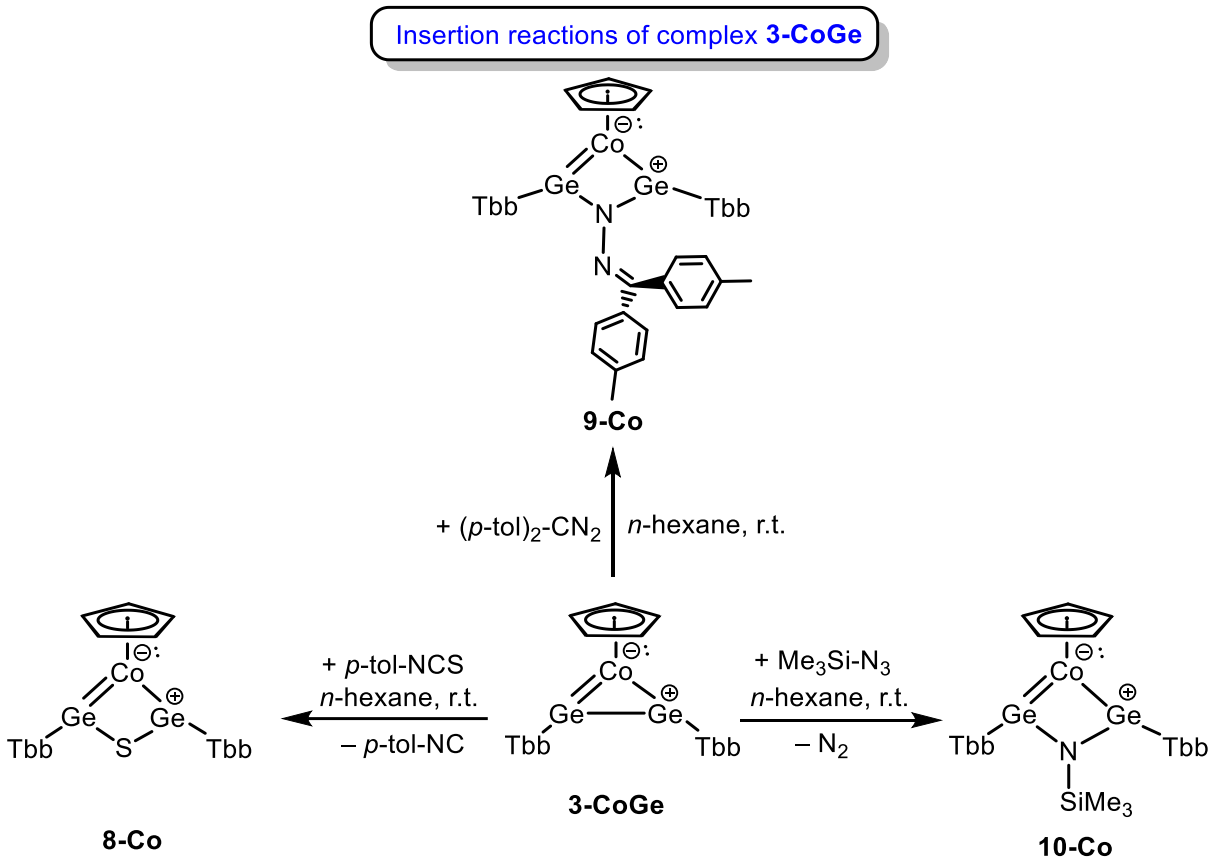

Scheme 5. Synthesis of inserted mechanism pathway products of **3-CoGe** to afford **8-Co, 9-Co** and **10-Co**.

with *p*-tol-NCS, this reaction proceeded slowly, with no immediate colour change. After stirring for 1 hour, the mixture turned dark brown, and ^{1}H NMR spectroscopy confirmed the complete consumption of the starting materials and the selective formation of the product **9-Co** (***Scheme 5***). An intense brown solid was isolated after workup and crystallization from diethyl ether (Et_2O), yielding **9-Co** as a diethyl ether solvate (**9-Co**·$\mathbf{C_4H_{10}O}$) with an 82% yield. The complexes **8-Co** and **9-Co**, both derived from the Ge-centered insertion reactivity of **3-CoGe** with polar unsaturated organic substrates, exhibit remarkable similarities in their handling and stability profiles yet differ in their thermal properties. Both compounds are susceptible to air and moisture, necessitating strict handling under inert conditions to prevent degradation. However, when stored under an argon atmosphere, they demonstrate exceptional stability.

Additionally, both **8-Co** and **9-Co** show good solubility in common organic solvents, facilitating their use in various synthetic and analytical procedures. Despite these similarities, their thermal behaviours diverge significantly. Thermal decomposition analysis, conducted using vacuum-sealed glass capillaries, revealed that **8-Co** undergoes decomposition upon melting at 249 °C, indicating relatively high thermal

stability. In contrast, **9-Co** decomposes at a lower temperature of 176 °C, suggesting a more thermally labile nature.

In a series of carefully orchestrated experiments, the reactivity of the complex **3-CoGe** was explored with two distinct reagents: trimethylsilyl azide (TMS-N_3) and white phosphorus (P_4). The first reaction began with the slow addition of a colourless *n*-hexane solution of TMS-N_3 to an *n*-hexane solution of **3-CoGe**. Almost immediately, a striking colour change occurred as the solution transitioned to a deep green-black. This dramatic shift signalled the onset of the reaction, which was meticulously monitored by ^{1}H NMR spectroscopy. The NMR data confirmed the selective formation of a new product, **10-Co** (***Scheme 5***). After a careful workup, black crystalline solids of **10-Co** were successfully isolated through crystallization from *n*-pentane at −30 °C, yielding a respectable 54% of the desired product. **10-Co** exhibits sensitivity towards air and moisture and shows good solubility in common organic solvents and deteriorates to a dark black mass upon melting at temperatures of 141 °C.

Complex **8-Co** was thoroughly characterized using single-crystal X-ray diffraction (scXRD) analysis and multinuclear NMR spectroscopy. High-quality single crystals of **8-Co**, appearing as clear violet plates, were obtained by slow cooling of a saturated

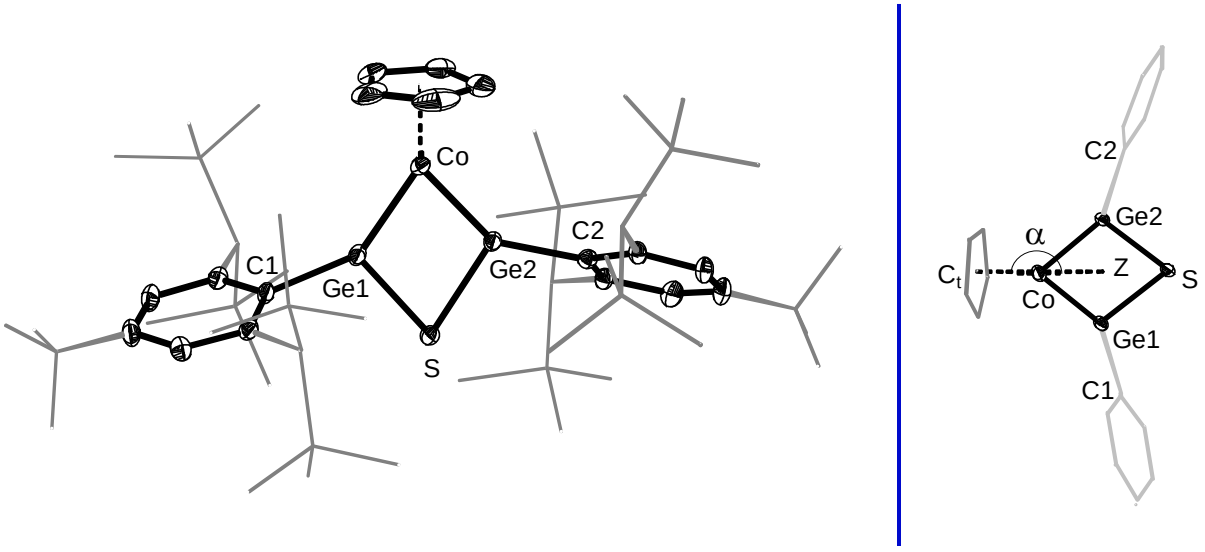

Figure 36. (***left***) DIAMOND plot of the molecular structure of **8-Co**. Thermal ellipsoids are set at 30 % probability level. Hydrogen atoms are omitted and the Dsi and ^{t}Bu substituents of the Tbb ligand are presented in wire-frame for clarity. Selected bond lengths [Å] and bond angles [°]: Co-Ge1 2.1990(4), Co-Ge2 2.1817(4), Ge1-S 2.2709(6), Ge1-C1 1.961(2), Ge2-S 2.2781(6), Ge1-C2 1.952(2), Co-Ge1-C1 146.05(6), Co-Ge1-S 104.737(17), Co-Ge2-C2 145.12(6), Co-Ge2-S 105.067(19). (***right***) A side-on view of the truncated molecular structure of **5-Co**; α = 177.2(7)°, C_t and Z is the centroid of the Cp and the cobaltacycle, respectively.

solution at −30 °C. The complex crystallized in the triclinic space group $P\bar{1}$. The molecular structure of **8-Co** (***Figure 36***) reveals an almost planar four-membered $CoGe_2S$ heterometallacyclic ring, with the sum of internal bond angles equal to 360°. Both germanium centers exhibit perfect trigonal planar coordination (∑∢(Ge1/Ge2) = 360°). The Co−Ge bond distances in **8-Co** (*d*(Co−Ge1) = 2.169(2) Å, *d*(Co−Ge2) = 2.175(6) Å) are consistent with those of a Co=Ge double bond, as observed in the literature-known bis-germylidene complex $CpCo(Ge_2Br_2Tbb_2)$ (*d*(Co−Ge)mean = 2.175(2) Å)[226]. These distances are significantly shorter than those of Co−Ge single bonds in Co(I)-germyl complexes, which typically range from 2.294 Å to 2.525 Å (based on a Cambridge Structural Database (CSD) search). Additionally, the Ge−S bond distances in **8-Co** (*d*(Ge−S) = 2.270(9) Å) closely match those reported for an amidinate-stabilized bis-germylene sulfide (*d*(Ge−S) = 2.262(6) Å)[238]. Based on these comparative analyses, it can be concluded that the lone pairs of the heteroatom (sulfur) do not participate in conjugation with the Co=Ge double bond to form a 6π-electron aromatic system

The cobalt complexes **9-Co** and **10-Co** were thoroughly characterized using advanced analytical techniques, including single-crystal X-ray diffraction (scXRD) and multinuclear NMR spectroscopy. High-quality single crystals suitable for X-ray diffraction analysis were successfully grown under controlled conditions. Specifically, **9-Co** (clear brown blocks) was crystallized from slow cooling of saturated ether (Et_2O) solution at −30 °C. In contrast, **10-Co** (clear pinkish-brown plates) was crystallized from saturated *n*-pentane solutions under the same temperature conditions. Crystallographic analysis revealed that **9-Co** and **10-Co** adopt a triclinic crystal system, crystallizing in the space group $P\bar{1}$.

The molecular structures of **9-Co** and **10-Co** (***Figure 37***) reveal an almost planar four-membered $CoGe_2N$ heterometallacyclic ring, with the sum of internal bond angles equal to 360°. Both germanium centers possess perfect trigonal planar coordination (∑∢(Ge1/Ge2) = 360°). The Co−Ge double bond distances in **9-Co** and **10-Co** are (*d*(Co−Ge1) = 2.1980(5) Å, *d*(Co−Ge2) = 2.1911(6) Å); (*d*(Co−Ge1) = 2.2155(7) Å, *d*(Co−Ge2) = 2.1926(6) Å) are bit elongated because of the nitrogen lone pair conjugation with Co=Ge double bond and also deviates with the literature-known bis-germylidene complex $CpCo(Ge_2Br_2Tbb_2)$ (*d*(Co−Ge)mean = 2.175(2) Å))[226] aligns close to the literature reported singlet biradicaloid germanium (*d*(Ge−N) = 1.870(2) Å) [198] by Philip P. Power. In the case of **9-Co** nitrogen present in the planar $CoGe_2N$ heterometallacyclic ring also conjugating with the in-plane *p*-tol ring, The

hetrometallacyclic ring plane is nearly orthogonal to the Cp Plane with pyramidal angle (α): 177.2(1)° (**9-Co**), 174.0(1)° (**10-Co**).

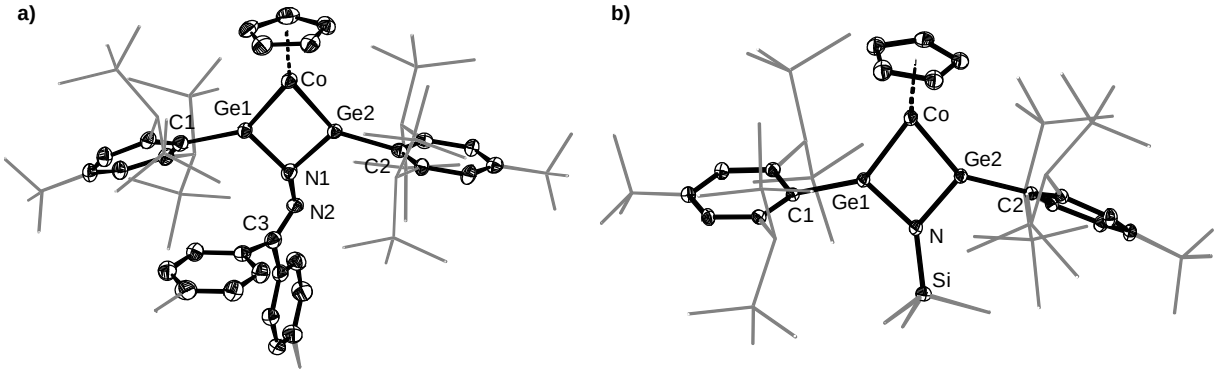

Figure 37. DIAMOND plot of the molecular structure of **9-Co** (***left***) and **10-Co** (***right***). Thermal ellipsoids are set at 30 % probability level. Hydrogen atoms are omitted and the Dsi and ^{t}Bu substituents of the Tbb ligand are presented in wire-frame for clarity. Selected bond lengths [Å] and bond angles [°]: **a)** Co-Ge1 2.1980(5), Co-Ge2 2.1911(6), Ge1-C1 1.974(3), Ge1-C2 1.979(3), Ge1-N1 1.900(2), Ge2-N1 1.904(3), N1-N2 1.402(3), N2-C3 1.286(4), Co-Ge1-N1 97.86(8), Co-Ge1-C1 144.46(9), Co-Ge2-N1 97.95(8), Co-Ge2-C2 146.11(8), Ge1-N1-Ge2 88.85(11), N1-N2-C3 119.6(3); **b)** Co-Ge1 2.2155(7), Co-Ge2 2.1926(6), Ge1-C1 1.990(2), Ge2-C2 1.975(2), Ge1-N 1.920(2), Ge2-N 1.894(2), N-Si 1.727(2), Co-Ge1-C1 142.88(8), Co-Ge1-N 99.44(7), Co-Ge2-C2 145.84(8), Co-Ge2-N 1001.07(7), Ge1-N-Ge2 86.65(9).

Further structural characterization of the complexes **8-Co**, **9-Co** and **10-Co** was achieved through comprehensive multinuclear NMR spectroscopy and the ^{1}H and ^{13}C{^{1}H} NMR spectra of all complexes were recorded in (D_6)benzene at 298 K. In solution, complex **8-Co** adopts a time-averaged *pseudo*-C_{2V}-symmetric structure, with the rotational axis passing the heterometallacyclic ring through C_t, Co, and S (where C_t represents the centroid of the Cp ring). The pyramidal angle (the angle between Cp-centroid (C_t), Co and the centroid of the 4-membered ring) (α) is close to 180°. This symmetry operation renders the two germanium centers and Tbb groups homotopic, where the sterically demanding Tbb substituents to undergo free rotation around the Ge–C^{ipso} bond axis at ambient temperature. This dynamic behaviour is evidenced by the sharp signals observed in the TMS, Dsi, and aromatic $C^{3,5}$-H region of free Tbb substituent in the ^{1}H NMR spectra supporting the time-averaged *pseudo*-C_{2V}-symmetric structure. Notably, complex **9-Co** and **10-Co** adopt a time-averaged C_s-symmetric structure, where the symmetry plane passes through C_t, Co, and N atoms making both the germanium centers and the sterically demanding Tbb substituents enantiotopic. This dynamic behaviour is evidenced by the sharp signals corresponding to the TMS group in the ^{1}H NMR spectra. The ^{1}H and ^{13}C{^{1}H} NMR spectral assignments were further supported by ^{13}C–^{1}H HSQC and HMBC correlation experiments.

Isolation of a crystalline Ge_2P_4 Dewar Benzene Complex

The degradation and direct functionalization of white phosphorus (P_4) into molecular phosphorus compounds hold significant fundamental importance in both academic research and industrial application.[239] In contrast to the extensively explored coordination chemistry of white phosphorus has evolved into a well-established field over the past five decades, achieving a comprehensive understanding of the mechanisms that drive the transition metal-mediated, chlorine-free functionalization of P_4.[262,263] The activation of P_4 facilitated by main-group elements in low oxidation states remains relatively less developed.[264,265] Recent advancements have highlighted the potential of low-valent Group 14 species, such as cyclic (alkyl)(amino)carbenes (cAACs), N-heterocyclic carbenes (NHCs), and N-heterocyclic silylenes (NHSis), as versatile building blocks for accessing functional phosphorus compounds with diverse structural motifs.[243] For instance, through the degradation or aggregation of P_4 in the presence of NHCs and cAACs, a variety of carbene-functionalized P_n (n=1, 2, 4, 8, 12) adducts have been successfully synthesized.[266,267] As discussed activation or degradation of molecular phosphorus (P_4) *via* metal complexes is well explored in an intriguing activation mode, while the activation *via* low-valent main-group elements are relatively scares and still unclear, prompting us to investigate their potential interactions, reaction mechanisms, and the resulting products to gain a deeper understanding of their chemical behaviour. In fact, treatment of digermyne complex (**3-CoGe**) with P_4 in molar ratio of 1:1 in *n*-hexane at ambient temperature furnishes a clean orange-brown solution of **11-Co**. Subsequent workup and crystallization of the reaction mixture leads to the isolation of **11-Co** as an analytically pure brown crystalline solid, with an impressive 74 % yield (***Scheme 6***). **11-Co** exhibits high sensitivity towards air and moisture, necessitating handling under strictly inert conditions and exhibits good solubility in common organic solvents and deteriorates to a dark mass upon melting at 241 °C.

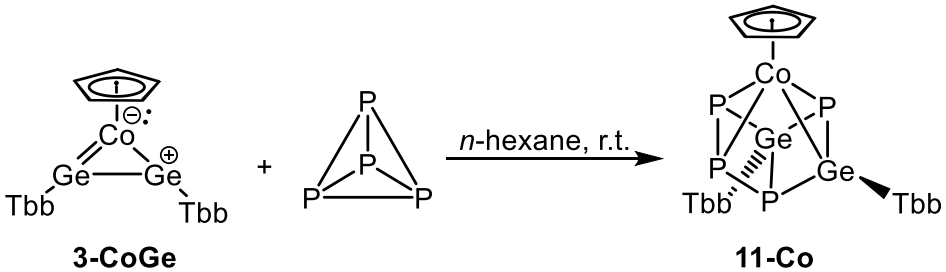

3-CoGe **11-Co**

Scheme 6. Non-metal mediated white phosphorous (P_4) activation from digermyne complex (**3-CoGe**) to afford **11-Co**.

11-Co represents the first P_4 functionalized low-valent main-group transition metal complex featuring a higher analogue of the dewar benzene framework ($Ge_2P_4R_2$), which is generated through the reaction of a digermyne complex (**3-CoGe**) with white phosphorus (P_4) under ambient conditions. This unique complex has been comprehensively characterized using single-crystal X-ray diffraction (scXRD) and multinuclear nuclear magnetic resonance (NMR) spectroscopy. Single crystals of **11-Co**, exhibiting a clear brown block morphology, were successfully obtained by slow cooling of a saturated diethyl ether (Et_2O) solution at −30 °C under meticulously controlled conditions. Detailed crystallographic analysis demonstrated that **11-Co** crystallizes in the monoclinic crystal system, adopting the space group $P2_1/c$.

Activation or degradation of molecular phosphorus (P_4) *via* metal complexes is well explored in an intriguing activation mode, while the activation *via* low-valent main-group transition metal complex is relatively scarce. The insertion of a P_4 unit around the germanium and cobalt centers in the **11-Co** complex results in the formation of a novel class of coordination compounds, which can be classified as a higher analogue of dewar benzene ($Ge_2P_4R_2$) where P is isolable to GeR fragment. In the molecular structure of **11-Co**, the orientation of the sterically demanding Tbb substituents adopts a *cis*-bent configuration, as indicated by the *syn-periplanarity* of the C1−Ge1−Ge2−C2 skeleton (ϕ = −27.47(1)°). Furthermore, one germanium center (Ge1) adopts an almost trigonal planar geometry, as evidenced by the sum of bond angles around Ge1 ($\sum\measuredangle$(Ge1) = 356.44°) whereas, the second germanium center (Ge2) exhibits a distorted tetrahedral geometry and are connected to Co and P respectively unveiling a molecular structure where CpCo fragment coordinates to the tetraphospadigerma dewar benzene core, forming an open-book-like structure (***Figure 38***, *right*) through the bond distances mentioned as follows: *d*(Co−Ge1) = 2.467(1) Å is significantly longer than Co−Ge (2.32 Å) single bond. Similarly, *d*(Co−P3) = 2.355(1) Å, *d*(Co−P1) = 2.350(1) Å, and *d*(Co−P3) = 2.323(1) Å are also exceeding the single-bond covalent radii for Co−P (2.22 Å). Notably, *d*(Ge1−P3) = 2.2542(15) Å and *d*(P1−P2) = 2.159(2) Å also exceed the double-bond covalent radii for Ge−P (2.13 Å) and P−P (2.04 Å) indicating significant π-type metal-ligand interactions. The $(Co-P)_{mean}$ = 2.342(1) Å bond distance in **11-Co** closely aligns with the literature reported *cyclo*-P_4 sandwich complex (Cp***Co(η^4-P_4) where * represent TMS groups attached on the Cp ring) with a $(Co-P)_{mean}$ bond length of 2.313(1) Å.[246]

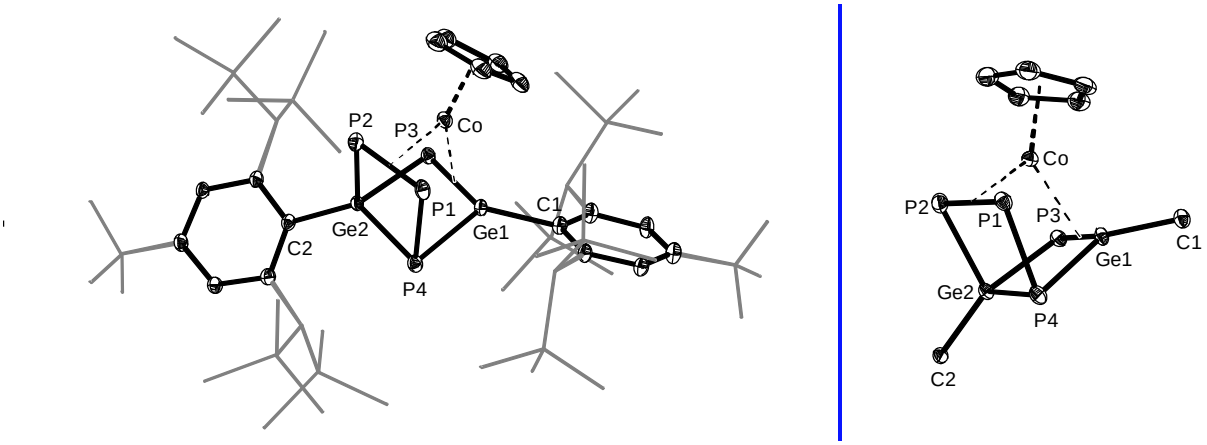

Figure 38. DIAMOND plot of the molecular structure of **11-Co** (***left***) and concentrated view of **11-Co** (***right***). Thermal ellipsoids are set at 30 % probability level. Hydrogen atoms are omitted and the Dsi and ^{t}Bu substituents of the Tbb ligand are presented in wire-frame for clarity. Selected bond lengths [Å] and bond angles [°]: Co-Ge1 2.4671(9), Co-P1 2.3504(17), Co-P2 2.3236(17), Co-P3 2.3553(16), Ge1-P3 2.2542(15), Ge2-P4 2.3764(16), P1-P2 2.159(2), Ge1-C1 1.961(5), Ge2-C2 1.966(5), P1-Ge1-C1 123.15(16), P1-Ge1-P4 53.23(5), P2-Ge2-P4 90.71(6), C1-Ge1-P4 123.15(16), C25-Ge2-P4 126.50(16), Ge1-P4-Ge2 80.10(5), C1-Ge1-Ge2-C2 –27.47(1).

Complex **11-Co** exhibits a C_1-symmetric structure due to the unsymmetrical P_4 insertion around the germanium and cobalt center, which makes both germanium centers heterotopic. In this case, one sterically demanding Tbb substituent rotates freely, while the other remains completely frozen in rotation around the Ge–C^{ipso} bond axis at ambient temperature. This dynamic behaviour is evidenced by the multiple sharp and broad signals observed in the TMS (9:18:18:18:9), Dsi (1:2:1), and aromatic regions (2:1:1) of the Tbb substituent in the ^{1}H NMR spectra. The ^{1}H and ^{13}C{^{1}H} NMR spectral assignments were further supported by ^{13}C–^{1}H HSQC and HMBC correlation experiments. Whereas the ^{31}P{^{1}H} NMR spectra gives four different type of phosphorus signals in the chemical shift range from +40 to -140 ppm (***Figure 39***) as compare to white phosphorous (–560 ppm) revealing the unsymmetrical insertion of phosphorus around the germanium and cobalt center. The phosphorus assignment was done carefully by analyzing the coupling constant.

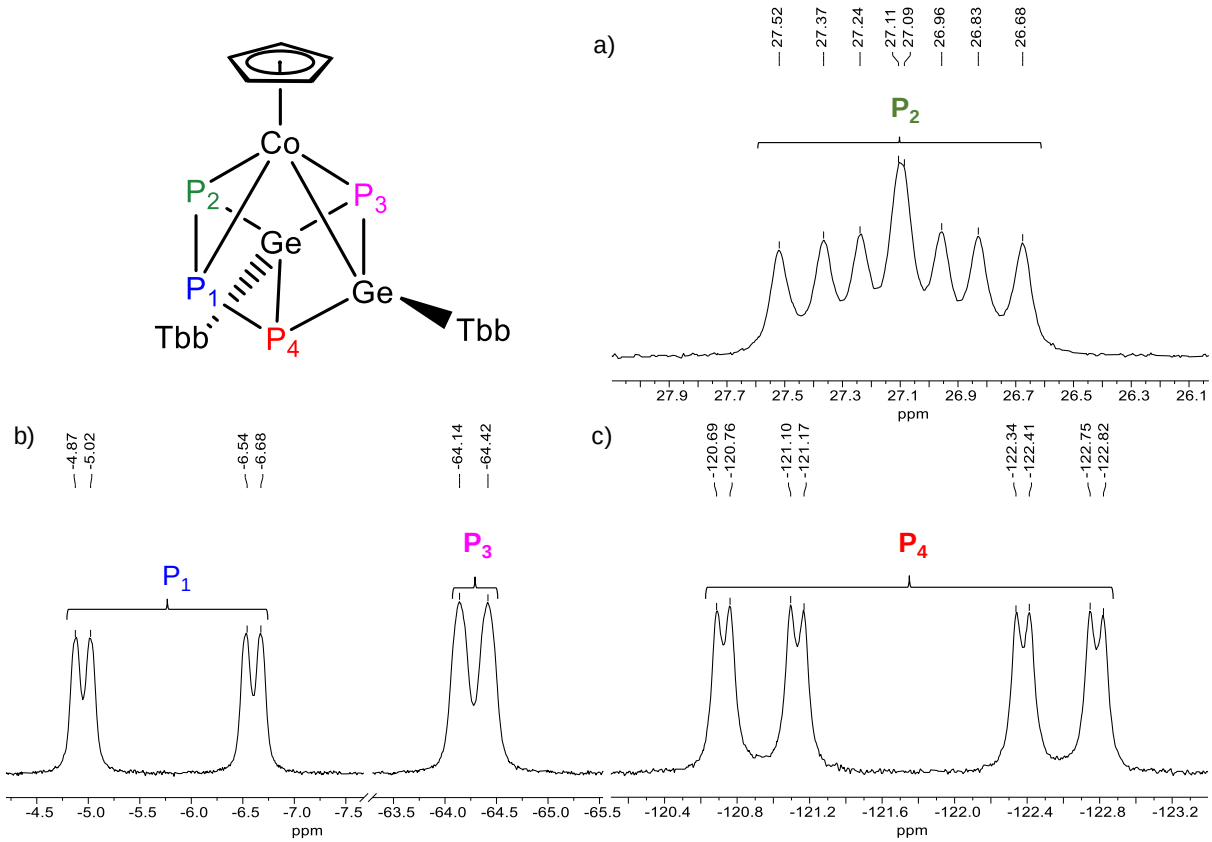

Figure 39. $^{31}P\{^{1}H\}$ NMR spectrum excerpts of **11-Co** in (D_6)benzene at 298 K.

2.2. Diverse downstream chemistry of ditetrelynes with unsaturated non-polar/polar molecules

As underscored in the introductory section, stable, heavier group 14 element multiple-bonded species have attracted considerable attention over the last four decades because of their unusual bonding and structural motifs.[9,10,12,247] The structures of these compounds disclosed a trans-bent rather than linear geometry in which the R−E−E angle decreases from silicon to lead.[8,34,206,207] This trend indicates an increase in the lone pair character and a decrease in the E−E bond order upon descending the group, and this finding is well correlated with computational results.[5,248,249] To investigate the unique bonding in these multiply bonded species, researchers have conducted extensive experimental studies using both unsaturated polar reagents (alkene and alkynes)[250,251] and non-polar reagents (like isocyanide)[57,237,252] to unravel cycloaddition and inserted coupling products. The reductive coupling of isocyanides represents an efficient and economical strategy for constructing diverse C−C bonds. However, in contrast to isoelectronic CO, which readily undergoes reductive coupling in molten potassium to yield small carbocycles such as delicate ($C_3O_3^{2-}$), squarate ($C_4O_4^{2-}$), croconate ($C_5O_5^{2-}$), rhodizonate ($C_6O_6^{2-}$) - reports on the reductive coupling of isocyanides to form cyclic frameworks remain scarce. A notable exception is the cyclization of the unsaturated quintuply bound chromium dimer [LCr−CrL] (L = N,N′-bis(2,6-diisopropylphenyl)-1,4-diazadiene) with cyclohexyl isocyanide (CyNC), leading to a series of heterocycles.[253] In this context, low-valent main-group systems have demonstrated the ability to access a variety of C2- and C3-coupled isocyanide products, with Al(I) species emerging as particularly effective due to pioneering contributions from the groups of Cowley, Cui, Coles, and others.[232,254–256] Additionally, Braunschweig,[257] Jones,[258] and Inoue[259] have demonstrated that other main-group compounds in low oxidation states, including metalloborylenes, magnesium(I) dimers, and silylenes, can facilitate the reductive coupling of isocyanides.

Despite significant recent advancements in the chemistry of low-oxidation-state germanium,[260,261,262] the reactivity of digermyne (heavier alkyne analogue, RGe≡GeR) with isocyanides (R—N≡C) is indeed a fascinating and active area of research in main-group chemistry. For instance, Power and coworkers demonstrated that the digermyne, ArGeGeAr (Ar = C_6H_3-2,6-(C_6H_3-2,6-^{i}Pr$_2$)$_2$), forms only a 1:1 adduct with *tert*-butyl isocyanide (^{t}BuNC),[251] highlighting the controlled reactivity of such complexes under stoichiometric conditions whereas Jones and co-workers

reported that a *bis*-germylene reacts with ^{t}BuNC to yield a green-coloured reductively coupled product.[263] Subsequently, Power and coworkers demonstrated that the diarylgermylene $Ge(Ar^{Mes})_2$ [Ar^{Mes} = C_6H_3-2,6-(C_6H_2-2,4,6-Me_3)$_2$] forms an adduct, $(Ar^{Mes})_2Ge{=}CN^{t}Bu$, which undergoes a facile C−H activation to afford selectively diaryl(hydrido)(cyno)germane, $(Ar^{Mes})_2Ge(H)CN$, with subsequent liberation of isobutene.[264] Later, the same group extended this reactivity to acetonitrile (MeCN), reporting its reductive coupling with diarylgermylene.[265] Notably, germylene-mediated C-C bond formation and insertion reactions remains rare, with only a limited number of examples reported to date.[291,292,293] Furthermore, to elucidate the nature of the bonding in a silicon−silicon triple bond, Sekiguchi and coworkers reported the first reactivity of RSi≡SiR (R = $Si^{i}Pr_2Dsi_2$) with Me_3SiCN, yielding a *bis*-adduct ($RSiSiR(CNSiMe_3)_2$) as minor component, exhibiting a dominant bis(silaketenimine) character with considerable zwitterionic nature. Although 1,4-diaza-2,3-disilabenzene analogue was also isolated as major component in the aforementioned reaction and could be regarded as the non-metal mediated C−C coupling product of respective cyanides.[266] Subsequently, the same group described the formation of a disilyne-isocyanide adduct [$RSiSiR(CNR')_2$] (R = $Si^{i}PrDsi_2$, R′ = ^{t}Bu or $CMe_2CH_2{}^{t}Bu$), which remains stable below − 30 °C and undergoes thermal decomposition upon warming to room temperature.[135] To date, these represents the only reported reactivites of disilyne leading to stable or metastable adducts, involving C-C reductive coupling silyl cyanides. Notably, there have been no documented instances of reductive coupling of isocyanides mediated by a ditetrelyne core center to afford cyclic low-coordinate tetrels coupling products.

2.2.1. Synthesis and characterization of 1,2-disile/germetene

Allenic compounds (X=Y=Z), such as allenes ($R_2C{=}C{=}CR_2$) and ketenimines ($R_2C{=}C{=}NR$), have been extensively explored because of their unique structures, properties and diversity as potent synthons.[267] Their heavier analogues are also of considerable interest due to their distinct bonding modes and applicability as diverse reagent in contemporary molecular inorganic chemistry.[143] Silicon compounds with multiple bonds have long generated interest because of their unique chemical and physical properties. Since the first syntheses of silene and disilene,[247] several silicon compounds with multiple bonds have been reported.[143] The successful isolation of dicoordinated silicon compounds (termed as silylenes) have opened new avenues for reactions with unsaturated molecules, leading to the development of new reaction modes and access to novel silicon compounds with multiple bonds, which seems

intricate without these aforementioned silicon compounds.[268] However, the reaction with polar unsaturated compounds (isocyanides) is the most promising one because of the amphiphilic behaviour of isocyanides as strong σ-donor and weak π-acceptor, isoelectronic with CO (carbon-end amphiphilicity). Additionally, the structural characteristics of silylene-isocyanide complexes have demonstrated that the substituents play a pivotal role in the contribution of two dominant resonance forms: an allenic form ($R_2Si=C=NR$) and a zwitterionic form ($R_2Si^{-}–C\equiv N^{+}R$) (***Figure 40***).

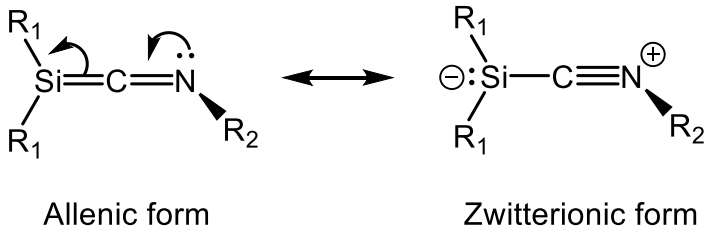

Figure 40. Two dominant resonance structures of silylene-isocyanide adduct (R1 and R2 are any substituents except hydrogen atom).

In 1990, Weidenbruch and coworkers reported that the photoreaction of $(^{t}Bu_2Si)_3$ with phenyl isocyanide exclusively yields two dimeric species with a Si_2C_2 ring structure.[269] In addition, by employing a sterically demanding silylene in reactions with isocyanides, Okazaki and coworkers were able to isolate Lewis acid–base complexes **I-73** (***Figure 41***), in which the isocyanide acts as a Lewis base, as indicated by the reaction of bulky isocyanide with disilene $(TbtSiMes)_2$ (Tbt = 2,4,6-tris[bis- (trimethylsilyl)methyl]pheny and Mes = 2,4,6-MeC_6H_2) and theoretical calculations (Optimized structure of $Ph_2SiCNPh$ at the B3LYP/6-31D(d) level of theory).[270] The research groups of Kira and Sekiguchi, respectively, reported reactions of a cyclic dialkylsilylene and an isolable disilyne with isocyanides yielding compounds **I-74** and **I-75**, which have been predicted to feature some degree of allenic character on the basis of their structural matrices.[134,135] Notably, controlled coupling of isocyanides *via* group 14 low-valent complexes are underexplored, and only a few examples (**I-76** and **I-77)**[138,139] are known so far (***Figure 41***), and only one example is known for isocyanide coupling of anion silicon(0) complex (**I-77)** reported by Cui and coworkers.[138] There have been no reports on the reductive homocoupling of isocyanides initiated by the neutral silicon(0) complex and ditetrelynes.

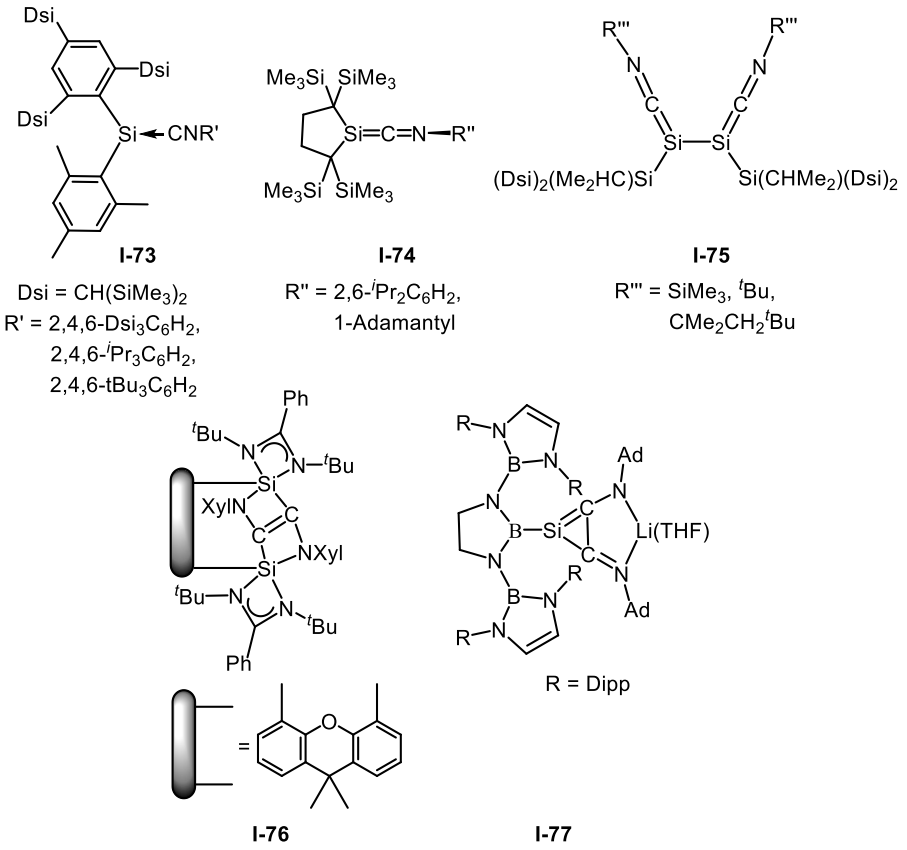

Figure 41. Reported neutral silylene–isocyanide complexes and isocyanide coupling of neutral and anion silicon(0) complex.

Intriguingly, in our endeavour to incorporate ditetrel centers into four-membered ring systems, we aimed to explore the reactivity of TbbE≡ETbb (E = Si, Ge) with isocyanides (e.g., Mes-NC). In fact, the dropwise addition of an *n*-hexane solution of Mes-NC to a red-orange *n*-hexane solution of TbbSi≡SiTbb in a 2:1 molar ratio induced an immediate colour change to red. The reaction progress was rigorously monitored using ^{1}H NMR spectroscopy, which indicated the complete consumption of the starting materials and the exclusive formation of an unprecedented reductive isocyanide coupling product, designated as **12-Si** (***Scheme 7***). In contrast, the analogous reaction involving Mes-NC and TbbGe≡GeTbb in a 2:1 molar ratio exhibited a distinct colour evolution. The solution initially transitioned to a dark green hue before rapidly turning dark brown, indicating the formation of a mono-isocyanide adduct intermediate, as observed by ^{1}H NMR spectroscopy but the pure mono-adduct of digermyne could not be isolated due to the competitive formation of the unprecedented reductive isocyanide coupling product **12-Ge** (***Scheme 7***). These findings represent the first documented examples of reductive isocyanide coupling reactions mediated by ditetrelynes especially by Si(I) and Ge(I) tetrel centers.

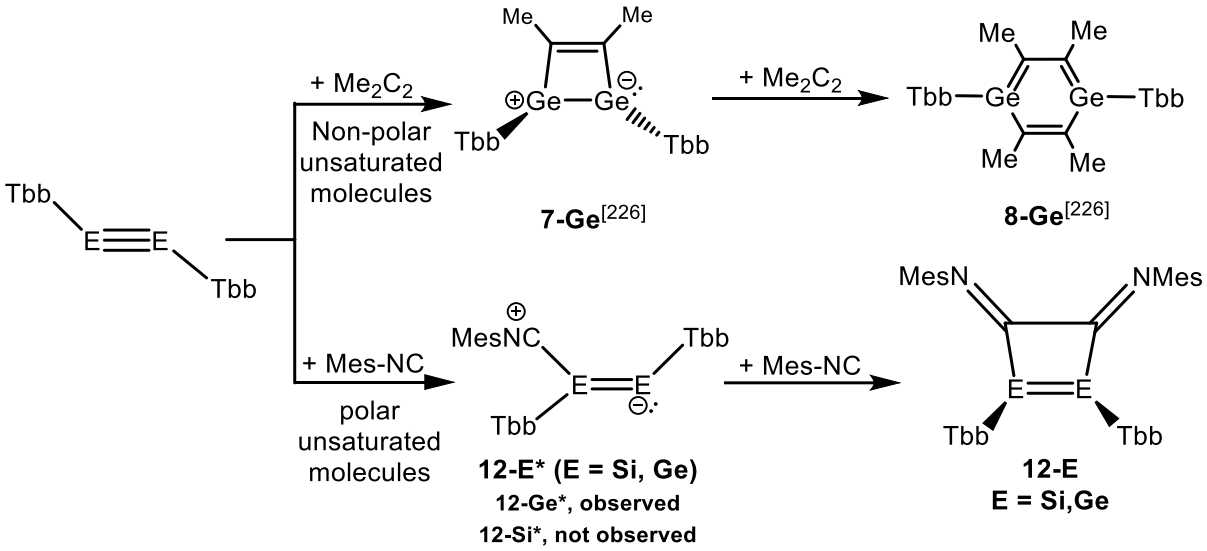

Scheme 7. Reaction of homonuclear ditetrelynes with non-polar and polar unsaturated molecules.

Both compounds, **12-Si** and **12-Ge**, were isolated as intensely coloured crystalline solids: **12-Si** as a red-brown crystal and **12-Ge** as a brown crystalline solid, following work-up and crystallization from *n*-pentane at −30 °C. Each complex was obtained with a yield of 68%. These complexes exhibit pronounced sensitivity to atmospheric oxygen and moisture, necessitating storage under an inert argon atmosphere. Both compounds reveal good solubility in all common organic solvents. The thermal decomposition behaviour was investigated using *vacuum*-sealed glass capillaries, revealing that **12-Si** undergoes unselective decomposition upon melting at 257 °C, while **12-Ge** decomposes at a lower temperature of 146 °C.

Compounds **12-Si** and **12-Ge** represent the first reported examples of reductive isocyanide coupling reactions facilitated by ditetrelynes that demostrate the 1,2-disiletene and 1,2-digermetene ring system. These compounds were thoroughly characterized using single-crystal X-ray diffraction (scXRD) and multinuclear NMR spectroscopy. Crystals suitable for scXRD analysis were grown by slow cooling of their respective *n*-pentane saturated solutions at −30 °C. Specifically, **12- Si·(*n*- pentane)$_{0.5}$** formed clear orange plank-shaped crystals, while **12-Ge** yielded plate-shaped red crystals.

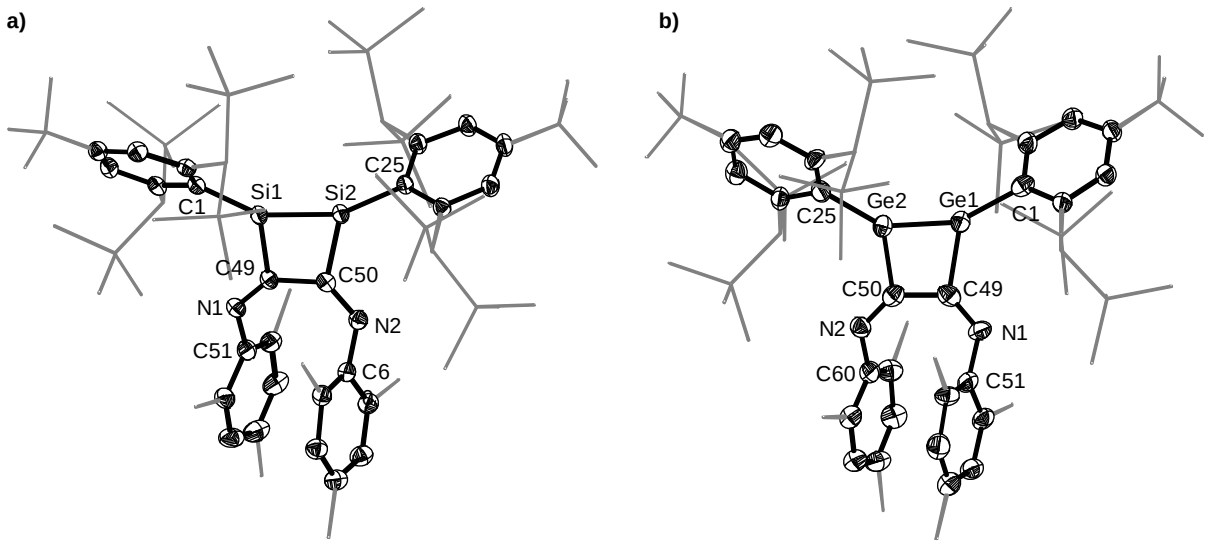

Figure 42. DIAMOND plot of the molecular structure of **12-Si (*left*)** and **12-Ge (*right*)**. Thermal ellipsoids are set at 30 % probability level. Hydrogen atoms are omitted and the Dsi and ^{t}Bu substituents of the Tbb ligand are presented in wire-frame for clarity. Selected bond lengths [Å], bond angles [°] and torsion angle [°]: **a)** Si1-Si2 2.1753(7), Si1-C49 1.1887(2), Si2-C50 1.887(2), C49-N1 1.286(3), N1-C51 1.421(3), C50-N2 1.289(3), N2-C60 1.414(3), C49-C50 1.522(3), C1-Si1-Si2 154.35(7), C1-Si1-C49 126.16(9), C49-Si1-Si2 79.30(6), C25-Si2-C50 125.45(9), C25-Si2-Si1 154.50(7), Si1-Si2-C50 79.84(7), Si1-C49-C50 99.40(13), Si2-C50-C49 99.34(13); **b)** Ge1-Ge2 2.2755(11), Ge1-C49 1.976(7), Ge2-C50 1.986(7), C49-N1 1.282(9), N1-C51 1.415(9), C50-N2 1.296(9), N2-C60 1.405(9), C49-C50 1.501(10), C1-Ge1-Ge2 147.2(2), C1-Ge1-C49 127.9(3), C49-Ge1-Ge2 77.4(2), C25-Ge2-C50 128.5(3), C25-Ge2-Ge1 146.5(2), Ge1-Ge2-C50 77.1(2), Ge1-C49-C50 99.2(5), Si2-C50-C49 98.9(5).

Crystallographic analysis revealed that **12-Si** crystallizes in the triclinic space group $P\bar{1}$, whereas **12-Ge** adopts the monoclinic space group $P2_1/c$. Both compounds illustrate nearly identical skeletal arrangements and adopt a *pseudo*-C_{2v}-symmetric structure in the solid state. The molecular structures of **12-Si** and **12-Ge** (***Figure 42***), demonstrate that the tetrel centers undergo isocyanide coupling to form an almost planar E_2C_2 ring (E = Si, Ge). The sum of the angles around the tetrel centers further highlights the structural similarities and subtle differences between the two compounds. For **12-Si**, the sum of angles around the silicon centers, ∑∢(Si1) and ∑∢(Si2), is exactly 360°, indicating a perfectly planar arrangement. In contrast, for **12-Ge**, the sum of angles around the germanium centers, ∑∢(Ge1) = 352.44° and ∑∢(Ge2) = 352.04°, deviates slightly from ideal planarity. The sum of the angle of the E_2C_2 ring is 357.9° (**12- Si**), which varies to 352.6° (**12-Ge**), showing a decrease in the ring strain when silicon (Si) is replaced by germanium (Ge). In **12-Si**, the Tbb groups adopt a *synperiplanar* configuration and **12-Ge** reveals a synclinical conformation, as evidenced by the torsion angles C1−Si1−Si2−C25 = 4.2° (**12-Si**) and C1−Ge1−Ge2−C25 = 55.4° (**12-Ge**). The Si1−Si2 bond distance in **12-Si** is 2.1753(7) Å, which is comparable to the reported value of 2.1632(11) Å in *trans*-3,4-dimethyl-

1,2-disilacyclobutene.[250] The Si1−C49 and Si2−C50 bond lengths are 1.887(2) Å and 1.877(2) Å, respectively, consistent with the single-bond covalent radii of silicon and carbon.[228] The C49−C50 distance of 1.522(2) Å corresponds to a typical C−C single bond, while the C49−N1 and C50−N2 bond lengths of 1.286(3) Å and 1.289(3) Å, respectively, align well with the double-bond covalent radii of carbon and nitrogen.[228] In the case of **12-Ge**, the Ge1−Ge2 bond distance is 2.2755(11) Å, which compare well with reported digermene (DmaSiR'$_2$)RGe=GeR(SiR'$_2$Dma) (R = Tip= 2,4,6-^{i}PrC$_6$H$_2$; R' = Ph; Dma = 2-Me$_2$NC$_6$H$_4$) (2.2604(6) Å)[271] by D. Scheschkewitz and coworkers.The Ge1−C49 and Ge2−C50 bond lengths are 1.976(7) Å and 1.986(7) Å, respectively, matching the single-bond covalent radii of germanium and carbon. The C49−C50 distance of 1.501(10) Å is consistent with a C−C single bond, while the C49−N1 and C50−N2 bond lengths of 1.282(9) Å and 1.296(9) Å, respectively, are in good agreement with the double-bond covalent radii of carbon and nitrogen.

A detailed structural elucidation of the compounds **12-Si** and **12-Ge** was achieved through multinuclear NMR and IR spectroscopic techniques. The ^{1}H and ^{13}C{^{1}H} NMR spectra of **12-Si** were recorded in (D$_8$)THF at 263 K, while those of **12- Ge** were recorded in (D$_6$)benzene at 298 K. These analyses revealed a time-averaged C_{2v}-symmetric structure in solution, characterized by a two-fold rotational axis passing through the center of the E=E bond, the centroid of the E$_2$C$_2$ ring and bisecting the reductively coupled C−C bond. This symmetry operation renders the silicon and germanium centers homotopic, as well as the Tbb groups. However, in the case of **12-Si**, the rotation of the sterically bulky Tbb substituent is frozen at low temperatures, whereas for **12-Ge**, this dynamic process remains active, facilitating rotation around the E−C^{ipso} (E = Si, Ge) bond axis. This dynamic behaviour is distinctly observable in the ^{1}H and ^{13}C{^{1}H} NMR spectra. The spectral assignments were further corroborated through ^{13}C−^{1}H HSQC and HMBC correlation experiments. Notably, the ^{29}Si{^{1}H} NMR spectrum of **12-Si** in (D$_8$)THF at 263 K displayed a signal at 89.79 ppm, corresponding to the unsaturated silicon center. This contrasts with the reported chemical shift of 152.1 ppm for the unsaturated silicon in *trans*-3,4-dimethyl-1,2-disilacyclobutene [250] in (D$_6$)benzene at 298 K. Additionally, the ^{13}C{^{1}H} NMR spectra of **12-Si** and **12-Ge** exhibited distinct resonances for the unsaturated carbon atoms at 183.88 ppm and 190.93 ppm respectively. These chemical shifts closely align with those observed in the isocyanide adduct of reported germanium analogues compound (Ar′Ge←NC-Mes)$_2$ (where Ar′ = C$_6$H$_3$–2,6(C$_6$H$_3$–2,6-^{i}Pr$_2$)$_2$), which display unsaturated carbon resonances at 196.06 ppm.[237]

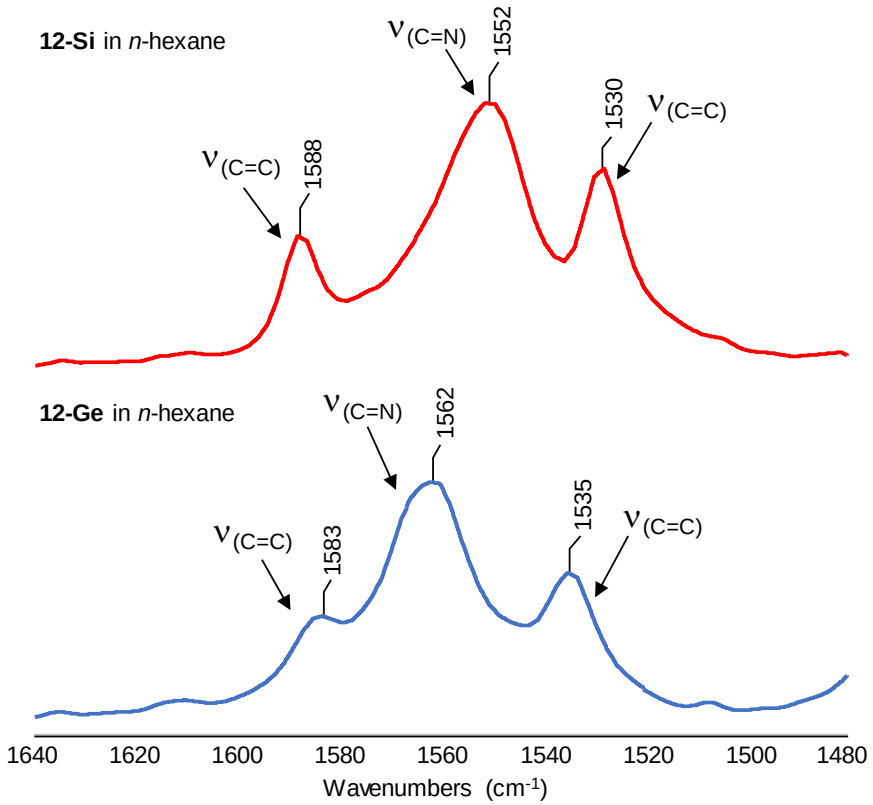

Figure 43. Excerpts of the solution state IR spectrum of the reductive coupling of isocyanide mediated by ditetrelynes **12-Si** (***top***) and **12-Ge** (***bottom***) recorded in *n*-hexane at 298 K.

The solution IR spectra of both compounds in *n*-hexane display a strong absorption band at 1552 cm^{-1} (**12-Si**) and 1562 cm^{-1} (**12-Ge**) (***Figure 43***).

Despite the successful isolation of **12-Si** and **12-Ge**, subsequent attempts to react these compounds with two equivalents of Mes-NC under both ambient and elevated temperature conditions proved unsuccessful in yielding the desired 1,4-ditetrel benzene derivatives. Instead, the reactions resulted in either non-selective mixtures or extensive decomposition of the starting materials at higher temperatures, thereby preventing the formation of the anticipated products.

To further explore the reactivity of **12-E**, both compounds were subsequently treated with $GeBr_2$(1,4-dioxane) in an effort to introduce an additional tetrel center into the core framework. In the case of **12-Si**, the reaction proceeded with notable selectivity, affording **13-Si** as a germylene species substituted with bis-amino groups. In contrast, the reaction involving **12-Ge** yielded a non-selective mixture of products, highlighting the divergent reactivity between the silicon and germanium analogues under these conditions (***Scheme 8***). **13-Si** represents the first instance of the formation of novel five- and four-membered fused ring system thus, this unique structure has been extensively characterized to elucidate its properties and significance.

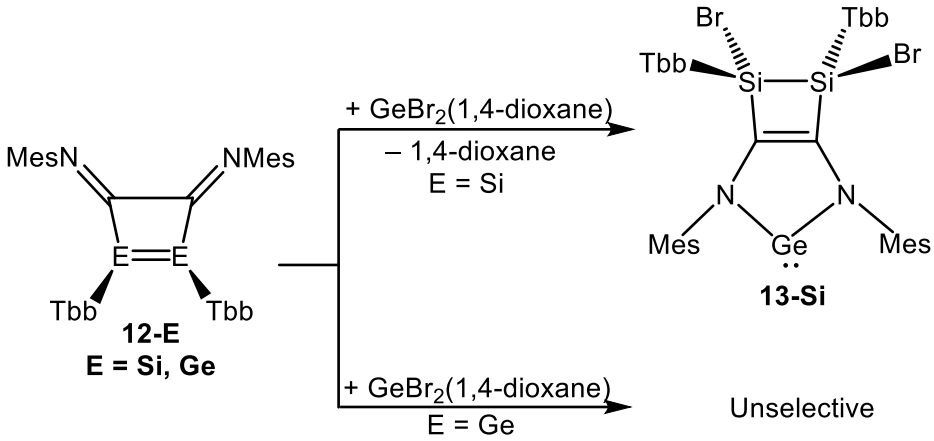

Scheme 8. Reaction of **12-E** (**E = Si, Ge**) with $GeBr_2$(1,4-dioxane).

The molecular structure of **13-Si** was determined by sc-XRD analysis of block-shaped, yellow crystals, grown by slow cooling of its saturated toluene solution at −30°C. Complex **13-Si** crystallizes as a solvate **13-Si** (**toluene**)$_2$ (**benzene**)$_{0.5}$. in the $P\bar{1}$ space group. It features almost a planar five-membered GeN_2C_2 ring fused with disilene that has distorted tetrahedral geometry around the silicon centers where the orientation of both the sterically demanding Tbb substituent is trans configuration, as evidenced by the torsion angles (φ) C1−Si1−Si2−C25 = −114.82° (***Figure 44***, ***left***). This spatial arrangement in the crystal lattice gives rise to a *pseudo*-C_{2V} symmetry of

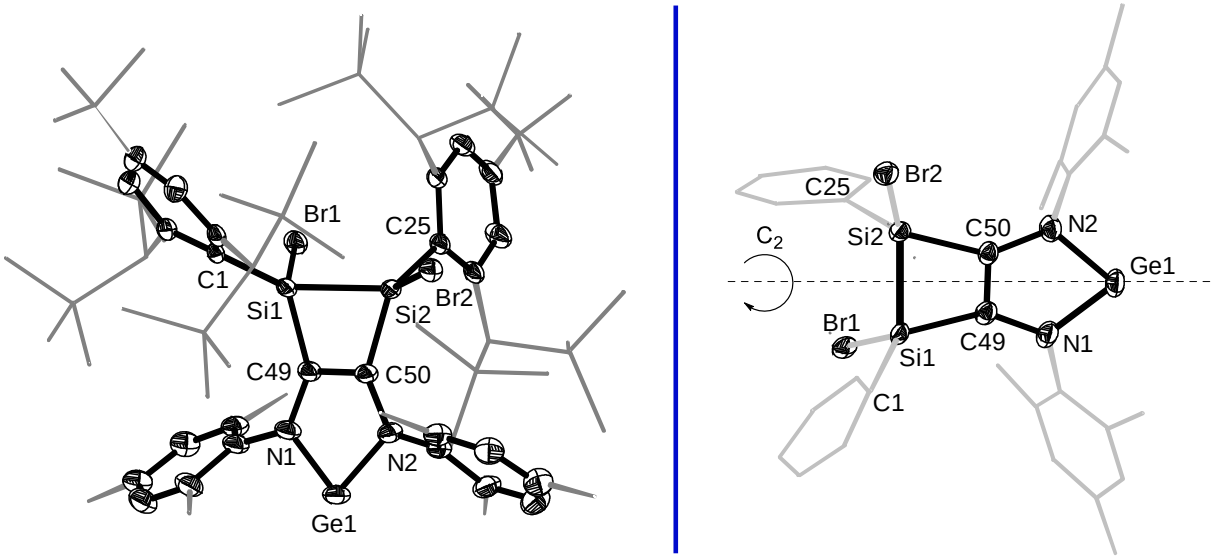

Figure 44. DIAMOND plot of the molecular structure of **13-Si** (***left***) and concentrated view of **13-Si** (***right***) showing 2-fold axis of rotation. Thermal ellipsoids are set at 30 % probability level. Hydrogen atoms are omitted and the Dsi and ^{t}Bu substituents of the Tbb ligand are presented in wire-frame for clarity. Selected bond lengths [Å], bond angles [°] and torsion angle [°]: Si1-Si2 2.360(2), Si1-C49 1.885(7), Si2-C50 1.899(7), C49-C50 1.400(9), C49-N1 1.407(9), C50-N2 1.406(8), N1-Ge1 1.861(5), N2-Ge2 1.887(15), Si1-Br1 2.2670(18), Si2-Br2 2.2444(19), C1-Si1-Si2 132.6(2), C1-Si1-Br1 106.4(2), C25-Si2-Si1 111.0(2), C25-Si2-Br2 105.3(2), Si1-Si2-C50 79.3(2), Si2-Si1-C49 75.5(2), N1-Ge1-N2 84.9(6), Si1-C49-C50 103.5(5), Si2-C50-C49 104.5(5).

13- Si with a C_2-axis through the midpoint of Si−Si, C=C and Ge (***Figure 44***, ***right***). The Si−Si (2.360(2)) Å single bond distance is in good agreement with most organosilicon compounds (2.32 to 2.37 Å). The Si−C bond length (1.894(6) and 1.910(7) Å) align well with the typical single bond range (1.87–1.89 Å). The Ge−N (1.861(15) and 1.887(15) Å) single bond distance also falls in range of typical organogermanium compounds (1.85 to 1.95 Å) as per CSD.

2.2.2. Reactivity of 1,2-digermabutadiene and 1,4-digermabenzene

In pursuit of synthesizing a cyclic compound bearing a tetrel center 1,2-digermabutadiene (**7-Ge**)[226] was chosen as a suitable starting material. A series of reactions were investigated with low-valent silicon, germanium, and tin halide precursors to construct a five-membered ring framework. Notably, the reaction of **7-Ge** with $SiBr_2$(SIDipp) proceeded with poor selectivity, as indicated by the complex mixture observed in the ^{1}H NMR spectrum. In contrast, treatment of **7-Ge** with $GeBr_2$(1,4-dioxane) and $SnCl_2$ successfully afforded *cyclo*-bis(germyl)germylene (**14-Ge**) as a colourless solid in 63% yield and *cyclo*-bis(germyl)stannylene (**14-Sn**) as an off-white solid in 56% yield, respectively (***Scheme 9***) enables us to further explore the chemistry of these intriguing complexes.

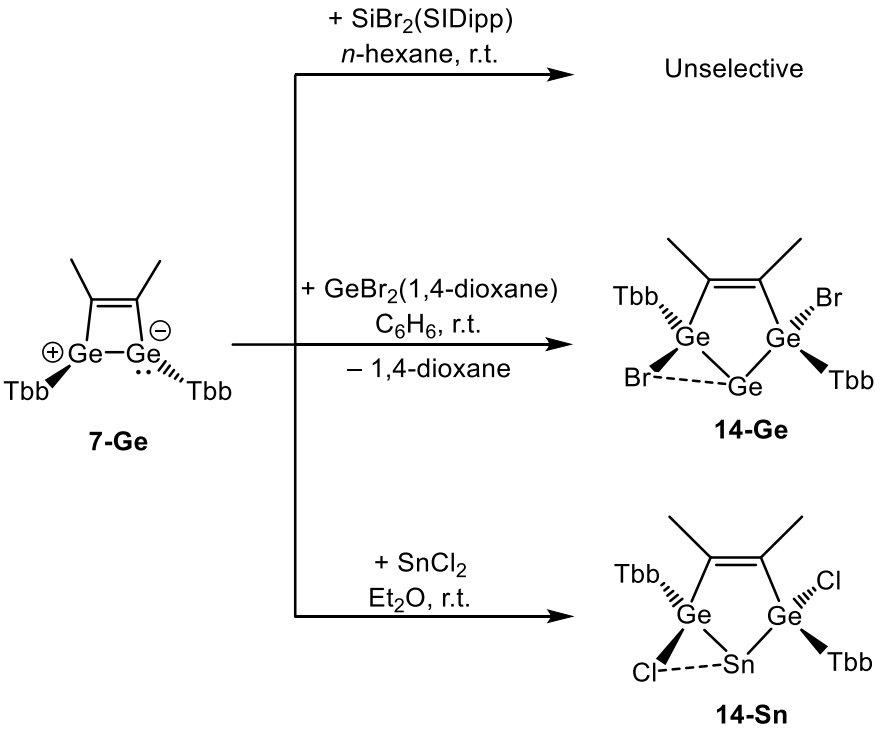

Scheme 9. Synthesis of *cyclo*-bis(germyl)germylene (**14-Ge**) and its tin analogue (**14-Sn**); the dotted lines represent the agostic interaction of dicoordinated tetrel centers with *vicinal*-halo substituents.

The compounds **14-Ge** and **14-Sn** are highly air-sensitive and exhibit moderate solubility in aliphatic solvents (*n*-pentane, *n*-hexane and petrolether) but good

solubility in Et_2O, THF, benzene, and toluene. Thermal decomposition studies of **14- Ge** and **14-Sn**, performed in *vacuum*-sealed glass capillaries, demonstrated that both compounds decompose upon melting at 230 °C and at 240 °C, respectively.

The compounds were comprehensively characterized by single-crystal X-ray diffraction (scXRD) and multinuclear NMR spectroscopy. Suitable single crystals of **14-Ge** (colourless plates) were obtained by slow cooling of a saturated Et_2O solution, yielding an Et_2O hemi-solvate (**14-Ge** $(\mathbf{Et_2O})_{0.5}$), while **14-Sn** (pale yellow plates) crystallized from a saturated *n*-hexane solution at −30 °C. X-ray diffraction analysis revealed that **14-Ge** crystallizes in the triclinic space group $P\bar{1}$, whereas **14-Sn** adopts the monoclinic space group $P2_1$. Both compounds exhibit nearly identical skeleton arrangement, featuring a *pseudo*-C_2-symmetric structure in the solid state. The primary structural characteristics of these compounds include:

i) Both compounds exhibit identical skeleton arrangements, featuring a nearly planar EGe_2C_2 (E = Ge, Sn) ring accompanied by two stereogenic germanium centers. Notably, the Ge/Sn centers exhibit agostic interactions with *vicinal*-halo atoms (Br/Cl), as evidenced by the elongated bond lengths between halo and tetrel centers (d(Ge−Br) = 2.8362(5) Å (**14-Ge**), d(Sn−Cl) = 2.722(5) Å (**14-Sn**))**.** These values significantly exceed the respective single-bond covalent radii (Ge−Br: 2.35 Å; Sn−Cl: 2.39 Å) yet remain well below their van der Waals radii (Ge−Br: 3.96 Å; Sn−Cl: 3.92 Å), suggesting a weak but considerable interaction (***Figure 45***).

ii) Both compounds **14-E** (E = Ge, Sn) possess considerable bending at the dicoorinated tetrel centes (Ge1–Ge2–Ge3 bond angle (80.10°) in **14-Ge** and the Ge1–Sn1–Ge2 angle (74.90°) in **14-Sn**), indicating the presence of lone-pair of electrons primarily in s-type orbital. Notably, the sterically encumbered Tbb substituents adopt a *anticlinical* conformation, reflected in the torsional angles (φ) C5−Ge1−Ge2−C29 = 118.50(3)° (**14-Ge**) and C1−Ge1−Ge2−C25 = 127.2(6)° (**14-Sn**) (***Figure 45***).

iii) In **14-Ge**, the Ge−Ge single-bond distances (d(Ge1−Ge2) = 2.4680(4) Å; d(Ge2−Ge3) = 2.4684(4) Å) compares well with the literature reported compound $Ge[GeCl_2\{(S{=}P^iPr_2CH)(S{=}P^iPr_2CH_2)C_5H_3N\text{-}2,6\}]_2$ (d(Ge−Ge) = 2.478(6) Å and 2.481(6) Å)[272]. Additionally, the C1−C2 bond length (1.333(4) Å) corresponds precisely to a typical $C^{(sp2)}{=}C^{(sp2)}$ double bond. Conversely, in **14-Sn**, the Ge−Sn bond distances (d(Ge1−Sn1) = 2.622(2) Å; d(Ge2−Sn1) = 2.690(2) Å) closely match the arithmetic mean of the Ge−Ge and Sn−Sn single-bond covalent radii (2.61 Å) (***Figure 45***). The C49−C50 bond (1.329(19) Å) further corroborates the presence of a C=C double bond, consistent with literature precedents.[273]

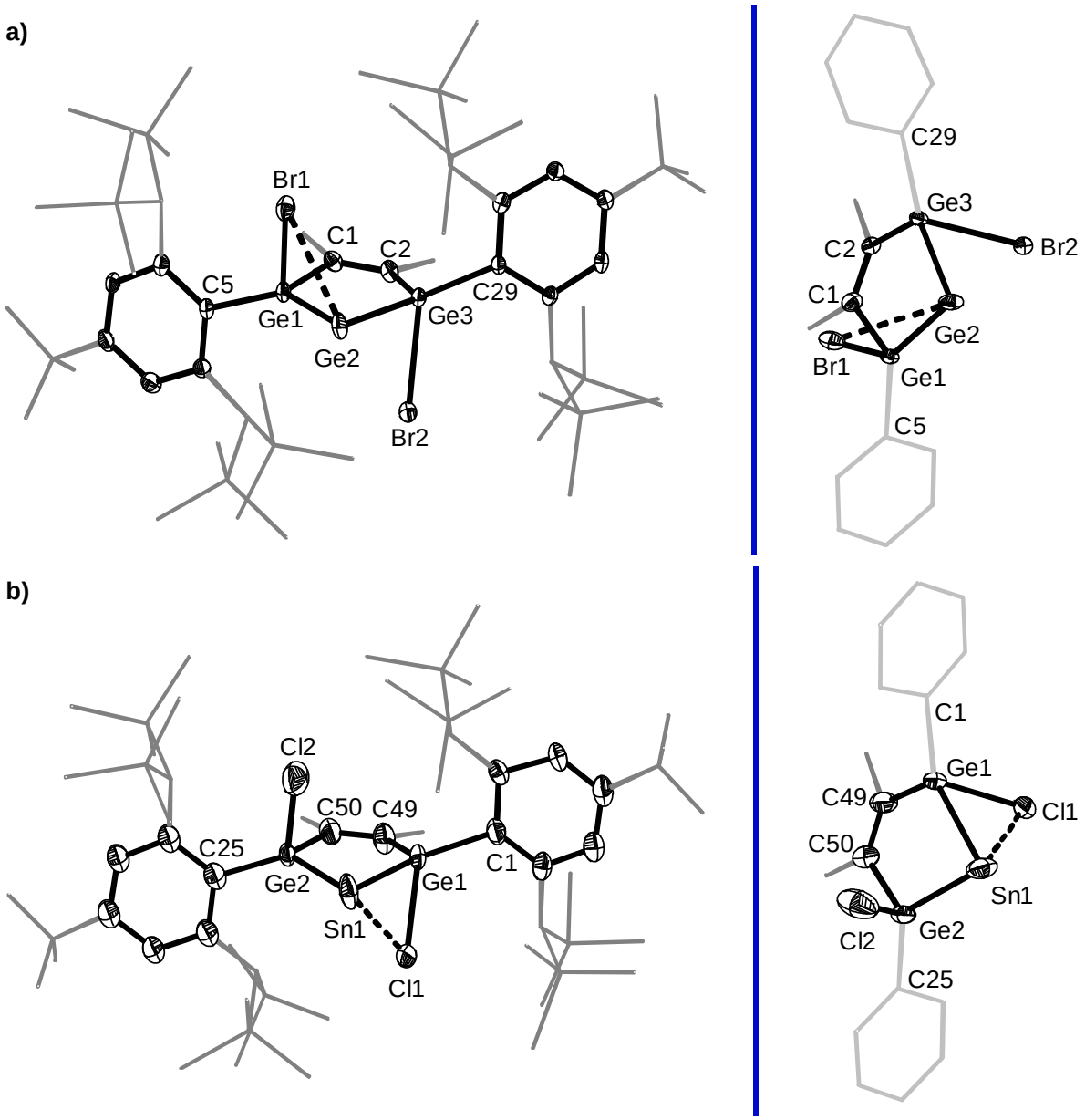

Figure 45. DIAMOND plot of the molecular structure of **14-Ge** (***top, left***) and **14-Sn** (***bottom, left***); concentrated view of **14-Ge** (***top, right***) and **14-Sn** (***bottom, right***). Thermal ellipsoids are set at 30 % probability level. Hydrogen atoms are omitted and the Dsi and ^{t}Bu substituents of the Tbb ligand are presented in wire-frame for clarity. Selected bond lengths [Å], bond angles [°] and torsion angle [°]: **a)** Ge1-Ge2 2.4680(4), Ge2-Ge3 2.4684(4), Ge1-Br1 2.5103(4), Ge3-Br2 2.4893(4), Ge1-C1 1.967(3), C1-C2 1.333(4), Ge3-C2 1.975(3), C1-Ge1-Ge2 111.79(8), C2-Ge3-Ge2 111.84(8), Ge1-Ge2-Ge3 80.081(3), Ge2-Ge1-Br1 69.454(14), Ge2-Ge3-Br2 71.884(13), C5-Ge1-Ge3-C29 118.50; **b)** Ge1-Sn1 2.622(2), Ge2-Sn1 2.690(2), Ge1-Cl1 2.340(4), Ge2-Cl2 2.335(6), Ge1-C49 1.960(14), C49-C50 1.329(19), Ge2-C50 1.961(14), C49-Ge1-Sn1 113.6(4), C50-Ge2-Sn1 112.6(4), Ge1-Sn1-Ge2 74.87(7), Sn1-Ge1-Cl1 66.24(13), Sn1-Ge2-Cl2 73.47(17), C1-Ge1-Ge2-C25 127.26(1).

The structural elucidation of **14-Ge** and **14-Sn** was further refined through comprehensive multinuclear NMR spectroscopy. ^{1}H and ^{13}C{^{1}H} NMR spectra, recorded in (D_6)benzene at 298 K, confirmed a time-averaged C_2-symmetric structure in solution. The C_2-symmetry axis passes through the unsaturated backbone (C=C),

the centroid (C_t) of the five-membered ring, and the Ge/Sn center. This symmetry renders the two germanium centers and Tbb groups homotopic, with the sterically encumbered Tbb substituents undergoing rapid rotation about the Sn–C^{ipso} bond axis. The dynamic behaviour is unambiguously evidenced by the sharp, well-resolved resonances in both ^{1}H and $^{13}C\{^{1}H\}$ NMR spectra. Complete spectral assignment was achieved through two-dimensional NMR spectroscopy, specifically $^{13}C-^{1}H$ HSQC and HMBC correlation experiments, which provided unambiguous connectivity mapping. Notably, the $^{119}Sn\{^{1}H\}$ NMR spectrum of **14-Sn** exhibits a characteristic resonance at – 486.57 ppm, a significant downfield shift compared to the analogous compound $CB(GeClAr^{Trip})_2Sn$ (Ar^{Trip} = 2,6-(2,4,6-^{i}Pr-C_6H_2)$_2C_6H_3$ and CB = *ortho*-C,C′-$C_2B_{10}H_{10}$) (– 217.90 ppm).[122]

A comparative investigation was conducted on the reactivity of ditetrelyne derivatives, specifically the coupling products (**12-Si** and **12-Ge**) and the cycloaddition product (**7-Ge**) - with Mes-NC (mesityl isocyanide). Exposure of **12-Si** and **12-Ge** to Mes-NC at ambient temperature yielded no observable reaction, whereas elevated temperatures led to a non-selective mixture of products or decomposition of the starting materials. In contrast, when a green *n*-hexane solution of **7-Ge** was treated with Mes-NC at room temperature, an immediate colour change to dark red-purple was observed, signalling the rapid formation of a new compound. This transformation was further corroborated by ^{1}H NMR spectroscopy, which confirmed the selective formation of **15-Ge**. Dark purple crystals of **15-Ge** were subsequently isolated *via* careful workup and crystallization from *n*-hexane at −30 °C. The isolated compound exhibits pronounced air sensitivity but demonstrates good solubility in most organic

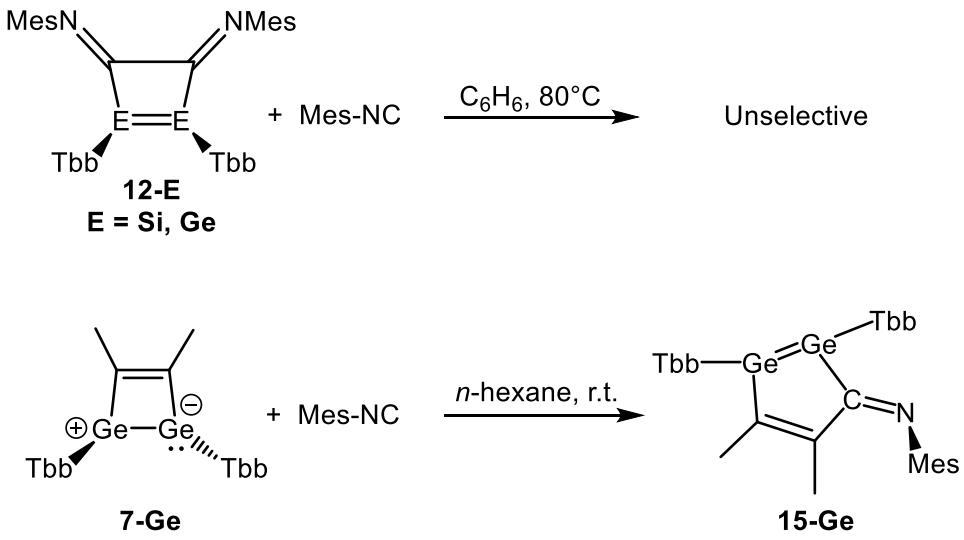

Scheme 10. Divergent reactivity of ditetrelyne coupling products (**12-Si** and **12-Ge**) and cycloaddition product (**7-Ge**) with Mes-NC to afford **15-Ge**

solvents. Thermal stability studies revealed that **15-Ge** decomposes upon melting at 169 °C.

The compound **15-Ge** was comprehensively characterized by single-crystal X-ray diffraction (scXRD) and multinuclear NMR spectroscopy. Suitable block-shaped orange-red crystals of **15-Ge** were obtained by slow cooling of the saturated *n*-hexane solution at −30 °C. X-ray diffraction analysis revealed that **15-Ge** crystallizes in the triclinic space group $P\bar{1}$. The molecular structure of **15-Ge** reveals a bent five-membered Ge_2C_3 ring (sum of internal angle = 516.65°) and two trigonal pyramidal germanium centers Ge1 and Ge2 with a degree of pyramidalization of 4.7 % and 7.9 % respectively (***Figure 46***).

i) The sterically more demanding Tbb substituents are arranged in *antiperiplanar* orientation (φ(C1−Ge1−Ge2−C25) = −94.55(1)°). The Ge1=Ge2 (2.3437(3) Å) bond lengths in **15-Ge** are a bit elongated as compared with previously reported Ge=Ge bond lengths in ArDip(H)Ge=Ge(H)ArDip (2.3026(3) Å).[274] The bond distance of Ge1-C49 (1.9745(19)) and Ge2-C51 (2.0326(18)) are found to be elongated than typical Ge=C^{sp2} double bond lengths of germaethenes reported in the Cambridge Structural Database (1.770 − 1.894 Å).

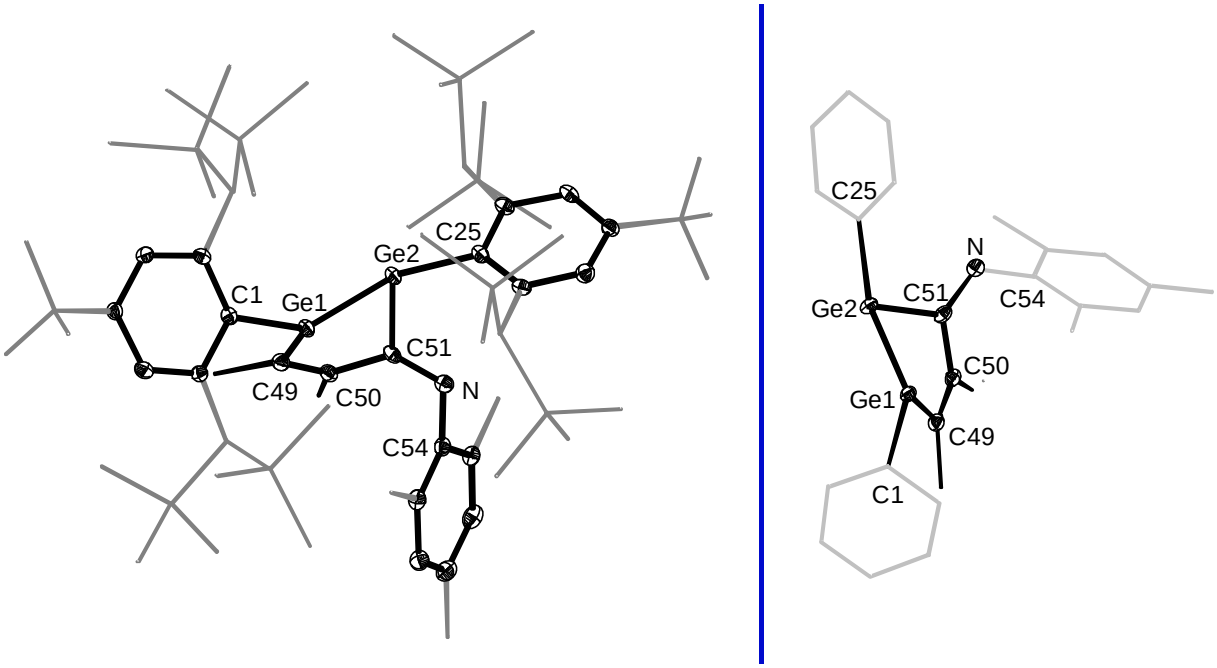

Figure 46. DIAMOND plot of the molecular structure of **15-Ge** (***left***) and concentrated view of **15-Ge** (***right***). Thermal ellipsoids are set at 30 % probability level. Hydrogen atoms are omitted and the Dsi and ^{t}Bu substituents of the Tbb ligand are presented in wire-frame for clarity. Selected bond lengths [Å], bond angles [°]: Ge1-Ge2 2.3437(3), Ge1-C1 1.9678(18), Ge2-C25 1.9772, Ge1-C49 1.9745(19), C49-C50 1.349(3), Ge2-C51 2.0326(18), C50-C51 1.486(2), C51-N 1.284(2), N-C54 1.429(2), C1-Ge1-Ge2 145.13(5), C1-Ge1-C49 107.13(8), C49-Ge1-Ge2 90.63(5), Ge1-Ge2-C51 83.09(5), C25-Ge2-Ge1 141.01(5), C51-Ge2-C25 107.44(7), C51-N-C54 119.73(16), C1-Ge1-Ge2-C25 −94.55(1)°.

Compound **15-Ge** was further characterized by comprehensive multinuclear NMR spectroscopic analysis. ^{1}H and $^{13}C\{^{1}H\}$ NMR spectra, acquired in (D_6)benzene at 298 K, revealed a time-averaged C_1-symmetric structure in solution. Notably, Ge2−C^{Tbb} bond rotation was found to be frozen on the NMR timescale at ambient temperature, as unequivocally demonstrated by the presence of two distinct singlets corresponding to the diastereotopic C^{2,6}-CH(Si*Me*$_3$)$_A$(Si*Me*$_3$)$_B$ groups. In contrast, Ge1−C^{Tbb} rotation remained rapid under these conditions, evidenced by the observation of a single sharp resonance for the $SiMe_3$ substituents. The dynamic behaviour is unambiguously evidenced by the sharp, well-resolved resonances in both ^{1}H and $^{13}C\{^{1}H\}$ NMR spectra.

The previously reported 1,2-digermabutadiene (**7-Ge**) serves as a versatile synthone, facilitating access to novel low-coordinate cyclic germanium compounds under standard laboratory conditions. Notably, upon treatment with $TMSN_3$ in *n*-hexane, **7-Ge** undergoes a distinct colour change from green to purple, indicative of a significant structural transformation. Monitoring the reaction progress *via* ^{1}H NMR spectroscopy in (D_6)benzene revealed the selective formation of a new compound, which was subsequently identified as the heavier germanium analogue of pyrrole, featuring a planar five-membered C_2Ge_2N core (**16-Ge**) (***Scheme 11***). Subsequent crystallization from *n*-hexane at −30 °C yielded **16-Ge** as an extremely air-sensitive, purple solid in 44% yield.

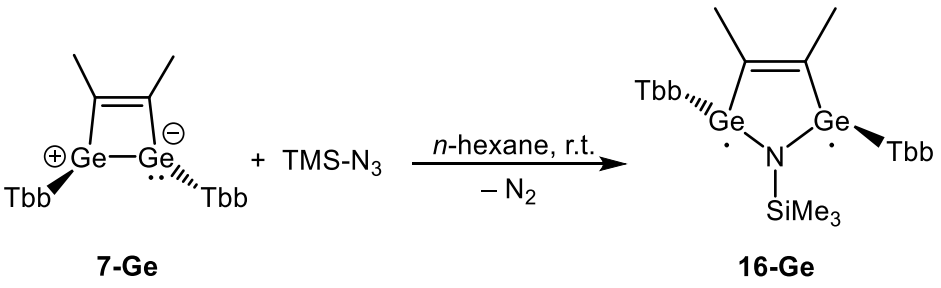

7-Ge **16-Ge**

Scheme 11. Reaction of 1,2-digermabutadiene (**7-Ge**) with $TMSN_3$ to afford heavier analogue of pyrrole **16-Ge**.

Consequently, a green *n*-hexane solution of **7-Ge** was treated with a purple *n*-hexane solution of (*p*-tol)$_2CN_2$ at ambient temperature, resulting in an initial colour change to purple, which gradually transitioned to a yellow-brown hue over an hour. ^{1}H NMR spectroscopic analysis of an aliquot of the reaction mixture revealed the complete and selective formation of a new compound, which was identified as the *p*-tolyl-activated product **17-Ge** (***Scheme 12***). Following careful workup and crystallization from *n*-pentane at −30 °C, the target compound was isolated in 65% good yield as a yellow solid.

Compounds **16-Ge** and **17-Ge** exhibit good solubility in benzene, toluene, THF and Et_2O at ambient temperature. The thermal decomposition of both compounds was detected upon melting at 226 °C and 273 °C, respectively, in a *vacuum*-sealed glass capillary. Analysis of the soluble part of the respective melting residue in (D_6)benzene by ^{1}H NMR spectroscopy revealed unselective decomposition of **16-Ge** and **17-Ge**.

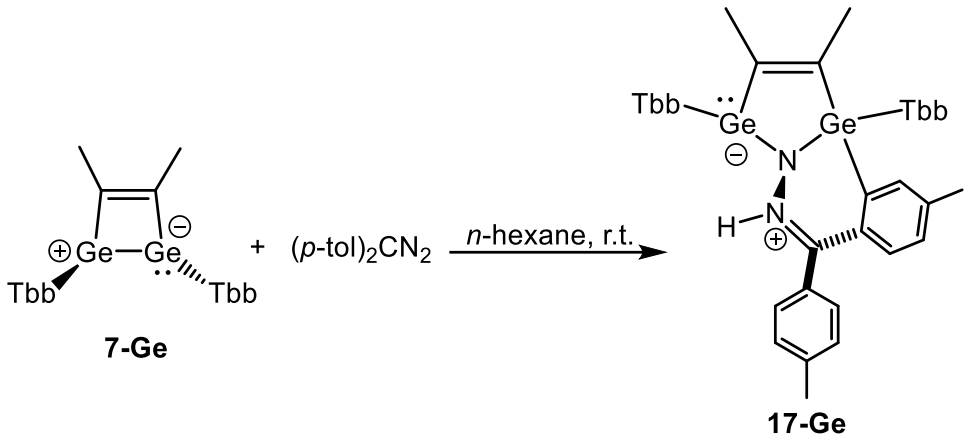

Scheme 12. Reaction of 1,2-digermabutadiene (**7-Ge**) with (p-tol)$_2$CN$_2$ to afford **17-Ge**.

Compound **16-Ge** is the first heavier germanium analogue of pyrrole and **17-Ge** bears the activated *p*-tol group and hence were characterized thoroughly by single crystal X-ray diffraction (sc-XRD) analysis and multinuclear NMR spectroscopy. Plate-shaped red crystals of **16-Ge**·(***n*-hexane**) and plate-shaped yellow crystals of **17-Ge**, suitable for sc-XRD analysis, were obtained by slow cooling of their saturated *n*-hexane and *n*-pentane solution at −30 °C, respectively. X-ray diffraction analysis revealed that **16-Ge** crystallizes in the triclinic space group $P\bar{1}$ and **17-Ge** crystallizes in the monoclinic $P2_1/c$.

The molecular structures of **16-Ge** (***Figure 47***) exhibit a planar Ge_2C_2N core (sum of internal angle = 540°) and two trigonal pyramidal germanium centers Ge1 ($\Sigma\measuredangle$ = 331.11(2)°) and Ge2 ($\Sigma\measuredangle$ = 334.11(2)°). The sterically encumbered Tbb substituents are arranged in *antiperiplanar*-orientation (φ(C1−Ge1−Ge2−C25) = −157.92(1)°). The Ge1−N and Ge2−N (1.860(2) and 1.856(2) Å) are within the range found in reported compound singlet biradicaloid Ar‘Ge(μ^2-NSiMe$_3$)$_2$GeAr‘ (Ar‘ = 2,6-Dipp$_2$C$_6$H$_3$, Dipp = 2,6-^{i}Pr$_2$C$_6$H$_3$)(1.8626(6) and 1.8741(6)[198] by P.P.Power. The Ge····Ge separation (3.035 Å) is about 0.6 Å longer than a normal Ge−Ge single bond (average 2.44 Å).[275] but it is 0.15 Å longer when compared to those found in the cyclic dimers (R‘GeNR‘‘)$_2$ (R‘ = 2,4,6-Me$_3$C$_6$H$_2$, R‘‘ = NCC$_{12}$H$_8$; R‘$_2$ = MeNCH$_2$CH$_2$NMe, R‘‘ = NSi(^{t}Bu)$_3$) and (GeNR)$_2$ (R = Mes*, 2,4,6-(CF$_3$)$_3$C$_6$H$_2$) (2.66−2.86 Å) in which there is no Ge−Ge bonding.[276] The long Ge····Ge separation is consistent with the biradical character of **16-Ge**. The well-

resolved ^{1}H and ^{13}C NMR spectra are consistent with the presence of a diamagnetic singlet ground state.

Whereas the structural characteristic of **17-Ge** display a *p*-tol activated product as illustrated (***Figure 47***) and exhibits a bent Ge_2C_2N core and one stereogenic germanium center (Ge1), and a trigonal pyramidal germanium center (Ge2) ($\Sigma\measuredangle$ = 338.04(1)°). The sterically encumbered Tbb substituents are arranged in *synperiplanar* orientation (φ(C1−Ge1−Ge2−C25) = −2.99(1)°). The Ge1−N and Ge2−N (1.8891(19) and 1.8999(19) Å) which is 0.03 Å more than what is observed in **16-Ge** and falls within the typical range of single Ge−N bond (1.85–2.00 Å). The C49=C50 (1.340(3) Å), C59=N2 (1.292(3)), N1−N2 (1.435(2)) and Ge1−C53 (1.955(2)) compares with the respective double bond and single bond covalent radii, respectively.

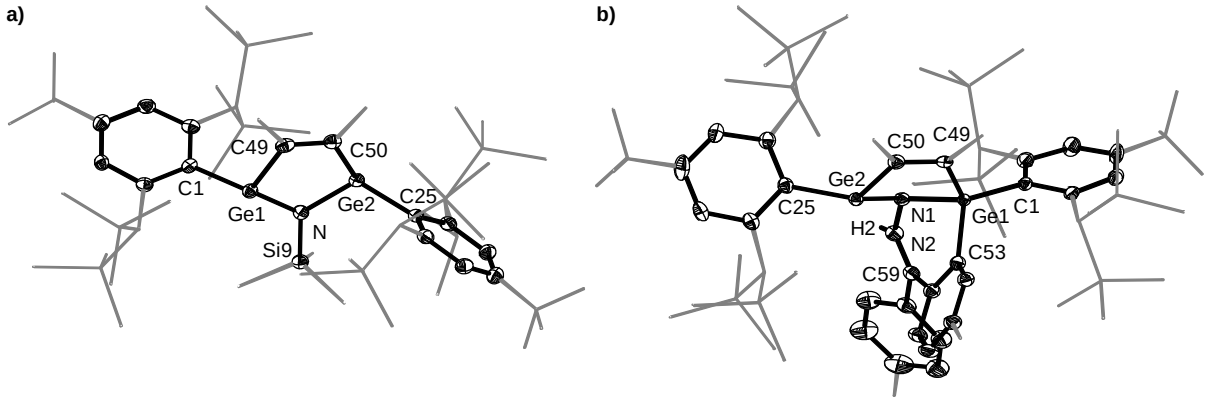

Figure 47. DIAMOND plot of the molecular structure of **16-Ge** (***left***) and **17-Ge** (***right***). Thermal ellipsoids are set at 30 % probability level. Hydrogen atoms are omitted and the Dsi and ^{t}Bu substituents of the Tbb ligand are presented in wire-frame for clarity. Selected bond lengths [Å], bond angles [°]: **a)** Ge1-N 1.860(2), Ge2-N 1.856(2), N-Si9 1.753(2), Ge1-C49 1.945(3), Ge2-C50 1.932(3), C49-C50 1.347(4), C49-Ge1-N 99.07(11), C50-Ge2-N 99.58(11), Ge1-N-Ge2 109.60(11), C1-Ge1-C49 109.42(10), C1-Ge1-N 122.03(10), C25-Ge2-C50 118.88(11), C25-Ge2-N 115.64(10), C1-Ge1-Ge2-C25 −157.92(1); **b)** Ge1-C1 1.977(2), Ge1-N1 1.8891(19), Ge1-C49 1.956(2), Ge2-C25 1.965(2), Ge2-C50 1.949(2), Ge2-N1 1.8999(19), N1-N2 1.435(2), N2-C59 1.292(3), Ge1-C53 1.955(2), C49-C50 1.340(3), C1-Ge1-C49 116.86(9), C1-Ge1-C53 116.59(9), N1-Ge1-C49 95.95(9), C25-Ge2-C50 118.56(9), C25-Ge2-N1 123.79(9), C50 Ge2-N1 95.70(9), Ge1-N1-Ge2 103.16(9), C1-Ge1-Ge2-C25 −2.99(1).

The structural elucidation of **16-Ge** was further refined through comprehensive multinuclear NMR spectroscopic analysis. ^{1}H and $^{13}C\{^{1}H\}$ NMR spectra, acquired in (D_6)benzene at 298 K, revealed a time-averaged C_{2v}-symmetric structure in solution. Notably, Ge−C^{Tbb} bond rotation was found to be rapid on the NMR timescale at ambient temperature, as unequivocally demonstrated by the presence of a single set of resonances corresponding to the homotopic $SiMe_3$ groups, indicative of fast dynamic averaging.

In contrast, for **17-Ge**, comprehensive multinuclear NMR spectroscopic analysis including ^{1}H and $^{13}C\{^{1}H\}$ NMR spectra acquired in $(D_2)DCM$ at 298 K revealed a C_1-symmetric structure with heterotopic germanium centers, rendering the Tbb substituents also heterotopic. Significantly, Ge−C^{Tbb} bond rotation was found to be frozen on the NMR timescale at ambient temperature, as conclusively evidenced by the presence of two distinct singlets corresponding to the diastereotopic $C^{2,6}$-$CH(SiMe_3)_A(SiMe_3)_B$ groups for each Tbb substituent. The static nature of the system was further corroborated by the sharp, well-resolved resonances in both ^{1}H and $^{13}C\{^{1}H\}$ NMR spectra, confirming the absence of dynamic averaging at this temperature.

The cycloaddition product 1,4-digerma benzene[226] acts as a versatile synthon due to its reactivity toward low-valent tetrel centers, enabling the isolation of rare bicyclic compounds, as evidenced by their scarcity in the Cambridge Structural Database (CSD) of the suitable structures. To explore this, **8-Ge** was treated with a series of low-valent tetrel compounds, including $SiBr_2$(SIDipp), $GeBr_2$(1,4-dioxane), and $SnCl_2$, yielding bicyclic derivatives.

Interestingly, a yellow benzene solution of **8-Ge** was initially treated with $SiBr_2$(SIDipp) at ambient temperature, but no reaction was observed. However, upon heating the mixture to 80 °C overnight, the solution turned light yellow, indicating the formation of a new compound. ^{1}H NMR spectroscopy confirmed the selective formation of **18-Si** (***Scheme 13***), along with the liberation of free SIDipp, which was removed by repeated washings with a 5:1 *n*-hexane/benzene mixture (6 × 3 mL). Subsequent workup and crystallization from *n*-hexane at −30°C yielded **18-Si**·(***n*-hexane**) as a colourless solid in 64% yield. In contrast, the reaction of **8-Ge** with $GeBr_2$(1,4 - dioxane) in benzene proceeded smoothly at room temperature**.** ^{1}H NMR analysis revealed the exclusive formation of **18-Ge** (***Scheme 13***) without any detectable byproducts. After workup, crystallization from *n*-hexane at −30 °C afforded **18-Ge** as a colourless crystalline solid in an excellent yield of 83 **%**, demonstrating the high efficiency of this transformation. When **8-Ge** was treated with $SnCl_2$ in diethyl ether (Et_2O), the mixture was sonicated for one hour, resulting in a light red-brown suspension. ^{1}H NMR spectroscopy confirmed the selective formation of **18-Sn** (***Scheme 13***). Following a careful workup, crystallization from Et_2O at −30 °C yielded **18-Sn** as an off-white, analytically pure solid in 52 % yield, reflecting somewhat lower efficiency compared to its lighter analogues.

All the compounds are highly sensitive to air but can be stored indefinitely under argon atmosphere and exhibit similar solubility behaviour, showing moderate

solubility in *n*-hexane, *n*-pentane and Et_2O but good solubility in THF and benzene. Thermal decomposition studies, conducted in *vacuum*-sealed glass capillaries, revealed that **18-Si**, **18-Ge**, and **18-Sn** undergo decomposition upon melting at 335 °C, 314 °C, and 203 °C, respectively. ^{1}H NMR analysis of the soluble part of the melted residues in (D_6)benzene indicated that all complexes undergo unselective decomposition.

Compounds **18-E** (E = Si, Ge, and Sn) constitute the heavier tetrel analogues featuring a bicyclic framework with the tetrel atoms located at the bridge position. These compounds were comprehensively characterized using single-crystal X-ray diffraction (scXRD) and multinuclear NMR spectroscopy, confirming their structural identity. Block-shaped colourless crystals of **18-Si** and **18-Sn**, along with plank-shaped colourless crystals of **18-Ge** suitable for the single-crystal X-ray diffraction

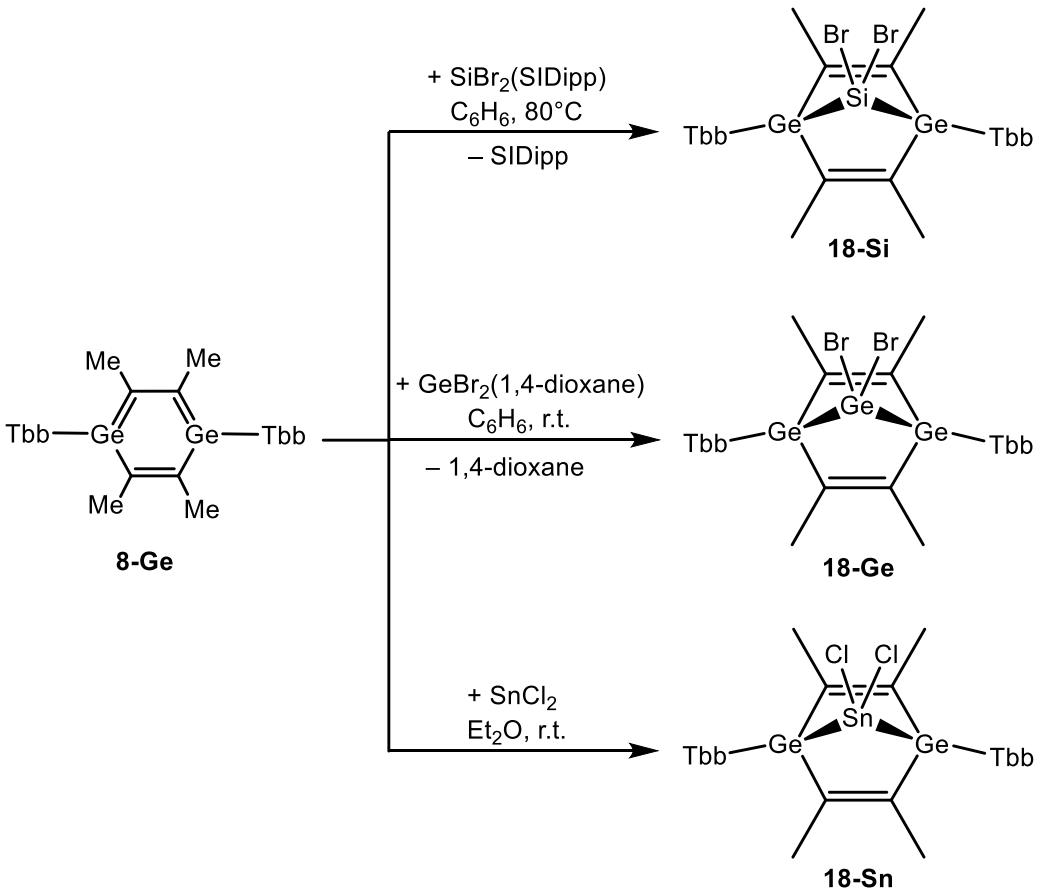

Scheme 13. Reactivity studies of **8-Ge** with $SiBr_2$(SIDipp), $GeBr_2$(1,4-dioxane) and $SnCl_2$ to afford **18- Si**, **18-Ge** and **18-Sn**.

(scXRD) analysis were obtained through the slow cooling of their saturated *n*-hexane (**18-Si** and **18-Sn**) and Et_2O (**18-Ge**) solutions at −30 °C. X-ray diffraction analysis revealed that **18-Si** and **18-Sn** crystallizes in the monoclinic space group $P2_1$, whereas **18-Ge** adopts the triclinic space group $P\bar{1}$.

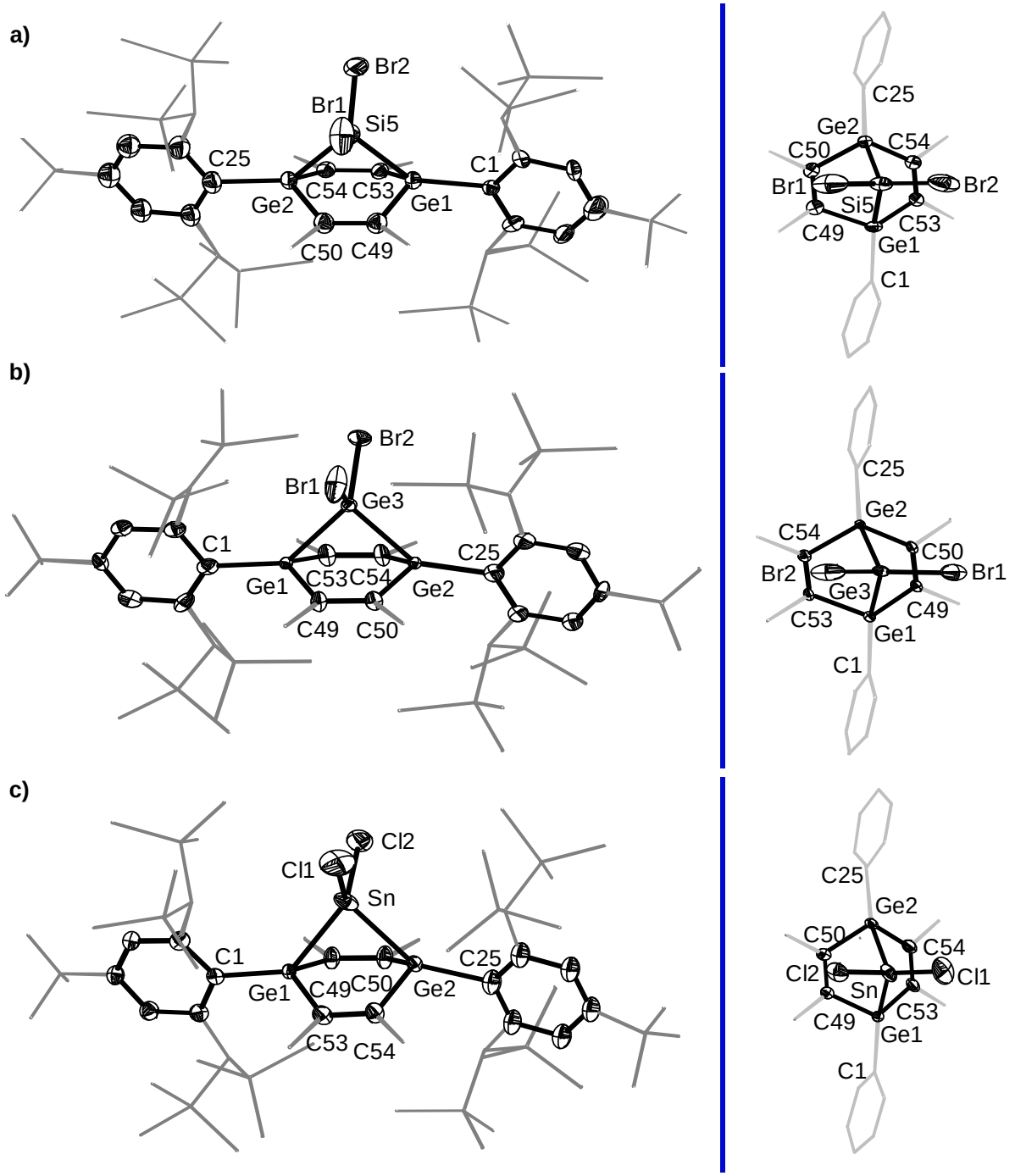

Figure 48. DIAMOND plot of the molecular structure of **18-E** (**E = Si**, **Ge**, and **Sn**) (***left***) and their respective concentrated view (***right***). Thermal ellipsoids are set at 30 % probability level. Hydrogen atoms are omitted and the Dsi and ^{t}Bu substituents of the Tbb ligand are presented in wire-frame for clarity. Selected bond lengths [Å], bond angles [°] and torsion angle [°]: **a)** Ge1-Si5 2.425(3), Ge2-Si5 2.421(3), Ge1-C49 1.963(11), Ge1-C53 1.940(9), Ge2-C50 1.957(11), Ge2-C54 1.947(9), Si5-Br1 2.243(3), Si5-Br2 2.241(4), C49-C50 1.355(15), C53-C54 1.344(13), Ge1-Si5-Ge2 79.97(10), C1-Ge1-C53 121.1(4), C1-Ge1-C49 108.9(4), C25-Ge2-C54 110.3(4), C25-Ge2-C50 120.0(5), C49-Ge1-C53 113.0(4), C50-Ge2-C54 112.3(4).C1-Ge1-Ge2-C25 −105.09(1); **b)** Ge1-Ge3 2.5019(12), Ge2-Ge3 2.5043(12), Ge1-C53 1.929(6), Ge1-C49 1.919(5), Ge2-C50 1.930(6), Ge2-C54 1.932(6), C53-C54 1.345(8), C49-C50 1.353(8), Ge3-Br1 2.3482(12), Ge3-Br2 2.3507(12), Ge1-Ge3-Ge2 79.15(4), C1-Ge1-C49 120.3(2), C1-Ge1-C53 111.7(2), C25-Ge2-C54 120.5(2), C25-Ge2-C50 112.5(2), C49-Ge1-C53 114.2(3), C50-Ge2-C54 113.3(2), C1-Ge1-Ge2-C25 −70.65(5); **c)** Ge1-Sn 2.678(4), Ge2-Sn 2.578(16), Ge1-C49 1.934(6), Ge1-C53 1.934(6), Ge2-

C50 1.955(10), Ge2-C54 2.011(13), C49-C50 1.360(9), C53-C54 1.351(9), Sn-Cl1 2.352(6), Sn-Cl2 2.334(5), Ge1-Sn-Ge2 76.2(3), C1-Ge-C49 131.9(2), C1-Ge1-C53 121.6(3), C49-Ge1-C53 111.5(3), C25-Ge2-C50 116.2(7), C25-Ge2-C54 106.7(7), C50-Ge2-C54 107.9(6), C1-Ge1-Ge2-C25 −77.84(2).

The molecular architectures of **18-Si**, **18-Ge**, and **18-Sn** exhibit analogous structural motifs, with their key geometric and coordination features demonstrating significant similarity as follows:

i) All compounds exhibit a bent Ge_2C_4 core and two distorted tetrahedral stereogenic germanium centers (Ge1 and Ge2). The sterically encumbered Tbb substituents are arranged in *anticlinical* orientation (**18-Si**) and *synclinical* orientation (**18-E, E = Ge**, **Sn**) (***Figure 48***) as evidenced by the torsion angles (φ(C1−Ge1−Ge2−C25) = −105.09(1)° (**18-Si**), −70.65(5)° (**18-Ge**) and −77.84(2)° (**18- Sn**) respectively (***Figure 48***).

ii) The Ge1−E−Ge2 bond angle (E = Si, Ge, and Sn) exhibits significant variations compared to literature-reported compounds, highlighting distinct electronic and steric influences. For E = Si (**18-Si**), the observed angle of 79.97(10)° is notably larger than that in 1,4-digermatetrasilabenzene (68.8(8)°)(***Figure 48***).[277] In contrast, for E = Ge (**18-Ge**), the angle 79.15(10)° is substantially smaller than that in the subhalide cluster $Ge_{14}Br_8(PEt_3)_4$ (127.91(3)°)[278], reflecting differences in coordination geometry where the subhalide cluster adopts a more open, three-dimensional structure, while **18-Ge** maintains a constrained cyclic framework, For E = Sn (**18-Sn**), the angle of 76.27(10)° (***Figure 48***) is considerably reduced relative to the 104.78(8)° reported in 1-stanna-2,5-digermacyclopentasilane.[279] This ~28° reduction indicates a significant electronic perturbation, likely due to enhanced *p*-character in the Sn−Ge bonds or increased ring strain.

iii) The Ge1–Si5 and Ge2–Si5 bond distances in **18-Si** (2.425(3) Å and 2.421(3) Å, respectively) are consistent with the reported Ge–Si bond length in 1-disilagermirene (2.415(1) Å) [280], confirming the expected covalent interaction. For **18-Ge**, the observed Ge1–Ge3 and Ge2–Ge3 bond lengths (2.5019(12) Å and 2.5043(12) Å) align closely with those in the subhalide cluster $Ge_{14}Br_8(PEt_3)_4$ (2.48(3)–2.50(3) Å),[278] supporting their classification as typical Ge–Ge single bonds. Additionally, the Ge–Br bond lengths in **18-Ge** (2.3482(12) Å and 2.3507(12) Å) fall within the expected range for standard Ge–Br single bonds, as exemplified by Br–Ge$(GePh_3)_3$ (2.38 Å).[281] In the case of **18-Sn**, the Ge1–Sn and Ge2–Sn distances (2.678(4) Å and 2.578(16) Å) are in good agreement with the literature-reported average for stanna-disilacyclogermanes

(2.6120(16) Å),[279] further validating the structural similarities within this class of compounds (***Figure 48***).

iv) The measured bond lengths for C49=C50 and C53=C54 in the studied compounds - 1.344(13) Å and 1.355(15) Å (**18-Si**), 1.353(8) Å and 1.345(8) Å (**18- Ge**), and 1.360(9) Å and 1.351(9) Å (**18-Sn**) (***Figure 48***). - are consistent with the typical range for C=C double bonds (1.31−1.36 Å).[228]

The structural elucidation of **18-Si**, **18-Ge**, and **18-Sn** was further refined through comprehensive multinuclear NMR spectroscopic analysis. ^{1}H and $^{13}C\{^{1}H\}$ NMR spectra, recorded in (D_8)THF at 298 K for **18-Si** and **18-Ge** whereas for **18-Sn**, it was carried out in (D_6)benzene, revealed a time-averaged C_2-symmetric structure in solution. This symmetry renders both the germanium centers (Ge1 and Ge2) homotopic. Notably, Ge−C^{Tbb} bond rotation was found to be frozen on the NMR timescale at ambient temperature, as unequivocally demonstrated by the presence of a distinct set of resonance corresponding to the $C^{2,6}$-CH(Si*Me*$_3$)$_A$(Si*Me*$_3$)$_B$ groups of each Tbb, confirmed by the absence of dynamic averaging at this temperature. The $^{29}Si\{^{1}H\}$ for **18-Si** appears at 31.81 ppm, which aligns with the typical tetracoordinated silanes, and the literature reported compound 1,1,2,5-tetrachloro-2,5-digerma-1-silacyclopentane (16.03 ppm).[103] The $^{119}Sn\{^{1}H\}$ for **18-Sn** appears at 57.03 ppm, which appears very deshielded as compared to the literature-know compound 1-stanna-2,5-digermacyclopentasilane (−101.9 ppm).[279]

Table 2. Selected structural and spectroscopic parameters of **18-Si**, **18-Ge**, **18-Sn** and literature known analogous compounds.

Compound	*d*(Ge−E−Ge) (°) [a]	$\delta(^{29}Si)$ (ppm)	$\delta(^{119}Sn)$ (ppm)	*Ref.*
$Tbb_2Ge_2C_4Me_4SiBr_2$ (**18-Si**)	79.97(10)	31.91	–	This work
$Tbb_2Ge_2C_4Me_4GeBr_2$ (**18-Ge**)	79.15(10)	–	–	This work
$Tbb_2Ge_2C_4Me_4SnCl_2$ (**18-Sn**)	76.27(10)	–	57.03	This work
cyclo-$(BbtGeClCH_2)_2SiCl_2$ (**A**)	80.08(4)	16.03	–	[103]
$Ge_{14}Br_8(PEt_3)_4$ (**B**)	127.90(4)	–	–	[278]
cyclo-$((SiMe_3)_2GeSiMe_2)_2SnMe_2$ (**C**)	104.78(8)	–	-101.9	[279]

a: E represents Si (**18-Si** and **A**), Ge (**18-Ge** and **B**) and Sn (**18-Sn** and **C**).

Isolation of these compounds was followed by reduction attempts employing KC_8 in benzene, THF, and DME to generate the respective norborane-type silylene, germylene, and stannylene species - substituted with a bis-germyl moiety. Notably, successful crystallization and subsequent structural characterization were achieved only for **18-Ge** in benzene. However, reproducibility in this solvent system proved inconsistent upon scaling the reaction. For the remaining derivatives (**Si**, **Sn**), no observable reaction occurred at ambient temperature.

2.2.3. Synthesis and charatcterization of germylone and stannylone

The chemistry of zero-valent Group 14 element complexes have emerged as a focal point in contemporary main-group and organometallic chemistry following Frenking and coworkers groundbreaking 2006 reinterpretation of the non-classical C-P bonding in carbodiphosphorane $C(PPh_3)_2$ as a dative Lewis donor-acceptor interaction.[87] This conceptual breakthrough led to the formal recognition of tetrylones - a novel class of compounds adopting the general formulation $L:\rightarrow E^0\leftarrow:L$ (where L = σ-donor ligand; E = C (carbone), Si (silylone), Ge (germylone), Sn (stannylone), Pb (plumbylone)) through subsequent theoretical validation.[282] These species represent unique molecular allotropes of their constituent elements,[283] with several notable examples including N-heterocyclic carbene (NHC)-stabilized carbones,[90] cyclic (alkyl)(amino)carbene (CAAC)-supported silylones and germylones,[101,113] and bis-NHC-coordinated heavier tetrylones.[100],[112] While the chemistry of carbones is relatively well-developed, isolable examples of their heavier congeners remain remarkably scarce. Despite computational evidence suggesting the thermodynamic feasibility of NHC-Pb^0 adducts,[284] all synthetic endeavours toward such plumbylones have proven unsuccessful,[154] with their inherent kinetic instability and pronounced photo-lability inevitably resulting in ligand dissociation and elemental Pb formation.

Building on these challenges, Driess group recognized that N-heterocyclic silylenes (NHSi) - particularly three-coordinate, intramolecularly stabilized silicon (II) centers offer superior σ-donor capabilities compared to the typical NHCs. Leveraging the chelate effect and enhanced electron-donating properties of bis-NHSi ligands, the research group successfully isolated stable silylones [106,116] and germylones.[81,104] Most recently, this approach has enabled the isolation of a two-coordinate stannylone[120] and plumbylon.[121] As discussed above, over the past two decades, the chemistry of zero-valent Group 14 elements has undergone remarkable development, yielding a diverse array of complexes with fascinating bonding characteristics and immense synthetic potential.

Building upon these milestones, we have extended our investigations to explore the heaviest congener in this series, further advancing the burgeoning field of tetrylone chemistry. Following the successful isolation of **14-Ge** and **14-Sn**, versatile synthons for germylone and stannylone derivatives. An investigation into their reductive dehalogenation was conducted simultaneously. Interestingly, when a benzene solution of **14-Ge** was treated with 2.1 equivalents of KC_8 at room temperature,

sonicated for 5 hours, and subsequently stirred for 16 hours under ambient conditions, a distinct colour change to green was observed. ^{1}H NMR spectroscopy confirmed the complete consumption of the starting material and the selective conversion to **19-Ge** (***Scheme 14***). Following careful workup, crystallization from *n*-hexane at −30 °C afforded **19-Ge** as green crystals in 65% yield. Under analogous conditions, **14-Sn** was subjected to the same reduction reaction, with stirring for 5 hours at ambient temperature. ^{1}H NMR spectroscopic analysis of an aliquot revealed the clean and selective formation of a stannylone, **19-Sn** (***Scheme 14***). Subsequent workup and crystallization from *n*-pentane at −30 °C yielded **19-Sn** as red crystals in 56% yield. The isolated compounds exhibit pronounced air sensitivity but display excellent solubility in most organic solvents. Thermal stability studies indicated that **19-Ge** and **19-Sn** decompose upon melting at 267 °C and 264 °C, respectively.

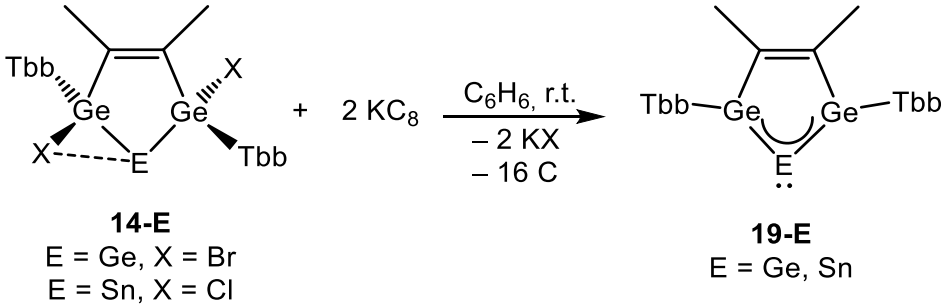

Scheme 14. Synthesis of the *cyclic*-germylone (**19-Ge**) and stannylone (**19-Sn**).

Tetrylones **19-Ge** and **19-Sn** were comprehensively characterized using single-crystal X-ray diffraction (scXRD) analysis and multinuclear NMR spectroscopy. Suitable crystals, block-shaped brownish-yellow crystals of **19-Ge** and plate-shaped red crystals of **19-Sn**·(***n*-pentane**), were obtained by slowly cooling their respective saturated *n*-hexane and *n*-pentane solutions at −30 °C. Both compounds crystallize in the triclinic space group $P\bar{1}$ and represent the class of bis(germylene)-supported germylone and stannylone incorporated into a five-membered ring system. **19-Ge** and **19-Sn** exhibit nearly identical skeleton arrangement and possess *pseudo*-C_{2v}-symmetric structures in the solid state. The molecular structures display the following key features (***Figure 49***).

i) The central germanium and tin engaged in bonds with two germanium atoms within a planar EGe_2C_2 (E = Ge and Sn) five-membered ring. The Ge···Ge distance in **19-Ge** and **19-Sn** (2.9182(10) and 2.997(9) Å) is longer than the sum of the covalent radii of Ge (2.48 Å) but shorter than that of the van der Waals radii (4.20 Å),[228] suggesting weak interactions between the Ge atoms (***Figure 49***). The Ge−Ge bond length in **19-Ge** (2.3606(10) and 2.3659(10) Å) is shorter than its precursor **14-Ge** (2.4680(4) and 2.4684(4)) and close to literature reported Ge=Ge in trigermaallene

(2.321(2) and 2.330(3) Å).[285] The structural parameters suggest a considerable delocalization of out-of-plane lone pair to the vicinal germaylene centers forming π_{oop}(3c−2e) bond and a in-plane dicoordinated germanium-centered lone-pair orbital. The tin analogue **19-Sn** also exhibits identical delocalization and possessses a Ge=Sn (2.5454(5) and 2.6871(5) Å), which aligns well with the literature known bis(germylene)-stabilized stannylone (2.5938 Å)[122] and longer than the Ge=Sn bond in a stannagermene (2.5065 Å) (***Figure 49***).[286]

ii) As discussed, **19-Ge** shows considerable bending at the dicoordinated germanium center (∠Ge1-Ge3-Ge2 = 76.25(3)°). It indicates the presence of in-plane lone-pair orbital mainly in s-type orbital, which agrees with the angle widening in acyclic-trigermaallene (122.61(6)°) due to increased orbital mixing and reduced "germylone-type" character in resonance hybrid.[285] Whereas the Ge1-Sn-Ge2 bond angle in **19-Sn** (69.829(14)°) is shifted by 9° when compared with reported bis(germylene)-stabilized stannylone (78.90°),[122] this decrease in bond angle around the central tin atom suggests enhanced Sn(0) character (***Figure 49***).

iii) The sterically demanding Tbb substituents are arranged *synclinical*-orientation as depicted by torsion angle (φ) C1−Ge1−Ge2−C25 = 80.21(8)° (**19-Ge**) and 80.12(7)° (**19-Sn**) and the sum of angles in the EGe_2C_2 (E = Ge and Sn) five-membered ring = 359.7° (**19-Ge**) and 360.0° (**19-Sn**). Indicating planarity in the ring system (***Figure 49***).

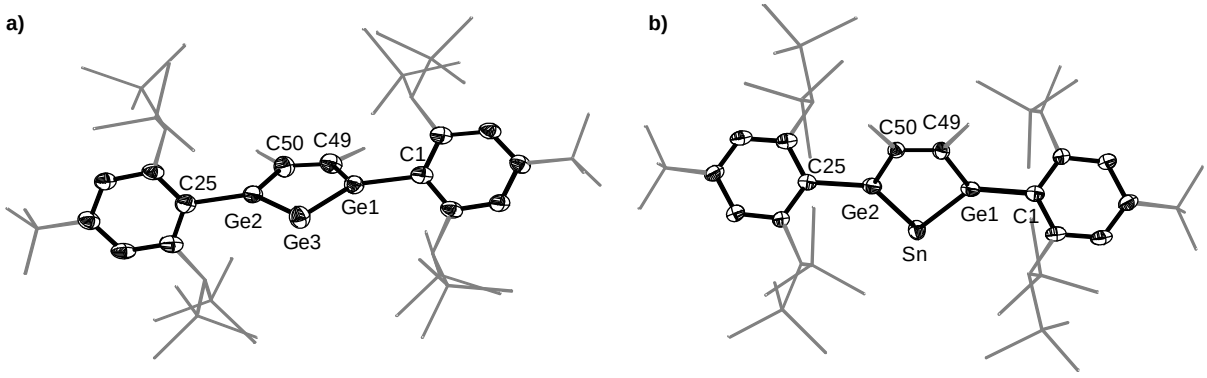

Figure 49. DIAMOND plot of the molecular structure of **19-Ge** (***left***) and **19-Sn** (***right***). Thermal ellipsoids are set at 30 % probability level. Hydrogen atoms are omitted and the Dsi and ^{t}Bu substituents of the Tbb ligand are presented in wire-frame for clarity. Selected bond lengths [Å], bond angles [°] and torsion angle [°]: **a)** Ge1-Ge2 2.9182(10), Ge1-Ge3 2.3606(10), Ge2-Ge3 2.3659(10), Ge2-C50 1.969(7), Ge1-C49 1.979(6), Ge1-Ge3-Ge2 76.25(3), C1-Ge1-Ge3 130.70(17), C1-Ge1-C49 110.7(3), C25-Ge2-C50 111.1(3), C25-Ge2-Ge3 130.28(17), C50-Ge2-Ge3 118.24(19), C49-Ge1-Ge3 118.5(2), C1-Ge1-Ge2-C25 80.21(8); **b)** Ge1-Sn 2.5454(4), Ge2-Sn 2.6871(5), Ge1-C1 1.878(5), Ge2-C25 1.935(6), C49-C50 1.359(7), Ge1-Sn-Ge2 69.829(14), C1-Ge1-Sn 124.17(15), C49-Ge-C1 110.95(16), Sn-Ge1-C1 125.16(1), C50-Ge2-Sn 114.75(1), C50-Ge2-C25 119.97(1), C1-Ge1-Ge2-C25 80.12(7).

The solution structures of compounds **19-Ge** and **19-Sn** were investigated using multinuclear NMR spectroscopy. The ^{1}H and ^{13}C NMR spectra of **19-Ge** and **19-Sn** at 298 K in (D_6)benzene exhibit a time-averaged C_{2v}-symmetric structure in solution. This symmetry renders both germanium centers (Ge1 and Ge2) homotopic as well as the Tbb substituents. Notably, Ge–C^{Tbb} bond rotation is frozen on the NMR timescale at ambient temperature, as unequivocally demonstrated by the presence of a distinct set of resonance corresponding to the $C^{2,6}$-CH(Si*Me*$_3$)$_A$(Si*Me*$_3$)$_B$ group of Tbb moiety, confirmed by the absence of dynamic averaging at this temperature. The $^{119}Sn\{^{1}H\}$ for **19-Sn** appears at −418.80 ppm, which is high-field shifted compared to the literature-known compound bis(germylene)-stabilized stannylone (−200.0 ppm).[122]

2.2.4. Reactivity and follow-up chemistry of germylone

The isolation of these compounds in substantial yields enabled further investigation of their reactivity. Preliminary reactivity studies probing the nature of the Ge=Ge bond in **19-Ge** was validated by reaction with $GeBr_2$(1,4-dioxane) in benzene at ambient conditions. The reaction proceeded rapidly, as indicated by an immediate colour change from green to orange, suggesting the formation of a new compound. Analysis of an aliquot by ^{1}H NMR spectroscopy confirmed the complete consumption of starting materials and the selective formation of the tetragerma[2,1,1]propellane **20- Ge** (***Scheme 15***). The orange product was isolated as an *n*-hexane solvate, **20- Ge** (***n*- hexane**), after workup and crystallization at −30 °C, yielding 59% of the analytically pure compound. The isolated compound is an air sensitive solid and shows moderate solubility in *n*-hexane, Et_2O and good solubility in solvents like benzene and toluene. Thermal stability studies revealed that **20-Ge** decomposes upon melting at 210 °C.

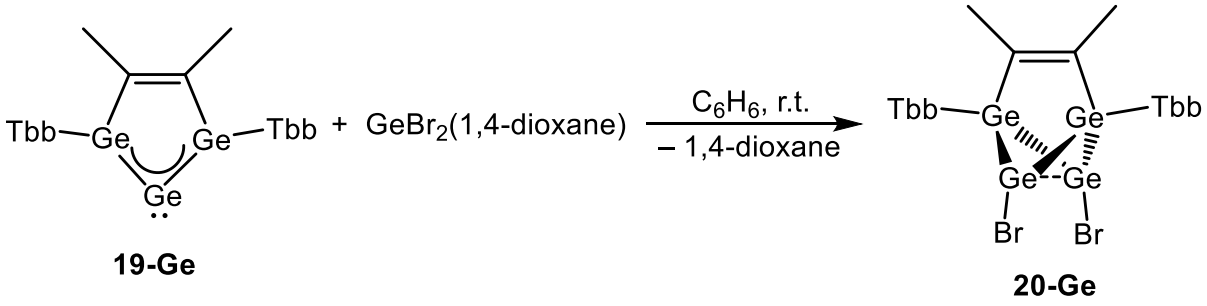

Scheme 15. Synthesis of the tetragerma[2,1,1]propellane (**20-Ge**).

The solid-state structure of compound **20-Ge** was elucidated through single-crystal X-ray diffraction analysis of clear orange block-shaped crystals by slow cooling of a saturated *n*-hexane solution at −30 °C and crystallized as a solvate of *n*-hexane **20- Ge**·(***n*-hexane**)$_{1.5}$. X-ray diffraction analysis revealed that **20-Ge** crystallizes in

the monoclinic space group $P2_1/n$ and possesses a *pseudo*-C_{2v}-symmetric structure in the solid state. Key structural characteristic features of **20-Ge** are as follows:

i) Ge1 and Ge2 adopt a distorted tetrahedral geometry, whereas Ge3 and Ge4 exhibit a trigonal pyramidal geometry ($\Sigma\measuredangle$(Ge3) = 313.60° and $\Sigma\measuredangle$(Ge4) = 313.25°(***Figure 50***).

ii) The sterically demanding Tbb substituents are arranged in synclinical conformation, as evident by the torsion angle (φ(C1−Ge1−Ge2−C25) = −31.55°).

iii) The Ge3···Ge4 distance in **20-Ge** (3.240(1) Å) (***Figure 50***) is approximately 2.7 Å more than that reported for pentagerma[1,1,1]propellane (2.9697(8) Å).[287] This distance is longer than the sum of the covalent radii of Ge (2.48 Å) but shorter than the van der Waals radii (4.20 Å),[228] suggesting weak interactions between the Ge atoms.

iv) The single-bond distances (Ge1−Ge3 = 2.4848(3) Å; Ge1−Ge4 = 2.4564(3) Å; Ge2−Ge3 = 2.4734(3) Å and Ge2−Ge4 = 2.4651(3) Å) are consistent with the reported mean Ge−Ge bond length in pentagerma[1,1,1]propellane (2.4910(5) Å).[287] and fall within the typical range for a Ge−Ge single bond.

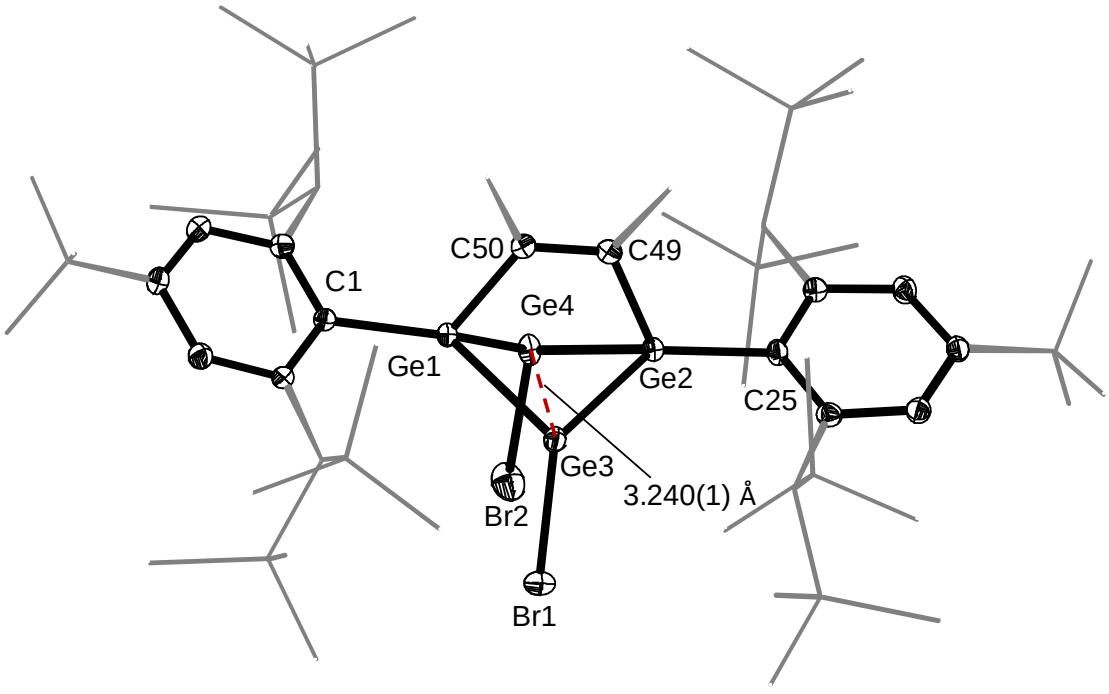

Figure 50. DIAMOND plot of the molecular structure of **20-Ge**. Thermal ellipsoids are set at 30 % probability level. Hydrogen atoms are omitted and the Dsi and ^{t}Bu substituents of the Tbb ligand are presented in wire-frame for clarity. Selected bond lengths [Å], bond angles [°] and torsion angle [°]: Ge1-Ge4 2.4564(3), Ge1-Ge3 2.4848(3), Ge2-Ge4 2.4651(3), Ge2-Ge3 2.4734(3), Ge1-C50 1.9582(19), Ge2-C49 1.9558(19), Ge3-Br1 2.3650(3), Ge4-Br2 2.3510(3), C49-C50 1.366(3), Ge1-Ge4-Ge2 82.947(9), Ge1-Ge3-Ge2 82.198(9), Ge4-Ge1-Ge3 81.946(9), Ge4-Ge2-Ge3 82.003(9), C1-Ge1-Ge4 134.68(5), C1-Ge1-Ge3 131.88(5), C25-Ge2-C49 116.41(8), C25-Ge2-Ge3 132.62(5); C1-Ge1-Ge2-C25 −31.55.

The solution-state structure of **20-Ge** was characterized using multinuclear NMR spectroscopy. The ^{1}H and ^{13}C NMR spectra recorded at 298 K in (D_6)benzene reveal a time-averaged C_{2v}-symmetric structure in solution, consistent with the symmetry observed in the solid state. This symmetry renders the germanium centers (Ge1 and Ge2) homotopic, as well as the Tbb substituents. Notably, Ge−C^{Tbb} bond rotation is restricted on the NMR timescale at ambient temperature, as evidenced by the presence of distinct resonance sets corresponding to the Si*Me*$_3$ in a 36:36 integral ratio and a single set of resonances for the $C^{3,5}$-*H* protons of Tbb moiety. This observation highlights the steric hindrance imposed by the bulky Tbb groups, which restricts conformational exchange and maintains the rigid molecular framework in solution.

The coordinatively unsaturated compound **19-Ge** exhibits multiple reactive sites suitable for further functionalization due to its zwitterionic form. Its reactivity with sterically less demanding diazoolifin is particularly interesting and offers significant potential for modifications. Notably, when a green solution of **19-Ge** was treated with one equivalent of a diazoloifin (IMe_4)CN_2 in benzene at ambient temperature, the reaction solution's colour gradually shifted from green to yellow-brown. After stirring for 1 hour, analysis of an aliquot of the reaction solution by ^{1}H NMR spectroscopy in (D_6)benzene revealed complete consumption of the starting material **19-Ge** and selective formation of bicyclo[2.1.1.]*bis*-germyl germylene **21-Ge** (***Scheme 16***, Pathway A).

Compound **21-Ge** was also synthesized through a non atom-economical, less-yield pathway involving the reaction of 2-butyne with coordinatively unsaturated NHC-supported 2,3,4-trigerma-cyclobutenyne type derivative (Ge_3C-1,2-diradicaloid) (**52-GeGe**) (***Scheme 16***, Pathway B).[2] to afford two products in 1.0 : 0.3 where the formation of **21-Ge** can be understood as a [2+2]cycloaddition reaction accompanied by the rearrangement of vinylidene fragments and the byproduct (**48-GeGe**) could be attributed to the loss of atomic germanium from **21-Ge.** Compound **21-Ge** was isolated as an analytically pure, air-sensitive, yellow solid with a 43 % yield after workup (From pathway A). The yellow solid decomposes upon melting to a brown

[2] Compounds **48-GeGe** and **52-GeGe** were thoroughly characterized and reported in the following doctoral thesis; Sandeep Kumar, "*Low-Valent Heavier Tetrel Compounds Supported by N-heterocyclic Carbenes: A Comprehensive Experimental and Theoretical Perusal*", *Dissertation*, Rheinische Friedrich-Wilhelms-Universität Bonn, **2025.**

liquid at 169 °C. Compound **21-Ge** is very well soluble in *n*-hexane, Et_2O, benzene and toluene at ambient temperature.

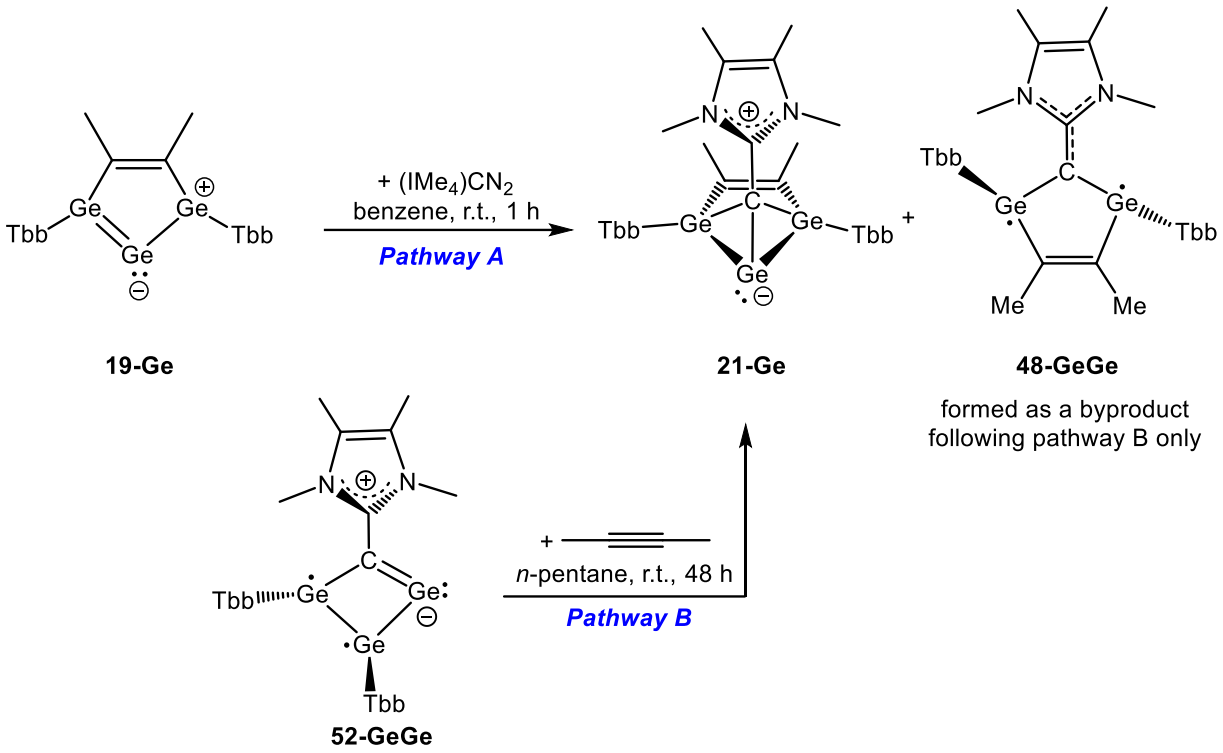

Scheme 16. Synthesis of the bicyclo[2.1.1] bis-germyl germylene **21-Ge** from two divergent reaction pathways.

The molecular structure of **21-Ge** was determined by single-crystal X-ray diffraction analysis. Yellow planks of **21-Ge**·(***n*-hexane**) were grown by storing a saturated solution of **54-Ge** in *n*-hexane at +4 °C. Compound **21-Ge** crystallized in monoclinic space group *C*2/c.

The molecular structure of **21-Ge** features a bicyclo[2.1.1] Ge_3C_3 ring with two distorted tetrahedral stereogenic germanium centers, **Ge1** and **Ge2** (***Figure 51***). These centers are connected to a V-shaped, dicoordinated germanium atom (Ge3) *via* Ge–Ge single bonds (Ge1–Ge3 = 2.443(2) Å; Ge2–Ge3 = 2.447(2) Å). The acute bending angle at Ge3 (Ge1–Ge3–Ge2 = 71.1(1)°) indicates a predominantly *s*-type lone pair localized on this germanium center. The observed Ge–Ge bond lengths are consistent with the expected single-bond distance of 2.42 Å (as derived from the Pyykkö table) [228] and closely match the average Ge–Ge bond length ($d(Ge–Ge)_{av}$ = 2.427(2) Å) reported for hexamethyldigermane, $(CH_3)_3Ge–Ge(CH_3)_3$.[288] The Ge–C bond lengths between the tetracoordinated germanium centers and the vinyl carbon (Ge1–C^{VNL} = 2.031(5) Å; Ge2–C^{VNL} = 2.030(5) Å) align well with the Ge–C_{sp2} single bond length in Ge(Terphenyl)$_2$ (2.033(2) Å),[289] suggesting negligible negative hyperconjugation from the vinyl carbon lone pair into σ*(Ge–Ge) or σ*(Ge–C^{Ar}/$C^{alkenic}$)

antibonding orbitals. Additionally, the C^{VNL}–C^{NHC} bond length (1.424(6) Å) closely resembles a typical $C^{(sp2)}$–$C^{(sp2)}$ single bond (1.460 Å),[290] indicating minimal π-character between the vinyl and carbenic carbons.

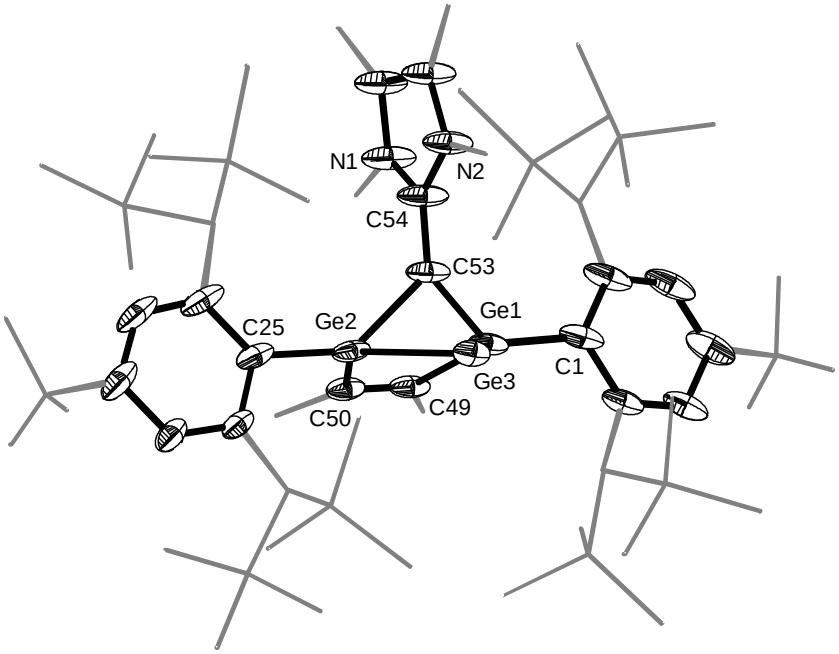

Figure 51. DIAMOND plot of the molecular structure of **21-Ge**. Thermal ellipsoids are set at 30 % probability level. Hydrogen atoms are omitted and the Dsi and *t*Bu substituents of the Tbb ligand are presented in wire-frame for clarity. Selected bond lengths [Å], bond angles [°] and torsion angle [°]: Ge1-Ge3 2.4438(5), Ge2-Ge3 2.4505(5), Ge1-C53 2.035(4), Ge2-C53 2.039(4), Ge3-C53 2.153(3), Ge1-C49 1.986(3), Ge2-C50 1.975(3) C49-C50 1.336(6), C53–C54 1.424(6); Ge1-Ge3-Ge2 71.281(16), Ge1-C53-Ge2 88.84(11), C1-Ge1-C53 133.91(14), C25-Ge2-C53 134.49(14), C49-Ge1-C53 99.78(14), C50-Ge2-C53 99.83(14), C49-Ge1-C1 111.27(14), C50-Ge2-C25 111.78(14).

The NMR spectroscopic data further corroborate with the solid-state structure of compound **21-Ge**. Both the ^{1}H and $^{13}C\{^{1}H\}$ NMR spectra reveal a C_s-symmetric structure in solution, where the sterically demanding Tbb substituents rotate freely around the Ge–C^{Tbb} bond axis. This dynamic behaviour is confirmed by the presence of two distinct Si*Me*$_3$ signals in a 36:36 integral ratio and a single set of resonances for the $C^{3,5}$-*H* protons. In the $^{13}C\{^{1}H\}$ NMR spectrum, the most notable signal corresponds to the vinyl carbon (C^{VNL}), which appears significantly upfield-shifted ($\delta_{(CVNL)}$ = 39.8 ppm) within the typical alkane region. This chemical shift is comparable to that observed in the four-membered puckered ring compound [(^{Me}IPrCH)GeCl]$_2$ ($\delta_{(C(VNL))}$ = 49.4 ppm in (D_6)benzene),[236] where the Ge–Cl bonds adopt a *syn*-orientation, and the vinylic carbon is coordinatively saturated.

Concluding investigation on the reactivity of **19-Ge**, unravel an addition product when treatment of **19-Ge** with the small N-heterocyclic carbene IMe$_4$ in benzene at ambient temperature resulted in an instantaneous colour change from green to red-

purple. ^{1}H NMR analysis of the reaction mixture confirmed the selective generation of the IMe_4 addition product, **22-Ge**. Isolation *via* standard workup procedures afforded **22-Ge** (***Scheme 17***) as an analytically pure red solid in 41% yield. The compound exhibits extreme air sensitivity, undergoing immediate decolourization upon exposure to air. It displays moderate solubility in *n*-hexane and high solubility in aromatic solvents (toluene, benzene) and THF at room temperature. Thermal decomposes analysis revealed that compound **22-Ge** decomposes upon melting to a black mass at 180 °C.

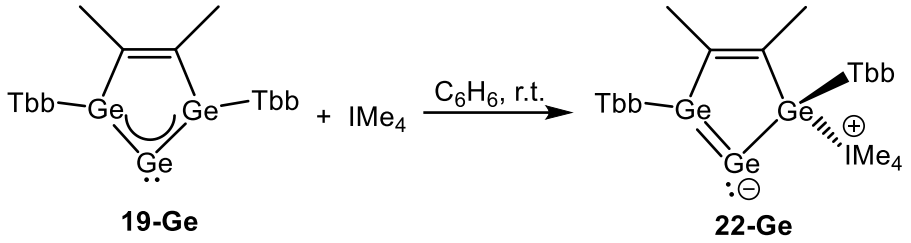

Scheme 17. Reaction of strong σ-donor IMe_4 with germylone (**19-Ge**) to afford **22-Ge.**

Full characterization was achieved through multinuclear NMR spectroscopy, elemental analysis (EA), and single-crystal X-ray diffraction (sc-XRD). Suitable single crystals of **22-Ge·(*n*-pentane)** (clear red blocks) were obtained by slow cooling of a saturated *n*-pentane solution at −30 °C, enabling definitive structural elucidation. Compound **22-Ge·(*n*-pentane)** crystallized in monoclinic space group $P2_1/c$ and showed C_1-symmetric structure in the solid state

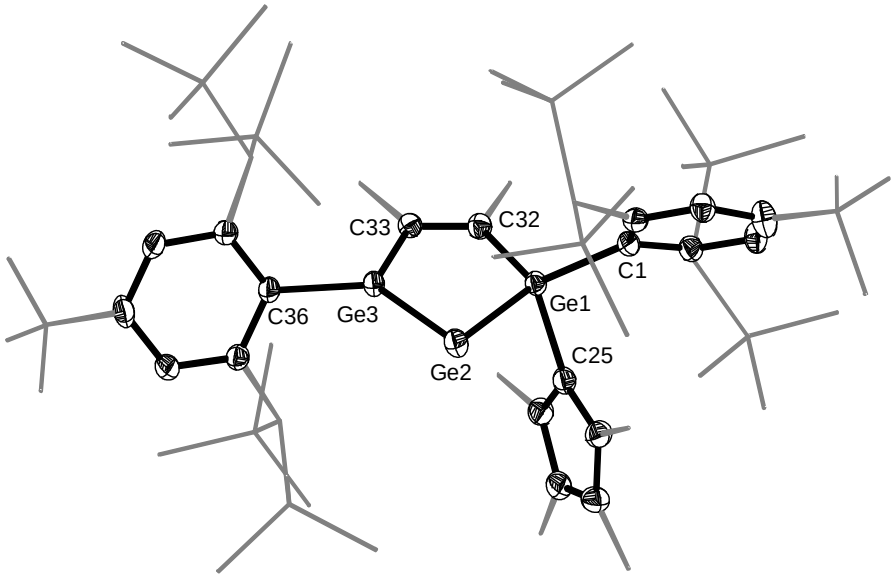

Figure 52. DIAMOND plot of the molecular structure of **22-Ge**. Thermal ellipsoids are set at 30 % probability level. Hydrogen atoms are omitted and the Dsi and ^{t}Bu substituents of the Tbb ligand are presented in wire-frame for clarity. Selected bond lengths [Å], bond angles [°] and torsion angle [°]: Ge1-Ge2 2.5019(4), Ge1-C32 2.034(2), Ge3-Ge2 2.3291(4), Ge3-C33 1.995(3), Ge1-C25 2.035(2), C32-C33 1.305(2), Ge1-Ge2-Ge3 77.323(13), Ge2-Ge3-C36 118.81(7), Ge2-Ge1-C32 113.44(7), Ge2-Ge3-C33

118.81(7), C1-Ge1-C25 102.21(9), C1-Ge1-C32 116.89(10), C25-Ge1-Ge2 93.42(7), C33-Ge3-C36 112.21(10).

Structural analysis reveals a nearly planar five-membered Ge_3C_2 ring, along with a significantly distorted tetrahedral Ge1 center and a nearly planar tri-coordinated Ge2 center (Σ∢(Ge2) = 359.75°). The Ge1–Ge2–Ge3 bond angle (77.323(13)°) closely matches that of its precursor, **19-Ge** (76.25(3)°). The sterically demanding Tbb substituents adopt a *antiperiplanar* conformation, as indicated by the torsion angle C1–Ge1–Ge3–C36 (163.43(1)° in **22-Ge**), which contrasts with the synclinical conformation observed in the precursor (80.21(8)° in **19-Ge**) (***Figure 52***). The Ge···Ge distance in **22-Ge** (3.021(1) Å) is 0.1 Å longer than in its precursor, suggesting weaker interactions between the Ge atoms. Notably, the Ge–Ge bond lengths in **22-Ge** (2.5019(4) Å and 2.329(1) Å) differ significantly from those in **19-Ge** (2.3606(10) Å and 2.3659(10) Å). One bond elongates, supporting single-bond character due to adduct formation, while the other shortens, approaching the typical Ge=Ge double-bond length—consistent with reported values for trigermaallene (2.321(2) Å and 2.330(3) Å).[285] Additionally, the elongated Ge1–C25 bond (2.035(2) Å) further corroborates adduct formation.

The NMR spectroscopic data corroborate the solid-state structure of compound **22-Ge**, revealing a C_1-symmetric architecture in solution. Both the ^1H and $^{13}C\{^1H\}$ NMR spectra indicate that the germanium centers are heterotopic, rendering the sterically demanding Tbb substituents chemically inequivalent. This dynamic behaviour arises from differential rotational freedom around the Ge–C^{Tbb} bonds: one Tbb group undergoes free rotation, while the other remains rotationally locked on the NMR timescale. This phenomenon is further evidenced by the presence of five distinct Si*Me*$_3$ signals in a 9:9:18:18:18 integral ratio, along with three distinct sets of resonances for the $C^{3,5}$–*H* protons in a 1:1:2 integral ratio. In the $^{13}C\{^1H\}$ NMR spectrum, the most diagnostically significant signal corresponds to the carbenic carbon (N*C*N), which resonates at δ = 163.30 ppm, well within the characteristic range for carbene centers. Notably, this chemical shift is upfield-shifted compared to that of the dicationic five-membered ring species (δ = 176.6 ppm) generated by the reaction of an N-heterocyclic germylene with two equivalents of MeOTf.[114]

The aforementioned tetragerma[2,1,1]propellane (**20-Ge**) is a powerful synthon that enables access to unprecedented germanium cluster compounds under standard laboratory conditions. Notably, the reduction of **20-Ge** with two equivalents of KC_8 in benzene was accompanied by a colour change from orange to yellow-orange. Reaction monitoring by ^1H NMR spectroscopy revealed the selective formation of a new

compound, which turned out to be the unprecedented η^5-Ge(0) half sandwich compound, **23-Ge**, and no intermediate could be observed by NMR spectroscopy at ambient temperature during the conversion of **20-Ge** to **23-Ge**. Subsequent crystallization from *n*-pentane at −30 °C afforded **23-Ge** as an extremely air-sensitive, yellow solid in 74 % yield. Compounds **23-Ge** exhibit good solubility in benzene, toluene, THF and moderately soluble in *n*-hexane and Et_2O at ambient temperature. Thermal decomposition of **23-Ge** in a *vacuum*-sealed glass capillary was detected upon melting at 309 °C. Analysis of the soluble part of the respective melting residue in (D_6)benzene by ^{1}H NMR spectroscopy revealed unselective decomposition of **23-Ge**.

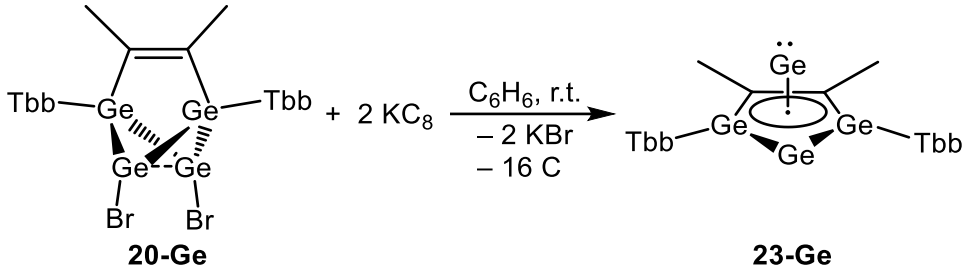

Figure 53. Synthesis of unprecedented η^5-Ge(0) half sandwich complex (**23-Ge**).

Complex **23-Ge** is the first η^5-Ge(0) half-sandwich complex to be reported and hence was characterized thoroughly by single crystal X-ray diffraction (scXRD) analysis and multinuclear NMR spectroscopy. Block-shaped clear light-yellow crystals of **23-Ge**, suitable for scXRD analysis, were obtained by slow cooling of their saturated *n*-pentane solution at −30 °C. X-ray diffraction analysis revealed that **23-Ge** crystallizes in the triclinic space group $P\bar{1}$.

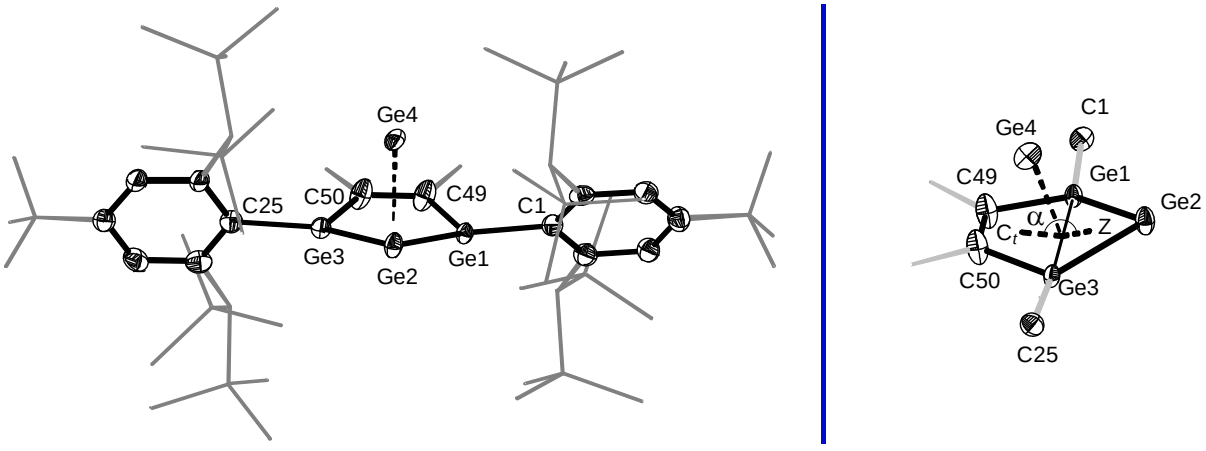

Figure 54. DIAMOND plot of the molecular structure of **23-Ge** (***left***). Thermal ellipsoids are set at 30 % probability level. Hydrogen atoms are omitted and the Dsi and ^{t}Bu substituents of the Tbb ligand are presented in wire-frame for clarity. Selected bond lengths [Å], bond angles [°] and torsion angle [°]: Ge1-Ge2 2.420(2), Ge3-Ge2 2.412(5), Ge1-Ge4 2.642(3), Ge2-Ge4 2.8481(11), Ge3-Ge4 2.597(5), Ge1-Ge2-Ge3 82.62(15), Ge2-Ge3-C50 109.1(3), Ge2-Ge1-C49 108.9(2), C1-Ge1-Ge2 132.16(16), C1-Ge1-C49 114.3(2),C25-Ge3-Ge2 134.5(3), C25-Ge3-Ge50 114.1(3). (***right***) A side-on view of the truncated

molecular structure of **23-Ge**; α = 162.17°, C_t is the centroid of (Ge1, Ge3, C49 and C50) and Z is the centroid of (Ge1, Ge2 and Ge3).

The molecular architecture of **23-Ge** features a pyramidal geometry, comprising a nearly planar five-membered Ge_3C_2 ring (deviation from planarity indicated by angle α = 162.17°) and an η^5-coordinated apical germanium atom (***Figure 54***). For context, the analogous η^5-aminoborole complex of germanium(II) exhibits a more planar ring (α = 170°), highlighting the subtle structural differences induced by coordination environments.[291]

The Ge1−Ge2−Ge3 angle in **23-Ge** (82.64°) is notably wider than that in **19-Ge** (76.26°), reflecting significant ring expansion due to the steric and electronic influence of the apical germanium center. Furthermore, the bond metrics within the Ge_3C_2 ring suggest a delocalized 6π-electron system, supported by comparative bond length analysis: The Ge−Ge bonds for **23-Ge** (Ge1−Ge2 2.420(2) Å, Ge2−Ge3 2.412(5) Å) and C49−C50 (1.403(7) Å) are elongated relative to **19-Ge** (Ge1−Ge2 2.361(3) Å, Ge2−Ge3 2.366(9) Å, C49−C50: 1.350(9) Å), while the Ge1−C49 (1.923(6) Å) and Ge3−C50 (1.916(7) Å) bonds are shortened compared to **19-Ge** (1.969(4) Å, 1.979(8) Å). This contraction and elongation pattern imply enhanced π-backdonation from the germylone ring to the germanium center, further corroborated by the Ge−Ge apical distances (Ge4−Ge1/Ge2/Ge3: 2.642(3) Å, 2.8481(11) Å, 2.597(5) Å), which exhibit marked variability compared to **19-Ge** (2.36 Å). The Ge−C distances (Ge−C49/C50: 2.263(5) Å, 2.252(6) Å) in **22-Ge** are notably elongated relative to standard Ge−C single bonds (1.96 Å), reinforcing the delocalized bonding framework.[228]

Collectively, these structural insights support the classification of **23-Ge** as, an η^5-germylone half-sandwich complex**.** This formulation aligns with the structural parallels observed in isoelectronic silicon cations,[292] germanium cations,[293] and Group 13 half-sandwich complexes, underscoring its unique electronic and coordinative properties.[294]

The ^1H and $^{13}C\{^1H\}$ NMR spectra of **23-Ge** in (D_6)benzene at 298 K exhibit time-averaged C_S-symmetry on the NMR timescale, as evidenced by a single set of resonances in both spectra. This observation is consistent with the C_S-symmetry observed in the solid state. Due to this symmetry, the germanium centers (Ge1 and Ge3) are enantiotopic, and the sterically demanding Tbb substituents are rendered equivalent. Notably, Ge−C^{Tbb} bond rotation is frozen on the NMR timescale at ambient temperature. This is unambiguously confirmed by the presence of distinct resonances for the $C^{2,6}$-CH(SiMe_3)$_A$(SiMe_3)$_B$groups, as demonstrated by the SiMe_3

signals appearing in an 18:18:18:18 ratio. Additionally, the aromatic $C^{3,5}$–*H* protons are split into two 2:2 signal groups, corresponding to a Tbb substituents. In the $^{13}C\{^1H\}$ NMR spectrum, the most diagnostically significant signal corresponds to the unsaturated backbone carbon, which appears at δ = 145.81 ppm a chemical shift well within the characteristic range for alkenic carbons. Notably, this resonance is upfield-shifted compared to that observed in the germylone **19-Ge** (δ = 159.93 ppm), indicating coordination of the backbone carbon to the apical germanium atom upon complexation.

Following the isolation of **23-Ge**, we investigated the effects of increasing the number of germanium atoms incorporated into the ring system. The reactivity of the resulting compound was then experimentally demonstrated by the treatment of one equivalent of $GeBr_2$(1,4-dioxane) in benzene at ambient temperature, which was accompanied by a colour change from orange-yellow to red. Reaction monitoring by ^1H NMR spectroscopy revealed the selective formation of a new compound, which turned out to be the unprecedented pentagerma[1.1.1]propellane (**24-Ge**) (***Scheme 18***). Subsequent crystallization from *n*-pentane at −30 °C afforded **24-Ge** as an extremely air-sensitive, red solid in 70 % yield.

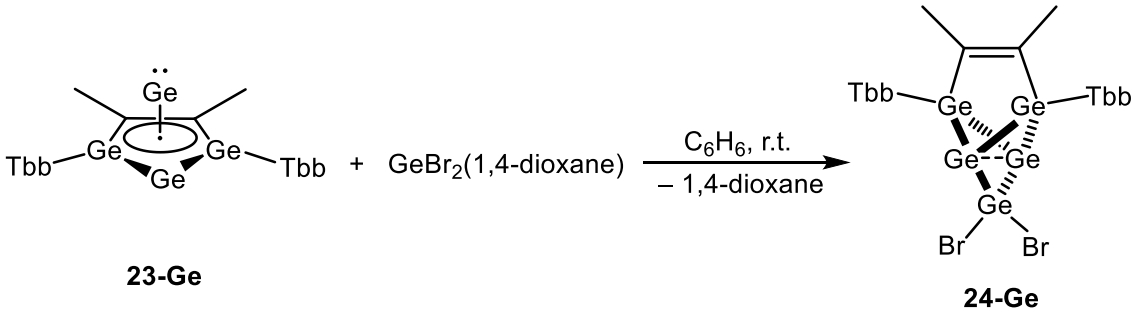

23-Ge **24-Ge**

Scheme 18. Synthetically accessible pentagerma[1.1.1]propellane (**24-Ge**).

The compounds **24-Ge** demonstrate excellent solubility in aromatic solvents (benzene, toluene) and ethereal solvents (THF, Et_2O) at ambient temperature. Thermal analysis performed in a *vacuum*-sealed glass capillary revealed decomposition concomitant with melting at 262 °C, indicating the robust nature of compound **24-Ge**. Furthermore, these compounds exhibit gradual decomposition in solution, with unselective degradation observed after 8 hours, suggesting limited stability under prolonged solvation.

Compound **24-Ge** represents one of the rarest synthetically accessible metalla[1.1.1]propellanes (***Figure 55***) among the heavier Group 14 elements reported to date. Its structural and electronic properties were comprehensively characterized using single-crystal X-ray diffraction (scXRD) and multinuclear NMR spectroscopy,

confirming its unique molecular architecture. Block-shaped red crystals of the solvated adduct **24-Ge**·(***n*-pentane**), suitable for high-resolution scXRD analysis, were obtained by slow cooling of a saturated *n*-pentane solution at −30 °C. Subsequent crystallographic studies revealed that **24-Ge** crystallizes in the monoclinic space group $P2_1/n$.

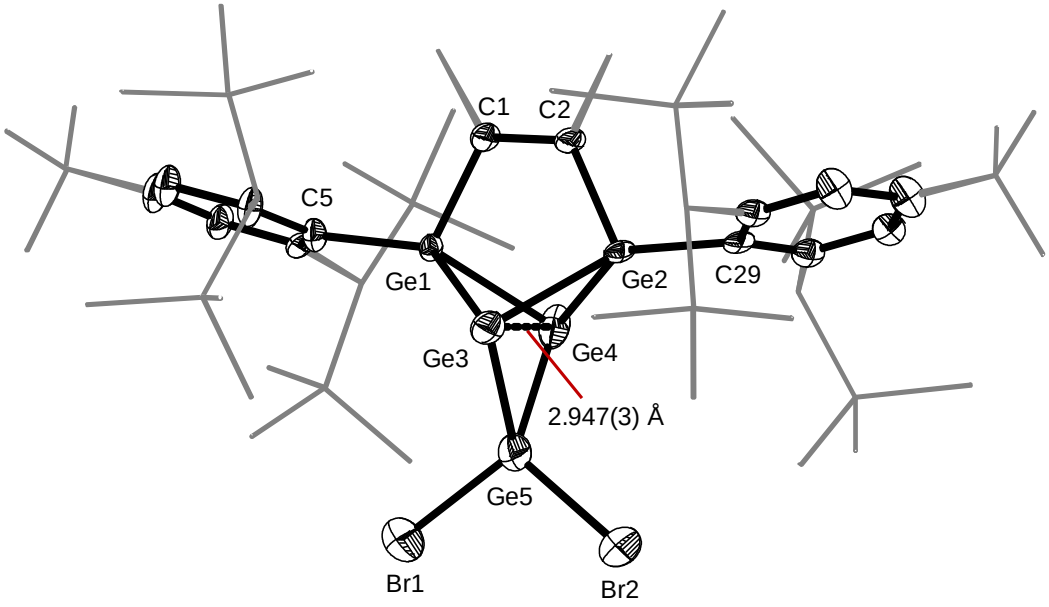

Figure 55. DIAMOND plot of the molecular structure of **24-Ge**. Thermal ellipsoids are set at 30 % probability level. Hydrogen atoms are omitted and the Dsi and ^{t}Bu substituents of the Tbb ligand are presented in wire-frame for clarity. Selected bond lengths [Å], bond angles [°] and torsion angle [°]: Ge1-Ge3 2.496(3), Ge1-Ge4 2.442(3), Ge2-Ge3 2.519(3), Ge2-Ge4 2.481(3), Ge3-Ge5 2.421(4), Ge4-Ge5 2.476(4), Ge5-Br1 2.322(4), Ge5-Br2 2.302(4), C1-C2 1.41(3), Ge1-Ge3-Ge2 78.31(9), Ge1-Ge4-Ge2 92.67(2), Ge1-Ge3-Ge5 91.29(12), Ge1-Ge4-Ge5 91.28(12), Ge2-Ge3-Ge5 93.06(12), Ge2-Ge4-Ge5 93.06(12), Ge2-Ge4-Ge5 92.67(12), Ge3-Ge5-Ge4 73.98(11), Ge3-Ge2-Ge4 72.21(10), Ge4-Ge1-Ge3 73.26(10).

The molecular structure of **24-Ge** confirms the formation of a quite rare pentagerma[1.1.1]propellane featuring two ligand-free bridgehead germanium centers (Ge3 and Ge4, ***Figure 55***). The latter are bonded to three bridging germanium centers (Ge1, Ge2 and Ge5) at distances (Ge1−Ge3/Ge4 = 2.496(3) Å, 2.442(3) Å; Ge2−Ge3/Ge4 = 2.519(3) Å, 2.481 (3) Å and Ge5−Ge3/Ge4 = 2.421(4) Å, 2.476(4) Å). compares well with the literature reported Ge_5Mes_6 (Ge1−Ge3/Ge4 = 2.476(3) Å, 2.485(3) Å; Ge2−Ge3/Ge4 = 2.453(1) Å, 2.501(1) Å and Ge5−Ge3/Ge4 = 2.489(2) Å, 2.466(1) Å).[234] The Ge3···Ge4 distance in **20-Ge** (2.947(3) Å) is comparable to that reported for pentagerma[1,1,1]propellane (2.9697(8) Å).[287] and also aligns close to the structurally analogue compound Ge_5Mes_6 (2.86(9) Å).[234] This distance is longer than the sum of the covalent radii of Ge (2.48 Å) but shorter than the van der Waals radii (4.20 Å),[228] suggesting weak interactions between the Ge centers. The sterically

demanding Tbb substituents are arranged in acute orientation, as evident by the torsion angle (φ(C1−Ge1−Ge2−C25) = −18.31°).

The ^{1}H and ^{13}C{^{1}H} NMR spectra of **24-Ge** in (D_6)benzene at 298 K exhibit time-averaged C_{2v}-symmetry on the NMR timescale, as evidenced by a single set of resonances in the respective spectrum. This observation aligns with the C_{2v}-symmetry observed in the solid state, confirming structural retention in the solution. Within this symmetric framework, the germanium centers (Ge1 and Ge3) are homotopic, and the sterically encumbered Tbb substituents are rendered chemically equivalent. Notably, Ge–C^{Tbb} bond rotation occurs rapidly on the NMR timescale at ambient temperature. This dynamic behaviour is unambiguously corroborated by the presence of distinct resonances for the Si*Me*$_3$, ^{t}Bu, Dsi, and aromatic C^{3,5}–*H* protons associated with the Tbb substituents, indicating free rotation that remains observable. In the ^{13}C{^{1}H} NMR spectrum, the most distinct signal corresponds to the unsaturated backbone carbon, appearing as a sharp resonance at δ = 162.50 ppm. This chemical shift is remarkably consistent with that observed for the germylone **19-Ge** (δ = 159.93 ppm), further supporting the no involvement of the backbone unsaturated carbon in the electronic delocalization between the two systems.

2.3. Base-supported heteroditetrelynes: Synthesis and reactivity

The synthesis of homonuclear ditetrelynes (RE≡ER; E = Si – Pb) is commonly achieved through the reductive dehalogenation of tetrel(II) or tetrel(IV) precursors.[58,167] However, the analogues strategy has proven ineffective for the successful isolation of heteronuclear congeners (RE≡E'R; E and E' = Si – Pb) , with no successful reports so far.[58,167,168] A notable breakthrough was reported by Filippou and coworkers,[3] developing a novel approach involving the irreversible metathetical exchange/cross-coupling between distannyne ($Sn_2Ar^{Dipp}_2$) and a germanium(II) halide ($Ar^{Dipp}GeCl$) at ambient temperature. This reaction selectively yields the dark purple stannagermyne ($Ar^{Dipp}Sn{\equiv}GeAr^{Dipp}$), representing the first successful synthesis of a heteronuclear ditetrelyne (***Scheme 19***).

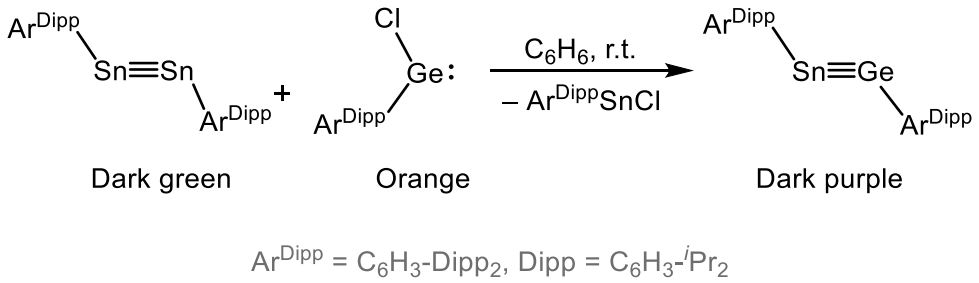

Scheme 19. Synthesis of a stannagermyne following the cross coupling of a distannyne with a Ge(II) precursor.

The molecular chemistry of silicon and germanium has undergone a notable resurgence, propelled by the recognition that *N*-heterocyclic carbenes (NHCs) and cyclic(alkyl)(amino)carbenes (CAACs) function as highly effective Lewis bases. These ligands have enabled the thermodynamic and kinetic stabilization of low-oxidation-state Si and Ge species, which exhibit unconventional bonding motifs and substantial synthetic utility.[130,170–176] While base-free heteronuclear ditetrelynes remain exceedingly rare, Filippou and coworkers recently reported the isolation of the first room temperature stable NHC-supported heteronuclear ditetrelyne, germasilyne (SIDipp)(Cl)Si=Ge(Ar^{Mes}).[130] Leveraging NHC coordination, the synthesis and structural characterization of the two-coordinate Si^0 isocyanide complex (SIDipp)Si=C=N(Ar^{Mes}) (SIDipp = C[N(Dipp)CH_2]$_2$; Ar^{Mes} = 2,6-bis(2,4,6-trimethylphenyl)phenyl) was achieved. Subsequent treatment of NHC-supported

[3] The compound ($Ar^{Dipp}Sn{\equiv}GeAr^{Dipp}$) is reported in the following doctoral thesis; David Hoffmann, "*Novel synthetic routes for multiple bond formation between Si, Ge and Sn and the d- and p-block elements*", *Dissertation*, Rheinische Friedrich-Wilhelms-Universität Bonn, **2021**.

iminosilenylidene (SIDipp)Si=C=N)(Ar^{Mes}) with Ar^{Mes}GeCl, affording the unprecedented NHC-supported heteronuclear ditetrelyne [(NHC)Si(Cl)GeAr^{Mes}], the only reported example of its class (***Scheme 20***).

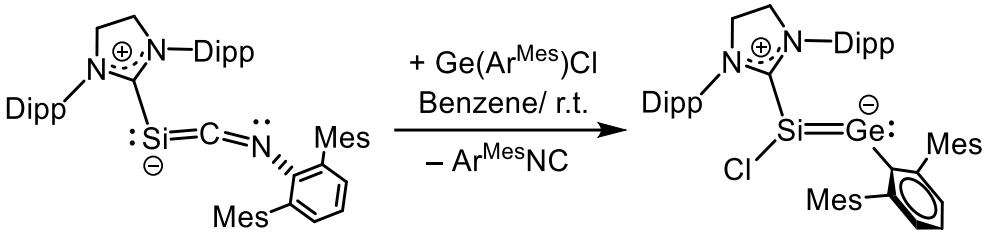

Dipp = C_6H_3-2,6-^{i}Pr$_2$; Mes = C_6H_2-2,4,6-Me$_3$

Scheme 20. Synthesis of an NHC-supported germasilyne (SIDipp)(Cl)Si=Ge(Ar^{Mes}).

In the pursuit of synthesizing base-supported heteroditetrelynes, the SnR transfer reagent (Ar^{Dipp}SnSnAr^{Dipp}) was chosen as a suitable starting material. In fact, the addition of a clear orange solution of (*E*)-(Tbb)BrSi=SiBr(Tbb) and 4−DMAP to a stirred green solution of Ar^{Dipp}Sn≡SnAr^{Dipp} in toluene at ambient temperature was accompanied by a slow transition of colour to intense green within two hours. Analysis of the reaction solution by ^{1}H NMR spectroscopy in (D_6)benzene revealed the selective elimination of Ar^{Dipp}SnBr(DMAP)[4] and formation of the DMAP-supported stannasilyne Ar^{Dipp}Sn=Si(DMAP)Tbb (**25-SnSi**) (***Scheme 21***) and trace amount of ArDipp-H was observed. The crude mixture was evaporated, taken up in *n*-hexane, and cooled to −30°C, precipitating the colourless Ar^{Dipp}SnBr(DMAP). Subsequent filtration removed this byproduct, and the remaining green filtrate was concentrated and subjected to recrystallization at −30 °C to further purify the product. Slow concentration ultimately afforded **25-SnSi**·(***n*-hexane**) as green crystals in 42% isolated yield.

---

[4] NMR spectroscopic data of Ar^{Dipp}SnBr(DMAP)): **^{1}H NMR** (500.1 MHz, (D_6)benzene, 298 K): δ (ppm)= 1.12(m, 12H, 1.10-1.13, 2×C^{2,6}-CH*Me*$_A$Me$_B$, 2×Dipp), 1.43(br,s, $\Delta\nu_{1/2}$ = 60.96 Hz, 12 H, 2×C^{2,6}-CHMe$_A$*Me*$_B$, 2×Dipp), 1.99(s, 6H, C^4-N*Me*$_2$, DMAP), 3.35(sept, 4H, C^{2,6}-C*H*Me$_A$Me$_B$, 2×Dipp), 5.51(d, ^3J(H,H) = 7.2 Hz, 2H, C^{3,5}-H, DMAP), 7.09-7.22(m, 9H, 2×Dipp + C_6H_3(Ar^{Dipp})) 7.58(d, ^3J(H,H) = 7.2 Hz, 2H, C^{2,6}-H, DMAP). **^{13}C{^{1}H} NMR** (125.8 MHz, (D_6)benzene, 298 K): δ (ppm) = 23.4(s, 4C, 2×C^{2,6}-CHMe$_A$*Me*$_B$, 2×Dipp), 26.2(s, 4C, 2×C^{2,6}-CH*Me*$_A$Me$_B$, 2×Dipp), 30.9 (s, 4C, 2×C^{2,6}- *C*HMe$_A$Me$_B$, 2×Dipp), 38.2(s, 2C, C^4-N*Me*$_2$, DMAP), 106.5(s, 2C, *C*^{3,5}-H, DMAP), 123.0(s, 4C, *C*^{3,5}-H, 2×Dipp), 126.2(s, 1C, C^4, C_6H_3(Ar^{Dipp}), 128.6(s, 1C, *C*^{4}-H, C_6H_3(Ar^{Dipp})), 130.7(s, 1C, *C*^{4}-H, 2×Dipp), 141.20(s, 2C, 2×C^1, 2×Dipp), 146.7(s, 4C, 2×*C*^{2,6}- CHMe$_A$Me$_B$, 2×Dipp), 147.7(s, 2C, *C*^{2,6}-H, DMAP), 148.0(s, 1C, *C*^{2,6}-CHMe$_A$Me$_B$, C_6H_3(Ar^{Dipp})), 154.2(s, 1C, *C*^{4}-NMe$_2$, DMAP), 172.4(s, 1C, C^1, C_6H_3(Ar^{Dipp}).

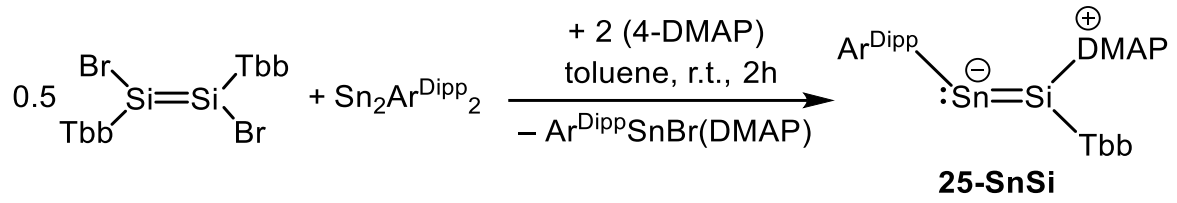

Dipp = C_6H_3-2,6-$^i Pr_2$; DMAP = N,N-Dimethylpyridin-4-amine

Scheme 21. Synthesis of the DMAP-supported stannasilyne (**25-SnSi**).

25-SnSi is a highly air- and moisture-sensitive green solid that rapidly decolourizes upon exposure to air. It is soluble in *n*-pentane, *n*-hexane, benzene, toluene and Et_2O at ambient temperature and melts with decomposition at 157 °C. In an inert atmosphere, solutions in (D_6)benzene remain stable for at least one week without any decomposition.

The structural and electronic properties of **25-SnSi** were meticulously elucidated through a combination of single-crystal X-ray diffraction (scXRD) and multinuclear NMR spectroscopy, unequivocally confirming its distinctive molecular architecture. Block-shaped green crystals of the solvated adduct **25-SnSi**·(***n*-hexane**), suitable for sc-XRD analysis, were successfully grown *via* controlled slow cooling of a saturated *n*-hexane solution at −60 °C. Subsequent crystallographic characterization revealed that **25-SnSi**·(***n*-hexane**) crystallizes in the triclinic crystal system, adopting $P\bar{1}$ space group.

The molecular structure of **25-SnSi** (***Figure 56***) possesses a *pseudo*-C_s-symmetry with the mirror plane passing through the *trans-bent* C^{ipso}-Sn-Si-C^{ipso} (φ(C32−Sn1−Si1−C1) = −179.98°) core and bisecting the central aryl ring of Ar^{Dipp} and Tbb substituents as well as passing through the DMAP ring. The planar core consists of atoms C32, Sn, Si1, C1. The trigonal planar coordinate Si atom ($\Sigma\measuredangle$(Si) = 359.9(5)°) is connected to a V-shaped dicoordinated Sn atom *via* a Sn=Si double bond (2.4580(7) Å). Notably, the DMAP six-membered ring is arranged coplanar to the core of the molecule, as evidenced by the dihedral angle φ_{DMAP} of (3.85(1)°) between the plane of the DMAP ring and the plane passing through the atoms C32, Sn1, Si1 and C1. This allows for the conjugation of the Sn=Si π-bond with the N_{DMAP}-centered acceptor orbital and the formation of a (3c-2e) π_{oop}-bond, leading to an elongation of the Sn=Si bond. In fact, the Sn−Si bond length (2.4580(7) Å) in **25-SnSi** is longer than the literature reported silastannene (2.4188(14) Å).[295]

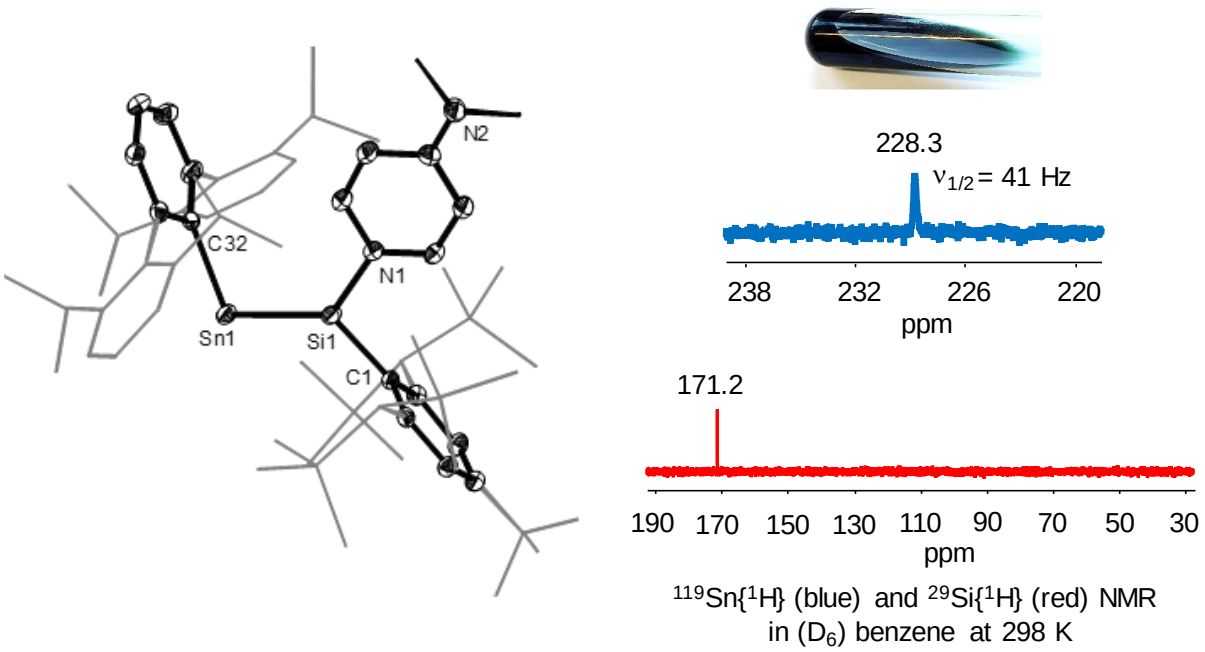

Figure 56. DIAMOND plot of the molecular structure of **25-SnSi**. Thermal ellipsoids are set at 30 % probability level. Hydrogen atoms are omitted and the Dsi and ^{t}Bu substituents of the Tbb ligand and Dipp Substituent of Ar^{Dipp} are presented in wire-frame for clarity. Selected bond lengths [Å], bond angles [°] and torsion angle [°]: Sn1-Si1 2.4580(7), Si1-C1 1.901(3), Sn1-C32 2.238(2), Si1-N1 1.865(2), Sn1-Si1-N1 128.22(7), C32-Sn1-Si1 105.74(6), Sn1-Si1-C1 127.10(8), C1-Si1-N1 103.13(10), C1-Si1-Sn1-C32 179.98(10).); (***top right***) picture of a solution sample of **25-SnSi** in benzene at ambient temperature and (***middle*** and ***bottom right***) selected excerpt of the ^{119}Sn{^{1}H} and ^{29}Si{^{1}H} NMR spectrum of **25-SiSn**, respectively.

The molecular structure of **25-SnSi** possesses a pseudo-C_s-symmetry in the solid state. However, the solution ^{1}H and ^{13}C{^{1}H} NMR spectral features of **25-SnSi** are in accordance with a higher local time average symmetry (C_{2v}) of the Ar^{Dipp} groups than that in the solid-state leading to a chemical equivalence of some diastereotopic nuclei. The spectral features can be rationalized by the following chemical exchange process: a fast Ar^{Dipp}-rotation about the Sn−C^{ipso} bond, a hindered rotation about the Si−C^{ipso} bond on the NMR time-scale. Accordingly, the time-averaged topicity relationship is assigned as follows: Dipp groups of each Ar^{Dipp} are homotopic, and the methyl groups of each isopropyl group of Dipp are diastereotopic, which are labelled as C^{2,6}-CHMe_AMe_B and the SiMe$_3$ groups of each disyl groups are diastereotopic, which are labelled as C^{2,6}-CH(SiMe_3)$_A$(SiMe_3)$_B$.

Compound **25-SnSi** represents an unprecedented class of base-supported stannasilyne featuring multiple reactive sites for its functionalization, allowing for the exploration of its reactivity. A broad range of electrophilic and nucleophilic reagents was therefore screened. However, in most cases, including boranes, nitriles, alkynes,

CO, $CpCo(C_2H_4)_2$, $CpCo(CO)_2$, $IMe_2{}^iPr_2$ and MindGeBr the reactions either proceeded unselectively or failed entirely, highlighting the compound's divergent reactivity.

In an effort to explore alternative pathways, **25-SnSi** was treated with organic arylisocyanide in *n*-hexane under prolonged stirring at ambient temperature. The reaction progress was monitored by a distinct colour change of the solution from dark green to dark blue. ^{1}H NMR analysis of an aliquot in (D_6)benzene confirmed the complete consumption of the starting materials and the selective formation of **26-SnSi** (***Scheme 22***), wherein the DMAP ligand was replaced by Mes-NC, yielding an isocyanide-supported stannasilyne. A parallel reaction was conducted using sterically less demanding N-heterocyclic carbene IMe_4 under identical conditions, resulting in a similar colour transition. ^{1}H NMR spectroscopy in (D_6)benzene unequivocally confirmed the selective formation of the NHC-supported stannasilyne (**27-SnSi**) (***Scheme 22***), demonstrating the generality of this ligand substitution pathway. Both compounds were isolated in analytically pure form as dark blue solids in a 56% isolated yield after careful separation of DMAP at low temperature followed by filtration and crystallization from *n*-pentane at −30 °C. The highly air-sensitive solids **26-SnSi** and **27-SnSi** undergo immediate decolourization upon exposure to air. Both compounds exhibit good solubility in all common organic solvents, including *n*-hexane, Et_2O, toluene, benzene, and THF at ambient temperature. Thermal decomposition studies revealed that **26-SnSi** and **27-SnSi** decompose upon melting at 187 °C and 169 °C, respectively.

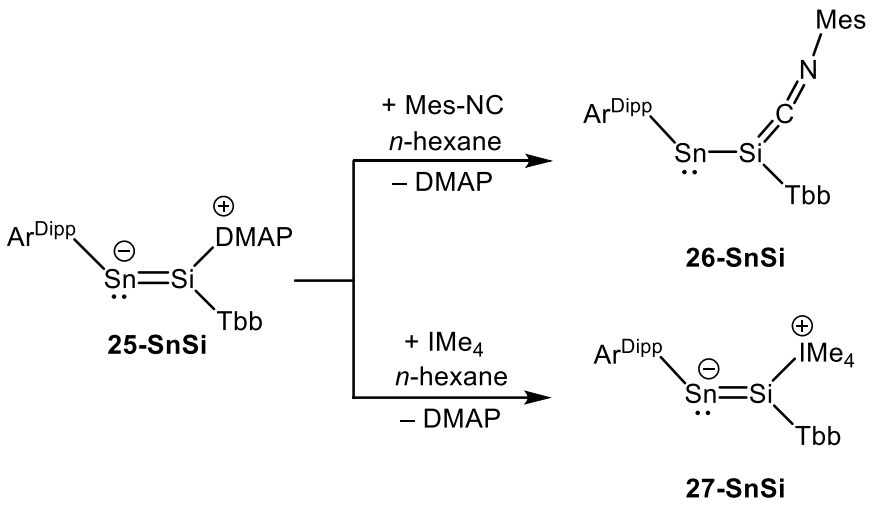

Scheme 22. Isolation of Mes-NC (**26-SnSi**) and IMe_4 (**27-SnSi**) supported stannasilyne.

Compounds **26-SnSi** and **27-SnSi** represent the first examples of an NHC and isocyanide base-supported stannasilyne. These complexes were comprehensively characterized using single-crystal X-ray diffraction (scXRD) analysis and multinuclear NMR spectroscopy. Suitable crystals (plate-shaped blue crystals of

26- SnSi and block-shaped dark-green crystals of **27-SnSi**·(**DMAP**) as the mono adduct with DMAP[5] for scXRD analysis were obtained by slowly cooling their respective saturated *n*-hexane solutions at −30 °C. Compound **26-SnSi**, crystallizes in the monoclinic space group $P2_1/c$ and **27-SnSi**·(**DMAP**) crystallize in the triclinic space group $P\bar{1}$. Both compounds exhibit nearly identical skeleton arrangement and possess a *pseudo*-C_s-symmetric structure in the solid state.

The molecular structures of **26-SnSi** and **27-SnSi** feature a *trans*-bent C^{ipso}–Sn–Si–C^{ipso} core, as evidenced by the torsion angles (φ(C32–Sn1–Si1–C1) = 177.15° (**26-SnSi**); −179.23°(**27-SnSi**)) (***Figure 57***). This arrangement positions the Sn–Si axis in a near-perfect orthogonal orientation relative to the central phenyl rings of the *m*-terphenyl substituent and the Tbb phenyl ring. The silicon center adopts a perfectly trigonal-planar geometry (Σ∢(Si) = 359.2(3)° (**26-SnSi**) and 359.7(2)° (**27-SnSi**)(***Figure 57***)), while the tin atom exhibits V-shaped coordination. The two tetrels are bonded by a robust Sn=Si double bond, with the overall architecture remaining isostructural with their precursor, **25-SnSi**, but exhibits notable variations in bonding metrics, reflecting the distinct σ-donor/π-acceptor properties of MesNC and IMe_4. For instance, the molecular structure of **26-SiSn** features a significantly elongated Si−Sn bond (2.516(1) Å) and a more acute bond angle at the dicordinated Sn center (101.8(1)°) compared to **27-SiSn** (2.475(1) Å and 113.3(1)°). Additionally, the notably short Si−$C^{isocyanide}$ bond (1.799(5) Å) in **26-SiSn** suggests a pronounced stannylene character, indicative of enhanced lone pair localization at Sn. Both **26-SnSi** and **27- SnSi** display elongated Si−Sn bonds (2.516(1) Å and 2.475(1) Å, respectively) relative to the only reported silastannene (^{t}Bu$_2$SiMe)$_2$Si=SnTip$_2$ (2.4188(4) Å),[295] further corroborating the weakening of the Si–Sn interaction due to base coordination at tricoordinated silicon. This trend underscores the influence of ligand electronics on bond perturbation, where MesNC (a weak π-acceptor) induces greater bond lengthening in **26-SiSn** compared to the more σ-donating IMe_4 in **27-SiSn**.

[5] The compound **27-SnSi** contains one molecule of DMAP in a crystal lattice in very close proximity to the IMe_4 unit in **27-SnSi**. This was confirmed by the scXRD measurement. In fact, all possible methods for separation of DMAP have remained unsuccessful so far.

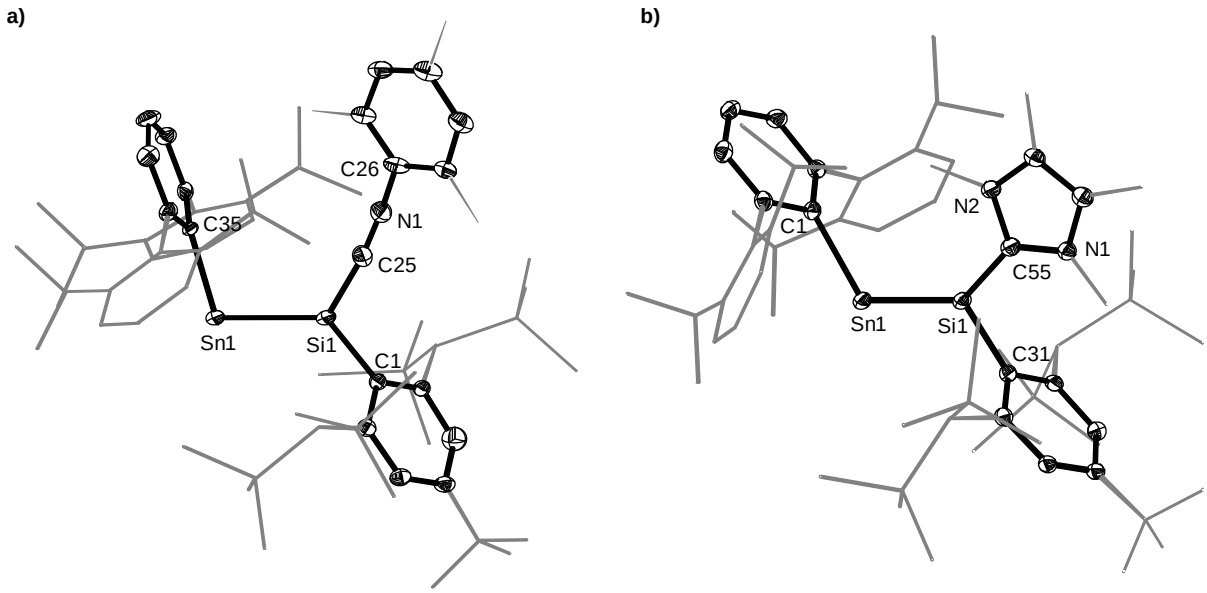

Figure 57. DIAMOND plot of the molecular structure of **26-SnSi** (***left***) and **27-SnSi** (***right***). Thermal ellipsoids are set at 30 % probability level. Hydrogen atoms are omitted and the Dsi and ^{t}Bu substituents of the Tbb ligand, Dipp Substituent of Ar^{Dipp}, Mes and IMe_4 are presented in wire-frame for clarity. Selected bond lengths [Å], bond angles [°] and torsion angle [°]: **a)** Sn1-Si1 2.5166(14), Sn1-C35 2.214(4), Si1-C1 1.901(5), Si1-C25 1.799(5), C25-N1 1.183(6), N1-C26 1.398(6), C35-Sn1-Si1 101.89(12), C1-Si1-Sn1 125.36(15), Sn1-Si1-C25 121.41(17), C1-Si1-C25 112.9(2), C35-Sn1-Si1-C1 177.15(1), C1-Sn1-Si1-C35 177.15; **b)** Sn1-Si1 2.4754(6), Sn1-C1 2.2517(19), Si1-C31 1.895(2), Si1-C55 1.888(2), C1-Sn1-Si1 113.37(5), Sn1-Si1-C31 116.56(6), Sn1-Si1-C55 138.90(6), C55-Si1-C31 104.54(8), C1-Sn1-Si1-C32 179.23.

Compound **26-SnSi** was further characterized by IR spectroscopy, which revealed a strong red-shifted ν(C≡N) band (2016 cm^{-1}, ***Figure 58***) compared to that of free MesNC (ν(C≡N) = 2114 cm^{-1} in THF). This significant shift strongly suggests substantial stannylene character in **26-SnSi** (***Figure 57***).

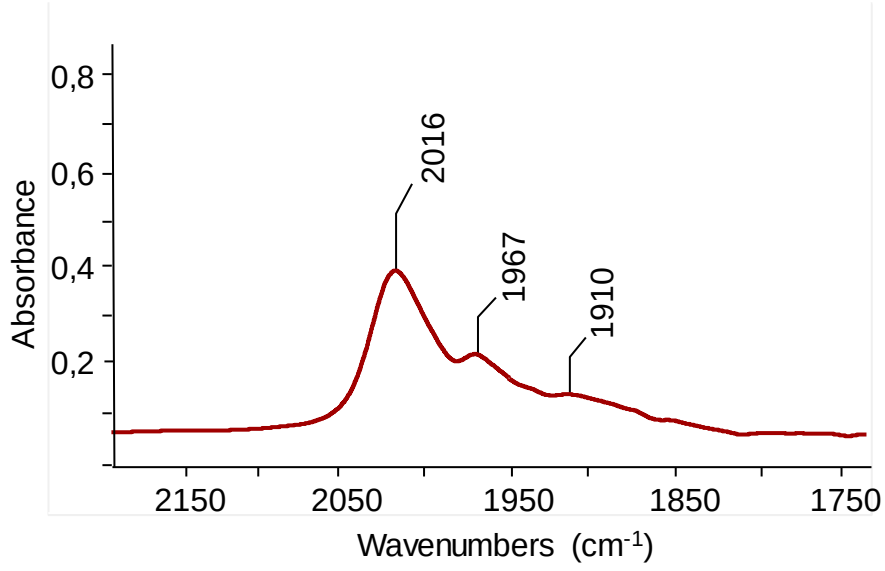

Figure 58. Solution state IR spectrum of **26-SiSn** in THF at 298 K.

The molecular structures of **26-SnSi** and **27-SnSi** possess a C_s-symmetry with the symmetry plane passing through the *trans-bent* C^{ipso}-Sn-Si-C^{ipso} core and bisecting the central phenyl ring of the *m*-terphenyl substituent (Ar^{Dipp}) and the phenyl ring of Tbb. This structural arrangement gives rise to the following topicity relationship: the Dipp groups of each Ar^{Dipp} are enantiotopic, the $C^{2,6}$ and $C^{3,5}$ positions of each Dipp are diastereotopic, the methyl groups of each isopropyl group are diastereotopic, the disyl groups are enantiotopic ($CH(SiMe_3)_2$) and the $SiMe_3$ groups of each disyl group are diastereotopic. Therefore, four doublets and two septet signals are expected for each Ar^{Dipp} group in the ^1H and ^{13}C NMR spectra. However, the solution ^1H and $^{13}C\{^1H\}$ NMR spectral features of **26-SnSi** and **27-SnSi** are in accordance with a higher local time average symmetry (C_{2v}) of the Ar^{Dipp} groups than that in the solid-state leading to a chemical equivalence of diastereotopic nuclei. The spectral features can be rationalized by the following chemical exchange process: a fast Ar^{Dipp}-rotation about the Sn−C^{ipso} bonds, a hindered rotation and rapid rotaion rotation about the Si−C^{ipso} bond on the NMR time-scale for **26-SnSi** and **27-SnSi** at ambient temperature respectively. Accordingly, the time averaged topicity relationship is assigned as follows: Dipp groups of each Ar^{Dipp} are homotopic, and the methyl groups of each isopropyl group of Dipp are diastereotopic, which are labelled as $C^{2,6}$-CHMe_AMe_B and the $SiMe_3$ groups of each disyl groups are homotopic.

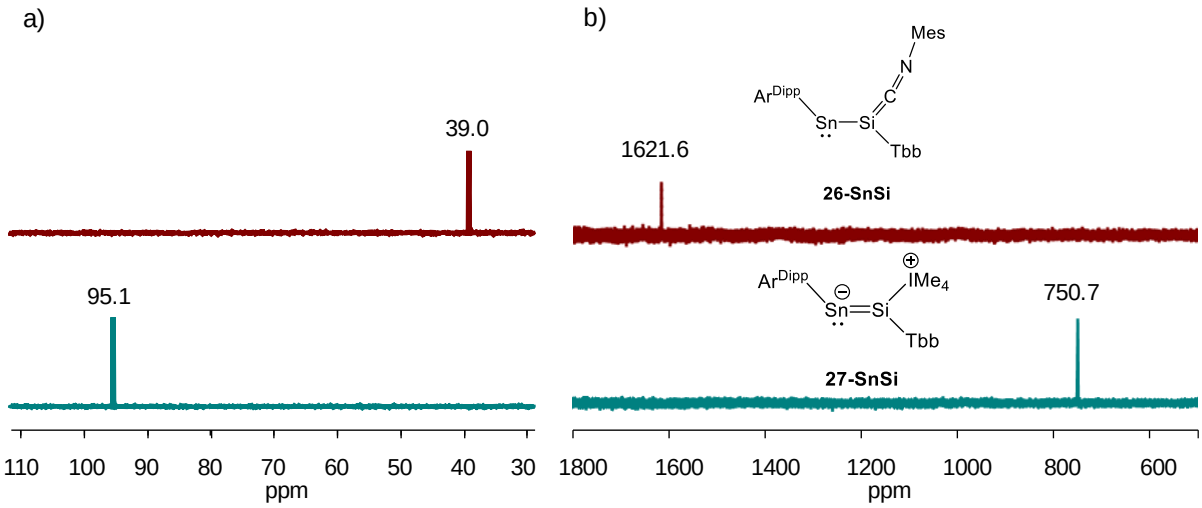

Figure 59. Stack plots of the selected exerpts of the $^{29}Si\{^1H\}$ (***left***) and $^{119}Sn\{^1H\}$ (***right***) NMR spectra of the coumpound **26-SnSi** (***top***) and **27-SnSi** (***bottom***).

Notably, compounds **25-SnSi**, **26-SnSi** and **27-SnSi** are distinguished by a ^{29}Si NMR signal for unsaturated Si at δ = 171.2, 39.00 and 95.10 ppm (***Figure 56*** *and* ***Figure 59***), respectively, which appears at lower field than those of the compound reported by Sekiguchi and coworkers ((^{t}Bu$_2$SiMe)$_2$Si=SnTip$_2$) (Tip = 2,4,6-triisopropylphenyl) (δ = 27.4 ppm).[295]

Table 3. A comparative assessment of selected structural and spectroscopic paramaters of base-supported silastannynes **25-SnSi**, **26-SnSi**, **27-SnSi** and literature known base-free and base-supported hetero/homo ditetrelynes.

Compound	d(E–E')/ (Å)[a]	φ(C^{i1}–E-E'–C^{i2}) (°)[b]	∢(C$^{i1/i2}$–E/E'–E/E') (°)[c]	Σ∢(E, E') (°)[d]	Φ (°)[e]	δ(^{29}Si) (ppm)	δ(^{119}Sn) (ppm)	*Ref.*
Ar^{Dipp}SnSi(DMAP)Tbb (**25-SnSi**)	2.458(1)	178.92(1)	105.7(1)	359.9(5)	3.85(1)	171.2	228.3	This work
Ar^{Dipp}SnSi(CN-Mes)Tbb (**26-SnSi**)	2.516(1)	177.15(2)	101.8(1)	359.2(3)	17.2(2)	39.0	1621.6	This work
Ar^{Dipp}SnSi(IMe$_4$)Tbb(**27-SnSi**)	2.475(1)	179.23(5)	113.3(1)	359.7(2)	1.85(7)	95.1	750.7	This work
Ar^{Dipp}SnGeAr^{Dipp}(**28**)	2.472(1)	179.97(3)	127.2(2)	–	–	–	182.6	[169]
(SIDipp)Si(Br)GeTbb(**15-SiGe**)	2.272(2)	176.73(1)	101.3	359.9(2)	3.6487(5)	48.2	–	[296]
(SIDipp)Si(Br)SnTbb(**17-SiSn**)	2.493(7)	161.81(1)	98.7	357	3.9(5)	63.5	378.6	[336]
(SIDipp)SiGe(Me)Tbb(**18-SiGe**)	2.219(2)	178.81(1)	99.46(1)	359.6(2)	95.14(3)	67.9	–	[336]
(Tbb)SiSi(Tbb)	2.105(2)	178.41	131.42(9)	–	–	16.2		[43]
Ar^{Dipp}SnSnAr^{Dipp}	2.6675(4)	3.2	125.24(7)	–	–	–	383.1	[35]

a: E = E'; for homoditetrelynes and E ≠ E' for heteroditetylynes; b: *i*1 represents the *ipso*-carbon of E bonded substituents and *i*2 represents the *ipso*-carbon of E' bonded substituents; c: angle at thedicoordinated tetrel center; d: Sum of bond angles at tricoordinated tertrel center; e: Φ defines the torsion angles of the mean planes defined by homo/hetero-ditetrelynes core (by atoms C^{i1}, E, E' and C^{i2}) and central ring atoms of coordinated ligand

Compounds **25-SnSi**, **26-SnSi** and **27-SnSi** were also characterized by UV-Vis-NIR spectroscopy (***Section 5.4,*** *Page 253*). Dark-green solution of **25-SnSi** in *n*-hexane at ambient temperature displays one intense absorption band at λ = 299 nm (ε_λ = 1.7578 × 10^4 L·mol^{-1}·cm^{-1}), a weaker band at λ = 533 nm (ε_λ = 2.744 × 10^3 L·mol^{-1}·cm^{-1}) as well as shoulders at λ = 767 nm (ε_λ = 8.808 × 10^3 L·mol^{-1}·cm^{-1}), λ = 678 nm (ε_λ = 6.174 × 10^3 L·mol^{-1}·cm^{-1}) and λ = 432 nm (ε_λ = 4.507 × 10^3 L·mol^{-1}·cm^{-1}) (***Figure 88****, Page 254*), Dark-blue solution of **26-SnSi** in *n*-hexane at ambient temperature displays one intense absorption band at λ = 292 nm (ε_λ = 1.6069 × 10^4 L·mol^{-1}·cm^{-1}), a weaker band at λ = 502 nm (ε_λ = 1.997 × 10^3 L·mol^{-1}·cm^{-1}) as well as shoulders at λ = 670 nm (ε_λ = 7.029 × 10^3 L·mol^{-1}·cm^{-1}), λ = 574 nm (ε_λ = 2.555 × 10^3 L·mol^{-1}·cm^{-1}), λ = 378 nm (ε_λ = 1.4431 × 10^4 L·mol^{-1}·cm^{-1}) and λ = 332 nm (ε_λ = 8.405 × 10^3 L·mol^{-1}·cm^{-1}) (***Figure 91****, Page 256*) and Dark-blue solution of **26-SnSi** in *n*-hexane at ambient temperature displays one intense absorption band at λ = 326 nm (ε_λ = 1.0407 × 10^4 L·mol^{-1}·cm^{-1}), a weaker band at λ = 400 nm (ε_λ = 2.648 × 10^3 L·mol^{-1}·cm^{-1}) as well as shoulders at λ = 614 nm (ε_λ = 9.146 × 10^3 L·mol^{-1}·cm^{-1}), λ = 544 nm (ε_λ = 3.201 × 10^3 L·mol^{-1}·cm^{-1}), and λ = 456 nm (ε_λ = 5.128 × 10^3 L·mol^{-1}·cm^{-1}) (***Figure 94***, *Page 258*).

2.4. Quest for base free Germyne / Silyne

2.4.1 Introduction

Alkynes, organic compounds featuring a carbon-carbon triple bond, are highly versatile in forming a wide range of functional groups and structures. Replacing the triple-bonded carbons with heavier group 14 elements (Si–Pb; ***Figure 60***) yields homonuclear analogues like disilyne,[36,206] digermyne,[34] distannyne,[35] and diplumyne [33] (R_1–E≡E–R_2). Pioneering work by Power,[33,34,35] Sekiguchi [36] and Wiberg [206] isolated these compounds, revealing unique *trans*-bent geometries due to the second-order Jahn-Teller (SOJT) effect.[11,248,297,298] This distortion results in slipped π-bonds and amphiphilic reactivity, enabling interactions with small molecules.[11,13,20,41,167,274,299,300,301]

By substituting one carbon atom in alkynes with a heavier group 14 element, their heteronuclear analogues silynes, germynes, stannynes, and plumbynes (R^1–C≡E–R^2, E = Si–Pb; ***Figure 60***) are obtained. Theoretical studies indicate that, like their homonuclear counterparts (R^1–E≡E–R^2), these R^1–C≡E–R^2 compounds adopt a *trans*-bent geometry about the core triple bond. [208–210,302–305] However, their isolation necessitates stabilization by Lewis bases. A significant synthetic challenge arises from the thermodynamically favoured isomerization of R^1–C≡E–R^2 to the corresponding 1-tetrelavinylidene R^1R^2C=E species, particularly when R^1 and R^2 are small substituents.[208–210,302–305]

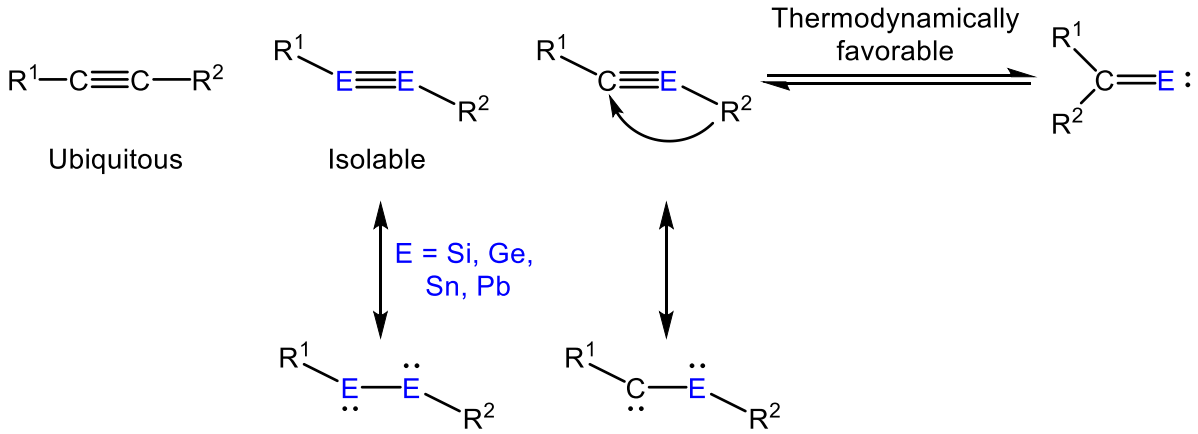

Figure 60. Comparative illustration of alkynes and their heavier group 14 congners.

To date, the only neutral R^1–C≡E–R^2 species characterized structurally below −30 °C are the base-stabilized silyne **I-79**[223] and two germynes **I-80**[306], reported over a decade ago (***Figure 61***). These compounds undergo intramolecular rearrangement reactions above this temperature threshold.[233,306] More recently, a cationic silyne (**I-**

81)[224] stabilized by a Lewis base was isolated, exhibiting moderate stability at room temperature ($t_{1/2}$ = 7 days in THF). In contrast, plumbynes remain elusive, even with Lewis base stabilization. UV–vis spectroscopic evidence suggests the transient formation of stannyne **I-83**[307] during low-temperature photolysis (−196 °C) of its diazo precursor, but this species is highly reactive at room temperature, precluding direct observation.[307,308] These observations highlight the pronounced instability of these compounds under ambient conditions. Liu group recently reported the isolation of base-free stannyne (R^1-C≡Sn-R^2)(**I-72**, ***Figure 26***)[225] at room temperature, achieved through the strategic use of a bulky cyclic phosphino ligand in combination with a bulky terphenyl substituent.

Landmark studies, including the work reported by Bertrand *et. al.* [309], as well as more recent investigations by the Liu group[225,310] and others,[310,311] have demonstrated the exceptional utility of phosphinodiazomethyl anion salts as versatile synthons for transferring singlet carbyne anion (R–C⁻) fragments to both main-group and transition-metal centers. This reactivity has enabled the synthesis of unusual species, including singlet carbenes (**I-78**) and carbyne complexes (**I-79**–**I-82**, ***Figure 61***). Liu group in their earlier work, reported the isolation of a copper phosphinocarbyne anion complex (**I-82**) using a sterically demanding phosphino substituent, [310] and transient stannyne **I-83**.[307]

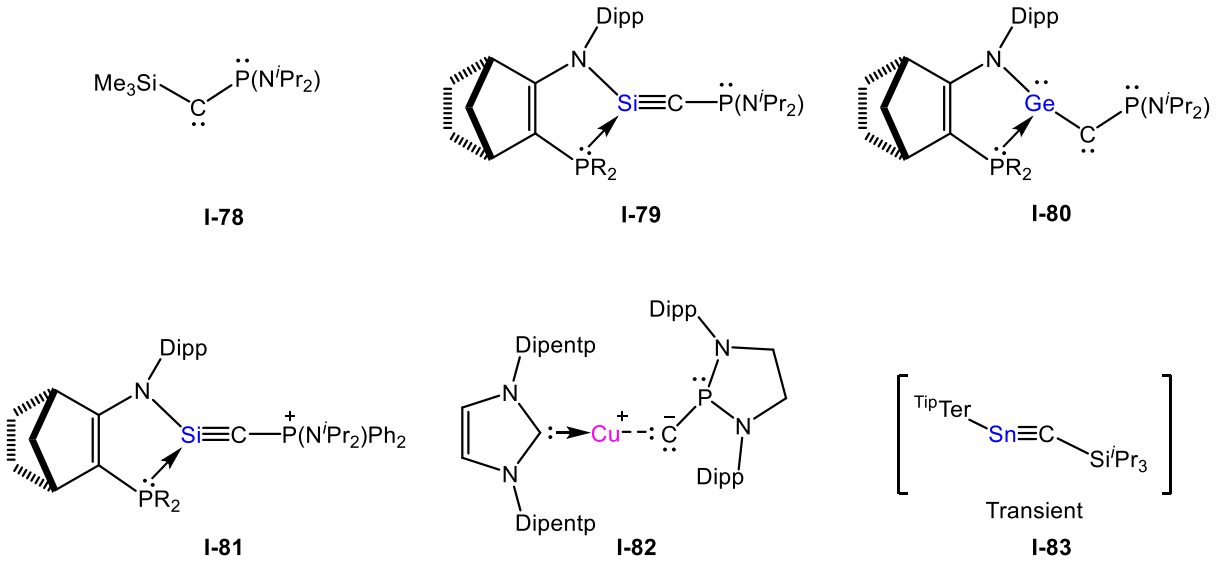

Figure 61. A selection of known compounds: singlet carbene **A**, base-stabilized silynes **B** and **D**, base-stabilized germynes **C**, copper carbyne anion complex **E** and transient stannyne **F**. PR_2 = $P(N^tBu)_2SiMe_2$ or $P(N^iPrCH_2)_2$; ^{Tip}Ter = 2,6-Tip_2-C_6H_3 (Tip = 2,4,6-^{i}Pr$_3$-C_6H_2); Dipp = 2,6-diisopropylphenyl; Dipentp = 2,6-di-(3-pentyl)phenyl.

2.4.2 Synthesis and characterization of η^1-N-bound diazomethanide complex

Our investigation into this field begins with the strategic design of a sterically encumbered diazomethane precursor to achieve enhanced stability and control over-reactivity. To this end, we synthesized a Tbb-substituted diazomethane derivative **28**, featuring a sterically demanding Tbb substituent at the carbon center. This compound was efficiently prepared by treating a Tbb-functionalized tosylhydrazone with sodium in THF under ambient conditions. Upon stirring at room temperature for one hour, the reaction mixture underwent a rapid colourimetric transition from yellow to orange, indicative of diazo compound formation. Quantitative conversion to **28** was unequivocally confirmed by ^{1}H NMR spectroscopic analysis in (D_6)benzene, while IR spectroscopy revealed a characteristic $\nu(CN_2)$ stretching frequency at 2055 cm^{-1} in THF. The crude mixture was subsequently concentrated *in vacuo*, and the residue was extracted with *n*-hexane. Crystallization from *n*-hexane afforded **28** as an orange-brown precipitate, which was isolated *via* filtration at −60 °C in an exceptional 96% yield (***Scheme 23***). After successful isolation, compound **28** was deprotonated using LDA in diethyl ether at −60 °C, generating the corresponding lithium diazomethanide complex **29** as a light-yellow solid (***Scheme 23***). A new $\nu(CN_2)$ IR absorption was observed at 1989 cm^{-1} in THF, which corroborated the formation of lithium diazomethanide complex, particularly evident by the lowering in the stretching frequency because of diminishing or reducing percentage contribution of the ylide form. To ensure stability, **29** was stored under an inert atmosphere at low temperatures, thereby mitigating decomposition and preserving its utility for subsequent transformations.

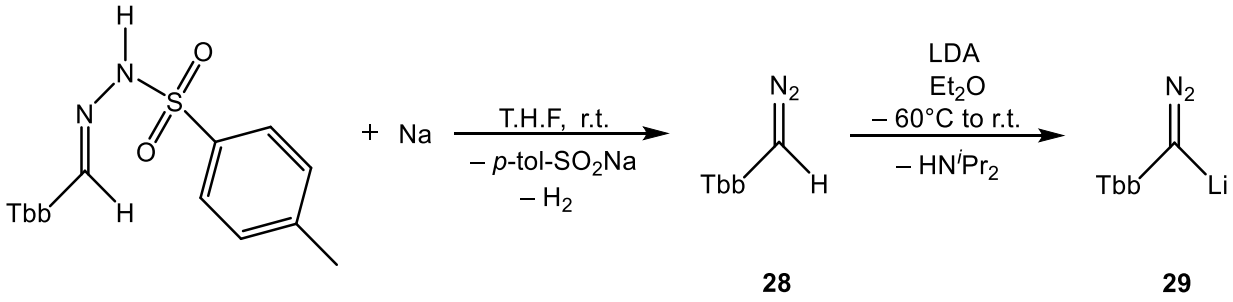

Scheme 23 Synthesis of sterically encumbered Tbb-diazomethane precursor (**28**) and diazomethanide complex of Li (**29**).

Following the isolation of lithium diazomethanide (**29**), the compound was immediately subjected to a reaction with halotetrylenes. Specifically, a yellow-orange *n*-pentane solution of *(E)*-(Tbb)BrGe=GeBr(Tbb) was added to a suspension of lithium diazomethanide, **29** in *n*-pentane at ambient temperature. The reaction proceeded

instantaneously, as evidenced by a distinct colour change from yellow to yellow-brown, indicative of new product formation. Initial characterization *via* ^{1}H NMR spectroscopy of an aliquot in (D_6)benzene confirmed the quantitative formation of the product, **30-Ge** (***Scheme 24***) alongside minor Tbb-containing impurities. After workup, including purification by crystallization from *n*-pentane at −30 °C, yellow-brown crystals of **30-Ge** were obtained *via* cold filtration at −30 °C. This procedure yielded **30-Ge** in acceptable purity with an isolated yield of 46%, reflecting moderate efficiency, likely due to competing side reactions or solubility limitations during crystallization. The compound is a moisture-sensitive brown solid exhibiting good solubility in ethereal solvents (Et_2O and THF), aliphatic hydrocarbons (*n*-hexane and *n*-pentane), and aromatic solvents (benzene and toluene) at ambient temperature. Clear prismatic-shaped light-orange coloured single crystals of **30-Ge** were obtained *via* slow cooling of a saturated *n*-pentane solution at −30 °C.

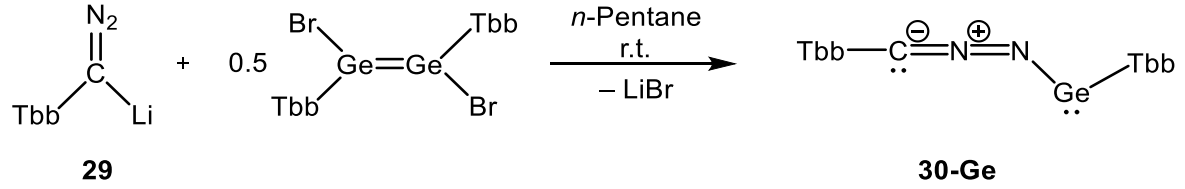

29 **30-Ge**

Scheme 24. Synthesis of η^1-N-bound diazomethanide complex of Ge (**30-Ge**).

Thermal decomposition studies of **30-Ge**, performed in *vacuum*-sealed glass capillaries, demonstrated that compound decomposes upon melting at 198 °C. Analysis of the soluble part of the respective melting residue in (D_6)benzene by ^{1}H NMR spectroscopy revealed unselective decomposition of **30-Ge**.

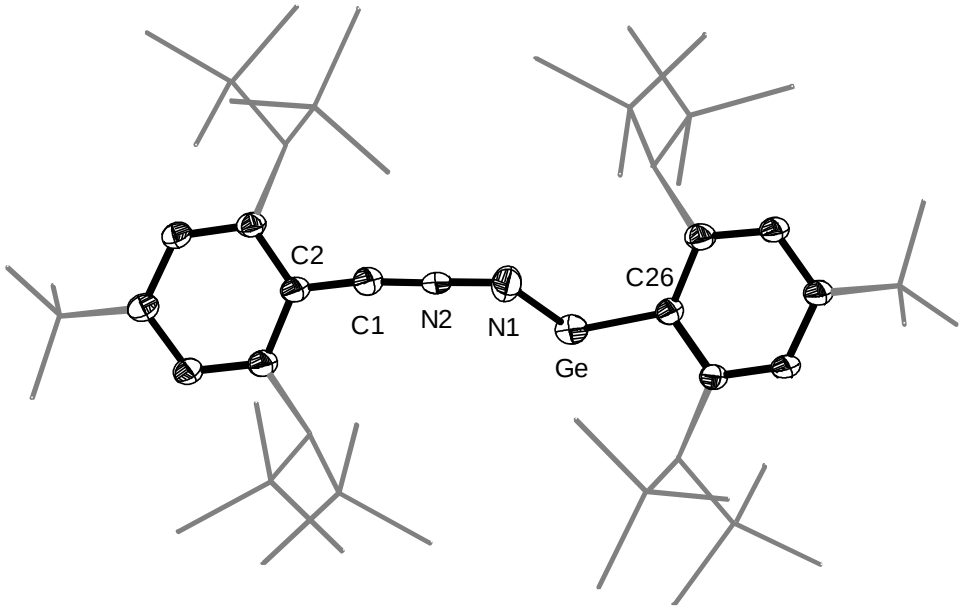

Figure 62. DIAMOND plot of the molecular structure of **30-Ge**. Thermal ellipsoids are set at 30 % probability level. Hydrogen atoms are omitted and the Dsi and ^{t}Bu substituents of the Tbb ligand are

presented in wire-frame for clarity. Selected bond lengths [Å], bond angles [°]: C1-C2 1.330(15), C1-N2 1.235(16), N2-N1 1.266(14), N1-Ge 1.838(10), Ge-C26 2.006(5), C2-C1-N2 172.1(11), C1-N2-N1 179.1(11), N2-N1-Ge 115.2(8), N1-Ge-C26 96.6(3).

The molecular structure of **30-Ge** (***Figure 62***) exhibits a rare η^1-N-bound diazomethanide complex coordinated to a Ge center. Such coordination is typically stabilized by transition metals [312,313] or alkali metals.[310] It features: (a) a nearly planar C_2–C_1–N_2–N_1 core (φ = 176.85°), bonded to a bent, dicoordinated germanium center ($\angle N_1$–Ge–C_{26} = 96.64(1)°), indicative of enhanced germylene character; (b) the orientation of sterically demanding Tbb substituents is trans as evidenced by torsion angle (φ = 179.19°); (c) a slightly elongated C1−C2 bond (1.330(4) Å), consistent with C^{sp2}=C^{sp2} character, suggesting delocalization within the ring.[228]

In solution, the ^{1}H and $^{13}C\{^1H\}$ NMR spectra of **30-Ge** in (D_6)benzene are well corroborating its C_S-symmetric structure. Free rotation around the C–C^{Tbb} and Ge–C^{Tbb} bonds on the NMR timescale is evident, as is the presence of distinct singlets for the enantiotopic Si*Me*$_3$ groups on each Tbb substituent. The $^{13}C\{^1H\}$ NMR spectrum of **30-Ge** exhibits a broad signal at δ = 87.56 ppm for the diazomethanide carbon, which is significantly deshielded compared to **28** (δ = 39.83 ppm) and **29** (where the signal was too broad to be observed). **30-Ge** converted into its activated product after standing (D_6)benzene solution at ambient temperature for three days, and the compound was also treated with UV light, showing unselective decomposition as per ^{1}H NMR spectrum.

2.4.3 Chemistry of Phosphino(silyl)carbene with low valent tetrel compounds

Parental carbene CH_2 possesses a natural triplet ground state with a considerable energy separation between triplet and singlet state ($\Delta E_{S\rightarrow T}$ = 9.05 kcal/mol). Due to its intrinsic high reactivity, it can only be isolated under matrix conditions or trapped at low temperatures. The nature of the substituents installed on the dicooordinated carbon highly influences the nature of the natural ground state and their energy separation. Taking advantage of substituents, Ardeungo and coworkers successfully isolated the first crystalline cyclic diamino carbene in 1991 in a singlet ground state. The aforementioned conceptualization of introducing heteroatom/substituents also unveils the isolation of a wide variety of cyclic and acyclic carbenes.[314,315] These stable singlet ground state carbene can be categorized into the following class, based on the electron-donating or accepting nature of their substituents (***Figure 63***): (a) Push-Pull carbenes (**A**) having electron-donating and withdrawing substituents. Carbenes **A** have quasi-linear geometry at the dicoordinated carbon and exhibits a

polarized allene-type resonance hybrid, resulting from the interaction of the lone pair of the electron-donating group (D) with the carbene carbon-centered vacant p-orbital and subsequent interaction of the filled lone-pair electron density of carbene carbon to the vacant orbital on the electron-withdrawing group (W) with appropriate symmetry. The most striking example of this class of carbenes are (phosphino)(silyl)carbenes[316,309] (b) Push-Push carbenes (**B**) having both electron-donating substituents and demonstrate noticeable bending at the carbene carbon. The competitive π-conjugation from the lone pair of the D substituents leads to a polarized (3c-4e) out-of-plane π-cloud. The representative carbenes of this class are diaminocarbenes,[317] (c) Push-Spectator carbenes (**C**), possessing only one strong electron-donating substituents which also causes significant bending at the carbene carbon. Nevertheless, cyclic(alkyl)(amino)carbenes (CAAC) and its phosphorus analogue cyclic(phosphino)(alkyl)carbenes reported by Bertrand and coworkers are astonishing examples of this class.[318]

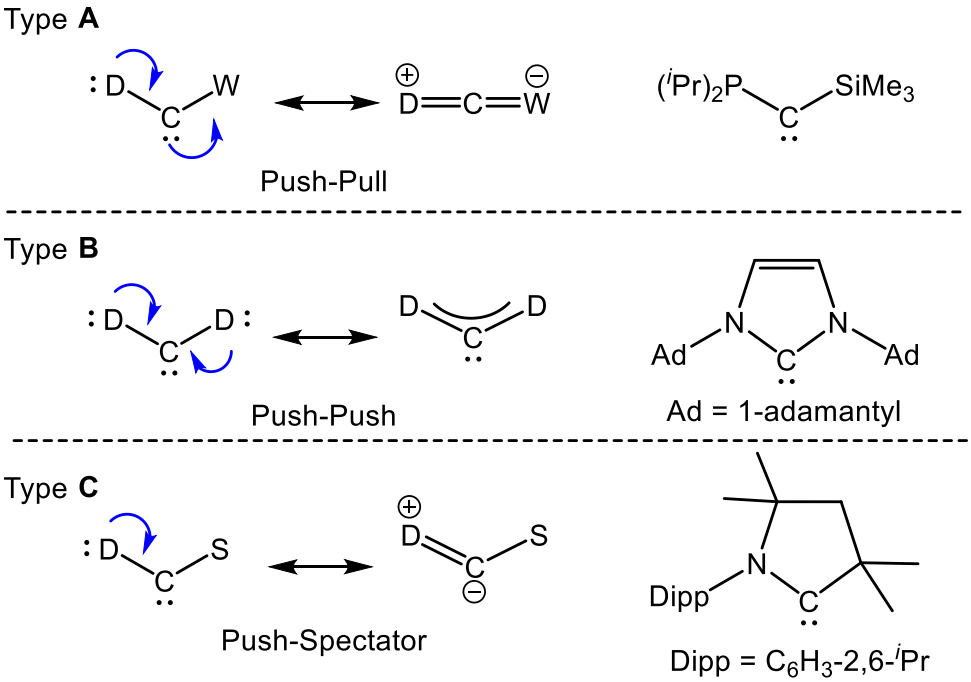

Figure 63. Electronic effects of the substituents in carbenes **A–C**. D = electron-donating group; W = electron-withdrawing group; S = spectator group.

Diazo compounds of the class $R_1R_2C{=}N_2$ (diazoalkanes) have proven their rich chemistry as a pivotal reagent in organic and organometallic chemistry thanks to their diverse reactivity profile and promising precedented for functionalization. Foremost, photo- or thermal-induced dinitrogen liberation from diazo compounds is considered a more synthetically appealing pathway for in situ carbene generation and has witnessed a renaissance in contemporary molecular chemistry. Recently, Liu and

coworkers demonstrated the synthetic applicability of sterically encumbered diazoalkane [{(NDippCH$_2$)$_2$P}(SiMe$_3$)C=N$_2$][311] *via* introducing sterically encumbered phosphino and silyl groups (Push-Pull carbene type **A**; ***Figure 63***), which suppress undesirable dimerization. The discussed diazoalkane [{(NDippCH$_2$)$_2$P}(SiMe$_3$)C=N$_2$] could demonstrate its synthetic versatility due to the presence of a labile silyl group at the carbene center and act as a carbyne equivalent. The strong σ-donation ability of carbenes to stabilize novel low-coordinate open and closed-shell complexs is well established. Based on these findings, we speculated a synthetic strategy to access the tetrelenes {(NDippCH$_2$)$_2$P}(SiMe$_3$)C=E(X)R *via* synergetic coordination of amphiphilic (halo)(aryl)tetrylenes R(E)X (E = Si – Pb) to Push-Pull carbene (type **A**) (***Scheme 25***). Intriguingly, conceptualized tetrelenes could undergo thermally or base-induced elimination (α,β-SiMe$_3$X elimination; X = F – I) to afford the long-standing and so far *in-silico* studied tetrylynes {(NDippCH$_2$)$_2$P}C≡E(R) (***Scheme 25***).

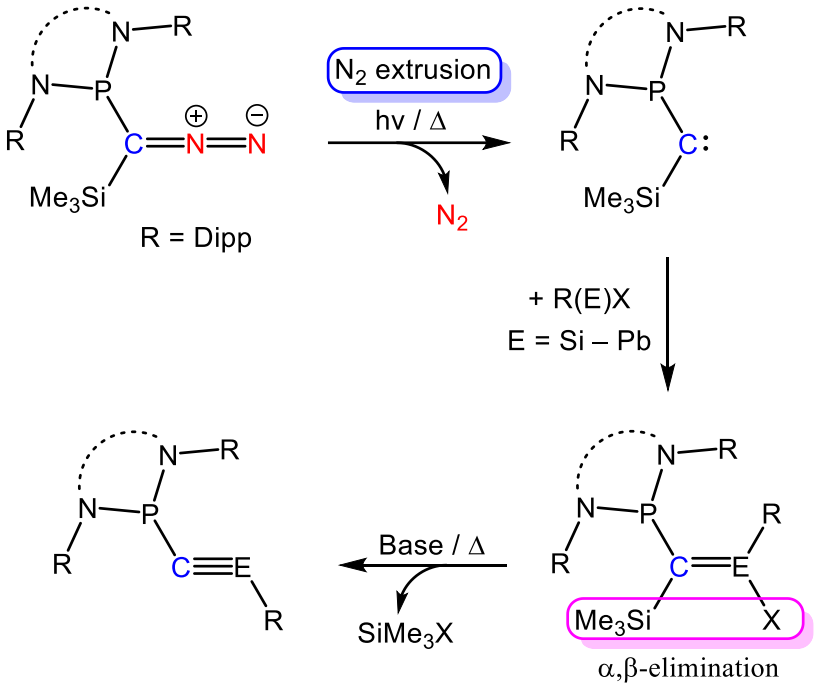

Scheme 25. Speculated scheme for the synthesis of tetrelynes.

In the pursuits of synthesizing tetrelynes, the aforementioned push-pull carbene (NDippCH2)$_2$P(SiMe$_3$)C: was selected as a suitable starting material which can be isolated in pure form as an off-white solid by heating its diazo precursor at 80 °C for 2 hours in the benzene. The addition of Ge$_2$Br$_2$(R)$_2$ (R = Tbb and Mind) to a light-yellow solution of carbene in *n*-hexane at ambient temperature was accompanied by an instantaneous intensification of colour from light-yellow to dark-yellow. Analysis of the reaction solution by ^{1}H and ^{31}P{^{1}H} NMR spectroscopy revealed the selective formation of anticipated products **31-Ge** and **32-Ge** (***Scheme 26***). Work-up and crystallization from *n*-pentane led to the isolation of **31-Ge** as *n*-pentane solvate **31-**

Ge·(*n*-pentane)$_{1.5}$ and **32-Ge** as analytically pure yellow solids in 70 % and 72 % yield, respectively. Both compounds are extremely air- and moisture-sensitive but thermally robust ($T_{melt.}$ = 150 °C for **31-Ge** and $T_{melt.}$ = 207 °C for **32-Ge**), solids turning immediately colourless upon contact with air. Both compounds are well soluble in *n*-pentane, toluene, benzene and Et_2O at ambient temperature.

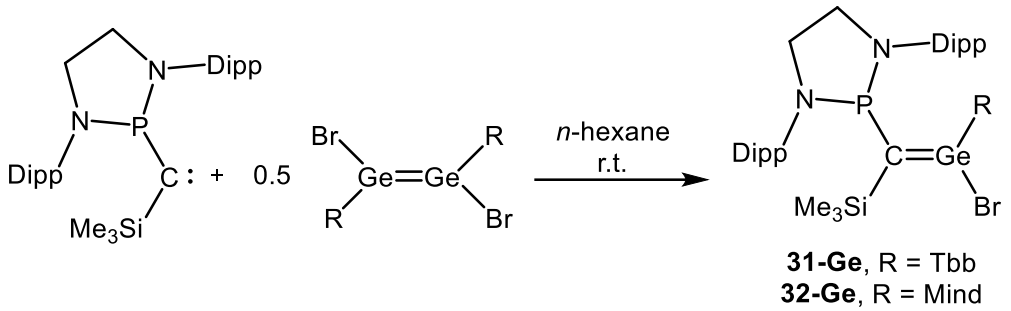

Scheme 26. Synthesis of **31-Ge** and **32-Ge** from Push-Pull type **A** carbene.

Clear block-shaped yellow crystals were obtained of **31-Ge** and **32-Ge** from a saturated solution of *n*-pentane and *n*-hexane upon slow cooling at −30 °C respectively, where **32-Ge** crystallized as hemi-solvate of *n*-hexane **32- Ge·(*n*- hexane)$_{0.5}$**. X-ray diffraction analysis revealed that **31-Ge** crystallizes in the monoclinic space group $P2_1/n$ and **32-Ge** crystallizes in the orthorhombic space group $Pna2_1$ and possesses a *pseudo*-C_S-symmetric structure in the solid state (***Figure 64***).

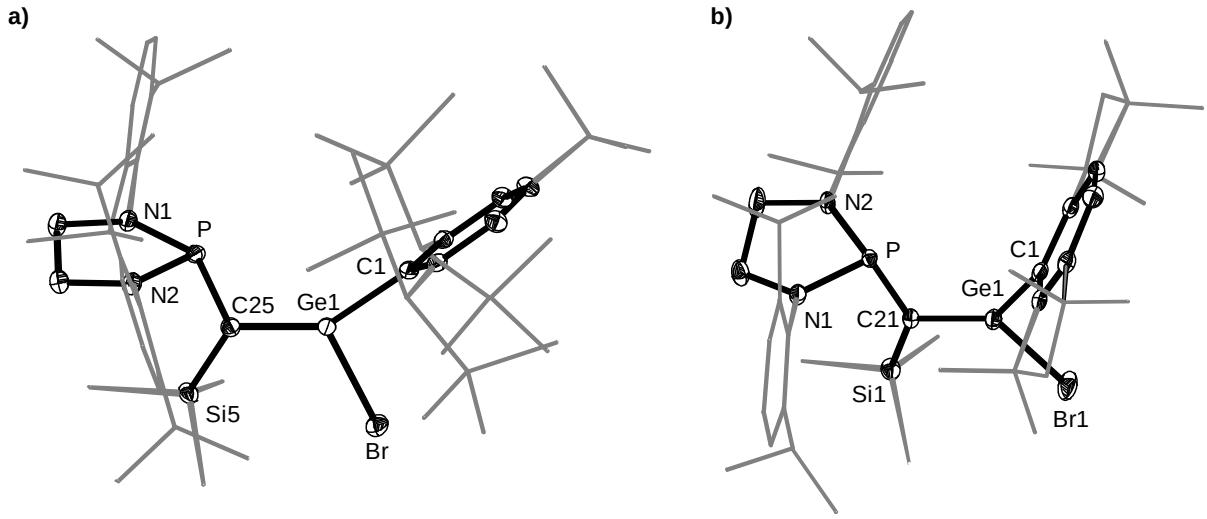

Figure 64. DIAMOND plot of the molecular structure of **31-Ge** (***left***) and **32-Ge** (***right***). Thermal ellipsoids are set at 30 % probability level. Hydrogen atoms are omitted and the Dsi and ^{t}Bu substituents of the Tbb and Dipp Substituent of NHP ligand are presented in wire-frame for clarity. Selected bond lengths [Å], bond angles [°] and torsion angle [°]: **a)** C25-Ge1 1.1889(16), C25-P 1.8372(17), C25-Si5 1.8948(17), Ge1-Br 2.3358(2), C1-Ge1 1.9500(16), C25-P-N1 104.01(7), C25-P-N2 108.74(7), C25-Ge1-Br 112.39(5), C1-Ge1-Br 103.19(5), Ge1-C25-Si5 117.35(8), Ge1-C25-P 109.33(8), P-C25-Ge1-C1 −18.92; **b)** C21-Ge1 1.806(4), C21- Si1 1.880(4), C21-P 1.824(4), Ge1-Br1 2.3210(6), Ge1-C1 1.939(4), P-N1 1.739(3), P-N2 1.722(3), P-C21-Ge1 103.63(18), P-C21-Si1 137.4(2), Si1-C21-Ge1 118.9(2), C21-

Ge1-C1 134.66(16), C1-Ge1-Br1 108.11(11), C21-P-N1 107.49(18), C21-P-N2 107.57(17), P-C21-Ge1-C1 −0.11(1).

The molecular structures of compounds **31-Ge** and **32-Ge** are isostructural and reveal nearly similar bonding matrices. Nearly trigonal planar central carbon (C^{cent}) ($\Sigma\measuredangle(C)$ = 359.76° (**31-Ge**), $\Sigma\measuredangle(C)$ = 359.79° (**32-Ge**)) are bonded to the trigonal planar germanium centers ($\Sigma\measuredangle(Ge)$ = 359.41°, $\Sigma\measuredangle(Ge)$ = 359.97°) *via* a Ge=C double bond (*d*(Ge=C) = 1.8189(16) Å) (**31-Ge**); (1.824(4) Å (**32-Ge**)). These structural features are in good agreement with the naturally polarized germenes, possessing a trigonal planar core carbon C^{cent} and germanium center as well as a naturally polarized $Ge^{(\delta+)}$–$C^{cent(\delta-)}$ double bond.[319] The sterically demanding NHP and aryl substituents (Tbb and Mind) are arranged in a *cis*-orientation with torsion angles (P^{NHP}–C^{cent}–Ge–C^{ipso}) φ of −18.92° (**31-Ge**) and −0.11(1)° (**32-Ge**). Notably, the NHP phosphorus atom in both derivatized germaethenes (**31-Ge** and **32-Ge**) is markedly pyramidalized ($\Sigma\measuredangle(P)$ = 302.79° (DP = 64%) (**31-Ge**); $\Sigma\measuredangle(Ge)$ = 304.55° (DP = 62%) (**32-Ge**)), suggesting no considerable delocalization of the P-centered lone pairs to the π* of C^{cent}=Ge. This is also reflected in the P^{NHP}–C^{cent} bond length (1.8372(17) (**31-Ge**) and 1.82(4) (**32-Ge**)), which compares well with the typical P–C single bond length. Notably, P^{NHP}–C^{cent} bond lengths are considerably elongated than the literature known bent germaphospha allene.[306]

Table 4. Selected structural and spectroscopic parameters of **31-Ge**, **32-Ge**, and literature known germaethenes and base-supported germyne.

Compound	*d*(Ge–C^{cent}) (pm)	$\Sigma\measuredangle(C^{cent})$ (°)	$\Sigma\measuredangle(Ge)$ (°)	$\delta(^{31}P)$ (ppm)[c,d]	*Ref.*
(NHP)($SiMe_3$)C=GeBr(Tbb)(**31-Ge**)	181.8(2)	359.8	359	100.6[c]	This work
(NHP)($SiMe_3$)C=GeBr(Mind)(**32-Ge**)	182.4(4)	359.8	360	105.8[c]	This work
$(SiMe_3)_2C(B^tBu)_2C$=Ge($N(SiMe_3)_2)_2$	182.7(4)	359.2	360	–	[319]
2-(R_1)-3-(R_2)GeCP($N^iPr_2)_2$[a]	188.7(5)[b]	–	299	82.1[d,e]	[306]
TbtTipGe=C{*cyclo*-$(S)_2$GeTbtTip}	177.0(2)	360	360	–	[320]

a: R_1 = ($P(N^tBu)_2SiMe_3$) and R_2 = ((Dipp)N-(norborane); b: dicoordinated carbon atom bonded to phosphino-base supported germanium center; c: (D_6)benzene, 298 K; d: (D_8)THF, 213 K; e: The ^{31}P signal corresponds to the dicoordinated carbon bonded phosphorous center.

The ^1H and $^{13}C\{^1H\}$ NMR spectra of **31-Ge** and **32-Ge** indicate a time-averaged C_s-symmetric structure in solution, akin to their solid-state. The Ge–C^{ipso} rotation is frozen out on the NMR time scale for both germaethenes, as clearly evident by the two signals observed for the diastereotopic $SiMe_3$ and four doublets for the Dipp

substituents of the NHP group in the case of **31-Ge** and the Mind derivative, which replicate the same symmetry pattern. Notably, $^{31}P\{^{1}H\}$ NMR of both compounds exhibit a sharp singlet at nearly similar chemical shift $\delta(^{31}P)$ = 100.6 ppm (**31-Ge**) and 105.8 ppm (**32-Ge**) (***Figure 65***), which is slightly low-field shifted then then literature know phosphino-supported germyne 2-(R_1)-3-(R_2)GeCP(N^iPr_2)$_2$ (R_1 = (P(N^tBu)$_2$$SiMe_3$) and R_2 = ((Dipp)N-(norborane)) $\delta(^{31}P)$ = 82.1 ppm ((D_8)THF, 213 K) despite of having significant triple bond character between core carbon and germanium center.[306]

As discussed above, isolated gemaethens **31-Ge** and **32-Ge** could be promising precursors for the synthetic accessibility of so far unknow base-free tetrylynes in heating or photochemical conditions. Molecular structures of germaethenes also reveal the *synclinical*-conformation of the silyl ($SiMe_3$) and Br group and pre-indicate the concomitant formation of $SiMe_3Br$. However, prolonged heating of toluene solutions of germaethenes **31-Ge** and **32-Ge** under an argon condition only leads to the formulation of a complicated mixture of products. Unfortunately, the low intensity of the colour of discussed germaethenes (**31-Ge** and **32-Ge**) does not allow for the precise determination of the nature of radiation required for the photolytic generation of tetrylynes.

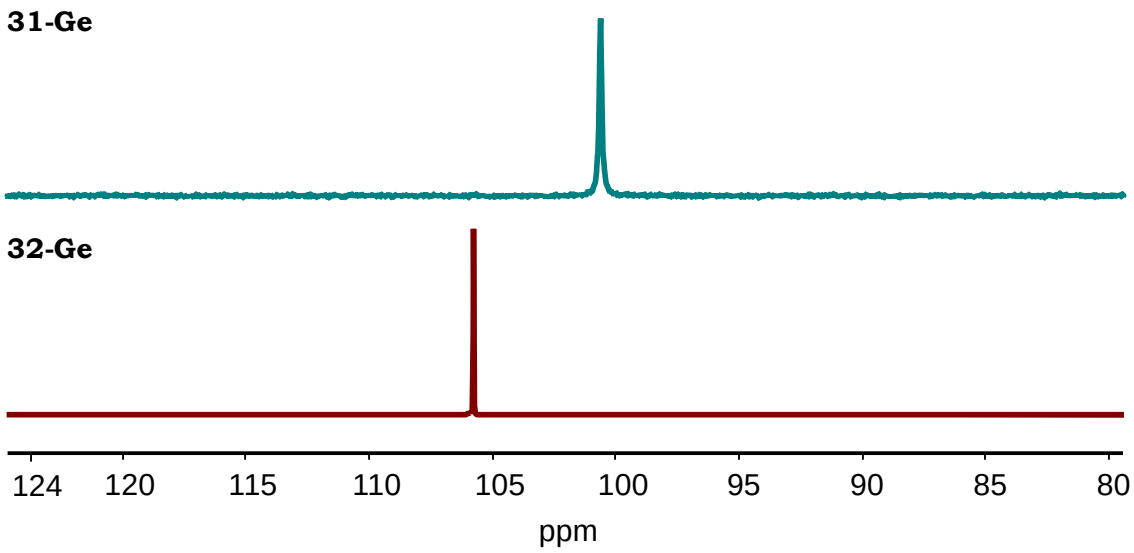

Figure 65. A stack plot of the selected excerpt of the $^{31}P\{^{1}H\}$ NMR spectra of the compounds **31-Ge** and **32-Ge** in (D_6)benzene.

Aforementioned, carbene was later treated with base-supported Si(II) precursors (for instance, $SiBr_2$(SIDipp) and $SiBr_2$($CAAC^{Me}$). Interestingly, the light-yellow solution of $SiBr_2$(SIDipp) was treated with the light-yellow benzene solution of carbene, showing no significant colour change at ambient temperature. ^{1}H and $^{31}P\{^{1}H\}$ NMR revealed no reaction at ambient temperature prompted us to heat the reaction solution at 80 °C for overnight upon which solution gradually turned from light-yellow to red-

brown. Furthermore, ^{1}H NMR spectroscopic analysis confirmed the complete consumption of the starting material and selective formation of **33-Si** (***Figure 66***) along with the release of free SIDipp. After careful separation of free SIDipp, **33-Si** was isolated as colourless solid in overall yield of 60 %. Then $SiBr_2(CAAC^{Me})$ was treated with a light-yellow benzene solution of the carbene, where the reaction proceeded smoothly at ambient temperature and completed in 2 hours to selectively give **34-Si**, as depicted by a colour transition from light-yellow to intense purple, and further confirmed by ^{1}H and $^{31}P\{^{1}H\}$ NMR spectroscopic analyses. The purple analytically pure solid, **34-Si** (***Figure 66***), was isolated after workup and crystallization from *n*-pentane at −30 °C in 70% yield. Both compounds, **33-Si** and **34-Si**, exhibit extreme sensitivity to air and moisture. However, they can be stored under an argon atmosphere at ambient temperature for several months. Upon heating, they begin to decompose during melting at 205 °C and 157 °C respectively. **33-Si** and **34-Si** are well soluble in benzene and toluene and moderately soluble in *n*-hexane and *n*-pentane at room temperature.

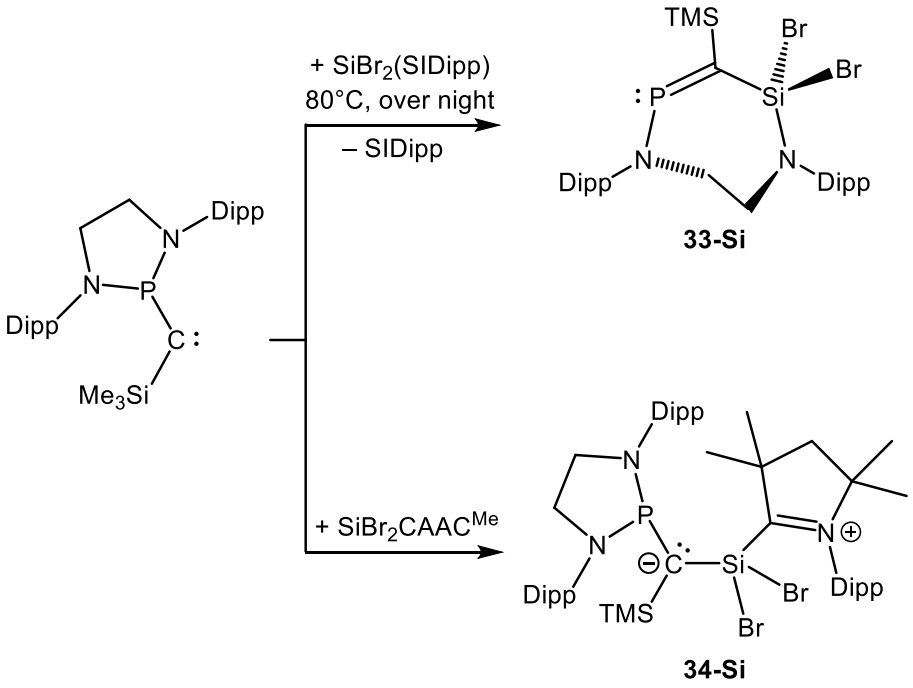

Figure 66. Reaction of $SiBr_2$(SIDipp) and $SiBr_2CAAC^{Me}$ with Push-Pull carbene to successfully afford **33-Si** and **34-Si**.

Compounds **33-Si** and **34-Si** exhibit striking variation in both colour and ^{31}P NMR spectra. While **33-Si** is colourless, **34-Si** appears purple. Additionally, their ^{31}P NMR signals in (D_6)benzene show a significant shift, with **33-Si** resonating at 318.50 ppm and **34-Si** at 120.71 ppm (***Figure 67***).

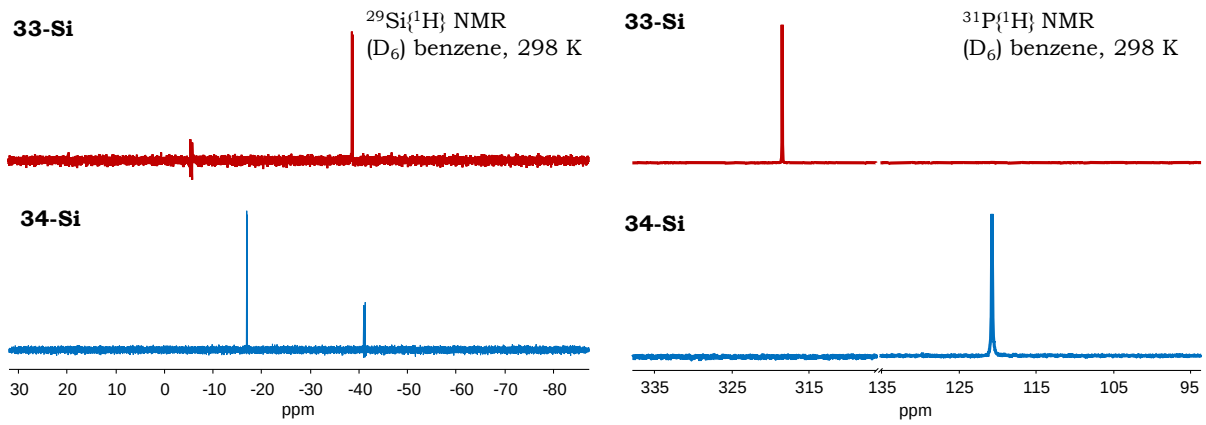

Figure 67. A stack plot of the selected excerpts of the $^{29}Si\{^{1}H\}$ and $^{31}P\{^{1}H\}$ NMR spectra of the compounds **33-Si** and **34-Si**.

These notable variations piqued our interest in their structural properties. Further investigation using single-crystal X-ray diffraction (scXRD) and multinuclear NMR spectroscopy uncovered distinct structural features: **33-Si** adopts a cyclic structure (***Figure 68***, a), whereas **34-Si** forms an anticipated adduct of $SiBr_2(CAAC^{Me})$ and carbene (***Figure 68***, b). Suitable colourless plate-shaped single crystals of **33-Si** and blue plate-shaped crystals of **34-Si** were successfully grown through slow evaporation of their *n*-hexane saturated solution at −30 °C. The molecular structures display the following:

i) **33-Si** revealed a non-planar cyclic structure of phosphaalkene formed *via* an opening of the NHP ring followed by insertion of $SiBr_2$ unit. Whereas **34-Si** exhibits an adduct formation of $SiBr_2(CAAC^{Me})$ and carbene to form silaethene.

ii) The molecular structures of compounds **33-Si** and **34-Si** exhibiting perfectly trigonal planar central carbon (C^{cent}) ($\Sigma\measuredangle(C)$ = 360° (**33-Si**), $\Sigma\measuredangle(C)$ = 359.42° (**34-Si**)) are bonded to the distorted tetrahedral silicon centers *via* a Si−C single bond (*d*(Si−C) = 1.822(2) Å) (**33-Si**) and polarized (*d*(Si=C) = (1.772(0) Å (**34-Si**)). The structural features of **33-Si** are in good agreement with the literature reported trichlorophosphasilapropene (*d*(Si−C) = 1.850(3) Å).[321] Whereas in the case of **34-Si**, the trigonal planar carbon C^{cent} core shows an elongated polarized double bond with silicon which aligns slightly with the reported compound with (*d*(Si=C) = (1.7286(18) Å).[322]

iii) In the case of **34-Si**, the sterically demanding NHP and CAAC substituents adopt a synclinical conformation with a torsion angle (P^{NHP}−C^{cent}−Si−$C^{carbene}$) φ of −52.22°. Notably, the phosphorus atom of the NHP group in the CAAC-supported silaethene derivative exhibits significant pyramidalization ($\Sigma\measuredangle(P)$ = 307.15°), corresponding to a 59% deviation from ideal trigonal planar geometry. This structural

feature suggests minimal delocalization of the lone pair on phosphorus into the π*-orbital of the C^{cent}=Si. Consistent with this observation, the P^{NHP}–C^{cent} bond length (1.773(2) Å), closely matches that of a typical P–C single bond.

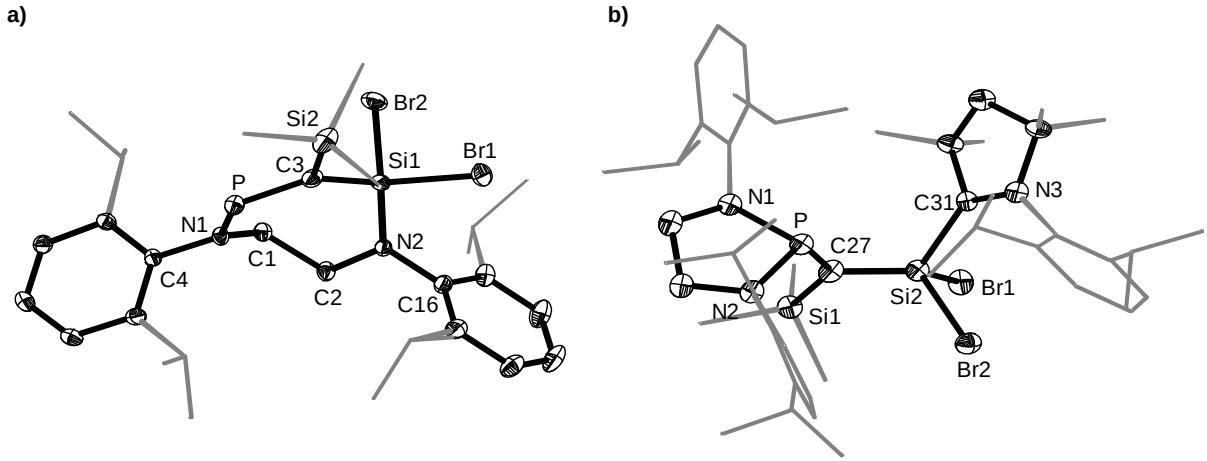

Figure 68. DIAMOND plot of the molecular structure of **33-Si** (***left***) and **34-Si** (***right***) Thermal ellipsoids are set at 30 % probability level. Hydrogen atoms are omitted and the Dipp substituents are presented in wire-frame for clarity. Selected bond lengths [Å], bond angles [°]: **a)** C1-C2 1.5239(19), C1-N1 1.4770(17), N1-P 1.6663(11), P-C3 1.6760(15), C3-Si1 1.8217(15), C2-N2 1.4687(17), N2-Si1 1.6980(12), Si1-Br1 2.2165(4), Si1-Br2 2.2556(4), C3-Si2 1.8887(14), C4-N1-P 115.19(9), C4-N1-C1 114.98(10), C1-N1-P 128.44(9), C3-Si1-N2 115.15(6), C2-N2-C16 111.89(10), C2-N2-Si1 123.61(9), N1-P-C3 112.13(6), Si1-N2-C16 124.45(9), Br1-Si-Br2 103.553(17); **b)** C27-Si2 1.772(5), C27-P 1.774(5), C27-Si1 1.858(5), Si2-C31 1.967(4), Si2-Br1 2.2604(13), Si2-Br2 2.2506(14), C27-Si2-C31 120.7(2), P-C27-Si2 110.7(2), Si1-C27-Si2 116.2(2), Si1-C27-P 132.5(3), C27-P-N1 105.52(19), C27-P-N2 113.1(2), Br1-Si2-Br2 99.55(5).

The successful isolation of **33-Si** and **34-Si** in considerable yields prompted us to study the reducing properties of these peculiar compounds. Notably, the 2e$^-$ reduction of **33-Si** with KC_8 in benzene at ambient temperature yielded only Dipp-H as an identifiable compound according to NMR spectroscopy. However, the 2e$^-$ reduction of **34-Si** with KC_8 in benzene at ambient temperature yielded selectively bis-ligand supported silasiliryne **35-Si** (***Scheme 27***), which was isolated after careful workup and crystallization from *n*-pentane as a light-blue solid with an isolated yield of 32%.

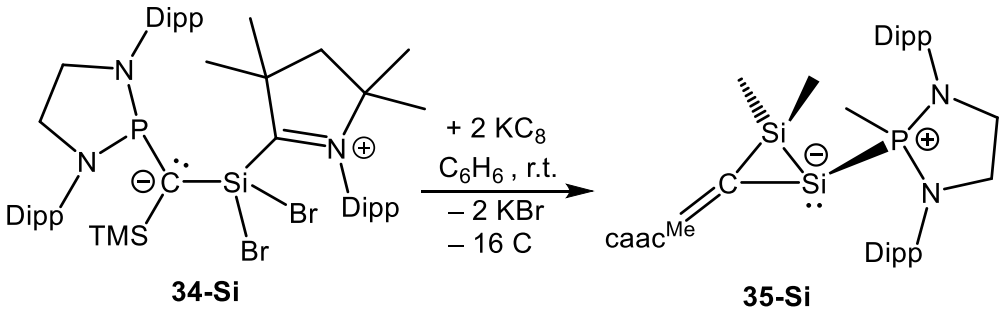

Scheme 27. Reductive dehalogenation of **34-Si** to afford **35-Si**.

Compound **35-Si** represents the first reported bis-ligand-supported silasiliryne, as confirmed by a search of the CCDC structural database and was comprehensively characterised by single crystal X-ray crystallography and multinuclear NMR spectroscopy. Colourless, plank-shaped crystals were obtained after slow cooling of a *n*-pentane saturated solution at −30 °C, which were suitable for X-ray diffraction analysis. The compound **35-Si** crystallized in the triclinic space group $P\bar{1}$. The molecular structure shows key structural features as follows:

i) reveals a three-membered cyclic scalene CSi_2 core (***Figure 69***) supported by It the sterically encumbered $CAAC^{Me}$ and phosphane ligands with a Si1−Si2 bond length of 2.228(5) Å, which is 0.1 Å less as compared to the reported compound $Mes_2Si(C{=}C(SiMe_3)Ph)SiMes_2$ (2.327(2) Å).[323] Shortening of a bond can be explained by the pyramidalization observed at the Si1 center and compared well with the Robinson $Si_2(0)$ compound (2.2294(11) Å).[150]

ii) The molecular architecture also exhibits one tetrahedral (Si2) and one stereogenic trigonal pyramidal Si center ($\Sigma\measuredangle$(Si1) = 258.08°) with a considerably higher degree of pyramidalization (DP) (~ 100 %). This suggests a higher s-character in the pyramidalized silicon-centered lone pair orbital.

iii) Exocyclic sterically more demanding $CAAC^{Me}$ and Phosphine ligands adopt an anticlinical conformation as indicated by the C^{CAAC}−C28−Si1−P torsion angle of 91.85(2)°(***Figure 69***). The C28−C29 bond length of 1.333(5) Å compares well with the typical $C^{sp2}{=}C^{sp2}$ bond length. And also corroborates well the literature known compound $(Mes)_2Si(C{=}CPhSiMe_3)Si(Mes)_2$ (1.339(2) Å).[323]

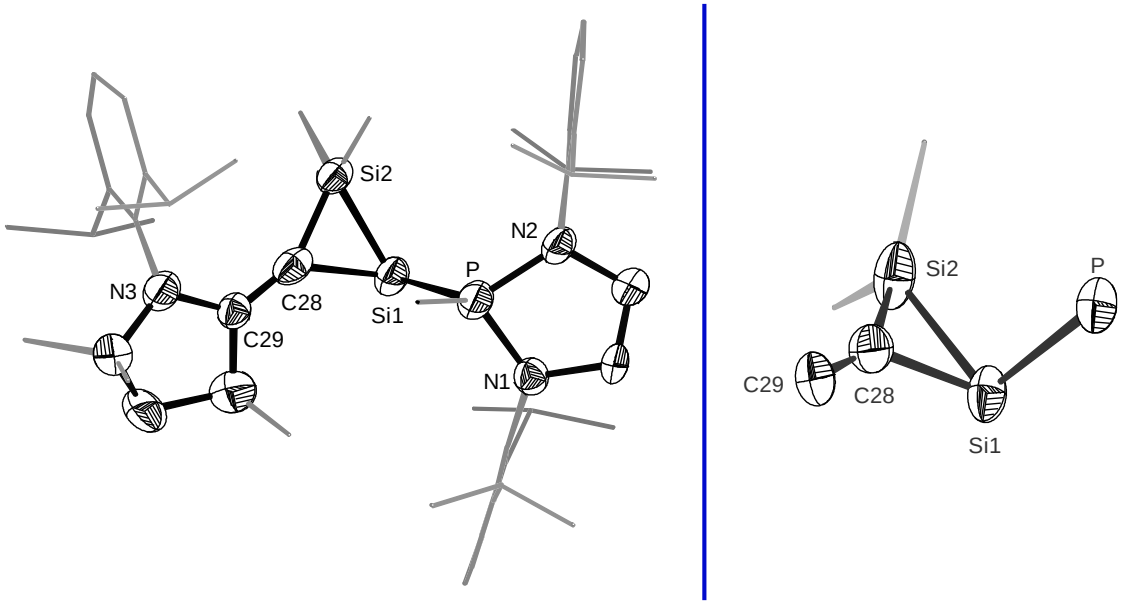

Figure 69. DIAMOND plot of the molecular structure of **35-Si** (***left***) and and its condensed side view (***right***). Thermal ellipsoids are set at 30 % probability level. Hydrogen atoms are omitted and the Dipp

substituents are presented in wire-frame for clarity. Selected bond lengths [Å], bond angles [°]:C28-Si1 1.877(9), P-Si1 2-263(3), Si1-Si2 2.228(3), Si2-C28 1.827(9), C28-C29 1.333(11), C29-C28-Si1 133.5(6), Si1-C28-Si2 73.9(3), C29-C28-Si2 152.2(6), P-Si1-Si2 101.72(12), Si2-Si1-C28 52.0(3), C28-Si1-P 104.4(3); C29-C28-Si1-P 91.85(2).

Based on the single-crystal X-ray diffraction (scXRD) parameters and comparison with literature data, compound **35-Si** can probably be best described as a bis-ligand supported sila siliryne, where the cyclic scalene CSi_2 core is supported by the $CAAC^{Me}$ and phosphane ligands at the respective carbon and silicon center (***Figure 69***).

The multinuclear NMR spectroscopic analysis of **35-Si** indicates the presence of a C_1-symmetric structure, where restricted rotational dynamics of the carbene and phosphine ligands around their respective $C–C^{carbene}$ and $Si–P^{phosphane}$ bond axes on the NMR timescale results in highly complex ^{1}H and $^{13}C\{^{1}H\}$ NMR spectra. The combination of C_1-symmetry and hindered rotation of both the carbene and phosphine ligands generates distinct chemical environments, leading to eight doublets for each methyl group of the Dipp substituents in the phosphane ligand and four doublets for the methyl group of the Dipp substituents in the $CAAC^{Me}$ ligand. These signals were unambiguously assigned through a comprehensive analysis using ^{13}C-^{1}H correlation NMR spectroscopy (e.g., HSQC or HMBC), which provided precise structural elucidation by correlating proton and carbon resonances. The $^{29}Si\{^{1}H\}$ NMR spectrum exhibits two doublets at δ = −69.17 ppm ($^{2}J(^{31}P,^{29}Si)$ = 25.3 Hz) for the $SiMe_3$ group and δ = 3.58 ppm ($^{1}J(^{31}P,^{29}Si)$ = 92.8 Hz) for the pyramidalized silicon center (***Figure 70***). These chemical shifts are markedly different from those of the precursor **34-Si**, which displays resonances at δ = −45.50 ppm ($^{2}J(^{31}P,^{29}Si)$ = 105.5 Hz) for the $SiBr_2$ group and δ = −17.11 ppm ($^{2}J(^{31}P,^{29}Si)$ = 10.6 Hz) for the $SiMe_3$ group.

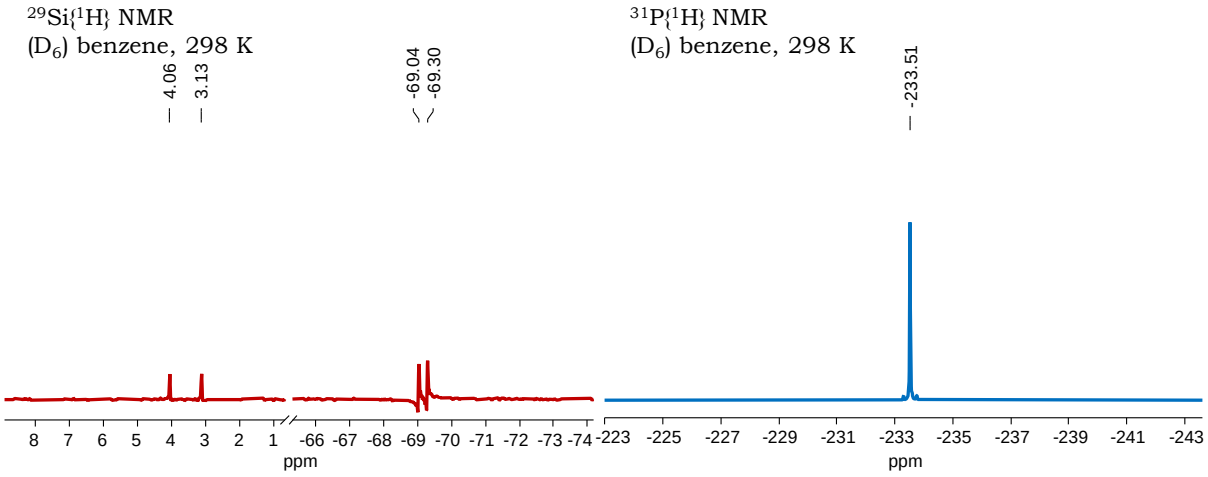

Figure 70. $^{29}Si\{^{1}H\}$ (***left***) and $^{31}P\{^{1}H\}$ (***right***) NMR of compound **35-Si**.

The significant deviation in chemical shift likely reflects the decrease in coordination number at the pyramidalized silicon atom. Additionally, the $^{31}P\{^{1}H\}$ NMR spectrum

shows a pronounced upfield shift, with a resonance at δ = −233.5 ppm (***Figure 70***), compared to its precursor, which appears at δ = 120.7 ppm in (D_6)benzene.

2.5. Chemistry of small diazoolefin with low valent tetrel elements

2.5.1. Introduction

Investigations into the stabilization of reactive intermediates have profoundly reshaped modern bonding theories, revealing limitations in the classical Lewis formalism and prompting the development of more advanced electronic structure descriptions. Diazoalkanes ($R_2C{=}N_2$, **I-84**; ***Figure 71***) and their cyclic isomers, diazirines (**I-85**), have been known for over a century and serve as versatile synthetic building blocks in organic chemistry.[324,325,326,327] In contrast, their higher homologs, diazoalkenes ($R_2C{=}C{=}N_2$, **I-86**; ***Figure 71***), also referred to as diazoolefins are highly unstable and are typically observed only as transient intermediates in organic reactions. The electronic structure of diazoalkenes can be represented by several resonance forms: a cumulenic structure with consecutive

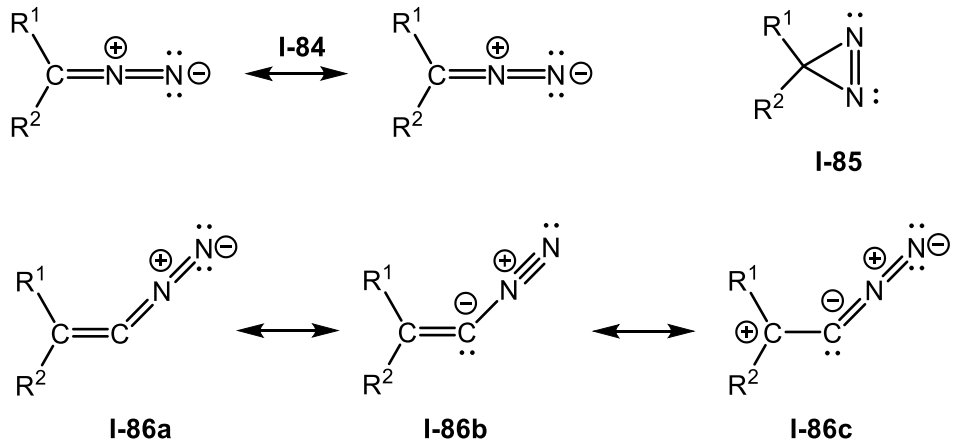

Figure 71. Comparison between diazoalkane (**I-84**), diazirine (**I-85**) and diazoalkenes (**I-86**).

double bonds (**I-86a**), a zwitterionic form depicting a vinyl anion paired with a diazonium cation (**I-86b**), or a polarized Lewis structure emphasizing the C=N=N fragment (**I-86c**).[328] These representations highlight the delocalized and highly reactive nature of diazoalkenes, underscoring their role as key yet elusive intermediates in mechanistic studies.

The Lewis structure **I-86b** (***Figure 71***), featuring a vinyl diazonium moiety, underscores the inherent instability of diazoalkenes due to the strong thermodynamic driving force for N_2 liberation, necessitating low-temperature conditions for their detection and characterization. Matrix-isolation studies of $F_2C{=}C{=}N_2$ at a few Kelvin have successfully demonstrated its generation *via* two pathways: (i) photochemical excitation of difluoropropadienone with concomitant CO elimination or (ii) reaction of dinitrogen with difluorovinylidene, the latter produced through photochemically induced rearrangement of difluoroacetylene (***Figure 72***). The presence of difluoro

substituents is critical, as they kinetically stabilize the vinylidene intermediate (F_2C=C:) against rapid 1,2-migration - a process that occurs much more readily in the parent system (H_2C=C:) thereby enabling the isolation and characterization of this reactive species.[329,330,331]

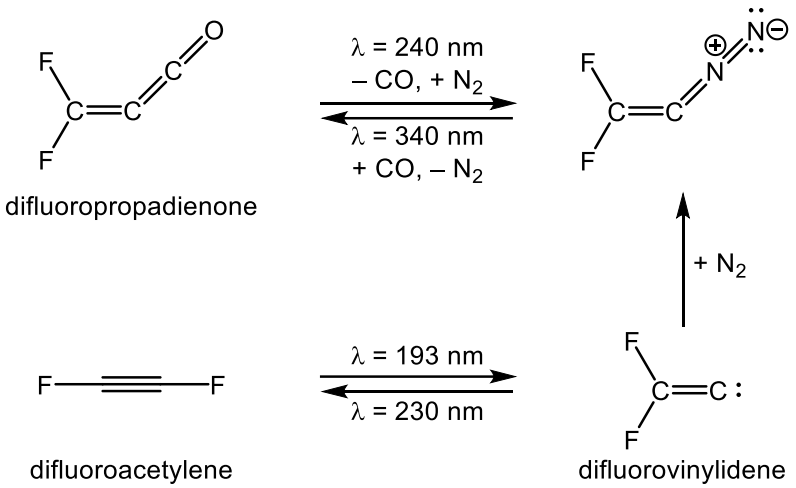

Figure 72. Matrix-isolation study of a diazoalkene.

In 2021, the research group of Severin and Hansmann made a breakthrough by independently achieving the first successful isolation of several ambient temperature stable diazoolefins by incorporating an N-heterocyclic scaffold (**I-87** [332] to **I-91** [333]) were built on N-heterocyclic scaffolds, a key factor in their stability. Following this discovery, chemists expanded the range of diazoolefins to include triazole-based **(I-92** to **I-93**)[334] and pyridine-based (**I-94** and **I-95**) structures.[335]

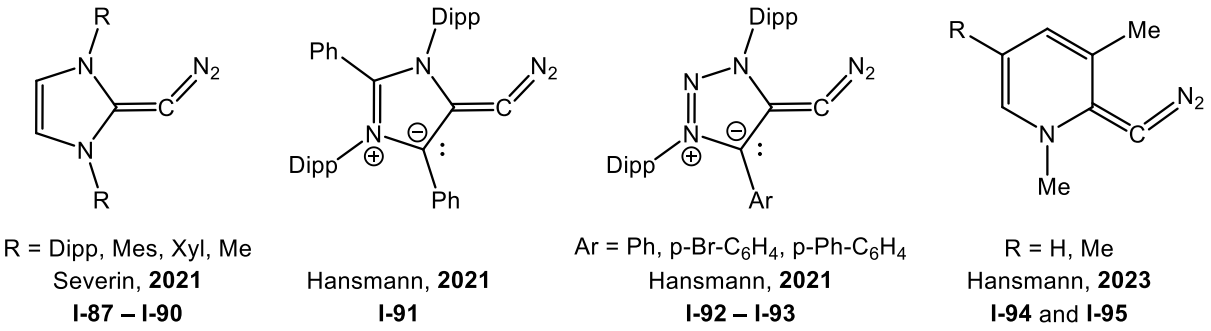

Figure 73. Literature known examples of diazoolefin possessing N-heterocyclic (**I-87** to **I-91**), triazole (**I-92** to **I-93**), and pyridine scaffolds (**I-94** and **I-95**).

Resonance and electron delocalization are key reasons for stabilization of these systems (***Figure 74***),[332],[333] allowing them to persist at room temperature for several months without any noticeable signs of decomposition.

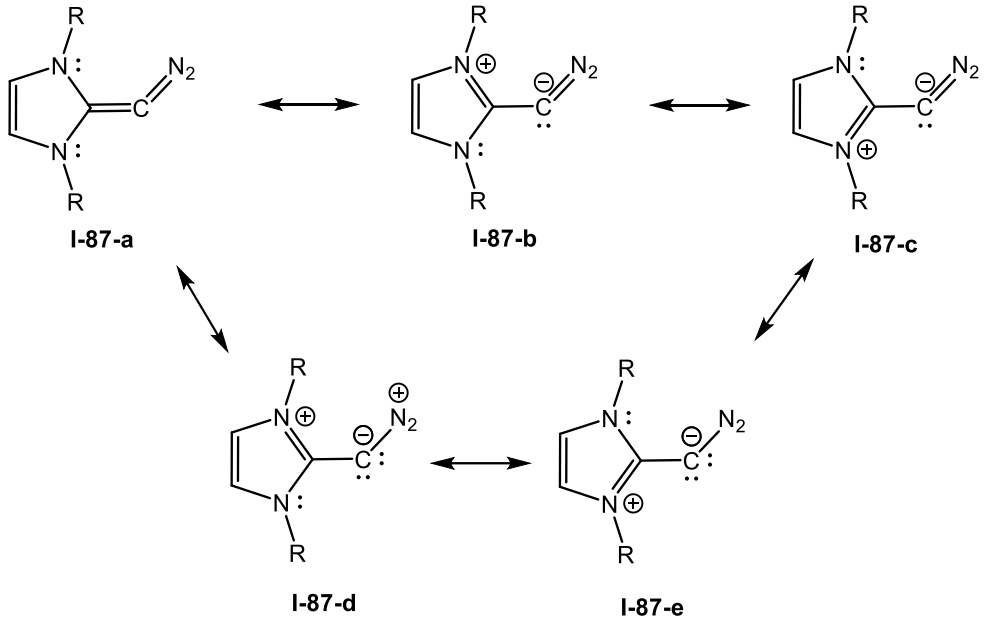

Figure 74. Description of mesomeric Lewis structures of N-heterocyclic diazoolefin **I-87**.

In addition to their well-documented reactivity with small molecules (e.g., CO, CS_2, and isocyanides)[332,333] and organic substrates (e.g., dimethylacetylene dicarboxylate

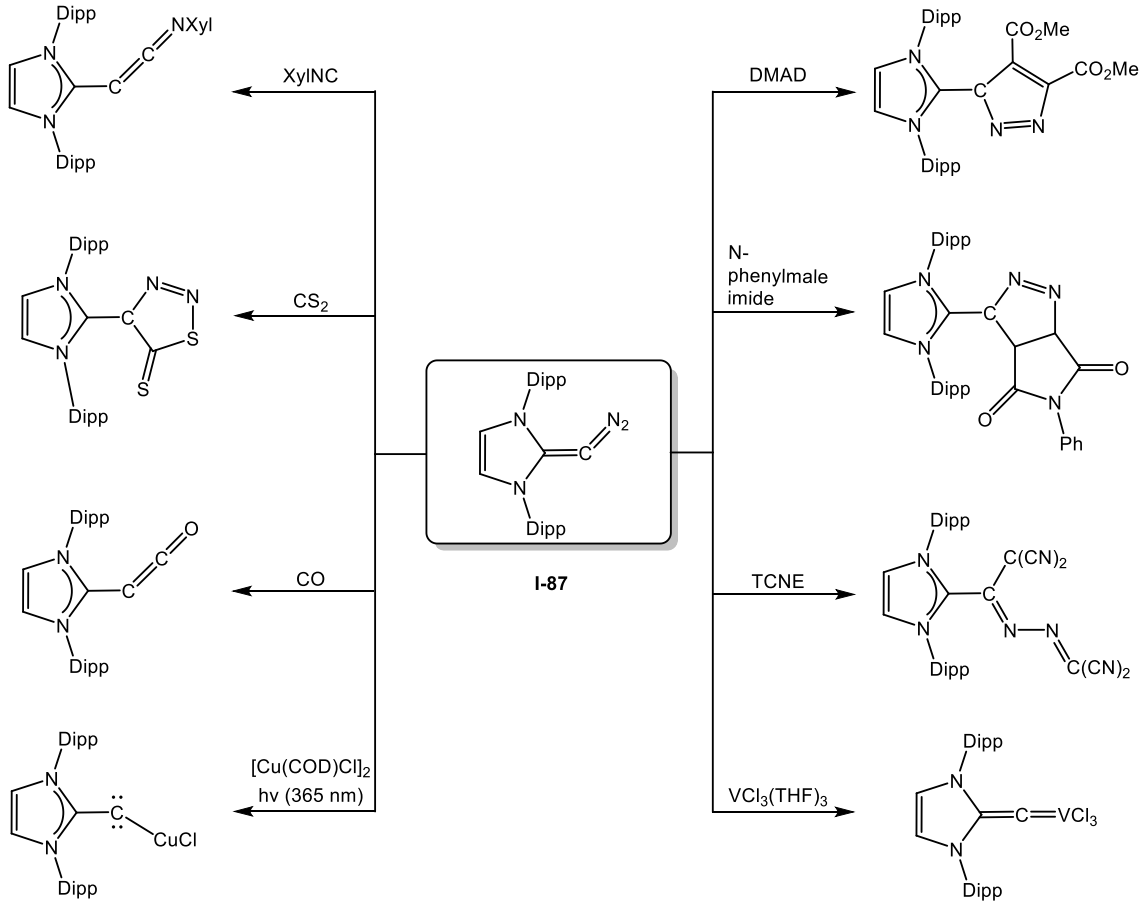

Figure 75. Selected reactivity study of Severin's diazoolefin **I-87** with small molecules (CO, CS_2 and isocyanide), organic substrates (dimethyl acetylene dicarboxylate DMAD, N-phenyl maleimide, or tetracyanoethylene), and metal complexes. Formal charges were omitted for clarity.

(DMAD), *N*-phenylmaleimide, and tetracyanoethylene),[332] diazoolefins have been shown to form stable complexes with transition metals as well as triel complexes (particularly boron and aluminum).[332] Furthermore, diazoolefins undergo photochemical activation upon irradiation with UV light (350–390 nm), leading to the extrusion of dinitrogen and the formation of a transient vinylidene intermediate. [336] Given this reactivity, diazoolefins have emerged as promising precursors for the synthesis of vinylidene metal complexes. This potential was recently validated by Severin and coworkers, who successfully isolated and characterized alkenylidene complexes of vanadium and copper derived from diazoolefin precursors.[337,338]

2.5.2. Non-metal mediated cleavage of Ge≡Ge triple bond

The impact of transition metal-mediated bond activation processes in chemical science is profound, as evidenced by their role as fundamental steps in homogeneous catalysis. These reactions have been extensively studied across nearly all transition metals in the periodic table (***Figure 76***). Among the most notable textbook examples is the transition metal-mediated activation of strong, nonpolar σ-bonds A–B (A, B = H or C, ***Figure 76*** (i)), which highlights the remarkable ability of transition metals to cleave such bonds. This process occurs through four distinct mechanisms (***Figure 76*** (i); (a) – (d)) where the synergistic donor-acceptor interaction between the metal center and the σ* and σ orbitals of the A–B bond plays a pivotal role in facilitating bond cleavage.

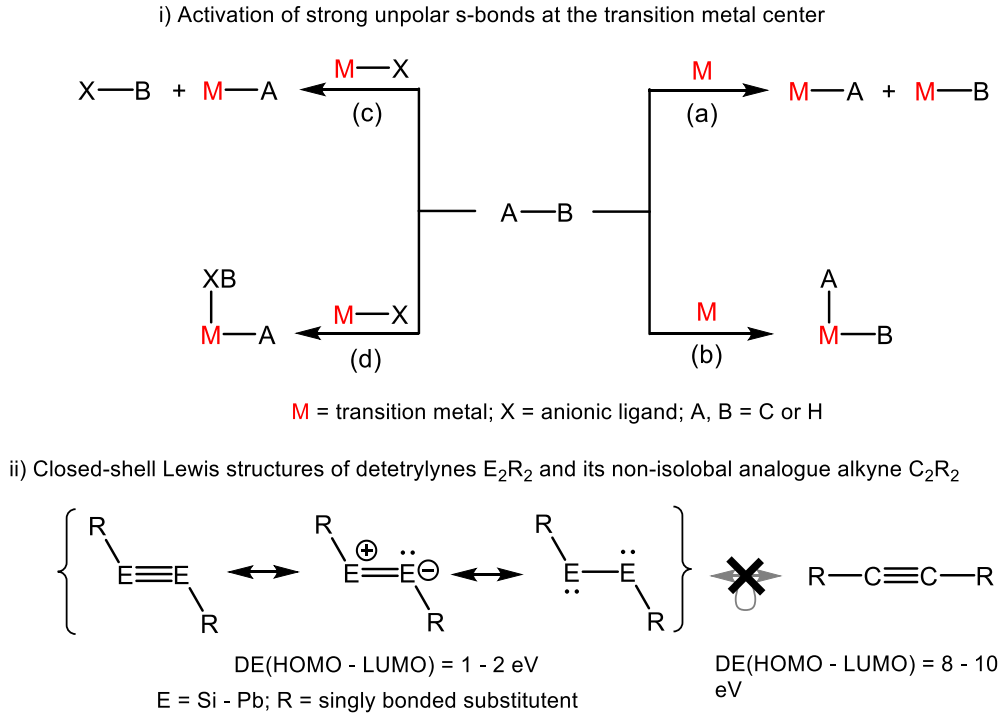

Figure 76. i) Schematic representation of the mechanism of the unpolar σ-bond activation at the metal center; ii) comparison of alkynes with their heavier analogues.

The lower HOMO-LUMO gap of digermynes (~2 eV) compared to alkynes (~9 − 11 eV), combined with the Ge-centered ambiphilicity of Ge_2R_2, enables novel coordination modes. The distinct, synergistic donor-acceptor interactions with transition metals may lead to unique reactivity. However, the bulky substituents typically required to stabilize the reactive E≡E triple bond in ditetrelynes kinetically pose significant challenges in harnessing their synthetic potential and exploring their reactivity. However, our research group has reported the Co- and Rh(I)-mediated E≡E triple bond activation chemistry, mimicking transition metal–assisted σ-bond activation reactions, leading to a series of unprecedented Co complexes (***Figure 77***). Nevertheless, non-metal-mediated cleavage of the Ge≡Ge triple bond has also been experimentally realised in our group and presented as the first example of non-metal-mediated cleavage of a Ge≡Ge triple bond, achieved using the sterically undemanding diazoolefin $(IMe_4)CN_2$ as a suitable reagent for displacing metal complexes (***Figure 77***).

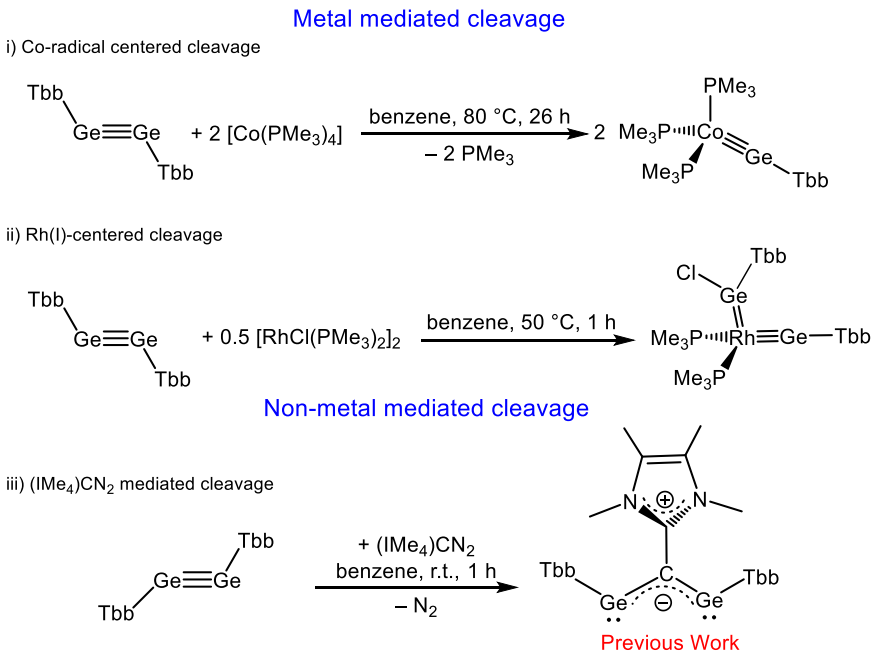

Figure 77. i) Co-centered Ge≡Ge triple bond cleavage;[226],[6] ii) Rh(I)-centerd Ge≡Ge triple bond cleavage;[7] and $(IMe_4)CN_2$ mediated Ge≡Ge triple bond cleavage.[8]

---

[6] T. Deckstein personal communication.

[7] K. Tomer, "*Metal-Centered Cleavage of E≡E Triple Bonds (E = Si, Ge): A Leap in Metal-Tetrel Triple Bond Chemistry*", *Dissertation*, Rheinische Friedrich-Wilhelms-Universität Bonn, **2025.**

[8] S. Kumar, "*Low-Valent Heavier Tetrel Compounds Supported by N-heterocyclic Carbenes: A Comprehensive Experimental and Theoretical Perusal*", *Dissertation*, Rheinische Friedrich-Wilhelms-Universität Bonn, **2025.**

Our exploration of this work begins with the synthesis of a new, less sterically demanding diazoolefin ($IMe_2{}^iPr_2)CN_2$ (**36**), which is, however, bulkier than the previous one, ($(IMe_4)CN_2$). This compound is used to screen for similar non-metal-mediated cleavage of the Ge≡Ge bond. Treatment of a solid mixture of orange-brown Ge_2Tbb_2 and brown $(IMe_2{}^iPr_2)CN_2$ with benzene under ambient conditions results in a gradual colour change to violet over 30 minutes. Reaction monitoring by ^{1}H NMR spectroscopy revealed the selective formation of a new compound, identified as the Ge_2C_2 diradicaloid (**37-Ge**) (***Scheme 28***), alongside unreacted Ge_2Tbb_2 (50%). This observation indicates the rapid formation of the Ge_2Tbb_2 diradicaloid rather than the 1,3-digermapropargylene species observed in our group's previous reaction of Ge_2Tbb_2 with $(IMe_4)CN_2$ under stoichiometric conditions (***Figure 77***).

To ensure complete consumption of the remaining Ge_2Tbb_2, an additional equivalent of $(IMe_2{}^iPr_2)CN_2$ was introduced, leading to the exclusive formation of **37-Ge**. Subsequent crystallization from *n*-pentane at −30 °C afforded **37-Ge** in 58% yield as a dark violet, highly air-sensitive crystalline solid, which decomposes instantaneously to a white powder upon exposure to air. Despite its sensitivity, **37-Ge** remains stable at ambient temperature for several months without observable decomposition, as confirmed by visual inspection and ^{1}H NMR spectroscopy. The compound exhibits high solubility in *n*-pentane, benzene, diethyl ether, and THF. The thermal decomposition of **37-Ge** was investigated in a vacuum-sealed glass capillary, where melting at 216 °C resulted in a black residue. Analysis of the soluble fraction of this residue by ^{1}H NMR spectroscopy ((D_6)benzene) indicated unselective decomposition.

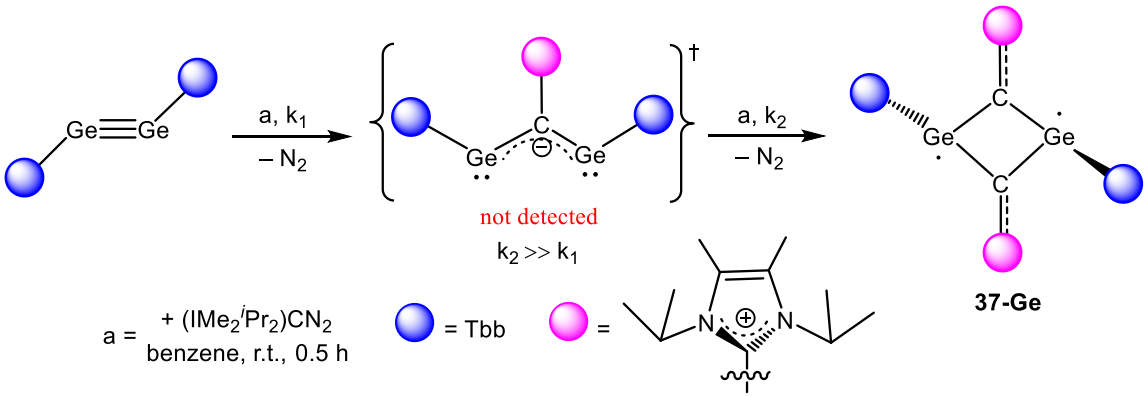

Scheme 28. Synthesis of the Ge_2C_2-diradicaloid **37-Ge**.

Clear violet plate-shaped single crystals of the Ge_2C_2-diradicaloid **37-Ge** were obtained by slowly cooling a saturated solution in *n*-pentane at −30 °C.

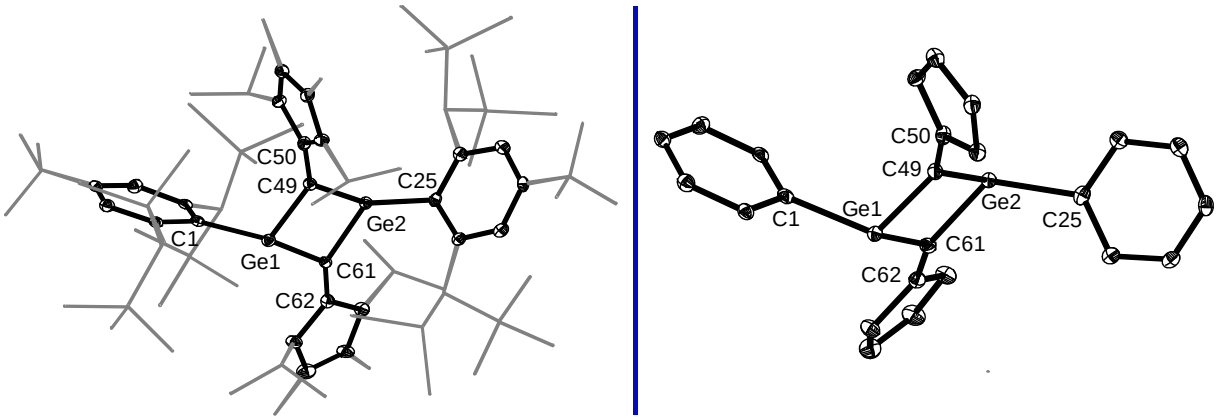

Figure 78. DIAMOND plot of the molecular structure of the Ge_2C_2-diradicaloid **37-Ge** with a top-view (***left***) and a condensed side-view (***right***) about the Ge_2C_2 ring; thermal ellipsoids are set at 30% probability level and the H atoms are omitted and Dsi, Me and ^{t}Bu groups are shown in wire frame for the sake of clarity; selected bond lengths in (Å), bond angles and torsion angles in (°): Ge1-C1 2.039(3), Ge1-C49 1.914(3), Ge1-C61 1.980(3), Ge2-C49 1.909(3), Ge2-C61 1.981(3), Ge2-C25 2.055(3), C49-C50 1.428(4), C61-C62 1.378(4),Ge1-C49-Ge2 95.39(12), Ge1-C61-Ge2 91.08(11), C1-Ge1-C49 111.38(11), C1-Ge1-C61 123.48(12), C49-Ge1-C61 86.72(12), C25-Ge2-C49 111.21(11), C25-Ge2-C61 126.51(12), C49-Ge2-C61 86.81(12)), $\varphi^{NHC(C49)}$ = 94.43(9), $\varphi^{NHC(C62)}$ = 12.80(9), Ge1···Ge2 = 2.8275(8).

Notably, the molecular framework of **37-Ge** exhibits a striking resemblance to Power's isolobal non-Kekulè singlet biradicaloid, $Ar^{Dipp}Ge(\mu\text{-}NSiMe_3)_2GeAr^{Dipp}$.[198] in terms of its skeletal arrangement. X-ray crystallographic analysis reveals that **37-Ge** adopts a *pseudo*-centrosymmetric structure in the solid state, enforced by crystallographic symmetry. The molecule features a perfectly planar four-membered Ge_2C_2 ring (Σ internal angles = 360°), with germanium centers occupying the 1,3-positions. (***Figure 78***).

The tri-coordinated germanium centers in **37-Ge** exhibit distinct pyramidalization, with bond angle sums of Σ∢(Ge1) = 321.6° and Σ∢(Ge2) = 324.6°, while the trans-annular Ge1····Ge2 distance of 2.8275(8) Å lies between the sum of covalent (2.42 Å) [339] and van der Waals (4.22 Å) [340] radii, indicating a weak through-space interaction. This elongated separation aligns with Power's biradical ArDippGe(μ-$NSiMe_3)_2$GeArDipp (2.755 Å), underscoring the pronounced biradical character of **37-Ge**. A Cambridge Structural Database (CSD) survey of tri-coordinated Ge····Ge separations (2.80–2.90 Å) reveals diverse bonding descriptions, including a π-single bond,[231] ultra-long σ-bond,[232] multicenter π(3c-2e) interaction,[341] stretched-bond with singlet diradicaloid character,[234] or even no bond.[235,236] The sterically hindered Tbb substituents adopt a trans-configuration (C1–Ge1–Ge2–C25 torsion angle = 155.1°), while the vinylic carbons (C^{VNL}) are nearly trigonal planar (Σ∢($C^{VNL1/2}$) = 359.9°) and feature elongated Ge–C^{VNL} bonds (avg. 1.946 Å vs. 1.943 Å in the case

of a similar analogue compound isolated in our group TbbGe{C(IMe$_4$)}$_2$GeTbb [9], despite the coplanar NHC-Ge$_2$C$_2$ arrangement. Bond matrix analysis strongly supports the resonance hybrid of diradical (**37-Ge-a/b**) and zwitterionic (**37-Ge-c/d**) forms, corroborating the complex electronic structure of **37-Ge** (***Figure 79***).

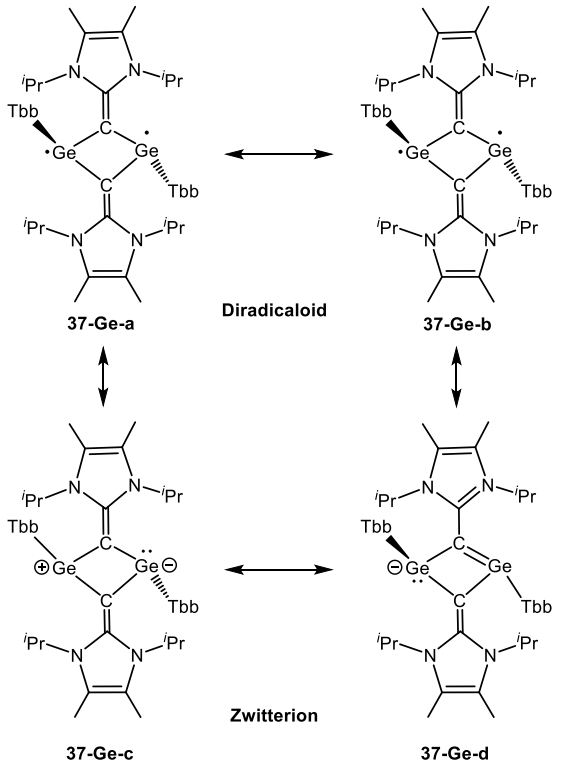

Figure 79. Representative diradicaloid (**37-Ge-a** and **37-Ge-b**) and zwitterion (**37-Ge-c** and **37-Ge-d**) resonance form of **37-Ge**.

The compound **37-Ge** exhibits a singlet ground-state diradicaloid character, as evidenced by detailed ^{1}H and ^{13}C{^{1}H} NMR spectroscopic analyses. NMR studies performed in (D$_8$)toluene at 239 K reveal a C_2-symmetric structure in solution, with hindered rotation of the sterically demanding Tbb groups around the Ge–C^{Tbb} bond axis. This rotational restriction is attributed to steric congestion imposed by the flanking IMe$_2$^{i}Pr$_2$ ligand moieties. Consequently, the ^{1}H NMR spectrum of **37-Ge** at 239 K displays two distinct SiMe$_3$ signals for each Tbb, indicative of a frozen conformational state on the NMR timescale. Further support for the diradicaloid nature of **37-Ge** comes from its ^{13}C{^{1}H} NMR spectrum, where the vinylic carbon atom (tri-coordinated within the ring) appears as a sharp resonance at

[9] The compound was thoroughly characterized and reported in the following doctoral thesis; Sandeep Kumar, "*Low-Valent Heavier Tetrel Compounds Supported by N-heterocyclic Carbenes: A Comprehensive Experimental and Theoretical Perusal*", Dissertation, Rheinische Friedrich-Wilhelms-Universität Bonn, **2025.**

δ(C^{VNL}) = 154.95 ppm and δ = 155.93 ppm. These signals compare well the similar analogue compound isolated in our group TbbGe{C(IMe$_4$)}$_2$GeTbb, where the vinylic carbon atom appears as a broad signal ($\Delta\nu_{1/2}$ = 12.96 Hz) at δ = 153.9 ppm) as it exhibits C_{2h}-symmetric structure in solution making both vinylic carbon atom enantiotopic in nature in contrast to our case.

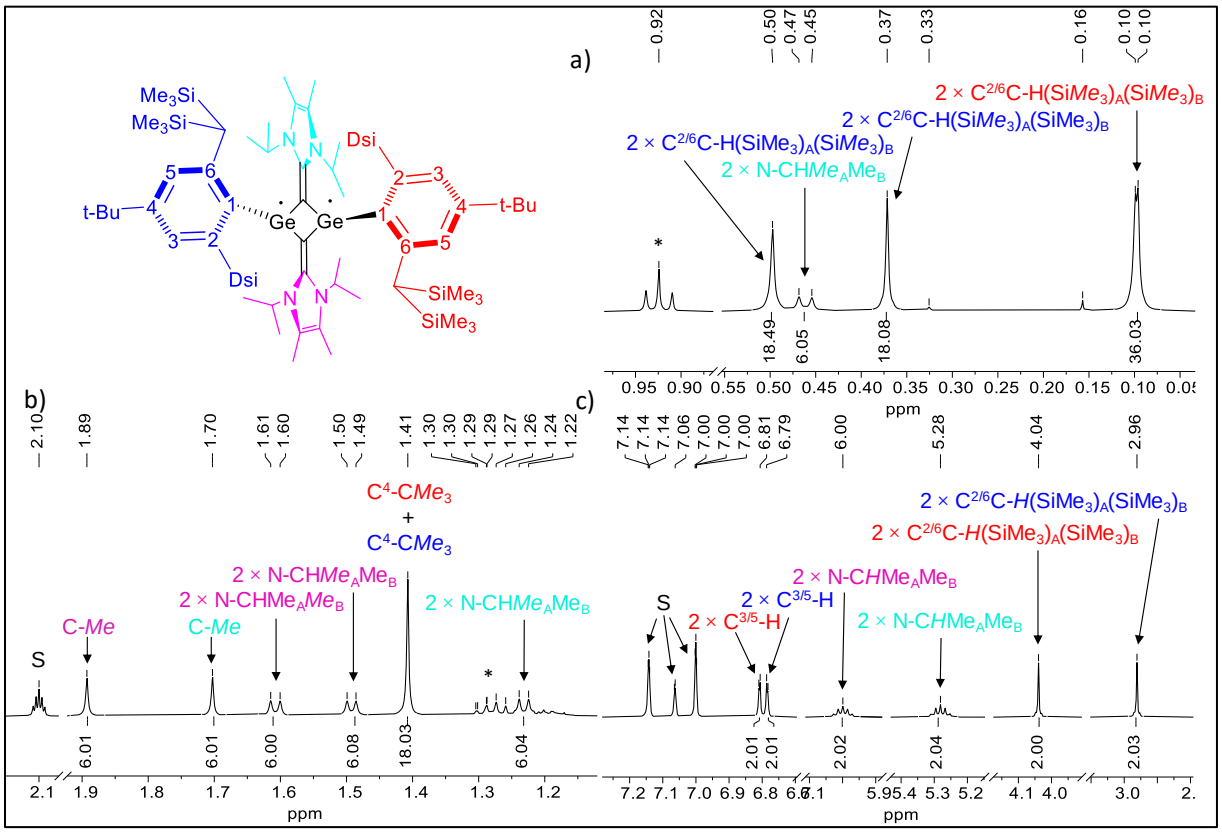

Figure 80. ^{1}H NMR spectrum excerpts of **37-Ge** in (D$_8$)toluene at 239 K; the residual proton signal of the deuterated solvent is marked with the character S.

2.5.3. Synthesis and characterization of heavier analogue of Imidazole

The reactivity of diazoolefins with low-valent main group complexes is highly influenced by electronic and steric factors. The sterically demanding diazoolefin (IDipp)CN$_2$ promotes the formation of the first NHC-supported 2-tetrelavinylidenes (NHC)C=EBr(Tbb) (E = Ge, Si) when reacted with suitable halo(aryl)tetrylenes. [217] Surprisingly, the less sterically hindered diazoolefin (IMe$_2$^{t}Pr$_2$)CN$_2$ (**36**) leads to markedly different products upon treatment with halo(aryl)tetrelenes. When an equimolar mixture of (IMe$_2$^{t}Pr$_2$)CN$_2$ (**36**) and 1,2-dibromodisilene (E)-(Tbb)BrSi=SiBr(Tbb) is treated in benzene at ambient temperature, the reaction solution undergoes a gradual colour change from yellow-orange to brown immediately. ^{1}H spectrum of an aliquot of the reaction solution revealed the formation of a [3+2] cycloaddition product, resulting from the insertion of the Si=Si double bond and yielding the metal-free cyclic bis-silyl amide (**38-Si**) (***Scheme 29***). After workup,

38-Si was isolated as an extremely air-sensitive light-yellow solid in 57% yield. This compound exhibits notable thermal stability as a solid but decomposes upon melting in a vacuum-sealed glass capillary at 210 °C.

In contrast, treatment of an equimolar mixture of $(IMe_2{}^iPr_2)CN_2$ (**36**) and 1,2-dibromodigermene (E)-(Tbb)BrGe=GeBr(Tbb) under identical conditions produced a complex mixture of products in which NHC-supported germynes, **39-Ge** was the major one (***Scheme 29***), highlighting the divergent reactivity between silicon and germanium analogues. Compound **39-Ge** was isolated as a yellow-brown solid in considerable purity after multiple crystallization from *n*-hexane at −30 °C. The compound exhibits air and moisture sensitivity but displays relatively high thermal stability in the solid state, decomposing upon melting at 160 °C.

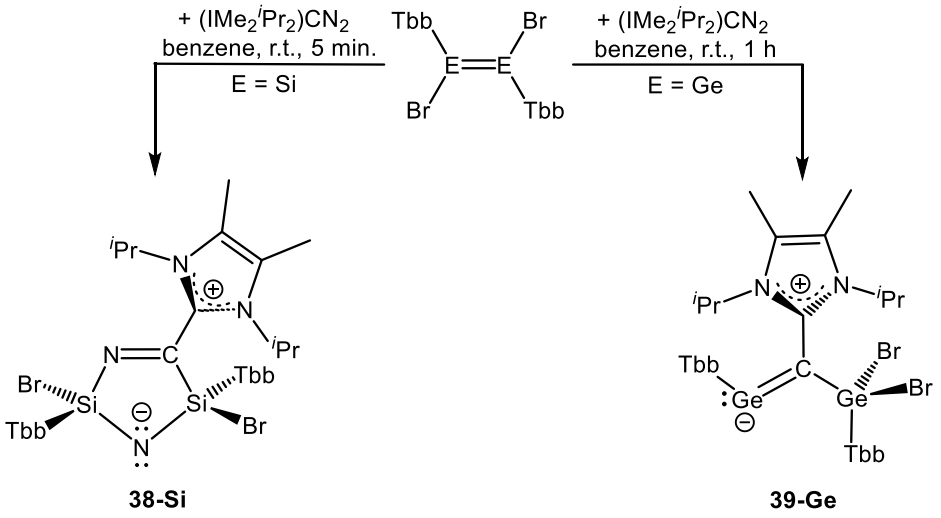

Scheme 29. Synthesis of the cyclic bis-silyl amide (**38-Si**) and NHC-supported germyne (**39-Ge**).

The molecular structure of cyclic bis-silylamide **38-Si** was determined by single-crystal X-ray diffraction analyses of the light-yellow plate-shaped crystals of **38-Si•($C_4H_{10}O$)**. Compound **38-Si** crystallized out in the monoclinic space group $P2_1/n$. The molecular structure of cyclic bis-silyl amide **38-Si** reveals a planar five-membered Si_2CN_2 ring (sum of interior angles = 540°) and two stereogenic distorted tetrahedral silicon centers Si1 and Si2 (***Figure 81***).

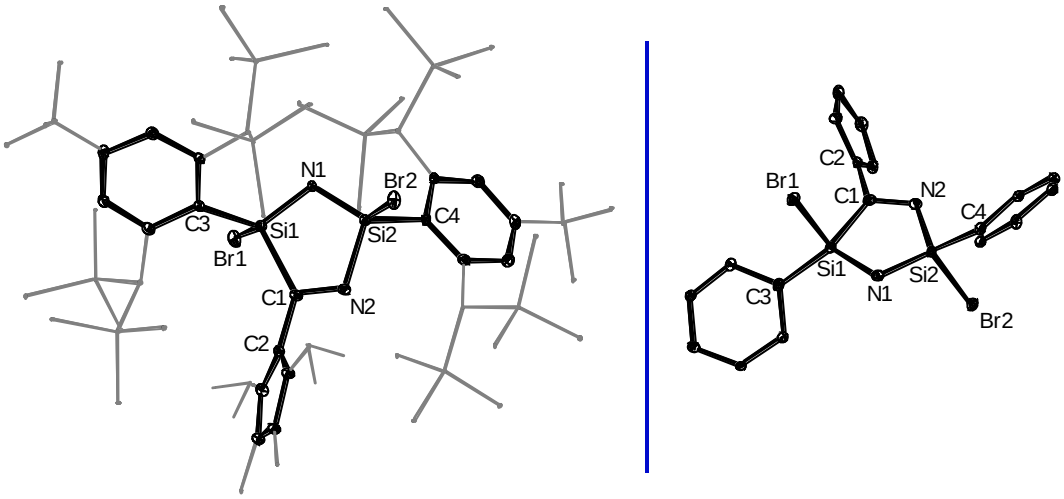

Figure 81. DIAMOND plot of the molecular structure of the cyclic bis-silylamide **38-Si** (left) and its condensed form (right); thermal ellipsoids are set at 30% probability level and the H atoms are omitted and Dipp, ^{t}Bu, Me and Dsi groups are shown in wire frame for the sake of clarity; selected bond lengths in (Å), bond angles and torsion angles in (°): Si1−N1 1.6593(12), Si1−Br1 2.2912(4), Si1−C3 1.9002(14), Si1−C1 1.9752(14), C1−C2 1.5008(18), Si2−N2 1.8091(12), Si2−N1 1.6550(12), Si2−Br2 2.2945(4), Si2−C4 1.8928(14); Si1−N1−Si2 111.11(7), Si1−C1−C2 136.33(10), Si1−C1−N2 112.93(10), C2−C1−N2 110.58(12); φ^{NHC} = 65.2(1)°; ∑∢(C1) = 359.84°.

The sterically more demanding Tbb substituents are arranged in trans-orientation (torsion angle C3−Si1−Si2−C4 = −154.49(1)°). The Si1−N1 and Si2−N1 bond lengths (1.659(1) Å and 1.655(1) Å, respectively) in **38-Si** compare well with previously reported metal bonded bis-silylamide Li(thf)[(SiMe$_3$)Si(CH$_2$^{t}Bu)$_2$-C$_6$H$_4$-1,2] (1.672(3) Å) [342] reported by Lappert *et. al.*. Both Si1−Br1 and Si2−Br2 bond lengths (2.2912(4) Å and 2.2945(4) Å, respectively) are slightly elongated than a typical Si$^{(sp3)}$−Br bond length, indicating some delocalization N(n_π)→Br(σ*). Notably, The C^{VNL}−C^{NHC} bond length (1.431(2) Å) corroborate well with the literature known NHC-supported bromogermynes ((IDipp)(SiBr$_2$Tbb)C=GeBr (1.444(2) Å) and (IDipp)(GeBr$_2$Tbb)C=GeBr (1.447(2) Å)),[217] equivalent to C$^{(sp3)}$−C$^{(sp2)}$ single bond distance [290] and C^{VNL} center shows trigonal planar coordination (Σ∢(C^{VNL}) = 359.82°). The NHC ring is a bit orientated (φ^{NHC} = 40.10(7)°) to the central five-membered ring Si$_2$CN$_2$.

The solution integrity of cyclic bis-silylamide **38-Si** was confirmed using multinuclear NMR spectroscopy in (D$_8$)thf at 263 K. The ^{1}H and ^{13}C{^{1}H} NMR spectra of **38-Si** indicate a time-averaged C_1-symmetric structure in solution due to the presence of two stereogenic silicon centers and fast rotation of Tbb around their Si−C^{Tbb} bond axis at 263 K. The most prominent spectroscopic feature of **38-Si** is its ^{29}Si NMR chemical shift at −34.7 and −20 ppm which is in good agreement with the ^{29}Si NMR chemical shift at −34.1 and −16.7 ppm of similar analogous compound

[N(SiBrTbb)$_2$NC(IMe$_4$)] isolated in our group[10], assigned to the two heterotopic stereogenic silicon centers in planar five-membered Si_2N_2C ring. These two signals are characteristic of a coordinatively saturated silicon(IV) center. In the $^{13}C\{^1H\}$ NMR spectrum, the chemical shift of the vinylidene carbon atom C^{VNL} appears at a slightly lower field (δ_{CVNL} = 194.2 ppm) compared to NHC-supported bromogermynes (IDipp)(EBr$_2$Tbb)C=GeBr (δ_{CVNL} = 133.6 ppm (**E = Si**) and 139.6 ppm (**E = Ge**))[217] and align well with vinylidene carbon atom C^{VNL} of [N(SiBrTbb)$_2$NC(IMe$_4$)] (δ_{CVNL} = 189.1 ppm).

The molecular architecture of NHC-supported germynes **39-Ge** was determined by single-crystal X-ray diffraction analyses of the clear orange block-shaped crystals of **39-Ge•(benzene)**. Compound **39-Ge** crystallized out in the orthorhombic space group *P*na2$_1$. The molecular structure of **39-Ge** features a dicoordinated V-shaped Ge-center ($\measuredangle(C^{VNL}–Ge–C^{ipso})$ = 108.49° suggesting the presence of a stereochemically active lone pair at the Ge center. The germyne cores display a slightly distorted *trans-bent* geometry, as evidenced by the torsion angle C^{Ipso}–Ge2/Ge2–C^{VNL}–Ge1 of 139.4(1)°. The C^{VNL} center is trigonal planar coordinated ($\Sigma\measuredangle(C^{VNL})$ = 358°), and the NHC five-membered ring mean-plane is tilted out of the plane defined by the C^{NHC}, C^{VNL} and Ge atoms with an interplane angle φ^{NHC} of 86.81(6)°. This conformation is very different from the N-heterocyclic vinyl tetrylenes (NHC=CH)$_2$E and ((NHC)=CH)ER, which display coplanar arrangement of the NHC ligand (φ^{NHC} ≈ 0°),[343],[344] but similar to those found for NHC-supported ditetrelynes R(NHC)E=ER (φ^{NHC} = 42.48(9)° – 82.14(7)°). The C^{VNL}–C^{NHC} bond lengths of **39-Ge** are 1.446(1) Å and resemble those of the typical $C^{(sp2)}$–$C^{(sp2)}$ single bond lengths (1.460 Å).[290] The Ge2–C^{VNL} bond lengths (1.905(1) Å (**32-SiGe**), 1.921(5) Å (**32-GeGe**)) are *ca.* 0.15 Å ($\Delta d_{Ge=C}$) longer than that of the calculated Ge≡C triple bond length (1.754 Å) of the germyne (Tbt)Ge≡C(Tbt) (Tbt = C$_6$H$_2$-2,4,6-(CH(SiMe$_3$)$_2$)$_3$).[303] A comparison of the $d_{E=E}$ bond lengths of NHC-coordinated ditetrelynes R(NHC)E=ER with that of NHC-free ditetrelynes E_2R_2 shows that the magnitude of bond length elongation follows the following trend: ($\Delta d_{Ge=C}$ (0.17 Å) > $\Delta d_{Si=Si}$ (0.14 Å) > $\Delta d_{Ge=Ge}$ (0.06 Å) (***Table 5***). Thus, Ge/Ge2–C^{VNL} bond lengths are closer to the upper end of the range of Ge=C^{sp^2} double

[10] The compound was thoroughly characterized and reported in the following doctoral thesis; Sandeep Kumar, "*Low-Valent Heavier Tetrel Compounds Supported by N-heterocyclic Carbenes: A Comprehensive Experimental and Theoretical Perusal*", *Dissertation*, Rheinische Friedrich-Wilhelms-Universität Bonn, **2025.**

bond lengths (*vide infra*) of germaethanes reported in the Cambridge Structural Database (1.770 − 1.894 Å).

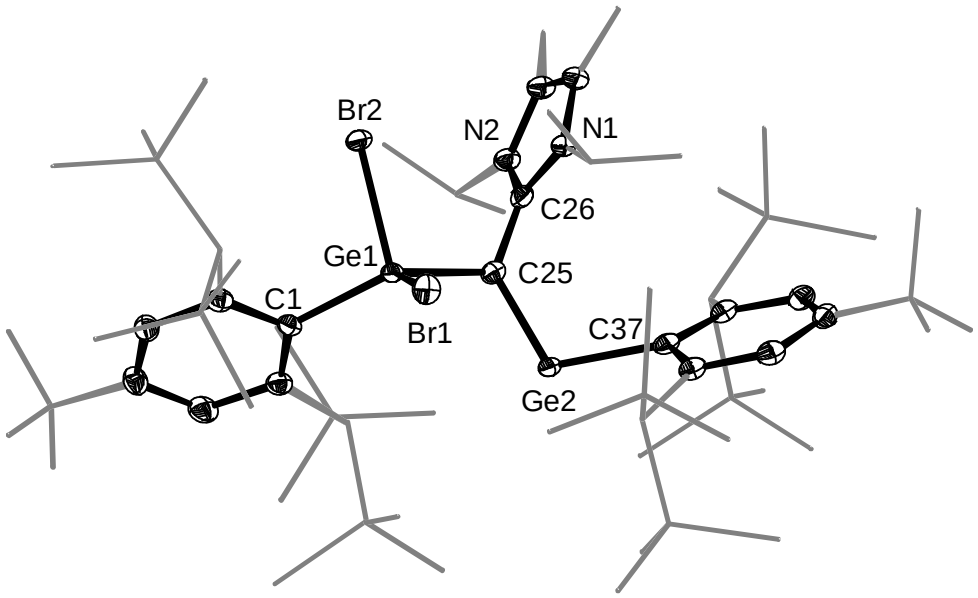

Figure 82. DIAMOND plots of the molecular structures of the unprecedented NHC-supported germyne **39-Ge**; thermal ellipsoids are set at 50% probability level and the H-atoms are omitted ^{i}Pr, ^{t}Bu and Dsi groups are shown in wire frame for the sake of clarity; selected bond lengths (Å) and bond angles (°): Ge1-C25 1.9047(18), Ge1-C1 1.9876(19), Ge2-C25 1.9233(19), Ge2-C37 2.0423(19), Ge1-Br1 2.3856(3), Ge2-Br2 2.3669(3), C25-C26 1.446(3), C1-Ge1-C25 135.63(8), C25-Ge2-C37 108.49(8), Ge1-C25-C26 113.41(13), Ge2-C25-C26 130.22(14), Ge1-C25-Ge2 114.11(9).; φ^{NHC} = 86.81(6), ∑∠(C25) = 358°.

Table 5. Comparison of E=E'/E≡E bond lengths, E'−E−R bond angles and interplanar angles (φ^{NHC}) of **39-Ge**, NHC-supported ditetrelynes, tetrelynes, ditetrelynes and (E, = C, Si, Ge; E' = Si, Ge).

Compound	E=E'/E≡E (Å)	E'−E−R (°)[a]	φ^{NHC} (°)[a]	*Ref.*
TbbGe=C(GeBr$_2$Tbb)(IMe$_2$^{i}Pr$_2$)(**39-Ge**)	1.905(1)	114.1(1)	75.2(1)	This work
(Tbt)Ge≡C(Tbt)[b]	1.754	130.7	–	[303]
(SiR$_3$)Si=Si(SiR$_3$)(IMe$_4$)[c,e]	2.1989(6)	120.35(2)	82.14(7)	[345]
(SiR$_3$)Si≡Si(SiR$_3$)[c]	2.0622(9)	137.44(4)	–	[36]
(Tbb)Si=Si(Tbb)(IMe$_4$)[d,e]	2.2120(7)	110.79(6)	42.48(9)	[130]
(Tbb)Si=Si(Tbb)(IMe$_2$^{i}Pr$_2$)[d,f]	2.214(3)	111.0(2)	59.9(4)	[130]
(Tbb)Si≡Si(Tbb)[d]	2.105(2)	131.42(9)	–	[43]
(Tbb)Ge=Ge(Tbb)(IMe$_4$)[d,e]	2.3039(6)	113.25(8)	43.1(1)	[130]
(Tbb)Ge≡Ge(Tbb)[d]	2.2410(9)	130.5(1)	–	[227]
	2.222(9)[g]	130.7(1)[g]		

[a]: E'−E−R denotes the angle at the dicoordinated tetrel atom and φ^{NHC} the angle between the least-squares plane of the NHC five-membered ring and the plane defined by the C^{NHC} and the two multiply-

bonded tetrel atoms; [b]: Tbt = C_6H_2-2,4,6-$(CH(SiMe_3)_2)_3$, bonding parameters predicted by theory; [c]: SiR_3 = $Si^iPr(CH(SiMe_3)_2)_2$; [d]: Tbb = C_6H_2-2,6-$(CH(SiMe_3)_2)_2$-4-^{t}Bu; [e]: IMe_4 = $C[N(Me)C(Me)]_2$; [f]: $IMe_2{}^iPr_2$ = $C[N(^iPr)C(Me)]_2$; [g] experimental bonding parameters of the second independent molecule.

The solution structures of **39-Ge** were determined by multi-nuclear NMR spectroscopy. In the $^{13}C\{^1H\}$ NMR spectrum, the chemical shift of the vinylic carbon atom C^{VNL} appears at higher field δ (**39-Ge**: C^{VNL} = 143.83 ppm, C^{NHC} = 155.03 ppm), suggesting a $C^{VNL(\delta-)}$–$C^{NHC(\delta+)}$ bond polarization. The ^1H and ^{13}C NMR spectral features can be rationalized by considering an overall C_1-symmetry with hindered rotations of the NHC ligand and the Tbb substituents about the respective C^{VNL}–C^{NHC} and Ge–C^{Tbb} bonds on the NMR time-scale.

As aforementioned, compounds **38-Si** and **39-Ge** serve as versatile synthons, enabling access to unprecedented constitutional isomers of heavier imidazole and C_3H_2-type frameworks under standard laboratory conditions. Reduction of **38-Si** with two equivalents of KC_8 in benzene resulted in a distinct colour change from light yellow to red, suggesting the formation of a new compound. Monitoring the reaction by ^1H NMR spectroscopy after 7 hours revealed the selective formation of a novel compound, identified as the novel heavier imidazole analogue **40-Si**. Notably, no intermediates were detected by NMR spectroscopy at ambient temperature during the conversion of **38-Si** to **40-Si**. Crystallization from *n*-hexane at −60 °C yielded **40-Si** as an intensely air-sensitive, red solid in 58% yield. In contrast, the germanium analogue **39-Ge** exhibited poor selectivity under identical conditions, as evidenced by a complex ^1H NMR spectrum at ambient temperature.

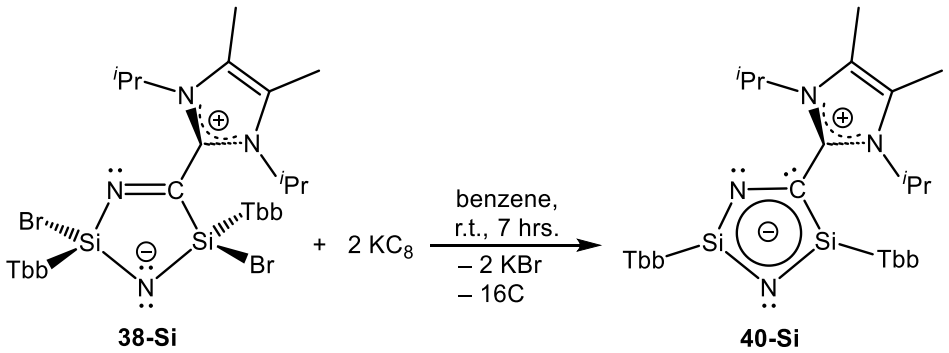

Scheme 30. Synthesis of unprecedented heavier analogue of Imidazole derivative **40-Si**

Compound **40-Si** exhibits good solubility in benzene, toluene, THF, Et_2O and *n*-hexane at ambient temperature. Thermal decomposition was detected upon melting at 145 °C in a vacuum-sealed glass capillary. Analysis of the soluble part of the respective melting residue in (D_6)benzene by ^1H NMR spectroscopy revealed unselective decomposition of **40-Si**.

Complex **40-Si** is the first heavier analogue of imidazole to be reported and was characterised thoroughly by single-crystal X-ray diffraction (sc-XRD) analysis and multinuclear NMR spectroscopy. Block-shaped red crystals of **40-Si**·(***n*-hexane**)$_{1.5}$, suitable for sc-XRD analysis, were obtained by slow cooling of their saturated *n*-hexane solution at −30 °C. Compound **40-Si** crystallized out in the triclinic space group $P\bar{1}$. The molecular structure of the heavier analogue of imidazole **40-Si** reveals a planar five-membered Si_2CN_2 ring (sum of interior angles = 540°) and two trigonal planar silicon centers (∡(Si1) = 359.9° and ∡(Si2) = 359.1°) (***Figure 83***).

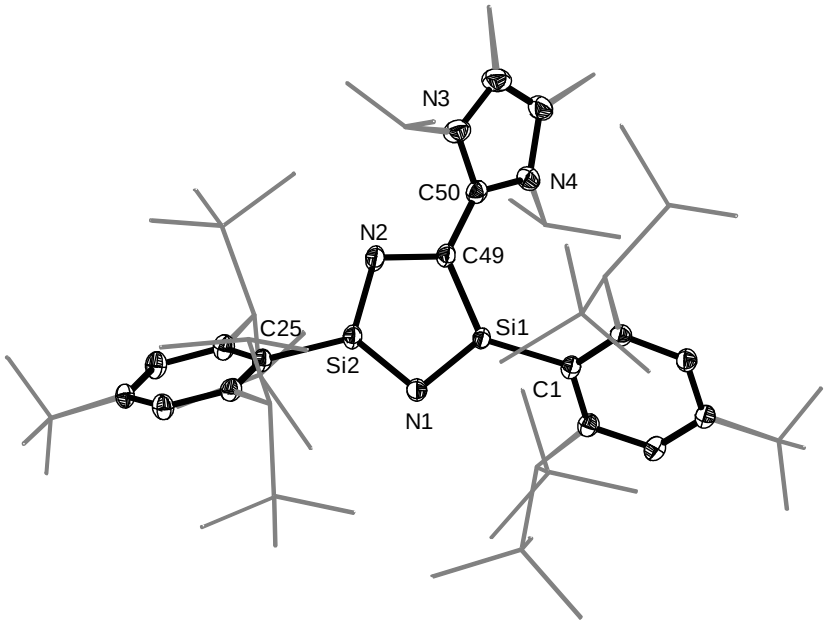

Figure 83. DIAMOND plot of the molecular structure of **40-Si**. Thermal ellipsoids are set at 30 % probability level. Hydrogen atoms are omitted and the Dsi and ^{t}Bu substituents of the Tbb ligand and, ^{i}Pr of NHC are presented in wire-frame for clarity. Selected bond lengths [Å], bond angles [°]: Si1-N1 1.6736(15), Si1-C49 1.7914(18), Si1-C1 1.8633(17), Si2-N1 1.6671(15), Si2-N2 1.6616(16), Si2-C25 1.8492(17), N2-C49 1.423(2), C49-C50 1.431(2), N1-Si1-C1 122.29(8), C49-Si1-C1 131.21(8), C49-Si-N1 106.39(8), N1-Si2-C25 126.04(8), N2-Si2-C25 119.82(8), N1-Si2-N2 113.23(8), N2-C49-Si1 110.67(17); φ^{NHC} = 40.10(7)°; ∑∡(C49) = 359.92°.

The sterically more demanding Tbb substituents are arranged in acute orientation (torsion angle C1−Si1−Si2−C25 = 41.85(1)°) as compared trans oriented to its precursor **38-Si** (torsion angle C1−Si1−Si2−C25 = −154.49(1)°). The Si1−N1 and Si2−N1 bond lengths (1.674(2) Å and 1.667(3) Å, respectively) in **40-Si** compare well with previously reported metal-bonded bis-silylamide Li(thf)[(SiMe$_3$)Si(CH$_2$^{t}Bu)$_2$-C$_6$H$_4$-1,2] (1.672(3) Å)[342] reported by Lappert and coworkers and abit enolgated to its precursor **38-Si** (1.659(1) Å and 1.655(1) Å) suggesting double bond character in the Si_2N_2C ring. Notably, The C^{VNL}–C^{NHC} bond length (1.431(2) Å) corroborate well with the literature known NHC-supported bromogermynes ((IDipp)(SiBr$_2$Tbb)C=GeBr (1.444(2) Å) and (IDipp)(GeBr$_2$Tbb)C=GeBr (1.447(2) Å)),[217] equivalent to $C^{(sp3)}$–$C^{(sp2)}$

single bond distance[290] and C^{VNL} center shows trigonal planar coordination ($\Sigma\measuredangle(C^{VNL})$ = 359.82°). The NHC ring is a bit orientated (φ^{NHC} = 40.10(7)°) to the central five-membered ring Si_2CN_2.

The solution integrity of the heavier analogue of imidazole **40-Si** was confirmed using multinuclear NMR spectroscopy in (D_6)benzene at 298 K. The ^{1}H and $^{13}C\{^{1}H\}$ NMR spectra of **40-Si** indicate a time-averaged C_1-symmetric structure in solution due to the presence of two stereogenic silicon centers and fast rotation of Tbb around their Si–C^{Tbb} bond axis at 298 K. The most prominent spectroscopic feature of **40-Si** is its ^{29}Si NMR chemical shift at 67.33 and 62.34 ppm, assigned to the two heterotopic stereogenic silicon centers in a planar five-membered Si_2N_2C ring. These two signals are downfield shifted as compare to their precursor **38-Si** (−34.7 and −20 ppm in (D_8)thf at 263 K) (***Figure 84***) due to electron delocalization in the planar five-membered Si_2N_2C ring. In the $^{13}C\{^{1}H\}$ NMR spectrum, the chemical shift of the vinylidene carbon atom C^{VNL} appears at an upfield shifted (δ_{CVNL} = 121.16 ppm in (D_6)benzene at 298 K) compared to its precursor **38-Si** (δ_{CVNL} = 194.2 ppm in (D_8)thf at 263 K) and align close with NHC-supported bromogermynes ((IDipp)($SiBr_2$Tbb)C=GeBr (δ_{CVNL} = 133.6 ppm).[217]

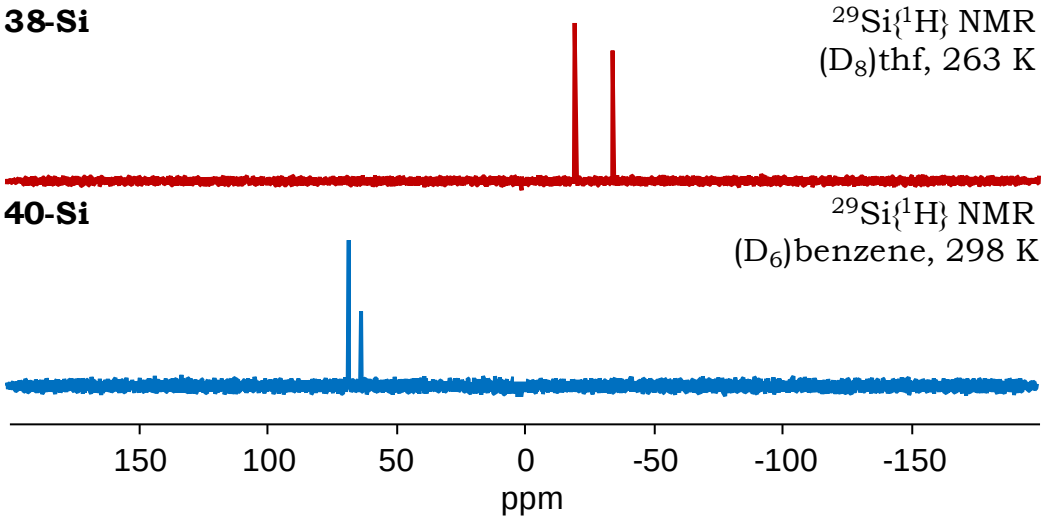

Figure 84. $^{29}Si\{^{1}H\}$ NMR of compound **38-Si** (***top***) and **40-Si** (***bottom***).

3. Summary and Outlook

3.1. Summary

Within the framework of this dissertation, the synthesis of unprecedented metallo-bis-stannylene complexes of cobalt and rhodium was investigated. Furthermore, the versatile reactivity of a digermyne cobalt complex with polar unsaturated organic molecules was systematically explored, leading to the discovery of a series of novel transformations and the isolation of unique products. Additionally, the reductive coupling chemistry of Mes-NC with (Tbb)E≡E(Tbb) (where E = Si and Ge), extending the scope of their reactivity followed by an in-depth exploration of the reactivity of 1,2-digermabutadiene (**7-Ge**)[226] and 1,4-digermabenzene (**8-Ge**)[226], which yielded a multitude of novel reactions and unique products with significant chemical implications. Afterwards, the versatile chemistry of base-supported heteroditetrelynes was experimentally examined within the context of this thesis.

Furthermore, the chemistry of Push-Pull carbene ($(NDippCH_2)_2P\}(SiMe_3)C$:) with (halo)(aryl)tetrylenes (R)GeX (where R = Tbb and Mind), as well as NHC and $CAAC^{Me}$ adducts of $SiBr_2$, was investigated, revealing a broad spectrum of intriguing transformations. Lastly, the reactivity of sterically non-demanding diazoolefin (**36**) with (Tbb)E≡E(Tbb) (where E = Si and Ge) and (E)-(Tbb)BrE=EBr(Tbb) (where E = Si and Ge) was explored, providing new insights into their chemical behaviour through the lens of this research endeavour.

Metallo-bis-stannylene complex of Co and Rh

The initial section of the thesis (***section 2.1.1***) focuses on the investigation into the reactivity of $Sn_2Ar^{Dipp}{}_2$ with $CpM(CO)_2$ (M = Co, Rh), revealing markedly divergent reaction pathways. These pathways culminated in the formation of novel metallo-bis-stannylene complexes, **2-Co** and **2-Rh** (***Scheme 31***), through the elimination of one CO ligand and the cleavage of the Sn−Sn bond. However, decarbonylation of **2-Co** / **2-Rh** under thermal or photochemical conditions failed to yield the desired CO-free product**.** Attempts were made to synthesize a CO-free **2-Co**/**2-Rh** derivative *via* a two-step procedure starting from $CpCo(C_2H_4)_2$. The first step involved a ligand exchange reaction with $[Tbb(\mu^2\text{-}Br)Sn]_2$, yielding a bis-bromostannylidene complex as per ^{1}H-NMR although the mentioned compound was not isolated due to its prolong instability in the solution and subsequent reduction of this intermediate with KC_8 was attempted; however, the desired CO-free derivative could not be isolated

successfully in contrast to the two-steps synthesis of digermyne complex of Co (**3-CoGe, *Scheme 2***).[226]

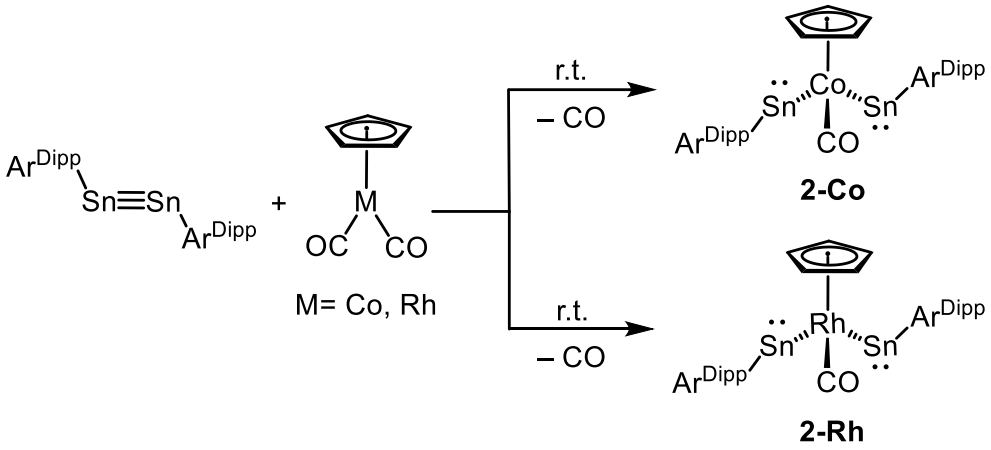

Scheme 31. Reactivity of $Sn_2Ar^{Dipp}{}_2$ with $CpM(CO)_2$ (M = Co, Rh)

Reactivity of digermyne complex of cobalt

Section 2.1.2 focuses on the reactivity of the aforementioned *cis*-digermyne complex (**3-CoGe**)[226] exhibiting dual centered reactivity, as demonstrated through systematic investigations with polar unsaturated organic molecules (e.g., aryl nitriles, isocyanates, ketones, CO_2, and isothiocyanates) and small polar molecules. These reactions were systematically explored and classified into three distinct categories: (i) addition reaction (**3-Co**), (ii) [2+2] cycloaddition reactions (**4-Co** to **7-Co**) and (iii) insertion reactions (**8-Co** to**11-Co**) (***Scheme 32***).

Initial reactivity studies of digermyne complex (**3-CoGe**) with the small phosphane (PMe_3) reveal Co-centered reactivity, yielding an addition product (**3-Co**) in which PMe_3 does not show dissociation/association dynamic equilibrium (***Scheme 32***). In contrast, reactions with a non-polar unsaturated substrate including *p*-tol-CN, (*p*-tol)$_2$CO, CO_2, and Mes-NCO proceed *via* [2+2] cycloaddition pathways, affording the corresponding cycloaddition products (**4-Co**, **5-Co**, **6-Co**, and **7-Co**, respectively) (***Scheme 32***). Notably, the reaction with *p*-tol-NCS deviates from this trend, producing an unexpected insertion product (**8-Co**), where elemental sulfur is incorporated between the two germanium centers. Further investigations demonstrate divergent reactivity with diazo and azide reagents. Treatment with (*p*-tol)$_2CN_2$ results in an N-end addition product (**9-Co**), whereas reaction with TMS-N_3 leads to N_2 liberation, yielding transient nitrene (TMS–N) insertion complex **10-Co**. Additionally, exposure of the digermyne complex to P_4 generates an unprecedented tetraphosphadigerma Dewar benzene complex of the CpCo fragment (**11-Co**) (***Scheme 32***).

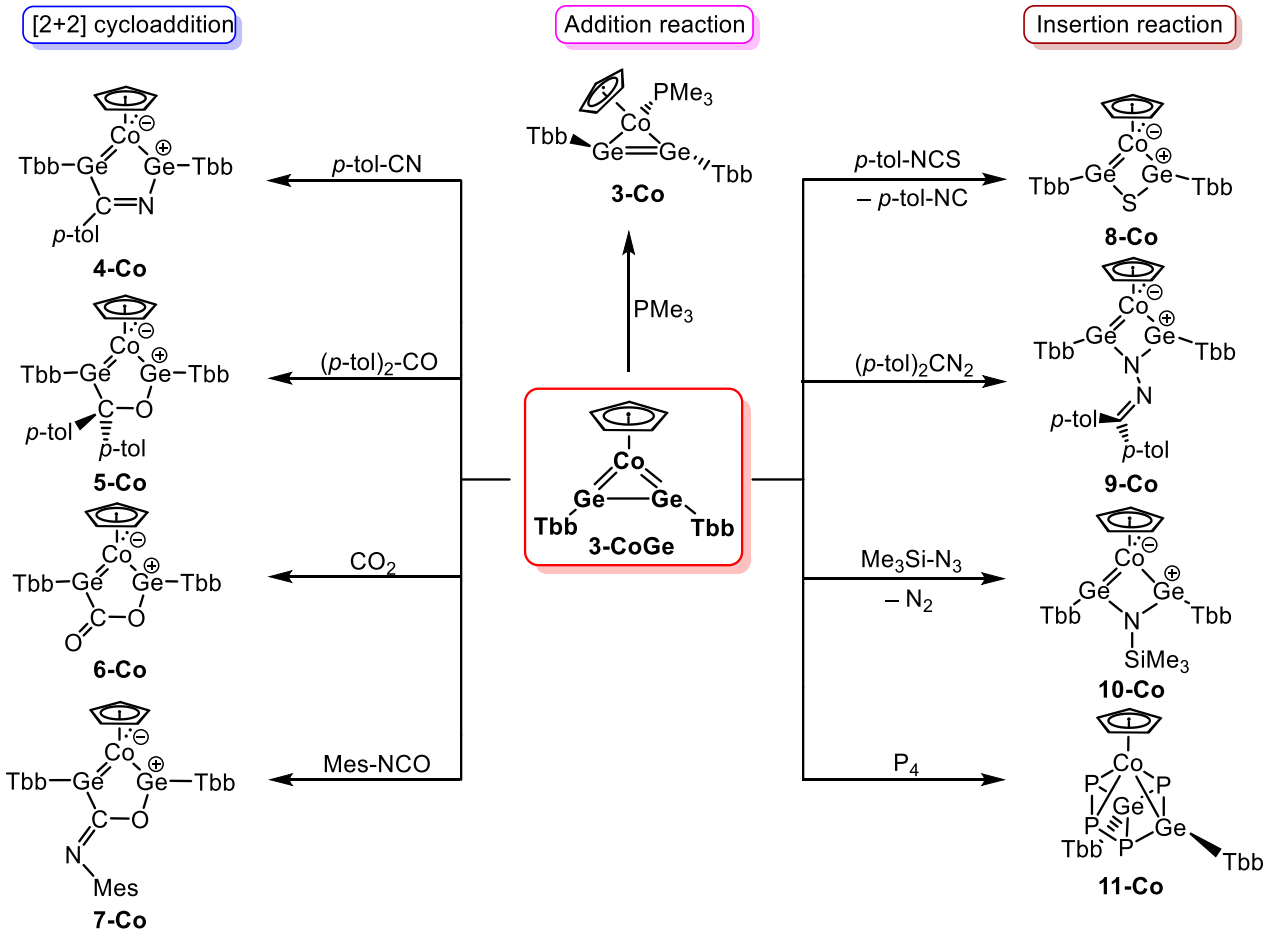

Scheme 32. Reactivity of digermyne complex **3-CoGe**.

Comparative studies of E_2Tbb_2 (E = Si, Ge) with Mesityl isocyanide

A comparative study of the reactivity of E_2Tbb_2 (E = Si, Ge) with Mes-NC, described in ***section* 2.2.1**, reveals a mechanistic distinct pathway compare to the previously reported Lewis acid-base bis–adduct formation of alkyl/aryl isocyanides with ditetrelynes, leading to the formation of the novel coupling products, 1,2-disiletene (**12-Si**) and 1,2-germetene (**12-Ge**) (***Scheme 33***). In both cases, the Tbb groups adopt a *cis* orientation, with the tetrel center exhibiting a trigonal planar geometry. The reaction of disilyne with one equivalent of Mes-NC at room temperature did not yield the mono-adduct, whereas under analogous conditions, digermyne formed a detectable mono-adduct as per ^{1}H-NMR. However, the pure mono-adduct of digermyne could not be isolated due to the competitive formation of a coupling product **12-Ge**. These observations demonstrate a notable divergence in reactivity between the silicon and germanium-based systems under identical reaction conditions.

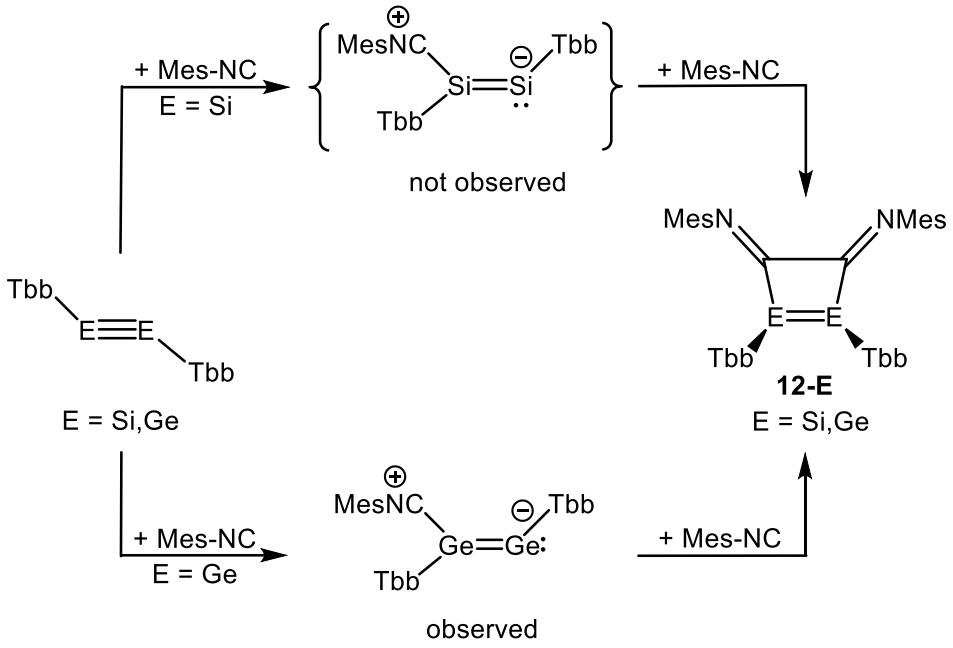

Scheme 33. A distinct reactivity profile of ditetrelynes E_2Tbb_2 (E = Si, Ge) with Mes-NC.

Upon isolation of **12-E** (E = Si, Ge), both ditetreletenes were subjected to reaction with $GeBr_2$(1,4-dioxane) at ambient temperature. In the case of **12-Si**, the reaction proceeded selectively to yield a novel compound, **13-Si** (***Scheme 34***), resulting Tbb in *anticlinical*-orientation and stereogenic silicon centers. In contrast, the reaction involving **12-Ge** exhibited poor selectivity, leading to a mixture of products without the formation of a well-defined structural motif analogous to that observed for **13-Si**. This divergence in reactivity highlights the distinct electronic and steric properties of silicon and germanium centers, influencing their behaviour in such transformations.

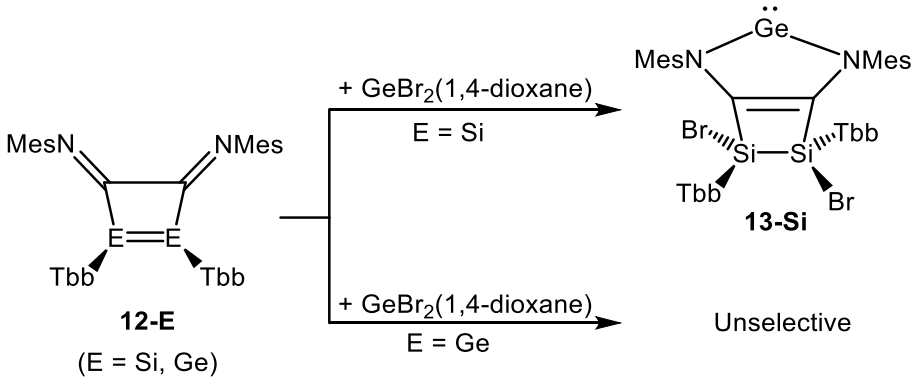

Scheme 34. Difference in the reactivity of **12-E** (**E** = **Si**, **Ge**) with $GeBr_2$(1,4-dioxane).

Downstream chemistry of 1,2-digermabutadiene (7-Ge) and 1,4-digermabenzene (8-Ge)

***Section* 2.2.2** to **2.2.4**, delves into the intricate reactivity profiles of 1,2-digermabutadiene (**7-Ge**)[226] and 1,4-digermabenzene (**8-Ge**)[226], exploring their unique structural and electronic characteristics. Additionally, the synthesis of

germylone (**19-Ge**) and stannylone (**19-Sn**), along with their distinctive reactivity patterns, is thoroughly investigated. These studies aim to uncover novel reaction pathways and generate intriguing compounds, thereby expanding the frontiers of main group low valent chemistry and offering new insights into the behaviour of heavy group 14 elements in complex molecular frameworks.

1,2-digermabutadiene (**7-Ge**)[226] undergoes insertion reaction of tetrel center associated with 1,2-halide migration to vicinal germanium centers with $GeBr_2$(1,4-dioxane) and $SnCl_2$ to facilitate *cyclo*-bis-germyl germylene **14-Ge** and *cyclo*-bis-germyl stannylene **14-Sn** (***Scheme 35***). In both cases, the sterically demanding Tbb groups adopt an *anticlinical*-orientation, as confirmed by structural analysis. This spatial arrangement is critical for stabilizing the resulting low-valent species. The discussed compounds **14-E** (E = Ge, Sn) could be potential precursors for the generation of bis-germylene-supported germylones and stannylones upon reductive dehalogenation with appropriate reducing agents, which are of considerable interest due to their unique electronic structures and potential applications in main-group catalysis and small-molecule activation.

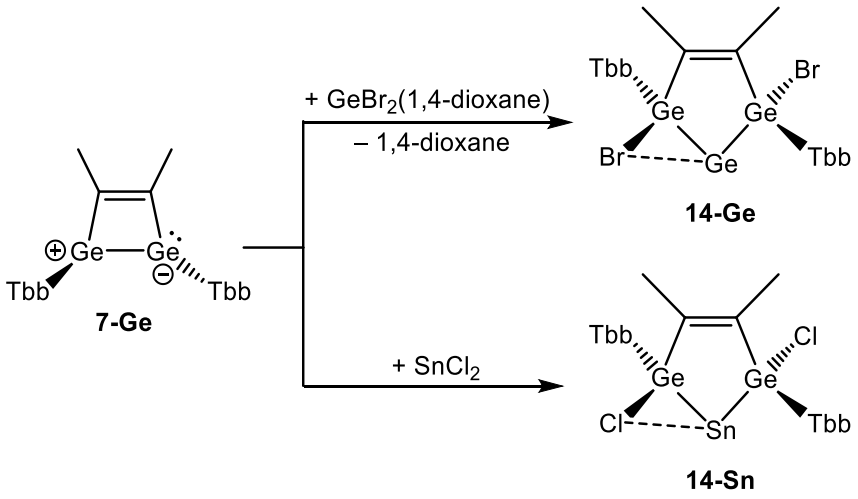

Scheme 35. Synthesis of *cyclo*-bis-germyl germylene (**14-Ge**) and *cyclo*-bis-germyl stannylene (**14-Sn**).

As mentioned, 1,2-digermabutadiene exhibits intriguing follow-up chemistry. Treating it with Mes-NC afforded **15-Ge**, featuring an inserted Mes-NC product formed by the cleavage of the Ge–C bond instead of the Ge–Ge bond (***Scheme 36***). The reaction of 1,2-digermabutadiene with silylazide (TMS-N_3) and diazomethane ((*p*-tol)$_2CN_2$) leads to the formation of **16-Ge** and **17-Ge** (***Scheme 36***). **16-Ge** represents a class of diradicaloid compounds with a predicted singlet ground state and can be interpreted as a heavier analogue of pyrrole. Whereas in **17-Ge**, one germanium center exhibits a trigonal pyramidal geometry whereas the other displays a distorted tetrahedral geometry, having being activated by the *p*-tol group.

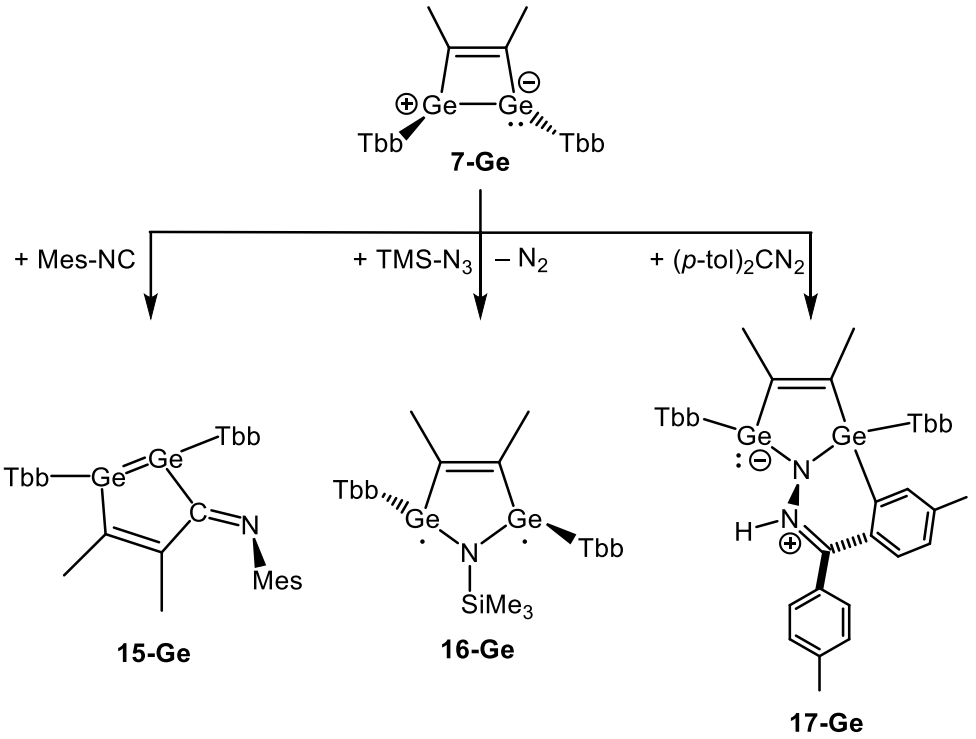

Scheme 36. Reactivity of 1,2-digermabutadiene (**7-Ge**).[226]

Compound 1,4-digermabenzene (**8-Ge**)[226] acts as a versatile synthon due to its reactivity towards amphiphile reagents, enabling the isolation of intriguing bicyclic compounds and notably, upon treating with a series of amphiphile reagents, including $SiBr_2$(SIDipp), $GeBr_2$(1,4-dioxane), and $SnCl_2$, yielding bicyclic derivatives of isostructural motifs **18-E** (E= Si, Ge, Sn) (***Scheme 37***).

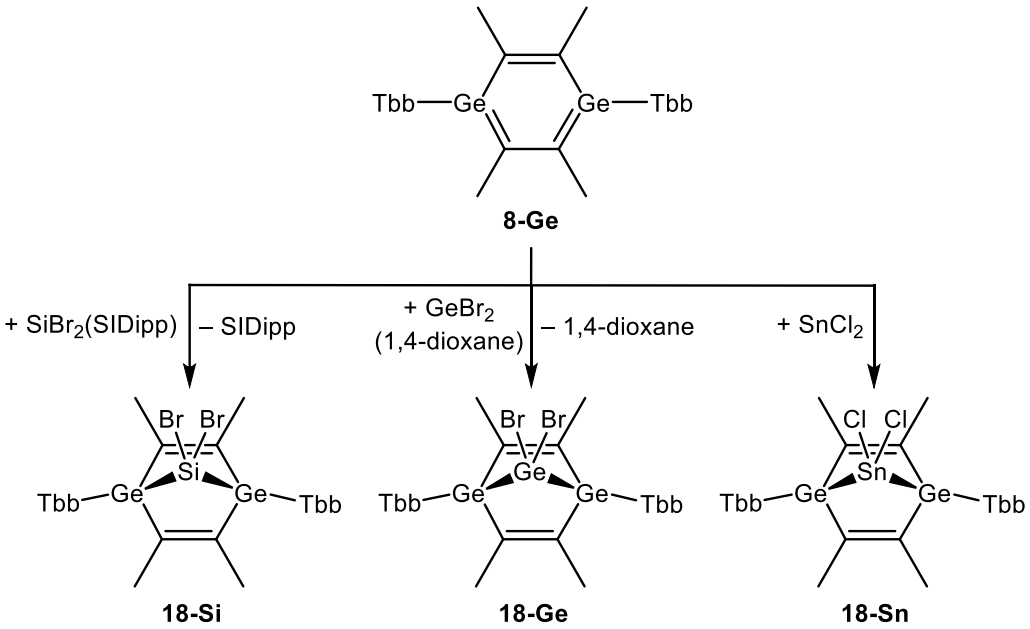

Scheme 37. Reactivity of 1,4-digermabenzene **8-Ge**.[226]

Reductive dehalogenation of *cyclo*-bis-germyl germylene **14-Ge** and *cyclo*-bis-germyl stannylene **14-Sn** with KC_8 successfully afforded *iso*-typic bis-germylene stabilized germylone (**19-Ge**) and stannylone (**19-Sn**) respectively (***Scheme 38***). The synthesized tetrylones exhibit the *iso*-typic electronic and structural features of literature known bis-tetylene-supported tetrylones.[122,285]

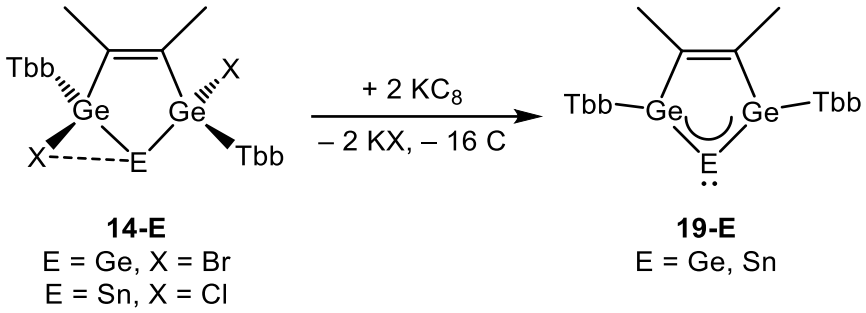

Scheme 38. Synthesis of bis-germylene stabilized germylone (**19-Ge**) and stannylone(**19-Sn**).

The isolation of these compounds enabled further investigation of their reactivity, allowing for the testing of multiple reactive sites for additional functionalization. Interestingly, the reaction of **19-Ge** with $GeBr_2$(1,4-dioxane) leads to the formation of unprecedented compound tetragerma[2,1,1]propellane **20-Ge** featuring two distorted tetrahedral germanium centers and two trigonal pyramidal germanium centers. Notably, **19-Ge** was treated with sterically non-demanding diazoolefin $(IMe_4)CN_2$ to yield bicyclo[2.1.1.]bis-germyl germylene **21-Ge**. At last, NHC (IMe_4) was treated with **19-Ge**, leading to the formation of the IMe_4 adduct **22-Ge** (***Scheme 39***).

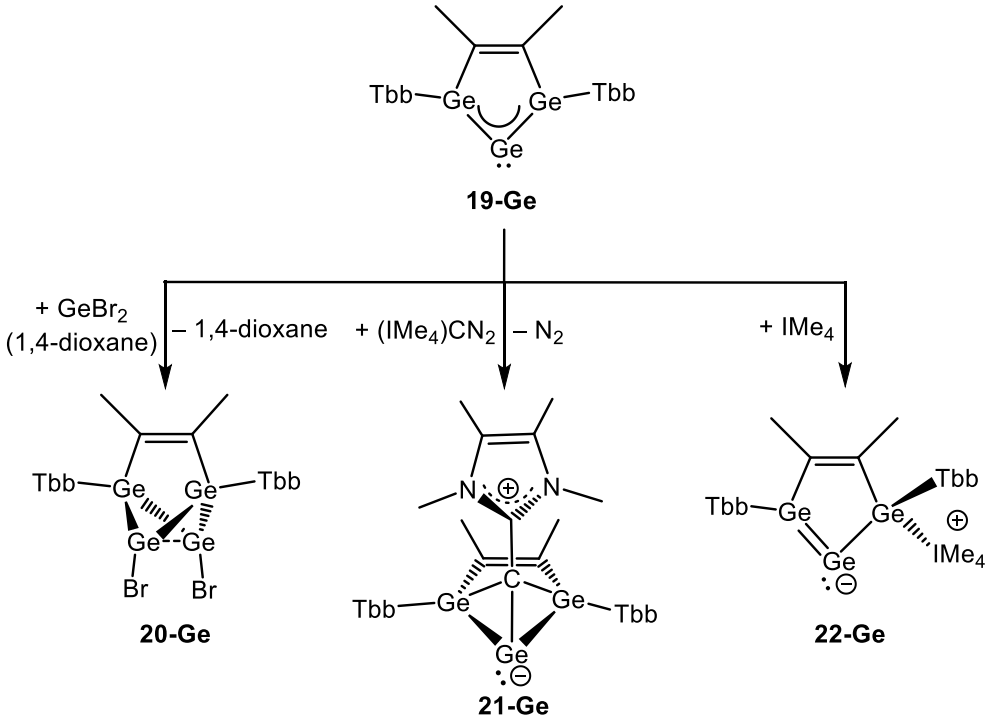

Scheme 39. Reactivity of germylone (**19-Ge**).

Compound tetragerma[2,1,1]propellane (**20-Ge**) is a powerful synthon that enables access to novel germanium cluster compounds under standard laboratory conditions. Notably**,** **20-Ge** undergoes further functionalization through the reductive dehalogenation *via* 2e-reduction to afford the unprecedented η^5-Ge(0) half-sandwich complex (**23-Ge**) featuring a slightly bent Ge_3C_2 core with an apical Ge atom (***Scheme 40***).

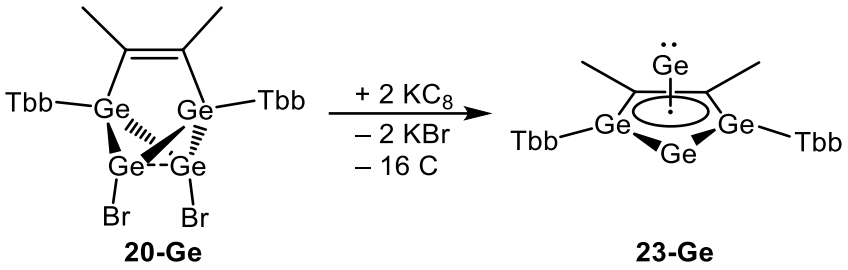

Scheme 40. Synthesis of unprecedented η^5-Ge(0) half sandwich complex (**23-Ge**).

Complex **23-Ge** was further treated with the $GeBr_2$(1,4-dioxane) to unravel the pentagerma[1.1.1]propellane **24-Ge** (***Scheme 41***). Compound **24-Ge** represents one of the rarest synthetically accessible metalla[1.1.1]propellanes,[234] whose further reductive dehalogenation turned out to be unselective.

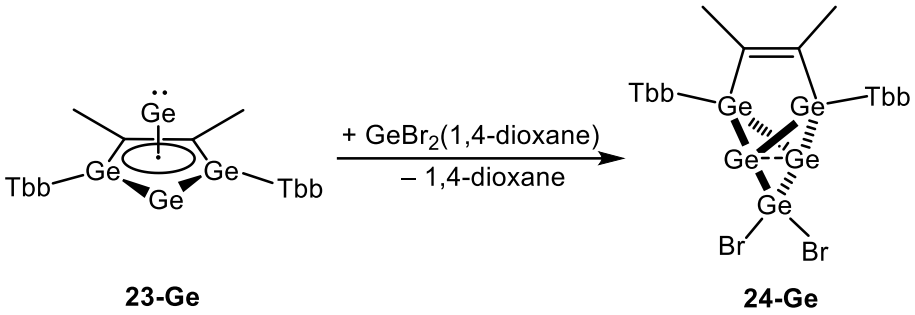

Scheme 41. Synthetically accessible pentagerma[1.1.1]propellane (**24-Ge**).

Isolation and Reactivity of DMAP-supported stannasilyne

Section* 2.3** of this thesis delves into the synthesis and reactivity profiles of heteroditetrelynes. The reaction of $Sn_2Ar^{Dipp}_2$ with the DMAP adduct of (*E*)-(Tbb)BrSi=SiBr(Tbb) facilitated the straightforward synthesis of the DMAP-supported stannasilyne **25-SnSi** (Scheme 42***), along with the equimolar amount of DMAP-supported $Ar^{Dipp}SnBr$. **25-SnSi** was subsequently isolated through low temperature crystallization and washing, effectively separating it from the byproduct. The DMAP supported stannasilyne **25-SnSi** exhibits notable thermal stability, remaining intact in solution at 110 °C in toluene for several hours.

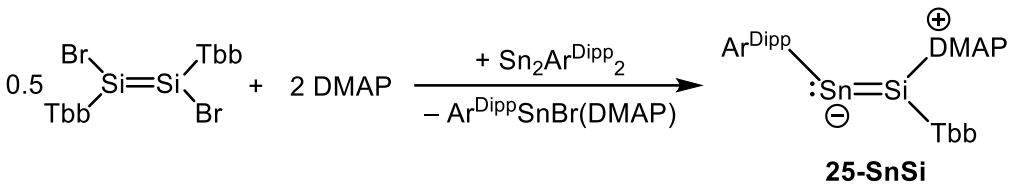

Scheme 42. Isolation of DMAP-supported stannasilyne **25-SnSi**.

The reactivity of **25-SnSi** with weak π-acceptor and strong σ-donor ligand like mesityl isocyanide (Mes-NC) and IMe_4 (1,3,4,5-tetramethylimidazol-2-ylidene) respectively was investigated at ambient temperature, leading to the facile synthesis of the unprecedented mesityl isocyanide-supported stannasilyne **26-SnSi** and IMe_4-supported stannasilyne **27-SnSi** (***Scheme 43***). The reaction involved ligand exchange, wherein the original base was replaced by Mes-NC or IMe_4, accompanied by the elimination of an equimolar amount of DMAP (4-dimethylaminopyridine).

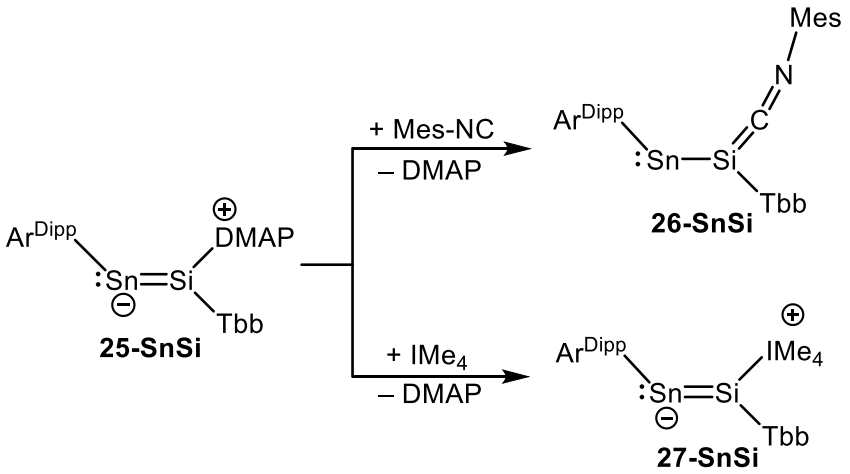

Scheme 43. Reactivity of DMAP-supported stannasilyne **25-SnSi** to afford base-supported stannasilyne **26-SnSi** and **27-SnSi**.

Section 2.4 focuses on the efforts to isolate base-free germynes/silynes through the synthesis of sterically encumbered diazomethane derivatives, such as (Tbb)HC=N_2) (**28**). Subsequent lithiation of **28** yielded the lithium diazomethanide (**29**). Treatment of **29** with (*E*)-(Tbb)BrGe=GeBr(Tbb) resulted in the formation of a novel η^1-N-bound diazomethanide germanium complex (**30-Ge**, ***Scheme 44***), demonstrating a rare coordination mode in low-valent germanium chemistry.

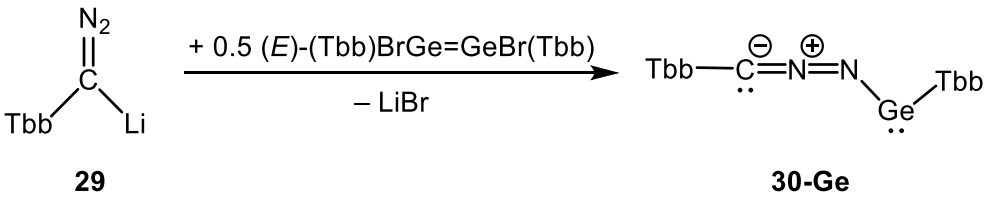

Scheme 44. Synthesis of η^1-N-bound diazomethanide complex of Ge (**30-Ge**).

In pursuits of synthesizing tetrelynes, the sterically encumbered diazoalkane [{(NDippCH$_2$)$_2$P}(SiMe$_3$)C=N$_2$][311] was selected as a suitable starting material to afford a straightforward push-pull carbene (NDippCH$_2$)$_2$P(SiMe$_3$)C: by heating its diazo precursor at 80 °C for 2 hours in benzene, which was later treated with (*E*)-(R)BrGe=GeBr(R) (R = Tbb, Mind) to afford germene **31-Ge** (R = Tbb) and **32-Ge** (R = Mind) featuring *iso*-typic structural architecture around the germene (Ge=C) core (***Scheme 45***).

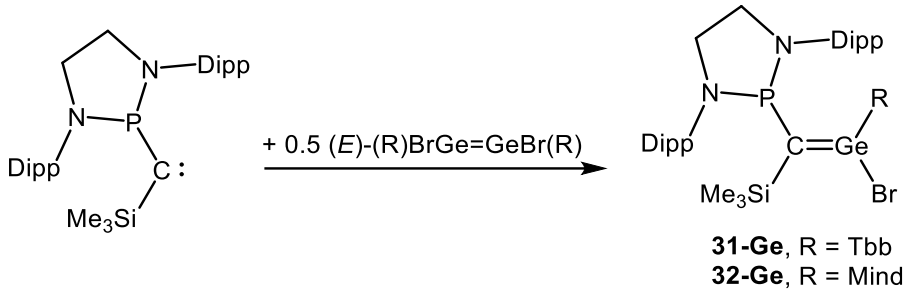

Scheme 45. Synthesis of germenes (**31-Ge** and **32-Ge**) from push-pull type-A carbene.

Type A push-pull carbene (NDippCH$_2$)$_2$P(SiMe$_3$)C: was later treated with base-supported Si(II) precursors (for instance SiBr$_2$(SIDipp) and SiBr$_2$(CAAC^{Me})) leading to **33-Si** and **34-Si** respectively. **33-Si** undergoes SiBr$_2$ insertion accompanied by ring opening of five-membered NHP substituent, resulting in the concomitant elimination of free SIDipp. However, in the case of **34-Si**, straightforward stable adduct formation of SiBr$_2$CAAC^{Me} and the carbene was observed, featuring a trigonal planar carbon center and a distorted tetrahedral silicon center supported by the CAAC^{Me} ligand (***Scheme 46***).

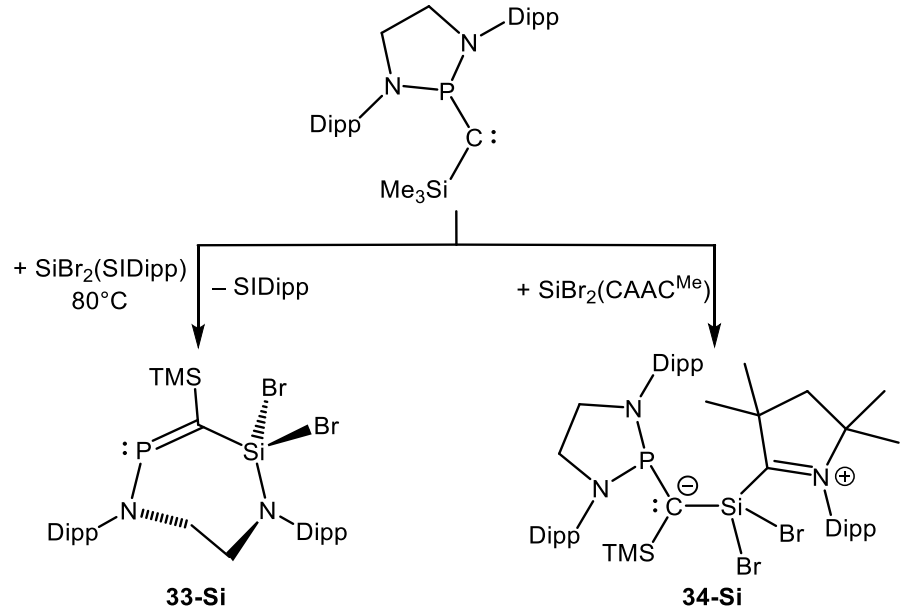

Scheme 46. Synthesis of **33-Si** and **34-Si** from push-pull type A carbene.

Compound **34-Si** features multiple reactive sites amenable to further functionalization. In pursuit of this, **34-Si** underwent reductive dehalogenation to afford the unprecedented bis-ligand-supported silasiliryne **35-Si**, featuring a three-membered Si_2C core supported by $CAAC^{Me}$ and the sterically encumbered phosphane ligand at the carbon and silicon center, respectively (***Scheme 47***).

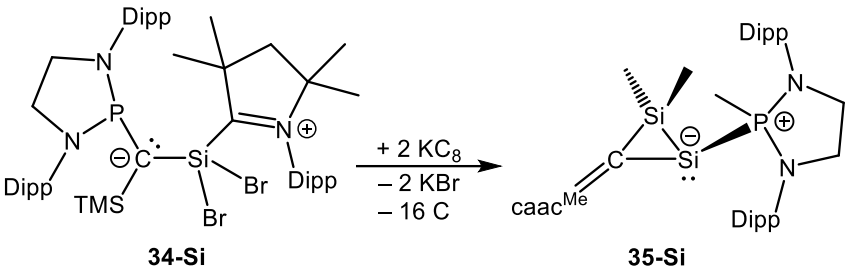

Scheme 47. 2e$^-$ reduction of **34-Si** to afford bis-ligand-supported silasiliryne **35-Si**.

***Section* 2.5** explores a series of novel reactions centered on low-valent Ge, Si and carbon compounds. The sterically less demanding diazolefin ($(IMe_2{}^iPr_2)CN_2$ (**36**)) has emerged as a pivotal synthon with its reactivity towards low-valent main group complexes being primarily driven by both electronic and steric factors employed by the diazooelfin.

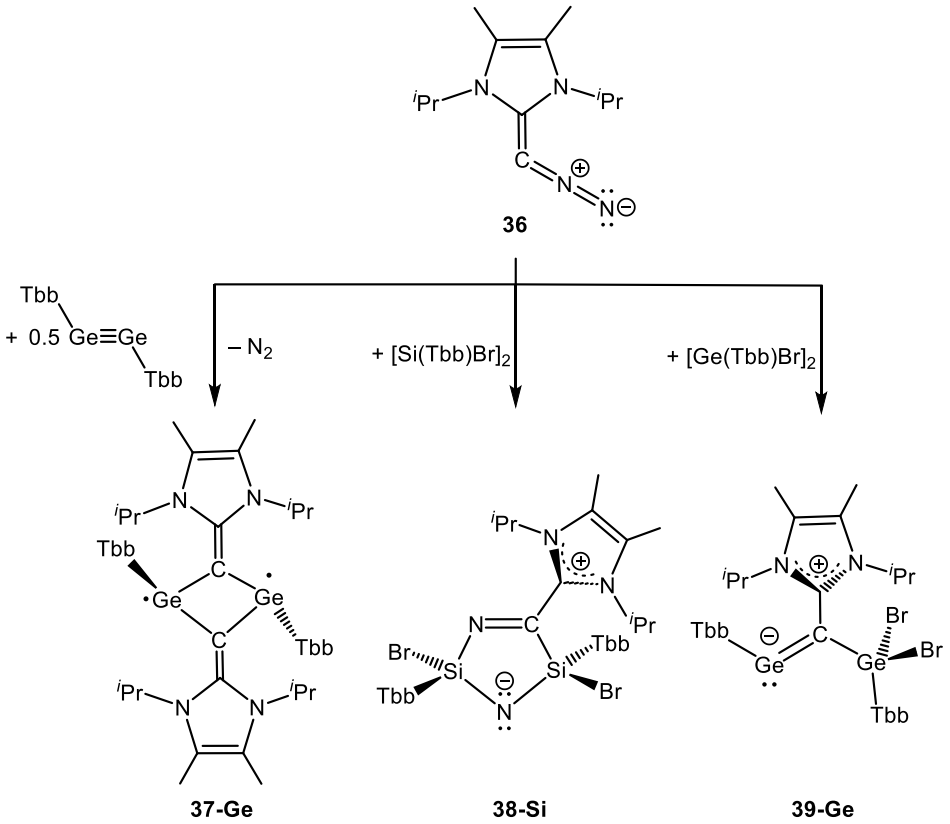

Scheme 48. Synthesis of Ge_2C_2-diradicaloid (**37-Ge**), bis(silyl)amide (**38-Si**) and unprecedented NHC-supported germyne (**39-Ge**).

Notably, the less hindered diazoolefin ($IMe_2^iPr_2$)CN_2 (**36**) yields markedly distinct reaction products compared to its bulkier counterpart upon interaction with tetrylynes and halo(aryl)tetrelenes. Specifically, the reaction of ($IMe_2^iPr_2$)CN_2 (**36**) with TbbGe≡GeTbb results in the formation of Ge_2C_2-diradicaloid **37-Ge** (***Scheme 48***), representing a rare instance of a non-metal mediated cleavage of a Ge≡Ge triple bond. In comparison treatment of ($IMe_2^iPr_2$)CN_2 (**36**) with $[Si(Tbb)Br]_2$ leads to the formation of the metal-free mediated cyclic bis-silyl amide **38-Si** (***Scheme 48***). In contrast the analogous reaction with $[Ge(Tbb)Br]_2$ proceeds probably *via* the NHC-supported 2-germavinylidene ($IMe_2^iPr_2$)C=Ge(Br)Tbb, which undergoes 1,2-addition reaction across the Ge=C double bond with an additional equivalent of "TbbGeBr" to afford the NHC-supported germyne **39-Ge**(***Scheme 48***).

Compounds **38-Ge** and **39-Ge** exhibit multiple reactive sites amenable to further functionalization, with dehalogenation representing a particularly promising pathway. Notably, **38-Si** undergoes a selective two-electron reduction to afford the unprecedented heavier analogue of Imidazole derivative **40-Si**, featuring a planar Si_2N_2C core (***Scheme 49***). In contrast, the analogous reaction with **39-Ge** was rather unselective.

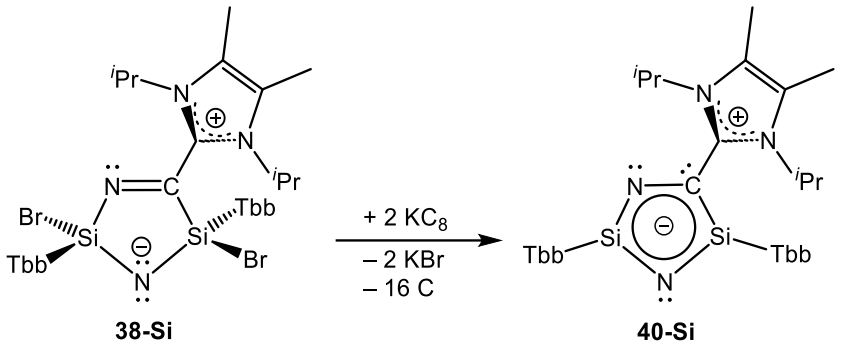

38-Si **40-Si**

Scheme 49. Synthesis of unprecedented heavier analogue of Imidazole derivative **40-Si**.

3.2. Outlook

The successful isolation of 1,2-disile/digermetene compounds (**12-Si** and **12-Ge**) has marked a significant advancement in the C−C coupling mediated by ditetrelynes (TbbE≡ETbb, where E = Si, Ge). Further studies reveal that **12-Si** reacts with $GeBr_2$(1,4-dioxane), yielding the "bis-amino stabilized germelene" **13-Si** through the halogen migration over the functionalized Si=Si double bond. This finding suggests that both **12-Si** and **12-Ge** exhibit reactive multiple bonds between the tetrel centers, potentially expanding their use in reactions with a broad array of organic reagents (for instance alkynes), sterically non-demanding diazoolefin, $CpCo(C_2H_4)_2$ and small tetrylenes (REX) which further reduced by 1e- to get anion radical (***Scheme 50***).

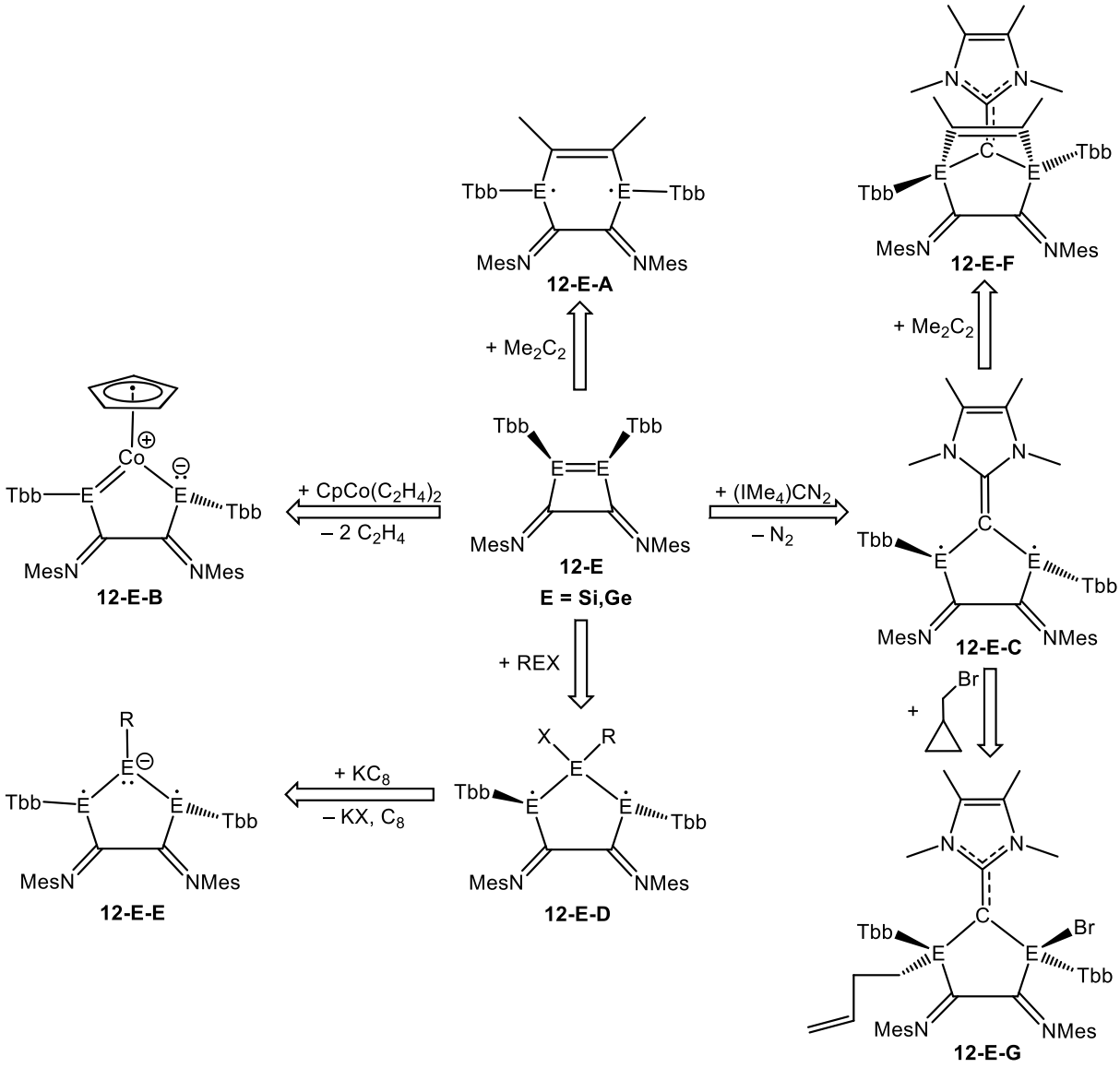

Scheme 50. Possible reactivity of 1,2-disile/germetene compounds (**12-Si** and **12-Ge**) towards organic alkyne, sterically non-demanding diazoolefin $(IMe_4)CN_2$, Co-based metal complex and small alkyl tetrel halide..

The bis-germylene-supported stannylone facilitated a comprehensive investigation of its reactivity, enabling a systematic exploration of electrophilic and nucleophilic sites for subsequent functionalization based on the chemical transformations observed in the case of analogous bis-germylene-supported germylone. Stannylone (**19-Sn**) potentially expands its use in reactions with a wide array of reagents like $Fe_2(CO)_9$, IMe_4, $(IMe_4)CN_2$ and $GeBr_2$(1,4-dioxane) whose potential reduced product might behave and geranium or tin atom transfer reagent (***Scheme 51***).

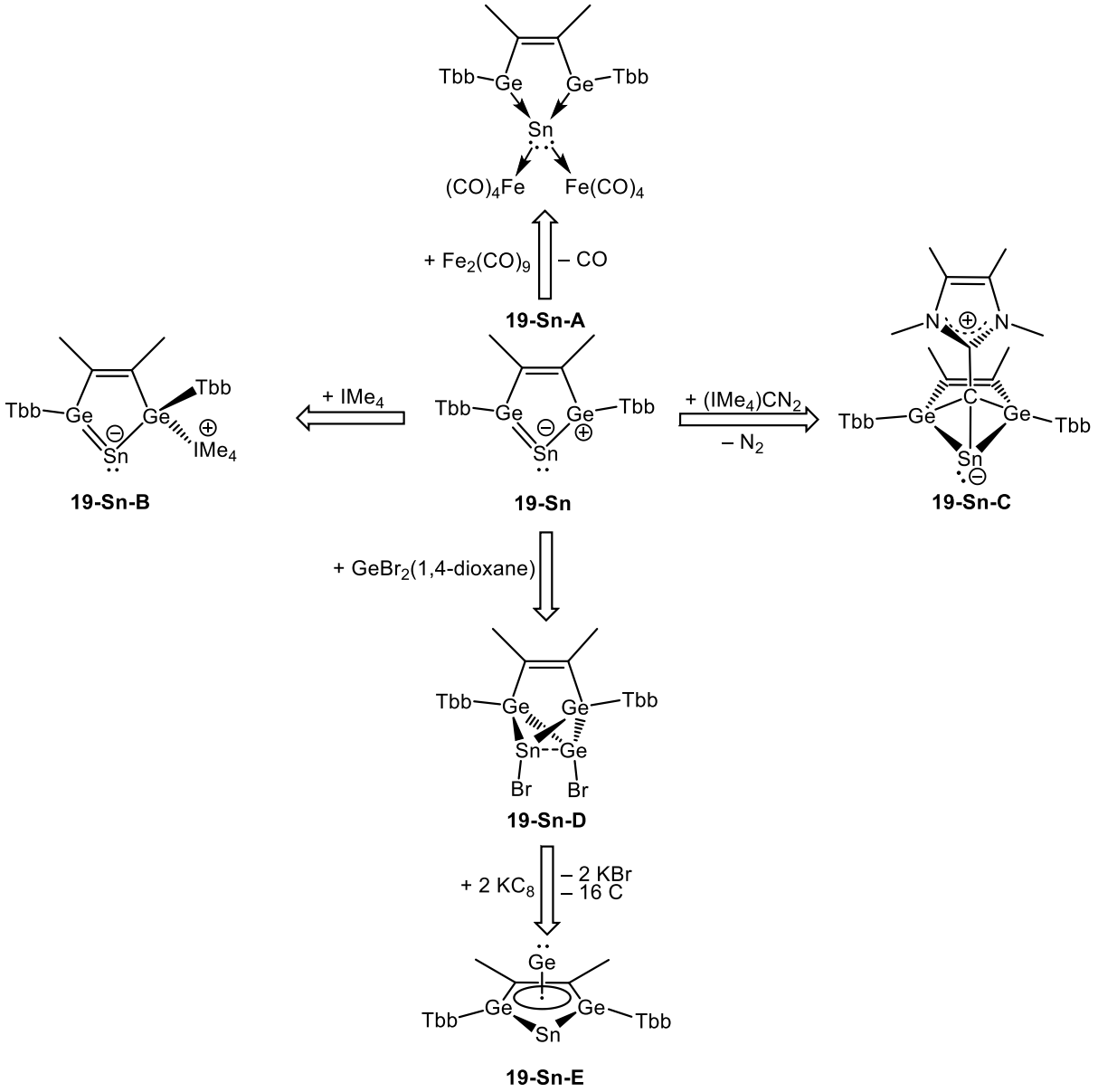

Scheme 51. Possible reactivity of stannylone (**19-Sn**) towards IMe_4, sterically non-demanding diazoolefin $(IMe_4)CN_2$, $Fe_2(CO)_9$ and $GeBr_2$(1,4-dioxane) and its further dehalogenation.

The germaethenes **31-Ge** and **32-Ge** exhibit a *synperiplanar*-orientation of $SiMe_3$ and Br substituents, hinting at possible $SiMe_3Br$ elimination. However, prolonged heating in toluene yields only decomposition products, making this route ineffective. As an alternative strategy, derivatization of both compounds *via* salt metathesis, followed

by thermally or base-induced α,β-elimination of $O(SiMe_3)_2$, could be pursued. This pathway may provide access to the long-sought tetrylyne species $\{(NDippCH_2)_2P\}C{\equiv}Ge(R)$, which has been studied *in silico* thus far (***Scheme 52***).

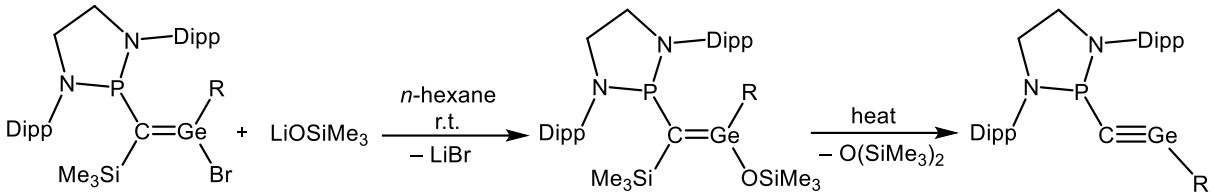

31-Ge, R = Tbb
32-Ge, R = Mind

Scheme 52. Possible accessible approach to synthesize base free germyne.

4. Experimental Section

4.1. General Part

All experiments were carried out under strict exclusion of air and moisture in an atmosphere of argon using Schlenk or glove box techniques. Argon was commercially received with a purity of ≥ 99.998 % and passed through a gas purification system composed of two consecutive columns to remove traces of oxygen and water. The first column was filled with the BTS copper catalyst R3−11G from BASF and operating at ca. 80 °C, whereas the second column was filled with 4 Å molecular sieves and kept at room temperature. All glassware was cleaned by storage in a KOH/isopropanol bath for 2 – 3 days, followed by thoroughly washing with tap water, then storage in the dilute HCl bath for 1 – 2 hours and finally cleaned with tap water, acetone and distilled water. All cleaned glassware was dried in a drying oven at approximately 110 °C and baked in fine vacuum (10^{-2} mbar) prior to use. Stainless steel transfer and filter cannulas (∅ = 1 or 2 mm) were used for the transfer of liquids and filtrations through Glass Microfiber filters (GF/B) from Whatman™ filters respectively. Fritted glass (porosity: *P3*) was used for the filtrations carried out inside the glove boxes.
All solvents were dried upon refluxing over suitable drying agents, were purged several times with argon during reflux and distilled under argon. The following drying agents were used for the solvents:

Solvents	Prior storage over	Predrying agents	Drying agents
n-hexane, *n*-pentane and PE		Na-wire	sodium-wire/tetraglyme (0.5 vol%)
Tetrahydrofuran (THF)[a]	KOH	Na-wire	Na-wire/benzophenone dianion ($Na_2[Ph_2CO]$)[a]
Dimethoxyethane (DME)[a]	KOH	Na-wire	Na-wire/benzophenone dianion ($Na_2[Ph_2CO]$)
Diethyl ether (Et_2O)[a]	KOH	Na-wire	Na-wire/benzophenone dianion ($Na_2[Ph_2CO]$)
Benzene, toluene		Na-wire	Na-wire
Chloroform ($CHCl_3$)		Sicapent	CaH_2
Dichloromethane (CH_2Cl_2)[b]	$CaCl_2$	Sicapent	CaH_2
Fluorobenzene[C]		CaH_2	$LiAlH_4$[C]

[a]: THF, DME and Et_2O are typically dried by distillation over Na/benzophenone ketyl ($Na_2[Ph_2CO]$), see references [346] and [347]. For the synthesis and characterization of $Na_2[Ph_2CO]$ see [348]. [b]: Commercially available dichloromethane (CH_2Cl_2) depending on the supplier contained either traces of ethanol or amylenes, which were removed upon extraction of the solvent with sulfuric acid and water. Therefore, a thoroughly drying procedure needed to be carried out, involving the distillation from two sicapent predryer flasks. [c]:

Commercially available fluorobenzene contained traces of acetone, which were removed upon stirring the predried solvent over $LiAlH_4$ for atleast 3 h and freshly trap to trap recondensed prior to use.

After distillation all solvents were degassed by freeze-pump-thaw cycles and stored in glove boxes in SCHOTT DURAN® laboratory glass bottles. For extremely air sensitive compounds, the solvents *n*-pentane and benzene were stirred overnight over KC_8 and filtered inside the glovebox prior to use. For air-stable compounds, commercially available solvents were used without purification.

4.2. Analytical Methods

4.2.1. IR Spectroscopy

IR spectra of solutions were recorded on a Nicolet 380 or Vector 22 FT-IR spectrometer in the range of 2400 – 1500 cm^{-1} using a cell of either NaCl or CaF_2 windows. IR spectra of the pure solids were recorded on a Bruker Alpha FT-IR spectrometer in the range of 4000 – 400 cm^{-1} in the glovebox using the platinum single reflection diamond ATR module. The following abbreviations were used for the intensities of absorption bands: vs = very strong, s = strong, m = medium, w = weak, vw = very weak, sh = shoulder, br = broad.

4.2.2. NMR Spectroscopy

The NMR spectra were recorded either on a Bruker Avance 300 MHz or a Bruker Avance IIID 500 MHz NMR spectrometer in dry deoxygenated deuterated solvents, using Ø = 5 mm NMR tubes equipped with J. Young valves. The deuterated solvents were dried by stirring over sodium-potassium alloy (D_6)benzene, (D_8)toluene, (D_8)THF) or CaH_2 (D_2)dichloromethane degassed and then trap-to-trap condensed and stored over molecular sieves (4 Å) in Schlenk flasks equipped with J. Young valves. The ^{1}H and $^{13}C\{^{1}H\}$ NMR spectra were calibrated against the residual proton and natural abundance ^{13}C resonances of the deuterated solvent relative to tetramethyl silane set at δ = 0 ppm ((D_6)benzene: δ_H = 7.15 ppm and δ_C = 128.0 ppm; (D_8)toluene: δ_H = 2.08 ppm and δ_C = 20.43 ppm; (D_8)THF: δ_H = 1.73 ppm and δ_C = 25.3 ppm; (D_2)dichloromethane: δ_H = 5.32 ppm and δ_C = 53.8 ppm), respectively. The recently reported ^{1}H no-D NMR method was employed at the Bruker Avance IIID 500 MHz NMR spectrometer and was used for monitoring reaction mixture solutions in benzene(C_6H_6), fluorobenzene (C_6H_5F) and *m*-difluorobenzene (C_6H_4-1,3-F_2).[349] The $^{31}P\{^{1}H\}$ and ^{29}Si NMR spectra were calibrated using the ^{2}H frequency of the deuterated solvent (lock frequency) and the frequency ratio value $\Xi(^{31}P)$ = 40.480742 and $\Xi(^{29}Si)$ = 19.867187 as recommended by IUPAC for H_3PO_4 (85% aqueous solution), and $SiMe_4$ (φ(volume fraction) = 1% in (D_1)chloroform) respectively as external

reference.[350] The ^{15}N NMR spectra were calibrated using the ^{2}H frequency of the deuterated solvent (lock frequency) and the frequency ratio value $\Xi(^{15}N)$ = 10.132912 as recommended by IUPAC for neat liquid ammonia as external reference.[350] All lock frequencies were calibrated internally against the ^{1}H NMR signals of the solution of tetramethylsilane (δ_H = 0 ppm) with a volume fraction of ≤ 1 % in the corresponding degassed deuterated solvent. The ^{15}N NMR signals of the compounds were obtained by inverse detected 2D NMR (^{1}H-^{15}N HMBC pulse sequence) experiments. The following abbreviations were used for the forms and multiplicities of the NMR signals: s − singlet, d − doublet, t − triplet, sept − septet, m − multiplet, br − broad. The full width at half maximum of broad signals was designated with $\Delta\nu_{1/2}$ and is given in Hz. All coupling constants are given in Hz as absolute values regardless of their signs. The ^{1}H and ^{13}C NMR signals of all compounds were assigned by a combination of ^{1}H-^{1}H COSY, ^{1}H-^{13}C HMQC and HMBC experiments.

4.2.3. X-ray Crystallography

Typically, crystals for the X-ray diffraction analysis were filtered from their supernatant solution at the temperature of crystallization and covered with Fomblin Y® lubricant to protect from air and moisture. A crystal suitable for the measurement was selected on a microscope and transferred to the diffractometers. The data collection was performed on Bruker X8-Kappa ApexII, Bruker D8-Venture, STOE IDPS-2T and STOE STADIVARI diffractometers using either graphite monochromated Mo-K_α radiation (λ = 0.7107 Å) or Cu- K_α radiation (λ = 1.54178 Å). The diffractometers were equipped with a low-temperature device (Oxford Cryostream 700er series, 100.0 K). Intensities were measured by fine-slicing ω and φ-scans and corrected for background, polarization and Lorentz effects. An absorption correction by integration was applied for all data sets.[11] The structures were solved by direct methods and refined anisotropically by the least-squares procedure implemented in the SHELX program system.[12] Hydrogen atoms except the silicon/germanium-bonded hydrogen atom were included using the riding model on the bound carbon atoms. The silicon/germanium-bonded hydrogen atom was found on the difference Fourier map and anisotropically refined. Selected crystallographic refinement data are listed in Section **5.2**. The sample handling and solution/refinement measurement was done by the central X-ray crystallographic facility of the Institute.

---

[11] SADABS, 2009/2, AXS, 2009.

[12] G. M. Sheldrick, SHELXS97 and SHELXL97, *University of Göttingen*, Germany, **1997**.

4.2.4. Elemental Analysis

The C, H, N analyses were carried out in triplicate for each sample using an Elementar Vario Micro elemental analyzer. The individual C, H and N values did not differ by more than ± 0.3 %, and the mean C, H, N values are given for each compound. The sample handling and measurement was done by the central EA facility of the Institute.

4.2.5. Melting Point Determination

The melting points were determined of analytically pure samples in duplicate using a Büchi melting point apparatus M-560, which was calibrated by using the following melting points standards: 4-nitrotoluene (52.5 +/– 0.2 °C at 0.5 °C/min), diphenylacetic acid (147.7 +/– 0.2 °C at 0.5 °C/min), caffeine (236.5 +/– 0.2 °C at 0.5 °C/min), and potassium nitrate (334.5 +/– 0.2 °C at 0.5 °C/min). The samples were sealed in glass capillaries under vacuum and heated once with a gradient of 10 °C/min for a rough determination of the melting point or temperature of starting decomposition. Heating of the second and third samples was then repeated with a gradient of 2 °C/min starting 25 °C below the temperature of melting or decomposition determined in the first experiment. The onset temperature of melting or decomposition of the samples is given without correction for the temperature gradient. The thermally treated samples were cooled to ambient temperature and analyzed either by No-D ^{1}H NMR spectroscopy[349] in fluorobenzene or ^{1}H/^{31}P NMR spectroscopy in (D_6)benzene to elucidate whether decomposition had occurred.

4.2.6. Cyclic Voltammetry

The cyclic voltammetry studies were performed using a Metrohm Autolab PGSTAT100N potentiostat/galvanostat (compliance voltage = 100 V), further equipped with a SCAN250 true linear scan generator module and an ADC10M ultra-fast sampling module. The results were analyzed with the NOVA software version 2.1.5. All experiments were carried out inside a glove box under argon in a gas-tight, specially designed full-glass three-electrode electrochemical cell at ambient temperature. The electrochemical cell used for the CV experiments was composed of a glassy-carbon disk electrode (Ø = 2 mm) as a working electrode (WE), a Pt wire (Ø = 1 mm) as a counter electrode (CE) and a second Pt wire (Ø = 1 mm) as a reference electrode (RE). All potentials are given relative to the half-wave potential ($E_{1/2}$) of the redox couple $[Fe(C_5Me_5)_2]^{+/0}$ ($DMFc^{+/0}$), which was determined at the end of the experiment under the same experimental condition.[351] The CV experiments were

carried out in fluorobenzene using 1.3 mmol/L of the analyte and 60 mmol/L $[N(^{n}Bu)_4][Al(OC(CF_3)_3)_4$[352,353] as conductivity salt. An automatic ohmic drop (iR-drop) compensation for the uncompensated resistance (R_u) of the electrolyte solution existing between the WE and RE was applied for all voltammograms by experimentally determining the R_u during the experiments. The assignment of electrochemical processes as oxidation or reduction was done by comparing the $E_{1/2}$ values of the redox couple with the open circuit potential (OCP) of the analyte, which is defined as the equilibrium potential of the solution of analyte and electrolyte at zero current flow and was determined before the experiment. An $E_{1/2}$ greater than OPC indicates electrochemical oxidation and an $E_{1/2}$ lower than OPC indicates electrochemical reduction process of the analyte. The electrochemical processes - reversible (E_r), quasi-reversible (E_q), irreversible (E_i) and a reversible electrochemical process coupled with irreversible chemical reaction (E_rC_i) were distinguished according to the criteria given in reference [354,355].

4.2.7. UV-Vis NIR Spectroscopy

The UV-Vis-NIR spectra of analytically pure compounds were recorded on a Thermo Scientific Evolution 300 spectrometer in a special designed quartz cuvette under inert conditions. The sample solutions were prepared inside the glove box using pure samples and extremely dry and degassed toluene. The measurements were performed using three different path lengths (d = 1 mm, 5 mm and 10 mm) and four different concentrations (ranging from 400 µmol L^{-1} to 10 µmol L^{-1}) at ambient temperature. the extinction coefficient (ε) were determined by plotting absorbance to concentration of the appropriate absorbance band, and determining the gradient of the linear regressed line through the data points using Microsoft Excel programme.

4.3. List of compounds prepared according to literature

Compound	Experimenter	Reference
$GeBr_2$(1,4-dioxane)	Singh/Kumar	[356]
Tbb-Br	Filippou group members	[357,358]
$[TbbGeBr]_2$	Singh	[227]
Ge_2Tbb_2	Singh	[227]
$[TbbSiBr]_2$	Filippou group members	[359]
Si_2Tbb_2	Palui/Singh	[43]
$caac^{Me}$	Gstrein	[177]
$SiBr_2(caac^{Me})$	Palui/Gstrein	[177]
$Si_2Br_2(caac^{Me})_2$	Palui/Singh	[177]
KC_8	Palui/Kumar/Singh	[360,361]
$Na[B(C_6H_3\text{-}3,5\text{-}(CF_3)_2)_4]$	Tewes/Kumar	[362,363]
MesLi	Gstrein	[364]
$CpRh(CO)_2$	Palui	[365]
$Co(PMe_3)_3Cl$	Palui	[366]
$Ni(PMe_3)Cl_2$	Singh	[367]
IMe_4	Filippou group members	[368]
PMe_3	Filippou group members	[369]
MesNC	Singh/Kumar	[370]
$[MindGeBr]_2$	Deckstein	[217]

4.4. List of commercially available reagents

Compound	Supplier	Purification
n-butyl lithium (1.6 M in *n*-hexane)	Chemetall	used as received
tert.-butyl lithium (1.9 M in *n*-pentane)	Acros	used as received
$AlMe_3$ (2 M in Tol)	Sigma-aldrich	used as received
Mesityl acetylene	TCI	used as received
Phenyl acetylene	Fluka	Stirring over K_2CO_3 followed by a distillation
2-butyne	ABCR	Stirring over CaH_2 followed by a trap to trap condensation
1,5-cyclooctadiene	TCI	Stirring over CaH_2 followed by a trap to trap condensation
$CpCo(CO)_2$	ABCR	used as received
$Ni(COD)_2$	Sigma-aldrich	used as received
CO (99.9997 %)	Air Liquide	used as received
C_2H_4 (99.5 %)	Air Liquide	used as received
naphthalene	Across	Sublimation at 70 °C
Trimethylsilyldiazomethane (2 M in *n*-hexane)	Sigma-aldrich	used as received
TlCp	Sigma-aldrich	Sublimation at 60 °C

4.5. Synthesis and analytical/spectroscopic data of compounds

4.5.1. [CpCo(CO)$Sn_2Ar^{Dipp}_2$] (**2-Co**)

A yellow-brown 0.58 M stock solution of $CpCo(CO)_2$ in *n*-hexane (0.83 mL, 0.484 mmol, 1 equiv.) was added slowly to a stirred green suspension of ArDippSn≡SnArDipp (500 mg, 0.484 mmol, 1 equiv.) in 20 mL of *n*-hexane at ambient temperature. No instant colour change was observed, and the reaction mixture was stirred overnight at ambient temperature. Upon stirring, the colour changed to yellow-brown. A ^1H spectrum of an aliquot of the reaction solution in (D_6)benzene revealed the selective formation of **2-Co** with a trace amount of starting material *ca.* 4% $CpCo(CO)_2$. The yellow-brown solution was filtered off, followed by the removal of all volatiles to dryness under vacuum, resulting in a brown crude product. This product was then crystallised from Et_2O (1.8 mL) at −30 °C. [13] The resulting brown crystals were isolated by filtration at −30 °C and dried under a fine vacuum at 40 °C for 1 hour to obtain **2-Co** as a mono-ether solvate, **2-Co·$C_4H_{10}O$**. Yield: 347 mg (0.29 mmol, 60 % from ArDippSn≡SnArDipp).

Properties: Compound **2-Co·$C_4H_{10}O$** is a highly air-sensitive, brown solid, turning immediately pale yellow upon contact with air. Upon heating, it begins to decompose during melting at 207 °C. It can be stored under an argon atmosphere at ambient temperature for several months. **2-Co·$C_4H_{10}O$** is very well soluble in *n*-pentane, benzene, toluene, Et_2O and THF at ambient temperature. Under strict exclusion of air, solutions of **2-Co·$C_4H_{10}O$** in (D_6)benzene is stable for at least 72 hours without any sign of decomposition at ambient temperature.

Elemental analysis: 2-Co·$C_4H_{10}O$ ($C_{66}H_{79}OCoSn_2(C_4H_{10}O)$, 1184.69 g mol^{-1}): Calcd. /%: C 66.84, H 6.97; found /%: C 66.42, H 7.07.

IR (Et_2O): $\tilde{\nu}$ (cm^{-1}) = 1934 (s) [ν(CO)], 1582 (w) and 1528 (w) [$\nu(CC)_{aryl}$].

IR (*n*-hexane): $\tilde{\nu}$ (cm^{-1}) = 1936 (s) [ν(CO)], 1583 (w) and 1528 (w) [$\nu(CC)_{aryl}$].

ATR-IR (solid): $\tilde{\nu}$ (cm^{-1}) = 2957 (m), 2924 (w), 2863 (w),1930 (s) [ν(CO)], 1887(vw), 1591 (w) and 1571 (w) [$\nu(CC)_{aryl}$], 1552 (vw), 1458 (m), 1441 (m), 1424 (w), 1382 (w), 1360 (w), 1322 (w), 1305 (vw), 1284 (w), 1180 (w), 1061 (vw), 1146 (w), 1116 (m), 1093 (w), 1076 (w), 1057 (w), 1044 (vw), 1006 (vw), 998 (vw), 844 (s), 836 (sh), 818 (w), 818 (s), 803 (m), 790 (m), 757 (s), 744 (w), 583 (m), 517 (m), 495 (m), 457 (w).

---

[13] I would like to acknowledge Tobis Deckstein for preliminary structural findings of the compound.

^{1}H NMR (500.1 MHz, (D_8)thf, 253 K): δ (ppm) = 0.68 (br s, $\Delta\nu_{½}$ = ca. 16.49 Hz, 6H, 2 × C^2-$C^{2'}$-CH*Me*$_A$Me$_B$, Dipp^1), 0.74 (d, ^3J(H,H) = 6.7 Hz, 6H, 2 × C^6-$C^{2'}$-CH*Me*$_A$Me$_B$, Dipp^2), 0.94 (d, ^3J(H,H) = 6.7 Hz, 12H, 2 × C^6-$C^{2'}$-CHMe$_A$*Me*$_B$, Dipp^2 and 2 × C^2-$C^{6'}$-CH*Me*$_A$Me$_B$, Dipp^1), 1.01 (d, ^3J(H,H) = 6.9 Hz, 6H, 2 × C^2-$C^{2'}$-CHMe$_A$*Me*$_B$, Dipp^1), 1.23 (d, ^3J(H,H) = 6.9 Hz, 6H, 2 × C^2-$C^{6'}$-CHMe$_A$*Me*$_B$, Dipp^1), 1.33 (d, ^3J(H,H) = 6.7 Hz, 6H, 2 × C^6-$C^{6'}$-CH*Me*$_A$Me$_B$, Dipp^2), 1.40 (d, ^3J(H,H) = 7.0 Hz, 6H, 2 × C^6-$C^{6'}$-CHMe$_A$*Me*$_B$, Dipp^2), 2.72 (sept, ^3J(H,H) = 6.7 Hz, 2H, 2 × C^2-$C^{6'}$-C*H*Me$_A$Me$_B$, Dipp^1), 3.03 (sept, 2H, ^3J(H,H) = 6.7 Hz, 2 × C^2-$C^{2'}$-C*H*Me$_A$Me$_B$, Dipp^1), 3.14 (sept, ^3J(H,H) = 6.7 Hz, 2H, 2 × C^6-$C^{2'}$-C*H*Me$_A$Me$_B$, Dipp^2), 3.43 (s, 5H, Cp), 3.56 (sept, ^3J(H,H) = 6.7 Hz, 2H, 2 × C^6-$C^{6'}$-C*H*Me$_A$Me$_B$, Dipp^2), 6.89 (d, ^3J(H,H) = 7.7 Hz, 2H, 2 × C^2-$C^{5'}$-*H*, Dipp^1), 7.00 (d, ^3J(H,H) = 6.7 Hz, 4H, 2 × C^6-$C^{3'}$-*H*, Dipp^2 and 2 × C^2-$C^{3'}$-*H*, Dipp^1), 7.07 (t, ^3J(H,H) = 7.5 Hz, 4H, 2 × $C^{3/5}$-*H* cent. ring and 2 × C^2-$C^{4'}$-*H*, Dipp^1), 7.18 (t, ^3J(H,H) = 7.6 Hz, 2H, 2 × C^6-C^4-H, Dipp^2), 7.33 (d, ^3J(H,H) = 6.9 Hz, 4H, 2 × $C^{3/5}$-*H* cent. ring and 2 × C^6-$C^{5'}$-*H*, Dipp^2), 7.49 (t, ^3J(H,H) = 7.5 Hz, 2H, 2 × C^4-*H* cent. ring).

^{13}C{^{1}H} NMR (125.8 MHz, (D_8)thf, 253 K): δ (ppm) = 23.22 (s, 2C, 2 × C^6-$C^{6'}$-CHMe$_A$*Me*$_B$, Dipp^2), 23.55 (s, 2C, 2 × C^2-$C^{2'}$-CH*Me*$_A$Me$_B$, Dipp^1), 23.65 (s, 2C, 2 × C^6-$C^{2'}$-CHMe$_A$*Me*$_B$, Dipp^2), 24.15 (s, 2C, 2 × C^2-$C^{6'}$-CHMe$_A$*Me*$_B$, Dipp^1), 26.29 (s, 2C, 2 × C^2-$C^{6'}$-CH*Me*$_A$Me$_B$, Dipp^1), 26.59 (s, 2C, 2 × C^6-$C^{2'}$-CHMe$_A$*Me*$_B$, Dipp^2), 27.22 (s, 2C, 2 × C^2-$C^{2'}$-CHMe$_A$*Me*$_B$, Dipp^1), 28.58 (s, 2C, 2 × C^6-$C^{6'}$-CH*Me*$_A$Me$_B$, Dipp^2), 30.81 (s, 2C, 2 × C^6-$C^{2'}$-*C*HMe$_A$Me$_B$, Dipp^2), 31.11 (s, 2C, 2 × C^2-$C^{2'}$-*C*HMe$_A$Me$_B$, Dipp^1), 31.40 (s, 2C, 2 × C^2-$C^{6'}$-*C*HMe$_A$Me$_B$, Dipp^1), 31.54 (s, 2C, 2 × C^6-$C^{6'}$-*C*HMe$_A$Me$_B$, Dipp^2), 87.74 (s, 5*C*, *C*$_5$H$_5$), 123.13 (s, 2C, 2 × C^6-*C*$^{3'}$-H, Dipp^2), 123.69 (s, 4C, 2 × C^2-*C*$^{5'}$-H, Dipp^1 and 2 × C^2-*C*$^{3'}$-H, Dipp^1), 123.98 (s, 2C, 2 × C^6-*C*$^{2'}$, Dipp^2), 124.15 (s, 2C, 2 × C^2-*C*$^{1'}$, Dipp^1), 125.06 (s, 2C, 2 × C^6-*C*$^{5'}$-H, Dipp^2), 127.24 (s, 2C, 2 × C^4-H, cent. ring), 129.06 (s, 2C, 2 × C^6-*C*$^{4'}$-H, Dipp^2), 129.87 (s, 2C, 2 × *C*^{3}-H, cent. ring), 130.03 (s, 2C, 2 × C^2-*C*$^{4'}$-H, Dipp^1), 131.59 (s, 2C, 2 × C^5-H, cent. ring), 139.46 (s, 2C, 2 × C^6-*C*$^{1'}$, Dipp^2), 144.11 (s, 2C, 2 × C^2, cent. ring), 146.83 (s, 2C, 2 × C^6, cent. ring), 147.30 (s, 4C, 2 × C^2-*C*$^{2'}$, Dipp^1 + C^2-*C*$^{6'}$, Dipp^1), 148.14 (s, 2C, 2 × C^6-$C^{6'}$, Dipp^2), 177.42 (s br, $\Delta\nu_{1/2}$ = 43 Hz, 2C, 2 × *C*^{1}, cent. ring), 198.48 (s, 1C, *C*O).

^{119}Sn{^{1}H} signal was not obtained at 298 K and 253 K due to dynamics.

4.5.2. [CpRh(CO)Sn$_2$Ar$^{Dipp}_2$] (2-Rh)

A yellow-brown 0.39 M stock solution of $CpRh(CO)_2$ in *n*-hexane (0.74 mL, 0.29 mmol, 1 equiv.) was added slowly to a stirred green suspension of Ar^{Dipp}Sn≡SnAr^{Dipp} (300 mg, 0.29 mmol, 1 equiv.) in 20 mL of *n*-hexane at ambient temperature. No instant colour change was observed, and the reaction mixture was stirred overnight

at ambient temperature, upon which the colour changed to the green solution. A ^{1}H spectrum of an aliquot of the reaction solution in (D_6)benzene revealed the selective formation of **10-Rh** with a trace amount of starting material *ca.* 4% $CpCo(CO)_2$. The green solution was filtered off, followed by all volatiles were removed to dryness in a vacuum, resulting green solid. This solid was then crystallised from *n*-hexane (2 mL) at −30 °C. The resulting green crystals were isolated by filtration at −30 °C and dried under a fine vacuum at ambient temperature for one hour to obtain **2-Rh** as an analytically pure green solid compound. Yield: 236 mg (0.29 mmol, 60 % from $Ar^{Dipp}Sn{\equiv}SnAr^{Dipp}$).

Properties: Compound **2-Rh** is a highly air-sensitive, green solid that turns immediately colourless upon contact with air. Upon heating, it begins to decompose during melting at 169 °C. It can be stored under an argon atmosphere at ambient temperature for several months. **2-Rh** is very well soluble in *n*-pentane, benzene, toluene, Et_2O and THF at ambient temperature. Under strict exclusion of air, solutions of **2-Rh** in (D_6)benzene and (D_8)thf is stable for at least 72 hours without any sign of decomposition at ambient temperature.

Elemental analysis: 2-Rh ($C_{66}H_{79}ORhSn_2$, 1184.69 g mol^{-1}): Calcd. /%: C 65.04, H 6.75; found: /%: C 64.69, H 6.68.

IR (*n*-hexane): $\tilde{\nu}$ (cm^{-1}) = 1957 (s) [ν(CO)], 1583 (w) and 1528 (w) [$\nu(CC)_{aryl}$].
ATR-IR (solid): $\tilde{\nu}$ (cm^{-1}) = 2956 (m), 2923 (w), 2864 (w), 1952 (s) [ν(CO)], 1910 (vw), 1572 (w) and 1553 (w) [$\nu(CC)_{aryl}$], 1457 (m), 1441 (vw), 1424 (vw, sh), 1381 (m), 1359 (m), 1321 (vw), 1247 (s), 1178 (vw), 1160 (w), 1092 (w), 1055 (vw), 1005 (w), 995 (w), 934 (w), 817 (w), 803 (w), 753 (w), 756 (w), 744 (vs), 558 (m), 574 (sh), 505 (s), 485 (m), 457 (m), 440.

^{1}H NMR (500.1 MHz, (D_8)thf, 263 K): δ (ppm) = 0.75 (d, ^{3}J(H,H) = 6.9 Hz, 12H, 2 × C^{6}-C^{2}'-CH*Me*$_A$$Me_B$, $Dipp^2$ + 2 × C^{2}-C^{2}'-CH*Me*$_A$$Me_B$, $Dipp^1$), 0.94 (d, ^{3}J(H,H) = 6.9 Hz, 6H, 2 × C^{2}-C^{6}'-CHMe_A*Me*$_B$, $Dipp^1$), 1.02 (d, ^{3}J(H,H) = 6.9 Hz, 12H, 2 × C^{6}-C^{2}'-CHMe_A*Me*$_B$, $Dipp^2$ + 2 × C^{2}-C^{2}'-CHMe_A*Me*$_B$, $Dipp^1$), 1.28 (d, ^{3}J(H,H) = 6.7 Hz, 6H, 2 × C^{2}-C^{6}'-CH*Me*$_A$$Me_B$, $Dipp^1$), 1.29 (d, ^{3}J(H,H) = 6.9 Hz, 6H, 2 × C^{6}-C^{6}'-CH*Me*$_A$$Me_B$, $Dipp^2$), 1.34 (d, ^{3}J(H,H) = 8.8 Hz, 6H, 2 × C^{6}-C^{6}'-CHMe_A*Me*$_B$, $Dipp^2$), 2.74 (sept, ^{3}J(H,H) = 6.7 Hz, 2H, 2 × C^{2}-C^{6}'-C*H*$Me_A$$Me_B$, $Dipp^1$), 3.00 (sept, ^{3}J(H,H) = 6.7 Hz, 2H, 2 × C^{2}-C^{2}'-C*H*$Me_A$$Me_B$, $Dipp^1$), 3.20 (sept, ^{3}J(H,H) = 6.6 Hz, 2H, 2 × C^{6}-C^{2}'-C*H*$Me_A$$Me_B$, $Dipp^2$), 3.38 (sept, ^{3}J(H,H) = 6.7 Hz, 2H, 2 × C^{6}-C^{6}'-C*H*$Me_A$$Me_B$, $Dipp^2$), 3.95 (s, 5H, C_5H_5, *Cp*), 6.95 (d, ^{3}J(H,H) = 7.3 Hz, 2H, 2 × C^{2}-C^{5}'-*H*, $Dipp^1$), 7.03 (d, ^{3}J(H,H) = 7.4 Hz, 4H, 2 × C^{6}-C^{3}'-*H*, $Dipp^2$ and 2 × C^{2}-C^{3}'-*H*, $Dipp^1$), 7.10 (d, 2H, 2 × $C^{3/5}$-*H*, cent. ring), 7.19 (t,

^{3}J(H,H) = 7.6 Hz, 2H, 2 × C^{6}-C'^{4}-H, Dipp^{2}), 7.30 (d, ^{3}J(H,H) = 7.9 Hz, 4H, 2 × C$^{3/5}$-*H* cent. ring + 2 × C^{6}-C^{5}'-*H*, Dipp^{2}), 7.42 (t, ^{3}J(H,H) = 7.5 Hz, 2H, 2 × C^{4}-*H* cent. ring).

^{13}C{^{1}H} NMR (125.8 MHz, (D_8)thf, 263 K): δ (ppm) = 23.20 (s, 2C, 2 × C^{6}-C^{6}'-CHMe$_A$*Me*$_B$, Dipp^{2}), 23.63 (s, 2C, 2 × C^{2}-C^{2}'-CH*Me*$_A$Me$_B$, Dipp^{1}), 24.04 (s, 2C, 2 × C^{6}-C^{2}'-CHMe$_A$*Me*$_B$, Dipp^{2}), 24.33 (s, 2C, 2 × C^{2}-C^{6}'-CHMe$_A$*Me*$_B$, Dipp^{1}), 26.33 (s, 2C, 2 × C^{2}-C^{6}'-CH*Me*$_A$Me$_B$, Dipp^{1}), 26.65 (s, 2C, 2 × C^{6}-C^{2}'-CHMe$_A$*Me*$_B$, Dipp^{2}), 26.65 (s, 2C, 2 × C^{2}-C^{2}'-CHMe$_A$*Me*$_B$, Dipp^{1}), 28.71 (s, 2C, 2 × C^{6}-C^{6}'-CH*Me*$_A$Me$_B$, Dipp^{2}), 31.16 (s, 2C, 2 × C^{6}-C^{2}'-*C*HMe$_A$Me$_B$, Dipp^{2}), 31.34 (s, 2C, 2 × C^{2}-C^{2}'-*C*HMe$_A$Me$_B$, Dipp^{1}), 31.38 (s, 2C, 2 × C^{2}-C^{6}'-*C*HMe$_A$Me$_B$, Dipp^{1}), 31.49 (s, 2C, 2 × C^{6}-C^{6}'-*C*HMe$_A$Me$_B$, Dipp^{2}), 92.85 (d, ^{1}J(^{103}Rh,^{13}C) = 1.80 Hz, 5C, *C*$_5$H$_5$), 123.86 (s, 4C, 2 × C^{6}-*C*^{3}'-H, Dipp^{2} and 2 × C^{2}-*C*^{5}'-H, Dipp^{1}), 124.25 (s, 4C, 2 × C^{6}-*C*^{2}', Dipp^{2} and 2 × C^{2}-*C*^{3}'-H, Dipp^{1}), 124.99 (s, 4C, 2 × C^{2}-*C*^{1}', Dipp^{1} and 2 × C^{6}-*C*^{5}'-H, Dipp^{2}), 127.10 (s, 2C, 2 × *C*^{4}-H, cent. ring), 129.10 (s, 2C, 2 × C^{6}-*C*^{4}'-H, Dipp^{2}), 130.09 (s, 4C, 2 × *C*^{3}-H, cent. ring and 2 × C^{2}-*C*^{4}'-H, Dipp^{1}), 131.42 (s, 2C, 2 × *C*^{5}-H, cent. ring), 139.52 (s, 2C, 2 × C^{6}-*C*^{1}', Dipp^{2}), 144.57 (s, 2C, 2 × *C*^{2}, cent. ring), 146.70 (s, 2C, 2 × *C*^{6}, cent. ring), 147.79 (s, 4C, 2 × C^{2}-*C*^{2}', Dipp^{1} and C^{2}-*C*^{6}', Dipp^{1}), 148.21 (s, 2C, 2 × C^{6}-*C*^{6}', Dipp^{2}), 175.71 (s, 2C, 2 × *C*^{1}, cent. ring), 192.62 (d, ^{1}J(^{103}Rh,^{13}C) = 88 Hz, 1C, Rh-*C*O).

^{119}Sn{^{1}H} signal was not obtained at 298 K and 263 K due to dynamics.

4.5.3. [CpCo(PMe$_3$)Ge$_2$Tbb$_2$] (3-Co)

A colourless 0.89 M stock solution of PMe_3 in *n*-hexane (0.84 mL, 0.342 mmol, 1 equiv.) was added to a stirred orange-brown solution of CpCo(Ge_2(Tbb)$_2$) (400 mg, 0.342 mmol, 1 equiv.) in 15 mL of *n*-hexane at ambient temperature. The colour of reaction the solution turned immediately to dark green. The solution was stirred for 1 h at ambient temperature. A ^{1}H and ^{31}P-NMR spectrum of an aliquot of the reaction solution in (D_6)benzene revealed the complete consumption of the starting materials and the selective formation of compound **3-Co**. The dark green solution was filtered off, followed by the removal of all volatiles to dryness in a vacuum, resulting in a green crude product. This product was then dissolved in Et_2O (1.3 mL) and cooled at 0 °C for 30 min. This is followed by filtration and drying under a fine vacuum at ambient temperature for 30 min. to obtain **3-Co** as a mono-ether solvate **3-Co·C$_4$H$_{10}$O**.Yield: 313 mg (0.25 mmol, 73 % from CpCo(Ge_2(Tbb)$_2$).

Properties: Compound **3-Co** is a highly air-sensitive, dark green solid turning immediately colourless upon contact with air. Upon heating, it begins to decompose during melting at 189 °C. It can be stored under an argon atmosphere at ambient temperature for several months. **3-Co** is very well soluble in *n*-pentane, benzene,

toluene, Et_2O and THF at ambient temperature. Under strict exclusion of air, solutions of **3-Co** in (D_6)benzene is stable for at least 48 hours without any sign of decomposition at ambient temperature.

Elemental analysis: 3-Co·$C_4H_{10}O$ ($C_{56}H_{112}CoGe_2PSi_8(C_4H_{10}O)$, 1317.20 $gmol^{-1}$): Calcd. /%: C 54.60, H 9.31; found /%: C 54.2, H 9.26.

^{1}H NMR (500.1 MHz, (D_8)thf, 243 K): δ (ppm) = 0.03 (s, 9H, C²-CH(Si*Me₃*)$_A$(SiMe$_3$)$_B$, Tbb$_Y$), 0.07 (s, 9H, C²-CH(Si*Me₃*)$_A$(SiMe$_3$)$_B$, Tbb$_X$), 0.08 (s, 9H, C⁶-CH(Si*Me₃*)$_A$(SiMe$_3$)$_B$, Tbb$_Y$), 0.09 (s, 9H, C⁶-CH(Si*Me₃*)$_A$(SiMe$_3$)$_B$, Tbb$_X$), 0.09 (s, 9H, C²-CH(SiMe$_3$)$_A$(Si*Me₃*)$_B$, Tbb$_X$), 0.17 (s, 9H, C²-CH(SiMe$_3$)$_A$(Si*Me₃*)$_B$, Tbb$_Y$), 0.30 (s, 18H, C⁶-CH(SiMe$_3$)$_A$(Si*Me₃*)$_B$, Tbb$_Y$ and Tbb$_X$), 1.12 (s,1H, C²-C*H*(SiMe$_3$)$_A$(SiMe$_3$)$_B$, Tbb$_Y$)*, 1.32 (s, 9H, C⁴-C*Me*$_3$, Tbb$_X$), 1.38 (s, 9H, C⁴-C*Me*$_3$, Tbb$_Y$), 1.55 (d, $^2J(^{31}P,^1H)$ = 8.8Hz, 9H, P*Me*$_3$), 1.73 (s,1H, C²-C*H*(SiMe$_3$)$_A$(SiMe$_3$)$_B$, Tbb$_X$)*, 2.15 (s,1H, C⁶-C*H*(SiMe$_3$)$_A$(SiMe$_3$)$_B$, Tbb$_Y$), 2.76 (s,1H, C⁶-C*H*(SiMe$_3$)$_A$(SiMe$_3$)$_B$, Tbb$_X$), 4.57 (s, 5H, C_5H_5, Cp), 6.62 (s, 1H, C³-*H*, Tbb$_X$), 6.64 (s, 1H, C⁵-*H*, Tbb$_X$), 6.70 (s, 1H, C³-*H*, Tbb$_Y$), 6.89 (s, 1H, C⁵-*H*, Tbb$_Y$).(* signal appers underneath Et_2O and (D_8)THF signal).

^{13}C{^{1}H} NMR (125.8 MHz, (D_8)thf, 243 K): δ (ppm) = 0.95 - 2.78 (m, 24C, 2 × C^{2,6}- CH(Si*Me₃*)$_A$(Si*Me₃*)$_B$, Tbb$_X$ and Tbb$_Y$), 25.62 (s, 3C, P*Me₃*), 29.56 (s, 1C, C²-*C*H(Si*Me₃*)$_A$(Si*Me₃*)$_B$, Tbb$_Y$), 30.62 (s, 1C, C²-*C*H(Si*Me₃*)$_A$(Si*Me₃*)$_B$, Tbb$_X$), 31.21 (s, 3C, C⁴-C*Me₃*, Tbb$_X$), 31.44 (s, 3C, C⁴-C*Me₃*, Tbb$_Y$), 33.35 (s, 1C, C⁶-*C*H(SiMe₃)$_A$(SiMe₃)$_B$, Tbb$_X$), 34.69 (s, 1C, C⁶-*C*H(SiMe₃)$_A$(SiMe₃)$_B$, Tbb$_Y$), 34.75 (s, 1C,C⁴-*C*Me$_3$, Tbb$_X$), 34.77 (s, 1C, C⁴-*C*Me$_3$, Tbb$_Y$), 85.54 (s, 5C, C_5H_5, Cp), 121.81 (s, 1C, *C*³/⁵-H, Tbb$_X$), 121.90 (s, 1C, *C*³/⁵-H, Tbb$_Y$), 122.02 (s, 1C, *C*³/⁵-H, Tbb$_Y$), 124.40 (s, 1C, *C*³/⁵-H, Tbb$_X$), 145.16 (s, 1C, *C*⁶-CH(SiMe₃)$_A$(SiMe₃)$_B$, Tbb$_Y$), 145.34 (s, 1C, *C*⁶-CH(SiMe₃)$_A$(SiMe₃)$_B$, Tbb$_X$), 146.90 (s, 1C, *C*²-CH(SiMe₃)$_A$(SiMe₃)$_B$, Tbb$_X$), 147.39 (s, 1C, *C*²-CH(SiMe₃)$_A$(SiMe₃)$_B$, Tbb$_y$), 147.74 (s, 1C, *C*⁴-CMe$_3$, Tbb$_X$), 148.35 (s, 1C, *C*⁴-CMe$_3$, Tbb$_Y$), 152.51 (s, 1C, *C*¹, Tbb$_Y$), 152.66 (s, 1C, *C*¹, Tbb$_X$).

^{31}P{^{1}H} NMR (202.44 MHz, (D_8)thf, 243 K): δ (ppm) = 4.03(br s, $\Delta\nu_{1/2}$ = ca. 53 Hz, 1 × *P*Me$_3$).

4.5.4. [CpCo(CN)(*p*-tol)Ge₂Tbb₂] (4-Co)

A colourless solution of *p*-tolyl nitrile (40 mg, 0.342 mmol, 1 equiv.) in 2 mL of *n*-hexane was added slowly to a stirred orange-brown solution of CpCo(Ge$_2$(Tbb)$_2$) (400 mg, 0.342 mmol, 1 equiv.) in 15 mL of *n*-hexane at ambient temperature. The colour of the reaction mixture immediately turned dark green. The reaction solution was stirred for 30 min. at ambient temperature. A ^{1}H NMR spectrum of an aliquot of

the reaction solution in (D_6)benzene revealed the complete consumption of the starting materials and the selective formation of compound **4-Co**. The dark green solution was filtered off, and all volatiles were removed to dryness under a vacuum, followed by crystallisation of the greenish-black crude product from *n*-hexane (0.6 mL) at −30 °C. The resulting greenish-black crystals were isolated by filtration at −30 °C and dried under a fine vacuum at at 60 °C for 30 min. to afford hemi-solvate **4-Co**·(C_6H_{14})$_{0.5}$. Yield: 365 mg (0.28 mmol, 82 % from CpCo(Ge_2(Tbb)$_2$)).

Attempts to obtain the solvate-free form of **4-Co** upon drying in a fine vacuum at 60 °C for two hrs. failed, leading only to a partial loss of *n*-hexane and extensive decomposition.

Properties: Compound **4-Co** is a highly air-sensitive, greenish-black solid, turning immediately pale yellow upon contact with air. Upon heating, it begins to decompose during melting at 171 °C. It can be stored under an argon atmosphere at ambient temperature for several months. **4-Co** is very well soluble in *n*-pentane, benzene, toluene, Et_2O and THF at ambient temperature. Under strict exclusion of air, solutions of **4-Co** in (D_6)benzene and (D_8)toluene are stable for at least 36 hours without any sign of decomposition at ambient temperature.

Elemental analysis: 4-Co·(C_6H_{14})$_{0.5}$ ($C_{61}H_{110}CoGe_2NSi_8(C_6H_{14})_{0.5}$, 1286.37 gmol^{-1}): calcd. /%: C 57.82, H 8.87, N 1.05; found /%: C 57.42, H 8.35, N 1.06.

ATR-IR (solid, RT): $\tilde{\nu}$ (cm^{-1}) = 2953 (s), 2899 (w), 2862 (w), 2784 (w), 1604 (w), 1582 (m), 1544 (vw), 1527 (w)[ν (CC)$_{aryl}$], 1517 (vw), 1475 (vw), 1460 (vw), 1393 (w), 1360 (w), 1260 (vw), 1246 (s), 1201 (vw), 1172 (w), 1158 (vw), 1110 (w), 1028 (m), 992 (m), 965 (w), 950 (w), 883 (m), 834 (s), 802 (vw), 761 (w), 739 (w), 718 (w), 684 (w), 670 (w), 641 (w), 622 (w), 608 (vw), 553 (m), 520 (m), 491 (m), 446 (m).

^{1}H NMR (500.1 MHz, (D_6)benzene, 298 K): δ (ppm) = 0.02 (s, 18H, $C^{2,6}$ - CH(Si*Me*$_3$)$_A$(SiMe$_3$)$_B$, Tbb_X), 0.22 (s, 18H, $C^{2,6}$-CH(Si*Me*$_3$)$_A$(SiMe$_3$)$_B$, Tbb_Y), 0.27 (s, 18H, $C^{2,6}$-CH(SiMe$_3$)$_A$(Si*Me*$_3$)$_B$, Tbb_X), 0.29 (s, 18H, $C^{2,6}$-CH(SiMe$_3$)$_A$(Si*Me*$_3$)$_B$, Tbb_Y), 1.40 (s, 9H, C^4-C*Me*$_3$,Tbb_X), 1.41 (s, 9H, C^4-C*Me*$_3$,Tbb_Y), 1.93 (s, 3H, C^4-*Me*, *p*-Tol-CN), 2.59 (s, 2H, $C^{2,6}$-C*H*(SiMe$_3$)$_A$(SiMe$_3$)$_B$,Tbb_Y), 2.62 (s, 2H, $C^{2,6}$-C*H*(SiMe$_3$)$_A$(SiMe$_3$)$_B$, Tbb_X), 5.15 (s, 5H, C_5H_5, Cp), 6.85 (d, ^3J (H,H)=7.9 Hz, 2H, $C^{3,5}$-*H*, *p*-Tol-CN), 6.94 (s, 2H, $C^{3,5}$-*H*, Tbb_X), 7.04 (s, 2H, $C^{3,5}$-*H*, Tbb_Y), 7.74 (d, ^3J (H,H)=8.2 Hz, 2H, $C^{2,6}$-*H*, *p*- Tol- CN).

^{13}C{^{1}H} NMR (125.8 MHz, (D_6)benzene, 298 K): δ (ppm) = 1.03 (s, 6C, C^2- CH(Si*Me*$_3$)$_A$(Si*Me*$_3$)$_B$, Tbb_Y), 1.09 (s, 6C, C^6-CH (Si*Me*$_3$)$_A$(Si*Me*$_3$)$_B$, Tbb_Y), 1.50 (s, 6C,

C^2-CH (Si*Me*$_3$)$_A$(Si*Me*$_3$)$_B$, Tbb$_X$), 1.89 (s, 6C, C^6-CH (Si*Me*$_3$)$_A$(Si*Me*$_3$)$_B$,Tbb$_X$), 21.26 (s, 1C, C^4-*Me*, *p*-Tol-CN), 29.36 (s, 2C, $C^{2,6}$-*C*H(SiMe$_3$)$_A$(SiMe$_3$)$_B$,Tbb$_X$), 30.75 (s, 2C, $C^{2,6}$- *C*H(SiMe$_3$)$_A$(SiMe$_3$)$_B$,Tbb$_Y$), 31.39 (s, 3C, C^4-C*Me*$_3$, Tbb$_X$), 31.41 (s, 3C, C^4-C*Me*$_3$, Tbb$_Y$), 34.63 (s, 1C, C^4-*C*Me$_3$, Tbb$_X$), 34.69 (s, 1C, C^4-*C*Me$_3$, Tbb$_Y$), 80.41 (s, 5C, C_5H_5, Cp), 121.73 (s, 2C, $C^{3,5}$-H, Tbb$_Y$), 123.14 (s, 2C, $C^{3,5}$-H, Tbb$_X$), 129.14 (s, 2C, $C^{3,5}$-H, *p*- Tol- CN), 131.72 (s, 2C, $C^{2,6}$-H, *p*-Tol-CN), 135.80 (s, 1C, C^1, *p*-Tol-CN), 140.80 (s, 1C, C^4, *p*-Tol-CN), 144.91 (s, 2C, $C^{2,6}$-CH(SiMe$_3$)$_A$(SiMe$_3$)$_B$, Tbb$_X$), 146.41 (s, 2C, $C^{2,6}$- CH(SiMe$_3$)$_A$(SiMe$_3$)$_B$, Tbb$_Y$), 151.08 (s, 1C, C^4, Tbb$_Y$), 151.79 (s,1C, C^1, Tbb$_Y$),151.81 (s, 1C, C^4, Tbb$_X$), 157.05 (s, 1C, C^1, Tbb$_X$), 192.07 (s, 1C, -*C*N, *p*-Tol-CN).

4.5.5. [CpCo(CO)(*p*-tol)$_2$Ge$_2$Tbb$_2$] (5-Co)

A colourless solution of (*p*-tolyl)$_2$CO (72 mg, 0.342 mmol, 1 equiv.) in 3 mL of *n*- hexane was added slowly to a stirred orange-brown solution of CpCo(Ge$_2$(Tbb)$_2$) (400 mg, 0.342 mmol, 1 equiv.) in 20 mL of *n*-hexane at ambient temperature. The colour of the reaction solution immediately turned orange-red. The reaction solution was stirred at ambient temperature for 30 min. ^{1}H NMR spectrum of an aliquot of the reaction solution in (D$_6$)benzene revealed the complete consumption of the starting materials and the selective formation of compound **5-Co**. The orange-red solution was filtered off, and all volatiles were removed to dryness in a vacuum, resulting in the orange-red crude product, which was dried for 30 min. at ambient temperature, followed by crystallisation of the orange-red crude product from (1:3) CH_3CN:Et_2O as *n*-hexane and Et_2O solvents forms an oily solution. The entire compound was dissolved in a 4 mL solution of (1:3) CH_3CN:Et_2O and left at room temperature for diffusion. The resulting red crystals were isolated by filtration at ambient temperature and dried under a fine vacuum at 60 °C for 2 hours to afford **5-Co** as an analytically pure solid. Yield: 333 mg (0.24 mmol, 70 % from CpCo(Ge$_2$(Tbb)$_2$)).

Properties: Compound **5-Co** is a highly air-sensitive, red solid turning immediately colourless upon contact with air. Upon heating, it begins to decompose during melting at 214 °C. It can be stored under an argon atmosphere at ambient temperature for several months. **5-Co** is very well soluble in *n*-pentane, benzene, toluene, Et_2O and THF at ambient temperature. Under strict exclusion of air, solutions of **5-Co** in (D$_6$)benzene and (D$_8$)toluene are stable for at least 48 hours without any sign of decomposition at ambient temperature.

Elemental analysis: 5-Co ($C_{68}H_{117}OCoGe_2Si_8$, 1379.49 gmol^{-1}): calcd. /%: C 59.20, H 8.55; found /%: C 59.19, H 8.62.

ATR-IR (solid, RT): $\tilde{\nu}$ (cm^{-1}) = 2951 (s), 2899 (m), 2868 (w), 1585 (m), 1531 (m), 1507 (w), 1476 (w), 1461 (w), 1424 (w), 1393 (m), 1360 (w), 1245 (s), 1204 (vw), 1192 (vw), 1172 (w), 1169 (w), 1011 (w), 998 (w), 972 (w), 957 (w), 937 (w), 885 (w), 833 (s), 764 (s), 740 (w), 722 (w), 686 (m), 663 (w), 624 (w), 608 (w), 594 (w), 579 (w), 554 (w), 522 (w), 491 (w), 465 (w), 444 (w).

^{1}H NMR (500.1 MHz, (D_8)toluene, 243 K): δ (ppm) = − 0.06 (s, 18H, $C^{2,6}$- CH(Si*Me*$_3$)$_A$(SiMe$_3$)$_B$, Tbb$_X$), 0.10 (s, 18H, $C^{2,6}$-CH(Si*Me*$_3$)$_A$(SiMe$_3$)$_B$, Tbb$_Y$), 0.31 (s, 18H, $C^{2,6}$-CH(Si*Me*$_3$)$_A$(Si*Me*$_3$)$_B$, Tbb$_X$), 0.32 (s, 18H, $C^{2,6}$-CH(Si*Me*$_3$)$_A$(Si*Me*$_3$)$_B$, Tbb$_Y$) 1.39 (s, 9H, C^4-C*Me*$_3$, Tbb$_Y$), 1.43 (s, 9H, C^4-C*Me*$_3$, Tbb$_X$), 2.15 (s, 6H, 2 × C^4-*Me*, *p*- Tol), 2.37 (s, 2H, $C^{2,6}$-C*H*(SiMe$_3$)$_A$(SiMe$_3$)$_B$, Tbb$_Y$), 2.57 (br s, $\Delta\nu_{1/2}$ = 35 Hz, 2H, $C^{2,6}$-C*H*(SiMe$_3$)$_A$(SiMe$_3$)$_B$, Tbb$_X$), 5.14 (s, 5H, C_5H_5, Cp), 6.90 (d, ^3J (H,H)= 8.3 Hz, 4H, 2 × $C^{3,5}$-*H*, *p*-Tol), 6.97 (s, 2H, $C^{3,5}$-*H*, Tbb$_Y$), 7.07 (s, 2H, $C^{3,5}$-*H*, Tbb$_X$), 7.65 (br s, $\Delta\nu_{1/2}$ = 38 Hz, 4H, 2 × $C^{2,6}$-*H*, *p*-Tol).

^{1}H NMR (500.1 MHz, (D_6)benzene, 298 K): δ (ppm) = − 0.06 (s, 18H, $C^{2,6}$- CH (Si*Me*$_3$)$_A$(SiMe$_3$)$_B$, Tbb$_X$), 0.10 (br s, $\Delta\nu_{1/2}$ = 37 Hz 18H, $C^{2,6}$- CH(Si*Me*$_3$)$_A$(SiMe$_3$)$_B$, Tbb$_Y$), 0.30 (s, 36H, $C^{2,6}$-CH(Si*Me*$_3$)$_A$(Si*Me*$_3$)$_B$, Tbb$_X$ and Tbb$_Y$), 1.37 (s, 9H, C^4-C*Me*$_3$, Tbb$_Y$), 1.41 (s, 9H, C^4-C*Me*$_3$, Tbb$_X$), 2.12 (s, 6H, 2 × C^4-*Me*, *p*- Tol), 2.40 (s, 2H, $C^{2,6}$-C*H*(SiMe$_3$)$_A$(SiMe$_3$)$_B$, Tbb$_Y$), 2.56 (s, 2H, $C^{2,6}$- C*H*(SiMe$_3$)$_A$(SiMe$_3$)$_B$, Tbb$_X$), 5.13 (s, 5H, C_5H_5, Cp), 6.91 (d, ^3J (H,H)= 8.3 Hz, 4H, 2 × $C^{3,5}$-*H*, *p*-Tol), 6.97 (s, 2H, $C^{3,5}$-*H*, Tbb$_Y$), 7.05 (s, 2H, $C^{3,5}$-*H*, Tbb$_X$), 7.66 (d, ^3J (H,H)= 7.8 Hz, 4H, 2 × $C^{2,6}$-*H*, *p*-Tol).

^{13}C{^{1}H} NMR (125.8 MHz, (D_8)toluene, 243 K): δ (ppm) = 0.53 (s, 6C, C^2- CH(Si*Me*$_3$)$_A$(Si*Me*$_3$)$_B$, Tbb$_X$), 1.34 (s, 6C, C^6-CH(Si*Me*$_3$)$_A$(Si*Me*$_3$)$_B$, Tbb$_X$), 1.93 (s, 6C, C^2-CH(Si*Me*$_3$)$_A$(Si*Me*$_3$)$_B$, Tbb$_Y$), 2.08 (s, 6C, C^6-CH(Si*Me*$_3$)$_A$(Si*Me*$_3$)$_B$, Tbb$_Y$), 20.99 (s, 2C, 2 × C^4-*Me*, *p*-Tol.), 28.68 (s, 2C, $C^{2,6}$-*C*H(Si*Me*$_3$)$_A$(Si*Me*$_3$)$_B$, Tbb$_X$), 30.34 (s, 2C, $C^{2,6}$- *C*H(Si*Me*$_3$)$_A$(Si*Me*$_3$)$_B$, Tbb$_Y$), 31.18 (s, 3C, C^4-C*Me*$_3$, Tbb$_X$), 31.33 (s, 3C, C^4-C*Me*$_3$, Tbb$_Y$), 34.54 (s, 1C, C^4-*C*Me$_3$, Tbb$_Y$), 34.61 (s, 1C, C^4-*C*Me$_3$, Tbb$_X$), 79.21 (s, 5C, C_5H_5, Cp), 98.06 (s, 1C, (*p*-Tol.)$_2$*C*O), 122.08 (s, 2C, *C*^{3,5}-H, Tbb$_Y$), 123.21 (s, 2C, *C*^{3,5}-H, Tbb$_X$), 128.19 (s, 4C, 2 × *C*^{3,5}-H, *p*-Tol.), 129.13 (s, 4C, 2 × *C*^{2,6}-H, *p*-Tol.), 135.83 (s, 2C, 2 × *C*^{4}-Me, *p*-Tol.), 143.57 (s, 2C, 2 × *C*^{1}, *p*-Tol.), 146.08 (s, 2C, *C*^{2,6}- CH(Si*Me*$_3$)$_A$(Si*Me*$_3$)$_B$, Tbb$_Y$), 146.51 (s, 2C, *C*^{2,6}-CH(Si*Me*$_3$)$_A$(Si*Me*$_3$)$_B$,Tbb$_X$), 149.89 (s, 1C, *C*^{1}, Tbb$_Y$), 150.37 (s, 1C, *C*^{4}-CMe$_3$, Tbb$_X$), 151.35 (s, 1C, *C*^{4}-CMe$_3$, Tbb$_Y$), 156.11 (s, 1C, *C*^{1}, Tbb$_X$).

^{13}C{^{1}H} NMR (125.8 MHz, (D_6)benzene, 298 K): δ (ppm) = 0.76 (s, 6C, C^2- CH(Si*Me*$_3$)$_A$(Si*Me*$_3$)$_B$, Tbb$_Y$), 1.51 (s, 6C, C^6-CH(Si*Me*$_3$)$_A$(Si*Me*$_3$)$_B$, Tbb$_Y$), 2.16 (s, 6C,

C^2-CH(Si*Me*$_3$)$_A$(Si*Me*$_3$)$_B$, Tbb$_X$), 2.23 (s, 6C, C^6-CH(Si*Me*$_3$)$_A$(Si*Me*$_3$)$_B$, Tbb$_X$), 21.00 (s, 2C, 2 × C^4-*Me*, *p*-Tol.), 29.12 (s, 2C, $C^{2,6}$-*C*H(Si*Me*$_3$)$_A$(Si*Me*$_3$)$_B$, Tbb$_X$), 30.65 (s, 2C, $C^{2,6}$- *C*H(Si*Me*$_3$)$_A$(Si*Me*$_3$)$_B$, Tbb$_Y$), 31.27 (s, 3C, C^4-C*Me*$_3$, Tbb$_Y$), 31.40 (s, 3C, C^4-C*Me*$_3$, Tbb$_X$), 34.61 (s, 1C, C^4-*C*Me$_3$, Tbb$_Y$), 34.66 (s, 1C, C^4-*C*Me$_3$, Tbb$_X$), 79.35 (s, 5C, C_5H_5, Cp), 98.49 (s, 1C, (*p*-Tol.)$_2$*C*O), 122.36 (s, 2C, *C*^{3,5}-H, Tbb$_Y$), 123.62 (s, 2C, *C*^{3,5}-H, Tbb$_X$), 129.02 (s, 4C, 2 × *C*^{3,5}-H, *p*-Tol.), 129.26 (s, 4C, 2 × *C*^{2,6}-H, *p*-Tol.), 135.94 (s, 2C, 2 × *C*^{4}-Me, *p*-Tol.), 143.74 (s, 2C, 2 × *C*^{1}, *p*-tol.), 146.41 (s, 2C, *C*^{2,6}- CH(Si*Me*$_3$)$_A$(Si*Me*$_3$)$_B$, Tbb$_Y$), 146.72 (s, 2C, *C*^{2,6}-CH(Si*Me*$_3$)$_A$(Si*Me*$_3$)$_B$, Tbb$_X$), 150.22 (s, 1C, *C*^{1}, Tbb$_Y$), 150.48 (s, 1C, *C*^{4}-CMe$_3$, Tbb$_X$), 151.60 (s, 1C, *C*^{4}-CMe$_3$, Tbb$_Y$), 156.35 (s, 1C, *C*^{1}, Tbb$_X$).

4.5.6. [CpCo(CO)(O)Ge$_2$Tbb$_2$] (6-Co)

Colourless gas CO2 (12 mg, 0.273 mmol, 1 equiv.) was passed to a stirred orange-brown solution of CpCo(Ge$_2$(Tbb)$_2$) (320 mg, 0.273 mmol, 1 equiv.) in 15 mL of *n*- hexane at −78°C upon which no colour change was observed, let it warm up to room temperature, the reaction solution colour changed to red-brown. ^{1}H NMR spectrum of an aliquot of the reaction solution in (D$_6$)benzene after 6 hours revealed the complete consumption of the starting materials and the selective formation of compound **6-Co.** The red-brown solution was filtered off, followed by the removal of all volatiles to dryness in a vacuum, resulting in a red-brown crude product. This product was then crystallised from *n*-hexane (2 mL) at −30 °C. The resulting red crystals were isolated by filtration at −30 °C and dried under a fine vacuum at ambient temperature for 2 hours to afford **6-Co** as an analytically pure solid. Yield: 196 mg (0.16 mmol, 59 % from CpCo(Ge$_2$(Tbb)$_2$)).

Properties: Compound **6-Co** is a highly air-sensitive, red solid turning immediately colourless upon contact with air. Upon heating, it begins to decompose during melting at 253 °C. It can be stored under an argon atmosphere at ambient temperature for several months. **6-Co** is very well soluble in *n*-pentane, benzene, toluene, Et$_2$O and THF at ambient temperature. Under strict exclusion of air, solutions of **6-Co** in (D$_6$)benzene and (D$_8$)toluene are stable for at least 72 hours without any sign of decomposition at ambient temperature.

Elemental analysis: 6-Co ($C_{54}H_{103}CoGe_2O_2Si_8$, 1213.23 gmol^{-1}): calcd. /%: C 53.46, H 8.56; found /%: C 53.13, H 8.58.

ATR-IR (solid, 298 K): $\tilde{\nu}$ (cm^{-1}) = 2951 (m), 2899 (w), 2772 (vw),1681 (s),1581 (m), 1533 (m), 1475 (vw), 1463 (vw), 1463 (w), 1395 (s), 1362 (vw), 1246 (s), 1172 (m), 1059 (vw), 1026 (vw), 997 (w), 959 (m), 935 (w), 883 (m), 834 (m), 808 (w), 762 (s),

739 (w), 721 (vw), 686 (s), 662 (m), 644 (vw), 623 (vw), 608 (w), 553 (m), 472 (s), 445 (vw), 418 (s).

^{1}H NMR (500.1 MHz, (D_6)benzene, 298 K): δ (ppm) = 0.24 (s, 54H, $C^{2,6}$- CH(Si*Me*$_3$)$_A$(Si*Me*$_3$)$_B$, Tbb_Y + $C^{2,6}$-CH(Si*Me*$_3$)$_A$(SiMe$_3$)$_B$, Tbb_X), 0.29 (s, 18H, $C^{2,6}$- CH(SiMe$_3$)$_A$(Si*Me*$_3$)$_B$, Tbb_X), 1.31 (s, 9H, C^4-C*Me*$_3$, Tbb_X), 1.37 (s, 9H, C^4-C*Me*$_3$, Tbb_Y), 2.32 (s, 2H, $C^{2,6}$-C*H*(SiMe$_3$)$_A$(SiMe$_3$)$_B$, Tbb_X), 2.53 (s, 2H, $C^{2,6}$-C*H*(SiMe$_3$)$_A$(SiMe$_3$)$_B$, Tbb_Y) 5.02 (s, 5H, C_5H_5, Cp), 6.95 (s, 2H, $C^{3,5}$-*H*, Tbb_Y), 6.96 (s, 2H, $C^{3,5}$-*H*, Tbb_X).

^{13}C{^{1}H} NMR (125.8 MHz, (D_6)benzene, 298 K): δ (ppm) = 0.87 (s, 6C, $C^{2,6}$- CH(Si*Me*$_3$)$_A$(Si*Me*$_3$)$_B$, Tbb_Y), 1.15 (s, 6C, $C^{2,6}$-CH(Si*Me*$_3$)$_A$(Si*Me*$_3$)$_B$, Tbb_X), 31.31 (s, 2C, $C^{2,6}$-*C*H(SiMe$_3$)$_A$(SiMe$_3$)$_B$, Tbb_X), 31.22 (s, 3C, C^4-C*Me*$_3$, Tbb_X), 31.27 (s, 3C, C^4-C*Me*$_3$, Tbb_Y), 31.95 (s, 2C, $C^{2,6}$-*C*H(SiMe$_3$)$_A$(SiMe$_3$)$_B$, Tbb_Y), 34.62 (s, 1C, C^4-*C*Me$_3$, Tbb_X), 34.71 (s, 1C, C^4-*C*Me$_3$, Tbb_Y), 79.32 (s, 5C, C_5H_5, Cp), 121.73 (s, 2C, $C^{3,5}$-H, Tbb_Y), 122.32 (s, 2C, $C^{3,5}$-H, Tbb_X), 146.79 (s, 2C, $C^{2,6}$-CH(Si*Me*$_3$)$_A$(Si*Me*$_3$)$_B$, Tbb_X), 146.99 (s, 1C, C^1, Tbb_Y), 147.25 (s, 2C, $C^{2,6}$-CH(Si*Me*$_3$)$_A$(Si*Me*$_3$)$_B$, Tbb_Y), 148.43 (s, 1C, C^1, Tbb_X), 151.90 (s, 1C, C^4-CMe$_3$, Tbb_Y), 153.23 (s, 1C, C^4-CMe$_3$, Tbb_X), 188.78 (s, 1C, Ge−O*C*–O).

4.5.7. [CpCo(CO)(NMes)Ge$_2$Tbb$_2$] (7-Co)

A colourless solution of Mes-NCO (56 mg, 0.345 mmol, 1 equiv.) in 3 mL of *n*-hexane was added slowly to a stirred orange-brown solution of CpCo(Ge$_2$(Tbb)$_2$) (400 mg, 0.345 mmol, 1 equiv.) in 20 mL of *n*-hexane at ambient temperature. No immediate colour change was observed. The solution was stirred for 7 hours at ambient temperature; then, the colour turned from orange-brown to red-brown. ^{1}H NMR spectrum of an aliquot of the reaction solution in (D_6)benzene revealed the complete consumption of the starting materials and the selective formation of compound **7-Co**. The red-brown solution was filtered off, followed by all volatiles being removed to dryness in a vacuum, resulting in an orange-brown crude product. This product was then crystallised from *n*-pentane (2 mL) at −30 °C. The resulting red crystals were isolated by filtration at −30 °C and dried under a fine vacuum at 40 °C for 2 hours to afford **7-Co** as an analytically pure solid. Yield: 310 mg (0.23 mmol, 67 % from CpCo(Ge$_2$(Tbb)$_2$)).

Properties: Compound **7-Co** is a highly air-sensitive, red solid turning immediately colourless upon contact with air. Upon heating, it begins to decompose during melting at 221 °C. It can be stored under an argon atmosphere at ambient temperature for several months. **7-Co** is very well soluble in *n*-pentane, benzene,

toluene, Et_2O and THF at ambient temperature. Under strict exclusion of air, solutions of **7-Co** in (D_6)benzene and (D_8)toluene are stable for at least 48 hours without any sign of decomposition at ambient temperature.

Elemental analysis: 7-Co ($C_{63}H_{114}CoGe_2NOSi_8$, 1330.42 gmol^{-1}): calcd. /%: C 56.87, H 8.64, N 1.05; found /%: C 56.70, H 8.67, N 1.07.

ATR-IR (solid, 298 K): $\tilde{\nu}$ (cm^{-1}) = 2952 (m), 2901 (w), 2862 (w), 2776 (vw) 1614 (w), 1591 (m), 1532 (m), 1475 (w), 1395 (m), 1361 (w), 1260 (w), 1246 (s), 1201 (w), 1175 (w), 1053 (m), 1010 (m), 964 (w), 949 (w), 936 (w), 881 (w), 831 (vs), 807 (w), 761 (m), 739 (w), 720 (m), 684 (w), 661 (w), 642 (w), 623 (m), 607 (w), 581 (w), 572 (w), 553 (w), 509 (m), 481 (w), 451 (w), 424 (s).

^{1}H NMR (500.1 MHz, (D_8)toluene, 236 K): δ (ppm) = 0.07 (s, 18H, C^2- CH(Si*Me*$_3$)$_A$(Si*Me*$_3$)$_B$, Tbb$_Y$), 0.24 (s, 18H, C^2-CH(Si*Me*$_3$)$_A$(Si*Me*$_3$)$_B$, Tbb$_X$), 0.25 (s, 18H, C^6-CH(Si*Me*$_3$)$_A$(Si*Me*$_3$)$_B$, Tbb$_Y$), 0.36 (s, 18H, C^6-CH(Si*Me*$_3$)$_A$(Si*Me*$_3$)$_B$, Tbb$_X$), 1.29 (s, 9H, C^4-C*Me*$_3$, Tbb$_Y$), 1.42 (s, 9H, C^4-C*Me*$_3$, Tbb$_X$), 2.20 (s, 3H, C^4-*Me*, Mes), 2.25 (s, 6H, $C^{2,6}$-*Me*, Mes), 2.49 (s, 2H, $C^{2,6}$-C*H*(SiMe$_3$)$_A$(SiMe$_3$)$_B$, Tbb$_Y$), 2.97 (s, 2H, $C^{2,6}$- C*H*(SiMe$_3$)$_A$(SiMe$_3$)$_B$, Tbb$_x$), 5.02 (s, 5H, C_5H_5, Cp), 6.78 (s, 2H, $C^{3,5}$-*H*, Mes), 6.89(s, 2H, $C^{3,5}$-*H*, Tbb$_Y$), 7.09 (s, 2H, $C^{3,5}$-*H*, Tbb$_X$).

^{13}C{^{1}H} NMR (125.8 MHz, (D_8)toluene, 236 K): δ (ppm) = 0.73 (s, 6C, C^2-CH(Si*Me*$_3$)$_A$(Si*Me*$_3$)$_B$, Tbb$_Y$), 1.01 ((s, 6C, C^2-CH(Si*Me*$_3$)$_A$(Si*Me*$_3$)$_B$, Tbb$_X$), 1.16 (s, 6C, C^6- CH(Si*Me*$_3$)$_A$(Si*Me*$_3$)$_B$, Tbb$_Y$), 1.56 (s, 6C, C^6-CH(Si*Me*$_3$)$_A$(Si*Me*$_3$)$_B$, Tbb$_X$), 20.85 (s, 2C, $C^{2,6}$-*Me*, Mes), 20.94 (s, 1C, C^4-*Me*, Mes), 29.84 (s, 2C, $C^{2,6}$-*C*H(SiMe$_3$)$_A$(SiMe$_3$)$_B$, Tbb$_X$), 31.03 (s, 2C, $C^{2,6}$-*C*H(SiMe$_3$)$_A$(SiMe$_3$)$_B$, Tbb$_Y$), 31.03 (s, 3C, C^4-C*Me*$_3$, Tbb$_y$), 31.19 (s, 3C, C^4-C*Me*$_3$, Tbb$_X$), 34.52 (s, 1C, C^4-*C*Me$_3$, Tbb$_Y$), 34.57 (s, 1C, C^4-*C*Me$_3$, Tbb$_X$), 79.58 (s, 5C, *C*$_5$H$_5$, Cp), 121.55 (s, 2C, *C*^{3,5}-H, Tbb$_Y$), 123.06 (s, 2C, *C*^{3,5}-H, Tbb$_X$), 127.21 (s, 1C, *C*^{1}, Mes), 128.19 (s, 2C, *C*^{2,6}-Me, Mes), 129.12 (s, 2C, *C*^{3,5}-H, Mes), 130.99 (s, 1C, *C*^{4}-Me, Mes), 146.09 (s, 2C, *C*^{2,6}-CH(SiMe$_3$)$_A$(SiMe$_3$)$_B$, Tbb$_X$), 146.96 (s, 2C, *C*^{2,6}-CH(SiMe$_3$)$_A$(SiMe$_3$)$_B$, Tbb$_Y$), 147.73 (s, 1C, *C*^{1}, Tbb$_Y$), 150.15 (s, 1C, *C*^{1}, Tbb$_X$), 150.88 (s, 1C, *C*^{4}-CMe$_3$, Tbb$_X$), 152.41 (s, 1C, *C*^{4}-CMe$_3$, Tbb$_Y$), 176.50 (s, 1C, N*C*O, Mes).

4.5.8. [CpCo(S)Ge$_2$Tbb$_2$] (8-Co)

Colourless solution *p*-tol-NCS (51 mg, 0.342 mmol, 1 equiv.) was added to a stirred orange-brown solution of CpCo(Ge$_2$(Tbb)$_2$) (400 mg, 0.342 mmol, 1 equiv.) in 15 mL of *n*-hexane at ambient temperature. The colour of the reaction mixture changed to an intense brown-black. The ^{1}H NMR spectrum of an aliquot of the reaction solution in (D_6)benzene after 30 min. reveals that the reaction was completed, yielding 4 to 5

Cp-containing products and compound **8-Co** was present in a 50% amount**.** The intense black-brown solution was filtered off, followed by all volatiles being removed to dryness in a vacuum, resulting in a black-brown crude product. This product was then crystallised from *n*-hexane (3 mL) at −30 °C. The resulting purple-black crystals were isolated by filtration at −30 °C and dried under a fine vacuum at 60 °C for 1 hour to afford **8-Co** as an analytically pure solid. Yield: 120 mg (0.10 mmol, 30 % from $CpCo(Ge_2(Tbb)_2)$).

Properties: Compound **8-Co** is a highly air-sensitive, purple black solid turning immediately colourless upon contact with air. Upon heating, it begins to decompose during melting at 249 °C. It can be stored under an argon atmosphere at ambient temperature for several months. **8-Co** is very well soluble in *n*-pentane, benzene, toluene, Et_2O and THF at ambient temperature. Under strict exclusion of air, solutions of **8-Co** in (D_6)benzene and (D_8)toluene are stable for at least 72 hours without any sign of decomposition at ambient temperature.

Elemental analysis: 8-Co ($C_{53}H_{103}CoGe_2SSi_8$, 1201.29 $gmol^{-1}$): calcd. /%: C 52.99, H 8.64, S 2.67; found /%: C 53.21, H 8.51, S 2.46.

ATR-IR (solid, 298 K): $\tilde{\nu}$ (cm^{-1}) = 2951 (m), 2900 (w), 2159 (vw), 2084 (s), 2073 (vw), 2056 (vw), 2027 (vw), 1580 (w), 1532 (w), 1476 (vw), 1394 (m), 1362 (vw), 1259 (m), 1247 (s), 1172 (m), 1108 (vw), 1069 (vw), 1009 (m), 959 (m), 935 (w), 884 (m), 837 (vs), 799 (w), 761 (w), 738 (w), 721 (w), 686 (m), 660 (vw), 643 (vw), 622 (vw), 607 (vw), 582 (vw), 566 (vw), 552 (vw), 535 (vw), 519 (vw), 511 (vw), 485 (vw), 477 (vw), 462 (vw), 444 (vw).

^{1}H NMR (500.1 MHz, (D_6)benzene, 298 K): δ (ppm) = 0.32 (s, 72H, 2 × $C^{2,6}$- $CH(SiMe_3)_A(SiMe_3)_B$, Tbb), 1.30 (s, 18H, 2 × C^4-CMe_3, Tbb), 2.68 (s, 4H, 2 × $C^{2,6}$- $CH(SiMe_3)_A(SiMe_3)_B$, Tbb), 4.82 (s, 5H, C_5H_5, Cp), 6.89 (s, 4H, 2 × $C^{3,5}$-*H*, Tbb).

^{13}C{^{1}H} NMR (125.8 MHz, (D_6)benzene, 298 K): δ (ppm) = 1.07 (s, 12C, 2 × $C^{2,6}$- $CH(SiMe_3)_A(SiMe_3)_B$, Tbb), 30.85 (s, 4C, 2 × $C^{2,6}$-CH$(SiMe_3)_A(SiMe_3)_B$, Tbb), 31.28 (s, 6C, 2 × C^4-CMe_3, Tbb), 34.60 (s, 2C, 2 × C^4-CMe$_3$, Tbb), 77.24 (s, 5C, C_5H_5, Cp), 121.41 (s, 4C, 2 × $C^{3,5}$-H, Tbb), 146.04 (s, 4C, 2 × $C^{2,6}$-$CH(SiMe_3)_A(SiMe_3)_B$, Tbb), 148.85 (s, 2C, 2 × C^1, Tbb), 152.62 (s, 2C, 2 × C^4-CMe_3,Tbb).

4.5.9. [CpCo(N)NC(*p*-tol)$_2$Ge$_2$Tbb$_2$] (9-Co)

A purple colour solution of (*p*-tol)2CN2 (76 mg, 0.342 mmol, 1 equiv.) in 5 mL of *n*-hexane was added slowly to a stirred orange-brown solution of $CpCo(Ge_2(Tbb)_2)$ (400 mg, 0.342 mmol, 1 equiv.) in 15 mL of *n*-hexane at ambient temperature. No

instant colour change was observed. The reaction solution was stirred for 1 hour at ambient temperature, and then the colour turned from orange-brown to intense brown. A ^{1}H NMR spectrum of an aliquot of the reaction solution in (D_6)benzene revealed the complete consumption of the starting materials and the selective formation of compound **9-Co**. The intense-brown solution was filtered off, followed by all volatiles being removed to dryness in a vacuum, resulting in an intense brown crude product, which was then crystallised from Et_2O (3 mL) at −30 °C. Compound. The resulting intense brown crystals were isolated by filtration at −30 °C and dried under a fine vacuum at ambient temperature for 30 min. to afford the mono-ether solvate **9-Co·$C_4H_{10}O$**. Yield: 390 mg (0.28 mmol, 82 % from CpCo(Ge_2(Tbb)$_2$)).

Properties: Compound **9-Co** is a highly air-sensitive, brown solid turning immediately colourless upon contact with air. Upon heating, it begins to decompose during melting at 249 °C. It can be stored under an argon atmosphere at ambient temperature for several months. **9-Co** is very well soluble in *n*-pentane, benzene, toluene, Et_2O and THF at ambient temperature. Under strict exclusion of air, solutions of **9-Co** in (D_6)benzene and (D_8)toluene are stable for at least 72 hours without any sign of decomposition at ambient temperature.

Elemental analysis: 9-Co·$C_4H_{10}O$ ($C_{68}H_{117}CoGe_2N_2Si_8(C_4H_{10}O)$, 1465.63 gmol^{-1}): calcd. /%: C 59.00, H 8.73, N 1.91; found /%: C 57.63, H 8.48, N 1.98.

ATR-IR (solid, 298 K): $\tilde{\nu}$ (cm^{-1}) = 2951 (m), 2898 (w), 2865 (w), 2785 (vw), 1611 (vw), 1582 (w), 1525 (m), 1506 (w), 1475 (w), 1463 (w), 1393 (s), 1360 (w), 1246 (s), 1164 (m), 1121 (vw), 1109 (vw), 1040 (w), 1012 (m), 987 (vw), 965 (w), 936 (m), 879 (w), 833 (vs), 794 (m), 763 (m), 737 (w), 721 (m), 684 (s), 662 (w), 622 (w), 610 (vw), 590 (m), 562 (vw), 472 (m), 441 (m).

^{1}H NMR (500.1 MHz, (D_6)benzene, 298 K): δ (ppm) = 0.25 (s, 36H, C^{2,6}- CH(Si*Me*$_3$)$_A$(Si*Me*$_3$)$_B$, Tbb$_X$), 0.33 (s, 36H, C^{2,6}-CH(Si*Me*$_3$)$_A$(Si*Me*$_3$)$_B$, Tbb$_Y$), 1.35 (s,18H, 2 × C^4-C*Me*$_3$, Tbb$_X$ and Tbb$_Y$), 1.91 (s, 3H, C^4-*Me*, *p*-tol^1), 2.13 (s, 3H, C^4-*Me*, *p*-tol^2), 2.81 (s, 4H, 2 × C^{2,6}-C*H*(SiMe$_3$)$_A$(SiMe$_3$)$_B$, Tbb$_X$ and Tbb$_Y$), 4.80 (s, 5H, C$_5$*H*$_5$, Cp), 6.69 (d, ^{3}*J*(H,H)=7.8 Hz, 2H, C^{2,6}-*H*, *p*-tol^2), 6.76 (d, ^{3}*J*(H,H)=8.6 Hz, 2H, C^{3,5}-*H*, *p*-tol^1), 6.85 (d, ^{3}*J*(H,H)=7.8 Hz, 2H, C$^{3;5}$-*H*, *p*-tol^2), 6.97 (s, 4H, 2 × C^{3,5}-*H*, Tbb$_X$ and Tbb$_Y$), 7.29 (d, ^{3}*J*(H,H)=8.6 Hz, 2H,C^{2,6}-*H*, *p*-tol^1).

^{13}C{^{1}H} NMR (125.8 MHz, (D_6)benzene, 298 K): δ (ppm) = 1.71 (s, 12C, C^{2,6}- CH(Si*Me*$_3$)$_A$(Si*Me*$_3$)$_B$, Tbb$_X$), 1.78 (s, 12C, C^{2,6}-CH(Si*Me*$_3$)$_A$(Si*Me*$_3$)$_B$, Tbb$_Y$), 21.14 (s, 1C, C^4-*Me*, *p*-tol^1), 21.51 (s, 1C, C^4-*Me*, *p*-tol^2), 29.57 (s, 4C, 2 × C^{2,6}- *C*H(SiMe$_3$)$_A$(SiMe$_3$)$_B$, Tbb$_X$ and Tbb$_Y$), 31.30 (s, 6C, 2 × C^4-C*Me*$_3$, Tbb$_X$ and Tbb$_Y$),

34.67 (s, 2C, 2 × C^{4}-*C*Me$_3$, Tbb$_x$ and Tbb$_y$), 78.16 (s, 5C, *C*$_5$H$_5$, Cp), 122.86 (s, 4C, 2 × *C*^{3,5}-H, Tbb$_X$ and Tbb$_Y$), 127.91 (s, 2C, *C*^{2,6}-H, *p*-tol^{1}), 128.29 (s, 2C, *C*^{3,5}-H, *p*-tol^{1}), 129.39 (s, 2C, *C*^{2,6}-H, *p*-tol^{2}), 129.96 (s, 2C, *C*^{3,5}-H, *p*-tol^{2}), 134.38 (s, 1C, *C*^{1}, *p*-tol^{2}), 136.86 (s, 1C,*C*^{4}-Me, *p*-tol^{2}), 137.72 (s, 1C,*C*^{4}-Me, *p*-tol^{1}), 138.54 (s, 1C, *C*^{1}, *p*-tol^{1}), 146.96 (s, 4C, 2 × *C*^{2,6}-CH(SiMe$_3$)$_A$(SiMe$_3$)$_B$, Tbb$_X$ and Tbb$_Y$), 147.89 (s, 2C, 2 × *C*^{1}, Tbb$_X$ and Tbb$_Y$), 151.74 (s, 2C, 2 × *C*^{4}-CMe$_3$, Tbb$_X$ and Tbb$_Y$), 156.19 (s, 1C, *C*N, CN(*p*-tol^{1})(*p*-tol^{2})).

4.5.10. [CpCo(N)(SiMe$_3$)Ge$_2$Tbb$_2$] (10-Co)

A colourless solution of Me3Si-N3 (40 mg, 0.342 mmol, 1 equiv.) in 1 mL of *n*-hexane was added slowly to a stirred orange-brown solution of CpCo(Ge$_2$(Tbb)$_2$) (400 mg, 0.342 mmol, 1 equiv.) in 15 mL of *n*-hexane at ambient temperature. The colour of the reaction solution instantly turned greenish-black. The solution was stirred for 1 h at ambient temperature. A ^{1}H NMR spectrum of an aliquot of the reaction solution in (D6)benzene revealed the complete consumption of the starting materials and the selective formation of compound **10-Co**. The greenish-black solution was filtered off, followed by all volatiles being removed to dryness in a vacuum, resulting in a black crude product, which was crystallised from *n*-pentane (2 mL) at −30 °C. The resulting intense green crystals were isolated by filtration at −30 °C and dried under a fine vacuum at 40 °C for 2 hours to afford **10-Co** as an analytically pure solid. Yield: 238 mg (0.19 mmol, 54 % from CpCo(Ge$_2$(Tbb)$_2$)).

Properties: Compound **10-Co** is a highly air-sensitive, intense green solid that turns immediately colourless upon contact with air. Upon heating, it begins to decompose during melting at 141 °C. It can be stored under an argon atmosphere at ambient temperature for several months. **10-Co**. It is very well soluble in *n*-pentane, benzene, toluene, Et$_2$O and THF at ambient temperature. Under strict exclusion of air, solutions of **10-Co** in (D$_6$)benzene is stable for at least 48 hours without any sign of decomposition at ambient temperature.

Elemental analysis: 10-Co (C$_{56}$H$_{112}$CoGe$_2$NSi$_9$, 1256.42 gmol^{-1}): calcd. /%: C 53.53, H 8.98, N 1.11; found /%: C 53.26, H 8.98, N 1.10.

ATR-IR (solid, RT): $\tilde{\nu}$ (cm^{-1}) = 2952 (m), 2900 (w), 2868 (w), 2862 (vw), 2820 (vw), 1584 (m), 1528 (m), 1476 (w), 1461 (vw), 1393 (m), 1361 (w), 1246 (s), 1174 (vw), 1160 (w), 1133 (w), 1112 (vw), 1007 (m), 990 (w), 938 (s), 879 (w), 831 (vs), 798 (m), 761 (m), 739 (w), 719 (w), 681 (m), 662 (w), 642 (w), 623 (w), 609 (vw), 565 (vw), 553 (w), 534 (m), 468 (w), 442 (m).

^{1}H NMR (500.1 MHz, (D_6)benzene, 298 K): δ (ppm) = −0.04 (s, 9H, Si*Me*$_3$), 0.37 (s, 36H, $C^{2,6}$-CH(Si*Me*$_3$)$_A$(Si*Me*$_3$)$_B$, Tbb_Y), 0.40 (s, 36H, $C^{2,6}$-CH(Si*Me*$_3$)$_A$(Si*Me*$_3$)$_B$, Tbb_X), 1.31 (s, 18H, 2 × C^4-C*Me*$_3$, Tbb_X and Tbb_Y), 2.77 (s, 4H, 2 × $C^{2,6}$-C*H*(SiMe$_3$)$_A$(SiMe$_3$)$_B$, Tbb_X and Tbb_Y), 4.78 (s, 5H, C_5*H*$_5$, Cp), 6.92 (s, 4H, 2 × $C^{3,5}$-*H*, Tbb_X and Tbb_Y).

^{13}C{^{1}H} NMR (125.8 MHz, (D_6)benzene, 298 K): δ (ppm) = 2.11 (s, 12C, $C^{2,6}$- CH(Si*Me*$_3$)$_A$(Si*Me*$_3$)$_B$, Tbb_Y), 2.77 (s, 12C, $C^{2,6}$-CH(Si*Me*$_3$)$_A$(Si*Me*$_3$)$_B$, Tbb_X), 5.28 (s, 3C, Si*Me*$_3$), 29.14 (s, 4C, 2 × $C^{2,6}$-*C*H(SiMe$_3$)$_A$(SiMe$_3$)$_B$, Tbb_X and Tbb_Y), 31.26 (s, 6C, 2 × C^4-C*Me*$_3$, Tbb_X and Tbb_Y), 34.51 (s, 2C, 2 × C^4-*C*Me$_3$, Tbb_X and Tbb_Y), 78.57 (s, 5C, *C*$_5$H$_5$, Cp), 122.93 (s, 4C, 2 × *C*^{3,5}-H, Tbb_X and Tbb_Y), 146.44 (s, 4C, 2 × *C*^{2,6}- CH(Si*Me*$_3$)$_A$(Si*Me*$_3$)$_B$, Tbb_X and Tbb_Y), 147.79 (s, 2C, 2 × *C*^{1}, Tbb_X and Tbb_Y), 151.51 (s, 2C, 2 × *C*^{4}, Tbb_X and Tbb_Y).

4.5.11. [CpCo(P$_4$)Ge$_2$Tbb$_2$] (11-Co)

An orange suspension of P_4 (35 mg, 0.278 mmol, 1 equiv.) in 3 mL of *n*-hexane was added slowly to a stirred orange-brown solution of CpCo(Ge$_2$(Tbb)$_2$) (325 mg, 0.278 mmol, 1 equiv.) in 15 mL of *n*-hexane at ambient temperature. No colour change was observed. The solution was stirred for 1 hour at ambient temperature. A ^{1}H and ^{31}P NMR spectrum of an aliquot of the reaction solution in (D_6)benzene revealed the complete consumption of the starting materials and the selective formation of compound **11-Co**. The brown solution was filtered off, followed by all volatiles being removed to dryness in a vacuum, resulting in a brown crude product. This product was then crystallised from *n*-hexane (2 mL) at −30 °C. The resulting brown crystals were isolated by filtration at −30 °C and dried under a fine vacuum at 60 °C for 2 hours to afford the hemi-*n*-hexane solvate **11-Co**·(**C$_6$H$_{14}$)$_{0.5}$**. Yield: 264 mg (0.20 mmol, 74 % from CpCo(Ge$_2$(Tbb)$_2$)).

Properties: Compound **11-Co** is a highly air-sensitive, brown solid, turning immediately pale yellow upon contact with air. Upon heating, it begins to decompose during melting at 241 °C. It can be stored under an argon atmosphere at ambient temperature for several months. **11-Co** is very well soluble in *n*-pentane, benzene, toluene, Et_2O and THF at ambient temperature. Under strict exclusion of air, solutions of **11-Co** in (D6)benzene is stable for at least 48 hours without any sign of decomposition at ambient temperature.

Elemental analysis: 11-Co·(C$_6$H$_{14}$)$_{0.5}$ ($C_{53}H_{103}CoGe_2P_4Si_8(C_6H_{14})_{0.5}$, 1293,12 gmol^{-1}): Calcd. /%: C 50.34, H 8.30; found /%: C 50.44, H 8.33.

^{1}H NMR (500.1 MHz, (D_6)benzene, 298 K): δ (ppm) = 0.24 (s, 9H, C^2- CH(Si*Me*$_3$)$_A$(SiMe$_3$)$_B$, Tbb_X), 0.32 (s, 18H, C^2-CH(Si*Me*$_3$)$_A$(SiMe$_3$)$_B$, Tbb_Y), 0.33 (s,

18H, C^{6}-CH(SiMe$_3$)$_A$(Si*Me$_3$*)$_B$, Tbb$_X$), 0.36 (s, 18H, C^{6}-CH(SiMe$_3$)$_A$(Si*Me$_3$*)$_B$, Tbb$_Y$), 0.43 (s, 9H, C^{2}-CH(Si*Me$_3$*)$_A$(SiMe$_3$)$_B$, Tbb$_X$),1.25 (s, 9H, C^{4}-C*Me$_3$*, Tbb$_Y$), 1.29 (s, 9H, C^{4}- C*Me$_3$*, Tbb$_X$), 1.81 (s, 1H, C^{2}-C*H*(SiMe$_3$)$_A$(SiMe$_3$)$_B$, Tbb$_X$), 2.16 (s, 2H, C^{2,6}-C*H*(SiMe$_3$)$_A$(SiMe$_3$)$_B$, Tbb$_Y$), 2.56 (s, 1H, C^{6}-C*H*(SiMe$_3$)$_A$(SiMe$_3$)$_B$, Tbb$_X$), 5.08 (s, 5H, C$_5$*H$_5$*, Cp), 6.79 (s, 2H, C^{3,5}-*H,* Tbb$_Y$),6.85 (s, 1H, C^{3}-*H,* Tbb$_X$), 6.99 (s, 1H, C^{5}-*H,* Tbb$_X$).

^{13}C{^{1}H} NMR (125.8 MHz, (D$_6$)benzene, 298 K): δ (ppm) = 0.93-1.73 (m, 24C, 2 × C^{2,6}- CH(Si*Me$_3$*)$_A$(Si*Me$_3$*)$_B$), Tbb$_Y$), 27.94 (s, 1C, C^{2}-*C*H(SiMe$_3$)$_A$(SiMe$_3$)$_B$, Tbb$_X$), 29.58 (s, 2C, C^{2,6}-*C*H(SiMe$_3$)$_A$(SiMe$_3$)$_B$, Tbb$_Y$), 30.06 (s, 1C, C^{6}-*C*H(SiMe$_3$)$_A$(SiMe$_3$)$_B$, Tbb$_X$), 31.13 (s, 3C, C^{4}-C*Me$_3$*, Tbb$_Y$), 31.17 (s, 3C, C^{4}-C*Me$_3$*, Tbb$_X$), 34.43 (s, 1C, C^{4}-*C*Me$_3$, Tbb$_Y$), 34.45 (s, 1C, C^{4}-*C*Me$_3$, Tbb$_X$), 84.24 (s, 5C, *C$_5$*H$_5$, Cp), 121.40 (s, 2C, *C^{3,5}*-H, Tbb$_Y$), 122.31 (s, 1C, *C^{3}*-H, Tbb$_X$), 123.45 (s, 1C, *C^{5}*-H, Tbb$_X$), 128.40 (s, 1C, *C^{1}*, Tbb$_X$), 138.23 (s, 1C, *C^{1}*, Tbb$_Y$), 148.67 (s, 2C, *C^{2,6}*-CH(SiMe$_3$)$_A$(SiMe$_3$)$_B$, Tbb$_Y$), 151.46 (s, 1C, *C^{2}*-CH(SiMe$_3$)$_A$(SiMe$_3$)$_B$, Tbb$_X$), 151.72 (s, *C^{4}*-CMe$_3$, Tbb$_Y$), 151.99 (s, *C^{4}*-CMe$_3$, Tbb$_X$), 153.07(s, 1C, *C^{6}*-CH(SiMe$_3$)$_A$(SiMe$_3$)$_B$, Tbb$_X$).

^{31}P{^{1}H} NMR (202.44 MHz, (D$_6$)benzene, 298 K): δ (ppm) = −121.75(ddd, ^{1}J(^{31}P$_D$-^{31}P$_A$) = 334.35 Hz, ^{2}J(^{31}P$_D$-^{31}P$_B$) = 82.78 Hz, ^{2}J(^{31}P$_B$-^{31}P$_C$) = 14.95 Hz, 1P, Ge*P$_D$*P$_A$), −64.28(d, ^{2}J(^{31}P$_C$-^{31}P$_B$) = 55.8 Hz, 1P, Ge*P$_C$*P$_B$), −5.78(dd, ^{1}J(^{31}P$_A$-^{31}P$_D$) = 334.35 Hz, ^{1}J(^{31}P$_A$-^{31}P$_B$) = 28.5 Hz, 1P, GeP$_D$*P$_A$*), 27.67−26.50(m, 1P Ge*P$_B$*P$_A$).

4.5.12. [Tbb$_2$Si$_2$(CNMes)$_2$] (12-Si)

A light-yellow solution of Mes-NC (30 mg, 0.20 mmol, 2 equiv.) in 2 mL of *n*-pentane was added slowly to a stirred orange solution of TbbSi≡SiTbb (100 mg, 0.10 mmol, 1 equiv.) in 10 mL of *n*-pentane at ambient temperature. The colour of the reaction solution turned yellow-brown immediately. A ^{1}H spectrum of an aliquot of the reaction solution in (D$_6$)benzene revealed the complete and selective formation of **12-Si**, along with 10 mol% free Mes-NC. The yellow-brown solution was filtered off, followed by the removal of all volatiles to dryness in a vacuum, resulting in a brown solid. This solid was then crystallised from *n*-pentane (0.5 mL) at −30 °C. The resulting brown crystals were isolated by filtration at −30 °C and dried under a fine vacuum at ambient temperature for one hour to obtain **12-Si** as an analytically pure brown solid compound. Yield: 78 mg (0.070 mmol, 68 % from TbbSi≡SiTbb).

Properties: Compound **12-Si** is a highly air-sensitive, brown solid that turns immediately colourless upon contact with air. Upon heating, it begins to decompose during melting at 253 °C. It can be stored under an argon atmosphere at ambient temperature for several months. **12-Si** is very well soluble in *n*-pentane, benzene, toluene, Et$_2$O and THF at ambient temperature. Under strict exclusion of air,

solutions of **12-Si** in (D_6)benzene and (D_8)thf is stable for at least 72 hours without any sign of decomposition at ambient temperature.

Elemental analysis: 12-Si ($C_{68}H_{120}N_2Si_{10}$, 1282.62 g mol^{-1}): Calcd. /%: C 66.02, H 9.90, N 2.18; found: /%: C 65.95, H 9.89, N 2.14.

IR (*n*-hexane): $\tilde{\nu}$ (cm^{-1}) = 1588 (w) [$\nu(CC)_{aryl}$], 1552 (s) [$\nu(CN)$], and 1530 (w) [$\nu(CC)_{aryl}$]. **ATR-IR** (solid): $\tilde{\nu}$ (cm^{-1}) = 2954 (w), 2899 (vw), 1588 (vw) [$\nu(CC)_{aryl}$],1551 (w) [$\nu(CN)$], 1530 (w) [$\nu(CC)_{aryl}$], 1463 (vw), 1425 (vw), 1396 (w), 1428 (vw), 1396 (w), 1309 (vw), 1297 (vw), 1247 (s), 1198 (w), 1176 (vw), 1157 (w), 1098 (vw), 1052 (w), 1026 (w), 1009 (w), 990 (w), 952 (w), 889 (w), 840 (w), 762 (w), 743 (w), 684 (m), 663 (w), 640 (w), 625 (w), 603 (w), 578 (vw), 559 (w), 526 (w), 494 (m), 475 (w), 452 (vw), 423 (w).

^{1}H NMR (500.1 MHz, (D_6)benzene, 298 K): δ (ppm) = 0.20 (s, 36H, 2 × $C^{2,6}$C- H(Si*Me*$_3$)$_A$(SiMe$_3$)$_B$, 2 × Tbb), 0.28 (s, 36H, 2 × $C^{2,6}$C-H(SiMe$_3$)$_A$(Si*Me*$_3$)$_B$, 2 × Tbb) 1.28 (s, 18H, 2 × C^4-C*Me*$_3$, 2 × Tbb), 2.10 (s, 6H, 2 × C^4-*Me*, 2 × Mes), 2.19 (s, 12H, 2 × $C^{2,6}$-*Me*, 2 × Mes), 2.78 (s, 4H, 2 × $C^{2,6}$C-*H*(SiMe$_3$)$_A$(SiMe$_3$)$_B$, 2 × Tbb), 6.43 (s, 4H, 2 × $C^{3,5}$-*H*, 2 × Mes), 7.04 (s, 4H, 2 × $C^{3,5}$-*H*, 2 × Tbb).

^{1}H NMR (500.1 MHz, (D_8)thf, 263 K): δ (ppm) = 0.00 (s, 36H, 2 × $C^{2,6}$C- H(Si*Me*$_3$)$_A$(SiMe$_3$)$_B$, 2 × Tbb), 0.15 (s, 36H, 2 × $C^{2,6}$C-H(SiMe$_3$)$_A$(Si*Me*$_3$)$_B$, 2 × Tbb) 1.32 (s, 18H, 2 × C^4-C*Me*$_3$, 2 × Tbb), 1.86 (s, 12H, 2 × $C^{2,6}$-*Me*, 2 × Mes), 2.02 (s, 6H, 2 × C^4-*Me*, 2 × Mes), 2.55 (s, 4H, 2 × $C^{2,6}$C-*H*(SiMe$_3$)$_A$(SiMe$_3$)$_B$, 2 × Tbb), 6.21 (s, 4H, 2 × $C^{3,5}$-*H*, 2 × Mes), 7.91 (s, 4H, 2 × $C^{3,5}$-*H*, 2 × Tbb).

^{13}C{^{1}H} NMR (125.8 MHz, (D_6)benzene, 298 K): δ (ppm) = 1.09 (s, 12C, 2 × $C^{2,6}$C- H(SiMe$_3$)$_A$(Si*Me*$_3$)$_B$, 2 × Tbb), 2.05 (s, 12C, 2 × $C^{2,6}$C- H(Si*Me*$_3$)$_A$(SiMe$_3$)$_B$, 2 × Tbb), 20.21 (s, 4C, 2 × $C^{2,6}$-*Me*, 2 × Mes), 20.85 (s, 2C, 2 × C^4-*Me*, 2 × Mes), 31.00 (s, 6C, 2 × C^4-C*Me*$_3$, 2 × Tbb), 33.46 (s, 4C, 2 × *C*^{2,6}*C*- H(SiMe$_3$)$_A$(SiMe$_3$)$_B$, 2 × Tbb), 34.70 (s, 2C, 2 × C^4-*C*Me$_3$, 2 × Tbb), 122.85 (s, 4C, 2 × *C*^{3,5}-H, 2 × Tbb), 124.96 (s, 4C, 2 × *C*^{2,6}- Me, 2 × Mes), 126.84 (s, 4C, 2 × *C*^{2,6}-H(SiMe$_3$)$_A$(SiMe$_3$)$_B$, 2 × Tbb), 128.75 (s, 4C, 2 × *C*^{3,5}-H, 2 × Mes), 130.18 (s, 2C, 2 × *C*^{4}-Me, 2 × Mes), 149.39 (s, 2C, 2 × *C*^{1}, 2 × Mes), 152.65 (s, 2C, 2 × *C*^{1}, 2 × Tbb), 153.43 (s, 2C, 2 × *C*^{4}-CMe$_3$, 2 × Tbb), 183.50 (s, 2C, 2 × Si-*C*-N-Mes).

^{13}C{^{1}H} NMR (125.8 MHz, (D_8)thf, 263 K): δ (ppm) = 1.11 (s, 12C, 2 × $C^{2,6}$C- H(SiMe$_3$)$_A$(Si*Me*$_3$)$_B$, 2 × Tbb), 2.08 (s, 12C, 2 × $C^{2,6}$C- H(Si*Me*$_3$)$_A$(SiMe$_3$)$_B$, 2 × Tbb), 20.38 (s, 4C, 2 × $C^{2,6}$-*Me*, 2 × Mes), 20.92 (s, 2C, 2 × C^4-*Me*, 2 × Mes), 31.26 (s, 6C, 2 × C^4-C*Me*$_3$, 2 × Tbb), 33.79 (s, 4C, 2 × *C*^{2,6}*C*- H(SiMe$_3$)$_A$(SiMe$_3$)$_B$, 2 × Tbb), 35.31 (s, 2C, 2 × C^4-*C*Me$_3$, 2 × Tbb), 123.31 (s, 4C, 2 × *C*^{3,5}-H, 2 × Tbb), 125.23 (s, 4C, 2 × *C*^{2,6}-Me,

2 × Mes), 127.03 (s, 4C, 2 × *C*^{2,6}-H(SiMe$_3$)$_A$(SiMe$_3$)$_B$, 2 × Tbb), 128.91 (s, 4C, 2 × *C*^{3,5}- H, 2 × Mes), 130.28 (s, 2C, 2 × *C*^{4}-Me, 2 × Mes), 149.69 (s, 2C, 2 × *C*^{1}, 2 × Mes), 152.98 (s, 2C, 2 × *C*^{1}, 2 × Tbb), 153.88 (s, 2C, 2 × *C*^{4}-CMe$_3$, 2 × Tbb), 183.88 (s, 2C, 2 × Si- *C*- N-Mes).

^{29}Si{^{1}H} NMR (99.33 MHz, (D$_6$)benzene, 298 K): δ (ppm) = 1.84 and 3.42 (s, 8Si, 2 × C^{2,6}C-H(*Si*Me$_3$)$_2$, 2 × Tbb), 90.17 (s, 2Si, 2 × *Si*-C-N-Mes).

^{29}Si{^{1}H} NMR (99.33 MHz, (D$_8$)thf, 263 K): δ (ppm) = 1.95 and 3.38 (s, 8Si, 2 × C^{2,6}C-H(*Si*Me$_3$)$_2$, 2 × Tbb), 89.79 (s, 2Si, 2 × *Si*-C-N-Mes).

4.5.13. [Tbb$_2$Ge$_2$(CNMes)$_2$] (12-Ge)

A light-yellow solution of Mes-NC (97 mg, 0.66 mmol, 2 equiv.) in 3 mL of *n*-pentane was added slowly to a stirred yellow-orange solution of TbbGe≡GeTbb (350 mg, 0.33 mmol, 1 equiv) in 10 mL of *n*-pentane at ambient temperature. The colour of the reaction solution turned first green, then immediately red-brown. A ^{1}H spectrum of an aliquot of the reaction solution in (D$_6$)benzene revealed the complete and selective formation of **12-Ge**. The red-brown solution was filtered off, followed by all volatiles being removed to dryness in a vacuum, resulting in a brown solid. This solid was then crystallised from *n*-pentane (2.8 mL) at −30 °C. The resulting brown crystals were isolated by filtration at −30 °C and dried under a fine vacuum at ambient temperature for one hour to obtain **12-Ge** as an analytically pure brown solid compound. Yield: 305 mg (0.228 mmol, 68 % from TbbGe≡GeTbb).

Properties: Compound **12-Ge** is a highly air-sensitive, brown solid turning immediately colourless upon contact with air. Upon heating, it begins to decompose during melting at 148 °C. It can be stored under an argon atmosphere at ambient temperature for several months. **12-Ge** is very well soluble in *n*-pentane, benzene, toluene, Et$_2$O and THF at ambient temperature. Under strict exclusion of air, solutions of **12-Ge** in (D$_6$)benzene and (D$_8$)thf is stable for at least 72 hours without any sign of decomposition at ambient temperature.

Elemental analysis: 12-Ge (C$_{68}$H$_{120}$Ge$_2$N$_2$Si$_8$, 1335.60 g mol^{-1}): Calcd. /%: C 61.15, H 9.06, N 2.09; found /%: C 61.02, H 8.94, N 1.90.

IR (*n*-hexane): $\tilde{\nu}$ (cm^{-1}) = 1583 (w) [ν(CC)$_{aryl}$], 1562 (s) [ν(CN)] and 1530 (w) [ν(CC)$_{aryl}$].

ATR-IR (solid): $\tilde{\nu}$ (cm^{-1}) = 2952 (w), 2901 (vw), 2888 (vw), 1583 (vw) [ν(CC)$_{aryl}$],1558 (w) [ν(CN)], 1526 (w) [ν(CC)$_{aryl}$], 1476 (vw), 1465 (vw), 1442 (vw, sh), 1428 (vw), 1396 (w), 1362 (vw), 1247 (s), 1218 (vw), 1199 (w), 1122 (w), 1175 (vw), 1161 (w), 1143 (w), 1026 (w), 1012 (w), 955 (w), 938 (w), 887 (w), 833 (vs), 762 (sh), 739 (s), 717 (m), 685

(m), 677 (w), 663 (w), 643 (w), 625 (w), 609 (w), 599 (w), 584 (w), 575 (m), 454 (w), 420 (vw), 410 (m).

^{1}H NMR (500.1 MHz, (D_6)benzene, 298K): δ (ppm) = 0.25 (s, 72H, 2 × $C^{2,6}$C- H(Si*Me*$_3$)$_A$(SiMe$_3$)$_B$, 2 × Tbb), 1.30 (s, 18H, 2 × C^4-C*Me*$_3$, 2 × Tbb), 2.08 (s, 6H, 2 × C^4-*Me*, 2 × Mes), 2.16 (s, 12H, 2 × $C^{2,6}$-*Me*, 2 × Mes), 2.67 (s, 4H, 2 × $C^{2,6}$C- *H*(SiMe$_3$)$_A$(SiMe$_3$)$_B$, 2 × Tbb), 6.72 (s, 4H, 2 × $C^{3,5}$-*H*, 2 × Mes), 7.07 (s, 4H, 2 × $C^{3,5}$-*H*, 2 × Tbb).

^{13}C{^{1}H} NMR (125.8 MHz, (D_6)benzene, 298 K): δ (ppm) = 1.44 (s, 24C, 2 × $C^{2,6}$C- H(Si*Me*$_3$)$_A$(Si*Me*$_3$)$_B$, 2 × Tbb), 20.19 (s, 4C, 2 × $C^{2,6}$-*Me*, 2 × Mes), 20.80 (s, 2C, 2 × C^4-*Me*, 2 × Mes), 31.16 (s, 6C, 2 × C^4-C*Me*$_3$, 2 × Tbb), 33.28 (s, 4C, 2 × *C*^{2,6}*C*- H(SiMe$_3$)$_A$(SiMe$_3$)$_B$, 2 × Tbb), 34.65 (s, 2C, 2 × C^4-*C*Me$_3$, 2 × Tbb), 122.80 (s, 4C, 2 × *C*^{3,5}-H, 2 × Tbb), 122.85 (s, 4C, 2 × *C*^{3,5}-H, 2 × Mes), 126.60 (s, 4C, 2 × *C*^{2,6}-Me, 2 × Mes.), 130.80 (s, 2C, 2 × *C*^{4}-H, 2 × Mes), 140.00 (s, 2C, 2 × *C*^{1}, 2 × Tbb), 148.87 (s, 2C, 2 × *C*^{1}, 2 × Mes), 149.77 (s, 4C, 2 × *C*^{2,6}C- H(SiMe$_3$)$_A$(SiMe$_3$)$_B$, 2 × Tbb), 152.38 (s, 2C, 2 × *C*^{4}-CMe$_3$, 2 × Tbb), 190.93 (s, 2C, 2 × Ge-*C*-N-Mes).

4.5.14. [Ge(TbbSiBr)$_2$(CNMes)$_2$] (13-Si)

A colourless solution of $GeBr_2$(1,4-dioxane) (50 mg, 0.15 mmol, 1 equiv.) in 5 mL of benzene was added slowly to a stirred red-orange solution of **12-Si** (200 mg, 0.15 mmol, 1 equiv.) in 10 mL of benzene at ambient temperature. No immediate colour change was observed, and the reaction solution was stirred for 5 hours at ambient temperature. Upon stirring, the colour transitioned from red-orange to light yellow. A ^{1}H spectrum of an aliquot of the reaction solution in (D_6)benzene after 5 hours revealed the complete and selective formation of **13-Si**. The light-yellow solution was filtered off, followed by all volatiles being removed to dryness in a vacuum, resulting in a light-yellow solid. This solid was then crystallised from *n*- hexane (4 mL) at −30 °C. The resulting light-yellow crystals were isolated by filtration at −30 °C and dried under a fine vacuum at ambient temperature for one hour to obtain **13-Si** as an analytically pure brown solid compound. Yield: 131 mg (0.228 mmol, 57 % from **12-Si**).

Properties: Compound **13-Si** is a highly air-sensitive, light-yellow solid turning immediately colourless upon contact with air. Upon heating, it begins to decompose during melting at 259 °C. It can be stored under an argon atmosphere at ambient temperature for several months. **13-Si** is moderately soluble in aliphatic solvents (*n*-pentane and *n*-hexane) and very well soluble in benzene, toluene, Et_2O and THF at ambient temperature. Under strict exclusion of air, solutions of **13-Si** in (D_8)toluene

is stable for at least 48 hours without any sign of decomposition at ambient temperature.

Elemental analysis: 13-Si ($C_{68}H_{120}GeBr_2N_2Si_{10}$, 1478.96 g mol^{-1}): Calcd. /%: C 56.85, H 8.57, N 1.81; found /%: C 55.83, H 8.58, N 1.85.

^{1}H NMR (500.1 MHz, (D_8)toluene, 243K): δ (ppm) = −0.22 (br s, $\Delta\nu_{1/2}$ = 22.50 Hz, 9H, C^2C- H(Si*Me*$_3$)$_A$(SiMe$_3$)$_B$, Tbb$_X$), 0.07 (s, 9H, C^2C-H(SiMe$_3$)$_A$(Si*Me*$_3$)$_B$, Tbb$_X$), 0.09 (s, 9H, C^6C-H(Si*Me*$_3$)$_A$(SiMe$_3$)$_B$, Tbb$_Y$), 0.13 (s, 9H, C^6C-H(Si*Me*$_3$)$_A$(SiMe$_3$)$_B$, Tbb$_X$), 0.31 (s, 9H, C^2C-H(Si*Me*$_3$)$_A$(SiMe$_3$)$_B$, Tbb$_Y$), 0.39 (s, 9H, C^6C-H(SiMe$_3$)$_A$(Si*Me*$_3$)$_B$, Tbb$_Y$), 0.66 (br s, $\Delta\nu_{1/2}$ = 8.85 Hz, 9H, C^2C-H(Si*Me*$_3$)$_A$(SiMe$_3$)$_B$, Tbb$_X$), 1.29 (s, 9H, C^4-C*Me*$_3$, Tbb$_X$), 1.33 (s, 9H, C^4-C*Me*$_3$, Tbb$_Y$), 1.81 (s, 1H, C^6C-*H*(SiMe$_3$)$_A$(SiMe$_3$)$_B$, Tbb$_X$), 1.96 (s, 1H, C^2C- *H*(SiMe$_3$)$_A$(SiMe$_3$)$_B$, Tbb$_Y$), 2.23 (s, 6H, C^4-*Me*, Mes^1 +Mes^2), 2.48 (s, 3H, C^2-*Me*, Mes^2), 2.50 (s, 3H, C^2-*Me*, Mes^1), 2.63 (s, 3H, C^6-*Me*, Mes^1), 2.69 (s, 1H, C^6C- *H*(SiMe$_3$)$_A$(SiMe$_3$)$_B$, Tbb$_Y$), 2.70 (s, 3H, C^6-*Me*, Mes^2), 2.78 (s, 1H, C^2C- *H*(SiMe$_3$)$_A$(SiMe$_3$)$_B$, Tbb$_X$), 6.69 (d, ^{4}*J*(H,H) = 2 Hz, 1H, C^5-*H*, Tbb$_X$), 6.74 (d, ^{4}*J*(H,H) = 2.7 Hz, 1H, C^3-*H*, Mes^1), 6.69 (d, ^{4}*J*(H,H) = 3 Hz, 1H, C^3-*H*, Tbb$_Y$), 6.83 (d, ^{4}*J*(H,H) = 3.5 Hz, 2H, 2 × C^5-*H*, Mes^1 + Mes^2), 6.86 (d, ^{4}*J*(H,H) = 3.0 Hz, 1H, C^3-*H*, Mes^2), 6.95 (d, ^{4}*J*(H,H) = 2.7 Hz, 1H, C^3-*H*, Tbb$_X$), 7.09 (d, ^{4}*J*(H,H) = 2 Hz, 1H, C^5-*H*, Tbb$_Y$).

^{13}C{^{1}H} NMR (125.8 MHz, (D_8)toluene, 243 K): δ (ppm) = 1.79 (s, 3C, C^6C-H(Si*Me*$_3$)$_A$(SiMe$_3$)$_B$, Tbb$_Y$), 2.31 (s, 3C, C^2C-H(SiMe$_3$)$_A$(Si*Me*$_3$)$_B$, Tbb$_X$), 2.86 (s, 3C, C^6C-H(Si*Me*$_3$)$_A$(SiMe$_3$)$_B$, Tbb$_X$), 3.60 (s, 3C, C^2C-H(Si*Me*$_3$)$_A$(SiMe$_3$)$_B$, Tbb$_Y$), 3.95 (s, 3C, C^6C-H(SiMe$_3$)$_A$(Si*Me*$_3$)$_B$, Tbb$_Y$), 20.40 (s, 1C, C^2-*Me*, Mes^1), 21.04 (s, 1C, C^6-*Me*, Mes^1), 22.18 (s, 1C, C^4-*Me*, Mes^1), 24.41 (s, 1C, C^5-*Me*, Mes^2), 24.93 (s, 1C, C^2-*Me*, Mes^2), 25.30 (s, 1C, C^4-*Me*, Mes^2), 27.37 (s, 1C, *C*^{2}*C*-H(SiMe$_3$)$_A$(SiMe$_3$)$_B$, Tbb$_X$), 29.38 (s, 1C, *C*^{2}*C*-H(SiMe$_3$)$_A$(SiMe$_3$)$_B$, Tbb$_Y$), 29.87 (s, 1C, *C*^{6}*C*-H(SiMe$_3$)$_A$(SiMe$_3$)$_B$, Tbb$_Y$), 30.89 (s, 1C, C^4-C*Me*$_3$, Tbb$_Y$), 31.02 (s, 1C, C^4-C*Me*$_3$, Tbb$_X$), 34.20 (s, 1C, C^4-*C*Me$_3$, Tbb$_Y$), 34.26 (s, 1C, C^4-*C*Me$_3$, Tbb$_X$), 35.62(s, 1C, *C*^{6}*C*-H(SiMe$_3$)$_A$(SiMe$_3$)$_B$, Tbb$_X$), 124.07 (s, 1C, *C*^{5}-H, Tbb$_X$), 124.59 (s, 1C, *C*^{3}-H, Tbb$_X$), 125.76 (s, 1C, *C*^{5}-H, Tbb$_Y$), 124.07 (s, 1C, *C*^{3}-H, Tbb$_X$), 129.46 (s, 1C, *C*^{3}-H, Mes^2), 129.59(s, 1C, *C*^{4}-Me, Mes^1), 130.17 (s, 1C, *C*^{3}-H, Mes^1), 130.32(s, 1C, *C*^{5}-H, Mes^1), 130.74 (s, 1C, *C*^{5}-H, Mes^2), 131.10 (s, 1C, *C*^{4}-Me, Mes^2), 132.47(s, 1C, *C*^{1}, Tbb$_X$), 135.23 (s, 1C, *C*^{2}-Me, Mes^1), 135.43 (s, 1C, *C*^{2}-Me, Mes^2), 135.60 (s, 1C, *C*^{6}-Me, Mes^2), 135.83 (s, 1C, *C*^{5}-Me, Mes^1), 137.17 (s, 1C, *C*^{1}, Tbb$_Y$), 139.95 (s, 1C, *C*^{1}, Mes^1), 140.33 (s, 1C, *C*^{1}, Mes^1), 147.31 (s, 1C, *C*^{2} C- H(SiMe$_3$)$_A$(SiMe$_3$)$_B$, Tbb$_Y$), 148.56 (s, 1C, *C*^{4}-CMe$_3$, Tbb$_Y$), 150.41 (s, 1C, *C*^{2} C- H(SiMe$_3$)$_A$(SiMe$_3$)$_B$, Tbb$_X$), 150.52 (s, 1C, *C*^{4}-CMe$_3$, Tbb$_X$), 152.44 (s, 1C, *C*^{6}

C- H($SiMe_3$)$_A$($SiMe_3$)$_B$, Tbb$_Y$), 152.80 (s, 1C, Si*C*CSi), 155.38(s, 1C, *C*^{6} C- H($SiMe_3$)$_A$($SiMe_3$)$_B$, Tbb$_X$) 157.86 (s, 1C, SiC*C*Si).

4.5.15. [Tbb$_2$Ge$_3$Br$_2$C$_2$Me$_2$] (14-Ge)

A colourless solution of $GeBr_2$(1,4-dioxane) (48 mg, 0.15 mmol, 1 equiv.) in 3 mL of benzene was added slowly to a stirred green solution of $Tbb_2Ge_2C_2Me_2$ (165 mg, 0.15 mmol, 1 equiv.) in 7 mL of benzene at ambient temperature. The colour of the reaction solution immediately changes to brown. The reaction solution was stirred at ambient temperature for 30 min, and analysis of an aliquot of the reaction solution by ^{1}H NMR spectroscopy in (D_6)benzene revealed the complete consumption of all the starting materials and the selective formation of **14-Ge**. The reaction solution was filtered off, followed by evaporation of the solvent to dryness in a vacuum. Then, 4 mL of n-hexane was added, and the solvent was evaporated to dryness, resulting in a light-brown solid crude product. This product was crystallised from *n*-hexane (0.5 mL) at – 30 °C. The resulting colourless crystals were isolated by filtration at − 30°C and dried under a fine vacuum at 50 °C for 2 hours to afford **14-Ge.** Yield: 135 mg (0.10 mmol, 67 % from $Tbb_2Ge_2C_2Me_2$).

Properties: Compound **14-Ge** is an air-sensitive, colourless solid that immediately turns pale yellow upon contact with air. Upon heating, it begins to decompose during melting at 230 °C. It can be stored under an argon atmosphere at ambient temperature for several months. **14-Ge** is very well soluble in benzene, toluene, Et_2O and THF and partially soluble in *n*-hexane at ambient temperature. Under strict exclusion of air, solutions of **14-Ge** in (D_6)benzene is stable for at least 7 days without any sign of decomposition at ambient temperature.

Elemental analysis: 14-Ge ($C_{52}H_{104}Ge_3Br_2Si_8$, 1331.70 g mol^{-1}): Calcd. /%: C 46.90, H 7.87; found /%: C 46.72, H 7.46.

^{1}H NMR (500.1 MHz, (D_6)benzene, 298 K): δ (ppm) = 0.26 (s, 72H, 2 × C^{2,6}C-H(Si*Me*$_3$)$_2$, 2 × Tbb), 1.31 (s, 18H, 2 × C^4-C*Me*$_3$, 2 × Tbb), 2.18 (s, 6H, 2 × C-*Me*), 2.73(s, 4H, 2 × C^{2,6}C-*H*($SiMe_3$)$_2$, 2 × Tbb), 6.94 (s, 4H, 2 × C^{3,5}-*H*, 2 × Tbb).

^{13}C{^{1}H} NMR (125.8 MHz, (D_6)benzene, 298 K): δ (ppm) = 1.51 (s, 24C, 2 × C^{2,6}C- H(Si*Me*$_3$)$_2$, 2 × Tbb), 20.55 (s, 2C, 2 × C-*Me*), 31.04 (s, 4C, 2 × C^{2,6}*C*-H($SiMe_3$)$_2$), 2 × Tbb), 31.14 (s, 6C, 2 × C^4-C*Me*$_3$, 2 × Tbb), 34.39 (s, 2C, 2 × C^4-*C*Me$_3$, 2 × Tbb), 123.28 (s, 4C, 2 × *C*^{3,5}-H, 2 × Tbb), 133.88 (s, 2C, 2 × *C*^{1}, 2 × Tbb), 149.28 (s, 4C, 2 × *C*^{2,6}-CH($SiMe_3$)$_2$, 2 × Tbb), 151.30 (s, 2C, 2 × *C*^{4}-CMe$_3$, 2 × Tbb), 157.01 (s, 2C, 2 × *C*-Me).

4.5.16. [$Tbb_2Ge_2SnCl_2C_2Me_2$] (**14-Sn**)

A colourless solution of $SnCl_2$ (63 mg, 0.332 mmol, 1 equiv.) in 10 mL of Et_2O was added slowly to a stirred green solution of $Tbb_2Ge_2C_2Me_2$ (365 mg, 0.332 mmol, 1 equiv.) in 20 mL of Et_2O at ambient temperature, and then sonicated for 30 min. Upon which, the colour of the reaction solution changed to red-brown. Analysis of an aliquot of the reaction solution by ^{1}H NMR spectroscopy in (D_6)benzene revealed the complete consumption of the starting materials and the selective formation of **14-Sn**. The reaction solution was filtered off, followed by evaporation of the solvent to dryness in a vacuum. Then, 4 mL of *n*-hexane was added, and the solvent was evaporated to dryness, resulting in a light-brown solid crude product. This product was crystallised from *n*-hexane (2 mL) at – 30 °C. The resulting off-white crystals were isolated by filtration at − 30°C and dried under a fine vacuum at 60 °C for 2 hours to afford **14-Sn.** Yield: 228 mg (0.170 mmol, 53 % from $Tbb_2Ge_2C_2Me_2$).

Properties: Compound **14-Sn** is an air-sensitive, off-white solid that immediately turns pale yellow upon contact with air. Upon heating, it begins to decompose during melting at 240 °C. It can be stored under an argon atmosphere at ambient temperature for several months. **14-Sn** is very well soluble in benzene, toluene, Et_2O and THF and partially soluble in *n*-hexane and *n*-pentane at ambient temperature. Under strict exclusion of air, solutions of **14-Sn** in (D_6)benzene is stable for at least 7 days without any sign of decomposition at ambient temperature.

Elemental analysis: 14-Sn ($C_{52}H_{104}Ge_2SnCl_2Si_8$, 1336.94 g mol^{-1}): Calcd. /%: C 48.45, H 8.13; found /% C 48.53, H 8.22.

^{1}H NMR (500.1 MHz, (D_6)benzene, 298 K): δ (ppm) = 0.25 (s, 72H, 2 × C^{2,6}C-H(Si*Me*$_3$)$_2$, 2 × Tbb), 1.32 (s, 18H, 2 × C^4-C*Me*$_3$, 2 × Tbb), 2.27 (s, 6H, 2 × C-*Me*), 2.57 (s, 4H, 2 × C^{2,6}C-*H*(SiMe$_3$)$_2$, 2 × Tbb), 6.93 (s, 4H, 2 × C^{3,5}-*H*, 2 × Tbb).

^{13}C{^{1}H} NMR (125.8 MHz, (D_6)benzene, 298 K): δ (ppm) = 1.23-1.67 (br s, 24C, 2 × C^{2,6}C-H(Si*Me*$_3$)$_2$, 2 × Tbb), 20.97 (s, 2C, 2 × C-*Me*), 30.06 (s, 4C, 2 × C^{2,6}*C*-H(SiMe$_3$)$_2$), 2 × Tbb), 31.21 (s, 6C, 2 × C^4-C*Me*$_3$, 2 × Tbb), 34.39 (s, 2C, 2 × C^4-*C*Me$_3$, 2 × Tbb), 123.12 (s, 4C, 2 × *C*^{3,5}-H, 2 × Tbb), 136.77 (s, 2C, 2 × *C*^{1}, 2 × Tbb), 149.36 (s, 4C, 2 × *C*^{2,6}-CH(SiMe$_3$)$_2$), 2 × Tbb), 151.36 (s, 2C, 2 × *C*^{4}-CMe$_3$, 2 × Tbb), 157.12 (s, 2C, 2 × *C*- Me).

^{119}Sn{^{1}H} NMR (186.50 MHz, (D_6)benzene, 298 K): δ (ppm) = −486.57 (s, Sn, *Sn*Ge$_2$).

4.5.17. [$Tbb_2Ge_2(CNMes)C_2Me_2$] (**15-Ge**)

Light yellow solution of Mes-NC (27 mg, 0.18 mmol, 1 equiv.) in 3 mL of *n*-pentane was added to a stirred green solution of $Tbb_2Ge_2C_2Me_2$ (200 mg, 018 mmol, 1 equiv.) in 10 mL of *n*-pentane at ambient temperature. The colour of reaction solution immediately changed to dark purple. An analysis of an aliquot of the reaction solution by ^{1}H NMR spectroscopy in (D_6)benzene revealed a complete consumption of all the starting materials and the selective formation of **15-Ge**. The reaction solution was filtered off followed by evaporating the solvent to dryness in vacuum resulting purple solid crude product which was crystallized from *n*-hexane (0.7 mL) at – 30 °C. The resulting deep purple crystals were isolated by filtration at – 30 °C and dried under fine vacuum at ambient temperature for one hour to afford **15-Ge** with Tbb-H (*ca.* 4%). Yield: 112 mg (0.089 mmol, 49 % from $Tbb_2Ge_2C_2Me_2$).

Properties: Compound **15-Ge** is a very air-sensitive, deep purple solid turning immediately colourless upon contact with air. Upon heating it begins to decompose during melting at 169 °C. It can be stored under argon atmosphere at ambient temperature for several months. **15-Ge** is very well soluble in benzene, toluene, THF, *n*-hexane and Et_2O at ambient temperature. Under strict exclusion of air, solutions of **15-Ge** in (D_6)benzene is stable for at least 72 hours without any sign of decomposition at ambient temperature.

Elemental analysis: 15-Ge ($C_{62}H_{115}Ge_2NSi_8$, 1244.49 g mol^{-1}): Calcd. /%: C 59.84, H 9.31, N 1.12; found /%: C 59.55, H 9.42, N 1.32.

^{1}H NMR (500.1 MHz, (D_6)benzene, 298 K): δ (ppm) = 0.26 (s, 36H, 2 × $C^{2,6}$C- H(Si*Me*$_3$)$_A$(SiMe$_3$)$_B$, Tbb$_X$), 0.27 (s, 18H, $C^{2,6}$C-H(Si*Me*$_3$)$_A$(SiMe$_3$)$_B$, Tbb$_Y$), 0.29 (s, 18H, $C^{2,6}$C-H(SiMe$_3$)$_A$(Si*Me*$_3$)$_B$, Tbb$_Y$), 1.35 (s, 9H, C^4-C*Me*$_3$, Tbb$_X$), 1.36 (s, 3H, C- *Me*),1.37 (s, 9H, C^4-C*Me*$_3$, Tbb$_Y$), 2.14 (s, 6H, $C^{2,6}$-*Me*, Mes), 2.15 (s, 3H, C^4-*Me*, Mes), 2.42 (s, 2H, $C^{2,6}$C-*H*(SiMe$_3$)$_A$(SiMe$_3$)$_B$, Tbb$_X$), 2.70 (s, 2H, $C^{2,6}$C-*H*(SiMe$_3$)$_A$(SiMe$_3$)$_B$, Tbb$_Y$), 6.76 (s, 2H, 2 × $C^{3,5}$-*H*, Mes), 6.96 (s, 2H, $C^{3,5}$-*H*, Tbb$_X$), 7.01 (s, 2H, $C^{3,5}$-*H*, Tbb$_Y$).

^{13}C{^{1}H} NMR (125.8 MHz, (D_6)benzene, 298 K): δ (ppm) = 1.72 and 1.85 (s, 12C, 2 × $C^{2,6}$C- H(Si*Me*$_3$)$_A$(Si*Me*$_3$)$_B$, Tbb$_X$), 1.79 and 1.99 (s, 12C, 2 × $C^{2,6}$C-H(Si*Me*$_3$)$_A$(Si*Me*$_3$)$_B$, Tbb$_Y$), 15.39 (s, 1C, C-*Me*), 20.37 (s, 1C, C-*Me*), 20.40 (s, 2C, $C^{2,6}$-*Me*, Mes), 20.86 (s, 1C, C^4-*Me*), 31.28 (s, 3C, C^4-C*Me*$_3$, Tbb$_X$), 31.34 (s, 3C, C^4-C*Me*$_3$, Tbb$_Y$), 33.58 (s, 2C, *C*^{2,6}*C*-H(SiMe$_3$)$_A$(SiMe$_3$)$_B$, Tbb$_X$), 33.92 (s, 2C, *C*^{2,6}*C*-H(SiMe$_3$)$_A$(SiMe$_3$)$_B$, Tbb$_Y$), 34.42 (s, 1C, C^4-*C*Me$_3$, Tbb$_X$), 34.42 (s, 1C, C^4-*C*Me$_3$, Tbb$_Y$), 122.86 (s, 2C, *C*^{3,5}-H, Tbb$_Y$), 122.85 (s, 2C, *C*^{3,5}-H, Tbb$_X$), 126.60 (s, 2C, *C*^{2,6}-Me, Mes.), 128.85 (s, 2C, *C*^{3,5}-H, Mes), 132.85

(s, 1C, *C*^{4}-Me, Mes), 144.57 (s, 1C, *C*^{1}, Tbb$_{X}$), 145.89 (s, 1C, *C*^{1}, Tbb$_{Y}$), 147.73 (s, 2C, *C*^{2,6}C-H(SiMe$_3$)$_A$(SiMe$_3$)$_B$, Tbb$_{Y}$), 147.81 (s, 2C, *C*^{2,6}C-H(SiMe$_3$)$_A$(SiMe$_3$)$_B$, Tbb$_{X}$), 148.03 (s, 1C, *C*-Me), 149.46 (s, 1C, *C*^{1}, Mes), 149.86 (s, 2C, *C*^{4}-CMe$_3$, Tbb$_{Y}$), 150.20 (s, 2C, *C*^{4}-CMe$_3$, Tbb$_{X}$), 155.19 (s, 1C, *C*-Me), 195.51 (s, 1C, Ge-*C*-N-Mes).

4.5.18. [Tbb$_2$Ge$_2$(N-SiMe$_3$)C$_2$Me$_2$] (16-Ge)

A colourless solution of Me$_3$Si-N$_3$ (26 mg, 0.21 mmol, 1 equiv.) in 2 mL of *n*-hexane was added to a stirred green solution of Tbb$_2$Ge$_2$C$_2$Me$_2$ (250 mg, 021 mmol, 1 equiv.) in 10 mL of *n*-pentane at ambient temperature. The colour of the reaction solution changed to a brownish hue, which was observed after stirring for 30 min. and changed to purple. An analysis of an aliquot of the reaction solution by ^{1}H NMR spectroscopy in (D$_6$)benzene revealed the complete consumption of all the starting materials and the selective formation of **16-Ge**. The reaction solution was filtered off, followed by evaporation of the solvent to dryness in a vacuum, resulting in a purple crude product. This was then crystallised from *n*-hexane (1.5 mL) at –60 °C. The resulting purple crystals were isolated by filtration at – 60 °C and dried under a fine vacuum at ambient temperature for one hour to afford **16-Ge** as an *n*-hexane solvate **16-Ge·C$_6$H$_{14}$**. Yield: 120 mg (0.092 mmol, 44 % from Tbb$_2$Ge$_2$C$_2$Me$_2$).

Properties: Compound **16-Ge** is a very air-sensitive, purple solid, turning immediately colourless upon contact with air. Upon heating, it begins to decompose during melting at 226 °C. It can be stored under an argon atmosphere at ambient temperature for several months. **16-Ge** is very well soluble in benzene, toluene, THF, *n*-hexane and Et$_2$O at ambient temperature. Under strict exclusion of air, solutions of **16-Ge** in (D$_6$)benzene is stable for at least 48 hours without any sign of decomposition at ambient temperature.

Elemental analysis: 16-Ge·C$_6$H$_{14}$ (C$_{55}$H$_{113}$Ge$_2$NSi$_9$(C$_6$H$_{14}$), 1186.48 g mol^{-1}): Calcd. /%: C 57.57, H 10.06, N 1.10; found /%: C 55.11, H 9.68, N 1.25.

^{1}H NMR (500.1 MHz, (D$_6$)benzene, 298 K): δ (ppm) = 0.25 (br s, $\Delta\nu_{1/2}$ = 56 Hz, 72H, 2 × C^{2,6}C-H(Si*Me*$_3$)$_A$(SiMe$_3$)$_B$, 2 × Tbb), 0.46 (s, 9H, Si*Me*$_3$), 1.32 (s, 18H, C^{4}-C*Me*$_3$, 2 × Tbb), 2.53 (s, 6H, C-*Me*), 3.52 (br s, $\Delta\nu_{1/2}$ = 123 Hz , 4H, 2 × C^{2,6}C-*H*(SiMe$_3$)$_A$(SiMe$_3$)$_B$, 2 × Tbb), 6.89 (br s, $\Delta\nu_{1/2}$ = 17 Hz , 4H, 2 × C^{3,5}-*H*, 2 × Tbb).

^{13}C{^{1}H} NMR (125.8 MHz, (D$_6$)benzene, 298 K): δ (ppm) = 2.44 (s, 24C, 2 × C^{2,6}C- H(Si*Me*$_3$)$_A$(Si*Me*$_3$)$_B$, 2 × Tbb), 7.78 (s, 3C, Si*Me*$_3$), 20.56 (s, 2C, 2 × C-*Me*), 31.27 (s, 6C, 2 × C^{4}-C*Me*$_3$, 2 × Tbb), 31.91 (s, 4C, *C*^{2,6}*C*- H(SiMe$_3$)$_A$(SiMe$_3$)$_B$, 2 × Tbb), 34.39 (s, 2C, 2 × C^{4}-*C*Me$_3$, 2 × Tbb), 122.97 (s, 4C, 2 × *C*^{3,5}-H, 2 × Tbb), 143.48 (s, 2C, 2 ×

C^{1}, 2 × Tbb), 150.70 (s, 4C, 2 × *C*^{2,6}-H, 2 × Tbb), 150.79 (s, 2C, 2 × *C*^{4}, 2 × Tbb), 166.86 (s, 2C, 2 × *C*-Me, 2 × Tbb).

4.5.19. [Tbb$_2$Ge$_2$(N$_2$C(*p*-tol)$_2$)C$_2$Me$_2$] (**17-Ge**)

A purple solution of (*p*-tol)$_2$CN$_2$ (61 mg, 0.272 mmol, 1 equiv.) in 5 mL of C_6H_6 was added to a stirred green solution of $Tbb_2Ge_2C_2Me_2$ (300 mg, 0.272 mmol, 1 equiv.) in 10 mL of *n*-hexane at ambient temperature. The colour of the the reaction solution immediately changed to purple, then to yellow-brown. An analysis of an aliquot of the reaction solution by ^{1}H NMR spectroscopy in (D_6)benzene revealed the complete consumption of all the starting materials and the selective formation of **17-Ge**. The reaction solution was filtered off, followed by evaporation of the solvent to dryness in a vacuum, resulting in a light brown crude product. This product was then crystallised from *n*-pentane (5 mL) at –30 °C. The resulting yellow crystals were isolated by filtration at –30 °C and dried under a fine vacuum at ambient temperature for 1 hour to afford **17-Ge** as an *n*-hexane hemisolvate, **17-Ge**·(**C$_6$H$_{14}$**)$_{0.5}$. Yield: 235 mg (0.177 mmol, 65 % from $Tbb_2Ge_2C_2Me_2$).

Properties: Compound **17-Ge** is a very air-sensitive, purple solid turning immediately colourless upon contact with air. Upon heating, it begins to decompose during melting at 273 °C. It can be stored under an argon atmosphere at ambient temperature for several months. **17-Ge** is very well soluble in DCM, fluorobenzene and moderately soluble in *n*-pentane, *n*-hexane, benzene and Et_2O at ambient temperature. Under strict exclusion of air, solutions of **17-Ge** in (D_2)DCM is stable for at least 48 hours without any sign of decomposition at ambient temperature.

Elemental analysis: 17-Ge·(C$_6$H$_{14}$)$_{0.5}$ ($C_{67}H_{118}Ge_2N_2Si_8(C_6H_{14})_{0.5}$, 1321.57 g mol^{-1}): Calcd. /%: C 62.46, H 9.19, N 1.99; found /%: C 62.21, H 9.21, N 2.14.

^{1}H NMR (500.1 MHz, (D_2)DCM, 298 K): δ (ppm) = −0.10 (s, 18H, C^{2,6}C-H(Si*Me*$_3$)$_A$(SiMe$_3$)$_B$, Tbb$_X$), −0.04 (s, 18H, C^{2,6}C-H(Si*Me*$_3$)$_A$(SiMe$_3$)$_B$, Tbb$_Y$), −0.03 (s, 18H, C^{2,6}C-H(SiMe$_3$)$_A$(Si*Me*$_3$)$_B$, Tbb$_X$), 0.04 (s, 18H, C^{2,6}C-H(SiMe$_3$)$_A$(Si*Me*$_3$)$_B$, Tbb$_Y$), 1.23 (s, 9H, C^{4}-C*Me*$_3$, Tbb$_X$), 1.26 (s, 9H, C^{4}-C*Me*$_3$, Tbb$_Y$), 1.79 (s, 3H, C-*Me*), 1.89 (s, 2H, C^{2,6}C-*H*(SiMe$_3$)$_A$(SiMe$_3$)$_B$, Tbb$_Y$), 2.17 (s, 3H, C-*Me*), 2.32 (s, 3H, C^{4}-*Me*, *p*-tol (non act.), 2.32 (s, 3H, C^{4}-*Me*, *p*-tol (act.), 2.80 (s, 2H, C^{2,6}C-*H*(SiMe$_3$)$_A$(SiMe$_3$)$_B$, Tbb$_X$), 4.68 (s, 1H, N- *H*), 6.64 (s, 2H, C^{3,5}-*H*, Tbb$_X$), 6.68 (s, 2H, C^{3,5}-*H*, Tbb$_Y$), 7.03 (d, ^{3}J(H,H)= 8.0 Hz, 2H, C^{3,5}-*H*, *p*-tol (non act.)), 7.13 (dd, ^{3}J(H,H) = 8.0 Hz, 1H, C^{5}-*H*, (act.)), 7.20 (d, ^{3}J(H,H) = 8.0 Hz, 1H, C^{6}-*H*, (act.)), 7.31 (s, 1H, C^{3}-*H*, (act.)), 7.57 (d, ^{3}J(H,H)= 8.3 Hz, 2H, C^{2,6}-*H*, (non act).).

$^{13}C\{^1H\}$ NMR (125.8 MHz, (D_2)DCM, 298 K): δ (ppm) = 1.26 and 1.33 (s, 12C, $C^{2,6}$C- H(Si*Me*$_3$)$_A$(Si*Me*$_3$)$_B$, Tbb$_Y$), 1.75 (s, 12C, $C^{2,6}$C-H(Si*Me*$_3$)$_A$(Si*Me*$_3$)$_B$, Tbb$_X$), 18.79 (s, 1C, C-*Me*), 19.98 (s, 1C, C-*Me*), 21.38 (s, 1C, C^4-*Me*, *p*-tol, (non act.)), 21.87 (s, 1C, C^4-*Me*, *p*-tol, (act.)), 28.14 (s, 2C, $C^{2,6}$*C*-H(SiMe$_3$)$_A$(SiMe$_3$)$_B$, Tbb$_X$), 29.99 (s, 2C, $C^{2,6}$*C*- H(SiMe$_3$)$_A$(SiMe$_3$)$_B$, Tbb$_Y$), 31.17(s, 3C, C^4-C*Me*$_3$, Tbb$_X$), 31.22(s, 3C, C^4-C*Me*$_3$, Tbb$_Y$) , 34.40 (s, 2C, C^4-*C*Me$_3$, Tbb$_X$), 34.50 (s, 2C, C^4-*C*Me$_3$, Tbb$_Y$), 123.06 (s, 2C, *C*^{3,5}- H, Tbb$_Y$), 123.93 (s, 2C, *C*^{3,5}-H, Tbb$_X$), 128.07 (s, 1C, *C*^{6}-H, *p*-tol, (act.)),128.17 (s, 1C, *C*^{3,5}-H, *p*-tol, (non act.)), 128.64 (s, 2C, *C*^{2,6}C-H(SiMe$_3$)$_A$(SiMe$_3$)$_B$, Tbb$_X$), 129.92 (s, 1C, *C*^{5}-H, *p*-tol, (act.)), 130.10 (s, 2C, *C*^{2,6}-H, *p*-tol, (non act)), 130.81 (s, 2C, *C*^{2,6}C- H(SiMe$_3$)$_A$(SiMe$_3$)$_B$, Tbb$_Y$), 132.61 (s, 1C, *C*^{1}, *p*-tol, act.), 134.28 (s, 1C, *C*^{3}-H), 136.55 (s, 1C, *C*^{1}, *p*-tol, (non act.)), 138.45 (s, 1C, *C*^{4}-Me, *p*-tol, (non act.)),139.97 (s, 1C, *C*^{2}-H, *p*-tol, (act.)), 140.03 (s, 1C, *C*^{4}-Me, *p*-tol, (act.)), 149.10 (s, 1C, *C*-Me), 149.87 (s, 1C, *C*^{4}-CMe$_3$, Tbb$_X$), 150.52 (s, 1C, *C*^{4}-CMe$_3$, Tbb$_Y$), 150.73 (s, 1C, *C*-Me), 150.90 (s, 1C, *C*^{1}, Tbb$_X$), 151.18(s, 1C, *C*^{1}, Tbb$_Y$), 167.22 (s, 1C, (*p*-tol)$_2$-*C*N).

4.5.20. [Tbb$_2$Ge$_2$(SiBr$_2$)C$_4$Me$_4$] (18-Si)

A yellow solution of $SiBr_2$(SIDipp) (201 mg, 0.34 mmol, 1 equiv.) in 10 ml of benzene was added slowly to a stirred orange solution of $Tbb_2Ge_2C_4Me_4$ (400 mg, 0.34 mmol, 1 equiv.) in 10 ml of benzene at ambient temperature. No instant colour change was observed at ambient temperature. The reaction solution was heated at 80 °C overnight to form a yellow suspension. Analysis of an aliquot of the reaction solution by ^{1}H NMR spectroscopy in (D_6)benzene revealed the complete consumption of all the starting materials and the selective formation of **18-Si,** along with free SIDipp. The reaction solution was worked up by evaporating the solvent to dryness in a vacuum, followed by adding three times 1:5 of benzene and *n*-hexane (approximately 6 mL). Then, filtration was performed, resulting in a colourless crude product, which was crystallised from *n*-pentane (4 mL) at –30 °C. The resulting colourless crystals were isolated by filtration at –30 °C and dried under a fine vacuum at ambient temperature for one hour to afford **18-Si** as *n*-pentane hemi-solvate **18-Si**·(**C$_5$H$_{12}$)$_{0.5}$**. Yield: 300 mg (0.220 mmol, 64 % from $Tbb_2Ge_2C_4Me_4$).

Properties: Compound **18-Si** is an air-sensitive colourless solid. Upon heating, it begins to decompose during melting at 335 °C. It can be stored under argon atmosphere at ambient temperature for several months. **18-Si** is very well soluble in THF and moderately soluble in *n*-pentane, *n*-hexane, benzene at ambient temperature. Under strict exclusion of air, solutions of **18-Si** in (D_8)thf is stable for at least 48 hours without any sign of decomposition at ambient temperature.

Elemental analysis: 18-Si·(C_5H_{12})$_{0.5}$ ($C_{56}H_{110}Ge_2Br_2Si_9(C_5H_{12})_{0.5}$, g mol^{-1}): Calcd. /%: C 51.01, H 8.49; found /%: C 50.64, H 8.31.

^{1}H NMR (500.1 MHz, (D_8)thf, 298 K): δ (ppm) = 0.13 (s, 36H, 2 × C^{2}C-H(Si*Me*$_3$)$_2$, 2 × Tbb), 0.17 (s, 36H, 2 × C^{6}C-H(Si*Me*$_3$)$_2$, 2 × Tbb), 1.35 (s, 18H, 2 × C^4-C*Me*$_3$, 2 × Tbb), 1.87 (s, 12H, 4 × C-*Me*), 2.02 (s, 2H, 2 × C^{2}C-*H*(SiMe$_3$)$_2$, 2 × Tbb), 2.24 (s, 2H, 2 × C^{6}C-*H*(SiMe$_3$)$_2$, 2 × Tbb), 6.95 (d, ^{4}*J*(H,H) = 1.9 Hz, 2H, 2 × C^3-*H*, 2 × Tbb), 7.03 (d, ^{4}*J* (H, H) = 1.9 Hz, 2H, 2 × C^5-*H*, 2 × Tbb).

^{13}C{^{1}H} NMR (125.8 MHz, (D_8)thf, 298 K): δ (ppm) = 1.50 (s, 12C, 2 × C^{2}C-H(Si*Me*$_3$)$_2$, 2 × Tbb), 2.68 (s, 12C, 2 × C^{6}C-H(Si*Me*$_3$)$_2$, 2 × Tbb), 21,97 (s, 4C, 4 × C-*Me*), 29.95 (s, 2C, 2 × C^2*C*-H(SiMe$_3$)$_2$, 2 × Tbb), 31.36 (s, 6C, 2 × C^4-C*Me*$_3$, 2 × Tbb), 33.85 (s, 2C, 2 × C^6*C*-H(SiMe$_3$)$_2$, 2 × Tbb), 34.95 (s, 2C, 2 × C^4-*CMe*$_3$, 2 × Tbb), 123.08 (s, 2C, 2 × *C*^{5}- H, 2 × Tbb), 123.93 (s, 2C, 2 × *C*^{3}-H, 2 × Tbb), 129.34 (s, 2C, 2 × *C*^{1}, 2 × Tbb), 150.93 (s, 2C, 2 × *C*^{6}-CH(SiMe$_3$)$_2$, 2 × Tbb), 150.93 (s, 4C, 4 × *C*-Me), 151.36 (s, 2C, *C*^{4}-CMe$_3$, 2 × Tbb), 151.64 (s, 2C, 2 × *C*^{2}-CH(SiMe$_3$)$_2$, 2 × Tbb).

^{29}Si{^{1}H} NMR (99.33 MHz, (D_8)thf, 298 K): δ (ppm) = 2.57(s, 8Si, 2 × C^{2,6}C-H(*Si*Me$_3$)$_2$, 2 × Tbb), 31.81(s, 1Si, *Si*Br$_2$Ge$_2$).

4.5.21. [Tbb$_2$Ge$_2$(GeBr$_2$)C$_4$Me$_4$] (18-Ge)

A colourless solution of GeBr$_2$(1,4-dioxane) (84 mg, 0.26 mmol, 1 equiv.) in 4 ml of benzene was added slowly to a stirred orange solution of Tbb$_2$Ge$_2$C$_4$Me$_4$ (300 mg, 0.26 mmol, 1 equiv.) in 10 ml of benzene at ambient temperature upon which no instant colour change was observed. The reaction solution was stirred at ambient temperature for 2 hours to form a yellow suspension. Analysis of an aliquot of the reaction solution by ^{1}H NMR spectroscopy in (D_6)benzene was performed after 2 hours, revealing a complete consumption of all the starting materials and the selective formation of **18-Ge**. The reaction solution was worked up by evaporating the solvent to dryness in a vacuum, followed by the addition of 6 mL of *n*-hexane and then evaporating the solvent to dryness, resulting in a light-yellow crude product. This product was crystallised from THF (3 mL) at –30 °C. The resulting light-yellow crystals were isolated by filtration at –30 °C and dried under a fine vacuum at ambient temperature for 2 hours to afford **18-Ge** as the THF hemisolvate **18- Ge·(C_4H_8O)$_{2.5}$**. Yield: 300 mg (0.216 mmol, 83 % from Tbb$_2$Ge$_2$C$_4$Me$_4$).

Properties: Compound **18-Ge** is an air-sensitive light-yellow solid. Upon heating, it begins to decompose during melting at 314 °C. It can be stored under an argon atmosphere at ambient temperature for several months. **18-Ge** is very well soluble in

THF and moderately soluble in *n*-pentane, *n*-hexane, benzene, toluene and Et_2O at ambient temperature. Under strict exclusion of air, solutions of **18-Ge** in (D_8)thf is stable for at least 7 days without any sign of decomposition at ambient temperature.

Elemental analysis: 18-Ge·(C_4H_8O)$_{2.5}$ ($C_{56}H_{110}Ge_3Br_2Si_8(C_4H_8O)_{2.5}$, 1457.94 g mol^{-1}): Calcd. /%: C 50.62, H 8.36; found /%: C 50.49, H 8.34.

^{1}H NMR (500.1 MHz, (D_8)thf, 298 K): δ (ppm) = 0.14 (s, 36H, 2 × C^{2}C-H(Si*Me*$_3$)$_2$, 2 × Tbb), 0.19 (s, 36H, 2 × C^{6}C-H(Si*Me*$_3$)$_2$, 2 × Tbb), 1.36 (s, 18H, 2 × C^4-C*Me*$_3$, 2 × Tbb), 1.91 (s, 12H, 4 × C-*Me*), 2.02 (s, 2H, 2 × C^{2}C-*H*(SiMe$_3$)$_2$, 2 × Tbb), 2.38 (s, 2H, 2 × C^{6}C- *H*(SiMe$_3$)$_2$, 2 × Tbb), 6.98 (d, ^{4}*J*(H,H) = 2 Hz, 2H, 2 × C^3-*H*, 2 × Tbb), 7.06 (d, ^{4}*J*(H,H) = 2 Hz, 2H, 2 × C^5-*H*, 2 × Tbb).

^{13}C{^{1}H} NMR (125.8 MHz, (D_8)thf, 298 K): δ (ppm) = 1.56 (s, 12C, 2 × C^{2}C-H(Si*Me*$_3$)$_2$, 2 × Tbb), 2.43 (s, 12C, 2 × C^{6}C-H(Si*Me*$_3$)$_2$, 2 × Tbb), 22.30 (s, 4C, 4 × C-*Me*), 30.65 (s, 2C, 2 × C^2*C*-H(SiMe$_3$)$_2$, 2 × Tbb), 31.32 (s, 6C, 2 × C^4-C*Me*$_3$, 2 × Tbb), 34.12 (s, 2C, 2 × C^6*C*-H(SiMe$_3$)$_2$, 2 × Tbb), 35.00 (s, 2C, 2 × C^4-*C*Me$_3$, 2 × Tbb), 123.43 (s, 2C, 2 × *C*^{5}- H, 2 × Tbb), 123.90 (s, 2C, 2 × *C*^{3}-H, 2 × Tbb), 128.29 (s, 2C, 2 × *C*^{1}, 2 × Tbb), 151.19 (s, 2C, 2 × *C*^{2}-CH(SiMe$_3$)$_2$, 2 × Tbb), 151.43 (s, 2C, 2 × *C*^{6}-CH(SiMe$_3$)$_2$, 2 × Tbb), 151.87 (s, 2C, *C*^{4}-CMe$_3$, 2 × Tbb), 153.61 (s, 4C, 4 × *C*-Me).

4.5.22. [Tbb$_2$Ge$_2$(SnCl$_2$)C$_4$Me$_4$] (18-Sn)

A colourless solution of $SnCl_2$ (33 mg, 0.17 mmol, 1 equiv.) in 10 ml of Et_2O was added slowly to a stirred orange solution of $Tbb_2Ge_2C_4Me_4$ (200 mg, 0.17 mmol, 1 equiv.) in 15 ml of Et_2O at ambient temperature. The colour of the reaction solution changed to yellow-orange, and then the reaction mixture was maintained for 30 min. After this, the colour changed to a brown suspension. Analysis of an aliquot of the reaction solution by ^{1}H NMR spectroscopy in (D_6)benzene revealed the complete consumption of all the starting materials and the selective formation of **18-Sn**. The reaction solution was filtered to obtain a red-brown filtrate, followed by evaporation of the solvent to dryness under vacuum, resulting in a light-brown crude product. This product was then crystallised from Et_2O (4 mL) at −30 °C for 3 days. The resulting colourless crystals were isolated by filtration at –30°C and dried under a fine vacuum at ambient temperature for 2 hours to afford **18-Sn.** Yield: 123 mg (0.094 mmol, 52 % from $Tbb_2Ge_2C_4Me_4$).

Properties: Compound **18-Sn** is an air-sensitive colourless solid. Upon heating, it begins to decompose during melting at 203 °C. It can be stored under an argon atmosphere at ambient temperature for several months. **18-Sn** is very well soluble in THF, benzene, Et_2O and moderately soluble in aliphatic solvents like *n*-pentane and

n-hexane at ambient temperature. Under strict exclusion of air, solutions of **18-Sn** in (D_6)benzene is stable for at least 72 hours without any sign of decomposition at ambient temperature.

Elemental analysis: 18-Sn ($C_{56}H_{110}Ge_2SnCl_2Si_8$, 1294.95 g mol^{-1}): Calcd. /%: C 50.08, H 8.26; found /%: C 49.16, H 8.24.

^{1}H NMR (500.1 MHz, (D_6)benzene, 298 K): δ (ppm) = 0.16 (s, 36H, 2 × C^{2}C-H(Si*Me*$_3$)$_2$, 2 × Tbb), 0.37 (s, 36H, 2 × C^{6}C-H(Si*Me*$_3$)$_2$, 2 × Tbb), 1.33 (s, 18H, 2 × C^4-C*Me*$_3$, 2 × Tbb), 1.96 (s, 12H, 4 × C-*Me*), 2.15 (s, 2H, 2 × C^{2}C-*H*(SiMe$_3$)$_2$, 2 × Tbb), 3.10 (s, 2H, 2 × C^{6}C-*H*(SiMe$_3$)$_2$, 2 × Tbb), 7.05 (d, ^4J(H,H) = 1.9 Hz, 2H, 2 × C^3-*H*, 2 × Tbb), 7.14 (d, ^4J (H, H) = 1.9 Hz, 2H, 2 × C^5-*H*, 2 × Tbb).

^{13}C{^{1}H} NMR (125.8 MHz, (D_6)benzene, 298 K): δ (ppm) = 1.50 (s, 12C, 2 × C^{2}C- H(Si*Me*$_3$)$_2$, 2 × Tbb), 2.04 (s, 12C, 2 × C^{6}C-H(Si*Me*$_3$)$_2$, 2 × Tbb), 22,13 (s, 4C, 4 × C-*Me*), 30.97 (s, 2C, 2 × C^2*C*-H(SiMe$_3$)$_2$, 2 × Tbb), 31.17 (s, 6C, 2 × C^4-C*Me*$_3$, 2 × Tbb), 34.54 (s, 2C, 2 × C^6*C*-H(SiMe$_3$)$_2$, 2 × Tbb), 34.87 (s, 2C, 2 × C^4-*CMe*$_3$, 2 × Tbb), 123.28 (s, 4C, 2 × *C*^{3,5}-H, 2 × Tbb), 128.29 (s, 2C, 2 × *C*^{1}, 2 × Tbb), 150.43 (s, 2C, 2 × *C*^{6}- CH(SiMe$_3$)$_2$, 2 × Tbb), 151.61 (s, 2C, *C*^{2}-CH(SiMe$_3$)$_2$, 2 × Tbb), 151.65 (s, 2C, *C*^{4}-CMe$_3$, 2 × Tbb), 154.15 (s, 4C, 4 × C-Me).

^{119}Sn{^{1}H} NMR (186.50 MHz, (D_6)benzene, 298 K): δ (ppm) = 57.03 (s, Sn, *Sn*Cl$_2$Ge$_2$).

4.5.23. [Tbb$_2$Ge$_3$C$_2$Me$_2$] (19-Ge)

14-Ge (350 mg, 0.26 mmol, 1 equiv.) was dissolved in 15 mL of benzene, and KC_8 (75 mg, 0.55 mmol, 2.1 equiv.) was added in one portion at ambient temperature. The reaction mixture was sonicated for 5 hours and then stirred for 16 hours at room temperature. During this period, the colour of the reaction solution changed to green. A ^{1}H spectrum of an aliquot of the reaction solution in (D_6)benzene revealed the complete and selective conversion from **14-Ge** to **19-Ge**. The green solution was separated from the black insoluble part by filtration, and all volatiles were removed to dryness in a vacuum, resulting in a green crude product, which was crystallized from *n*-hexane (2 mL) at −30 °C. The resulting green crystals were isolated by filtration at −30°C and dried under a fine vacuum at ambient temperature for 2 hours to afford **19-Ge.** Yield: 200 mg (0.17 mmol, 65 % from **14-Ge**).

Properties: Compound **19-Ge** is a very air-sensitive, green solid that turns immediately colourless upon contact with air. Upon heating, it begins to decompose during melting at 267 °C. It can be stored under an argon atmosphere at ambient temperature for several months. **19-Ge** is very well soluble in benzene, toluene, THF

and partially soluble in *n*-hexane and Et_2O at ambient temperature. Under strict exclusion of air, solutions of **19-Ge** in (D_6)benzene is stable for at least 7 days without any sign of decomposition at ambient temperature.

Elemental analysis: 19-Ge ($C_{52}H_{104}Ge_3Si_8$, 1171.90 g mol^{-1}): Calcd. /%: C 53.29, H 8.94; found /%: C 53.11, H 8.72.

^{1}H NMR (500.1 MHz, (D_6)benzene, 298 K): δ (ppm) = 0.2 (s, 36H, 2 × $C^{2,6}$C- H($Si\mathit{Me}_3$)$_A$($SiMe_3$)$_B$, 2 × Tbb), 0.29 (s, 36H, 2 × $C^{2,6}$C-H($SiMe_3$)$_A$($Si\mathit{Me}_3$)$_B$, 2 × Tbb), 1.34 (s, 18H, 2 × C^4-$C\mathit{Me}_3$, 2 × Tbb), 2.01 (s, 6H, 2 × C-*Me*), 2.11 (s, 4H, 2 × $C^{2,6}$C- *H*($SiMe_3$)$_A$($SiMe_3$)$_B$, 2 × Tbb), 6.93 (s, 4H, 2 × $C^{3,5}$-*H*, 2 × Tbb).

^{13}C{^{1}H} NMR (125.8 MHz, (D_6)benzene, 298 K): δ (ppm) = 1.25 (s, 12C, 2 × $C^{2,6}$C- H($Si\mathit{Me}_3$)$_A$($SiMe_3$)$_B$, 2 × Tbb), 1.59 (s, 12C, 2 × $C^{2,6}$C-H($SiMe_3$)$_A$($Si\mathit{Me}_3$)$_B$, 2 × Tbb), 18.71 (s, 2C, 2 × C-*Me*), 31.33 (s, 6C, 2 × C^4-$C\mathit{Me}_3$, 2 × Tbb), 32.81 (s, 4C, 2 × $\mathit{C}^{2,6}$*C*- H($SiMe_3$)$_A$($SiMe_3$)$_B$, 2 × Tbb), 34.50 (s, 2C, 2 × C^4-*C*Me_3, 2 × Tbb), 121.99 (s, 4C, 2 × $\mathit{C}^{3,5}$-H, 2 × Tbb), 146.29 (s, 2C, 2 × C^1, 2 × Tbb), 147.12 (s, 4C, 2 × $\mathit{C}^{2,6}$C- H($SiMe_3$)$_A$ ($SiMe_3$)$_B$, 2 × Tbb), 151.84 (s, 2C, 2 × C^4-CMe_3, 2 × Tbb), 159.93 (s, 2C, 2 × *C*-Me).

4.5.24. [Tbb$_2$Ge$_2$SnC$_2$Me$_2$] (19-Sn)

14-Sn (200 mg, 0.15 mmol, 1 equiv.) was dissolved in 15 mL of benzene, and KC_8 (44 mg, 0.32 mmol, 2.1 equiv.) was added in one portion at ambient temperature. The reaction mixture was stirred for 5 hours at ambient temperature. During this period, the colour of the reaction solution changed to red. A ^{1}H spectrum of an aliquot of the reaction solution in (D_6)benzene revealed the complete and selective conversion of **14-Sn** to **19-Sn**. The red solution was separated from the black insoluble part by filtration, and all volatiles were removed to dryness in a vacuum, resulting in a red crude product, which was crystallized from *n*-pentane (2 mL) at −30 °C. The resulting red crystals were isolated by filtration at − 30°C and dried under a fine vacuum at ambient temperature for one hour to afford **19-Sn.** Yield: 106 mg (0.087 mmol, 56 % from **14- Sn**).

Properties: Compound **19-Sn** is a very air-sensitive, red solid, turning immediately turns colourless upon contact with air. Upon heating, it begins to decompose during melting at 264 °C. It can be stored under an argon atmosphere at ambient temperature for several months. **19-Sn** is very well soluble in benzene, toluene, THF and partially soluble in *n*-hexane and Et_2O at ambient temperature. Under strict exclusion of air, solutions of **19-Sn** in (D_6)benzene is stable for at least 48 hours without any sign of decomposition at ambient temperature.

Elemental analysis: 19-Sn ($C_{52}H_{104}Ge_2SnSi_8$, 1217.99 g mol^{-1}): Calcd. /%: C 51.27, H 8.60; found /%: C 50.96, H 8.46.

^{1}H NMR (500.1 MHz, (D_6)benzene, 298 K): δ (ppm) = 0.23 (s, 36H, 2 × $C^{2,6}$C- H(Si*Me*$_3$)$_A$(SiMe$_3$)$_B$, 2 × Tbb), 0.28 (s, 36H, 2 × $C^{2,6}$C-H(SiMe$_3$)$_A$(Si*Me*$_3$)$_B$, 2 × Tbb), 1.33 (s, 18H, 2 × C^4-C*Me*$_3$, 2 × Tbb), 2.01 (s, 6H, 2 × C-*Me*), 2.18 (s, 4H, 2 × $C^{2,6}$C- *H*(SiMe$_3$)$_A$(SiMe$_3$)$_B$, 2 × Tbb), 6.92 (s, 4H, 2 × $C^{3,5}$-*H*, 2 × Tbb).

^{13}C{^{1}H} NMR (125.8 MHz, (D_6)benzene, 298 K): δ (ppm) = 1.48 (s, 12C, 2 × $C^{2,6}$C- H(Si*Me*$_3$)$_A$(SiMe$_3$)$_B$, 2 × Tbb), 1.71 (s, 12C, 2 × $C^{2,6}$C-H(SiMe$_3$)$_A$(Si*Me*$_3$)$_B$, 2 × Tbb), 18.87 (s, 2C, 2 × C-*Me*), 31.32 (s, 6C, 2 × C^4-C*Me*$_3$, 2 × Tbb), 32.01 (s, 4C, 2 × *C*^{2,6}*C*- H(SiMe$_3$)$_A$(SiMe$_3$)$_B$, 2 × Tbb), 34.47 (s, 2C, 2 × C^4-*C*Me$_3$, 2 × Tbb), 122.53 (s, 4C, 2 × *C*^{3,5}-H, 2 × Tbb), 147.02 (s, 4C, 2 × *C*^{2,6}C-H(SiMe$_3$)$_A$(SiMe$_3$)$_B$, 2 × Tbb), 148.92 (s, 2C, 2 × *C*^{1}, 2 × Tbb),, 151.47 (s, 2C, 2 × *C*^{4}-CMe$_3$, 2 × Tbb), 162.22 (s, 2C, 2 × *C*-Me).

^{119}Sn{^{1}H} NMR (186.50 MHz, (D_6)benzene, 298 K): δ (ppm) = −418.86 (s, Sn, *Sn*Ge$_2$).

4.5.25. [Tbb$_2$Ge$_4$Br$_2$C$_2$Me$_2$] (20-Ge)

A colourless solution of $GeBr_2$(1,4-dioxane) (55 mg, 0.17 mmol, 1 equiv.) in 4 mL of benzene was added slowly to a stirred green solution of **19-Ge** (200 mg, 0.17 mmol, 1 equiv.) in 10 mL of benzene at ambient temperature. The colour of the reaction solution immediately changed to orange. The reaction solution was stirred at ambient temperature for 30 min., and an aliquot of the reaction solution was analysed by ^{1}H NMR spectroscopy in (D_6)benzene after 30 min., revealing the complete consumption of all the starting materials and the selective formation of **20-Ge**. The reaction solution was filtered off, followed by evaporation of the solvent to dryness in a vacuum. Then, 6 mL of *n*-hexane was added, and the solvent was evaporated to dryness, resulting in a light orange crude product. This product was crystallised from *n*-hexane (2 mL) at –30 °C. The resulting orange crystals were isolated by filtration at – 30 °C and dried under a fine vacuum at ambient temperature for 2 hours to afford **20-Ge**. Yield: 140 mg (0.10 mmol, 59 % from **19-Ge**).

Properties: Compound **20-Ge** is a very air-sensitive, orange solid that turns immediately colourless upon contact with air. Upon heating, it begins to decompose during melting at 210 °C. It can be stored under an argon atmosphere at ambient temperature for several months. **20-Ge** is very well soluble in benzene, toluene, THF and partially soluble in *n*-hexane and Et_2O at ambient temperature. Under strict exclusion of air, solutions of **20-Ge** in (D_6)benzene is stable for at least 48 hours without any sign of decomposition at ambient temperature.

Elemental analysis: 20-Ge ($C_{52}H_{104}Ge_4Br_2Si_8$, 1404.31 g mol^{-1}): Calcd. /%: C 46.00, H 7.83; found /%: C 45.35, H 7.51.

^{1}H NMR (500.1 MHz, (D_6)benzene, 298 K): δ (ppm) = 0.24 (s, 36H, 2 × $C^{2,6}$C- H(Si*Me*$_3$)$_A$(SiMe$_3$)$_B$, 2 × Tbb), 0.36 (s, 36H, 2 × $C^{2,6}$C-H(SiMe$_3$)$_A$(Si*Me*$_3$)$_B$, 2 × Tbb), 1.31 (s, 18H, 2 × C^4-C*Me*$_3$, 2 × Tbb), 1.68 (s, 6H, 2 × C-*Me*), 3.18 (s, 4H, 2 × $C^{2,6}$C- *H*(SiMe$_3$)$_A$(SiMe$_3$)$_B$, 2 × Tbb), 7.04 (s, 4H, 2 × $C^{3,5}$-*H*, 2 × Tbb).

^{13}C{^{1}H} NMR (125.8 MHz, (D_6)benzene, 298 K): δ (ppm) = 1.22 (s, 12C, 2 × $C^{2,6}$C- H(Si*Me*$_3$)$_A$(SiMe$_3$)$_B$, 2 × Tbb),1.94 (s, 12C, 2 × $C^{2,6}$C-H(SiMe$_3$)$_A$(Si*Me*$_3$)$_B$, 2 × Tbb), 23.02 (s, 2C, 2 × C-*Me*), 31.16 (s, 6C, 2 × C^4-C*Me*$_3$, 2 × Tbb), 34.40 (s, 2C, C^4-*C*Me$_3$, 2 × Tbb), 35.25 (s, 4C, 2 × $C^{2,6}$*C*-H(SiMe$_3$)$_A$(SiMe$_3$)$_B$, 2 × Tbb), 122.28 (s, 4C, 2 × *C*^{3,5}- H, 2 × Tbb), 136.44 (s, 2C, 2 × C^1, 2 × Tbb), 149.64 (s, 4C, 2 × *C*^{2,6}-CH(SiMe$_3$)$_A$(SiMe$_3$)$_B$, 2 × Tbb), 151.93 (s, 2C, 2 × *C*^{4}-CMe$_3$, 2 × Tbb), 163.80 (s, 2C, 2 × *C*-Me).

4.5.26. [Tbb$_2$Ge$_3$(C)(IMe$_4$)C$_2$Me$_2$] (21-Ge)

A light-yellow solution of IMe$_4$CN$_2$ (28 mg, 0.17 mmol, 1 equiv.) in 4 ml of benzene was added slowly to a stirred green solution of **19-Ge** (200 mg, 0.17 mmol, 1 equiv.) in 10 mL of benzene at ambient temperature. The colour of the reaction solution immediately changed to yellow-brown. The reaction solution was stirred at ambient temperature for 30 min., and analysis of an aliquot of the reaction solution by ^{1}H NMR spectroscopy in (D_6)benzene revealed the complete consumption of all the starting materials and the selective formation of **21-Ge**. The reaction solution was filtered off, followed by evaporation of the solvent to dryness in a vacuum. Then, 5 mL of *n*-pentane was added, and the solvent was evaporated to dryness, resulting in a brown crude product. This product was then crystallised from *n*-pentane (2 mL) at − 30 °C. The resulting brown crystals were isolated by filtration at –30 °C and dried under a fine vacuum at ambient temperature for 2 hours to afford **21-Ge**. Yield: 157 mg (0.120 mmol, 70 % from **19-Ge**).

Properties: Compound **21-Ge** is a very air-sensitive, brown solid, turning immediately colourless upon contact with air. Upon heating, it begins to decompose during melting at 169 °C. It can be stored under an argon atmosphere at ambient temperature for several months. **21-Ge** is very well soluble in benzene, toluene, THF, *n*-hexane and Et_2O at ambient temperature. Under strict exclusion of air, solutions of **21-Ge** in (D_6)benzene is stable for at least 4 days without any sign of decomposition at ambient temperature.

Elemental analysis: 21-Ge ($C_{60}H_{116}Ge_3N_2Si_8$, 1308.09 g mol^{-1}): Calcd. /%: C 55.09, H 8.94, N 2.14; found /%: C 54.73, H 8.66, N 3.64.

^{1}H NMR (500.1 MHz, (D_6)benzene, 298 K): δ (ppm) = 0.10 (br s, $\Delta\nu_{1/2}$ = 11.8 Hz, 36H, $C^{2,6}$-CH($SiMe_3$)$_A$($SiMe_3$)$_B$, 2 × Tbb), 0.34 (s, 36H, $C^{2,6}$-CH($SiMe_3$)$_A$($SiMe_3$)$_B$, 2 × Tbb), 1.38 (s, 18H, C^4-C(CH_3)$_3$, 2 × Tbb), 1.61 (s, 6H, $C^{4,5}$-Me, IMe_4), 1.97 (s, 6H, $C^{4,5}$-Me, Central Ring), 3.65 (s, 6H, $N^{1,3}$-Me, IMe_4), 6.96 (s, 4H, $C^{3,5}$-H, 2 × Tbb), The signal corresponds to $C^{2,6}$-CH($SiMe_3$)$_A$($SiMe_3$)$_B$ could not be found due to dynamics in solution.

^{13}C{^{1}H} NMR (125.8 MHz, (D_6)benzene, 298 K): *δ* (ppm) = 1.3 (br s, $\Delta\nu_{1/2}$ = 6.7 Hz, 12C, $C^{2,6}$-CH(Si*Me*$_3$)$_A$($SiMe_3$)$_B$, 2 × Tbb), 2.06 (s, ^{1}J(^{29}Si,^{13}C) = 52.0 Hz, 12C, $C^{2,6}$-CH($SiMe_3$)$_A$(Si*Me*$_3$)$_B$, 2 × Tbb), 9.0 (s, 2C, $C^{4,5}$-*Me*, IMe_4), 18.8 (s, 2C, $C^{4,5}$-*Me*, Central Ring), 31.4 (s, 6C, C^4-C*Me*$_3$, 2 × Tbb), 32.3 (br s, $\Delta\nu_{1/2}$ = 27.7 Hz, $C^{2,6}$-*C*H($SiMe_3$)$_A$($SiMe_3$)$_B$, 2 × Tbb), 33.2 (s, 2C, $N^{1,3}$-*Me*, IMe_4), 34.3 (s, 2C, C^4-*C*Me$_3$, 2 × Tbb), 39.8 (s, 1C, Ge*C*Ge), 121.4 (s, 2C, *C*^{4,5}-Me, IMe_4), 122.3 (br s, $\Delta\nu_{1/2}$ = 9.8 Hz, 4C, *C*^{3,5}-H, 2 × Tbb), 132.4 (s, 1C, Ge*C*Ge), 138.1 (s, 2C, *C*^{1}, 2 × Tbb), 144.2 (s, 2C, *C*^{4,5}-Me, Central Ring), 148.9 (s, 2C, *C*^{4}, 2 × Tbb), 158.7 (s, 1C, $N^1C^2N^3$, IMe_4).

^{29}Si{^{1}H} NMR (99.36 MHz, (D_6)benzene, 298 K): *δ* (ppm) = 1.4 (s, 4Si, $C^{2,6}$-CH($SiMe_3$)$_A$(*Si*Me$_3$)$_B$, 2 × Tbb), 1.5 (s, 4Si, $C^{2,6}$-CH(*Si*Me$_3$)$_A$($SiMe_3$)$_B$, 2 × Tbb).

4.5.27. [Tbb$_2$Ge$_3$(IMe_4)C_2Me_2] (22-Ge)

A colourless solution of IMe_4 (21 mg, 0.17 mmol, 1 equiv.) in 4 mL of benzene was added slowly to a stirred green solution of **19-Ge** (200 mg, 0.17 mmol, 1 equiv.) in 6 mL of benzene at ambient temperature. An immediate colour change was observed to a red-purple hue. The reaction solution was stirred at ambient temperature for 30 min., and an aliquot of the reaction solution was analysed by ^{1}H NMR spectroscopy in (D_6)benzene after 30 min., revealing the complete consumption of all the starting materials and the selective formation of **22-Ge**. The reaction solution was filtered off, followed by evaporation of the solvent to dryness in a vacuum. Then, 4 mL of *n*- pentane was added, and the solvent was evaporated to dry again, resulting in a red crude product. This product was crystallised from *n*-pentane (2 mL) at –30 °C. The resulting red crystals were isolated by filtration at –30 °C and dried under a fine vacuum at ambient temperature for 1 hour to afford the *n*-pentane mono-solvate **22- Ge·C_5H_{12}.** Yield: 90 mg (0.070 mmol, 41 % from **19-Ge**).

Attempts to obtain the solvate-free form upon drying of **22-Ge** in a fine vacuum for 4 hours at ambient temperature or 60 °C for 2 hours. Failed, leading only to a partial loss of *n*-pentane and extensive decomposition.

Properties: Compound **22-Ge** is a very air-sensitive, red solid, turning immediately turns colourless upon contact with air. Upon heating, it begins to decompose during melting at 180 °C. It can be stored under an argon atmosphere at ambient temperature for several months. **22-Ge** is very well soluble in benzene, toluene, THF, *n*-hexane and Et_2O at ambient temperature. Under strict exclusion of air, solutions of **22-Ge** in (D_6)benzene is stable for at least 5 days without any sign of decomposition at ambient temperature.

Elemental analysis: 22-Ge·C_5H_{12} ($C_{52}H_{104}Ge_5Br_2Si_8(C_5H_{12})$, 1476.92 g mol^{-1}): Calcd. /%: C 56.18, H 9.43, N 2.05; found /%: C 56.12, H 9.54, N 1.99.

^{1}H NMR (500.1 MHz, (D_6)benzene, 298 K): δ (ppm) = 0.08 (s, 18H, $C^{2,6}$C- H(Si*Me*$_3$)$_A$(SiMe$_3$)$_B$, Tbb$_X$), 0.22 (s, 18H, $C^{2,6}$C-H(Si*Me*$_3$)$_A$(SiMe$_3$)$_B$, Tbb$_Y$), 0.32 (s, 18H, $C^{2,6}$C-H(SiMe$_3$)$_A$(Si*Me*$_3$)$_B$, Tbb$_X$), 0.38 (s, 9H, $C^{2,6}$C-H(SiMe$_3$)$_A$(Si*Me*$_3$)$_B$, Tbb$_Y$), 0.46 (s, 9H, $C^{2,6}$C-H(SiMe$_3$)$_A$(Si*Me*$_3$)$_B$, Tbb$_Y$), 1.34 (s, 6H, $C^{4,5}$-*Me*, IMe$_4$), 1.39 (s, 9H, C^4- C*Me*$_3$, Tbb$_X$), 1.45 (s, 9H, C^4-C*Me*$_3$, Tbb$_Y$), 2.28 (s, 3H C^4-*Me*), 2.38 (s, 3H, C^5-*Me*), 3.09 (s, 2H, $C^{2,6}$C-*H*(SiMe$_3$)$_A$(SiMe$_3$)$_B$, Tbb$_X$), 3.21 (s, 2H, $C^{2,6}$C-*H*(SiMe$_3$)$_A$(SiMe$_3$)$_B$, Tbb$_Y$), 3.24 (s, 6H, $N^{1,3}$-*Me*, IMe$_4$), 6.93 (s, 2H, $C^{3,5}$-*H*, Tbb$_X$), 7.02 (s, 1H, $C^{3/5}$-*H*, Tbb$_Y$), 7.07 (s, 1H, $C^{3/5}$-*H*, Tbb$_Y$).

^{13}C{^{1}H} NMR (125.8 MHz, (D_6)benzene, 298 K): δ (ppm) = 1.37 (s, 3C, C^2C- H(Si*Me*$_3$)$_A$(SiMe$_3$)$_B$, Tbb$_Y$), 1.61 (s, 6C, 2 × $C^{2,6}$C- H(SiMe$_3$)$_A$(Si*Me*$_3$)$_B$, 2 × Tbb$_X$), 1.66 (s, 3C, C^6C-H(SiMe$_3$)$_A$(Si*Me*$_3$)$_B$, Tbb$_Y$), 2.00 (s, 3C, C^6C-H(Si*Me*$_3$)$_A$(SiMe$_3$)$_B$, Tbb$_Y$), 2.08 (s, 3C, C^2C-H(SiMe$_3$)$_A$(Si*Me*$_3$)$_B$, Tbb$_Y$), 2.47 (s, 6C, 2 × $C^{2,6}$C-H(Si*Me*$_3$)$_A$(SiMe$_3$)$_B$, 2 × Tbb$_X$), 8.29 (s, 2C, $C^{4,5}$-*Me*, IMe$_4$), 21.92 (s, 1C, C-*Me*),23.87 (s, 1C, C-*Me*), 30.67 (s, 2C, $C^{2,6}$*C*-H(SiMe$_3$)$_A$(SiMe$_3$)$_B$, Tbb$_X$), 31.39 (s, 1C, C^4-C*Me*$_3$, Tbb$_X$), 31.60 (s, 1C, C^4-C*Me*$_3$, Tbb$_Y$), 31.91(s, 2C, $C^{2/6}$*C*-H(SiMe$_3$)$_A$(SiMe$_3$)$_B$, Tbb$_Y$), 34.24 (s, 1C, C^4-*C*Me$_3$, Tbb$_X$), 34.40 (s, 1C, C^4-*C*Me$_3$, Tbb$_Y$), 35.23 (s, 2C, $N^{1,3}$-*Me*, IMe$_4$), 120.92(s, 2C, *C*$^{2/6}$C-H(SiMe$_3$)$_A$(SiMe$_3$)$_B$, Tbb$_Y$), 123.08 (s, 2C, *C*^{2,6}C-H(SiMe$_3$)$_A$(SiMe$_3$)$_B$, Tbb$_X$), 126.11 (s, 2C, 2 × *C*-Me, IMe$_4$), 138.59 (s, 1C, *C*^{1}, Tbb$_X$), 147.81 (s, 1C, *C*^{3}, Tbb$_Y$), 148.34 (s, 1C, *C*^{1}, Tbb$_Y$), 148.84 (s, 1C, *C*^{4}, Tbb$_Y$), 148.90 (s, 1C, *C*^{5}, Tbb$_Y$), 149.12 (s, 1C, *C*^{4}, Tbb$_X$), 150.41 (s, 1C, *C*-Me), 151.10 (s, 2C, *C*^{3,5}-H, Tbb$_X$), 163.30 (s, 1C, N*C*^{2}N, IMe$_4$), 168.00 (s, 1C, *C*-Me).

4.5.28. [$Tbb_2Ge_4C_2Me_2$] (23-Ge)

20-Ge (200 mg, 0.14 mmol, 1 equiv.) was dissolved in 15 mL of benzene, and KC_8 (40 mg, 0.29 mmol, 2.1 equiv.) was added in one portion at ambient temperature. The reaction mixture was sonicated for 5 hrs. During this period, the colour of the reaction solution changed to yellow-orange. Analysis of an aliquot of the reaction

solution by ^{1}H NMR spectroscopy in (D_6)benzene revealed the complete and selective conversion of **20-Ge** to **23-Ge**. The yellow-orange solution was separated from the black insoluble part by filtration and evaporated to dryness in a vacuum, resulting in a yellow-orange compound that was crystallised from *n*-pentane (2 mL) at −30 °C. The resulting yellow crystals were isolated by filtration at –30 °C and dried under a fine vacuum at ambient temperature for 1 hour to afford **23-Ge**. Yield: 110 mg (0.10 mmol, 71 % from **20-Ge**).

Properties: Compound **23-Ge** is a very air-sensitive, yellow solid that turns immediately colourless upon contact with air. Upon heating, it begins to decompose during melting at 309 °C. It can be stored under an argon atmosphere at ambient temperature for several months. **23-Ge** is very well soluble in benzene, toluene, THF and partially soluble in *n*-hexane and Et_2O at ambient temperature. Under strict exclusion of air, solutions of **23-Ge** in (D_6)benzene is stable for at least 4 days without any sign of decomposition at ambient temperature.

Elemental analysis: 23-Ge ($C_{52}H_{104}Ge_4Si_8$, 1244.51 g mol^{-1}): Calcd. /%: C 50.19, H 8.42; found /%: C 49.98, H 8.45.

^{1}H NMR (500.1 MHz, (D_6)benzene, 298 K): δ (ppm) = 0.22 (s, 18H, 2 × C^{2}C- H(Si*Me*$_3$)$_A$(SiMe$_3$)$_B$, 2 × Tbb), 0.23 (s, 18H, 2 × C^{2}C-H(SiMe$_3$)$_A$(Si*Me*$_3$)$_B$, 2 × Tbb), 0.28 (s, 18H, 2 × C^{6}C-H(Si*Me*$_3$)$_A$(SiMe$_3$)$_B$, 2 × Tbb), 0.30 (s, 18H, 2 × C^{6}C- H(SiMe$_3$)$_A$(Si*Me*$_3$)$_B$, 2 × Tbb), 1.36 (s, 18H, 2 × C^{4}-C*Me*$_3$, 2 × Tbb), 2.45 (s, 6H, 2 × C-*Me*), 2.87 (s, 2H, 2 × C^{2}C-*H*(SiMe$_3$)$_A$(SiMe$_3$)$_B$, 2 × Tbb), 3.26 (s, 2H, 2 × C^{6}C- *H*(SiMe$_3$)$_A$(SiMe$_3$)$_B$, 2 × Tbb), 7.01 (s, 2H, 2 × C^{3}-*H*, 2 × Tbb). 7.15 (s, 2H, 2 × C^{5}-*H*, 2 × Tbb).

^{13}C{^{1}H} NMR (125.8 MHz, (D_6)benzene, 298 K): δ (ppm) = 1.15 (s, 6C, 2 × C^{2}C- H(Si*Me*$_3$)$_A$(SiMe$_3$)$_B$, 2 × Tbb), 1.23 (s, 6C, 2 × C^{2}C-H(SiMe$_3$)$_A$(Si*Me*$_3$)$_B$, 2 × Tbb), 1.42 (s, 6C, 2 × C^{6}C-H(Si*Me*$_3$)$_A$(SiMe$_3$)$_B$, 2 × Tbb), 1.48 (s, 6C, 2 × C^{6}C- H(SiMe$_3$)$_A$(Si*Me*$_3$)$_B$, 2 × Tbb), 22.99 (s, 2C, 2 × C-*Me*), 31.34 (s, 6C, 2 × C^{4}-C*Me*$_3$, 2 × Tbb), 33.51 (s, 2C, 2 × C^{2}*C*-H(SiMe$_3$)$_A$(SiMe$_3$)$_B$, 2 × Tbb), 34.51 (s, 2C, 2 × C^{4}-*CMe*$_3$, 2 × Tbb), 37.82 (s, 2C, 2 × C^{6}*C*-H(SiMe$_3$)$_A$(SiMe$_3$)$_B$, 2 × Tbb), 120.84 (s, 2C, 2 × *C*^{5}-H, 2 × Tbb), 122.05 (s, 2C, 2 × *C*^{3}-H, 2 × Tbb), 139.38 (s, 2C, 2 × *C*^{1}, 2 × Tbb), 145.81 (s, 2C, 2 × *C*-Me), 148.31 (s, 2C, 2 × *C*^{6}-CH(SiMe$_3$)$_A$(SiMe$_3$)$_B$, 2 × Tbb), 150.06 (s, 2C, 2 × *C*^{2}-CH(SiMe$_3$)$_A$(SiMe$_3$)$_B$, 2 × Tbb), 151.41 (s, 2C, 2 × *C*^{4}-CMe$_3$, 2 × Tbb).

4.5.29. [Tbb$_2$Ge$_5$Br$_2$C$_2$Me$_2$] (24-Ge)

A colourless solution of $GeBr_2$(1,4-dioxane) (26 mg, 0.08 mmol, 1 equiv.) in 4 mL of benzene was added slowly to a stirred yellow-orange solution of **23-Ge** (100 mg,

0.08 mmol, 1 equiv.) in 10 mL of benzene at ambient temperature. The colour of the reaction solution instantly changed to red-purple. The reaction solution was stirred at ambient temperature for 30 min. Analysis of an aliquot of the reaction solution by ^{1}H NMR spectroscopy in (D_6)benzene was performed after 30 min., revealing the complete consumption of all the starting materials and the selective formation of **24- Ge**. The reaction solution was filtered off, followed by evaporation of the solvent to dryness in a vacuum. Then, 5 mL of *n*-hexane was added, and the solvent was evaporated to dryness, resulting in a red-purple crude product. This product was crystallised from *n*-hexane (2 mL) at –30 °C. The resulting red crystals were isolated by filtration at –30 °C and dried under a fine vacuum at 60 °C for 2 hours to afford **24-Ge.** Yield: 83 mg (0.056 mmol, 70 % from **23-Ge**).

Properties: Compound **24-Ge** is a very air-sensitive, red-purple solid that turns immediately colourless upon contact with air. Upon heating, it begins to decompose during melting at 353 °C. It can be stored under an argon atmosphere at ambient temperature for several months. **24-Ge** is very well soluble in benzene, toluene, THF, *n*-hexane and Et_2O at ambient temperature. Under strict exclusion of air, solutions of **24-Ge** in (D_6)benzene is stable for 8 hours after that compound sign of decomposition at ambient temperature.

Elemental analysis: 24-Ge ($C_{52}H_{104}Ge_5Br_2Si_8$, 1476.92 g mol^{-1}): Calcd. /%: C 42.29, H 7.87; found /%: C 46.72, H 7.46.

^{1}H NMR (500.1 MHz, (D_6)benzene, 298 K): δ (ppm) = 0.23 (s, 72H, 2 × C^{2,6}C-H(Si*Me*$_3$)$_2$, 2 × Tbb), 1.29 (s, 18H, 2 × C^4-C*Me*$_3$, 2 × Tbb), 1.72 (s, 6H, 2 × C-*Me*), 3.05 (s, 4H, 2 × C^{2,6}C-*H*(SiMe$_3$)$_2$, 2 × Tbb), 6.94 (s, 4H, 2 × C^{3,5}-*H*, 2 × Tbb).

^{13}C{^{1}H} NMR (125.8 MHz, (D_6)benzene, 298 K): δ (ppm) = 1.65 (s, 12C, 2 × C^{2}C- H(Si*Me*$_3$)$_2$, 2 × Tbb), 1.88 (s, 12C, 2 × C^{6}C-H(Si*Me*$_3$)$_2$, 2 × Tbb), 22.26 (s, 6H, 2 × C-*Me*), 31.12 (s, 6C, 2 × C^4-C*Me*$_3$, 2 × Tbb), 34.36 (s, 2C, 2 × C^4-*C*Me$_3$, 2 × Tbb), 34.83 (s, 4C, 2 × C^{2,6}*C*-H(SiMe$_3$)$_2$, 2 × Tbb), 122.23 (s, 4C, 2 × *C*^{3,5}-H, 2 × Tbb), 136.14 (s, 2C, 2 × *C*^{1}, 2 × Tbb), 149.19 (s, 4C, 2 × *C*^{2,6}-CH(SiMe$_3$)$_2$), 2 × Tbb), 151.23 (s, 2C, 2 × *C*^{4}-CMe$_3$, 2 × Tbb), 162.25 (s, 2C, 2 × *C*-Me).

4.5.30. [Ar^{Dipp}SnSi(DMAP)Tbb] (25-SnSi)

A clear orange solution of (*E*)-(Tbb)BrSi=SiBr(Tbb) (660 mg, 0.59 mmol, 1.0 equiv.) and 4−DMAP (145 mg, 1.18 mmol, 2.0 equiv) in 10 mL of toluene was added slowly to a stirred green solution of ArDippSn≡SnArDipp (610 mg, 0.59 mmol, 1 equiv.) in 20 mL of toluene at ambient temperature. The reaction solution was stirred at ambient temperature for 2 hours, and no distinguishable colour change was

observed. Analysis of an aliquot of the reaction solution by ^{1}H NMR spectroscopy in (D_6)benzene revealed a complete consumption of the starting materials and the formation of **25 - SnSi**, ArDippSnBr(DMAP), and ArDipp-H in a molar ratio of 0.41 : 0.55 : 0.04. The reaction solution was worked up by evaporating all volatiles and subsequently adding 20 mL of *n*-hexane to the intense green residue, which was then stored at −30 °C. After 30 min., the colourless precipitate was separated from the intense green solution by cannula filtration and extracted one time with 6 mL of *n*-hexane. The colourless residue contains $Ar^{Dipp}SnBr(DMAP)$[14] as a major component. The filtered *n*-hexane extract was evaporated to dryness and then dissolved in 20 mL of *n*-hexane. The solution was kept at −30 °C for 1 hour. The remaining content of ArDippSnBr(DMAP) was separated by cannula filtration, and the obtained green filtrate was concentrated up to 10 mL and kept at −30 °C. After 24 hours, the obtained green crystals were separated from the light green mother liquor by filtration at −30°C and dried under fine vacuum for 1 hour at ambient temperature. The resulting product was identified as a mono-solvate of *n*-hexane, **25- SnSi·C_6H_{14}**. Yield: 281 mg (0.25 mmol, 42 % from $Ar^{Dipp}Sn{\equiv}SnAr^{Dipp}$).

Properties: Compound **25-SnSi** is a highly air-sensitive, green solid turning immediately cololess upon contact with air. Upon heating, it begins to decompose during melting at 157 °C. It can be stored under an argon atmosphere at ambient temperature for several months. **25-SnSi** is very well soluble in *n*-pentane, benzene, toluene, Et_2O and THF at ambient temperature. Under strict exclusion of air, solutions of **25-SnSi** in (D_6)benzene is stable for at least 7 days without any sign of decomposition at ambient temperature.

---

[14] NMR spectroscopic data of $Ar^{Dipp}SnBr(DMAP)$): **^{1}H NMR** (500.1 MHz, (D_6)benzene, 298 K): δ (ppm)= 1.12(m, 12H, 1.10-1.13, 2×$C^{2,6}$-CH*Me*$_A$Me$_B$, 2×Dipp), 1.43(br,s, $\Delta\nu_{1/2}$ = 60.96 Hz, 12 H, 2×$C^{2,6}$-CHMe$_A$*Me*$_B$, 2×Dipp), 1.99(s, 6H, C^4-N*Me*$_2$, DMAP), 3.35(sept, 4H, $C^{2,6}$-C*H*Me$_A$Me$_B$, 2×Dipp), 5.51(d, ^{3}J(H,H) = 7.2 Hz, 2H, $C^{3,5}$-H, DMAP), 7.09-7.22(m, 9H, 2×Dipp + $C_6H_3(Ar^{Dipp})$) 7.58(d, ^{3}J(H,H) = 7.2 Hz, 2H, $C^{2,6}$-H, DMAP). **^{13}C{^{1}H} NMR** (125.8 MHz, (D_6)benzene, 298 K): δ (ppm) = 23.4(s, 4C, 2×$C^{2,6}$-CHMe$_A$*Me*$_B$, 2×Dipp), 26.2(s, 4C, 2×$C^{2,6}$-CH*Me*$_A$Me$_B$, 2×Dipp), 30.9 (s, 4C, 2×$C^{2,6}$- *C*HMe$_A$Me$_B$, 2×Dipp), 38.2(s, 2C, C^4-N*Me*$_2$, DMAP), 106.5(s, 2C, *C*^{3,5}-H, DMAP), 123.0(s, 4C, *C*^{3,5}-H, 2×Dipp), 126.2(s, 1C, C^4, $C_6H_3(Ar^{Dipp})$, 128.6(s, 1C, *C*^{4}-H, $C_6H_3(Ar^{Dipp})$), 130.7(s, 1C, *C*^{4}-H, 2×Dipp), 141.20(s, 2C, 2×C^1, 2×Dipp), 146.7(s, 4C, 2×*C*^{2,6}- CHMe$_A$Me$_B$, 2×Dipp), 147.7(s, 2C, *C*^{2,6}-H, DMAP), 148.0(s, 1C, *C*^{2,6}-CHMe$_A$Me$_B$, $C_6H_3(Ar^{Dipp})$), 154.2(s, 1C, *C*^{4}-NMe$_2$, DMAP), 172.4(s, 1C, C^1, $C_6H_3(Ar^{Dipp})$.

Elemental analysis: 25-SnSi·C_6H_{14} ($C_{66}H_{108}N_2Si_5Sn(C_6H_{14})$, 1188.71 g mol^{-1}): Calcd. /%: C 66.69, H 9.16, N 2.36; found: /%: C 65.95, H 9.01, N 2.51 %.

^{1}H NMR (500.1 MHz, (D_6) benzene, 298 K): δ (ppm) = 0.14 (s, 18H, $C^{2,6}$-CH(Si*Me*$_3$)$_A$(SiMe$_3$)$_B$, Tbb), 0.26 (s, 18H, $C^{2,6}$-CH(SiMe$_3$)$_A$(Si*Me*$_3$)$_B$, Tbb), 1.27 (d, ^3J(H,H) = 6.8 Hz, 12H, $C^{2,6}$-CH*Me*$_A$Me$_B$, 2 × Dipp), 1.34 (s, 9H, C^4-C*Me*$_3$, Tbb), 1.39 (br s, $\Delta\nu_{1/2}$ =11.04 Hz , $C^{2,6}$-CHMe$_A$*Me*$_B$, 2 × Dipp), 1.65 (s, 6H, C^4-N*Me*$_2$, DMAP), 3.34 (sept, ^3J(H,H) = 6.8 Hz, 4H, $C^{2,6}$-C*H*Me$_A$Me$_B$, 2 × Dipp), 3.50 (s, 2H, $C^{2,6}$-C*H*(SiMe$_3$)$_A$(SiMe$_3$)$_B$, Tbb), 5.73 (d, ^3J(H,H) = 7.6 Hz, 2H, $C^{3,5}$-*H*, DMAP), 7.0 (s, 2H, $C^{3,5}$-*H*, Tbb), 7.25 - 7.28*(dd, 1H, C^4-*H*, C_6H_3(Ar^{Dipp})), 7.30 - 7.33*(m, 4H, 2 × $C^{3,5}$-*H*, 2 × Dipp), 7.34 - 7.35*(m, 2H, 2 × C^4-*H*, 2 × Dipp), 7.38-7.41*(m, 2H, $C^{3,5}$-*H*, C_6H_3(Ar^{Dipp})), 7.93 (d, ^3J(H,H) = 6.7 Hz, 2H, $C^{2,6}$-*H*, DMAP). the signal marked with * show the multiplicity pattern of AB_2 spin.

^{13}C{^{1}H} NMR (125.8 MHz, (D_6) benzene, 298 K): δ (ppm) = 1.9 (s, 6C, $C^{2,6}$-CH(Si*Me*$_3$)$_A$(SiMe$_3$)$_B$, Tbb), 2.1 (s, 6C, $C^{2,6}$-CH(SiMe$_3$)$_A$(Si*Me*$_3$)$_B$, Tbb), 24.7 (s, 4C, $C^{2,6}$-CH*Me*$_A$Me$_B$, 2 × Dipp), 26.3 (s, 4C, $C^{2,6}$-CHMe$_A$*Me*$_B$, 2 × Dipp), 31.3 (s, 3C, C^4-C*Me*$_3$, Tbb), 31.4 (s, 4C, 2 × $C^{2,6}$-*C*HMe$_A$Me$_B$, 2 × Dipp), 31.9 (s, 2C, $C^{2,6}$-*C*H(SiMe$_3$)$_A$(SiMe$_3$)$_B$, Tbb), 34.5 (s, 3C, C^4-*C*Me$_3$, Tbb), 38.2 (s, 2C, C^4-N*Me*$_2$, DMAP), 106.4 (s, 2C, *C*^{3,5}-H, DMAP), 121.7 (s, 2C, *C*^{3,5}-H, Tbb), 123.4(s, 4C, 2 × *C*^{3,5}-H, 2 × Dipp), 125.3 (s, 1C, *C*^{4}-H, C_6H_3(Ar^{Dipp})), 128.2 (s, 2C, 2 × *C*^{4}-H, 2 × Dipp), 128.5 (s, 2C, *C*^{3,5}-H, C_6H_3(Ar^{Dipp})), 138.6 (s, 1C, *C*^{1}, Tbb), 144.2 (s, 2C, *C*^{2,6}-H, DMAP), 144.2 (s, 2C, 2 × *C*^{1}, 2 × Dipp), 146.6 (s, 4C, 2 × *C*^{2,6}, 2 × Dipp), 150.6 (s, 1C, *C*^{4}, Tbb), 151.0 (s, 2C, $C^{2,6}$-H, C_6H_3(Ar^{Dipp})), 151.9 (s, 2C, *C*^{2,6}, Tbb), 152.2 (s, 1C, *C*^{4}, DMAP), 163.5 (s, 1C, *C*^{1}, C_6H_3(Ar^{Dipp})).

^{29}Si{^{1}H} NMR (99.36 MHz, (D_6)benzene, 298 K): δ (ppm) = 0.4 (s, 2Si, $C^{2,6}$-CH(*Si*Me$_3$)$_A$(SiMe$_3$)$_B$, Tbb), 3.8 (s, 2Si, $C^{2,6}$-CH(SiMe$_3$)$_A$(*Si*Me$_3$)$_B$, Tbb), 171.2 (s, 1Si, *Si*=Sn).

^{119}Sn{^{1}H} NMR (186.6 MHz, (D_6)benzene, 298 K): δ (ppm) = 228.3 (br s, $\Delta\nu_{1/2}$ = 41 Hz).

4.5.31. [Ar^{Dipp}SnSi(Mes-NC)Tbb] (26-SnSi)

To a dark green solution of **25-SnSi** (500 mg, 0.45 mmol, 1.0 equiv.) in 15 mL of *n*-pentane was added a light-yellow solution of MesNC (65 mg, 0.45 mmol, 1.0 equiv.) in 4 mL of *n*-pentane in dropwise manner for 10 minutes at room temperature. The colour of the reaction solution gradually turned to blue during 36 hours. Analysis of an aliquot of the reaction solution by ^{1}H NMR spectroscopy in (D_6)benzene revealed the complete consumption of the starting materials and the selective formation of

26- SnSi, along with an equimolar amount of DMAP. All volatiles were removed from the intense blue solution, and the resulting residue was dried for 30 min. at 40 °C. The residue was suspended in 10 mL of *n*-pentane and stored at −30°C for 30 minutes. The colourless residue was separated from the blue mother liquor and extracted one time with 4 mL of *n*-pentane at −30°C. All volatiles were removed from the collected filtrate under reduced pressure, and the obtained residue was suspended again in 8 mL of *n*-pentane. After storing the suspension at −30°C for 1 hour, the remaining amount of precipitated DMAP was separated by cannula filtration. The filtrate was concentrated to approx. 3 mL and stored at −30 °C for 24 hours. The plate-shaped Blue crystals were separated from the light blue mother liquor by cannula filtration at −30 °C and dried under a fine vacuum for 1 hour to afford **26-SnSi** in analytically pure form. Yield: 285 mg (0.25 mmol, 56 % from **25-SnSi**).

Properties: Compound **26-SnSi** is a highly air-sensitive, blue solid that turns immediately colourless upon contact with air. Upon heating, it begins to decompose during melting at 187 °C. It can be stored under an argon atmosphere at ambient temperature for several months. **26-SnSi** is very well soluble in *n*-pentane, benzene, toluene, Et_2O and THF at ambient temperature. Under strict exclusion of air, solutions of **26-SnSi** in (D_6)benzene is stable for at least 72 hours without any sign of decomposition at ambient temperature.

Elemental analysis: 26-SnSi ($C_{64}H_{97}NSi_5Sn$, 1139.60 g mol^{-1}): Calcd. /%: C 67.45, H 8.58, N 1.23; found: /%: C 66.99, H 8.55, N 1.67.

ATR-IR (solid, RT): $\tilde{\nu}$ (cm^{-1}) = 2958 (s), 2926 (vw), 2898 (w), 2863 (w), 2002 (s), 1965 (s), 1912 (w), 1615 (s), 1589 (m), 1529 (s), 1461 (s), 1442 (vw), 1425 (vw), 1393 (vw), 1381 (w), 1359 (m), 1246 (s), 1202 (w), 1177 (w), 1146 (m), 1058 (w), 1033 (w), 1009 (w), 947 (s), 915 (w), 890 (m), 838 (s), 804 (m), 789 (w), 770 (vw), 745 (m), 726 (vw), 708 (w), 686 (s), 662 (w), 646 (w), 610 (w), 602 (w), 587 (w), 562 (m), 539 (s), 479 (m), 466.0 (w), 423.0 (s).

^{1}H NMR (500.1 MHz, (D_6)benzene, 298 K): δ (ppm) = 0.12 (br, s, $\Delta\nu_{1/2}$ = 64 Hz, 36H, $C^{2,6}$-CH(Si*Me*$_3$)$_2$, Tbb), 1.10 (d, ^3J(H,H) = 6.7 Hz 12H, 2 × $C^{2,6}$-CH*Me*$_A$Me$_B$, 2 × Dipp), 1.32 (s, 9H, C^4-C*Me*$_3$, Tbb), 1.40 (d, ^3J(H,H) = 6.9 Hz, 12H, 2 × $C^{2,6}$-CHMe$_A$*Me*$_B$, 2 × Dipp), 1.94 (s, 3H, C^4-*Me*, Mes), 1.96 (s, 6H, $C^{2,6}$-*Me*, Mes), 3.08 (s, 2H, $C^{2,6}$-C*H*(SiMe$_3$)$_2$, Tbb), 3.31 (sept, 4H, $C^{2,6}$-C*H*Me$_A$Me$_B$, 2 × Dipp), 6.56 (s, 2H, $C^{3,5}$-*H*, Mes), 7.02 (s, 2H, $C^{3,5}$-*H*, Tbb), 7.20-7.21(m, 7H, 2 × $C^{3,5}$-H + C^4-H + $C^{3,5}$-H, 2 × Dipp +

$C_6H_3(Ar^{Dipp})$ + $C_6H_3(Ar^{Dipp})$), 7.29*(m, 2H, 2 × C^4-*H*, 2 × Dipp), the signal marked with * show the multiplicity pattern of AB_2 spin.

^{1}H NMR (500.1 MHz, (D_8)toluene, 243 K): δ (ppm) = 0.05 (s, 18H, $C^{2,6}$-CH(Si*Me*$_3$)$_A$(SiMe$_3$)$_B$, Tbb), 0.22 (s, 18H, $C^{2,6}$-CH(SiMe$_3$)$_A$(Si*Me*$_3$)$_B$, Tbb), 1.12 (broad doublet, 12H, $C^{2,6}$-CH*Me*$_A$Me$_B$, 2 × Dipp), 1.35 (s, 9H, C^4-C*Me*$_3$, Tbb), 1.40 (broad doublet, 12H, $C^{2,6}$-CHMe$_A$*Me*$_B$, 2 × Dipp), 1.94 (s, 6H, $C^{2,6}$-*Me*, Mes), 1.96 (s, 3H, C^4-*Me*), 3.09 (s, 2H, $C^{2,6}$-C*H*(SiMe$_3$)$_A$(SiMe$_3$)$_B$, Tbb), 3.30 (sept, 4H, $C^{2,6}$-C*H*Me$_A$Me$_B$, 2 × Dipp), 6.49 (s, 2H, $C^{3,5}$-*H*, Mes), 7.03 (s, 2H, $C^{3,5}$-*H*, Tbb), 7.18(d, ^{3}*J*(H,H) = 7.8 Hz, 4H, 2 × $C^{3,5}$-*H*, 2 × Dipp), 7.23(s, 3H, C^4-*H* + $C^{3,5}$-*H*, $C_6H_3(Ar^{Dipp})$), 7.29*(m, 2H, 2 × C^4-*H*, 2 × Dipp), the signal marked with * show the multiplicity pattern of AB_2 spin.

^{13}C{^{1}H} NMR (125.8 MHz, (D_6) benzene, 298 K): δ (ppm) = 1.49 (s, 6C, $C^{2,6}$-CH(Si*Me*$_3$)$_2$, Tbb), 18.57 (s, 2C, $C^{2,6}$-*Me,* Mes), 20.82 (s, 1C, C^4-*Me,* Mes), 23.90 (s, 4C, $C^{2,6}$-CH*Me*$_A$Me$_B$, 2 × Dipp), 26.17 (s, 4C, $C^{2,6}$-CHMe$_A$*Me*$_B$, 2 × Dipp), 31.01 (s, 4C, 2 × $C^{2,6}$-*C*HMe$_A$Me$_B$, 2 × Dipp), 31.29 (s, 3C, C^4-C*Me*$_3$, Tbb), 34.39 (s, 2C, $C^{2,6}$-*C*H(SiMe$_3$)$_2$, Tbb), 35.24 (s, 3C, C^4-*C*Me$_3$, Tbb), 106.75 (s, 2C, 2 × *C*^{4}-H, 2 × Dipp), 121.59 (s, 2C, *C*^{3,5}-H, Tbb), 123.78 (s, 4C, 2 × *C*^{3,5}-H, 2 × Dipp), 126.48 (s, 1C, *C*^{1}, Mes), 128.77 (s, 2C, *C*^{3,5}-H, $C_6H_3(Ar^{Dipp})$), 129.10 (s, 2C, *C*^{3,5}-H, Mes), 129.27 (s, 2C, *C*^{2,6}-Me, Mes), 130.31 (s, 1C, *C*^{1}, Tbb), 130.47 (s,1C, *C*^{4}-H, $C_6H_3(Ar^{Dipp})$), 136.13 (s, 1C, *C*^{4}-Me, Mes), 140.43 (s, 4C, 2 × *C*^{2,6}-CHMe$_A$Me$_B$, $C_6H_3(Ar^{Dipp})$), 146.99 (s, 4C, 2 × *C*^{2,6}-CHMe$_A$Me$_B$, 2 × Dipp), 147.33 (s, 2C, C^1, 2 × Dipp), 150.60 (s, 1C, *C*^{4}-CMe$_3$, Tbb), 152.35 (s, 2C, *C*^{2,6} CH(SiMe$_3$)$_2$, Tbb), 171.24 (s, 1C, *C*^{1}, Ar), 187.26 (s, 1C, *C*=N, Mes-NC).

^{13}C{^{1}H} NMR (125.8 MHz, (D_8)toluene, 243 K): δ (ppm) = 1.30 (s, 6C, $C^{2,6}$-CH(Si*Me*$_3$)$_A$(SiMe$_3$)$_B$, Tbb), 1.32 (s, 6C, $C^{2,6}$-CH(SiMe$_3$)$_A$(Si*Me*$_3$)$_B$, Tbb), 18.5 (s, 2C, $C^{2,6}$-*Me,* Mes), 20.8 (s, 1C, C^4-*Me,* Mes), 23.7 (s, 4C, 2 × $C^{2,6}$-CH*Me*$_A$Me$_B$, 2 × Dipp), 26.2 (s, 4C, 2 × $C^{2,6}$-CHMe$_A$*Me*$_B$, 2 × Dipp), 30.9 (s, 4C, 2 × $C^{2,6}$-*C*HMe$_A$Me$_B$, 2 × Dipp), 31.2 (s, 3C, C^4-C*Me*$_3$, Tbb), 34.3 (s, 2C, $C^{2,6}$-*C*H(SiMe$_3$)$_A$(SiMe$_3$)$_B$, Tbb), 34.8 (s, 1C, C^4-*C*Me$_3$, Tbb), 106.5 (s, 2C, 2 × *C*^{4}, 2 × Dipp), 121.3 (s, 2C, *C*^{3,5}-H, Tbb), 123.6 (s, 4C, 2 × *C*^{3,5}-H, 2 × Dipp), 126.5 (s, 1C, *C*^{1}, Mes), 128.2 (s, 2C, *C*^{3,5}-H, $C_6H_3(Ar^{Dipp})$), 129.1 (s, 2C, *C*^{3,5}-H, Mes), 129.2 (s, 2C, *C*^{2,6}-Me, Mes), 130.0 (s, 1C, *C*^{1}, Tbb), 130.1 (s,1C, *C*^{4}-H, $C_6H_3(Ar^{Dipp})$), 135.8 (s, 1C, *C*^{4}-Me, Mes), 140.3 (s, 2C, *C*^{2,6}-CHMe$_A$Me$_B$, $C_6H_3(Ar^{Dipp})$), 146.6 (s, 4C, 2 × *C*^{2,6}-CHMe$_A$Me$_B$, 2 × Dipp), 147.2 (s, 2C, *C*^{1}, 2 × Dipp), 150.3 (s, 1C, *C*^{4}-CMe$_3$, Tbb), 152.1 (s, 2C, *C*^{2,6} CH(SiMe$_3$)$_A$(SiMe$_3$)$_B$, Tbb), 170.3 (s, 1C, *C*^{1}, $C_6H_3(Ar^{Dipp})$).

^{29}Si{^{1}H} NMR (99.36 MHz, (D_6)benzene, 298 K): δ (ppm) = 0.4 (s, 2Si, $C^{2,6}$-CH($SiMe_3$)$_A$($SiMe_3$)$_B$, Tbb), 3.8 (s, 2Si, $C^{2,6}$-CH($SiMe_3$)$_A$($SiMe_3$)$_B$, Tbb), 39.0 (s, 1Si, *Si*- Sn).

^{119}Sn{^{1}H} NMR(186.6 MHz, (D_6)benzene, 298 K): δ (ppm) = 1621.6 (br s, $\Delta\nu_{1/2}$ = 350 Hz).

4.5.32. [Ar^{Dipp}SnSi(IMe$_4$)Tbb] (27-SnSi)

A solid mixture of **25-SnSi** (200 mg, 0.18 mmol, 1 equiv.) and colourless IMe_4 (23 mg, 0.18 mmol, 1 equiv.) was treated with 20 mL of benzene at room temperature. The colour of the reaction mixture changed from green to intense blue within 6 hours. An aliquot of the reaction mixture was analysed in (D_6)benzene and showed complete consumption of the starting materials and the selective formation of **27-SnSi**, along with an equimolar amount of DMAP. All volatiles were removed from the intense blue solution, and the residue was dried for 2 hours at 40 °C. The residue was dissolved in *ca.* 1 mL of *n*-pentane at stored at −30 °C. After 24 hours, the block-shaped blue crystals were separated from the light blue mother liquor at the same temperature and dried under a fine vacuum for 1 hour at ambient temperature to afford **27-SnSi** as the monoadduct with DMAP.[15] Yield: 123 mg (0.11 mmol, 59 % from **25-SnSi**).

Properties: Compound **27-SnSi** is a highly air-sensitive, blue solid that turns immediately colourless upon contact with air. Upon heating, it begins to decompose during melting at 169 °C. It can be stored under an argon atmosphere at ambient temperature for several months. **27-SnSi** is very well soluble in *n*-pentane, benzene, toluene, Et_2O and THF at ambient temperature. Under strict exclusion of air, solutions of **27-SnSi** in (D_6)benzene is stable for at least 72 hours without any sign of decomposition at ambient temperature.

Elemental analysis: 27-SnSi ($C_{61}H_{98}N_2Si_5Sn(C_7H_{10}N_2)$, 1240.75 gmol^{-1}): Calcd. /%: C 65.82, H 8.77, N 4.52; found: /%: C 65.83, H 8.61, N 4.52.

^{1}H NMR (500.1 MHz, (D_6)benzene, 298 K): δ (ppm) = 0.10 (s, 36H, $C^{2,6}$-CH(SiMe_3)$_2$, Tbb), 1.21 - 1.22 (m, 18H, $C^{4,5}$-*Me* + 2 × $C^{2,6}$-CHMe_AMe$_B$, IMe_4 + 2 × Dipp), 1.33 – 1.34 (m, 21H, 2 × $C^{2,6}$- CHMe$_A$$Me_B$ + C^4-CMe_3, 2 × Dipp + Tbb), 2.23 (s, 6H, C^4-NMe_2, DMAP), 2.93 (br s, $\Delta\nu_{1/2}$ = 10.30 Hz, 6H, $N^{1,3}$-*Me*, IMe_4), 3.30 (sept, ^3J(H,H) = 6.8 Hz, 4H, 2 × $C^{2,6}$-C*H*Me$_A$Me$_B$, 2 × Dipp), 3.54 (s, 2H, $C^{2,6}$-C*H*($SiMe_3$)$_2$, Tbb), 6.09 – 6.11 (m, 2H, $C^{3,5}$-*H*, DMAP), 6.83 (s, 2H, $C^{3,5}$-*H*, Tbb), 7.25 (d, ^3J(H,H) = 7.7 Hz, 4H, 2 × $C^{3,5}$-

[15] The molecule **14-SnSi** contains one molecule of DMAP in a crystal lattice in very close proximity to the IMe_4 unit in **14-SnSi**. This was confirmed by the scXRD measurement. In fact, all the possible method for separation of DMAP remains unsuccessful so far.

H, 2 × Dipp), 7.27 (t, ^{3}J(H,H) = 7.2 Hz, 1H, C^{4}-*H*, $C_6H_3(Ar^{Dipp})$), 7.33 (d, ^{3}J(H,H) = 7.2 Hz, 2H, C^{3,5}-*H*, $C_6H_3(Ar^{Dipp})$), 7.35 (t, ^{3}J(H,H) = 7.7 Hz, 2H, 2 × C^{4}-*H*, 2 × Dipp), 8.44 - 8.46 (d, 2H, C^{2,6}-*H*, DMAP).

^{13}C{^{1}H} NMR (125.8 MHz, (D_6) benzene, 298 K): δ (ppm) = 2.2 (s, ^{1}J(^{29}Si,^{13}C) = 52.0 Hz, 12C, C^{2,6}-CH(Si*Me$_3$*)$_2$, Tbb), 8.1 (s, 2C, C^{4,5}-*Me*, IMe_4), 23.6 (s, 4C, 2 × C^{2,6}-CHMe$_A$*Me$_B$*, 2 × Dipp), 26.7 (s, 4C, 2 × C^{2,6}-CH*Me$_A$*Me$_B$, 2 × Dipp), 31.1 (s, 4C, 2 × C^{2,6}-*C*HMe$_A$Me$_B$, 2 × Dipp), 31.4 (s, 3C, C^{4}-C*Me$_3$*, Tbb), 32.7 (s, ^{1}J(^{29}Si,^{13}C) = 42.0 Hz, 2C, C^{2,6}-*C*H(SiMe$_3$)$_2$, Tbb), 34.2 (s, 1C, C^{4}-*C*Me$_3$,Tbb), 35.0 (s, 2C, N^{1,3}-*Me*, IMe_4), 38.3 (s, 2C, C^{4}-N*Me$_2$*, DMAP), 106.9 (s, 2C, *C*^{3,5}-H, DMAP), 121.9 (s, 2C, *C*^{3,5}-H, Tbb), 123.4 (s, 4C, 2 × *C*^{3,5}-H, 2 × Dipp), 124.2 (s, 2C, *C*^{4,5}-Me, IMe_4), 125.0 (s, 1C, *C*^{4}-H, $C_6H_3(Ar^{Dipp})$), 128.0 (s, 2C, 2 × *C*^{4}-H, 2 × Dipp)*, 129.3 (s, 2C, *C*^{3,5}-H, $C_6H_3(Ar^{Dipp})$), 140.3 (s, 1C, *C^{1}*, Tbb), 142.9 (s, 2C, *C^{2,6}*, $C_6H_3(Ar^{Dipp})$), 146.6 (s, 4C, 2 × *C^{2,6}*, 2 × Dipp), 148.3 (s, 1C, *C^{4}*, Tbb), 148.5 (s, 2C, 2 × *C^{1}*, 2 × Dipp), 150.2 (s, 2C, *C*^{2,6}, Tbb), 150.6 (s, 2C, *C*^{2,6}-H, DMAP), 154.0 (s, 1C, *C*^{4}-NMe_2, DMAP), 165.2 (s, 1C, N^{1}*C*^{2}N^{3}, IMe_4), 171.9 (s, 1C, *C^{1}*, $C_6H_3(Ar^{Dipp})$), * This peak was overlapping with the (D_6)benzene ^{13}C NMR signal, therefore assigned with the careful analysis of {^{13}C,^{1}H} HSQC correlation spectra.

^{29}Si{^{1}H} NMR (99.36 MHz, (D_6)benzene, 298 K): δ (ppm) = 2.06 (s, 2Si, C^{2,6}-CH(*Si*Me$_3$)$_A$(SiMe$_3$)$_B$, Tbb), 2.23 (s, 2Si, C^{2,6}-CH(SiMe$_3$)$_A$(*Si*Me$_3$)$_B$, Tbb), 95.1 (s, 1Si, *Si*- Sn).

^{119}Sn{^{1}H} NMR(186.6 MHz, (D_6)benzene, 298 K): δ (ppm) = 750.7 (br s, $\Delta\nu_{1/2}$ = 58 Hz).

4.5.33. [(Tbb)CHN$_2$] (28)

TbbCHNNHSO$_2$-*p*-tol (3.78 g, 5.84 mmol, 1 equiv.) was suspended in 150 mL of thf, and a colourless solid of NaH (435 mg, 18 mmol, 3.1 equiv.) was added in portions to the suspension at ambient temperature. The colour of the reaction mixture immediately changed from yellow to orange after 1 hour of stirring at ambient temperature. An aliquot of the reaction solution in (D_6)benzene was analyzed by ^{1}H NMR spectroscopy, revealing the quantitative formation of **28**. The reaction solution was evaporated to dryness and extracted with 110 mL of *n*-hexane. The solution was then evaporated under a vacuum, resulting in a brown residue. This residue was crystallised from *n*-hexane (2.6 mL) at −60 °C. The orange-brown precipitate of **28** was isolated by filtration at −60 °C followed by drying under a fine vacuum at ambient temperature for one hour to afford **28** in pure form. Yield: 2.750 g (5.60 mmol, 96 % from TbbCHNNHSO$_2$-*p*-tol).

Properties: Compound **28** is an air-sensitive orange brown solid turning light yellow upon contact with air within 5 min. Upon heating, it begins to decompose during

melting at 207 °C. It can be stored under an argon atmosphere at ambient temperature for several months **28** is very well soluble in benzene, toluene, n-pentane, *n*-hexane and Et_2O at ambient temperature. Under strict exclusion of air, solutions of **28** in (D_6)benzene is stable for at least 48 hours without any sign of decomposition at ambient temperature.

Elemental analysis: 28 ($C_{25}H_{50}N_2Si_4$, 491.02 g mol^{-1}): Calcd. /%: C 61.15, H 10.26, N 5:70; found /%: C 60.51, H 9.64, N 5:06.

^{1}H NMR (500.1 MHz, (D_6)benzene, 298 K, and): δ (ppm) = 0.10 (s, 36H, $C^{2,6}$C-H(Si*Me*$_3$)$_2$, Tbb), 1.29 (s, 9H, C^4-C*Me*$_3$, Tbb), 2.03 (s, 2H, $C^{2,6}$C-*H*(SiMe$_3$)$_2$, Tbb), 4.02 (s, 1H, C*H*N_2), 6.93 (s, 2H, $C^{3,5}$-*H*, Tbb).

^{13}C{^{1}H} NMR (125.8 MHz, (D_6)benzene, 298 K, and): δ (ppm) = 0.50 (s, 12C, $C^{2,6}$C- H(Si*Me*$_3$)$_2$, Tbb), 26.42 (s, 2C, *C*^{2,6}*C*-H(SiMe$_3$)$_2$, Tbb), 31.37 (s, 3C, C^4- C*Me*$_3$, Tbb), 34.36 (s, 1C, C^4-*C*Me$_3$, Tbb), 39.83 (s, 1C, *C*N_2), 121.06 (s, 1C, *C*^{1}, Tbb), 121.66 (s, 2C, *C*^{3,5}-H, Tbb), 143.72 (s, 2C, *C*^{2,6}C-H(SiMe$_3$)$_2$, Tbb), 149.66 (s, 2C, *C*^{4}-CMe$_3$, Tbb).

^{29}Si{^{1}H} NMR (99.3 MHz, (D_6)benzene, 298 K): δ (ppm) = 1.96 (s, 4Si, $C^{2,6}$C-H(*Si*Me$_3$)$_2$, Tbb).

4.5.34. [(Tbb)CLiN_2] (29)

An orange ethereal solution of (Tbb)CHN_2 (350 mg, 0.71 mmol, 0.5 equiv.) in anhydrous Et_2O (6 mL) and a colourless solution of LDA (76 mg, 0.71 mmol, 1.0 equiv.) in Et_2O (4 mL) were independently cooled to −60 °C and maintained at this temperature for 15 min under an inert atmosphere. The LDA solution was then slowly transferred *via* cannula into the vigorously stirred (Tbb)CHN_2 solution at −60 °C, with no observable colour change upon addition. The reaction mixture was allowed to warm gradually under continuous stirring over 3 hours. In situ, monitoring by ^{1}H NMR spectroscopy (in (D_8)THF) confirmed quantitative conversion to the desired product **29**, accompanied by 25% formation of Tbb-H as a side product. The crude reaction mixture was filtered through a filter cannula under reduced pressure, and the filtrate was concentrated in vacuo to afford a brown residue. This material was subsequently dissolved in anhydrous n-hexane (10 mL) and re-concentrated under reduced pressure to yield a yellow-brown solid. Purification was achieved by recrystallization from cold *n*-hexane (1.5 mL) at −30 °C, affording light-yellow crystals of **29** after filtration at low temperature. The isolated product was subjected to drying under high vacuum at ambient temperature for 30 min, yielding **29** in 85% purity (284 mg, 0.54 mmol, 76% yield based on (Tbb)CHN_2).

Properties: Compound **29** is an air-sensitive yellow. Upon heating, it begins to decompose during melting at 189 °C. It can be stored under an argon atmosphere at low temperature for several days. **29** is very well soluble in Et_2O and THF and moderately soluble in benzene, toluene and *n*-hexane at ambient temperature. Under strict exclusion of air, solutions of **29** in (D_8)THF is not stable at ambient temperature and get converted to decomposed product upon standing it for 1 day completely.

^{1}H NMR (500.1 MHz, (D_8)THF, 298 K): δ (ppm) = 0.02 (s, 36H, $C^{2,6}$C-H(Si*Me*$_3)_2$, Tbb), 1.24 (s, 9H, C^4-C*Me*$_3$, Tbb), 2.80 (s, 2H, $C^{2,6}$C-*H*$(SiMe_3)_2$, Tbb), 6.60 (s, 2H, $C^{3,5}$-*H*, Tbb).

^{13}C{^{1}H} NMR (125.8 MHz, (D_8)THF, 298 K): δ (ppm) = 0.56 (s, 12C, $C^{2,6}$C-H(Si*Me*$_3)_2$, Tbb), 25.93 (s, 2C, $C^{2,6}$*C*-H$(SiMe_3)_2$, Tbb), 31.75 (s, 3C, C^4-C*Me*$_3$, Tbb), 34.33 (s, 1C, C^4-*C*Me_3, Tbb), 120.99 (s, 2C, *C*^{3,5}-H, Tbb), 130.86 (br,s , $\Delta\nu_{1/2}$ = 31 Hz, 1C, *C*^{1}), 142.33 (s, 1C, *C*^{2,6}*C*-H$(SiMe_3)_2$, Tbb), 143.98(s, 1C, *C*^{4}-CMe_3, Tbb). * *C*-Tbb was not visible due to extreme broadness.

^{29}Si{^{1}H} NMR (99.3 MHz, (D_6)benzene, 298 K,): δ (ppm) = 0.84 (s, 4Si, $C^{2,6}$C-H(*Si*$Me_3)_2$, Tbb).

4.5.35. [(Tbb)CN_2Ge(Tbb)] (30-Ge)

A yellow-orange solution of (*E*)-(Tbb)BrGe=GeBr(Tbb) (364 mg, 0.30 mmol, 0.5 equiv.) in 15 mL of *n*-pentane was added to the light yellow suspension of TbbCN_2Li (300 mg, 0.60 mmol, 1 equiv.) in 10 mL of *n*-pentane at ambient temperature. The colour of the reaction solution turned yellow-brown immediately. After 5 min. of stirring at ambient temperature. An aliquot of the reaction solution in (D_6)benzene was analyzed by ^{1}H NMR spectroscopy, revealing the quantitative formation of **30-Ge** along with some Tbb-containing impurities. The reaction solution was filtered and evaporated to dryness under vacuum, yielding a brown crude product. This product was then crystallised from *n*-pentane (2 mL) at −30 °C. The yellow crystals of **30-Ge** were isolated by filtration at −30 °C followed by drying under a fine vacuum at ambient temperature for 30 min. to afford **30-Ge**. Yield: 284 mg (0.28 mmol, 46 % from (*E*)-(Tbb)BrGe=GeBr(Tbb)).

Properties: Compound **30-Ge** is an air-sensitive brown solid that turns colourless immediately upon contact with air. Upon heating, it begins to decompose during melting at 198 °C. It can be stored under an argon atmosphere at ambient temperature for several months **30-Ge** is very well soluble in benzene, toluene, *n*-pentane, *n*-hexane and Et_2O at ambient temperature. Under strict exclusion of air,

solutions of **30-Ge** in (D_6)benzene is not stable at ambient temperature and get converted to their activated product upon standing it for 3 days completely.

Elemental analysis: 30-Ge ($C_{49}H_{98}GeN_2Si_8$, 1012.60 g mol^{-1}): Calcd. /%: C 58.12, H 9.75, N 2.77; found /%: C 57.67, H 9.38, N 2.72.

^{1}H NMR (500.1 MHz, (D_6)benzene, 298 K): δ (ppm) = 0.15 (s, 36H, $C^{2,6}$C-H(Si*Me*$_3$)$_2$, C-Tbb), 0.28 (s, 36H, $C^{2,6}$C-H(Si*Me*$_3$)$_2$, Ge-Tbb), 1.22 (s, 9H, C^4-C*Me*$_3$, Ge-Tbb), 1.35 (s, 9H, C^4-C*Me*$_3$, C-Tbb), 2.05 (s, 2H, $C^{2,6}$C-*H*(SiMe$_3$)$_2$, Ge-Tbb), 2.05 (s, 2H, $C^{2,6}$C-*H*(SiMe$_3$)$_2$, Ge-Tbb), 2.28 (s, 2H, $C^{2,6}$C-*H*(SiMe$_3$)$_2$, Ge-Tbb), 6.86 (s, 2H, $C^{3,5}$-*H*, Ge-Tbb), 6.95 (s, 2H, $C^{3,5}$-*H*, C-Tbb).

^{13}C{^{1}H} NMR (125.8 MHz, (D_6)benzene, 298 K): δ (ppm) = 0.30 (s, 12C, $C^{2,6}$C-H(Si*Me*$_3$)$_2$, C-Tbb), 0.87 (s, 12C, $C^{2,6}$C-H(Si*Me*$_3$)$_2$, Ge-Tbb), 29.57 (s, 2C, $C^{2,6}$*C*-H(SiMe$_3$)$_2$, Ge-Tbb), 29.77 (s, 2C, $C^{2,6}$*C*-H(SiMe$_3$)$_2$, C-Tbb), 31.04 (s, 3C, C^4-C*Me*$_3$, Ge-Tbb), 31.49 (s, 3C, C^4-C*Me*$_3$, C-Tbb), 34.50 (s, 1C, C^4-*C*Me$_3$, Ge-Tbb), 34.69 (s, 1C, C^4-*C*Me$_3$, C-Tbb), 87.59 (br s, $\Delta\nu_{1/2}$ = 39 Hz, 1C, *C*-Tbb), 114.34 (s, 1C, C^1, C-Tbb), 121.15 (s, 2C, $C^{3,5}$-H, C-Tbb), 121.66 (s, 2C, $C^{3,5}$-H, Ge-Tbb), 146.13 (s, 2C, $C^{2,6}$C-H(SiMe$_3$)$_2$, Ge-Tbb), 146.24 (s, 2C, $C^{2,6}$-C-H(SiMe$_3$)$_2$, C-Tbb), 151.14 (s, 1C, C^4, C-Tbb), 152.30 (s, 1C, C^4, Ge-Tbb), 155.77 (s, 1C, C^1, Ge-Tbb).

^{29}Si{^{1}H} NMR (99.3 MHz, (D_6)benzene, 298 K,): δ (ppm) = 1.98 (s, 4Si, $C^{2,6}$C-H(*Si*Me$_3$)$_2$, Ge-Tbb), 2.49 (s, 4Si, $C^{2,6}$C-H(*Si*Me$_3$)$_2$, C-Tbb).

4.5.36. [(NHP)SiMe$_3$C=GeBr(Tbb)] (31-Ge)

A light-yellow solution of (NHP)CSiMe3 (400 mg, 0.808 mmol, 1 equiv.) in 10 mL of *n*-hexane was slowly added to a stirred yellow-orange suspension of (*E*)- (Tbb)BrGe=GeBr(Tbb) (490 mg, 0.404 mmol, 0.5 equiv.) in 20 mL of *n*-hexane at ambient temperature. The colour of the reaction solution turned yellow-orange immediately. After 2 h. of stirring at ambient temperature, an aliquot of the reaction solution in (D_6)benzene was analyzed by ^{1}H and ^{31}P NMR spectroscopy revealed the selective formation of **31-Ge** along with trace impurities. The reaction solution was filtered and evaporated to dryness in a vacuum, resulting in a yellow crude product, which was crystallized from *n*-pentane (4 mL) at −30 °C. The yellow crystals of **31-Ge** were isolated by filtration at −30 °C followed by drying under a fine vacuum at ambient temperature for 30 min. to afford **31-Ge** as *n*-pentane hemi-solvate **31-Ge (C$_5$H$_{12}$)$_{1.5}$**. Yield: 623 mg (0.567 mmol, 70 % from (*E*)-(Tbb)BrGe=GeBr(Tbb)).

Properties: Compound **31-Ge** is an air-sensitive yellow solid turning immediately colourless upon contact with air. Upon heating, it begins to decompose during

melting at 150 °C. It can be stored under an argon atmosphere at ambient temperature for several months. **31-Ge** is very well soluble in benzene, Et_2O, *n*-pentane and *n*-hexane at ambient temperature. Under strict exclusion of air, solutions of **31-Ge** in (D_6)benzene is stable for at least 12 hours without any sign of decomposition at ambient temperature.

Elemental analysis: 31-Ge ($C_{54}H_{96}BrGeN_2PSi_5 \cdot 1.5C_5H_{12}$, 1097.24 g mol^{-1}): Calcd. /%: C 59.87, H 9.07, N 2.47; found /%: C 59.83, H 9.12, N 2.31.

^{1}H NMR (500.1 MHz, (D_6)benzene, 298 K): δ (ppm) = −0.15 (s, 18H, $C^{2,6}$C- H(Si*Me*$_3$)$_A$(SiMe$_3$)$_B$, Tbb), 0.21 (s, 18H, $C^{2,6}$C-H(SiMe$_3$)$_A$(Si*Me*$_3$)$_B$, Tbb), 0.88 (s, 9H, SiMe$_3$), 1.17 (s, 9H, C^4-C*Me*$_3$, Tbb), 1.25 (d, ^3J(H,H) = 6.8 Hz, 6H, 2 × C^2-CH*Me*$_A$Me$_B$, 2 × Dipp), 1.33 (d, ^3J(H,H) = 6.8 Hz, 12H, 2 × C^6-CH*Me*$_A$*Me*$_B$, 2 × Dipp), 1.51 (d, ^3J(H,H) = 6.8 Hz, 6H, 2 × C^2-CHMe$_A$*Me*$_B$, 2 × Dipp), 1.71 (s, 2H, $C^{2,6}$C- *H*(SiMe$_3$)$_A$(SiMe$_3$)$_B$, Tbb), 3.19 (s, 2H, 2 × C^4-*H*$_A$H$_B$), 3.77 (sept, ^3J(H,H) = 4.5 Hz, 2H, 2 × C^2-C*H*Me$_A$Me$_B$, 2 × Dipp), 3.80 (br s, 2H, 2 × C^3-H$_A$*H*$_B$), 3.94 (sept, ^3J(H,H) = 4.0 Hz, 2H, 2 × C^6- C*H*Me$_A$Me$_B$, 2 × Dipp), 6.81 (s, 2H, $C^{3,5}$-*H*, Tbb), 7.14 (d, ^3J(H,H) = 6.2 Hz, 4H, 2 × $C^{3,5}$-*H*, 2 × Dipp), 7.17 (t, ^3J(H,H) = 6.2 Hz, 2H, 2 × C^4-*H*, 2 × Dipp).

^{13}C{^{1}H} NMR (125.8 MHz, (D_6)benzene, 298 K): δ (ppm) = 0.96(s, 6C, $C^{2,6}$C- H(Si*Me*$_3$)$_A$(SiMe$_3$)$_B$, Tbb), 0.96 (s, 6C, $C^{2,6}$C-H(SiMe$_3$)$_A$(Si*Me*$_3$)$_B$, Tbb), 6.98 (s, 3C, Si*Me*$_3$) , 24.97 (s, 2C, 2 × C^6-CH*Me*$_A$Me$_B$, 2 × Dipp), 26.25 (s, 2C, 2 × C^2-CHMe$_A$*Me*$_B$, 2 × Dipp), 26.99 (s, 2C, 2 × C^2-CH*Me*$_A$Me$_B$, 2 × Dipp), 27.15 (s, 2C, 2 × C^6-CHMe$_A$*Me*$_B$, 2 × Dipp), 28.43 (s, 4C, 2 × $C^{2,6}$-*C*HMe$_A$Me$_B$, 2 × Dipp), 30.99 (s, 3C, C^4-C*Me*$_3$, Tbb), 34.44 (s, 1C, C^4-*C*Me$_3$, Tbb), 35.08 (s, 2C, *C*^{2,6}*C*-H(SiMe$_3$)$_A$(SiMe$_3$)$_B$, Tbb), 56.63 (d, ^2J(^{31}p,^{13}C) = 8.6 Hz, 2C, *C*^{3,4}), 122.43 (s, 2C, *C*^{3,5}-H, Tbb), 124.84 (s, 2C, 2 × *C*^{4}-H, 2 × Dipp), 126.01 (s, 4C, 2 × *C*^{3,5}-H, 2 × Dipp), 127.45 (s, 4C, 2 × *C*^{2,6}-CHMe$_A$Me$_B$, 2 × Dipp), 142.48 (d, ^2J(^{31}p,^{13}C) = 16 Hz, 2C, 2 × *C*^{1}, 2 × Dipp), 144.68 (s, 1C, *C*^{1}, Tbb), 147.45 (s, 2C, *C*^{2,6}C-H(SiMe$_3$)$_A$(SiMe$_3$)$_B$, Tbb), 149.63 (d, ^1J(^{31}P,^{13}C) = 52 Hz, 1C, *C*Ge), 152.41 (s, 1C, *C*^{4}, Tbb).

^{29}Si{^{1}H} NMR (99.3 MHz, (D_6)benzene, 298 K): *δ* (ppm) = −12.30(s, 1Si, *Si*Me$_3$), 12.90(s, 2Si, $C^{2,6}$C-H(*Si*Me$_3$)$_A$(SiMe$_3$)$_B$, Tbb), 12.94(s, 2Si, $C^{2,6}$C-H(SiMe$_3$)$_A$(*Si*Me$_3$)$_B$, Tbb).

^{31}P{^{1}H} NMR (200.4 MHz, (D_6)benzene, 298 K): *δ* (ppm) = 100.60 (s, 1P, N*P*N).

4.5.37. [(NHP)SiMe$_3$C=GeBr(Mind)] (32-Ge)

A light-yellow solution of (NHP)CSiMe$_3$ (100 mg, 0.202 mmol, 1 equiv.) in 10 mL of *n*-hexane was slowly added to a stirred yellow suspension of (*E*)-(Tbb)BrGe=GeBr(Mind) (490 mg, 0.404 mmol, 0.5 equiv.) in 20 mL of *n*-hexane at

ambient temperature. The colour of the reaction solution turned clear yellow immediately. After 2 hours of stirring at ambient temperature, an aliquot of the reaction solution in (D_6)benzene was analysed by ^{1}H and ^{31}P NMR spectroscopy, which revealed the selective formation of **32-Ge** along with trace impurities. The reaction solution was filtered and evaporated to dryness in a vacuum, resulting in a yellow crude product, which was crystallised twice from *n*-pentane (1.5 mL) at −30 °C to obtain the pure compound. The yellow crystals of **32-Ge** were isolated by filtration at −30 °C, followed by drying under a fine vacuum at ambient temperature for one hour, to afford **32-Ge** as an analytically pure yellow solid. Yield: 623 mg (0.567 mmol, 70 % from (*E*)-(Tbb)BrGe=GeBr(Tbb)).

Properties: Compound **32-Ge** is an air-sensitive, yellow solid that turns immediately colourless upon contact with air. Upon heating, it begins to decompose during melting at 207 °C. It can be stored under an argon atmosphere at ambient temperature for several months. **32-Ge** is very well soluble in benzene, toluene, Et_2O and moderately soluble in *n*-pentane and *n*-hexane at ambient temperature. Under strict exclusion of air, solutions of **32-Ge** in (D_6)benzene is stable for at least 48 hours without any sign of decomposition at ambient temperature.

Elemental analysis: 32-Ge ($C_{50}H_{76}BrGeN_2PSi$, 916.72 g mol^{-1}): Calcd. /%: C 65.51, H 8.35, N 3.05; found /%: C 66.09, H 8.26, N 3.03.

^{1}H NMR (500.1 MHz, (D_6)benzene, 298 K): δ (ppm) = 0.84 (s, 9H, $SiMe_3$), 0.86 (s, 6H, $C^{3,5}$-*Me*$_A$Me$_B$, Mind), 0.97 (d, ^{3}J(H,H) = 6.8 Hz, 6H, 2 × C^{6}-CH*Me*$_A$Me$_B$, 2 × Dipp), 1.13 (s, 6H, $C^{1,7}$-Me$_A$*Me*$_B$, Mind), 1.16 (d, ^{3}J(H,H) = 6.8 Hz, 6H, 2 × C^{6}-CHMe$_A$*Me*$_B$, 2 × Dipp), 1.21 (s, 6H, $C^{1,7}$-*Me*$_A$Me$_B$, Mind), 1.31 (d, ^{3}J(H,H) = 6.8 Hz, 6H, 2 × C^{2}-CH*Me*$_A$Me$_B$, 2 × Dipp), 1.43 (s, 6H, $C^{3,5}$-*Me*$_A$Me$_B$, Mind), 1.45 (d, ^{3}J(H,H) = 6.8 Hz, 6H, 2 × C^{2}- CHMe$_A$*Me*$_B$, 2 × Dipp), 1.49 (d, ^{2}J(H,H) = 12.9 Hz, 2H, $C^{2,6}$-*H*$_A$H$_B$, Mind), 1.55 (d, ^{2}J(H,H) = 12.9 Hz, 2H, $C^{2,6}$-H$_A$*H*$_B$, Mind), 3.10−3.14 (m, 2H, $C^{3,4}$-*H*$_A$H$_B$), 3.65 (sept, ^{3}J(H,H) = 6.8 Hz, 2H, 2 × C^{6}-C*H*Me$_A$Me$_B$, 2 × Dipp), 3.83−3.86 (m, 2H, $C^{3,4}$-H$_A$*H*$_B$), 3.92 (sept, ^{3}J(H,H) = 6.8 Hz, 2H, 2 × C^{2}-C*H*Me$_A$Me$_B$, 2 × Dipp), 6.90 (s, 1H, *C*^{4}-H, Mind), 7.05−7.11 (m, 2H, 2 × C^{4}-*H*, 2 × Dipp), 7.15 (d, ^{3}J(H,H) = 6.2 Hz, 4H, 2 × *C*^{3,5}-*H*, 2 × Dipp).

$^{13}C\{^{1}H\}$ NMR (125.8 MHz, (D_6)benzene, 298 K): δ (ppm) = 4.87 (s, 3C, Si*Me*$_3$), 24.65 (s, 2C, 2 × C^{6}-CH*Me*$_A$Me$_B$, 2 × Dipp), 25.18 (s, 2C, 2 × C^{2}-CHMe$_A$*Me*$_B$, 2 × Dipp), 26.17 (s, 2C, 2 × C^{6}-CHMe$_A$*Me*$_B$, 2 × Dipp), 27.16 (s, 2C, 2 × C^{2}-CH*Me*$_A$Me$_B$, 2 × Dipp), 28.25 (s, 2C, 2 × C^{2}-*C*HMe$_A$Me$_B$, 2 × Dipp), 28.56 (d, ^{4}J(^{31}P,^{13}C) = 8.9 Hz, 6H, 2 × C^{6}- *C*HMe$_A$Me$_B$, 2 × Dipp), 31.26 (s, 2C, $C^{1,7}$-Me$_A$*Me*$_B$, Mind), 31.27 (s, 2C,

$C^{3,5}$- Me_A*Me*$_B$, Mind), 31.73 (s, 2C, $C^{1,7}$-*Me*$_A$Me$_B$, Mind), 33.52 (s, 2C, $C^{3,5}$-*Me*$_A$Me$_B$, Mind), 41.02 (s, 2C, *C*^{1,7}-Me$_A$Me$_B$, Mind), 44.80 (s, 2C, *C*^{3,5}-Me$_A$Me$_B$, Mind), 56.35 (d, ^1J(H,H) = 7.8 Hz, 2C, *C*^{3,4}-H$_A$H$_B$), 57.71 (s, 2C, *C*^{2,6}-H$_A$H$_B$, Mind), 120.41 (s, 1C, *C*^{8}-H, Mind), 124.26 (s, 2C, 2 × *C*^{3}-H, 2 × Dipp), 125.15 (s, 2C, 2 × *C*^{5}-H, 2 × Dipp), 126.99 (s, 2C, 2 × *C*^{4}-H, 2 × Dipp), 131.63 (d, ^3J(^{31}P,^{13}C) = 3 Hz, 1C, Ge-*C*^{4}), 140.05 (d, ^1J(^{31}P,^{13}C) = 113 Hz, 1C, Ge=*C*), 142.31 (d, ^2J(^{31}P,^{13}C) = 16 Hz, 2C, 2 × *C*^{1}, 2 × Dipp), 149.20 (s, 2C, 2 × *C*^{6}, 2 × Dipp), 149.20 (s, 2C, 2 × *C*^{2}, 2 × Dipp), 151.78 (s, 4C, *C*^{3a,4a,7a,8a}, Mind).

^{29}Si{^{1}H} NMR (99.3 MHz, (D$_6$)benzene, 298 K): δ (ppm) = −12.36 (s, 1Si, *Si*Me$_3$).

^{31}P{^{1}H} NMR (200.4 MHz, (D$_6$)benzene, 298 K): δ (ppm) = 105.75 (s, 1P, N*P*N).

4.5.38. [(DippNCH$_2$)P=CSiMe$_3$SiBr$_2$(DippNCH$_2$)] (33-Si)

A light-yellow solution of (NHP)CSiMe$_3$ (260 mg, 0.529 mmol, 1 equiv.) in 10 mL of benzene was added slowly to the yellow suspension of SiBr$_2$(SIDipp) (306 mg, 0.529 mmol, 1 equiv.) in 15 mL of benzene at ambient temperature. No instant colour change was observed, and the reaction solution was stirred overnight at ambient temperature. An aliquot of the reaction solution in (D$_6$)benzene was analyzed by ^{1}H and ^{31}P NMR spectroscopy, revealing the selective formation of **33-Si** along with free equimolar SIDipp. The reaction solution was filtered and evaporated to dryness in a vacuum, resulting in a pale-yellow crude product, which was washed from *n*-pentane (3 × 3 mL) at ambient temperature to remove free SIDipp to give a colourless residue, which was crystallized from *n*-pentane (3 mL) after forming a clear colourless solution by warming it up then stored it at −30 °C. The resulting colourless crystals of **33-Si** were isolated by filtration at −30 °C, followed by drying under a fine vacuum at ambient temperature for 1 hour, to afford **33-Si** as an analytically pure, colourless compound. Yield: 216 mg (0.316 mmol, 60 % from SiBr$_2$(SIDipp)).

Properties: Compound **33-Si** is an air-sensitive colourless solid. Upon heating, it begins to decompose during melting at 205 °C. It can be stored under an argon atmosphere at ambient temperature for several months. **33-Si** is very well soluble in benzene toluene and moderately soluble in *n*-pentane and *n*-hexane at ambient temperature. Under strict exclusion of air, solutions of **33-Si** in (D$_6$)benzene is stable for at least 24 hours without any sign of decomposition at ambient temperature.

Elemental analysis: 33-Si ($C_{30}H_{47}Br_2N_2PSi_2$, 682.66 g mol^{-1}): Calcd. /%: C 52.78, H 6.94, N 4.10; found /%: C 53.43, H 6.92, N 3.99.

^{1}H NMR (500.1 MHz, (D_6)benzene, 298 K): δ (ppm) = 0.52 (d, $^{4}J(^{31}P,^{1}H)$ = 2.1 Hz, 9H, Si*Me*$_3$), 1.10 (d, ^{3}J(H,H) = 6.8 Hz, 6H, 2 × C^{2,6}-CH*Me*$_A$Me$_B$, Dipp$_Y$),1.18 (d, ^{3}J(H,H) = 6.8 Hz, 6H, 2 × C^{2,6}-CHMe$_A$*Me*$_B$, Dipp$_Y$), 1.30 (d, ^{3}J(H,H) = 6.8 Hz, 6H, 2 × C^{2,6}- CH*Me*$_A$Me$_B$, Dipp$_X$), 1.47 (d, ^{3}J(H,H) = 6.8 Hz, 6H, 2 × C^{2,6}-CHMe$_A$*Me*$_B$, Dipp$_X$), 3.36 (sept, , ^{3}J(H,H) = 6.8 Hz, 2H, C^{2,6}-C*H*Me$_A$Me$_B$, Dipp$_Y$) 3.56−3.57 (m, 2H, C^{3,4}- *H*$_A$H$_B$), 3.74 (sept, ^{3}J(H,H) = 6.8 Hz, 2H, C^{2,6}-C*H*Me$_A$Me$_B$, Dipp$_X$), 6.99 (d, ^{3}J(H,H) = 7.7 Hz, 2H, *C*^{3,5}-H, Dipp$_Y$), 7.09 (t, ^{3}J(H,H) = 7.7 Hz, 2H, C^{4}-*H*, Dipp$_Y$), 7.14 (d, ^{3}J(H,H) = 7.6 Hz, 2H, *C*^{3,5}-*H*, Dipp$_X$), 7.20 (t, ^{3}J(H,H) = 7.7 Hz, 2H, C^{4}-*H*, Dipp$_Y$).* C^{3,4}-H$_A$*H*$_B$ signal was not visible due to dynamics at 298 K.

^{13}C{^{1}H} NMR (125.8 MHz, (D_6)benzene, 298 K): δ (ppm) = 4.87 (d, $^{4}J(^{31}P,^{1}H)$ = 13.6 Hz 3C, Si*Me*$_3$), 24.23 (s, 2C, C^{2,6}-CH*Me*$_A$Me$_B$, Dipp$_Y$), 25.01 (s, 2C, C^{2,6}-CHMe$_A$*Me*$_B$, Dipp$_Y$), 25.10 (s, 2C, C^{2,6}-CH*Me*$_A$Me$_B$, Dipp$_X$), 25.82 (s, 2C, C^{2,6}-CHMe$_A$*Me*$_B$, Dipp$_Y$), 28.67 (s, 2C, C^{2,6}-*C*HMe$_A$Me$_B$, Dipp$_X$), 28.95 (s, 2C, C^{2,6}-*C*HMe$_A$Me$_B$, Dipp$_Y$), 57.36 (d, $^{2}J(^{31}P,^{13}C)$ = 10.2 Hz, 1C, *C*^{3}-H$_A$H$_B$), 57.52 (s, 1C, *C*^{4}-H$_A$H$_B$), 124.79 (s, 1C, *C*^{1}, Dipp$_X$), 124.88 (s, 1C, *C*^{1}, Dipp$_Y$), 126.69 (d, $^{1}J(^{31}P,^{13}C)$ = 82.5 Hz, 1C, *C*^{7}-SiMe$_3$), 127.88 (s, 1C, *C*^{4}-H, Dipp$_Y$), 128.81 (s, 1C, *C*^{4}-H, Dipp$_X$), 142.63 (s, 2C, *C*^{3,5}-H, Dipp$_Y$), 143.98 (d, $^{4}J(^{31}P,^{13}C)$ = 15 Hz, 2C, *C*^{3,5}-H, Dipp$_X$), 147.17 (d, $^{3}J(^{31}P,^{13}C)$ = 4.2 Hz, 2C, *C*^{2,6}-H, Dipp$_X$), 148.23 (s, 2C, *C*^{2,6}-H, Dipp$_Y$).

^{29}Si{^{1}H} NMR (99.3 MHz, (D_6)benzene, 298 K): δ (ppm) = −36.59(d, $^{2}J(^{31}P,^{29}Si)$ = 14.5 Hz, 1Si, *Si*Br$_2$), −2.79(d, $^{2}J(^{31}P,^{29}Si)$ = 38.5 Hz, 1Si, *Si*Me$_3$).

^{31}P{^{1}H} NMR (200.4 MHz, (D_6)benzene, 298 K): δ (ppm) = 318.50(s, 1P, N*P*C).

4.5.39. [(NHP)SiMe$_3$C=SiBr$_2$(caac^{Me})] (34-Si)

A light-yellow solution of (NHP)CSiMe$_3$ (208 mg, 0.421 mmol, 1 equiv.) in 10 mL of benzene was slowly added to a yellow suspension of SiBr$_2$(caac^{Me}) (200 mg, 0.42 mmol, 1 equiv.) in 15 mL of benzene at ambient temperature. The colour of the reaction solution after 2 hours of stirring at ambient temperature changed to intense purple. An aliquot of the reaction solution in (D_6)benzene was analyzed by ^{1}H and ^{31}P NMR spectroscopy revealed the selective formation of **34-Si**. The reaction solution was filtered and evaporated to dryness under vacuum, yielding a dark purple crude product. This product was then crystallised from *n*-pentane (3 mL) at −30 °C. The resulting purple crystals of **34-Si** were isolated by filtration at −30 °C, followed by drying under a fine vacuum at ambient temperature for 1 hour, to afford **34-Si** as an analytically pure, dark purple solid. Yield: 285 mg (0.294 mmol, 70 % from SiBr$_2$(caac^{Me})).

Properties: Compound **34-Si** is an air-sensitive dark purple solid turning immediately colourless upon contact with air. Upon heating, it begins to decompose during melting at 157 °C. It can be stored under an argon atmosphere at ambient temperature for several months. **34-Si** is very well soluble in benzene, toluene and moderately soluble in *n*-pentane and *n*-hexane at ambient temperature. Under strict exclusion of air, solutions of **34-Si** in (D_6)benzene is stable for at least 72 hours without any sign of decomposition at ambient temperature.

Elemental analysis: 34-Si ($C_{50}H_{78}Br_2N_3PSi_2$, 968.13 g mol^{-1}): Calcd. /%: C 62.03, H 8.12, N 4.34; found /%: C 61.77, H 8.21, N 4.27.

^{1}H NMR (500.1 MHz, (D_6)benzene, 298 K): δ (ppm) = 0.64 (s, 6H, C^3*Me*$_2$, caac^{Me}), 0.88 (s, 9H, Si*Me*$_3$), 0.97 (d, ^3J(H,H) = 6.5 Hz, 6H, C^{2,6}-CHMe$_A$*Me*$_B$, caac^{Me}), 1.15 (s, 2H, C^4-*H*$_2$, caac^{Me}), 1.31 (d, ^3J(H,H) = 6.7 Hz, 6H, 2 × C^2-CH*Me*$_A$Me$_B$, 2 × Dipp),1.33 (d, ^3J(H,H) = 6.5 Hz, 6H, C^{2,6}-CH*Me*$_A$Me$_B$, caac^{Me}), 1.42 (d, ^3J(H,H) = 6.7 Hz, 12H, 2 × C^6- CH*Me*$_A$Me$_B$, Dipp + 2 × C^5-*Me*$_2$, caac^{Me}), 1.51 (d, ^3J(H,H) = 6.7 Hz, 6H, 2 × C^2- CHMe$_A$*Me*$_B$, 2 × Dipp), 1.58 (d, ^3J(H,H) = 6.7 Hz, 6H, 2 × C^6-CHMe$_A$*Me*$_B$, 2 × Dipp), 2.52 (sept, ^3J(H,H) = 6.8 Hz, 2H, C^{2,6}-C*H*Me$_A$Me$_B$, caac^{Me}), 3.42-3.43 (m, 2H, C^{3,4}-*H*$_A$H$_B$), 4.06 (sept, ^3J(H,H) = 6.8 Hz, 2H, C^2-C*H*Me$_A$Me$_B$, 2 × Dipp), 4.10−4.13 (m, 2H, C^{3,4}-H$_A$*H*$_B$), 4.38 (sept, , ^3J(H,H) = 6.8 Hz, 2H, 2 × C^6-C*H*Me$_A$Me$_B$, 2 × Dipp), 6.77−6.79 (m, 2H, 2 × *C*^{4}-H, 2 × Dipp), 6.88−6.90 (m, 1H, *C*^{4}-H, caac^{Me}), 7.18−7.21 (m, 2H, C^{3,5}-*H*, caac^{Me}), 7.22−7.24 (m, 2H, 2 × *C*^{3}-*H*, 2 × Dipp), 7.26−7.28 (m, 2H, 2 × C^5-*H*, 2 × Dipp).

^{13}C{^{1}H} NMR (125.8 MHz, (D_6)benzene, 298 K): δ (ppm) = 7.49 (s, 3C, Si*Me*$_3$), 24.67 (s, 2C, 2 × C^2-CH*Me*$_A$Me$_B$, 2 × Dipp), 24.73 (s, 2C, 2 × C^6-CH*Me*$_A$Me$_B$, 2 × Dipp), 25.34(s, 2C, C^{2,6}-CH*Me*$_A$Me$_B$, caac^{Me}), 27.55 (s, 2C, 2 × C^2-CHMe$_A$*Me*$_B$, 2 × Dipp), 28.12(s, 2C, C^6-CHMe$_A$*Me*$_B$, Dipp), 28.35 (s, 4C, 2 × C^{2,6}-CHMe$_A$Me$_B$, Dipp), 28.40 (s, 2C, C^{2,6}-CHMe$_A$*Me*$_B$, caac^{Me}), 28.45 (s, 2C, *C*^{3}-Me$_2$, caac^{Me}), 29.13 (s, 2C, C^{2,6}-*C*HMe$_A$Me$_B$, caac^{Me}), 31.28 (s, 2C, *C*^{5}-Me$_2$, caac^{Me}), 50.77 (s, 1C, *C*^{4}-H$_2$, caac^{Me}), 55.77 (d, ^2J(^{31}P,^{13}C) = 8 Hz, 2C, *C*^{3,4}-H$_A$H$_B$), 56.00 (s, 1C, *C*^{3}-Me$_2$, caac^{Me}), 57.77 (d, ^1J(^{31}P,^{13}C) = 83 Hz, 1C, Si=*C*), 82.32 (s, 1C, *C*^{5}-Me$_2$, caac^{Me}), 123.69 (s, 2C, 2 × *C*^{5}-H, 2 × Dipp), 124.50 (s, 2C, 2 × *C*^{3}-H, 2 × Dipp), 125.81 (s, 2C, 2 × *C*^{4}-H, 2 × Dipp), 126.27 (s, 2C, *C*^{3,5}-H, caac^{Me}), 130.47 (s, 1C, *C*^{4}-H, caac^{Me}), 132.68 (s, 1C, *C*^{1}, caac^{Me}), 145.00 (d, ^2J(^{31}P,^{13}C) = 15.2 Hz, 1C, *C*^{1}, Dipp), 145.55 (s, 2C, *C*^{2,6}-CHMe$_A$Me$_B$, caac^{Me}), 150.67 (s, 2C, 2 × *C*^{6}-CHMe$_A$Me$_B$, 2 × Dipp), 151.53 (s, 2C, 2 × *C*^{2}-CHMe$_A$Me$_B$, 2 × Dipp), 217.69 (d, ^3J(^{31}P,^{13}C) = 2.5 Hz, 1C, C^{2}N, caac^{Me}).

^{29}Si{^{1}H} NMR (99.3 MHz, (D_6)benzene, 298 K): δ (ppm) = −45.50 (d, $^{2}J(^{31}P,^{29}Si)$ = 105.5 Hz, 1Si, *Si*Br_2), −17.11 (d, $^{2}J(^{31}P,^{29}Si)$ = 10.6 Hz, 1Si, *Si*Me_3).

^{31}P{^{1}H} NMR (200.4 MHz, (D_6)benzene, 298 K): δ (ppm) = 120.71 (s, 1P, N*P*N).

4.5.40. [(NHPMe)SiSiMe$_2$C(caac^{Me})] (35-Si)

(NHP)$SiMe_3$C=$SiBr_2$(caacMe) (**34-Si**) (395 mg, 0.40 mmol, 1 equiv.) was dissolved in 20 mL of benzene, and KC_8(114 mg, 0.84 mmol, 2.1 equiv.) was added in one portion at ambient temperature to give a dark purple suspension. The reaction mixture was stirred for 16 hours at ambient temperature. During this period, the colour of the reaction solution changed gradually from dark purple to light blue. An aliquot of the reaction solution in (D_6)benzene was analyzed by ^{1}H, and ^{31}P NMR spectroscopy revealed the selective conversion of **34-Si** to **35-Si**. The light blue solution was separated from the black insoluble part by filtration and evaporated to dryness under vacuum, resulting in a light blue crude product, which was then crystallised from *n*- pentane (2 mL) at −30 °C. The resulting light blue crystals of **35-Si** were isolated by filtration at −30 °C, followed by drying under a fine vacuum at ambient temperature for 1 hour, to afford **35-Si** as an analytically pure light blue solid. Yield: 105 mg (0.129 mmol, 32 % from (NHP)$SiMe_3$C=$SiBr_2$(caacMe)).

Properties: Compound **35-Si** is an air-sensitive light-blue solid turning immediately colourless upon contact with air. Upon heating, it begins to decompose during melting at 272 °C. It can be stored under an argon atmosphere at ambient temperature for several months. **35-Si** is very well soluble in benzene, toluene, *n*-pentane, and *n*-hexane at ambient temperature. Under strict exclusion of air, solutions of **35-Si** in (D_6)benzene is stable for at least 72 hours without any sign of decomposition at ambient temperature.

Elemental analysis: 35-Si ($C_{50}H_{78}N_3PSi_2$, 808.32 g mol^{-1}): Calcd. /%: C 62.03, H 8.12, N 4.34; found /%: C 61.77, H 8.21, N 4.27.

^{1}H NMR (500.1 MHz, (D_6)benzene, 298 K): δ (ppm) = −0.08 (s, 3H, $SiMe_A$*Me*$_B$), 0.30 (d, $^{3}J(^{13}C,^{1}H)$ = 3.8 Hz, 3H, Si*Me*$_A$$Me_B$), 0.42 (d, ^{3}J(H,H) = 7.0 Hz, 3H, C^6-CH*Me*$_A$$Me_B$, caac^{Me}), 0.66 (s, 3H, P*Me*), 0.72(s, 3H, C^5-*Me*$_A$$Me_B$, caac^{Me}), 0.91 (d, ^{3}J(H,H) = 6.8 Hz, C^6-CH*Me*$_A$$Me_B$, Dipp$_x$), 1.05 (d, ^{3}J(H,H) = 6.8 Hz, C^6-CHMe_A*Me*$_B$, caac^{Me}), 1.13 (d, ^{3}J(H,H) = 7.2 Hz, 3H, C^2-CH*Me*$_A$$Me_B$, caac^{Me}), 1.14 (d, ^{3}J(H,H) = 7.1 Hz, 3H, C^6-CHMe_A*Me*$_B$, Dipp$_Y$), 1.15 (s, 3H, C^5-Me_A*Me*$_B$, caac^{Me}), 1.19 (s, 3H, C^3-*Me*$_A$$Me_B$, caac^{Me}), 1.20 (d, ^{3}J(H,H) = 6.8 Hz, 6H, C^2-CH*Me*$_A$$Me_B$, Dipp$_X$ + C^2-CH*Me*$_A$$Me_B$, Dipp$_Y$), 1.24 (1.19(s, 3H, C^3-Me_A*Me*$_B$, caac^{Me}), 1.31 (d, ^{3}J(H,H) = 6.8 Hz, 3H, C^6-CHMe_A*Me*$_B$, Dipp$_x$), 1.33 (d, ^{3}J(H,H) = 6.8 Hz, 3H, C^2-CH*Me*$_A$$Me_B$, caac^{Me}), 1.36 (d, ^{3}J(H,H) = 6.8 Hz, 3H,

C^2-CHMe$_A$*Me*$_B$, Dipp$_X$), 1.37 (d, ^3J(H,H) = 6.9 Hz, 3H, C^2-CHMe$_A$*Me*$_B$, Dipp$_Y$), 1.52 (d, ^3J(H,H) = 6.8 Hz, 3H, C^6-CHMe$_A$*Me*$_B$, Dipp$_Y$),1.59−1.68 (m, 2H, , Caac^{Me}), 2.76 (sept, ^3J(H,H) = 6.7 Hz, 1H, C^2-C*H*Me$_A$Me$_B$, caac^{Me}), 2.93-2.98 (m, 1H, C^3-*H*$_A$H$_B$), 3.01-3.05 (m, 1H, C^4-*H*$_A$H$_B$), 3.16 (sept, ^3J(H,H) = 7.0 Hz, 1H, C^6-C*H*Me$_A$Me$_B$, caac^{Me}), 3.58-3.63 (m, 1H, C^3-H$_A$*H*$_B$), 3.69 (sept, ^3J(H,H) = 6.8 Hz, 1H, C^2-C*H*Me$_A$Me$_B$, Dipp$_Y$), 3.82 (sept, ^3J(H,H) = 6.9 Hz, 1H, C^2-C*H*Me$_A$Me$_B$, Dipp$_X$), 3.87−3.98 (m, 3H, C^6-C*H*Me$_A$Me$_B$, Dipp$_X$ + C^4-H$_A$*H*$_B$ + C^6-C*H*Me$_A$Me$_B$, Dipp$_Y$), 6.84 (dd, ^3J(H,H) = 7.7, 1.6 Hz, 1H, C^5-*H*, caac^{Me}), 7.04 (dd, ^3J(H,H) = 7.7, 1.6 Hz, 1H, C^3-*H*, caac^{Me}), 7.10 (dd, ^3J(H,H) = 7.7, 1.6 Hz, 1H, C^3-H, caac^{Me}), 7.16−7.18 (m, 2H, C^3-*H*, Dipp$_X$ + C^4-*H*, caac^{Me}), 7.19−7.21 (m, 2H, C^3-*H*, Dipp$_X$ + C^4-*H*, Dipp$_Y$), 7.25 (dd, ^3J(H,H) = 7.6, 1.7 Hz, 1H, C^5-H, Dipp$_Y$), 7.29 (t, ^3J(H,H) = 7.6 Hz, 1H, C^4-*H*, Dipp$_X$).

^{13}C{^{1}H} NMR (125.8 MHz, (D$_6$)benzene, 298 K): δ (ppm) = 0.77 (s, 1C, SiMe$_A$*Me*$_B$), 2.88 (d, ^3J(^{13}C,^{1}H) = 12.1 Hz, 1C, Si*Me*$_A$Me$_B$), 4.22 (s, 1C, P-*Me*), 22.31(d, ^3J(^{13}C,^{1}H) = 6.2 Hz , 1C, C^6-CH*Me*$_A$Me$_B$, Dipp$_Y$), 22.94 (s, 1C, C^2-CH*Me*$_A$Me$_B$, Dipp$_Y$), 23.53 (s, 1C, C^6-CH*Me*$_A$Me$_B$, caac^{Me}), 23.72 (s, 1C, C^2-CH*Me*$_A$Me$_B$, Dipp$_X$), 25.22 (s, 1C, C^6-CH*Me*$_A$Me$_B$, Dipp$_X$), 26.01 (d, ^3J(^{13}C,^{1}H) = 6.0 Hz , 1C, C^2-CH*Me*$_A$Me$_B$, caac^{Me}), 26.12 (d, ^3J(^{13}C,^{1}H) = 8.0 Hz , 1C, C^2-CHMe$_A$*Me*$_B$, caac^{Me}), 26.47 (s, 1C, C^6-CHMe$_A$*Me*$_B$, caac^{Me}), 26.99 (s, 1C, C^2-CHMe$_A$*Me*$_B$, Dipp$_X$), 27.43 (s, 1C, C^2-CHMe$_A$*Me*$_B$, Dipp$_Y$), 27.86 (s, 1C, C^6-CHMe$_A$*Me*$_B$, Dipp$_X$), 28.03 (s, 1C, C^2-*C*HMe$_A$Me$_B$, Dipp$_X$), 28.18 (s, 1C, C^6-CHMe$_A$*Me*$_B$, Dipp$_Y$), 28.36 (s, 1C, C^2-*C*HMe$_A$Me$_B$, caac^{Me}), 28.44 (s, 1C, C^6-*C*HMe$_A$Me$_B$, caac^{Me}), 28.67 (d, ^3J(^{13}C,^{1}H) = 8.4 Hz , 1C, C^6-*C*HMe$_A$Me$_B$, Dipp$_X$), 28.78 (s, 1C, C^2-*C*HMe$_A$Me$_B$, Dipp$_Y$), 28.89 (s, 1C, C^5-*Me*$_A$Me$_B$, caac^{Me}), 29.96 (d, ^3J(^{13}C,^{1}H) = 9.5 Hz , 1C, C^6- *C*HMe$_A$Me$_B$, Dipp$_Y$), 31.06 (s, 1C, *C*^{5}-Me$_A$*Me*$_B$, caac^{Me}), 32.39 (s, 1C, C^3-*Me*$_A$Me$_B$, caac^{Me}), 32.46 (s, 1C, C^3-Me$_A$*Me*$_B$, caac^{Me}), 46.36 (s, 1C, *C*^{3}-Me$_A$Me$_B$, caac^{Me}), 54.49 (s, 1C, *C*^{3}-H$_A$H$_B$), 54.56 (s, 1C, *C*^{4}-H$_A$H$_B$), 54.67 (s, 1C, *C*^{4}-H$_A$H$_B$, caac^{Me}), 64.48 (s, 1C, *C*^{5}-Me$_A$Me$_B$, caac^{Me}), 68.88 (d, ^2J(^{31}P,^{13}C) = 63.2 Hz, 1C, *C*Si$_A$Si$_B$), 123.67 (s, 1C, *C*^{3}-H, Dipp$_Y$), 123.87 (s, 1C, *C*^{5}-H, Dipp$_Y$), 124.01 (s, 1C, *C*^{3}-H, caac^{Me}), 124.11 (s, 1C, *C*^{5}-H, Dipp$_X$), 124.52 (s, 1C, *C*^{3}-H, Dipp$_X$), 124.68 (s, 1C, *C*^{5}-H, caac^{Me}), 126.05(s, 1C, *C*^{4}-H, Dipp$_Y$), 126.14 (s, 1C, *C*^{4}-H, Dipp$_X$), 128.41 (s, 1C, *C*^{4}-H, caac^{Me}), 135.19 (s, 1C, *C*^{1}, caac^{Me}), 142.56 (s, 1C, *C*^{1}, Dipp$_x$), 144.41 (135.19(s, 1C, *C*^{1}, Dipp$_Y$), 148.55 (s, 1C, *C*^{6}-CHMe$_A$Me$_B$, caac^{Me}), 148.59 (s, 1C, *C*^{2}-CHMe$_A$Me$_B$, Dipp$_X$), 148.70 (s, 1C, *C*^{2}-CHMe$_A$Me$_B$, caac^{Me}), 149.13 (s, 1C, C^6-CHMe$_A$Me$_B$, Dipp$_Y$), 150.11 (s, 1C, *C*^{6}-CHMe$_A$Me$_B$, Dipp$_X$), 150.32 (s, 1C, *C*^{2}-CHMe$_A$Me$_B$, Dipp$_Y$), 167.96 (s, 1C, *C*^{2}, caac^{Me}).

^{29}Si{^{1}H} NMR (99.3 MHz, (D$_6$)benzene, 298 K): δ (ppm) = −69.17 (d, ^2J(^{31}P,^{29}Si) = 25.3 Hz, 1Si, *Si*Me$_2$), 3.58 (d, ^1J(^{31}P,^{29}Si) = 92.8 Hz, 1Si, *Si*PN$_2$).

^{31}P{^{1}H} NMR (200.4 MHz, (D$_6$)benzene, 298 K): δ (ppm) = −233.51 (s, 1P, N*P*N).

4.5.41. [(IMe$_2$^{i}Pr$_2$)CN$_2$] (**36**)

In a 200 mL Schlenk tube, a solid mixture of (IMe$_2$^{i}Pr$_2$)CH$_2$ (2.250 g, 11.57 mmol, 1.00 equiv.), KH (0.511 g, 12.73 mmol, 1.1 equiv.) and K^{t}BuO (0.029 g, 0.25 mmol, 0.022 equiv.) were suspended in *ca.* 100 mL of THF at ambient temperature. The suspension was freeze-pump-thawed twice and exposed to N_2O gas at a pressure of 1 bar and a temperature of 0 °C. The ice bath was removed, and the reaction mixture was stirred under the dynamic flow of N_2O gas for 1 hour. The reaction solution turned from light yellow to intense brown. An aliquot of the reaction solution in (D_6)benzene was analyzed by 1H NMR spectroscopy, revealing the complete and selective conversion of (IMe$_2$^{i}Pr$_2$)CH$_2$ to **36**. All volatiles were removed under vacuum until dry, and the resulting brown residue was dried for 1 hour at ambient temperature. The residue was extracted with 4 × 30 mL of benzene. The combined extract was then concentrated to approximately 20 mL, and the brown solid was precipitated out with approx. 100 mL of *n*-hexane at ambient temperature. The precipitate was filtered off and washed twice with 15 mL of Et_2O each at ambient temperature. The brown solid was dried under a fine vacuum for 2 hours. at ambient temperature to afford **36** in an analytically pure form. Yield: 1.97 g (8.94 mmol, 77 % from (IMe$_2$^{i}Pr$_2$)CH$_2$).

Properties: Compound **36** is an air-sensitive, brown solid that turns immediately colourless upon contact with air. Upon heating, it begins to decompose during melting at 220 °C. It can be stored under an argon atmosphere at ambient temperature for several months. It is very well soluble in benzene, toluene and moderately soluble in *n*-pentane and *n*-hexane at ambient temperature. Under strict exclusion of air, solutions of **36** in (D_6)benzene is stable for at least 48 hours without any sign of decomposition at ambient temperature.

Elemental analysis: 36 ($C_{12}H_{20}N_4$, 220.31 g mol^{-1}): Calcd. /%: C 65.42, H 9.15, N 25.43; found /%: C 64.96, H 9.24, N 24.95.

^{1}H NMR (500.1 MHz, (D_6)benzene, 298 K,): δ (ppm) = 1.18 (d, ^3J(H,H) = 7.2 Hz, 12H, N^{1,3}-CH*Me*$_2$, IMe$_2$*i*Pr$_2$), 1.49 (s, 6H, C^{4,5}-*Me*, IMe$_2$*i*Pr$_2$), 4.73 (s br, $\Delta\nu_{1/2}$ = 66 Hz, 2H, N^{1,3}-C*H*Me$_2$, IMe$_2$*i*Pr$_2$).

^{13}C{^{1}H} NMR (125.8 MHz, (D_6)benzene, 298 K,): δ (ppm) = 9.55 (s, 2C, C^{4,5}-*Me*, IMe$_2$*i*Pr$_2$), 21.21 (s, 4C, N^{1,3}-CH*Me*$_2$, IMe$_2$*i*Pr$_2$), 26.71 (s br, $\Delta\nu_{1/2}$ = 7 Hz, 1C, *C*N$_2$, IMe$_2$*i*Pr$_2$=*C*), 48.14 (s, 2C, N^{1,3}-*C*HMe$_2$, IMe$_2$*i*Pr$_2$) 119.63 (s, 2C, *C*^{4,5}-Me, IMe$_2$*i*Pr$_2$), 145.95 (s, 1C, , N^1*C*N^3, IMe$_2$*i*Pr$_2$).

^{1}H-^{15}N HMBC (500.1 MHz, 50.69 MHz, (D_6)benzene, 298K): δ_N(ppm) = 167.24 (2N, $N^{1,3}$, $IMe_2{}^iPr_2$).

4.5.42. [((IMe$_2{}^i$Pr$_2$)CGeTbb)$_2$] (37-Ge)

A brown suspension of ($IMe_2{}^iPr_2$)CN_2 (84 mg, 0.38 mmol, 2 equiv.) in 10 mL of *n*-pentane was added to a yellow-orange solution of TbbGe≡GeTbb (200, 0.19 mmol, 1 equiv.) in 15 mL of *n*-pentane at ambient temperature. The colour of the reaction solution turned dark violet immediately. After 5 min. of stirring at ambient temperature. An aliquot of the reaction solution in (D_6)benzene was analyzed by ^{1}H NMR spectroscopy, revealing the quantitative formation of **37-Ge**. The reaction solution was filtered and evaporated to dryness under vacuum, resulting in a violet crude product, which was then crystallised from *n*-pentane (2 mL) at −30 °C. The violet crystals of **37-Ge** were isolated by filtration at −30 °C, followed by drying under a fine vacuum at ambient temperature for 1 hour to afford **37-Ge** as *n*-pentane hemisolvate, **37-Ge**·(C_5H_{12})$_{1.5}$. Yield: 184 mg (0.128 mmol, 67 % from TbbGe≡GeTbb).

Attempts to obtain the solvate-free form of **37-Ge** by drying in fine a vacuum for 4 hours at ambient temperature or at 40 °C for 2 hours. failed leading only to partial loss of *n*-pentane and extensive decomposition.

Properties: Compound **37-Ge** is an air-sensitive violet solid turning immediately colourless upon contact with air. Upon heating, it begins to decompose during melting at 156 °C. It can be stored under an argon atmosphere at ambient temperature for several months **37-Ge** is very well soluble in benzene, toluene, *n*- pentane and Et_2O at ambient temperature. Under strict exclusion of air, solutions of **37-Ge** in (D_6)benzene is stable for at least 48 hours without any sign of decomposition at ambient temperature.

Elemental analysis: 37-Ge·(C_5H_{12})$_{1.5}$ ($C_{72}H_{138}Ge_2N_4Si_8(C_5H_{12})_{1.5}$, 1429.79 g mol^{-1}): Calcd. /%: C 61.57, H 10.06, N 3.73; found /%: C 60.97, H 9.97, N 3.87.

^{1}H NMR (500.1 MHz, (D_8)toluene, 239 K): δ (ppm) = 0.10 (s, 36H, 2 × $C^{2/6}$C- H(Si*Me*$_3$)$_A$(Si*Me*$_3$)$_B$, Tbb$_Y$), 0.37 (s, 18H, 2 ×$C^{2/6}$C-H(Si*Me*$_3$)$_A$(SiMe$_3$)$_B$, Tbb$_X$), 0.46 (d, ^{3}J(H,H) = 7.1 Hz, 6H, 2 × N-CH*Me*$_A$Me$_B$, (IMe_2iPr_2)$_A$)), 0.37 (s, 18H, 2 × $C^{2/6}$C- H(SiMe$_3$)$_A$(Si*Me*$_3$)$_B$, Tbb$_X$), 1.23 (d, ^{3}J(H,H) = 7.1 Hz, 6H, 2 × N-CHMe$_A$*Me*$_B$, (IMe_2iPr_2)$_A$)), 1.41 (s, 18H, 2 × C^4-C*Me*$_3$, Tbb$_x$ and Tbb$_Y$), 1.49 (d, ^{3}J(H,H) = 7.1 Hz, 6H, 2 × N-CHMe$_A$*Me*$_B$, (IMe_2iPr_2)$_B$)), 1.60 (d, ^{3}J(H,H) = 7.1 Hz, 6H, 2 × N-CHMe$_A$*Me*$_B$, (IMe_2iPr_2)$_B$)), 1.70 (s, 6H, 2 × C-*Me*, (IMe_2iPr_2)$_A$)), 1.89 (s, 6H, 2 × C-*Me*, (IMe_2iPr_2)$_B$)), 2.96(s, 2H, 2 × $C^{2/6}$C-*H*(SiMe$_3$)$_A$(SiMe$_3$)$_B$, Tbb$_X$), 4.04 (s, 2H, 2 × $C^{2/6}$C-*H*(SiMe$_3$)$_A$(SiMe$_3$)$_B$, Tbb$_Y$), 5.28 (sept, ^{3}J(H,H) = 7.1 Hz, 2H, 2 × N-C*H*Me$_A$Me$_B$,

($IMe_2iPr_2)_A$)), 6.00 (sept, ^3J(H,H) = 7.1 Hz, 2H, 2 × N-C*H*Me_AMe_B, ($IMe_2iPr_2)_B$)), 6.78 (d, ^3J(H,H) = 2.0 Hz, 2H, 2 × $C^{3/5}$-H, Tbb_X), 6.81 (d, ^3J(H,H) = 1.9 Hz, 2H, 2 × $C^{3/5}$-H, Tbb_Y).

$^{13}C\{^1H\}$ NMR (125.8 MHz, (D_8)toluene, 239 K): δ (ppm) = 2.28 (s, 6C, 2 × $C^{2/6}$C-H(Si*Me*$_3)_A$(SiMe$_3)_B$, Tbb_X), 2.46 (s, 6C, 2 × $C^{2/6}$C-H(Si*Me*$_3)_A$(SiMe$_3)_B$, Tbb_Y), 2.76 (s, 6C, 2 × $C^{2/6}$C-H(SiMe$_3)_A$(Si*Me*$_3)_B$, Tbb_Y), 4.27 (s, 6C, 2 × $C^{2/6}$C-H(SiMe$_3)_A$(Si*Me*$_3)_B$, Tbb_X), 9.87 (s, 2C, 2 × C-*Me*, ($IMe_2iPr_2)_A$)), 11.96 (s, 2C, 2 × C-*Me*, ($IMe_2iPr_2)_B$)), 19.61(s, 2C, 2 × N-CHMe$_A$*Me*$_B$, ($IMe_2iPr_2)_A$)), 23.23 (s, 2C, 2 × N-CH*Me*$_A$Me$_B$, ($IMe_2iPr_2)_A$)), 24.19 (s, 2C, 2 × N-CHMe$_A$*Me*$_B$, ($IMe_2iPr_2)_B$)), 24.72 (s, 2C, 2 × N-CH*Me*$_A$Me$_B$, ($IMe_2iPr_2)_B$)), 26.62 (s, 2C, 2 × $C^{2/6}$*C*-H(SiMe$_3)_A$(SiMe$_3)_B$, Tbb_X), 28.14 (s, 2C, 2 × $C^{2/6}$*C*-H(SiMe$_3)_A$(SiMe$_3)_B$, Tbb_Y), 31.49 (s, 6C, 2 × C^4-C*Me*$_3$, Tbb_X and Tbb_Y), 34.49 (s, 2C, 2 × C^4-*C*Me$_3$, Tbb_X and Tbb_Y), 49.09 (s, 2C, 2 × N-*C*HMe$_A$Me$_B$, ($IMe_2iPr_2)_A$)), 51.06 (s, 2C, 2 × N-*C*HMe$_A$Me$_B$, ($IMe_2iPr_2)_B$)), 119.08 (s, 2C, 2 × *C*-Me, ($IMe_2iPr_2)_B$)), 121.71 (s, 2C, 2 × *C*-Me, ($IMe_2iPr_2)_A$)), 122.70 (s, 2C, 2 × *C*$^{3/5}$-H, Tbb_X), 122.80 (s, 2C, 2 × *C*$^{3/5}$-H, Tbb_Y), 144.98 (s, 2C, *C*^{1}, Tbb_X and Tbb_Y), 146.17 (s, 1C, *C*^{4}, Tbb_X and Tbb_Y), 148.61 (s, 2C, 2 × *C*$^{2/6}$, Tbb_X), 148.63 (s, 2C, 2 × *C*$^{2/6}$, Tbb_Y), 154.95 (s, 1C, *C*^{2}, ($IMe_2iPr_2)_A$)), 155.93 (s, 2C, 2 × Ge*C*Ge), 156.16 (s, 1C, *C*^{2}, ($IMe_2iPr_2)_B$)).

$^{29}Si\{^1H\}$ NMR (99.3 MHz, (D_6)benzene, 298 K,): δ (ppm) = −2.49 (s, 2Si, $C^{2/6}$C-H(*Si*Me$_3)_A$(SiMe$_3)_B$, Tbb_X), 0.45 (s, 2Si, $C^{2/6}$C-H(*Si*Me$_3)_A$(SiMe$_3)_B$, Tbb_Y), −2.13 (s, 2Si, $C^{2/6}$C-H(SiMe$_3)_A$(*Si*Me$_3)_B$, Tbb_Y), 2.70 (s, 2Si, $C^{2/6}$C-H(SiMe$_3)_A$(*Si*Me$_3)_B$, Tbb_X).

^1H-^{15}N HMBC (500.1 MHz, 50.69 MHz, (D_6)benzene, 298K): δ_N(ppm) = 138.76 (2N, $N^{1,3}$, ($IMe_2iPr_2)_B$), 182.06 (2N, $N^{1,3}$, ($IMe_2iPr_2)_A$).

4.5.43. [N(SiBrTbb)$_2$NC(IMe$_2$^{i}Pr$_2$)] (38-Si)

A brown solution of (IMe_2iPr_2)CN_2 (118 mg, 0.537 mmol, 1 equiv.) in 10 mL of benzene was added to a bright yellow solution of (*E*)-(Tbb)BrSi=SiBr(Tbb) (600 mg, 0.537 mmol, 1 equiv.) in 20 mL of benzene at ambient temperature. The colour of the reaction mixture turned brown immediately after 2 hours of stirring at ambient temperature. An aliquot of the reaction solution in (D_6)benzene was analyzed by ^1H NMR spectroscopy, revealing the selective formation of **38-Si**. The reaction solution was filtered and evaporated to dryness under vacuum, resulting in a light brown crude product. The remaining amount of benzene was co-evaporated with 10 mL of *n*-hexane at 40 °C. The brown residue was extracted with 20 mL of *n*-pentane at ambient temperature, followed by evaporation of the solvent under vacuum at 40 °C to dryness. The resulting solid was then crystallised from *n*-pentane (6 mL) at −30 °C. The light-yellow crystals of **38-Si** were isolated by filtration at −30 °C, followed by

drying under a fine vacuum at ambient temperature for one hour, affording **38-Si** as an analytically pure light-yellow solid. Yield: 409 mg (0.306 mmol, 57 % from (*E*)-(Tbb)BrSi=SiBr(Tbb)).

Properties: Compound **38-Si** is an air-sensitive light-yellow solid turning immediately colourless upon contact with air. Upon heating, it begins to decompose during melting at 210 °C. It can be stored under an argon atmosphere at ambient temperature for several months **38-Si** is very well soluble in benzene, toluene and moderately soluble in *n*-pentane and *n*-hexane at ambient temperature. Under strict exclusion of air, solutions of **38-Si** in (D_6)benzene is stable for at least 24 hours without any sign of decomposition at ambient temperature.

Elemental analysis: 38-Si ($C_{60}H_{118}Br_2Si_{10}N_4$, 1336.27 g mol^{-1}): Calcd. /%: C 54.86, H 9.13, N 4.06; found /%: C 54.13, H 9.10, N 4.25.

^{1}H NMR (500.1 MHz, (D_8)thf, 263 K): δ (ppm) = −0.17 (s br, $\Delta\nu_{1/2}$ = 23 Hz, 9H, C^{6}C-H(Si*Me*$_3$)$_A$(SiMe$_3$)$_B$, Tbb$_Y$), −0.09 (s , 9H, C^{6}C-H(Si*Me*$_3$)$_A$(SiMe$_3$)$_B$, Tbb$_x$), 0.08−0.10 (m, 27H, C^{6}C-H(SiMe$_3$)$_A$(Si*Me*$_3$)$_B$, Tbb$_Y$ + C^{2}C-H(Si*Me*$_3$)$_A$(Si*Me*$_3$)$_B$, Tbb$_Y$), 0.15−0.18 (m, 27H, C^{6}C-H(SiMe$_3$)$_A$(Si*Me*$_3$)$_B$, Tbb$_X$ + C^{2}C-H(Si*Me*$_3$)$_A$(Si*Me*$_3$)$_B$, Tbb$_X$), 1.19 (s br, $\Delta\nu_{1/2}$ = 16 Hz , 3H, N^1-CH*Me*$_A$Me$_B$), 1.27 (s, 9H, C^4-C*Me*$_3$, Tbb$_Y$), 1.28 (s br, $\Delta\nu_{1/2}$ = 16 Hz , 3H, N^1-CHMe$_A$*Me*$_B$), 1.30 (s, 9H, C^4-C*Me*$_3$, Tbb$_Y$), 1.41 (d, ^3J(H,H) = 6.9, 3H, N^3-CH*Me*$_A$Me$_B$), 1.75 (d, ^3J(H,H) = 6.9, 3H, N^3-CHMe$_A$*Me*$_B$), 2.29 (s, 3H, C^5-Me), 2.43 (s, 3H, C^5-Me), 2.97 (br s, $\Delta\nu_{1/2}$ = 14 Hz, 1H, C^{2}C-*H*(SiMe$_3$)$_A$(SiMe$_3$)$_B$, Tbb$_X$), 3.67 (br s, $\Delta\nu_{1/2}$ = 23 Hz, 1H, C^{2}C-*H*(SiMe$_3$)$_A$(SiMe$_3$)$_B$, Tbb$_Y$), 4.18 (sept, ^3J(H,H) = 6.9 Hz, 1H, N^1-C*H*Me$_A$Me$_B$), 5.03−5.09 (m, 2H, N^3-C*H*Me$_A$Me$_B$ + C^{6}C-*H*(SiMe$_3$)$_A$(SiMe$_3$)$_B$, Tbb$_Y$), 5.38 (br s, $\Delta\nu_{1/2}$ = 18 Hz, 1H, C^{6}C-*H*(SiMe$_3$)$_A$(SiMe$_3$)$_B$, Tbb$_X$), 6.75 (s, 2H, C^{3,5}-*H*, Tbb$_X$), 6.77 (s, 1H, C^3-*H*, Tbb$_Y$), 6.90 (s, 1H, C^3-*H*, Tbb$_Y$).

^{13}C{^{1}H} NMR (125.8 MHz, (D_8)thf, 263 K): δ (ppm) = 1.63−1.78 (m, 12C, C^{2,6}C- *H*(SiMe$_3$)$_A$(SiMe$_3$)$_B$, Tbb$_Y$), 2.14 (s, 3C, C^{6}C-*H*(SiMe$_3$)$_A$(Si*Me*$_3$)$_B$, Tbb$_X$), 2.26 (s, 3C, C^{2}C-*H*(SiMe$_3$)$_A$(Si*Me*$_3$)$_B$, Tbb$_X$), 2.55 (s, 3C, C^{2}C-*H*(Si*Me*$_3$)$_A$(SiMe$_3$)$_B$, Tbb$_X$), 2.76 (s, 3C, C^{6}C-*H*(Si*Me*$_3$)$_A$(SiMe$_3$)$_B$, Tbb$_X$), 9.80 (s br, $\Delta\nu_{1/2}$ = 19 Hz, 1C, C^5-Me), 10.38 (s, 1C, C^4-Me), 20.89 (br s, $\Delta\nu_{1/2}$ = 43 Hz, 1C, N^1-CH*Me*$_A$Me$_B$), 22.29 (s, 1C, N^1-CHMe$_A$*Me*$_B$), 22.73 (s, 1C, N^3-CHMe$_A$*Me*$_B$), 24.52 (s, 1C, N^3-CH*Me*$_A$Me$_B$), 26.57 (s br, $\Delta\nu_{1/2}$ = 20 Hz, 1C, C^6*C*-H(SiMe$_3$)$_A$(SiMe$_3$)$_B$, Tbb$_Y$), 26.73 (s, 1C, C^{6}C-*H*(SiMe$_3$)$_A$(SiMe$_3$)$_B$, Tbb$_X$), 27.37 (br s, 1C, $\Delta\nu_{1/2}$ = 26 Hz, C^2*C*-H(SiMe$_3$)$_A$(SiMe$_3$)$_B$, Tbb$_Y$), 29.94 (s, 1C, C^2*C*-H(SiMe$_3$)$_A$(SiMe$_3$)$_B$, Tbb$_X$), 31.31 (s, 3C, C^4-C*Me*$_3$, Tbb$_Y$), 31.33 (s, 3C, C^4-C*Me*$_3$, Tbb$_X$), 34.67 (s, 3C, C^4-*C*Me$_3$, Tbb$_Y$), 34.79 (s, 3C, C^4-*C*Me$_3$, Tbb$_X$), 52.94 (s, 1C, N^3-*C*HMe$_A$Me$_B$), 53.14 (s, 1C, N^1-*C*HMe$_A$Me$_B$), 122.53 (br s, $\Delta\nu_{1/2}$ = 24 Hz, 1C, *C*^{3}-H, Tbb$_Y$), 123.58 (br s, $\Delta\nu_{1/2}$ = 22

Hz, 1C, *C*^{5}-H, Tbb$_{Y}$), 124.05 (s, 1C, *C*^{3}-H, Tbb$_{X}$), 126.57 (s, 1C, *C*^{5}-Me), 126.70 (s, 1C, *C*^{5}-H, Tbb$_{X}$), 126.89 (s, 1C, *C*^{1}, Tbb$_{Y}$), 128.44 (s, 1C, *C*^{5}-Me), 128.66 (s, 1C, *C*^{1}, Tbb$_{X}$), 149.56 (s, 1C, *C*^{2}, N*C*N), 150.13 (s, 1C, *C*^{4}-CMe$_3$, Tbb$_{Y}$), 150.54 (s, 1C, *C*^{4}-CMe$_3$, Tbb$_{X}$), 151.64 (s, 1C, *C*^{2}C-H(SiMe$_3$)$_A$(SiMe$_3$)$_B$, Tbb$_{X}$), 152.94 (br s, 1C, $\Delta\nu_{1/2}$ = 28 Hz, *C*^{2}C-H(SiMe$_3$)$_A$(SiMe$_3$)$_B$, Tbb$_{Y}$), 153.25 (br s, 1C, $\Delta\nu_{1/2}$ = 26 Hz, *C*^{6}C-H(SiMe$_3$)$_A$(SiMe$_3$)$_B$, Tbb$_{Y}$), 156.13 (s, 1C, *C*^{6}C-H(SiMe$_3$)$_A$(SiMe$_3$)$_B$, Tbb$_{X}$), 194.22 (s, 1C, Si*C*N).

^{29}Si{^{1}H} NMR (99.3 MHz, (D$_6$)benzene, 263 K): δ (ppm) = −34.74 (s, 1Si, *Si*-Tbb$_{Y}$), −21.87 (s, 2Si, C^{2,6}C-H(*Si*Me$_3$)$_A$(SiMe$_3$)$_B$, Tbb$_{Y}$), −20.04 (s, 1Si, *Si*-Tbb$_{X}$), 0.44 (s, 2Si, C^{2,6}C- H(*Si*Me$_3$)$_A$(SiMe$_3$)$_B$, Tbb$_{X}$), 0.94 (s, 2Si, C^{2,6}C-H(SiMe$_3$)$_A$(*Si*Me$_3$)$_B$, Tbb$_{Y}$), 2.46 (s, 2Si, C^{2,6}C-H(SiMe$_3$)$_A$(*Si*Me$_3$)$_B$, Tbb$_{X}$).

4.5.44. [TbbGe(IMe$_2$^{i}Pr$_2$)GeBr$_2$Tbb] (39-Ge)

A brown solution of (IMe$_2$^{i}Pr$_2$)CN$_2$ (110 mg, 0.50 mmol, 1 equiv.) in 10 mL of benzene was added to a bright yellow solution of (*E*)-(Tbb)BrGe=GeBr(Tbb) (600 mg, 0. 50mmol, 1 equiv.) in 20 mL of benzene at ambient temperature. The colour of the reaction mixture turned brown immediately after a night of stirring at ambient temperature. An aliquot of the reaction solution in (D$_6$)benzene was analyzed by ^{1}H NMR spectroscopy, revealing the selective formation of **39-Ge**. The reaction solution was filtered and evaporated to dryness under vacuum, resulting in a brown crude product. The remaining amount of benzene was co-evaporated with 10 mL of *n*-hexane at ambient temperature. The brown residue was extracted with 20 mL of *n*-hexane at ambient temperature, followed by evaporation of the solvent under vacuum at 40 °C to dryness; the resulting solid was then crystallised from *n*-hexane (4 mL) at 4 °C. The light-brown crystals of **39-Ge** were isolated by filtration at 0 °C, followed by drying under a fine vacuum at ambient temperature for 2 hours, affording **39-Ge** as an analytically pure, light-brown solid. Yield: 409 mg (0.293 mmol, 59 % from (*E*)-(Tbb)BrGe=GeBr(Tbb)).

Properties: Compound **39-Ge** is a brown, an air sensitive solid. It is moderately soluble in aliphatic solvents (*n*-pentane, *n*-hexane, Petroleum ether and Et$_2$O but well soluble in benzene, toluene and THF at ambient temperature. Upon strict exclusion of air, a solution of **39-Ge** in (D$_6$)benzene does not exhibit any signs of decomposition after 24 hours at ambient temperature.

^{1}H NMR (500.1 MHz, (D$_8$)toluene, 243 K): δ (ppm) = 0.06 (s, 9H, C^{2}C- H(SiMe$_3$)$_A$(Si*Me*$_3$)$_B$, Tbb$_{Y}$), 0.18 (s, 9H, C^{2}C- H(SiMe$_3$)$_A$(Si*Me*$_3$)$_B$, Tbb$_{X}$), 0.33 (s, 27H, C^{2}C-H(Si*Me*$_3$)$_A$(SiMe$_3$)$_B$, Tbb$_{X}$ + C^{6}C-H(Si*Me*$_3$)$_A$(SiMe$_3$)$_B$, Tbb$_{Y}$ + C^{6}C-H(SiMe$_3$)$_A$(Si*Me*$_3$)$_B$, Tbb$_{X}$), 0.40 (d, ^{3}J(H,H) = 7.0 Hz, 3H, N^{1}-CHMe$_A$*Me*$_B$), 0.45 (s , 9H,

C^2C-H($SiMe_3$)$_A$(Si*Me*$_3$)$_B$, Tbb$_X$), 0.46 (s , 18H, C^2C-H(Si*Me*$_3$)$_A$($SiMe_3$)$_B$, Tbb$_Y$ + C^6C-H($SiMe_3$)$_A$(Si*Me*$_3$)$_B$, Tbb$_Y$), 1.10 (s, 1H, C^6C-*H*($SiMe_3$)$_A$($SiMe_3$)$_B$, Tbb$_X$), 1.16 (d, ^3J(H,H) = 7.0 Hz, 3H, N^3-CHMe$_A$*Me*$_B$), 1.33 (d, ^3J(H,H) = 7.0 Hz, 3H, N^3-CH*Me*$_A$Me$_B$), 1.36 (s, 18H, 2 × C^4-C*Me*$_3$, Tbb$_X$ + Tbb$_Y$), 1.50 (d, ^3J(H,H) = 7.0 Hz, 3H, N^1-CH*Me*$_A$Me$_B$), 1.64 (s, 1H, C^6C-*H*($SiMe_3$)$_A$($SiMe_3$)$_B$, Tbb$_Y$), 1.64 (s, 3H, C^4-*Me*, IMe$_2$*i*Pr$_2$), 1.71 (s, 3H, C^5-*Me*, IMe$_2$*i*Pr$_2$), 3.36 (s, 1H, C^2C-*H*($SiMe_3$)$_A$($SiMe_3$)$_B$, Tbb$_X$), 4.11 (br s, $\Delta\nu_{1/2}$ = 78 Hz, 1H, C^2C-*H*($SiMe_3$)$_A$($SiMe_3$)$_B$, Tbb$_Y$), 5.35 (sept, ^3J(H,H) = 6.9 Hz, 4H, $C^{2,6}$-CHMe$_A$Me$_B$, IMe$_2$*i*Pr$_2$), 5.44 (sept, ^3J(H,H) = 6.9 Hz, 4H, $C^{2,6}$-CHMe$_A$Me$_B$, IMe$_2$*i*Pr$_2$), 6.82*(m, 2H, $C^{3,5}$-*H*, Tbb$_X$), 6.90 (s, 1H, C^3-*H*, Tbb$_Y$), 7.03 (s, 1H, C^5-*H*, Tbb$_Y$).* the signals marked with an asterisk show the multiplicity pattern of an AB_2 spin system.

^{13}C{^{1}H} NMR (125.8 MHz, (D_8)thf, 263 K): δ (ppm) = 1.79 (s, 3C, C^6C-H(Si*Me*$_3$)$_A$(Si*Me*$_3$)$_B$, Tbb$_X$), 1.91 (s, 3C, C^2C-H($SiMe_3$)$_A$(Si*Me*$_3$)$_B$, Tbb$_Y$), 2.01 (s, 3C, C^2C-H(Si*Me*$_3$)$_A$($SiMe_3$)$_B$, Tbb$_X$), 2.11 (s, 3C, C^6C-H(Si*Me*$_3$)$_A$($SiMe_3$)$_B$, Tbb$_Y$), 2.20 (s, 3C, C^6C-H($SiMe_3$)$_A$(Si*Me*$_3$)$_B$, Tbb$_X$), 2.33 (s, 3C, C^2C-H($SiMe_3$)$_A$(Si*Me*$_3$)$_B$, Tbb$_X$), 2.86 (s, 3C, C^6C-H($SiMe_3$)$_A$(Si*Me*$_3$)$_B$, Tbb$_Y$), 2.96 (s, 3C, C^2C-H(Si*Me*$_3$)$_A$($SiMe_3$)$_B$, Tbb$_Y$), 10.37 (s, 1C, C^4-*Me*), 10.49 (s, 1C, C^5-*Me*), 20.73 (s, 1C, N^3-CH*Me*$_A$Me$_B$, IMe$_2$*i*Pr$_2$), 20.96 (s, 1C, N^1-CHMe$_A$*Me*$_B$, IMe$_2$*i*Pr$_2$), 22.51 (s, 1C, N^1-CH*Me*$_A$Me$_B$, IMe$_2$*i*Pr$_2$), 23.62 (s, 1C, N^3-CHMe$_A$*Me*$_B$, IMe$_2$*i*Pr$_2$), 25.11 (s, 1C, C^2*C*-H($SiMe_3$)$_A$($SiMe_3$)$_B$, Tbb$_X$), 25.42 (s, 1C, C^2*C*-H($SiMe_3$)$_A$(Si*Me*$_3$)$_B$, Tbb$_Y$), 29.18 (s, 1C, C^6*C*-H($SiMe_3$)$_A$($SiMe_3$)$_B$, Tbb$_Y$), 29.50 (s, 1C, C^6*C*-H($SiMe_3$)$_A$($SiMe_3$)$_B$, Tbb$_X$), 31.02 (s, 3C, C^4-C*Me*$_3$, Tbb$_X$). 31.37 (s, 3C, C^4-C*Me*$_3$, Tbb$_Y$), 34.16 (s, C^4-*C*Me$_3$, Tbb$_X$), 34.30 (s, C^4-*C*Me$_3$, Tbb$_Y$), 48.31 (s, 1C, N^3-*C*H*Me*$_A$Me$_B$, IMe$_2$*i*Pr$_2$), 50.37 (s, 1C, N^1-*C*H*Me*$_A$Me$_B$, IMe$_2$*i*Pr$_2$), 122.38 (s, 1C, *C*^{3}-H, Tbb$_Y$), 123.13 (s, 1C, *C*^{3}-H, Tbb$_X$), 123.85 (s, 1C, *C*^{5}-H, Tbb$_X$), 123.88 (s, 1C, *C*^{5}-H, Tbb$_Y$), 135.05 (s, 1C, *C*^{1}, Tbb$_X$), 137.66 (s, 1C, *C*^{1}, Tbb$_Y$), 143.83 (s, 1C, Ge=*C*), 148.05 (s, 1C, *C*^{4}-CMe$_3$, Tbb$_X$), 148.79 (s, 1C, *C*^{2,6}-CH($SiMe_3$)$_A$($SiMe_3$)$_B$, Tbb$_Y$), 150.62 (s, 1C, *C*^{4}-CMe$_3$, Tbb$_Y$), 155.03 (s, 1C, *C*^{2}, N*C*N), 158.78 (s, 1C, *C*^{2,6}-CH($SiMe_3$)$_A$($SiMe_3$)$_B$, Tbb$_X$).

4.5.45. [N(SiTbb)$_2$NC(IMe$_2$*i*Pr$_2$)] (40-Si)

N(TbbSiBr)$_2$NC(IMe$_2$*i*Pr$_2$) (400 mg, 0.30 mmol, 1 equiv.) was dissolved in 20 mL of benzene, and KC_8(85 mg, 0.63 mmol, 2.1 equiv.) was added in one portion at ambient temperature. The colour of the reaction mixture turned red immediately after 7 hours of stirring at ambient temperature. An aliquot of the reaction solution in (D_6)benzene was analyzed by ^{1}H NMR spectroscopy, revealing the selective formation of **40-Si**. The red solution was separated from the black insoluble part by filtration and then evaporated to dryness under vacuum, yielding a red crude product. The remaining amount of benzene was co-evaporated with 15 mL of *n*-hexane at 40 °C. The red residue was extracted with 15 mL of *n*-pentane at ambient temperature, followed by

evaporation of the solvent under vacuum at 40 °C to dryness. The resulting solid was then crystallised from *n*-hexane (3 mL) at −60 °C. The red crystals of **40-Si** were isolated by filtration at −60 °C, followed by drying under a fine vacuum at ambient temperature for 2 hours, to afford **40-Si** as an analytically pure red solid. Yield: 204 mg (0.173 mmol, 58 % from $N(TbbSiBr)_2NC(IMe_2{}^iPr_2)$).

Properties: Compound **40-Si** is an air-sensitive, red solid that turns immediately colourless upon contact with air. Upon heating, it begins to decompose during melting at 145 °C. It can be stored under an argon atmosphere at ambient temperature for several months. **40-Si** is very well soluble in benzene, toluene, *n*-pentane, and *n*-hexane at ambient temperature. Under strict exclusion of air, solutions of **40-Si** in (D_6)benzene is stable for at least 72 hours without any sign of decomposition at ambient temperature.

Elemental analysis: 40-Si ($C_{60}H_{118}Si_{10}N_4$, 1176.46 g mol^{-1}): /%: C 61.25, H 10.11, N 4.76; found /%: C 60.27, H 10.21, N 4.68.

^{1}H NMR (500.1 MHz, (D_8)thf, 263 K): δ (ppm) = 0.19 (br s, $\Delta\nu_{1/2}$ = 13 Hz, 18H, $C^{2,6}$C- H(Si*Me*$_3$)$_A$(SiMe$_3$)$_B$, Tbb$_Y$), 0.28 (br s, $\Delta\nu_{1/2}$ = 13 Hz, 9H, $C^{2,6}$C-H(SiMe$_3$)$_A$(Si*Me*$_3$)$_B$, Tbb$_Y$) 0.33 (s , 36H, $C^{2,6}$C-H(Si*Me*$_3$)$_A$(Si*Me*$_3$)$_B$, Tbb$_X$), 1.22−1.30 (m, 6H, 2 × N-CH*Me*$_A$Me$_B$), 1.31−1.36 (m, 6H, 2 × N-CHMe$_A$*Me*$_B$), 1.37 (s, 9H, C^4-C*Me*$_3$, Tbb$_Y$), 1.40 (s, 9H, C^4-C*Me*$_3$, Tbb$_Y$), 1.74 (s, 6H, 2 × C-*Me*), 3.32 (s , 2H, $C^{2,6}$C-*H*(SiMe$_3$)$_A$(SiMe$_3$)$_B$, Tbb$_X$), 5.90 (s, 2H, $C^{2,6}$C-*H*(SiMe$_3$)$_A$(SiMe$_3$)$_B$, Tbb$_Y$), 7.00 (br s, $\Delta\nu_{1/2}$ = 13 Hz, 2H, $C^{3,5}$- *H*, Tbb$_Y$), 7.07(s, 2H, $C^{3,5}$-*H*, Tbb$_Y$).

^{13}C{^{1}H} NMR (125.8 MHz, (D_8)thf, 263 K): δ (ppm) = 0.91 (s, 12C, $C^{2,6}$C-H(Si*Me*$_3$)$_A$(Si*Me*$_3$)$_B$, Tbb$_X$), 1.25 (s, 6C, $C^{2,6}$C-H(Si*Me*$_3$)$_A$(SiMe$_3$)$_B$, Tbb$_Y$), 1.85 (s, 6C, $C^{2,6}$C-H(SiMe$_3$)$_A$(Si*Me*$_3$)$_B$, Tbb$_Y$), 10.28 (s, 2C, 2 × C-*Me*), 21.68 (s, 2C, 2 × N-CH*Me*$_A$Me$_B$), 22.10 (s, 2C, 2 × N-CHMe$_A$*Me*$_B$), 30.31 (br s, $\Delta\nu_{1/2}$ = 72 Hz, 2C, $C^{2,6}$*C*- H(SiMe$_3$)$_A$(SiMe$_3$)$_B$, Tbb$_Y$), 31.31 (s, 3C, C^4-C*Me*$_3$, Tbb$_Y$), 31.43 (s, 3C, C^4-C*Me*$_3$, Tbb$_X$), 34.08 (s, 2C, $C^{2,6}$*C*-H(SiMe$_3$)$_A$(SiMe$_3$)$_B$, Tbb$_X$), 34.56 (s, 1C, C^4-*C*Me$_3$, Tbb$_Y$), 34.64 (s, 1C, C^4-*C*Me$_3$, Tbb$_X$), 120.33 (s, 2C, *C*^{3,5}-H, Tbb$_X$), 121.16 (s, 1C, N*C*(IMe$_2$*i*Pr$_2$)), 122.61 (s, 2C, *C*^{3,5}-H, Tbb$_Y$), 123.02 (br s, $\Delta\nu_{1/2}$ = 71 Hz, 2 × *C*-Me), 130.69 (s, 1C, *C*^{1}, Tbb$_Y$), 132.19 (s, 1C, *C*^{1}, Tbb$_X$), 150.67 (s, 2C, *C*^{2,6}C- H(SiMe$_3$)$_A$(SiMe$_3$)$_B$, Tbb$_X$), 151.14 (s, 1C, *C*^{4}-CMe$_3$, Tbb$_Y$), 151.94 (s, 1C, *C*^{4}- CMe$_3$, Tbb$_X$), 155.84 (s, 1C, *C*^{2}, N*C*N). Due to dynamics ($C^{2,6}$C-H(SiMe$_3$)$_A$(SiMe$_3$)$_B$, Tbb$_Y$) was not visible at 298 K.

^{29}Si{^{1}H} NMR (99.3 MHz, (D_6)benzene, 298 K): δ (ppm) = 0.67 (s, 2Si, $C^{2,6}$C- H($SiMe_3$)$_A$($SiMe_3$)$_B$, Tbb_Y), 1.90 (s, 2Si, $C^{2,6}$C-H($SiMe_3$)$_A$($SiMe_3$)$_B$, Tbb_X), 62.34 (s, 1Si, *Si*-Tbb_Y), 67.33 (s, 1Si, *Si*-Tbb_X).

4.5.46. [(IDipp)C-GeBrAr^{Mes}] (**41-Ge**)

A light-yellow solution of (IDipp)CN_2 (429 mg, 1.0 mmol, 1 equiv.) in 10 mL of benzene was slowly added to the yellow suspension of Ar^{Mes}GeBr (466 mg, 1.0 mmol, 1 equiv.) in 15 mL of benzene at ambient temperature. The colour of the reaction mixture turned yellow-orange after 5 hours of stirring at ambient temperature. An aliquot of the reaction solution in (D_6)benzene was analyzed by ^{1}H NMR spectroscopy, revealing the selective formation of **41-Ge**. The reaction solution was filtered and evaporated to dryness under vacuum, resulting in a yellow crude product, which was then crystallised from toluene (3 mL) at −30 °C. The resulting yellow crystals of **41-Ge** were isolated by filtration at −30 °C, followed by drying under a fine vacuum at 80 °C for one hour to afford **41-Ge** as a toluene hemisolvate, **41-Ge**·(C_7H_8)$_{0.5}$. Yield: 500 mg (0.577 mmol, 57 % from Ar^{Mes}GeBr).

Properties: Compound **41-Ge** is an air-sensitive yellow solid turning immediately colourless upon contact with air. Upon heating, it begins to decompose during melting at 220 °C. It can be stored under an argon atmosphere at ambient temperature for several months. **41-Ge** is very well soluble in benzene, toluene and moderately soluble in *n*-pentane and *n*-hexane at ambient temperature. Under strict exclusion of air, solutions of **41-Ge** in (D_6)benzene is stable for at least 48 hours without any sign of decomposition at ambient temperature.

Elemental analysis: 41-Ge·(C_7H_8)$_{0.5}$ ($C_{52}H_{61}BrGeN_2(C_7H_8)_{0.5}$, 912.64 g mol^{-1}): Calcd. /%: C 73.04, H 7.18, N 3.07; found /%: C 72.78, H 7.18, N 3.16.

^{1}H NMR (500.1 MHz, (D_6)benzene, 298 K): δ (ppm) = 0.92 (d, ^{3}J(H,H) = 6.8 Hz, 6H, 2 × C^6-CH*Me*$_A$Me$_B$, 2 × Dipp), 0.98 (d, ^{3}J(H,H) = 6.8 Hz, 6H, 2 × C^6-CHMe$_A$*Me*$_B$, 2 × Dipp), 1.15−1.23 (m, 6H, 2 × C^2-CHMe$_A$*Me*$_B$, 2 × Dipp), 1.22 (d, ^{3}J(H,H) = 6.6 Hz, 6H, 2 × C^2-CH*Me*$_A$Me$_B$, 2 × Dipp), 2.14 (s, 3H, C^4-*Me*, Mes(Act.)), 2.20 (s, 3H, C^4-*Me*, Mes), 2.27(s, 3H, C^6-*Me*, Mes(Act.)), 2.35 (s, 3H, C^2-*Me*, Mes), 2.45 (s, 3H, C^6-*Me*, Mes), 2.52 (br s, $\Delta\nu_{1/2}$ = 34 Hz, 2H, 2 × C^2-C*H*Me$_A$Me$_B$, 2 × Dipp), 2.76−2.84 (m, 2H, C^2-CH_AH_B, Mes(Act.)), 2.85−2.90 (m, 2H, 2 × C^6-C*H*Me$_A$Me$_B$, 2 × Dipp), 3.59 (dd, ^{3}J(H,H) = 11.0, 1.2 Hz, 1H, C-*H*), 6.01 (br s, $\Delta\nu_{1/2}$ = 12.9 Hz, 2H, $C^{4,5}$-*H*, IDipp), 6.77 (s, 1H, C^3-*H*, Mes(Act.)), 6.81 (s, 1H, C^3-*H*, Mes), 6.92−6.93 (m, 4H, C^5-*H*, Mes, + C^5-*H*, Mes(Act.), + $C^{3,5}$-*H*, Ar^{Mes}), 6.98−7.04 (m, 4H, 2 × C^3-*H* + 2 × C^5-*H*, 2 × Dipp), 7.08−7.12 (m, 2H, C^4-*H*, Ar^{Mes} + C^4-*H*, Dipp), 7.16−7.18 (m, 1H, C^4-*H*, Dipp).

$^{13}C\{^1H\}$ NMR (125.8 MHz, (D_6)benzene, 298 K): δ (ppm) = 21.24 (s, 3C, C^2-*Me*, Mes + 2 × C^6-CH*Me*$_A$Me$_B$, 2 × Dipp), 21.31 (s, 1C, C^6-*Me*, Mes(Act.)), 21.84 (s, 1C, C^4-*Me*, Mes), 22.06 (s, 1C, C^4-*Me*, Mes(Act.)), 22.76 (s, 1C, C^6-*Me*, Mes), 22.89 (s, 2 × C^2-CH*Me*$_A$Me$_B$, 2 × Dipp), 25.74 (s, 2 × C^6-CHMe$_A$*Me*$_B$, 2 × Dipp), 26.31 (s, 2 × C^2-CHMe$_A$*Me*$_B$, 2 × Dipp), 29.24 (s, 2 × C^6-*C*HMe$_A$Me$_B$, 2 × Dipp), 29.65 (s, 2 × C^2-*C*H*Me*$_A$Me$_B$, 2 × Dipp), 32.47 (s, 1C, C^2-*C*H$_A$H$_B$, Mes(Act.)), 46.67 (s, 1C, *C*-Ge), 121.67 (s, 2C, *C*^{4,5}H, IDipp), 124.67 (s, 1C, *C*^{3}-H, Ar^{Mes}), 125.00 (s, 1C, *C*^{5}-H, Ar^{Mes}), 126.26 (s, *C*^{3}-H, Mes(Act.)), 127.32 (s, 2C, 2 × *C*^{4}-H, 2 × Dipp), 127.44 (s, 2C, 2 × *C*^{5}-H, 2 × Dipp), 127.51 (s, 1C, *C*^{5}-H, Mes), 129.11 (s, 1C, *C*^{3}-H, Mes), 129.33 (s, 2C, 2 × *C*^{3}-H, 2 × Dipp), 129.79 (s, 1C, *C*^{5}-H, Mes(Act.)), 131.47 (s, 1C, *C*^{4}-H, Ar^{Mes}), 132.77 (s, 1C, *C*^{2}-Mes, Ar^{Mes}), 133.91 (s, 1C, *C*^{6}-Me, Mes), 135.16 (s, 1C, *C*^{4}-Me, Mes(Act.)), 135.42 (s, 1C, *C*^{4}-Me, Mes), 137.83 (s, 1C, *C*^{2}-Me, Mes(Act.)), 138.07 (s, 1C, *C*^{6}-Me, Mes(Act.)), 139.29 (s, 1C, *C*^{2}- Me, Mes), 140.54 (s, 1C, *C*^{1}, Mes(Act.)), 141.20 (s, 1C, *C*^{1}, Mes), 144.27 (s, 1C, *C*^{6}- Mes, Ar^{Mes}), 145.87 (s, 2C, 2 × *C*^{2}-CHMe$_A$Me$_B$, 2 × Dipp), 146.50 (s, 1C, *C*^{1}, Ar^{Mes}), 148.06 (s, 2C, 2 × *C*^{6}-CHMe$_A$Me$_B$, 2 × Dipp), 159.31 (s, 2C, 2 × *C*^{1}, 2 × Dipp), 159.69(s, 1C, *C*^{2}, IDipp).

4.5.47. [$(PMe_3)_2$Ni(SiClTbb)$_2$] (42-Ni)

A red solution of $(PMe_3)_2NiCl_2$ (59 mg, 0.21 mmol, 1 equiv.) in 3 mL of benzene was added to a stirred yellow-orange solution of TbbSi≡SiTbb (200 mg, 0.21 mmol, 1 equiv.) in 10 mL of benzene at ambient temperature. The colour of the reaction solution was immediately changed to dark brown. After 1 hour of stirring at ambient temperature, an aliquot of the reaction solution in (D_6)benzene was analysed by ^1H and ^{31}P NMR spectroscopy, revealing the complete consumption of the starting materials and the formation of **42-Ni,** along with some Tbb-containing impurity. The reaction solution was filtered and evaporated to dryness in a vacuum followed by a freeze-pump-thaw resulting in a brown crude product which was crystallized from 5 mL of 2:3 (CH_3CN : Et_2O) mixture at −30 °C. The resulting dark-brown crystals were isolated by filtration at −30 °C followed by drying under a fine vacuum at ambient temperature for 30 min to afford **42-Ni**. Yield: 112 mg (0.090 mmol, 43 % from TbbSi≡SiTbb).

Properties: Compound **42-Ni** is an air-sensitive dark brown solid turning immediately colourless upon contact with air. Upon heating, it begins to decompose during melting at 114 °C. It can be stored under an argon atmosphere at ambient temperature for several months. **42-Ni** is very well soluble in THF, benzene, Et_2O, *n*- pentane and *n*-hexane and insoluble in CH_3CN at ambient temperature. Under

strict exclusion of air, solutions of **42-Ni** in (D_6)benzene is stable for at least 24 hours without any sign of decomposition at ambient temperature.

Elemental analysis: 42-Ni ($C_{54}H_{116}Cl_2NiP_2Si_{10}$, 1237.90 g mol^{-1}): Calcd. /%: C 52.75, H 9.56; found /%: C 52.32, H 9.43.

^{1}H NMR (500.1 MHz, (D_6)benzene, 298 K): δ (ppm) = 0.33 (s, 36H, 2 × $C^{2,6}$C-H(Si*Me*$_3$)$_A$(SiMe$_3$)$_B$, 2 × Tbb), 0.36 (s, 36H, 2 × $C^{2,6}$C-H(SiMe$_3$)$_A$(Si*Me*$_3$)$_B$, 2 × Tbb), 1.33 (s, 18H, 2 × C^4-C*Me*$_3$, 2 × Tbb),1.39 (d, ^2J(^{31}P-^{1}H) = 6 Hz, 18H, 2 × P*Me*$_3$), 2.54 (s, 4H, 2 × $C^{2,6}$C-*H*(SiMe$_3$)$_A$(SiMe$_3$)$_B$, 2 × Tbb), 6.85 (s, 4H, 2 × $C^{3,5}$-*H*, 2 × Tbb).

^{13}C{^{1}H} NMR (125.8 MHz, (D_6)benzene, 298 K): δ (ppm) = 1.86 (s, 12C, 2 × $C^{2,6}$C- H(Si*Me*$_3$)$_A$(SiMe$_3$)$_B$, 2 × Tbb), 2.30 (s, 12C, 2 × $C^{2,6}$C-H(Si*Me*$_3$)$_A$(SiMe$_3$)$_B$, 2 × Tbb), 24.59 (dd, ^1J(^{31}P-^{13}C) = 15 Hz, ^3J(^{31}P-^{13}C) = 11 Hz, 6C, 2 × P*Me*$_3$), 29.94 (s, 4C, 2 × *C*^{2,6}*C*- H(SiMe$_3$)$_A$(SiMe$_3$)$_B$, 2 × Tbb), 31.30 (s, 6C, 2 × C^4-C*Me*$_3$, 2 × Tbb), 34.43 (s, 2C, 2 × C^4-*C*Me$_3$, 2 × Tbb), 122.33 (s, 4C, 2 × *C*^{3,5}-H, 2 × Tbb), 146.27 (s, 4C, 2 × *C*^{2,6}C- H(SiMe$_3$)$_A$(SiMe$_3$)$_B$, 2 × Tbb), 147.55 (s, 2C, 2 × *C*^{4}-C*Me*$_3$, 2 × Tbb), 150.29 (s, 2C, 2 × *C*^{1} , 2 × Tbb).

^{31}P{^{1}H} NMR (200.4 MHz, (D_6)benzene, 298 K): δ (ppm) = −21.08 (s, 2P, 2 × *P*Me$_3$).

4.5.48. [Cp*Rh(TbbGeCl)$_2$)] (43-Rh)

To a stirred yellow-brown solution of TbbGe≡GeTbb (300 mg, 0.29 mmol, 1 equiv.) in 15 mL of toluene, a red solution of [Cp*RhCl$_2$]$_2$ (90 mg, 0.145 mmol, 0.5 equiv.) in 5 mL of toluene was added at ambient temperature. The colour of the reaction solution was immediately changed to dark brown. After 1 hour of stirring at ambient temperature, an aliquot of the reaction solution in (D_6)benzene was analyzed by ^{1}H spectroscopy, revealing complete consumption of the starting materials and selective formation of **43-Rh** along with some Tbb-containing impurity. The reaction solution was filtered and evaporated to dryness in a vacuum followed by a freeze-pump-thaw, resulting in a brown crude product, which was crystallized from *n*-pentane (2 mL) and stored at −30 °C. Dark-brown crystals were isolated by filtration at −30 °C followed by drying at ambient temperature for 30 min. Yield: 200 mg (0.147 mmol, 51 % from TbbGe≡GeTbb).

Properties: Compound **43-Rh** is an air-sensitive dark brown solid that turns immediately colourless upon contact with air. Upon heating, it begins to decompose during melting at 175 °C. It can be stored under an argon atmosphere at ambient temperature for several months. **43-Rh** is very well soluble in THF, benzene, Et$_2$O, *n*- pentane and *n*-hexane at ambient temperature. Under strict exclusion of air,

solutions of **43-Rh** in (D_6)benzene is stable for at least 24 hours without any sign of decomposition at ambient temperature.

Elemental analysis: 43-Rh ($C_{58}H_{113}Cl_2Ge_2RhSi_8$, 1354.23 g mol^{-1}): Calcd. /%: C 52.43, H 8.65; found: /%: C 52.62, H 8.60.

^{1}H NMR (500.1 MHz, (D_6)benzene, 298 K): δ (ppm) = 0.33 (s, 72H, 2 × $C^{2,6}$C-H(Si*Me*$_3$)$_2$, 2 × Tbb), 1.31 (s, 18H, 2 × C^4-C*Me*$_3$, 2 × Tbb), 2.06 (s, 15H, C_5*Me*$_5$, Cp*), 2.41 (s, 4H, 2 × $C^{2,6}$C-*H*(SiMe$_3$)$_2$, 2 × Tbb), 6.92 (s, 4H, 2 × $C^{3,5}$-*H*, 2 × Tbb).

^{13}C{^{1}H} NMR (125.8 MHz, (D_6)benzene, 298 K): δ (ppm) = 2.18 (s, 24C, 2 × $C^{2,6}$C- H(Si*Me*$_3$)$_2$, 2 × Tbb), 11.98 (s, 5C, C_5*Me*$_5$, Cp*), 28.96 (s, 4C, 2 × *C*^{2,6}*C*-H(SiMe$_3$)$_2$, 2 × Tbb), 31.22 (s, 6C, 2 × C^4-C*Me*$_3$, 2 × Tbb), 34.46 (s, 2C, 2 × C^4-*C*Me$_3$, 2 × Tbb), 98.64 (d, ^1J(^{103}Rh,^{13}C) = 4.60 Hz, 5C, *C*$_5$Me$_5$, Cp*), 124.19 (s, 4C, 2 × *C*^{3,5}-H, 2 × Tbb), 146.00 (s, 4C, 2 × *C*^{2,6}C-H(SiMe$_3$)$_2$, 2 × Tbb), 150.27 (s, 2C, 2 × *C*^{4}-C*Me*$_3$, 2 × Tbb), 155.55 (d, ^2J(^{103}Rh,^{13}C) = 14 Hz, 2C, 2 × *C*^{1} , 2 × Tbb).

5. Appendices

5.1. List of synthesized compounds

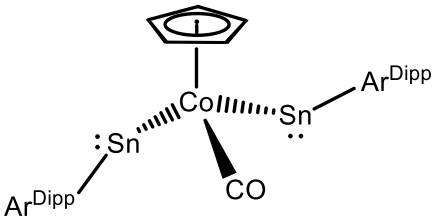

2-Co

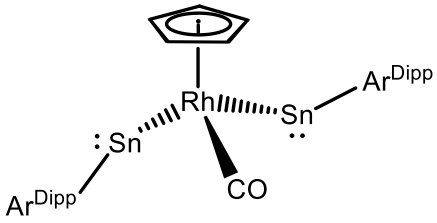

2-Rh

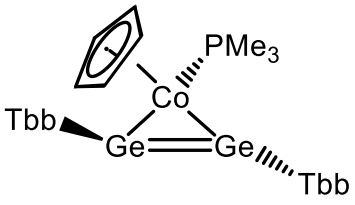

3-Co

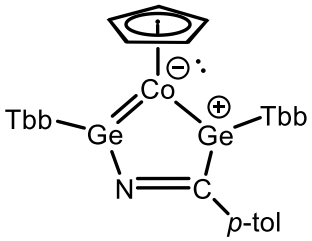

4-Co

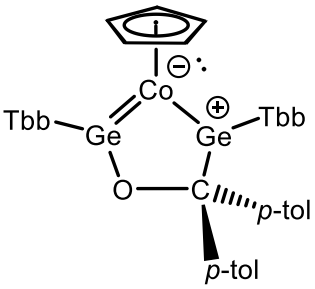

5-Co

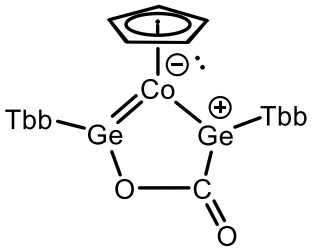

6-Co

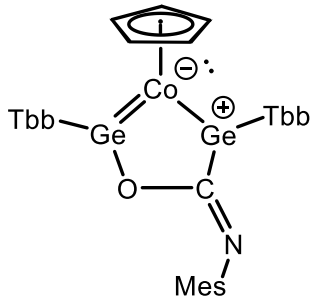

7-Co

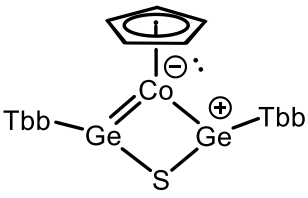

8-Co

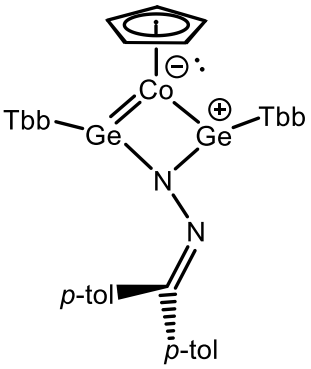

9-Co

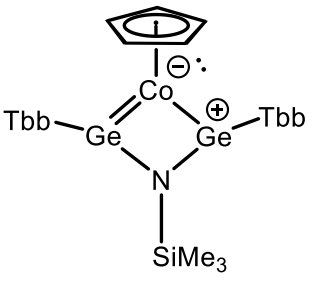

10-Co

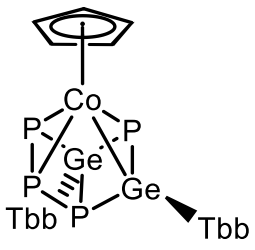

11-Co

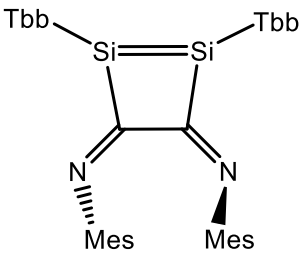

12-Si

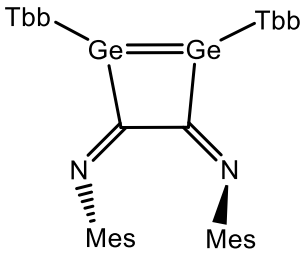

12-Ge

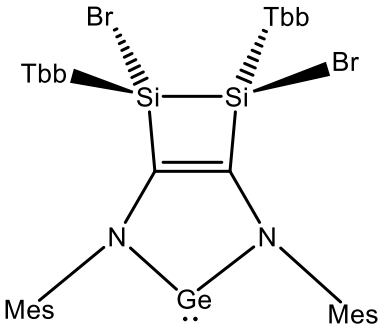

13-Si

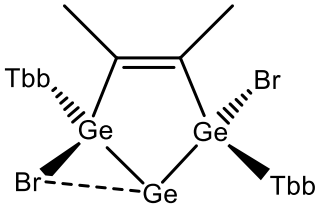

14-Ge

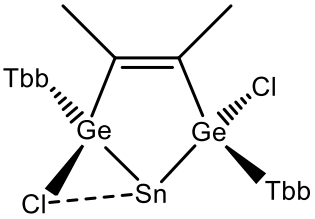

14-Sn

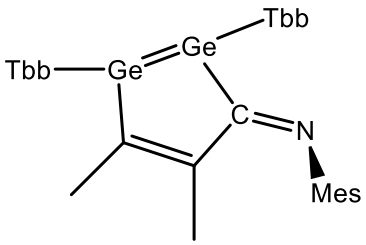

15-Ge

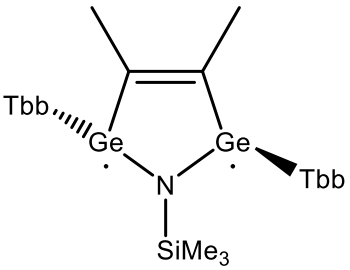

16-Ge

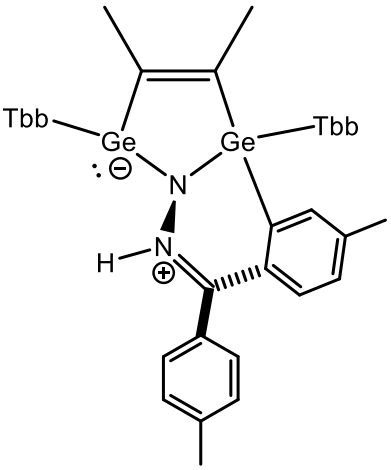

17-Ge

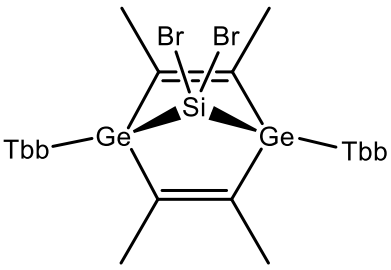

18-Si

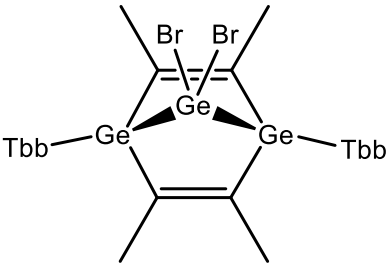

18-Ge

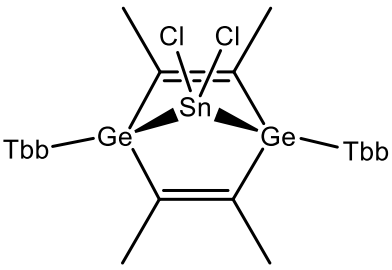

18-Sn

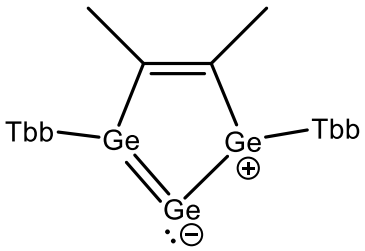

19-Ge

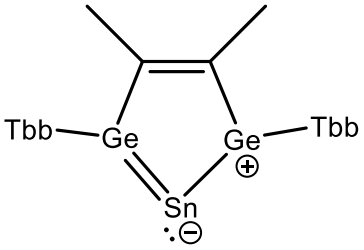

19-Sn

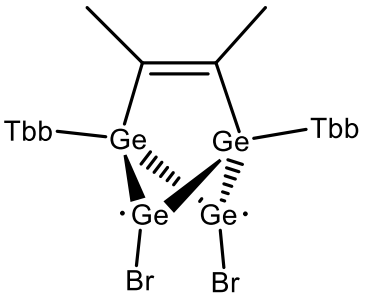

20-Ge

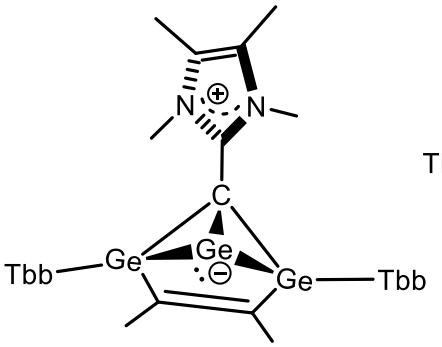

21-Ge

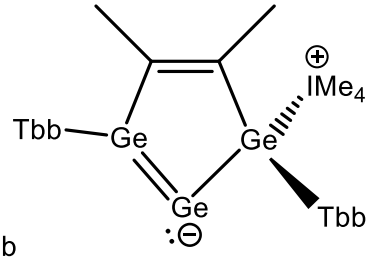

22-Ge

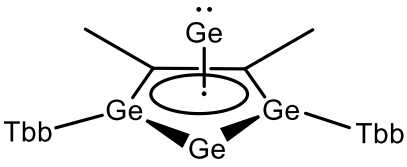

23-Ge

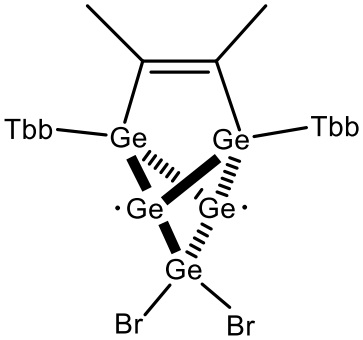

24-Ge

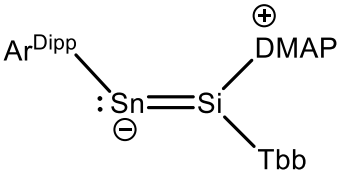

25-SnSi

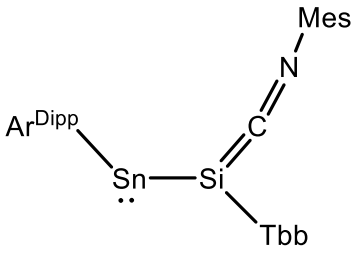

26-SnSi

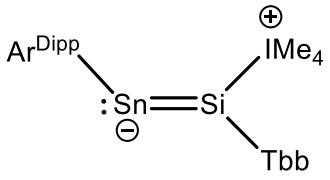

27-SnSi

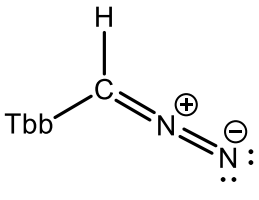

28

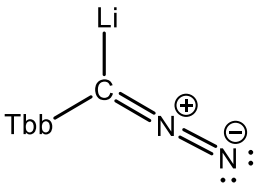

29

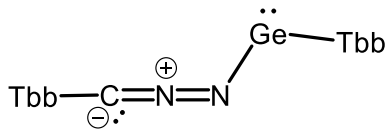

30-Ge

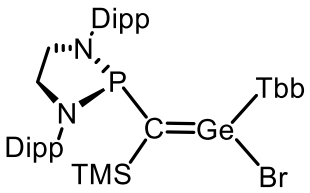

31-Ge

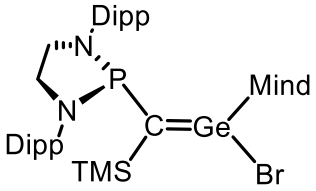

32-Ge

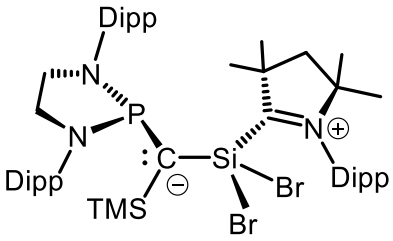

33-Si

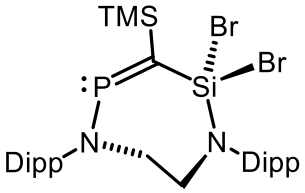

34-Si

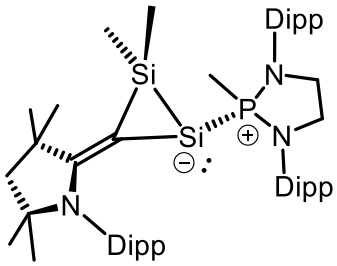

35-Si

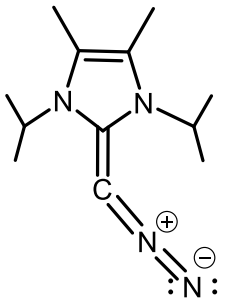

36

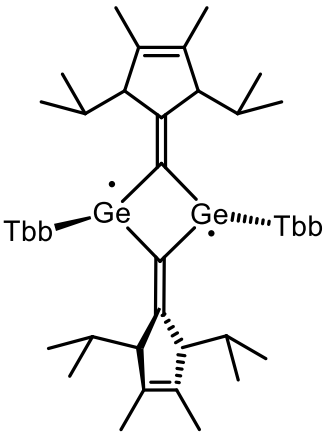

37-Ge

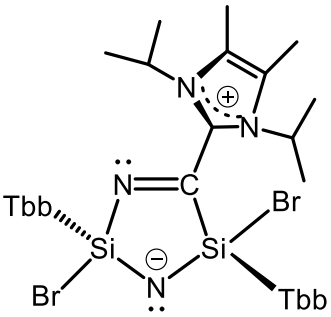

38-Si

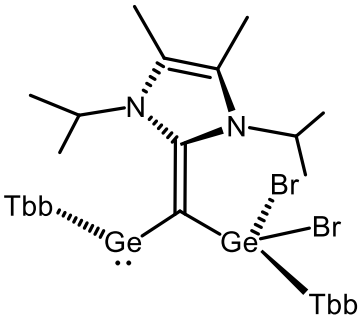

39-Ge

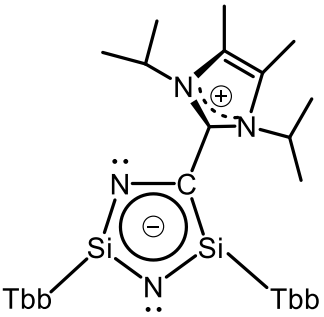

40-Si

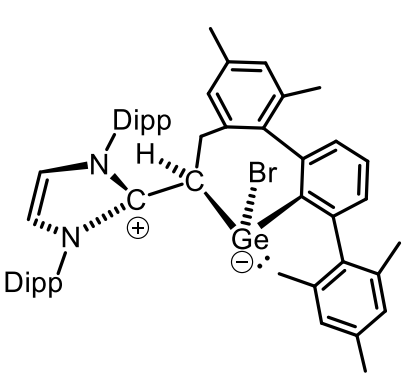

41-Ge

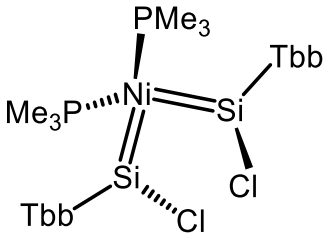

42-Ni

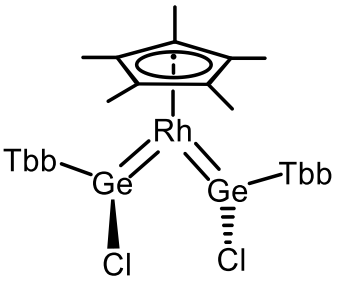

43-Rh

5.2. Crystallographic data of synthesized compounds

Table 6. Crystal data and structure refinement parameters of [$CpCoSn_2Ar^{Dipp}_2$] (**2-Co**) and [$CpRhSn_2Ar^{Dipp}_2$] (**2-Rh**).

	2-Co	**2-Rh**
Crystal Habitus	clear reddish brown needle	clear green plank
Device Type	Bruker X8-KappaApexII	Bruker D8 Venture
Empirical formula	$C_{70}H_{89}CoO_2Sn_2$	$C_{70}H_{89}O_2RhSn_2$
Moiety formula	$C_{66}H_{79}CoOSn_2$, $C_4H_{10}O$	$C_{66}H_{79}ORhSn_2$, $C_4H_{10}O$
Formula weight	1258.72	1302.70
Temperature/K	123	100.0
Crystal system	monoclinic	monoclinic
Space group	C2/c	C2/c
a/Å	22.544(6)	22.4814(12)
b/Å	11.523(3)	11.5602(6)
c/Å	48.691(13)	48.653(3)
α/°	90	90
β/°	91.447(6)	91.599(2)
γ/°	90	90
Volume/Å^3	12644(6)	12639.6(12)
Z	8	8
ρ_{calc}g/cm^3	1.322	1.369
μ/mm^{-1}	1.085	1.085
F(000)	5216.0	5360.0
Crystal size/mm^3	0.25 × 0.03 × 0.02	0.4 × 0.1 × 0.04
Absorption correction	empirical	multi-scan
Tmin; Tmax	0.246519; 0.746068	0.6590; 0.7461
Radiation	MoKα (λ = 0.71073)	MoKα (λ = 0.71073)
2Θ range for data collection/°	5.736 to 50.498°	3.962 to 56°
Completeness to theta	0.973	0.997
Index ranges	? ≤ h ≤ ?, ? ≤ k ≤ ?, ? ≤ l ≤ ?	-29 ≤ h ≤ 29, -15 ≤ k ≤ 15, -59 ≤ l ≤ 64
Reflections collected	11129	80069
Independent reflections	11129 [R_{int} = 0.2599, R_{sigma} = 0.1266]	15244 [R_{int} = 0.0346, R_{sigma} = 0.0246]
Data/restraints/parameters	11129/0/694	15244/2/676
Goodness-of-fit on F^2	1.035	1.033
Final R indexes [I>=2σ (I)]	R_1 = 0.0746, wR_2 = 0.1614	R_1 = 0.0248, wR_2 = 0.0590
Final R indexes [all data]	R_1 = 0.1162, wR_2 = 0.1809	R_1 = 0.0284, wR_2 = 0.0612
Largest diff. peak/hole / e Å^{-3}	1.05/-1.39	1.34/-0.59

Table 7. Crystal data and structure refinement parameters of [CpCo(PMe$_3$)Ge$_2$Tbb$_2$] (**3-Co**) and [CpCo(CN)(*p*-tol)Ge$_2$Tbb$_2$] (**4-Co**).

	3-Co	**4-Co**
Crystal Habitus	clear brown block	clear dark brown block
Device Type	STOE IPDS-2T	Bruker D8 Venture
Empirical formula	$C_{60}H_{122}CoGe_2OPSi_8$	$C_{65}H_{120}CoGe_2NOSi_8$
Moiety formula	$C_{56}H_{112}CoGe_2PSi_8$, $C_4H_{10}O$	$C_{61}H_{110}CoGe_2NSi_8$, ($C_4H_{10}O$)
Formula weight	1319.37	1360.44
Temperature/K	123(2)	100.0
Crystal system	orthorhombic	triclinic
Space group	Pbca	P-1
a/Å	17.4829(3)	12.9039(7)
b/Å	25.6016(3)	17.3085(8)
c/Å	33.7460(4)	19.2887(11)
α/°	90	81.584(2)
β/°	90	79.641(2)
γ/°	90	71.055(2)
Volume/Å^3	15104.4(4)	3990.3(4)
Z	8	2
ρ_{calc}g/cm^3	1.160	1.132
μ/mm^{-1}	1.190	1.109
F(000)	5664.0	1456.0
Crystal size/mm^3	0.6 × 0.48 × 0.36	0.24 × 0.16 × 0.14
Absorption correction	multi-scan	empirical
Tmin; Tmax	0.3800; 0.4623	0.6555; 0.7461
Radiation	MoKα (λ = 0.71073)	MoKα (λ = 0.71073)
2Θ range for data collection/°	3.994 to 56.998°	4.25 to 61.118°
Completeness to theta	0.999	0.999
Index ranges	-23 ≤ h ≤ 23, -34 ≤ k ≤ 32, -45 ≤ l ≤ 27	-18 ≤ h ≤ 18, -24 ≤ k ≤ 24, -27 ≤ l ≤ 27
Reflections collected	162870	184326
Independent reflections	19118 [R_{int} = 0.0546, R_{sigma} = 0.0383]	24403 [R_{int} = 0.0649, R_{sigma} = 0.0391]
Data/restraints/parameters	19118/881/818	24403/130/830
Goodness-of-fit on F^2	1.066	1.112
Final R indexes [I>=2σ (I)]	R_1 = 0.0526, wR_2 = 0.0933	R_1 = 0.0467, wR_2 = 0.1277
Final R indexes [all data]	R_1 = 0.0745, wR_2 = 0.0984	R_1 = 0.0641, wR_2 = 0.1478
Largest diff. peak/hole / e Å^{-3}	0.60/-0.53	1.52/-1.25

Table 8. Crystal data and structure refinement parameters of [CpCo(CO)(*p*-tol)$_2$Ge$_2$Tbb$_2$] (**5-Co**).and [CpCo(CO)(O)Ge$_2$Tbb$_2$] (**6-Co**).

	5-Co	**6-Co**
Crystal Habitus	clear red plate	clear dark orange plank
Device Type	STOE IPDS-2T	STOE Stadivari
Empirical formula	$C_{68}H_{117}CoGe_2OSi_8$	$C_{114}H_{216}Co_2Ge_4O_4Si_{16}$
Moiety formula	$C_{68}H_{117}CoGe_2OSi_8$	$2(C_{54}H_{103}CoGe_2O_2Si_8)$, C_6H_{10}
Formula weight	1379.44	2508.52
Temperature/K	123	100
Crystal system	triclinic	monoclinic
Space group	P-1	$P2_1$
a/Å	11.9827(9)	9.4856(3)
b/Å	17.559(2)	22.5802(5)
c/Å	20.5608(13)	33.4710(10)
α/°	72.300(8)	90.00
β/°	78.473(5)	90.439(3)
γ/°	70.752(7)	90.00
Volume/Å^3	3867.0(6)	7168.9(4)
Z	2	2
ρ_{calc}g/cm^3	1.185	1.162
μ/mm^{-1}	1.145	4.316
F(000)	1472.0	2676.0
Crystal size/mm^3	0.48 × 0.32 × 0.08	0.22 × 0.21 × 0.05
Absorption correction	integration	multi-scan
Tmin; Tmax	0.6813; 0.9047	0.2019; 0.3817
Radiation	MoKα (λ = 0.71073)	CuKα (λ = 1.54186)
2Θ range for data collection/°	4.976 to 55.998°	7.83 to 141.236°
Completeness to theta	0.994	0.995
Index ranges	-15 ≤ h ≤ 14, -23 ≤ k ≤ 23, -27 ≤ l ≤ 27	-11 ≤ h ≤ 11, -20 ≤ k ≤ 27, -40 ≤ l ≤ 31
Reflections collected	39713	59255
Independent reflections	18353 [R_{int} = 0.0484, R_{sigma} = 0.0926]	20842 [R_{int} = 0.0753, R_{sigma} = 0.0840]
Data/restraints/parameters	18353/12/793	20842/1/1324
Goodness-of-fit on F^2	0.808	1.025
Final R indexes [I>=2σ (I)]	R_1 = 0.0369, wR_2 = 0.0631	R_1 = 0.0777, wR_2 = 0.1915
Final R indexes [all data]	R_1 = 0.0807, wR_2 = 0.0711	R_1 = 0.1019, wR_2 = 0.2116
Largest diff. peak/hole / e Å^{-3}	0.40/-0.56	1.40/-0.92

Table 9. Crystal data and structure refinement parameters of [CpCo(CO)(NMes)Ge_2Tbb$_2$] (**7-Co**).and [CpCo(S)Ge_2Tbb$_2$] (**8-Co**).

	7-Co	**8-Co**
Crystal Habitus	clear dark yellow plate	clear violet plate
Device Type	Bruker D8 Venture	Bruker D8 Venture
Empirical formula	$C_{63}H_{114}NOSi_8CoGe_2$	$C_{53}H_{103}Si_8SCoGe_2$
Moiety formula	$C_{63}H_{114}CoGe_2NOSi_8$	$C_{53}H_{103}CoGe_2SSi_8$
Formula weight	1330.38	1201.24
Temperature/K	100.0	100.0
Crystal system	triclinic	triclinic
Space group	P-1	P-1
a/Å	14.929(2)	12.7968(14)
b/Å	16.292(2)	17.2537(19)
c/Å	17.352(3)	17.6772(19)
α/°	111.978(5)	96.339(5)
β/°	101.920(6)	106.479(4)
γ/°	90.886(6)	109.122(4)
Volume/Å^3	3809.2(10)	3446.0(7)
Z	2	2
ρ_{calc}g/cm^3	1.160	1.158
μ/mm^{-1}	1.160	1.303
F(000)	1420.0	1280.0
Crystal size/mm^3	0.02 × 0.01 × 0.01	0.32 × 0.16 × 0.02
Absorption correction	empirical	multi-scan
Tmin; Tmax	0.6175; 0.7461	0.6143; 0.7468
Radiation	MoKα (λ = 0.71073)	MoKα (λ = 0.71073)
2Θ range for data collection/°	3.694 to 56°	4.854 to 58.5°
Completeness to theta	0.999	0.999
Index ranges	-19 ≤ h ≤ 19, -21 ≤ k ≤ 21, -22 ≤ l ≤ 22	-17 ≤ h ≤ 17, -23 ≤ k ≤ 23, -24 ≤ l ≤ 24
Reflections collected	122565	100481
Independent reflections	18381 [R_{int} = 0.2991, R_{sigma} = 0.2005]	18779 [R_{int} = 0.0544, R_{sigma} = 0.0411]
Data/restraints/parameters	18381/0/718	18779/52/647
Goodness-of-fit on F^2	0.985	1.047
Final R indexes [I>=2σ (I)]	R_1 = 0.0725, wR_2 = 0.1438	R_1 = 0.0406, wR_2 = 0.0977
Final R indexes [all data]	R_1 = 0.1827, wR_2 = 0.1939	R_1 = 0.0611, wR_2 = 0.1101
Largest diff. peak/hole / e Å^{-3}	0.70/-0.85	1.46/-0.70

Table 10. Crystal data and structure refinement parameters of [CpCo(N)NC(*p*-tol)$_2$Ge$_2$Tbb$_2$] (**9-Co**) and [CpCo(N)(SiMe$_3$)Ge$_2$Tbb$_2$] (**10-Co**).

	9-Co	**10-Co**
Crystal Habitus	clear brown block	clear pinkish brown plate
Device Type	STOE IPDS-2T	Bruker D8 Venture
Empirical formula	$C_{72}H_{127}CoGe_2N_2OSi_8$	$C_{56}H_{112}NSi_9CoGe_2$
Moiety formula	$C_{68}H_{117}CoGe_2N_2Si_8$, $C_4H_{10}O$	$C_{56}H_{112}CoGe_2NSi_9$
Formula weight	1465.58	1256.38
Temperature/K	123	100.0
Crystal system	triclinic	triclinic
Space group	P-1	P-1
a/Å	12.7525(6)	13.1937(18)
b/Å	17.3326(12)	17.413(2)
c/Å	20.4941(10)	33.044(4)
α/°	80.638(5)	78.102(4)
β/°	86.219(4)	84.660(5)
γ/°	70.534(5)	73.948(4)
Volume/Å^3	4213.7(4)	7133.5(15)
Z	2	4
ρ_{calc}g/cm^3	1.155	1.170
μ/mm^{-1}	1.055	1.250
F(000)	1568.0	2688.0
Crystal size/mm^3	0.8 × 0.24 × 0.22	0.238 × 0.156 × 0.06
Absorption correction	integration	empirical
Tmin; Tmax	0.7612; 0.8890	0.6561; 0.7460
Radiation	MoKα (λ = 0.71073)	MoKα (λ = 0.71073)
2Θ range for data collection/°	5.232 to 52°	3.782 to 56.8°
Completeness to theta	0.979	0.999
Index ranges	-15 ≤ h ≤ 15, -21 ≤ k ≤ 21, -25 ≤ l ≤ 24	-17 ≤ h ≤ 17, -23 ≤ k ≤ 23, -44 ≤ l ≤ 44
Reflections collected	33967	191491
Independent reflections	16216 [R_{int} = 0.0651, R_{sigma} = 0.0996]	35778 [R_{int} = 0.0549, R_{sigma} = 0.0459]
Data/restraints/parameters	16216/61/861	35778/1245/1322
Goodness-of-fit on F^2	0.848	1.033
Final R indexes [I>=2σ (I)]	R_1 = 0.0408, wR_2 = 0.0722	R_1 = 0.0452, wR_2 = 0.1056
Final R indexes [all data]	R_1 = 0.0789, wR_2 = 0.0799	R_1 = 0.0624, wR_2 = 0.1138
Largest diff. peak/hole / e Å^{-3}	0.66/-0.56	1.90/-0.71

Table 11. Crystal data and structure refinement parameters of [CpCo(P_4)Ge_2Tbb$_2$] (**11-Co**) and [Tbb$_2$$Si_2$(CNMes)$_2$] (**12-Si**).

	11-Co	**12-Si**
Crystal Habitus	clear red plate	clear orange plank
Device Type	Bruker D8 Venture	STOE STADIVARI
Empirical formula	$C_{57}H_{113}CoGe_2OP_4Si_8$	$C_{141}H_{252}N_4Si_{20}$
Moiety formula	$C_{53}H_{103}CoGe_2P_4Si_8$, C_4 $H_{10}O$	2($C_{68}H_{120}N_2Si_{10}$), C_5H_{12}
Formula weight	1367.18	2565.25
Temperature/K	100.0	100.0
Crystal system	monoclinic	triclinic
Space group	$P2_1/c$	P-1
a/Å	14.7369(5)	13.6112(4)
b/Å	32.1583(9)	14.9401(4)
c/Å	17.1730(6)	21.8485(6)
α/°	90	78.726(2)
β/°	112.8810(10)	86.199(2)
γ/°	90	70.864(2)
Volume/Å^3	7498.1(4)	4116.4(2)
Z	4	1
ρ_{calc}g/cm^3	1.211	1.035
μ/mm^{-1}	1.262	1.772
F(000)	2904.0	1406.0
Crystal size/mm^3	0.28 × 0.26 × 0.12	0.6 × 0.353 × 0.22
Absorption correction	empirical	multi-scan
Tmin; Tmax	0.581101; 0.746069	0.4755; 0.5963
Radiation	MoKα (λ = 0.71073)	CuKα (λ = 1.54186)
2Θ range for data collection/°	4.82 to 57.998°	6.372 to 141.96°
Completeness to theta	0.999	0.993
Index ranges	-20 ≤ h ≤ 18, 0 ≤ k ≤ 43, 0 ≤ l ≤ 23	-8 ≤ h ≤ 16, -15 ≤ k ≤ 18, -26 ≤ l ≤ 26
Reflections collected	19775	104910
Independent reflections	19775 [R_{int} = ?, R_{sigma} = 0.1121]	15533 [R_{int} = 0.0564, R_{sigma} = 0.0374]
Data/restraints/parameters	19775/711/722	15533/700/804
Goodness-of-fit on F^2	1.107	1.039
Final R indexes [I>=2σ (I)]	R_1 = 0.0774, wR_2 = 0.1641	R_1 = 0.0467, wR_2 = 0.1158
Final R indexes [all data]	R_1 = 0.1466, wR_2 = 0.1933	R_1 = 0.0651, wR_2 = 0.1268
Largest diff. peak/hole / e Å^{-3}	1.23/-0.99	0.41/-0.38

Table 12. Crystal data and structure refinement parameters of [$Tbb_2Ge_2(CNMes)_2$] (**12-Ge**) and [$Ge(TbbSiBr)_2(CNMes)_2$] (**13-Si**).

	12-Ge	**13-Si**
Crystal Habitus	clear red plate	dull yellow block
Device Type	STOE STADIVARI	STOE Stadivari
Empirical formula	$C_{68}H_{120}N_2Ge_2Si_8$	$C_{170}H_{278}Br_4Ge_2N_4Si_{20}$
Moiety formula	$C_{68}H_{120}Ge_2N_2Si_8$	$2(C_{68}H_{120}Br_2GeN_2Si_{10})$, $4(C_7H_8)$, C_6H_6
Formula weight	1335.60	3404.68
Temperature/K	100	100.0
Crystal system	monoclinic	triclinic
Space group	$P2_1/c$	P-1
a/Å	15.1643(6)	13.70853(25)
b/Å	21.4625(6)	25.1449(4)
c/Å	24.5460(10)	29.6653(6)
α/°	90.00	108.2997(14)
β/°	91.219(3)	89.7550(16)
γ/°	90.00	104.5182(14)
Volume/$Å^3$	7987.0(5)	9367.6(3)
Z	4	2
$\rho_{calc}g/cm^3$	1.111	1.207
μ/mm^{-1}	2.34	2.971
F(000)	2872.0	3620.0
Crystal size/mm^3	0.12 × 0.09 × 0.02	0.15 × 0.1 × 0.08
Absorption correction	multi-scan	multi-scan
Tmin; Tmax	0.4929; 0.8720	0.4553; 0.6025
Radiation	CuKα (λ = 1.54186)	CuKα (λ = 1.54186)
2Θ range for data collection/°	7.138 to 142.706°	6.682 to 141.63°
Completeness to theta	0.997	0.985
Index ranges	-18 ≤ h ≤ 17, -24 ≤ k ≤ 26, -30 ≤ l ≤ 18	-16 ≤ h ≤ 16, -30 ≤ k ≤ 24, -18 ≤ l ≤ 36
Reflections collected	101158	115291
Independent reflections	15215 [R_{int} = 0.1593, R_{sigma} = 0.1005]	34973 [R_{int} = 0.0574, R_{sigma} = 0.0545]
Data/restraints/parameters	15215/0/757	34973/1843/1968
Goodness-of-fit on F^2	1.036	1.385
Final R indexes [I>=2σ (I)]	R_1 = 0.0858, wR_2 = 0.1852	R_1 = 0.1139, wR_2 = 0.3090
Final R indexes [all data]	R_1 = 0.1556, wR_2 = 0.2347	R_1 = 0.1394, wR_2 = 0.3387
Largest diff. peak/hole / e $Å^{-3}$	2.09/-1.24	5.11/-1.92

Table 13. Crystal data and structure refinement parameters of [Tbb$_2$Ge$_3$Br$_2$C$_2$Me$_2$] (**14-Ge**) and [Tbb$_2$Ge$_2$SnCl$_2$C$_2$Me$_2$] (**14-Sn**).

	14-Ge	**14-Sn**
Crystal Habitus	clear colourless plate	clear yellowish colourless plate
Device Type	Bruker D8 Venture	Bruker D8 Venture
Empirical formula	$C_{108}H_{218}Br_4Ge_6OSi_{16}$	$C_{52}H_{104}Cl_2Ge_2Si_8Sn$
Moiety formula	2($C_{52}H_{104}Br_2Ge_3Si_8$), $C_4H_{10}O$	$C_{52}H_{104}Cl_2Ge_2Si_8Sn_{0.76}$, 0.24(Sn)
Formula weight	2737.43	1288.84
Temperature/K	100	103.00
Crystal system	triclinic	monoclinic
Space group	P-1	$P2_1$
a/Å	13.4471(6)	15.1288(6)
b/Å	17.0341(8)	13.3394(5)
c/Å	18.3110(9)	17.3677(6)
α/°	115.497(2)	90
β/°	94.608(2)	91.6210(10)
γ/°	104.931(2)	90
Volume/Å^3	3569.0(3)	3503.6(2)
Z	1	2
ρ_{calc}g/cm^3	1.274	1.222
μ/mm^{-1}	2.540	1.448
F(000)	1430.0	1352.0
Crystal size/mm^3	0.48 × 0.38 × 0.08	0.2 × 0.12 × 0.08
Absorption correction	multi-scan	multi-scan
Tmin; Tmax	0.5223; 0.7464	0.6742; 0.7463
Radiation	MoKα (λ = 0.71073)	MoKα (λ = 0.71073)
2Θ range for data collection/°	3.954 to 58.5°	3.622 to 55.996°
Completeness to theta	0.999	0.999
Index ranges	-18 ≤ h ≤ 18, -23 ≤ k ≤ 23, -25 ≤ l ≤ 25	-19 ≤ h ≤ 19, -17 ≤ k ≤ 17, -22 ≤ l ≤ 22
Reflections collected	113037	95524
Independent reflections	19410 [R_{int} = 0.0845, R_{sigma} = 0.0582]	16892 [R_{int} = 0.0784, R_{sigma} = 0.0592]
Data/restraints/parameters	19410/76/665	16892/1207/1126
Goodness-of-fit on F^2	1.034	1.020
Final R indexes [I>=2σ (I)]	R_1 = 0.0400, wR_2 = 0.0851	R_1 = 0.0695, wR_2 = 0.1647
Final R indexes [all data]	R_1 = 0.0679, wR_2 = 0.0997	R_1 = 0.0993, wR_2 = 0.1882
Largest diff. peak/hole / e Å^{-3}	0.85/-1.19	2.15/-0.97

Table 14. Crystal data and structure refinement parameters of [Tbb$_2$Ge$_2$(CNMes)C$_2$Me$_2$] (**15-Ge**) and [Tbb$_2$Ge$_2$(N-SiMe$_3$)C$_2$Me$_2$] (**16-Ge**).

	15-Ge	**16-Ge**
Crystal Habitus	clear orangish red block	clear red plate
Device Type	Bruker D8 Venture	STOE STADIVARI
Empirical formula	$C_{62}H_{115}Ge_2NSi_8$	$C_{61}H_{127}Ge_2NSi_9$
Moiety formula	$C_{62}H_{115}Ge_2NSi_8$	$C_{55}H_{113}Ge_2NSi_9$, C_6H_{14}
Formula weight	1244.44	1272.62
Temperature/K	100.00	100
Crystal system	triclinic	triclinic
Space group	P-1	P-1
a/Å	13.0162(9)	16.2948(8)
b/Å	16.6680(11)	17.0655(13)
c/Å	17.8248(12)	17.7480(10)
α/°	78.011(3)	111.422(5)
β/°	78.042(3)	96.079(4)
γ/°	84.058(3)	117.313(5)
Volume/Å^3	3693.3(4)	3852.6(5)
Z	2	2
ρ_{calc}g/cm^3	1.119	1.097
μ/mm^{-1}	0.977	2.536
F(000)	1340.0	1380.0
Crystal size/mm^3	0.18 × 0.13 × 0.08	0.2 × 0.094 × 0.002
Absorption correction	multi-scan	multi-scan
Tmin; Tmax	0.7002; 0.7463	0.3523; 0.4680
Radiation	MoKα (λ = 0.71073)	Cu Kα (λ = 1.54186)
2Θ range for data collection/°	3.94 to 55.996°	9.084 to 142.216°
Completeness to theta	0.999	0.994
Index ranges	-17 ≤ h ≤ 17, -22 ≤ k ≤ 22, -23 ≤ l ≤ 23	-19 ≤ h ≤ 19, -20 ≤ k ≤ 16, -20 ≤ l ≤ 21
Reflections collected	203480	111474
Independent reflections	17817 [R_{int} = 0.0599, R_{sigma} = 0.0292]	14539 [R_{int} = 0.0544, R_{sigma} = 0.0373]
Data/restraints/parameters	17817/0/693	14539/112/757
Goodness-of-fit on F^2	1.101	1.045
Final R indexes [I>=2σ (I)]	R_1 = 0.0347, wR_2 = 0.0813	R_1 = 0.0431, wR_2 = 0.0976
Final R indexes [all data]	R_1 = 0.0463, wR_2 = 0.0874	R_1 = 0.0654, wR_2 = 0.1083
Largest diff. peak/hole / e Å^{-3}	1.91/-0.66	0.60/-0.74

Table 15. Crystal data and structure refinement parameters of [Tbb$_2$Ge$_2$(N$_2$C(*p*-tol)$_2$)C$_2$Me$_2$] (**17-Ge**) and [Tbb$_2$Ge$_2$(SiBr$_2$)C$_4$Me$_4$] (**18-Si**).

	17-Ge	**18-Si**
Crystal Habitus	clear yellow plate	clear colourless block
Device Type	Bruker D8 Venture	STOE Stadivari
Empirical formula	$C_{67}H_{118}Ge_2N_2Si_8$	$C_{56}H_{110}Ge_2Br_2Si_9$
Moiety formula	$C_{67}H_{118}Ge_2N_2Si_8$	$C_{56}H_{110}Br_2Ge_2Si_9$
Formula weight	1321.53	1341.24
Temperature/K	102.00	100
Crystal system	monoclinic	monoclinic
Space group	$P2_1/c$	$P2_1$
a/Å	20.5714(8)	9.82122(22)
b/Å	17.6718(6)	22.1213(4)
c/Å	24.3371(9)	16.8351(4)
α/°	90	90.00
β/°	113.1320(10)	102.3642(18)
γ/°	90	90.00
Volume/Å^3	8136.0(5)	3572.72(14)
Z	4	2
ρ_{calc}g/cm^3	1.079	1.247
μ/mm^{-1}	0.891	4.02
F(000)	2840.0	1412.0
Crystal size/mm^3	0.2 × 0.2 × 0.04	0.4 × 0.36 × 0.36
Absorption correction	multi-scan	multi-scan
Tmin; Tmax	0.6606; 0.7465	0.1104; 0.1540
Radiation	MoKα (λ = 0.71073)	CuKα (λ = 1.54186)
2Θ range for data collection/°	3.64 to 56°	6.698 to 141.586°
Completeness to theta	0.999	1.000
Index ranges	-27 ≤ h ≤ 27, -23 ≤ k ≤ 23, -30 ≤ l ≤ 32	-12 ≤ h ≤ 6, -26 ≤ k ≤ 24, -20 ≤ l ≤ 20
Reflections collected	186256	45230
Independent reflections	19624 [R_{int} = 0.0608, R_{sigma} = 0.0388]	12491 [R_{int} = 0.0316, R_{sigma} = 0.0295]
Data/restraints/parameters	19624/90/777	12491/751/657
Goodness-of-fit on F^2	1.036	1.033
Final R indexes [I>=2σ (I)]	R_1 = 0.0429, wR_2 = 0.1022	R_1 = 0.0759, wR_2 = 0.1949
Final R indexes [all data]	R_1 = 0.0574, wR_2 = 0.1104	R_1 = 0.0789, wR_2 = 0.1981
Largest diff. peak/hole / e Å^{-3}	0.94/-1.30	2.58/-1.50

Table 16. Crystal data and structure refinement parameters of [Tbb$_2$Ge$_2$(GeBr$_2$)C$_4$Me$_4$] (**18-Ge**) and [Tbb$_2$Ge$_2$(SnCl$_2$)C$_4$Me$_4$] (**18-Sn**).

	18-Ge	**18-Sn**
Crystal Habitus	clear colourless plank	clear colourless block
Device Type	Bruker D8 Venture	Bruker D8 Venture
Empirical formula	$C_{60}H_{118}Br_2Ge_3OSi_8$	$C_{56}H_{110}Cl_2Ge_2Si_8Sn$
Moiety formula	$C_{56}H_{110}Br_2Ge_3Si_8$, C_4H_8O	$C_{56}H_{110}Cl_2Ge_2Si_8Sn$
Formula weight	1457.85	1342.92
Temperature/K	100.0	100.00
Crystal system	triclinic	monoclinic
Space group	P-1	$P2_1$
a/Å	13.5456(9)	9.7760(3)
b/Å	17.4219(12)	22.3755(9)
c/Å	19.5015(12)	16.6851(6)
α/°	68.957(2)	90
β/°	88.408(3)	101.4140(10)
γ/°	69.455(3)	90
Volume/Å^3	3996.6(5)	3577.6(2)
Z	2	2
ρ_{calc}g/cm^3	1.211	1.247
μ/mm^{-1}	2.273	1.421
F(000)	1528.0	1412.0
Crystal size/mm^3	0.4 × 0.12 × 0.1	0.18 × 0.1 × 0.09
Absorption correction	multi-scan	multi-scan
Tmin; Tmax	0.5663; 0.7462	0.1104; 0.1540
Radiation	MoKα (λ = 0.71073)	MoKα (λ = 0.71073)
2Θ range for data collection/°	3.676 to 55.998°	4.412 to 56°
Completeness to theta	0.999	0.999
Index ranges	-17 ≤ h ≤ 17, -23 ≤ k ≤ 23, -25 ≤ l ≤ 25	-11 ≤ h ≤ 12, -29 ≤ k ≤ 29, -22 ≤ l ≤ 22
Reflections collected	157435	139209
Independent reflections	19274 [R_{int} = 0.0884, R_{sigma} = 0.0733]	17265 [R_{int} = 0.0754, R_{sigma} = 0.0473]
Data/restraints/parameters	19274/735/1006	17265/1584/1061
Goodness-of-fit on F^2	1.031	1.031
Final R indexes [I>=2σ (I)]	R_1 = 0.0980, wR_2 = 0.2395	R_1 = 0.0520, wR_2 = 0.1176
Final R indexes [all data]	R_1 = 0.1239, wR_2 = 0.2625	R_1 = 0.0594, wR_2 = 0.1236
Largest diff. peak/hole / e Å^{-3}	1.89/-2.74	1.04/-1.55

Table 17. Crystal data and structure refinement parameters of [Tbb$_2$Ge$_3$C$_2$Me$_2$] (**19-Ge**) and [Tbb$_2$Ge$_2$SnC$_2$Me$_2$] (**19-Sn**).

	19-Ge	**19-Sn**
Crystal Habitus	clear brownish yellow block	clear red plate
Device Type	STOE STADIVARI	STOE IPDS 2T
Empirical formula	$C_{52}H_{104}Ge_3Si_8$	$C_{57}H_{116}Ge_2Si_8Sn$
Moiety formula	$C_{52}H_{104}Ge_3Si_8$	$C_{52}H_{104}Ge_2Si_8Sn$, C_5H_{12}
Formula weight	1171.8516	1290.08
Temperature/K	100	100
Crystal system	triclinic	triclinic
Space group	P-1	P-1
a/Å	13.3055(4)	9.6762(5)
b/Å	17.3572(6)	12.0623(5)
c/Å	17.5712(6)	17.1432(9)
α/°	104.928(3)	101.161(4)
β/°	109.194(3)	100.532(4)
γ/°	106.613(3)	106.071(4)
Volume/Å^3	3383.97(20)	1826.09(16)
Z	2	1
ρ_{calc}g/cm^3	1.150	1.173
μ/mm^{-1}	3.137	1.319
F(000)	1248.0	684.0
Crystal size/mm^3	0.24 × 0.12 × 0.1	0.16 × 0.14 × 0.02
Absorption correction	multi-scan	multi-scan
Tmin; Tmax	0.3426; 0.6932	0.6543; 0.9067
Radiation	CuKα (λ = 1.54186)	Mo Kα (λ = 0.71073)
2Θ range for data collection/°	7.348 to 135.49°	4.526 to 59.338°
Completeness to theta	0.989	0.995
Index ranges	-15 ≤ h ≤ 15, -20 ≤ k ≤ 15, -21 ≤ l ≤ 19	-13 ≤ h ≤ 13, -16 ≤ k ≤ 16, -23 ≤ l ≤ 23
Reflections collected	44802	20408
Independent reflections	12115 [R_{int} = 0.0903, R_{sigma} = 0.0675]	10234 [R_{int} = 0.0300, R_{sigma} = 0.0326]
Data/restraints/parameters	12115/0/600	10234/420/529
Goodness-of-fit on F^2	1.050	1.093
Final R indexes [I>=2σ (I)]	R_1 = 0.0948, wR_2 = 0.2511	R_1 = 0.0501, wR_2 = 0.1075
Final R indexes [all data]	R_1 = 0.1108, wR_2 = 0.2687	R_1 = 0.0647, wR_2 = 0.1158
Largest diff. peak/hole / e Å^{-3}	2.48/-1.09	0.88/-0.47

Table 18. Crystal data and structure refinement parameters of [$Tbb_2Ge_5Br_2C_2Me_2$] (**20-Ge**) and [$Tbb_2Ge_3(ClMe_4)C_2Me_2$] (**21-Ge**).

	20-Ge	**21-Ge**
Crystal Habitus	clear orange block	clear yellow block
Device Type	Bruker D8 Venture	Bruker D8 Venture
Empirical formula	$C_{61}H_{125}Br_2Ge_4Si_8$	$C_{60}H_{116}Ge_3N_2Si_8$
Moiety formula	$C_{52}H_{104}Br_2Ge_4Si_8$, 1.5($C_6H_{14}$)	$C_{60}H_{116}Ge_3N_2Si_8$
Formula weight	1533.50	1308.03
Temperature/K	100.0	100.0
Crystal system	monoclinic	monoclinic
Space group	$P2_1/n$	C2/c
a/Å	15.1140(4)	42.1209(18)
b/Å	30.7321(8)	13.5986(6)
c/Å	17.1717(4)	34.271(2)
α/°	90	90
β/°	94.3860(10)	126.4890(10)
γ/°	90	90
Volume/Å^3	7952.6(3)	15781.8(14)
Z	4	8
ρ_{calc}g/cm^3	1.281	1.101
μ/mm^{-1}	2.655	1.289
F(000)	3204.0	5584.0
Crystal size/mm^3	0.34 × 0.26 × 0.24	0.24 × 0.22 × 0.16
Absorption correction	multi-scan	multi-scan
Tmin; Tmax	0.6336; 0.7462	0.6541; 0.7463
Radiation	MoKα (λ = 0.71073)	MoKα (λ = 0.71073)
2Θ range for data collection/°	4.58 to 58.5°	3.836 to 64.346°
Completeness to theta	0.999	0.999
Index ranges	-20 ≤ h ≤ 20, -42 ≤ k ≤ 42, -23 ≤ l ≤ 22	-62 ≤ h ≤ 62, -20 ≤ k ≤ 20, -51 ≤ l ≤ 51
Reflections collected	200498	407455
Independent reflections	21647 [R_{int} = 0.0436, R_{sigma} = 0.0235]	27568 [R_{int} = 0.1044, R_{sigma} = 0.0449]
Data/restraints/parameters	21647/175/763	27568/357/905
Goodness-of-fit on F^2	1.043	1.036
Final R indexes [I>=2σ (I)]	R_1 = 0.0313, wR_2 = 0.0754	R_1 = 0.0607, wR_2 = 0.1435
Final R indexes [all data]	R_1 = 0.0414, wR_2 = 0.0808	R_1 = 0.1003, wR_2 = 0.1729
Largest diff. peak/hole / e Å^{-3}	0.89/-0.70	1.09/-2.71

Table 19. Crystal data and structure refinement parameters of [Tbb$_2$Ge$_3$(IMe$_4$)C$_2$Me$_2$] (**22-Ge**) and [Tbb$_2$Ge$_4$C$_2$Me$_2$] (**23-Ge**).

	22-Ge	**23-Ge**
Crystal Habitus	clear red block	clear light yellow block
Device Type	STOE Stadivari	Bruker D8 Venture
Empirical formula	$C_{64}H_{128}Ge_3N_2Si_8$	$C_{52}H_{104}Ge_4Si_8$
Moiety formula	$C_{59}H_{116}Ge_3N_2Si_8$, C_5H_{12}	$C_{52}H_{104}Ge_4Si_8$
Formula weight	1368.1866	1244.43
Temperature/K	100	100.0
Crystal system	monoclinic	triclinic
Space group	$P2_1/c$	P-1
a/Å	16.7276(3)	13.2155(8)
b/Å	29.0875(4)	17.7872(11)
c/Å	17.2132(3)	17.8744(11)
α/°	90.00	107.479(2)
β/°	109.4293(12)	107.963(2)
γ/°	90.00	106.732(2)
Volume/Å^3	7898.38(20)	3460.8(4)
Z	4	2
ρ_{calc}g/cm^3	1.151	1.194
μ/mm^{-1}	2.761	1.888
F(000)	2936.0	1312.0
Crystal size/mm^3	0.35 × 0.237 × 0.16	0.2 × 0.18 × 0.16
Absorption correction	multi-scan	multi-scan
Tmin; Tmax	0.7177; 0.8006	0.6816; 0.7463
Radiation	CuKα (λ = 1.54186)	MoKα (λ = 0.71073)
2Θ range for data collection/°	6.078 to 151.612°	4.528 to 56°
Completeness to theta	0.992	0.998
Index ranges	-20 ≤ h ≤ 18, -34 ≤ k ≤ 35, -8 ≤ l ≤ 20	-17 ≤ h ≤ 17, -23 ≤ k ≤ 23, -23 ≤ l ≤ 23
Reflections collected	110493	161422
Independent reflections	14987 [R_{int} = 0.0378, R_{sigma} = 0.0235]	16694 [R_{int} = 0.0446, R_{sigma} = 0.0266]
Data/restraints/parameters	14987/255/811	16694/386/937
Goodness-of-fit on F^2	1.020	1.187
Final R indexes [I>=2σ (I)]	R_1 = 0.0378, wR_2 = 0.0911	R_1 = 0.0561, wR_2 = 0.1263
Final R indexes [all data]	R_1 = 0.0484, wR_2 = 0.0965	R_1 = 0.0655, wR_2 = 0.1310
Largest diff. peak/hole / e Å^{-3}	0.91/-1.02	1.46/-1.01

Table 20. Crystal data and structure refinement parameters of [$Tbb_2Ge_5Br_2C_2Me_2$] (**24-Ge**) and [$Ar^{Dipp}SnSi(DMAP)Tbb$] (**25-SnSi**).

	24-Ge	**25-SnSi**
Crystal Habitus	clear red block	clear green block
Device Type	Bruker D8 Venture	Bruker D8 Venture
Empirical formula	$C_{57}H_{116}Br_2Ge_5Si_8$	$C_{67}H_{110}N_2Si_5Sn$
Moiety formula	$C_{52}H_{104}Br_2Ge_5Si_8$, C_5H_{12}	$C_{61}H_{96}N_2Si_5Sn$, C_6H_{14}
Formula weight	1548.98	1202.70
Temperature/K	100.0	100.0
Crystal system	monoclinic	triclinic
Space group	$P2_1/n$	P-1
a/Å	15.342(2)	15.1899(6)
b/Å	30.894(4)	22.6558(10)
c/Å	17.350(2)	23.6278(9)
α/°	90	63.567(2)
β/°	93.160(4)	78.762(2)
γ/°	90	86.260(2)
Volume/Å^3	8210.8(18)	7139.4(5)
Z	4	4
ρ_{calc}g/cm^3	1.253	1.119
μ/mm^{-1}	2.928	0.478
F(000)	3200.0	2584.0
Crystal size/mm^3	0.26 × 0.22 × 0.08	0.18 × 0.1 × 0.06
Absorption correction	multi-scan	multi-scan
Tmin; Tmax	0.5385; 0.7462	0.6733; 0.7462
Radiation	MoKα (λ = 0.71073)	MoKα (λ = 0.71073)
2Θ range for data collection/°	3.644 to 54°	3.526 to 56°
Completeness to theta	0.976	0.999
Index ranges	-19 ≤ h ≤ 19, 0 ≤ k ≤ 39, 0 ≤ l ≤ 21	-20 ≤ h ≤ 20, -29 ≤ k ≤ 29, -31 ≤ l ≤ 31
Reflections collected	17456	238601
Independent reflections	17456 [R_{int} = ?, R_{sigma} = 0.0749]	34437 [R_{int} = 0.0828, R_{sigma} = 0.0488]
Data/restraints/parameters	17456/609/684	34437/67/1483
Goodness-of-fit on F^2	2.407	1.087
Final R indexes [I>=2σ (I)]	R_1 = 0.2026, wR_2 = 0.5466	R_1 = 0.0427, wR_2 = 0.1041
Final R indexes [all data]	R_1 = 0.2474, wR_2 = 0.5686	R_1 = 0.0657, wR_2 = 0.1211
Largest diff. peak/hole / e Å^{-3}	10.49/-3.50	1.72/-0.85

Table 21. Crystal data and structure refinement parameters of [Ar^{Dipp}SnSi(Mes-NC)Tbb] (**26-SnSi**) and [Ar^{Dipp}SnSi(IMe$_4$)Tbb] (**27-SnSi**).

	26-SnSi	**27-SnSi**
Crystal Habitus	clear blue plate	clear dark green block
Device Type	Bruker D8 Venture	Bruker D8 Venture
Empirical formula	$C_{64}H_{97}NSi_5Sn$	$C_{68}H_{108}N_4Si_5Sn$
Moiety formula	$C_{64}H_{97}NSi_5Sn$	$C_{61}H_{98}N_2Si_5Sn$, $C_7H_{10}N_2$
Formula weight	1139.56	1240.72
Temperature/K	100.0	100.0
Crystal system	triclinic	monoclinic
Space group	P-1	$P2_1/c$
a/Å	14.3981(18)	13.4296(8)
b/Å	14.8735(18)	22.9601(14)
c/Å	15.7775(18)	23.2751(15)
α/°	87.481(5)	90
β/°	87.035(5)	100.446(2)
γ/°	78.090(5)	90
Volume/Å^3	3299.7(7)	1240.72
Z	2	4
ρ_{calc}g/cm^3	1.147	1.168
μ/mm^{-1}	0.514	0.487
F(000)	1216.0	2656.0
Crystal size/mm^3	0.2 × 0.08 × 0.02	0.22 × 0.14 × 0.04
Absorption correction	multi-scan	multi-scan
Tmin; Tmax	0.4929; 0.8720	0.6648; 0.7462
Radiation	MoKα (λ = 0.71073)	MoKα (λ = 0.71073)
2Θ range for data collection/°	3.746 to 58.498°	3.97 to 56°
Completeness to theta	0.972	0.999
Index ranges	-19 ≤ h ≤ 19, -20 ≤ k ≤ 20, 0 ≤ l ≤ 21	-17 ≤ h ≤ 17, -30 ≤ k ≤ 30, -30 ≤ l ≤ 29
Reflections collected	16957	123227
Independent reflections	16957 [R_{int} = ?, R_{sigma} = 0.1096]	17044 [R_{int} = 0.0693, R_{sigma} = 0.0423]
Data/restraints/parameters	16957/0/667	17044/0/732
Goodness-of-fit on F^2	1.151	1.019
Final R indexes [I>=2σ (I)]	R_1 = 0.0739, wR_2 = 0.1200	R_1 = 0.0346, wR_2 = 0.0766
Final R indexes [all data]	R_1 = 0.1306, wR_2 = 0.1410	R_1 = 0.0536, wR_2 = 0.0861
Largest diff. peak/hole / e Å^{-3}	0.90/-0.65	0.46/-0.66

Table 22. Crystal data and structure refinement parameters of [(Tbb)CN_2Ge(Tbb)] (**30-Ge**) and [(NHP)$SiMe_3$C=GeBrTbb] (**31-Ge**).

	30-Ge	**31-Ge**
Crystal Habitus	clear light orange prisms	clear yellow block
Device Type	STOE IPDS 2T	Bruker D8 Venture
Empirical formula	$C_{49}H_{98}GeN_2Si_8$	$C_{54}H_{96}N_2Si_5PGeBr$
Moiety formula	$C_{49}H_{98}GeN_2Si_8$	$C_{54}H_{96}BrGeN_2PSi_5$
Formula weight	1012.60	1097.24
Temperature/K	100	100.0
Crystal system	triclinic	monoclinic
Space group	P-1	$P2_1/n$
a/Å	16.5085(8)	11.8185(3)
b/Å	16.8696(8)	23.8921(7)
c/Å	19.7291(9)	22.4746(7)
α/°	102.885(4)	90
β/°	92.952(4)	100.6790(10)
γ/°	114.758(4)	90
Volume/Å^3	4798.1(4)	6236.2(3)
Z	3	4
ρ_{calc}g/cm^3	1.051	1.169
μ/mm^{-1}	0.658	1.287
F(000)	1650.0	2344.0
Crystal size/mm^3	0.2 × 0.147 × 0.08	0.28 × 0.16 × 0.14
Absorption correction	multi-scan	multi-scan
Tmin; Tmax	0.6101; 0.9670	0.7009; 0.7463
Radiation	Mo Kα (λ = 0.71073)	MoKα (λ = 0.71073)
2Θ range for data collection/°	4.294 to 50.5°	3.876 to 55.996°
Completeness to theta	0.965	0.999
Index ranges	-19 ≤ h ≤ 19, -17 ≤ k ≤ 20, -23 ≤ l ≤ 23	-15 ≤ h ≤ 13, -31 ≤ k ≤ 31, -29 ≤ l ≤ 29
Reflections collected	29547	140515
Independent reflections	16769 [R_{int} = 0.0660, R_{sigma} = 0.0630]	15046 [R_{int} = 0.0532, R_{sigma} = 0.0268]
Data/restraints/parameters	16769/717/910	15046/88/634
Goodness-of-fit on F^2	1.083	1.049
Final R indexes [I>=2σ (I)]	R_1 = 0.0919, wR_2 = 0.2160	R_1 = 0.0325, wR_2 = 0.0818
Final R indexes [all data]	R_1 = 0.1264, wR_2 = 0.2387	R_1 = 0.0388, wR_2 = 0.0859
Largest diff. peak/hole / e Å^{-3}	2.04/-0.84	0.87/-1.04

Table 23. Crystal data and structure refinement parameters of [(NHP)SiMe$_3$C=GeBrMind] (**32-Ge**) and [(DippNCH$_2$)P=CSiMe$_3$SiBr2(DippNCH$_2$)] (**33-Si**).

	32-Ge	**33-Si**
Crystal Habitus	clear yellow block	clear colourless plate
Device Type	Bruker D8 Venture	Bruker D8 Venture
Empirical formula	$C_{106}H_{166}Br_2Ge_2N_4P_2Si_2$	$C_{30}H_{47}Br_2N_2PSi_2$
Moiety formula	$2(C_{50}H_{76}BrGeN_2PSi)$, C_6H_{14}	$C_{30}H_{47}Br_2N_2PSi_2$
Formula weight	1919.54	682.66
Temperature/K	100.00	100
Crystal system	orthorhombic	triclinic
Space group	$Pna2_1$	P-1
a/Å	19.4044(7)	10.5121(4)
b/Å	12.3671(4)	11.7216(5)
c/Å	43.2502(16)	15.5904(6)
α/°	90	88.200(2)
β/°	90	82.8090(10)
γ/°	90	63.5660(10)
Volume/Å^3	10379.0(6)	1706.01(12)
Z	4	2
ρ_{calc}g/cm^3	1.228	1.329
μ/mm^{-1}	1.449	2.514
F(000)	4088.0	708.0
Crystal size/mm^3	0.22 × 0.17 × 0.1	0.32 × 0.24 × 0.14
Absorption correction	multi-scan	multi-scan
Tmin; Tmax	0.6533; 0.7463	0.5547; 0.7463
Radiation	MoKα (λ = 0.71073)	MoKα (λ = 0.71073)
2Θ range for data collection/°	4.198 to 56°	3.882 to 56°
Completeness to theta	0.999	0.999
Index ranges	-25 ≤ h ≤ 25, -16 ≤ k ≤ 16, -57 ≤ l ≤ 57	-13 ≤ h ≤ 13, -15 ≤ k ≤ 15, -20 ≤ l ≤ 20
Reflections collected	369684	118552
Independent reflections	25064 [R_{int} = 0.0780, R_{sigma} = 0.0385]	8231 [R_{int} = 0.0596, R_{sigma} = 0.0216]
Data/restraints/parameters	25064/128/1100	8231/0/345
Goodness-of-fit on F^2	1.022	1.039
Final R indexes [I>=2σ (I)]	R_1 = 0.0347, wR_2 = 0.0806	R_1 = 0.0229, wR_2 = 0.0627
Final R indexes [all data]	R_1 = 0.0412, wR_2 = 0.0838	R_1 = 0.0264, wR_2 = 0.0638
Largest diff. peak/hole / e Å^{-3}	1.65/-0.86	0.98/-0.42

Table 24. Crystal data and structure refinement parameters of [(NHP)SiMe$_3$C=SiBr2(caac^{Me})] (**34-Si**) and [(NHPMe)SiSiMe$_2$C(caac^{Me})] (**35-Si**).

	34-Si	**35-Si**
Crystal Habitus	clear blue plate	clear colourless plate
Device Type	Bruker D8 Venture	Bruker D8 Venture
Empirical formula	$C_{50}H_{78}N_3Si_2PBr_2$	$C_{50}H_{78}N_3PSi_2$
Moiety formula	$C_{50}H_{78}Br_2N_3PSi_2$	$C_{50}H_{78}N_3PSi_2$
Formula weight	968.12	808.30
Temperature/K	100.00	100.00
Crystal system	monoclinic	triclinic
Space group	$P2_1/n$	P-1
a/Å	12.4859(12)	17.695(2)
b/Å	18.8007(19)	17.7523(16)
c/Å	21.208(2)	18.1304(18)
α/°	90	94.296(7)
β/°	100.613(3)	103.205(8)
γ/°	90	95.107(8)
Volume/Å^3	4893.3(8)	5495.9(10)
Z	4	4
ρ_{calc}g/cm^3	1.314	0.977
μ/mm^{-1}	1.775	1.083
F(000)	2048.0	1768.0
Crystal size/mm^3	0.18 × 0.1 × 0.05	0.16 × 0.14 × 0.02
Absorption correction	multi-scan	multi-scan
Tmin; Tmax	0.5785; 0.7463	0.5438; 0.7517
Radiation	MoKα (λ = 0.71073)	CuKα (λ = 1.54178)
2Θ range for data collection/°	3.964 to 55.998°	5.022 to 135.494°
Completeness to theta	0.999	0.982
Index ranges	-16 ≤ h ≤ 16, -24 ≤ k ≤ 24, -27 ≤ l ≤ 28	-21 ≤ h ≤ 21, -21 ≤ k ≤ 21, -21 ≤ l ≤ 21
Reflections collected	108684	213709
Independent reflections	11802 [R_{int} = 0.1621, R_{sigma} = 0.0996]	19556 [R_{int} = 0.2319, R_{sigma} = 0.1275]
Data/restraints/parameters	11802/0/542	19556/89/1046
Goodness-of-fit on F^2	1.035	1.713
Final R indexes [I>=2σ (I)]	R_1 = 0.0618, wR_2 = 0.1382	R_1 = 0.1930, wR_2 = 0.4550
Final R indexes [all data]	R_1 = 0.1172, wR_2 = 0.1707	R_1 = 0.2376, wR_2 = 0.4805
Largest diff. peak/hole / e Å^{-3}	0.82/-1.60	1.89/-0.68

Table 25. Crystal data and structure refinement parameters of [(IMe2^{i}Pr2)CN_2] (**36**) and [((IMe$_2$^{i}Pr$_2$)CGeTbb)$_2$] (**37-Ge**).

	36	**37-Ge**
Crystal Habitus	clear yellow plank	clear violet plate
Device Type	STOE STADIVARI	Bruker D8 Venture
Empirical formula	$C_{11}H_{20}N_4$	$C_{78}H_{144}Ge_2N_4Si_8$
Moiety formula	$C_{11}H_{20}N_4$	$C_{72}H_{138}Ge_2N_4Si_8$, C_6H_6
Formula weight	208.30	1507.86
Temperature/K	100	105.15
Crystal system	monoclinic	orthorhombic
Space group	$P2_1/c$	$Pna2_1$
a/Å	6.9462(5)	31.484(3)
b/Å	15.5914(11)	13.8781(10)
c/Å	16.1804(9)	20.0706(17)
α/°	90	90
β/°	99.256(5)	90
γ/°	90	90
Volume/Å^3	1729.5(2)	8769.6(13)
Z	8	4
ρ_{calc}g/cm^3	1.261	1.142
μ/mm^{-1}	0.656	0.835
F(000)	704.0	3264.0
Crystal size/mm^3	0.25 × 0.08 × 0.04	0.21 × 0.18 × 0.05
Absorption correction	multi-scan	multi-scan
Tmin; Tmax	0.5215; 0.9054	0.6714; 0.7377
Radiation	CuKα (λ = 1.54186)	MoKα (λ = 0.71073)
2Θ range for data collection/°	7.926 to 141.364°	4.814 to 55.996°
Completeness to theta	1.000	0.999
Index ranges	-8 ≤ h ≤ 8, -18 ≤ k ≤ 18, -18 ≤ l ≤ 19	-41 ≤ h ≤ 41, -18 ≤ k ≤ 18, -26 ≤ l ≤ 26
Reflections collected	42158	285190
Independent reflections	42158 [R_{int} = 0.1241, R_{sigma} = 0.1885]	21168 [R_{int} = 0.1088, R_{sigma} = 0.0519]
Data/restraints/parameters	42158/0/226	21168/1/872
Goodness-of-fit on F^2	0.930	1.037
Final R indexes [I>=2σ (I)]	R_1 = 0.0971, wR_2 = 0.2325	R_1 = 0.0312, wR_2 = 0.0658
Final R indexes [all data]	R_1 = 0.2146, wR_2 = 0.3098	R_1 = 0.0378, wR_2 = 0.0692
Largest diff. peak/hole / e Å^{-3}	0.33/-0.35	0.31/-0.34

Table 26. Crystal data and structure refinement parameters of [N(SiBrTbb)$_2$NC(IMe$_2$*i*Pr$_2$)] (**38-Si**) and [((IMe$_2$^{i}Pr$_2$)(GeTbb)GeBr$_2$Tbb] (**39-Ge**).

	38-Si	**39-Ge**
Crystal Habitus	clear light yellow plates	clear orange blocks
Device Type	Bruker D8 Venture	Bruker D8 Venture
Empirical formula	$C_{64}H_{128}Br_2N_4OSi_{10}$	$C_{64}H_{128}Br_2Ge_2N_2OSi_8$
Moiety formula	$C_{60}H_{118}Br_2N_4Si_{10}$, $C_4H_{10}O$	$C_{60}H_{118}Br_2Ge_2N_2Si_8$, $C_4H_{10}O$
Formula weight	1354.22	1471.40
Temperature/K	100	100.15
Crystal system	monoclinic	monoclinic
Space group	$P2_1/n$	$P2_1/n$
a/Å	22.0913(12)	14.9960(6)
b/Å	20.0046(12)	14.1378(6)
c/Å	22.2247(13)	37.7565(17)
α/°	90	90
β/°	113.891(4)	92.868(2)
γ/°	90	90
Volume/Å^3	8980.2(9)	7994.7(6)
Z	4	4
ρ_{calc}g/cm^3	1.105	1.222
μ/mm^{-1}	2.693	1.908
F(000)	3232.0	3120.0
Crystal size/mm^3	0.6 × 0.48 × 0.24	0.32 × 0.23 × 0.1
Absorption correction	multi-scan	multi-scan
Tmin; Tmax	0.1267; 0.2073	0.6057; 0.7463
Radiation	Cu Kα (λ = 1.54186)	MoKα (λ = 0.71073)
2Θ range for data collection/°	9.144 to 141.38°	4.07 to 56°
Completeness to theta	0.998	0.999
Index ranges	-26 ≤ h ≤ 25, -16 ≤ k ≤ 24, -27 ≤ l ≤ 25	-19 ≤ h ≤ 19, -18 ≤ k ≤ 18, -49 ≤ l ≤ 49
Reflections collected	111827	246599
Independent reflections	17036 [R_{int} = 0.0810, R_{sigma} = 0.0410]	19291 [R_{int} = 0.0452, R_{sigma} = 0.0216]
Data/restraints/parameters	17036/779/813	19291/180/784
Goodness-of-fit on F^2	2.242	1.042
Final R indexes [I>=2σ (I)]	R_1 = 0.1669, wR_2 = 0.4954	R_1 = 0.0316, wR_2 = 0.0852
Final R indexes [all data]	R_1 = 0.1895, wR_2 = 0.5202	R_1 = 0.0367, wR_2 = 0.0890
Largest diff. peak/hole / e Å^{-3}	3.67/-1.74	1.21/-1.04

Table 27. Crystal data and structure refinement parameters of [N(SiTbb)$_2$NC(IMe*2i*Pr$_2$)] (**40-Si**) and [(IDipp)C-GeBrAr^{Mes}] (**41-Ge**).

	40-Si	**41-Ge**
Crystal Habitus	clear dark red block	clear yellow plate
Device Type	Bruker D8 Venture	Bruker D8 Venture
Empirical formula	$C_{69}H_{139}N_4Si_{10}$	$C_{55}H_{64}BrGeN_2$
Moiety formula	$C_{60}H_{118}N_4Si_{10}$, 1.5(C_6H_{14})	$C_{52}H_{61}BrGeN_2$, 0.5(C_6H_6)
Formula weight	1305.73	905.58
Temperature/K	105.00	100
Crystal system	triclinic	monoclinic
Space group	P-1	$P2_1/n$
a/Å	12.3066(10)	14.3090(5)
b/Å	15.3905(12)	22.6461(7)
c/Å	24.6973(18)	15.6961(6)
α/°	96.492(3)	90
β/°	100.462(3)	100.027(2)
γ/°	110.747(3)	90
Volume/Å^3	4220.9(6)	5008.5(3)
Z	2	4
ρ_{calc}g/cm^3	1.027	1.201
μ/mm^{-1}	0.192	1.445
F(000)	1442.0	1900.0
Crystal size/mm^3	0.215 × 0.12 × 0.09	0.33 × 0.21 × 0.06
Absorption correction	multi-scan	multi-scan
Tmin; Tmax	0.7066; 0.7463	0.6491; 0.7464
Radiation	MoKα (λ = 0.71073)	MoKα (λ = 0.71073)
2Θ range for data collection/°	3.638 to 56°	3.596 to 65.226°
Completeness to theta	0.999	0.999
Index ranges	-16 ≤ h ≤ 16, -20 ≤ k ≤ 20, -32 ≤ l ≤ 32	-21 ≤ h ≤ 21, -34 ≤ k ≤ 34, -23 ≤ l ≤ 23
Reflections collected	251764	150814
Independent reflections	20358 [R_{int} = 0.0607, R_{sigma} = 0.0287]	18251 [R_{int} = 0.0482, R_{sigma} = 0.0299]
Data/restraints/parameters	20358/55/806	18251/761/785
Goodness-of-fit on F^2	1.042	1.319
Final R indexes [I>=2σ (I)]	R_1 = 0.0482, wR_2 = 0.1221	R_1 = 0.1036, wR_2 = 0.2460
Final R indexes [all data]	R_1 = 0.0604, wR_2 = 0.1310	R_1 = 0.1090, wR_2 = 0.2480
Largest diff. peak/hole / e Å^{-3}	1.41/-0.86	1.82/-3.50

Table 28. Crystal data and structure refinement parameters of $[(PMe_3)_2Ni(SiClTbb)_2]$ (**42-Ni**).

	42-Ni
Crystal Habitus	clear reddish brown block
Device Type	STOE STADIVARI
Empirical formula	$C_{58}H_{126}Cl_2NiOP_2Si_{10}$
Moiety formula	$C_{54}H_{116}Cl_2NiP_2Si_{10}$, $C_4H_{10}O$
Formula weight	1312.03
Temperature/K	100
Crystal system	monoclinic
Space group	$P2_1/c$
a/Å	14.76342(19)
b/Å	24.6247(3)
c/Å	22.5871(3)
α/°	90.00
β/°	104.7487(10)
γ/°	90.00
Volume/Å^3	7940.86(17)
Z	4
ρ_{calc}g/cm^3	1.097
μ/mm^{-1}	3.037
F(000)	2856.0
Crystal size/mm^3	0.25 × 0.21 × 0.18
Absorption correction	multi-scan
Tmin; Tmax	0.2873; 0.3596
Radiation	CuKα (λ = 1.54186)
2Θ range for data collection/°	7.18 to 141.13°
Completeness to theta	0.992
Index ranges	-17 ≤ h ≤ 18, -29 ≤ k ≤ 29, -16 ≤ l ≤ 27
Reflections collected	150340
Independent reflections	14949 [R_{int} = 0.0446, R_{sigma} = 0.0223]
Data/restraints/parameters	14949/23/753
Goodness-of-fit on F^2	1.028
Final R indexes [I>=2σ (I)]	R_1 = 0.0317, wR_2 = 0.0754
Final R indexes [all data]	R_1 = 0.0427, wR_2 = 0.0804
Largest diff. peak/hole / e Å^{-3}	0.70/-0.28

5.3. Supplementary molecular structures

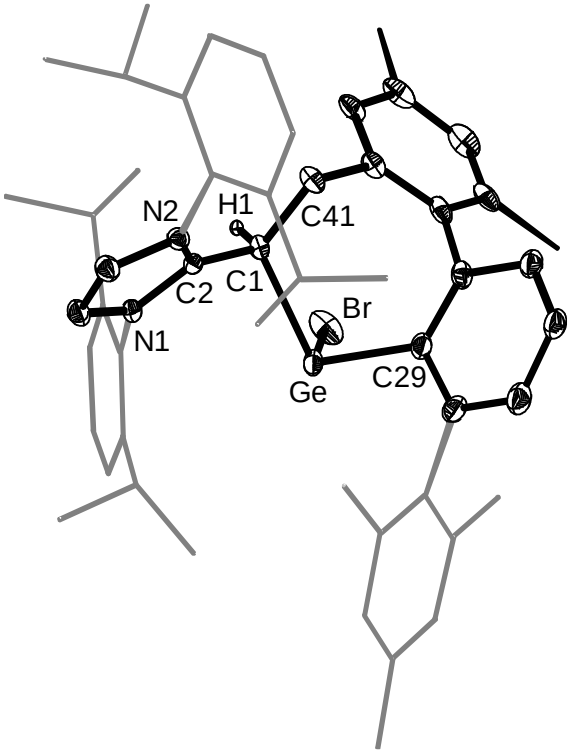

Figure 85. DIAMOND plot of the molecular structure of **41-Ge**. Thermal ellipsoids are set at 30 % probability level. Hydrogen atoms are omitted and the Dipp and Mes substituents of the Idipp ans Ar^{Mes} ligand are presented in wire-frame for clarity. Selected bond lengths [Å], bond angles [°]: Ge-C1 2.190(4), C1-C2 1.449(6), Ge-C29 2.018(15), Ge-Br 2.4927(7), C1-C41 1.540(6), C1-Ge-C29 100.9(5), C2-C1-C41 116.0(4), Ge-C1-C41 117.5(3), C1-Ge-Br 93.44(12), C29-Ge-Br 104.0(5).

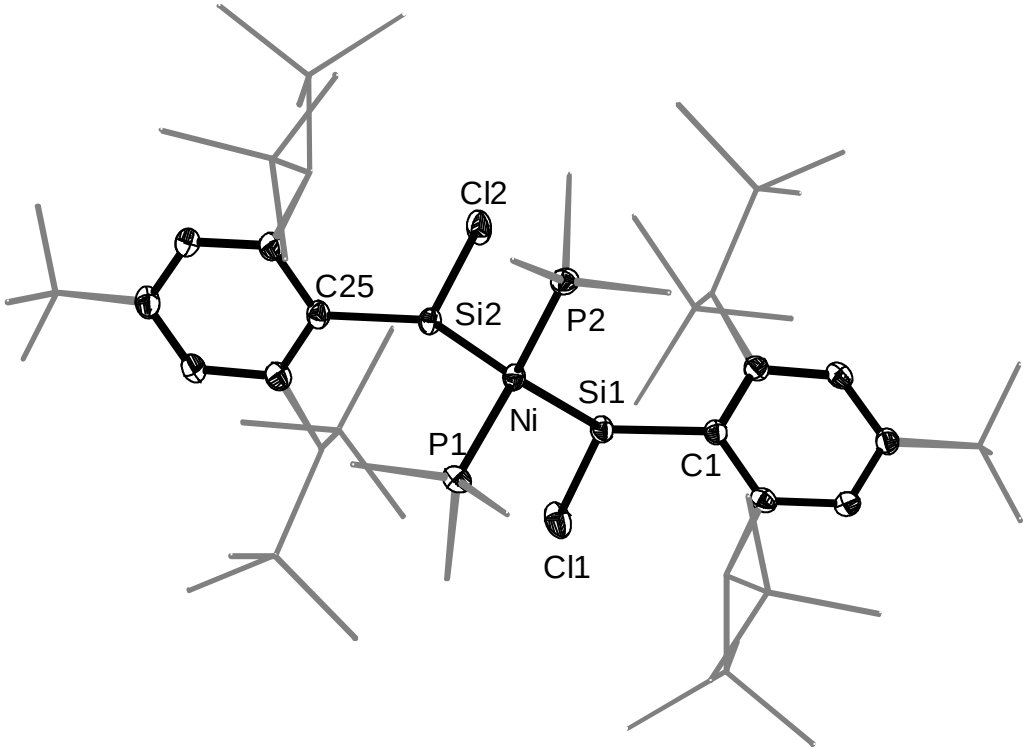

Figure 86. DIAMOND plot of the molecular structure of **8-Ge**. Thermal ellipsoids are set at 30 % probability level. Hydrogen atoms are omitted and the Dsi and ^{t}Bu substituents of the Tbb ligand are

presented in wire-frame for clarity. Selected bond lengths [Å], bond angles [°] and torsion angle [°]: Ni-P1 2.1794(5), Ni-P2 2.1785(5), Ni-Si1 2.1172(5), Ni-Si2 2.1125(5), Si1-Cl1 2.1309(6), Si2-Cl2 2.1272(6), Si1-Ni-P1 108.62(2), Si1-Ni-P2 112.34(2),Si2-Ni-P1 111.39(2), Si2-Ni-P2 108.17(2), Ni-Si1-Cl1 115.64(2), Ni-Si2-Cl2 116.04(2).

5.4. UV-Vis NIR spectroscopic studies of compounds

UV-Vis-NIR spectra of **25-SnSi**

The UV-Vis-NIR spectra of **25-SnSi** were recorded in *n*-hexane at ambient temperature and are depicted in ***Figure 87***. The absorption maxima and corresponding molar extinction coefficients (**ε**) are summarized in ***Table 29***. The absorption bands were determined by means of band deconvolution, assuming a Gaussian line profile. The corresponding deconvoluted absorption bands are displayed in ***Figure 88***, and the parameters used for the band deconvolution are summarized in ***Table 30***.

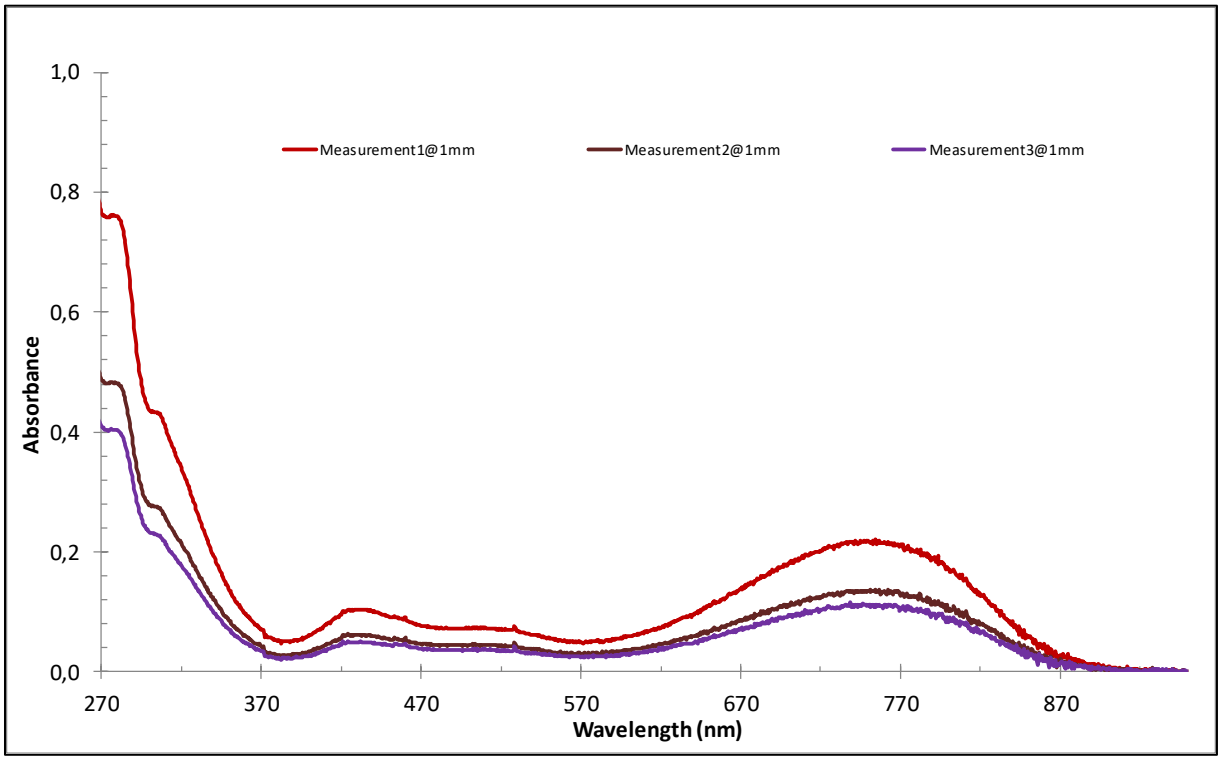

Figure 87. Experimental UV-Vis-NIR spectra of **25-SnSi** in *n*-hexane from 270 – 980 nm at different concentrations.

Table 29. Absorption maxima of the UV-Vis-NIR spectra of **25-SnSi** depicted in ***Figure 87*** and their corresponding molar extinction coefficients.

λ_{max}/nm	767	678	533	432	299
ε / L·mol^{-1}·cm^{-1}	8808	6174	2744	4507	17578

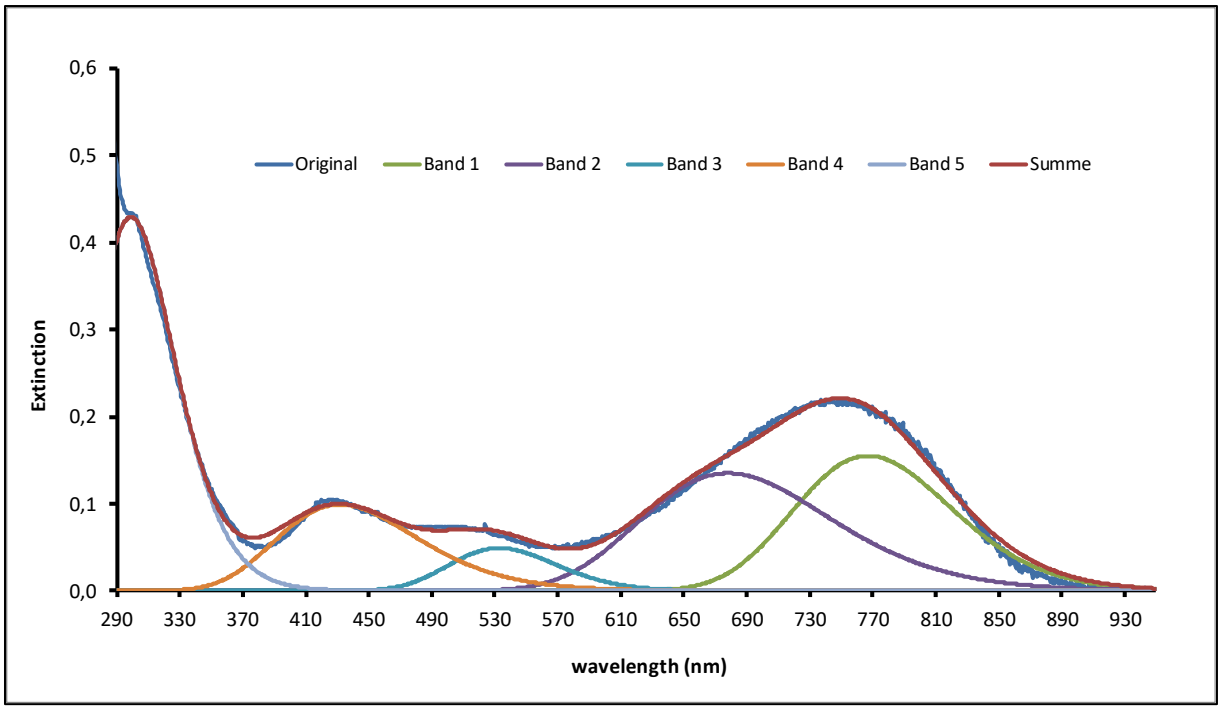

Figure 88. Deconvoluted and experimental UV-Vis-NIR spectra of **25-SnSi** in *n*-hexane at c = 10 µmol L^{-1} and d = 1 mm.

Table 30. Parameters used for the band deconvolution of the UV-Vis-NIR spectrum depicted in ***Figure 88***.

		Band 1	Band 2	Band 3	Band 4	Band 5
Absorbance	$\mathbf{A_{max}}$	0,155	0,135	0,049	0,099	0,429
Bandwidth	$\mathbf{\sigma_{max}}$	1200	1850	1690	3350	4100
Wavelength	$\mathbf{\lambda_{max}}$	767	678	533	432	299

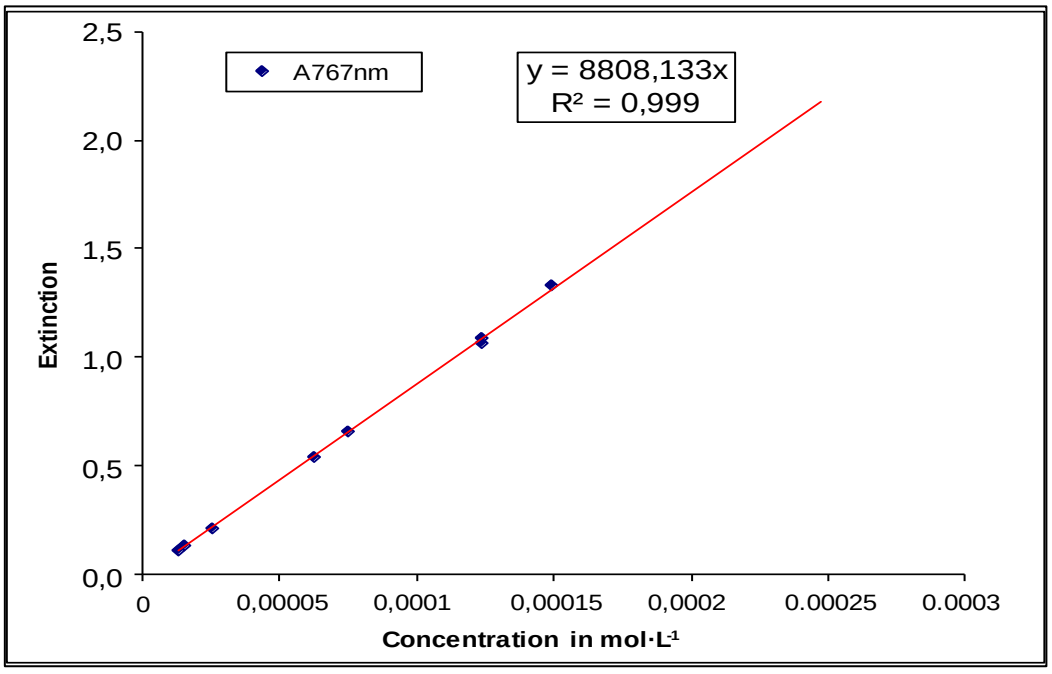

Figure 89. Plot of extinction vs concentration for the band at λ_{max} = 767 nm in the UV-Vis spectrum of **25-SnSi**.

UV-Vis-NIR spectra of **26-SnSi**

The UV-Vis-NIR spectra of **26-SnSi** were recorded in *n*-hexane at ambient temperature and are depicted in ***Figure 90***. The absorption maxima and corresponding molar extinction coefficients (**ε**) are summarized in ***Table 31***. The absorption bands were determined by means of band deconvolution, assuming a Gaussian line profile. The corresponding deconvoluted absorption bands are displayed in ***Figure 91***, and the parameters used for the band deconvolution are summarized in ***Table 32***.

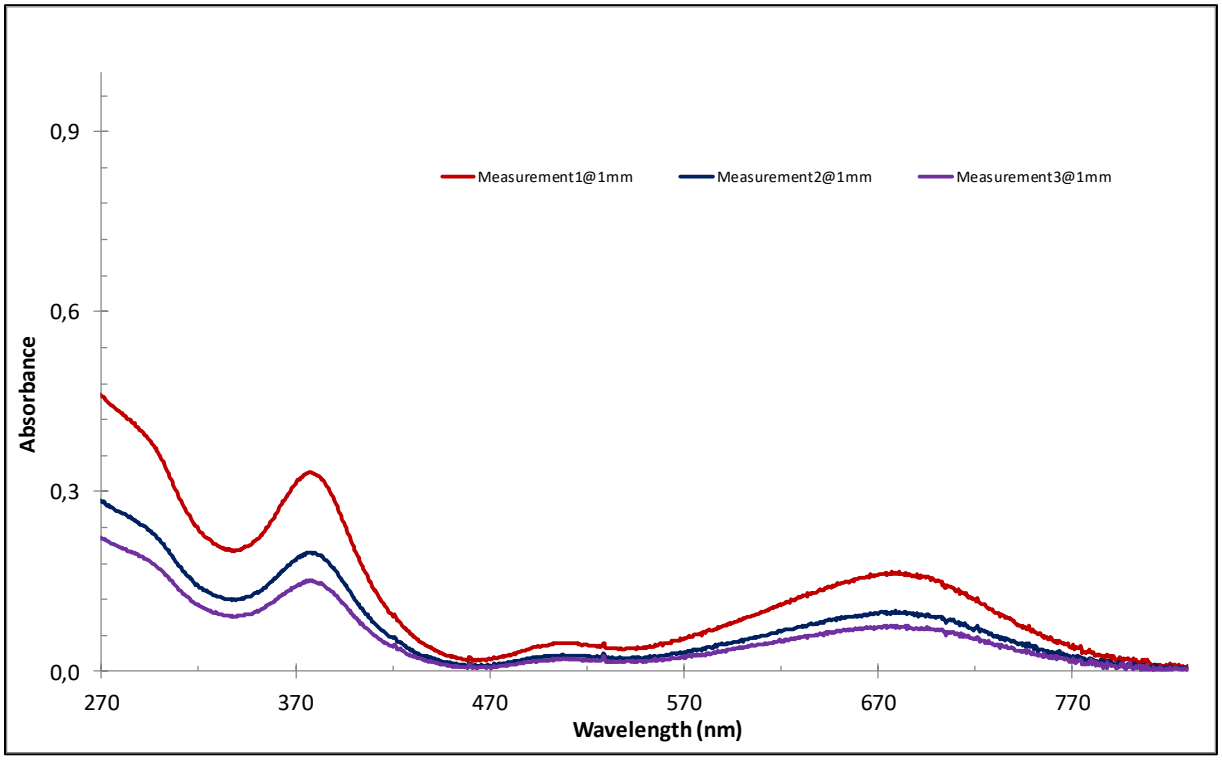

Figure 90. Experimental UV-Vis-NIR spectra of **26-SnSi** in *n*-hexane from 270 – 820 nm at different concentrations.

Table 31. Absorption maxima of the UV-Vis-NIR spectra of **26-SnSi** depicted in ***Figure 87*** and their corresponding molar extinction coefficients.

λ_{max}/nm	670	574	502	378	332	292
ε / L·mol^{-1}·cm^{-1}	7029	2555	1997	14431	8405	16069

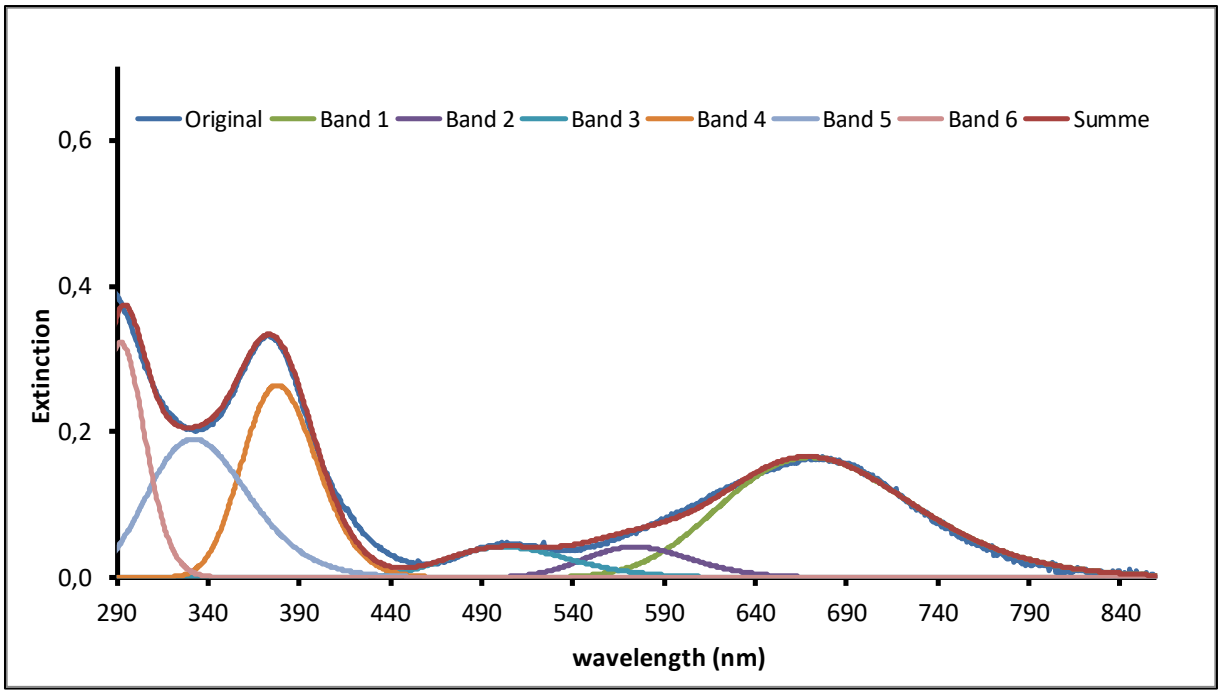

Figure 91. Deconvoluted and experimental UV-Vis-NIR spectra of **26-SnSi** in *n*-hexane at c = 20 µmol L^{-1} and d = 1 mm.

Table 32. Parameters used for the band deconvolution of the UV-Vis-NIR spectrum depicted in ***Figure 91***.

		Band 1	Band 2	Band 3	Band 4	Band 5	Band 6
Absorbance	$\mathbf{A_{max}}$	0,165	0,042	0,042	0,264	0,190	0,323
Bandwidth	σ_{max}	1650	1250	1870	2010	3500	2100
Wavelength	λ_{max}	670	574	502	378	332	292

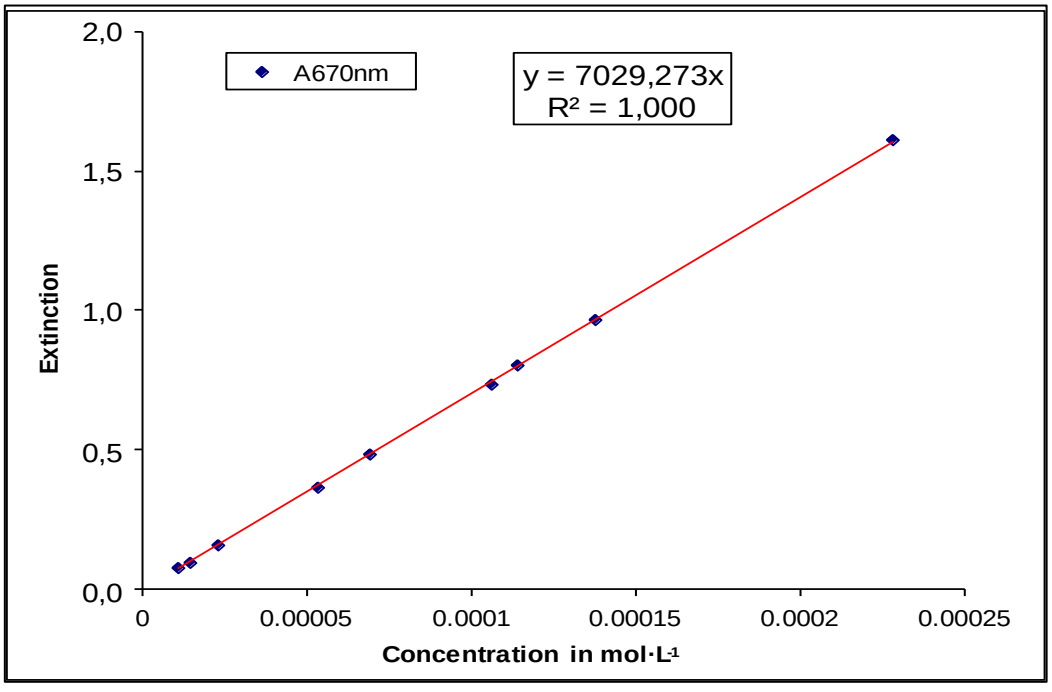

Figure 92. Plot of extinction vs concentration for the band at λ_{max} = 670 nm in the UV-Vis spectrum of **26-SnSi**.

UV-Vis-NIR spectra of 27-SnSi

The UV-Vis-NIR spectra of **27-SnSi** were recorded in *n*-hexane at ambient temperature and are depicted in ***Figure 93***. The absorption maxima and corresponding molar extinction coefficients (**ε**) are summarized in ***Table 33***. The absorption bands were determined by means of band deconvolution, assuming a Gaussian line profile. The corresponding deconvoluted absorption bands are displayed in ***Figure 94***, and the parameters used for the band deconvolution are summarized in ***Table 34***.

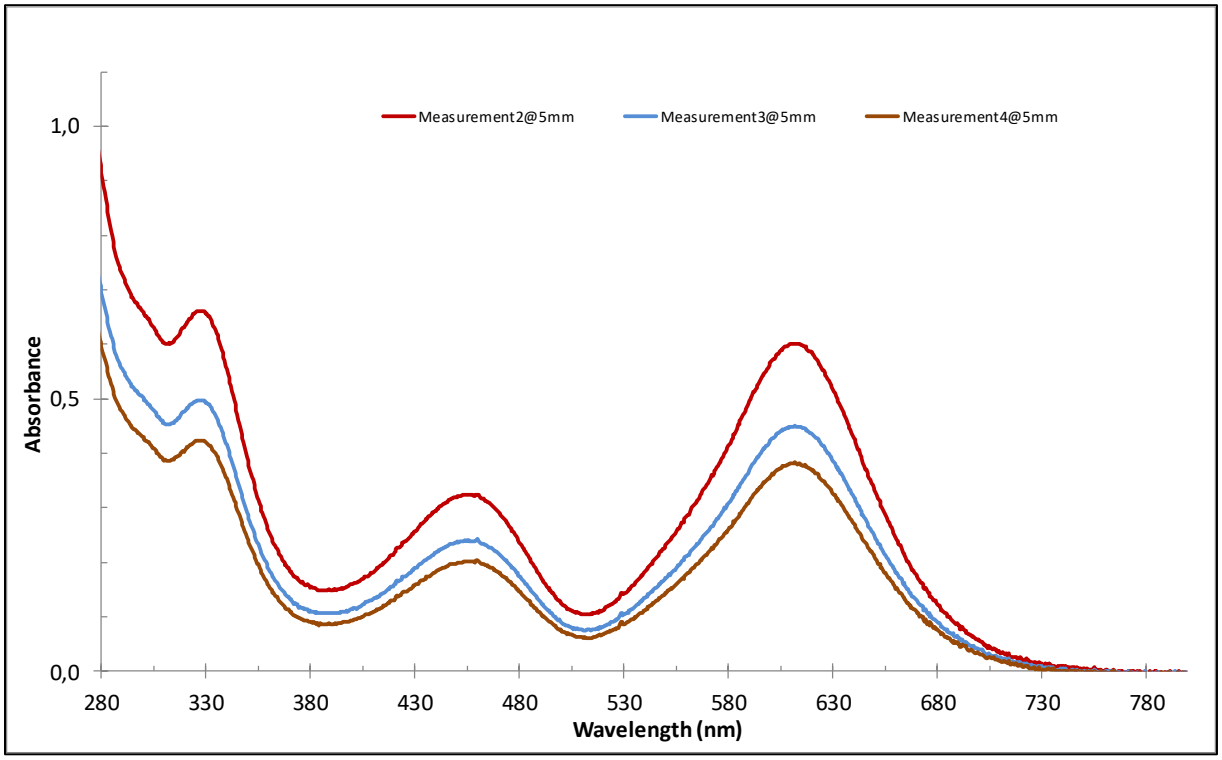

Figure 93. Experimental UV-Vis-NIR spectra of **27-SnSi** in *n*-hexane from 270 – 980 nm at different concentrations.

Table 33. Absorption maxima of the UV-Vis-NIR spectra of **27-SnSi** depicted in ***Figure 87*** and their corresponding molar extinction coefficients.

λ_{max}/nm	614	544	456	400	326
ε / $L \cdot mol^{-1} \cdot cm^{-1}$	9146	3201	5128	2648	10407

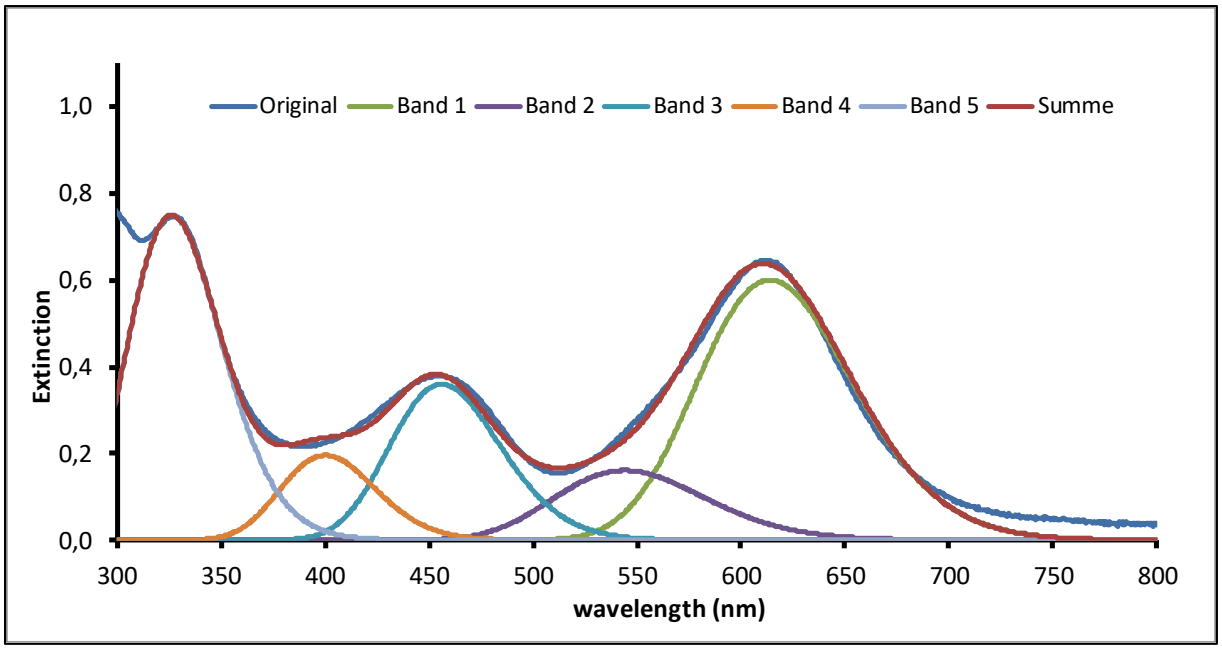

Figure 94. Deconvoluted and experimental UV-Vis-NIR spectra of **27-SnSi** in *n*-hexane at c = 50 µmol L^{-1} and d = 1 mm.

Table 34. Parameters used for the band deconvolution of the UV-Vis-NIR spectrum depicted in ***Figure 91***.

		Band 1	Band 2	Band 3	Band 4	Band 5
Absorbance	$\mathbf{A_{max}}$	0,600	0,161	0,360	0,196	0,750
Bandwidth	σ_{max}	1400	1720	1800	2000	3000
Wavelength	$\boldsymbol{\lambda_{max}}$	614	544	456	400	326

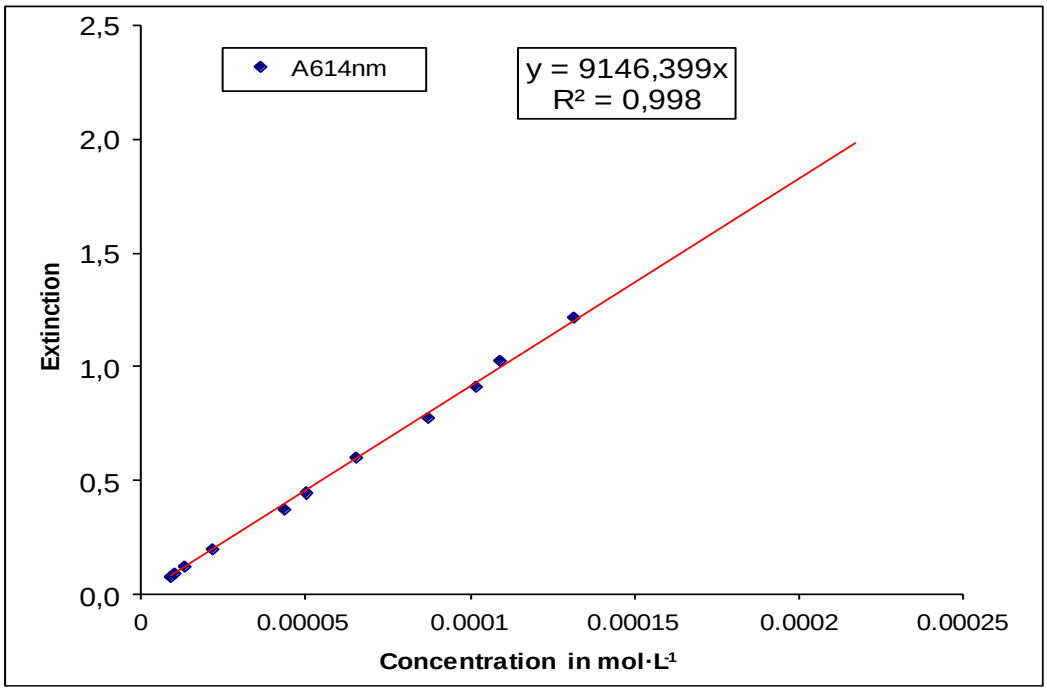

Figure 95. Plot of extinction vs concentration for the band at λ_{max} = 614 nm in the UV-Vis spectrum of **27-SnSi**.

5.5. Study of the dynamics of compound by the VT ^{1}H-NMR spectroscopy

5.5.1. General Part

The VT ^{1}H NMR spectra were recorded in a 300 MHz NMR spectrometer using the following acquisition parameters: Zg30 pulse, 16 scans, 1.0 second relaxation delay (d_1) and 3.0 second acquisition time (a_t). The FIDs were processed as follows: i) apodization using an exponential window function with a line broadening (LB) of 0.3 Hz, ii) zero-filling to 64K before Fourier transform, iii) automatic baseline (5th order polynomial) and phase correction (0th + 1st order polynomial). The probe temperatures were set using a BSVT temperature controller in combination with a liq. N_2 heat exchanger, which was used for the low temperature experiments. Temperature calibration of the BSVT was done using the following calibration standards recommended by Bruker: 4% (D_4)methanol in MeOH (calibration formula for the temperature range 190 − 298 K: T/ K = a·Δδ/ppm + b, where Δδ is the chemical shift difference of the signals of MeOH, and a and b are constants) and 80% ethylene glycol in (D_6)DMSO (calibration formula for the temperature range: 300 − 373 K: T/ K = 109.504·(4.218 − Δδ/ppm), where Δδ is the chemical shift difference of the signals of ethylene glycol). The NMR samples were thermally equilibrated for 10 minutes at each temperature to minimize NMR line-broadening due to temperature gradient and convection in the sample volume. Shimming was performed at each temperature to reduce distortions of the NMR lineshapes due to the magnetic field inhomogeneities caused by the temperature change of the sample. The VT NMR spectra were recorded in 10 K or 5 K steps. The temperature stability of the BSVT unit during the NMR measurement was within ±0.1 K ($\sigma_{sys}(T)$).

The temperature range for the VT NMR experiments was chosen so that the NMR spectra covered the slow, intermediate and fast exchange regime of the dynamic processes on the NMR time-scale ($k << \Delta\nu^{max}$ (slow), $k \approx \Delta\nu^{max}$ (intermediate), $k >> \Delta\nu^{max}$ (fast), where k is the exchange rate constant in Hz and $\Delta\nu^{max}$ is the peak-to-peak separation in Hz in the lower limit of the slow exchange regime).[16] This kinetic regime is indicated by the change in the lineshape of the exchanging signals as broadening-coalescencing-sharpening with increasing exchange rates. The exchange rate constants at different temperatures were obtained by full-lineshape analysis, which was carried out using the gNMR programme (version 5.0.6.0).[17] For this purpose, the

(16) J. Sandström, *Dynamic NMR Spectroscopy*, Academic Press, London, **1982**.

(17) gNMR, Version 5.0.6.0, P.H.M. Budzelaar, Ivorysoft, Centennial, USA, **2006**.

NMR data files were converted by gCVT (version 5.0.6.0) using the WINNMR filter prior to lineshape analysis. Inspection of the VT ^{1}H NMR spectra of all discussed molecules showed that the two exchanging signals have an 1 : 1 integration ratio in the slow exchange regime. Therefore, an equally populated two-site chemical exchange model, where $k_1 = k_{-1}$ (k_1, k_{-1} = exchange rate constant in Hz for the forward and backward reaction) and $\rho_1 = \rho_{-1} = 0.5$ (ρ_1, ρ_{-1} = mole fraction of each exchanging site) was used in the exchange calculation. A pseudo spin model with a pseudo spin parameter of $n{\cdot}I$ (n = number of J-coupled pseudo nuclei to the exchanging signal, I = nuclear spin) was used for the chemical exchange of multiplets with a multiplicity of $2n{\cdot}I + 1$. The line-shape of chemically exchanging signals is a function of the exchange rate constant (k), the peak positions (δ_i^{max}, i = 1, 2) and the peak-to-peak separation in the lower limit of the slow exchange regime ($\Delta\nu^{max} = \delta_1^{max} - \delta_2^{max}$), the natural full-linewidth at half-height ($\Delta\nu^{o}_{½}$) and the scalar coupling constant (J) in the absence of chemical exchange.[18] δ_i^{max} and $\Delta\nu^{max}$ were obtained from the lower limit of the slow exchange regime, which was assumed to be the spectrum with $\Delta\nu_{½} \approx n\Delta\nu^{o}_{½}$ or $|\Delta(\Delta\nu)| \approx n\Delta\nu^{o}_{½}$, where $n \leq 2$, $\Delta\nu_{½}$ is the linewidth of the exchanging signal and $\Delta(\Delta\nu)$ is the change in the peak-separation between two successive VT NMR spectra. A natural linewidth $\Delta\nu^{o}_{½}$ of 1.0 Hz was used for the line-shape analysis of the silyl group of $C^{2,6}$-CH(Si*Me*$_3$)$_A$(Si*Me*$_3$)$_B$ and $C^{3,5}$-*H* aromatic protons of Tbb of all compounds assuming the same T_1 (spin-lattice relaxation time) for these protons and a temperature independence of T_1 and T_2 (spin-spin relaxation time) within the temperature range of the VT NMR measurements. k and δ_i^{max} whereas, $\Delta\nu^{max}$ and $\Delta\nu^{o}_{½}$ were kept as constants. A Lorentzian lineshape, a tight convergence (final residual ≤ 1E−6) and a comparable magnitude within a factor of 10^3 of *singular values* of the singular value matrix obtained in error analysis were considered in the simulation. These criteria ensured relative errors in k ($\sigma(k)/k = \sigma(\ln k)$) in the range of 0.1% − 5% depending on the linewidths of the exchanging signals. Furthermore, spectra having linewidths similar in magnitude to the natural linewidth ($\Delta\nu^{o}_{½}$ = 1.0 Hz) gave exchange rate constants with very large errors despite tight-convergence. This is typically observed near the very slow-exchange and very fast-exchange regime. Therefore, these rate constants were not considered for the determination of the activation parameters by Eyring analysis. As a general trend, the relative errors $\sigma(k)/k$ were found to be < 5% for spectra with linewidths of the exchanging signals much higher than the natural linewidth, typically $\Delta\nu_{½} > 5{\cdot}\Delta\nu^{o}_{½}$. The gNMR lineshape

(18) H. S. Gutowsky, C. H. Holm, *J. Chem. Phys.* **1956**, *25*, 1228.

analysis gives a *pseudo*-first-order rate constant for the chemical exchange, that is $k_1 = k_{-1}$, but not the sum $k^{sum} = k_1 + k_{-1}$. Thus, the exchange rate constant k_c at the coalescence temperature (T_c) obtained from gNMR compares well with that calculated from the Gutowsky-Holm formula (***Eq. 1***), which is valid for the equally populated two-site chemical exchange of two singlets or two multiplets with $\Delta\nu^{max} > 3J$,[19] but differs from that obtained using ***Eq. 2***, which was proposed by M. L. H. Green *et. al.*[20] to correlate the NMR observed rate constant with the intramolecular chemical exchange.

$$k_c = 2.22(\Delta\nu^{max}) \qquad Eq.\ (1)$$

$$k_c{}^{sum} = 2k_c = 4.44(\Delta\nu^{max}) \qquad Eq.\ (2)$$

The temperature dependent exchange rate constants were used in the Eyring analysis for the determination of the standard activation parameters ($\Delta^{\ddagger}H^{\circ}$ *and* $\Delta^{\ddagger}S^{\circ}$). The data analyses were carried out in Excel. The data were plotted in a $\ln(k/T)$ versus $1/T$ plot, the Eyring plot, according to the linearized form of the Eyring equation (***Eq. 3***, k_B = Boltzmann's constant, h = Planck's constant, R = ideal gas constant; transmission coefficient $\kappa = 1$, $\Delta(C_p) = 0$ in the temperature range of the experiments). The error in $\ln(k/T)$ were approximated according to the error propagation formula for uncorrelated errors[21] as $\sigma(\ln k)$ by neglecting the error in T, because, $\sigma(\ln k)$ [$>10^{-2}$] >> ($\sigma_{sys}(T)/T_{av}$) [$\sim 10^{-4}$], where $\sigma_{sys}(T) = \pm 0.2$ K and T_{av} is the average temperature of the VT NMR experiment. The values of $\sigma(\ln k)$ was found to be negligible compared to k, hence were neglected in the regression analysis. The data were fitted using a linear regression instead of weighted linear regression. The standard activation enthalpy ($\Delta^{\ddagger}H^{\circ}$) and the standard activation entropy ($\Delta^{\ddagger}S^{\circ}$) was obtained from the slope and the intercept of the linear regression line using ***Eq. 4*** and ***Eq. 5***, respectively. The standard activation Gibbs free energy ($\Delta^{\ddagger}G^{\circ}$) and the Arrhenius activation energy (E_a) was then calculated using the ***Eq. 6*** and ***Eq. 7***, respectively. The activation Gibbs energy at the coalescence temperature ($\Delta^{\ddagger}G(T_c)$) was estimated from ***Eq. 8***, which was obtained by combining the Gutowsky-Holm formula (***Eq. 1***) with ***Eq. 3*** and ***Eq. 6***. The standard deviations $\sigma_{stat}(\Delta^{\ddagger}H^{\circ})$ and $\sigma_{stat}(\Delta^{\ddagger}S^{\circ})$ were calculated from the standard deviations in slope and intercept according to the variance formula for uncorrelated

(19) a) H. Kessler, *Angew. Chem. Int. Ed.* **1970**, *9*, 219; b) D. Kost, E. H. Carlson, M. Raban, *Chem. Commun.* **1971**, 656.

(20) M. L. H. Green, L. L. Wong, A. Sella, *Organometallics* **1992**, *11*, 2660.

(21) H. H. Ku, *J. Res. Nat. Stand. Sec. C: Engineering and Instrumentation*, **1966**, *70C*, 262.

errors, for which the ***Eq. 4*** and ***Eq. 5*** were used for partial derivatives. The $\sigma_{stat}(\Delta^{\ddagger}G°)$ and $\sigma_{stat}(E_a)$ were calculated from the $\sigma_{stat}(\Delta^{\ddagger}H°)$ and $\sigma_{stat}(\Delta^{\ddagger}S°)$ by error propagation assuming that $\sigma_{stat}(\Delta^{\ddagger}H°)$ and $\sigma_{stat}(\Delta^{\ddagger}S°)$ are small and uncorrelated, for which ***Eq. 6*** and ***Eq. 7*** were considered in the partial derivative assuming $\sigma_{sys}(T)$ = ±0.2 K. Finally, the total errors in the activation parameters were calculated as $\sigma_{total} = ((\sigma_{stat})^2+(\sigma_{sys}))^2)^{1/2}$ and given as two standard deviations from the mean (confidence interval 95%, probability factor Z = 1.96).

$$\ln\left(\frac{k}{T}\right) = \ln\left(\frac{k_B}{h}\right) + \left(\frac{\Delta^{\ddagger}S°}{R}\right) + \left(-\frac{\Delta^{\ddagger}H°}{R}\right)\cdot\frac{1}{T} \qquad \textit{Eq.}\ (3)$$

$$\Delta^{\ddagger}H° = -R \cdot \text{slope}\ [\text{J}\cdot\text{mol}^{-1}] \qquad \textit{Eq.}\ (4)$$

$$\Delta^{\ddagger}S° = R \cdot \left(\text{Intercept} - \ln\left(\frac{k_B}{h}\right)\right)\ [\text{J}\cdot\text{K}^{-1}\cdot\text{mol}^{-1}] \qquad \textit{Eq.}\ (5)$$

$$\Delta^{\ddagger}G° = \Delta^{\ddagger}H° - T\cdot\Delta^{\ddagger}S° \qquad \textit{Eq.}\ (6)$$

$$E_a = \Delta^{\ddagger}H° + R\,T \qquad \textit{Eq.}\ (7)$$

$$\Delta^{\ddagger}G(T_c) = 0.0191\cdot T_c\left[9.97 + \log\left(\frac{T_c}{\Delta\nu^{max}}\right)\right][\text{kJ}\cdot\text{mol}^{-1}] \qquad \textit{Eq.}\ (8)$$

5.5.2. VT ^{1}H NMR spectra and line shape analysis of complex 3-Co

In solution, the digermyne complex **3-Co** exists as a racemic mixture comprising two C_1-symmetric enantiomers, each defined by a stereochemically distinct (***R,R***) and (***S,S***) configuration at the pyramidalized germanium centers (***Figure 96***).

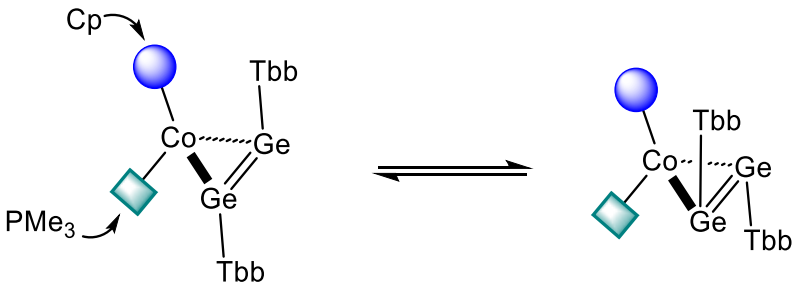

Figure 96. The two C_1-symmetric enantiomers of complex 3-Co undergoing stereomutation in solution.

The observed stereochemical configuration arises from the inherently *trans*-bent, nominally C_{2h}-symmetric geometry of the digermyne core (Ge_2Tbb_2), whose coordination to the cobalt center occurs *via* π_{oop}-bond. This interaction disrupts the symmetry and renders the Tbb substituents diastereotopic. Of these, one substituent, arbitrarily designated Tbb_X - projects toward the PMe_3 ligand (and away from the Cp ligand), while the other, denoted Tbb_Y, is oriented in the opposite direction, toward the Cp ligand. Consequently, in the slow exchange regime, distinct ^1H NMR resonances are observed for each of the diastereotopic Tbb substituents. For instance, two separate singlets corresponding to the ^tBu protons appear at δ = 1.31 ppm and 1.37 ppm at 193 K. Furthermore, at low temperatures, rotational freedom about the respective Ge–C^{ipso} bond vectors for both Tbb_X and Tbb_Y is effectively suppressed. This conformational rigidity results in the appearance of two sets of signals for the Dsi substituents bonded to C^2/C^6, as well as for the protons at C^3/C^5, in the ^1H NMR spectra recorded in (D_8)THF over the temperature range of 193 – 333 K. The observed dynamic behaviour can be effectively interpreted in three distinct and explanatory ways:

- **Tbb_X rotation around Ge–Tbb_X^{ipso} bond vector**

Compound **3-Co** exhibits hindered rotation of the Tbb_X substituent about the Ge–C^{ipso} bond axis, as evidenced by a pair of distinct resonances for the aromatic C^3/C^5 protons in the low-temperature ^1H NMR spectrum recorded at 193 K. These appear as narrowly split, roof-effect doublets at δ = 6.57 and 6.61 ppm (^4J(H,H) = 1.4 Hz, Δν = 13 Hz). This dynamic process was investigated *via* variable-temperature (VT) ^1H NMR spectroscopy over the range of 193 − 273 K (***Figure 97***), with coalescence of the two signals observed at 263 K. Using this temperature as the coalescence temperature (T_c), the activation barrier for rotation about the Ge–C^{ipso} bond in Tbb_X was calculated according to the Gutowsky Holm equation (***Eq. 1***), yielding a $\Delta^{\ddagger}G$ value of 56.80 kJ/mol based on a Δν of 13 Hz.

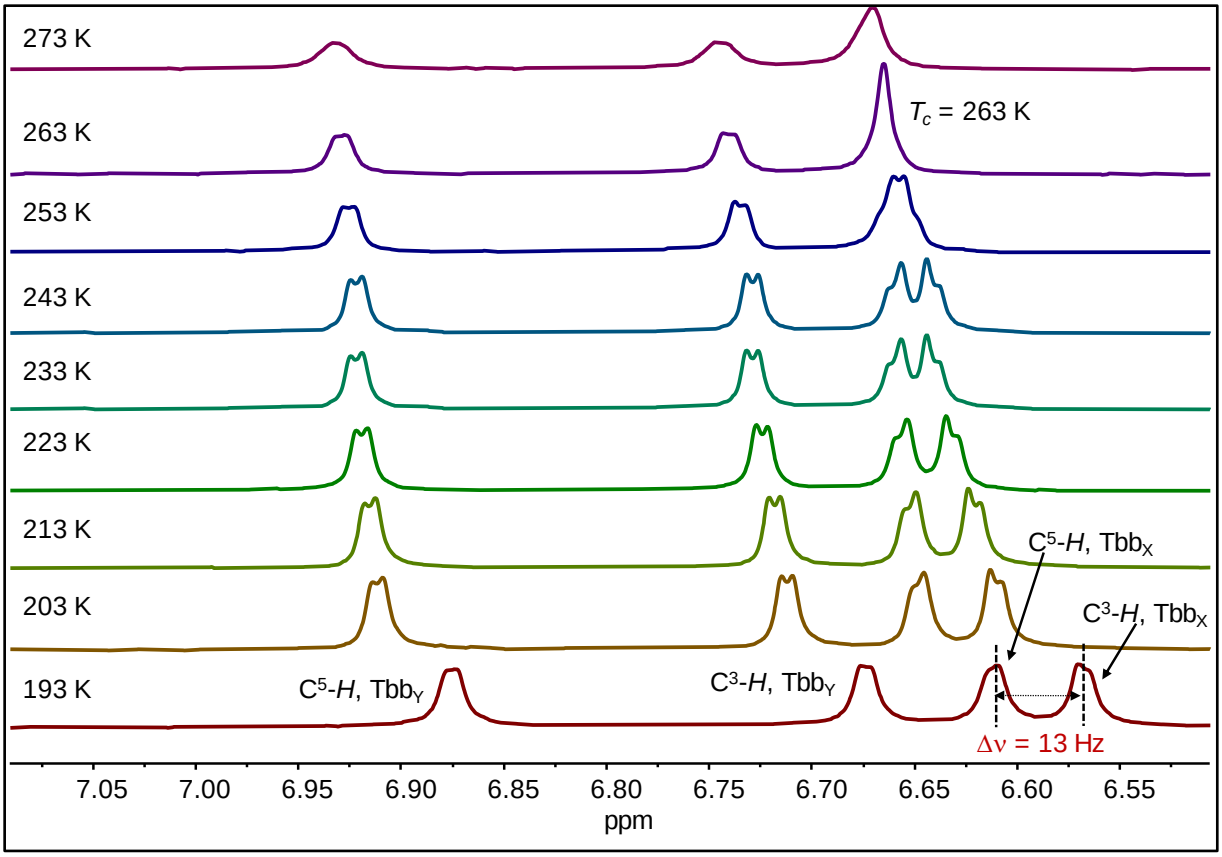

Figure 97. Excerpt of the VT ^{1}H NMR spectra (300.1 MHz) of **3-Co** in (D_8)THF (chemical shift range: 6.50 − 7.10 ppm) in temperature range 193 − 273 K showing the Tbb_X rotational dynamics.

- **Enantiomerization (Homotopomerization of Tbbb substituents)**

The second dynamic process of **3-Co** was studied taking advantage of the interchanging of ^{t}Bu methyl protons, which upon warming first broaden, then coalesce at ≈ 283 K (***Figure 98***) and finally merge to a sharp singlet at 333 K. This dynamic process (enantiomerization) is an example of an equally populated two-site chemical exchange. A comprehensive line-shape analysis of the NMR signals across the temperature range of 253 K − 303 K, performed using the gNMR simulation software, yielded the first-order rate constants for the exchange between the Tbb_X and Tbb_Y substituents, as summarized in ***Table 35***.

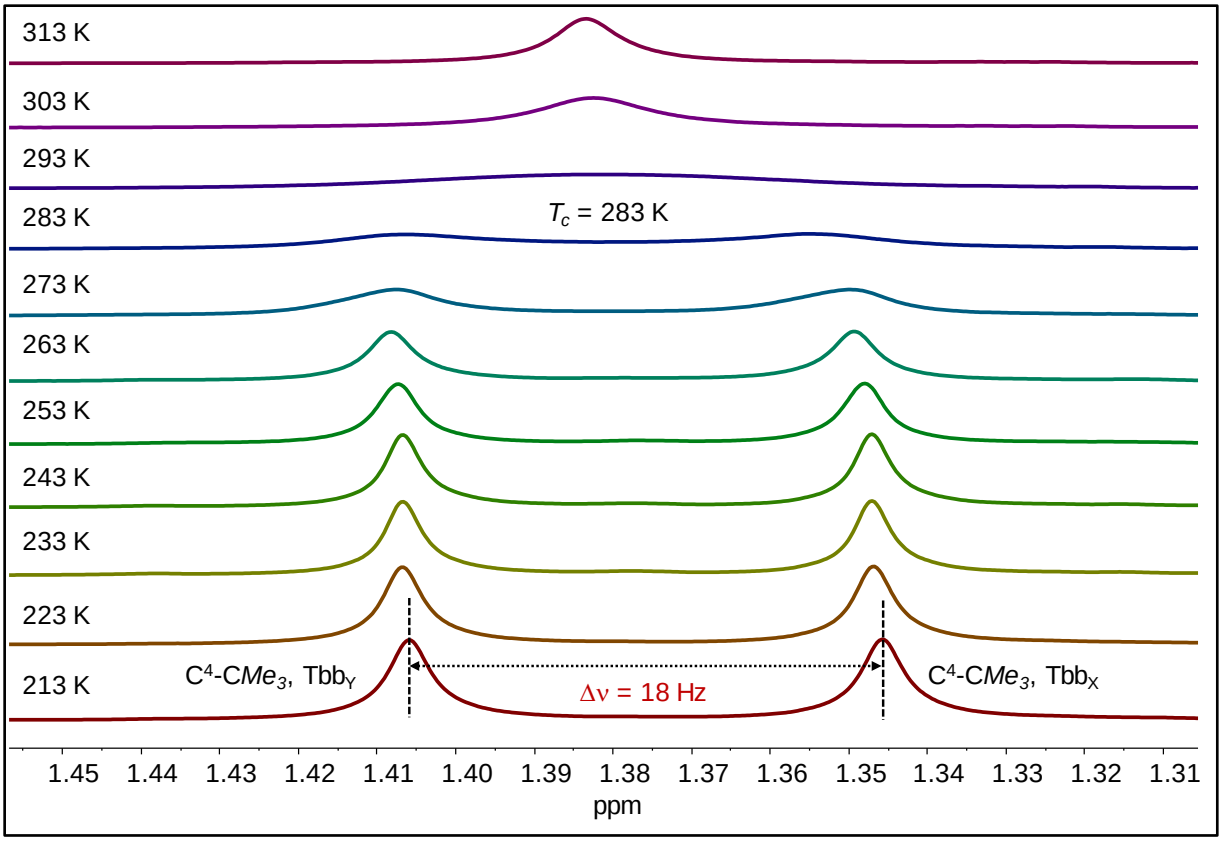

Figure 98. Excerpt of the VT ^{1}H NMR spectra (300.1 MHz) of **3-Co** in (D_8)THF (chemical shift range: 1.31 – 1.45 ppm) in temperature range 213 – 313 K showing the exchanging C^4-CMe_3 signals of the Tbb_X and Tbb_Y substituents.

Table 35. Exchange rate constants of the chemical exchange of the C^4-CMe_3 protons of the Tbb_X and Tbb_Y substituents at different temperature obtained from full line shape analysis of the VT ^{1}H NMR spectra.

T	K	K/T	ln(k/T)	1/T
253	0,395	0,001561	-6,46226	0,003953
263	6,65	0,025285	-3,67754	0,003802
273	17,9	0,065568	-2,72467	0,003663
283	52,1	0,184099	-1,69228	0,003534
293	206	0,703072	-0,3523	0,003413
303	934	3,082508	1,125744	0,0033

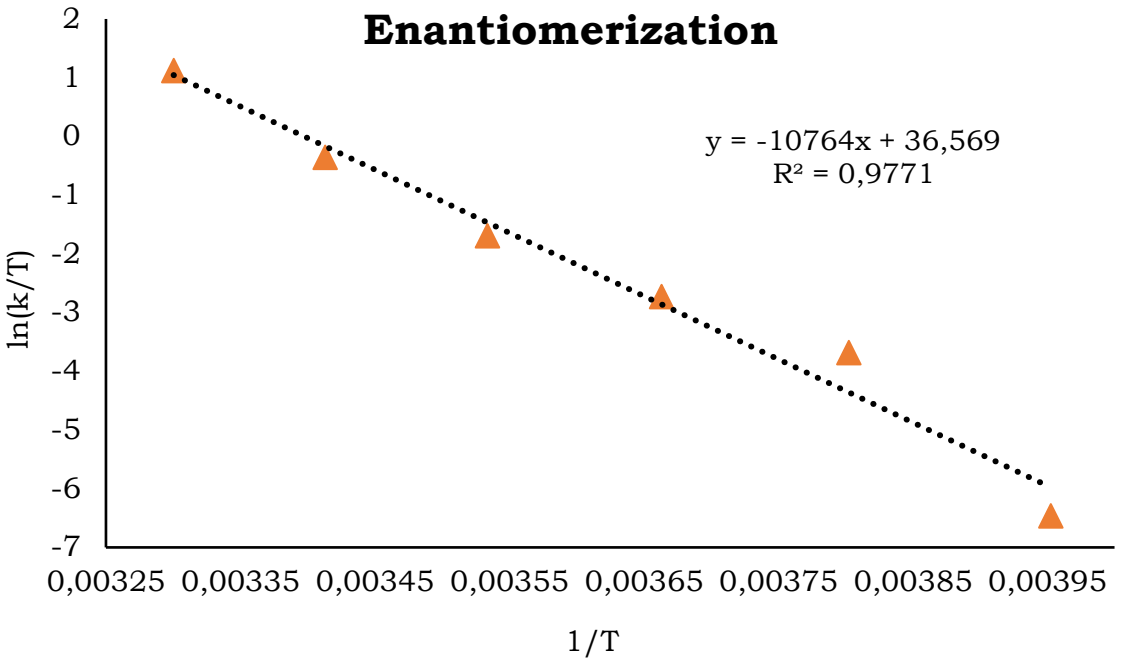

Figure 99. Eyring plot of the two-site degenerate chemical exchange of the two C^4-CMe_3 methyl protons of Tbb substituents (Tbb_X and Tbb_Y) in **3-Co**.

The tempertaure dependence of the exchange rate constant k was derived from a modified form of the linearized Eyring equastion (***Eq. 3***, k_B = Boltzmann constant, h = Plank's constant, R = universal gas constant) assuming that the transmission coefficient κ is equal to 1 and that the activation enthalpy ($\Delta^{\ddagger}H$) is constant over the temperature interval of the experiment ($\Delta^{\ddagger}C_p = d(\Delta^{\ddagger}H)/dT = 0$, $\Delta^{\ddagger}C_p$ = heat capacity of activation). The reulting thermodynamic activation parameter for the eneantiomerization process in 3-Co are tabulated in ***Table 36***.

Table 36. Thermodynamic parameters of the chemical exchange process of the two C^4-CMe_3 methyl protons of Tbb substituents (Tbb_X and Tbb_Y) in **3-Co** obtained from line shape analysis.

$\Delta^{\ddagger}H$ / kJ.mol^{-1}	$\Delta^{\ddagger}S$ / J.mol^{-1}.K^{-1}	$\Delta^{\ddagger}G$ at 298 K / kJ.mol^{-1}	$\Delta^{\ddagger}G$ at T_c / kJ.mol^{-1}	$\Delta E_a^{\ddagger}$ at 298 K / kJ.mol^{-1}
89.5(±2.4)	106.5(±12)	57.8(±4.3)	60.5[a)]	92.0(±3)

a) The $\Delta^{\ddagger}G$ at T_c was obtained from Gutowsky formula, $k_c = 2.22(\Delta\nu)$; where, T_c = 283 K, $\Delta\nu$ = 18 Hz.

- **Tbb_Y rotation around Ge–Tbb_Y^{ipso} bond vector**

Compound **3-Co** exhibits hindered rotation of the Tbb_Y substituent about the Ge–C^{ipso} bond axis, as evidenced by a pair of distinct resonances for the aromatic C^3/C^5 protons in the low-temperature ^{1}H NMR spectrum recorded at 243 K. This dynamic process was investigated *via* variable-temperature (VT) ^{1}H NMR spectroscopy over the range of 243 − 333 K (***Figure 100***), with coalescence of the two signals observed at

303 K. Using this temperature as the coalescence temperature (T_c), the activation barrier for rotation about the Ge–C^{ipso} bond in Tbb_X was calculated according to the Gutowsky Holm equation (***Eq. 1***), yielding a $\Delta^{\ddagger}G$ value of 64.1 kJ/mol based on a $\Delta\nu$ of 18 Hz.

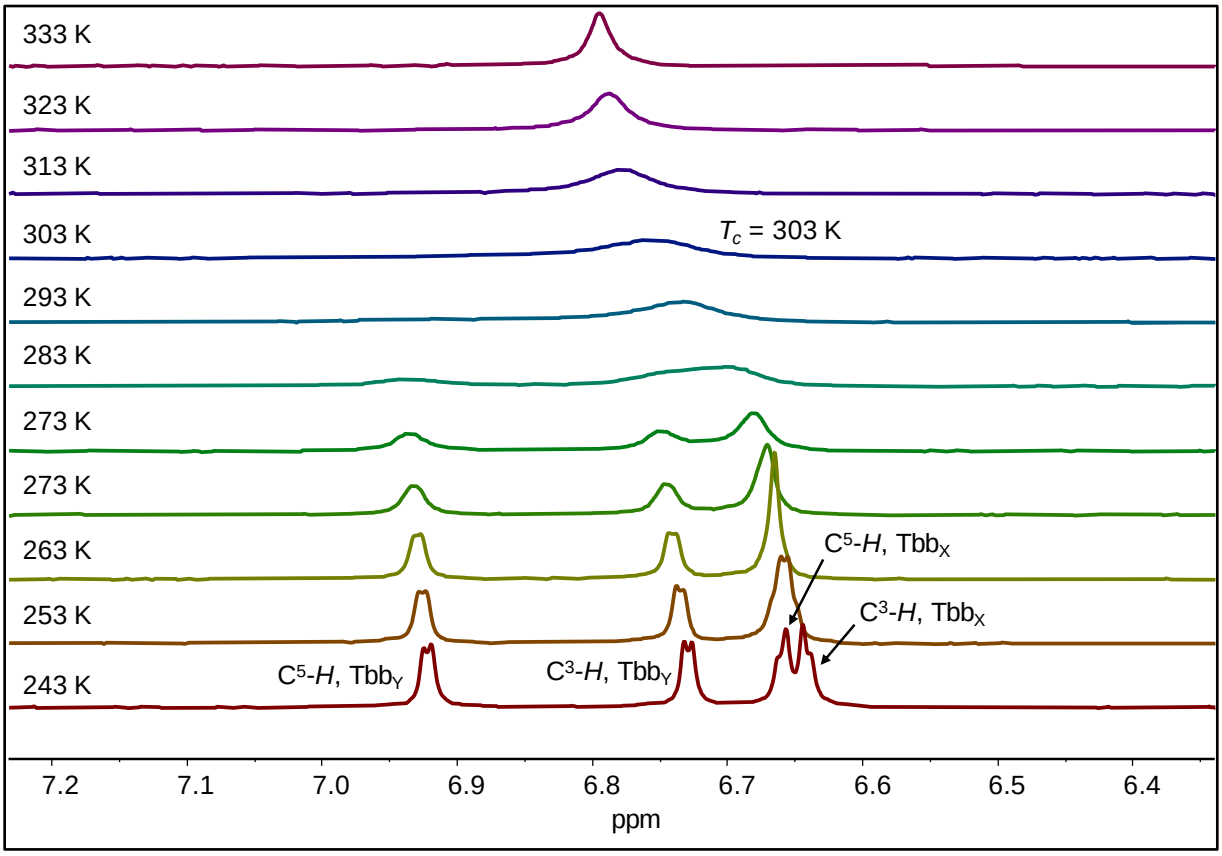

Figure 100. Excerpt of the VT ^{1}H NMR spectra (300.1 MHz) of **3-Co** in (D_8)THF (chemical shift range: 6.35 – 7.20 ppm) in temperature range 243 – 333 K showing the Tbb_Y rotational dynamics.

5.6. List of abbreviations

4-dmap	4-dimethylaminopyridine
ATR	Attenuated total reflection
br	broad
ca.	circa
calcd.	calculated
CAAC	cyclic(alkyl)(amino)carbene
caac^{Me}	:C[N(Dipp)(CMe_2)(CH_2)(CR_2)] R = Me
Cp	cyclopentadienyl
Cp*	pentamethylcyclopentadienyl
CV	Cyclic voltammetry
$\Delta\nu_{1/2}$	half height width
d	doublet
dec.	decomposition
DEPT	distortionless enhancement by polarisation transfer
DFT	Density functional theory
Dipp	2,6-$^{i}Pr_2$-C_6H_3
DME	dimethoxyethane
dmfc	Decamethylferrocene, [η^5-$C_5Me_5)_2$Fe]
Dsi	Disyl, $CH(SiMe_3)_2$
EA	elemental analysis
Eind	1,1,3,3,5,5,7,7-octaethyl-s-hydrindacen-4-yl
equiv.	equivalent(s)
EPR	electron paramagnetic resonance
Et_2O	diethylether
et al.	And others
FT	Fourier-transform
Fig.	figure
HMBC	Heteronuclear multiple bond correlation
HMQC	Heteronuclear multiple quantum coherence

HOMO	Highest occupied molecular orbital
in situ	in the reaction mixture
^{i}Pr	isopropyl
IMe$_4$	1,3,4,5-tetramethylimidazol-2-ylidene
I^{i}Pr$_2$Me$_2$	:C[N(*i*Pr)C(Me)]$_2$
IDipp	1,3-bis(2,6-diisopropylphenyl)imidazol-2-ylidene
IR	Infrared
Mes	mesityl, 2,4,6-Me$_3$-C$_6$H$_2$
Mind	1,3,3,5,5,7,7-octamethyl-*s*-hydrindacen-4-yl
NBO	natural bond orbital
NHC	N-heterocyclic carbene
NHP	N-heterocyclic Phosphine
NHI	N-heterocylcic imine
NMR	nuclear magnetic resonance
NRT	natural resonance theory
OTf	triflate, OSO$_2$(CF$_3$)
Ph	phenyl substituent
SIDipp	1,3-bis(2,6-diisopropylphenyl)imidazolidin-2-ylidene
t	triplet
Tbb	2,4-Dsi$_2$-4-^{t}Bu-C$_6$H$_2$
Tbt	2,4,6-(CH(SiMe$_3$)$_2$)$_3$-C$_6$H$_2$
^{t}*Bu*	tert.-butyl
THF	tetrahydrofuran
Tip	2,4,6-^{i}Pr$_2$-C$_6$H$_3$
TMS	SiMe$_3$
UV	ultra violet
Vis	visible
vs	very strong
vw	very weak
X	halogen

5.7. Scientific Contributions

Conference contributions

"Entry into Heteroditetrelyne Chemistry *via* Si(NHC) and SnR Transfer Reactions ".

A. Singh, S. Kumar, D. Hoffmann, G. Schnakenburg, U. Das* and A. C. Filippou*, GDCh Conference on Inorganic Chemistry, Munich, Germany, 16th – 18th September, **2024**, Book of Abstracts, W 132.

6. Oath of compliance with the principles of scientific integrity

I hereby affirm that this dissertation was prepared independently at the Institute of Inorganic Chemistry, University of Bonn under the supervision of Prof. Dr. Alexander C. Filippou, and all references and additional sources have been appropriately cited.

Avnish Singh

Bonn, 2025

7. References

[1] A. F. Holleman, E. Und Nils Wiberg, G. Fischer, *Lehrbuch der Anorganischen Chemie*, Walter De Gruyter, Berlin • New York, **2007**.

[2] P. Siffert, E. F. Krimmel, Eds., *Silicon*, Springer Berlin Heidelberg, Berlin, Heidelberg, **2004**.

[3] L. Gallagher, "Sand and sustainability: Finding new solutions for environmental governance of global sand resources" **2019**, DOI 10.13140/RG.2.2.33747.63526.

[4] A. Torres, J. Brandt, K. Lear, J. Liu, "A looming tragedy of the sand commons" *Science* **2017**, *357*, 970–971.

[5] S. Patai, Z. Rappoport, Y. Apeloig, Eds., *The chemistry of organic silicon compounds*, Wiley, Chichester [England]; New York, **1989**.

[6] J. P. Desclaux, "Relativistic Dirac-Fock expectation values for atoms with Z = 1 to Z = 120" *At. Data Nucl. Data Tables* **1973**, *12*, 311–406.

[7] A. L. Allred, "Electronegativity values from thermochemical data" *J. Inorg. Nucl. Chem.* **1961**, *17*, 215–221.

[8] P. P. Power, "π-Bonding and the Lone Pair Effect in Multiple Bonds between Heavier Main Group Elements" *Chem. Rev.* **1999**, *99*, 3463–3504.

[9] P. J. Davidson, M. F. Lappert, "Stabilisation of metals in a low co-ordinative environment using the bis(trimethylsilyl)methyl ligand; coloured Sn II and Pb II alkyls, $M[CH(SiMe_3)_2]_2$" *J. Chem. Soc. Chem. Commun.* **1973**, 317a.

[10] D. E. Goldberg, D. H. Harris, M. F. Lappert, K. M. Thomas, "A new synthesis of divalent group 4B alkyls $M[CH(SiMe_3)_2]_2$(M = Ge or Sn), and the crystal and molecular strcuture of the tin compound" *J. Chem. Soc. Chem. Commun.* **1976**, 261.

[11] P. P. Power, "An Update on Multiple Bonding between Heavier Main Group Elements: The Importance of Pauli Repulsion, Charge-Shift Character, and London Dispersion Force Effects" *Organometallics* **2020**, *39*, 4127–4138.

[12] R. West, M. J. Fink, J. Michl, "Tetramesityldisilene, a Stable Compound Containing a Silicon-Silicon Double Bond" *Science* **1981**, *214*, 1343–1344.

[13] R. C. Fischer, P. P. Power, "π-Bonding and the Lone Pair Effect in Multiple Bonds Involving Heavier Main Group Elements: Developments in the New Millennium" *Chem. Rev.* **2010**, *110*, 3877–3923.

[14] V. Ya. Lee, A. Sekiguchi, *Organometallic Compounds of Low-Coordinate Si, Ge, Sn and Pb: From Phantom Species to Stable Compounds*, Wiley, **2010**.

[15] C. Weetman, "Main Group Multiple Bonds for Bond Activations and Catalysis" *Chem. – Eur. J.* **2021**, *27*, 1941–1954.

[16] D. Scheschkewitz, Ed., *Functional Molecular Silicon Compounds II: Low Oxidation States*, Springer International Publishing, Cham, **2014**.

[17] C. R. Landis, F. Weinhold, "Origin of Trans-Bent Geometries in Maximally Bonded Transition Metal and Main Group Molecules" *J. Am. Chem. Soc.* **2006**, *128*, 7335–7345.

[18] R. A. Poirier, J. D. Goddard, "The isomers of Si_2H_4: disilene and silylsilylene" *Chem. Phys. Lett.* **1981**, *80*, 37–41.

[19] G. Trinquier, J. P. Malrieu, "Nonclassical distortions at multiple bonds" *J. Am. Chem. Soc.* **1987**, *109*, 5303–5315.

[20] P. P. Power, "Main-group elements as transition metals" *Nature* **2010**, *463*, 171–177.

[21] H. B. Wedler, P. Wendelboe, D. J. Tantillo, P. P. Power, "Second order Jahn–Teller interactions at unusually high molecular orbital energy separations" *Dalton Trans.* **2020**, *49*, 5175–5182.

[22] P. P. Power, "An Update on Multiple Bonding between Heavier Main Group Elements: The Importance of Pauli Repulsion, Charge-Shift Character, and London Dispersion Force Effects" *Organometallics* **2020**, *39*, 4127–4138.

[23] M. J. Fink, M. J. Michalczyk, K. J. Haller, R. West, J. Michl, "The X-ray crystal structure of tetramesityldisilene" *J. Chem. Soc. Chem. Commun.* **1983**, 1010.

[24] K. L. Hurni, P. A. Rupar, N. C. Payne, K. M. Baines, "On the Synthesis, Structure, and Reactivity of Tetramesityldigermene" *Organometallics* **2007**, *26*, 5569–5575.

[25] R. P. Singh, S. Kumar, S. Dubey, A. Singh, "A review on working and applications of oxy-acetylene gas welding" *Mater. Today Proc.* **2021**, *38*, 34–39.

[26] Y. Saeki, T. Emura, "Technical progresses for PVC production" *Prog. Polym. Sci.* **2002**, *27*, 2055–2131.

[27] K. C. Nicolaou, P. G. Nantermet, H. Ueno, R. K. Guy, E. A. Couladouros, E. J. Sorensen, "Total Synthesis of Taxol. 1. Retrosynthesis, Degradation, and Reconstitution" *J. Am. Chem. Soc.* **1995**, *117*, 624–633.

[28] R. Zhao, J. Zhu, X. Jiang, R. Bai, "Click chemistry-aided drug discovery: A retrospective and prospective outlook" *Eur. J. Med. Chem.* **2024**, *264*, 116037.

[29] H. Chen, L. Zhai, Y. Zuo, X. Qin, J. Zhang, K. Tian, P. Xu, "Simultaneous Dehalogenation and Hydrogenation in Sonogashira Coupling" *Precis. Chem.* **2023**, *1*, 602–607.

[30] D. Kumar, R. C. Sharma, "Advances in conductive polymers" *Eur. Polym. J.* **1998**, *34*, 1053–1060.

[31] K. J. Hughes, K. A. Iyer, R. E. Bird, J. Ivanov, S. Banerjee, G. Georges, Q. A. Zhou, "Review of Carbon Nanotube Research and Development: Materials and Emerging Applications" *ACS Appl. Nano Mater.* **2024**, *7*, 18695–18713.

[32] T. Tsukada, Y. Shoji, K. Takenouchi, H. Taka, T. Fukushima, "A carbon-functionality-appended diborylacetylene available for a component of organic synthesis and OLEDs" *Chem. Commun.* **2022**, *58*, 4973–4976.

[33] L. Pu, B. Twamley, P. P. Power, "Synthesis and Characterization of 2,6-$Trip_2H_3C_6PbPbC_6H_3$-2,6-$Trip_2$ (Trip = C_6H_2-2,4,6-$^iPr_3$): A Stable Heavier Group 14 Element Analogue of an Alkyne" *J. Am. Chem. Soc.* **2000**, *122*, 3524–3525.

[34] M. Stender, A. D. Phillips, R. J. Wright, P. P. Power, "Synthesis and Characterization of a Digermanium Analogue of an Alkyne" *Angew. Chem. Int. Ed.* **2002**, *41*, 1785–1787.

[35] A. D. Phillips, R. J. Wright, M. M. Olmstead, P. P. Power, "Synthesis and Characterization of 2,6-$Dipp_2$-$H_3C_6SnSnC_6H_3$-2,6-$Dipp_2$ (Dipp = C_6H_3-2,6-$^iPr_2$): A Tin Analogue of an Alkyne" *J. Am. Chem. Soc.* **2002**, *124*, 5930–5931.

[36] A. Sekiguchi, R. Kinjo, M. Ichinohe, "A Stable Compound Containing a Silicon-Silicon Triple Bond" *Science* **2004**, *305*, 1755–1757.

[37] N. Wiberg, W. Niedermayer, H. Nöth, M. Warchhold, "Auf dem Wege zu einem Disilin -Si≡Si-: Bildung von RHSi=SiHR und Hinweise auf die intermediäre Bildung von RSi≡SiR (R = $SiH(Si^tBu_3)_2$)" *Z. Für Anorg. Allg. Chem.* **2001**, *627*, 1717–1722.

[38] N. Wiberg, W. Niedermayer, G. Fischer, H. Nöth, M. Suter, "Synthesis, Structure and Dehalogenation of the Disilene RClSi=SiClR [R = $(^tBu_3Si)_2MeSi$]" *Eur. J. Inorg. Chem.* **2002**, *2002*, 1066–1070.

[39] E. A. Carter, W. A. Goddard, "Relation between singlet-triplet gaps and bond energies" *J. Phys. Chem.* **1986**, *90*, 998–1001.

[40] J. P. Malrieu, G. Trinquier, "Trans-bending at double bonds. Occurrence and extent" *J. Am. Chem. Soc.* **1989**, *111*, 5916–5921.

[41] P. P. Power, "Silicon, germanium, tin and lead analogues of acetylenes" *Chem. Commun.* **2003**, 2091.

[42] H. B. Wedler, P. Wendelboe, P. P. Power, "Second-Order Jahn–Teller (SOJT) Structural Distortions in Multiply Bonded Higher Main Group Compounds" *Organometallics* **2018**, *37*, 2929–2936.

[43] T. Sugahara, J.-D. Guo, D. Hashizume, T. Sasamori, S. Nagase, N. Tokitoh, "The selective formation of a 1,2-disilabenzene from the reaction of a disilyne with phenylacetylene" *Dalton Trans.* **2018**, *47*, 13318–13322.

[44] T. Sasamori, K. Hironaka, Y. Sugiyama, N. Takagi, S. Nagase, Y. Hosoi, Y. Furukawa, N. Tokitoh, "Synthesis and Reactions of a Stable 1,2-Diaryl-1,2-dibromodisilene: A Precursor for Substituted Disilenes and a 1,2-Diaryldisilyne" *J. Am. Chem. Soc.* **2008**, *130*, 13856–13857.

[45] Y. Murata, M. Ichinohe, A. Sekiguchi, "Unsymmetrically Substituted Disilyne $Dsi_2{}^tPrSi—Si{\equiv}Si—SiNpDsi_2$(Np = $CH_2{}^tBu$): Synthesis and Characterization" *J. Am. Chem. Soc.* **2010**, *132*, 16768–16770.

[46] S. Ishida, R. Sugawara, Y. Misawa, T. Iwamoto, "Palladium and Platinum η^2-Disilyne Complexes Bearing an Isolable Dialkyldisilyne as a Ligand" *Angew. Chem.* **2013**, *125*, 13107–13111.

[47] Y. Ding, J. Zhang, Y. Li, C. Cui, "Disilicon Dicarbonyl Complex: Synthesis and Protonation of CO with O–H Bond" *J. Am. Chem. Soc.* **2022**, *144*, 20566–20570.

[48] Y. Sugiyama, T. Sasamori, Y. Hosoi, Y. Furukawa, N. Takagi, S. Nagase, N. Tokitoh, "Synthesis and Properties of a New Kinetically Stabilized Digermyne: New Insights for a Germanium Analogue of an Alkyne" *J. Am. Chem. Soc.* **2006**, *128*, 1023–1031.

[49] Y. Peng, R. C. Fischer, W. A. Merrill, J. Fischer, L. Pu, B. D. Ellis, J. C. Fettinger, R. H. Herber, P. P. Power, "Substituent effects in ditetrel alkyne analogues: multiple vs. single bonded isomers" *Chem. Sci.* **2010**, *1*, 461.

[50] J. Li, C. Schenk, C. Goedecke, G. Frenking, C. Jones, "A Digermyne with a Ge–Ge Single Bond That Activates Dihydrogen in the Solid State" *J. Am. Chem. Soc.* **2011**, *133*, 18622–18625.

[51] T. J. Hadlington, M. Hermann, J. Li, G. Frenking, C. Jones, "Activation of H_2 by a Multiply Bonded Amido-Digermyne: Evidence for the Formation of a Hydrido-Germylene" *Angew. Chem. Int. Ed.* **2013**, *52*, 10199–10203.

[52] T. Sugahara, J.-D. Guo, T. Sasamori, Y. Karatsu, Y. Furukawa, A. E. Ferao, S. Nagase, N. Tokitoh, "Reaction of a Stable Digermyne with Acetylenes: Synthesis of a 1,2-Digermabenzene and a 1,4-Digermabarrelene" *Bull. Chem. Soc. Jpn.* **2016**, *89*, 1375–1384.

[53] J. A. Kelly, M. Juckel, T. J. Hadlington, I. Fernández, G. Frenking, C. Jones, "Synthesis and Reactivity Studies of Amido-Substituted Germanium(I)/Tin(I) Dimers and Clusters" *Chem. – Eur. J.* **2019**, *25*, 2773–2785.

[54] A. Caise, L. P. Griffin, A. Heilmann, C. McManus, J. Campos, S. Aldridge, "Controlling Catenation in Germanium(I) Chemistry through Hemilability" *Angew. Chem. Int. Ed.* **2021**, *60*, 15606–15612.

[55] R. C. Fischer, L. Pu, J. C. Fettinger, M. A. Brynda, P. P. Power, "Very Large Changes in Bond Length and Bond Angle in a Heavy Group 14 Element Alkyne Analogue by Modification of a Remote Ligand Substituent" *J. Am. Chem. Soc.* **2006**, *128*, 11366–11367.

[56] L. G. Perla, J. M. Kulenkampff, J. C. Fettinger, P. P. Power, "Steric and Electronic Properties of the Bulky Terphenyl Ligand Ar^{tBu6}(Ar^{tBu6} = C_6H_3-2,6(C_6H_2-2,4,6-$^tBu_3$)$_2$) and Synthesis of Its Tin Derivatives $Ar^{tBu6}SnCl$, $Ar^{tBu6}SnSn(H)_2Ar^{tBu6}$, and $Ar^{tBu6}SnSnAr^{tBu6}$: A New Route to a Distannyne via Thermolysis of the Asymmetric Hydride $Ar^{tBu6}SnSn(H)_2Ar^{tBu6}$" *Organometallics* **2018**, *37*, 4048–4054.

[57] T. J. Hadlington, C. Jones, "A singly bonded amido-distannyne: H_2 activation and isocyanide coordination" *Chem. Commun.* **2014**, *50*, 2321.

[58] J. Guo, T. Sasamori, "Activation of Small Molecules by Compounds that Contain Triple Bonds Between Heavier Group-14 Elements" *Chem. – Asian J.* **2018**, *13*, 3800–3817.

[59] T. Sugahara, J. Guo, T. Sasamori, S. Nagase, N. Tokitoh, "Regioselective Cyclotrimerization of Terminal Alkynes Using a Digermyne" *Angew. Chem. Int. Ed.* **2018**, *57*, 3499–3503.

[60] W. A. Herrmann, Ed., *Transition Metals Part 1*, Georg Thieme Verlag, Stuttgart, **1997**.

[61] W. Ma, C. Yu, T. Chen, L. Xu, W.-X. Zhang, Z. Xi, "Metallacyclopentadienes: synthesis, structure and reactivity" *Chem. Soc. Rev.* **2017**, *46*, 1160–1192.

[62] J. R. Bleeke, "Metallabenzene chemistry" *Acc. Chem. Res.* **1991**, *24*, 271–277.

[63] C. W. Landorf, M. M. Haley, "Recent Advances in Metallabenzene Chemistry" *Angew. Chem. Int. Ed.* **2006**, *45*, 3914–3936.

[64] M. Cui, R. Lin, G. Jia, "Chemistry of Metallacyclobutadienes" *Chem. – Asian J.* **2018**, *13*, 895–912.

[65] S. Ishida, T. Iwamoto, "Recent advances in η^2-disilene and η^2-disilyne mononuclear transition metal complexes and related compounds" *Coord. Chem. Rev.* **2016**, *314*, 34–63.

[66] M. Suginome, H. Oike, Y. Ito, "Novel Activation of Two Si-Si. sigma-Bonds in a Molecule by tert-Alkyl Isocyanide-Palladium Complexes" *Organometallics* **1994**, *13*, 4148–4150.

[67] M. Suginome, H. Oike, S.-S. Park, Y. Ito, "Reactions of Si–Si σ-Bonds with Bis(t-alkyl isocyanide)palladium(0) Complexes. Synthesis and Reactions of Cyclic Bis(organosilyl)palladium Complexes" *Bull. Chem. Soc. Jpn.* **1996**, *69*, 289–299.

[68] M. Zirngast, M. Flock, J. Baumgartner, C. Marschner, "Group 4 Metallocene Complexes of Disilenes, Digermenes, and a Silagermene" *J. Am. Chem. Soc.* **2009**, *131*, 15952–15962.

[69] C. Kayser, G. Kickelbick, C. Marschner, "Simple Synthesis of Oligosilyl-α,ω-dipotassium Compounds" *Angew. Chem. Int. Ed.* **2002**, *41*, 989–992.

[70] M. Tanabe, N. Ishikawa, M. Hanzawa, K. Osakada, "Mono- and Dinuclear Germapalladacycles Obtained via the Ge−Ge Bond Forming Reactions Promoted by Palladium Complexes" *Organometallics* **2008**, *27*, 5152–5158.

[71] K. Mochida, H. Karube, M. Nanjo, Y. Nakadaira, "Preparation and Structural Characterization of 1,4-Digerma-2-buten-1,4-diylplatinum(II) Complexes and Their Reactions with Alkynes, Carbon Monoxide, and Isocyanides" *Organometallics* **2005**, *24*, 4734–4741.

[72] M. Tanabe, J. Jiang, H. Yamazawa, K. Osakada, T. Ohmura, M. Suginome, "Dinuclear Palladium and Platinum Complexes with Bridging Silylene Ligands. Preparation Using (Aminosilyl)boronic Ester as the Ligand Precursor and Their Reactions with Alkynes" *Organometallics* **2011**, *30*, 3981–3991.

[73] C. Y. Lee, Y. Wang, C. S. Liu, "Stereochemical nonrigidity in six-coordinate monochelate complexes via polytopal rearrangement" *Inorg. Chem.* **1991**, *30*, 3893–3899.

[74] X. Wang, Y. Peng, M. M. Olmstead, H. Hope, P. P. Power, "A Ditetrylyne as a π-Electron Donor: Synthesis and Characterization of $[AgAr'GeGeAr']^+SbF_6^-$ and $[Ag_2Ar'GeGe(F)Ar']^+SbF_6^-$ (Ar′ = C_6H_3-2,6(C_6H_3-2,6-Pr^i_2)$_2$)" *J. Am. Chem. Soc.* **2010**, *132*, 13150–13151.

[75] S. Ishida, R. Sugawara, Y. Misawa, T. Iwamoto, "Palladium and Platinum η^2-Disilyne Complexes Bearing an Isolable Dialkyldisilyne as a Ligand" *Angew. Chem. Int. Ed.* **2013**, *52*, 12869–12873.

[76] A. Jana, V. Huch, H. S. Rzepa, D. Scheschkewitz, "A Molecular Complex with a Formally Neutral Iron Germanide Motif (Fe_2Ge_2)" *Organometallics* **2015**, *34*, 2130–2133.

[77] P. K. Majhi, M. Zimmer, B. Morgenstern, V. Huch, D. Scheschkewitz, "Transition Metal Complexes of Heavier Vinylidenes: Allylic Coordination vs Vinylidene–Alkyne Rearrangement at Nickel" *J. Am. Chem. Soc.* **2021**, *143*, 13350–13357.

[78] P. K. Majhi, M. Zimmer, B. Morgenstern, D. Scheschkewitz, "Transition-Metal Complexes of Heavier Cyclopropenes: Non-Dewar–Chatt–Duncanson Coordination and Facile Si=Ge Functionalization" *J. Am. Chem. Soc.* **2021**, *143*, 8981–8986.

[79] T. Yoshimoto, H. Hashimoto, M. Ray, N. Hayakawa, T. Matsuo, J. Chakrabarti, H. Tobita, "Products of [2+2] Cycloaddition between a W≡Si Triple-bonded Complex and Alkynes: Isolation, Structure, and Non-classical Bonding Interaction" *Chem. Lett.* **2020**, *49*, 311–314.

[80] P. G. Hayes, Z. Xu, C. Beddie, J. M. Keith, M. B. Hall, T. D. Tilley, "The Osmium–Silicon Triple Bond: Synthesis, Characterization, and Reactivity of an Osmium Silylyne Complex" *J. Am. Chem. Soc.* **2013**, *135*, 11780–11783.

[81] Y. Wang, M. Karni, S. Yao, Y. Apeloig, M. Driess, "An Isolable Bis(silylene)-Stabilized Germylone and Its Reactivity" *J. Am. Chem. Soc.* **2019**, *141*, 1655–1664.

[82] A. Jana, M. Majumdar, V. Huch, M. Zimmer, D. Scheschkewitz, "NHC-coordinated silagermenylidene functionalized in allylic position and its behaviour as a ligand" *Dalton Trans* **2014**, *43*, 5175–5181.

[83] B. Baars, *Dissertation*, "*Synthese und Reaktivität von kationischen Metallosilylidinen und Metallosilylenen*", Mensch Und Buch Verlag, Berlin, **2017**.

[84] Y. N. Lebedev, *Dissertation*, "*Multiple bonding of low-valent silicon and germanium to group 6 and 9 metals*", Verl. Dr. Hut, München, **2015**.

[85] L. Arizpe, *Dissertation*, "*Synthesis and characterization of complexes featuring tantalum-germanium multiple bonds*", Mensch & Buch, Berlin, **2019**.

[86] F. Ramirez, N. B. Desai, B. Hansen, N. McKelvie, "HEXAPHENYLCARBODIPHOSPHORANE, $(C_6H_5)_3PCP(C_6H_5)_3$" *J. Am. Chem. Soc.* **1961**, *83*, 3539–3540.

[87] R. Tonner, F. Öxler, B. Neumüller, W. Petz, G. Frenking, "Carbodiphosphoranes: The Chemistry of Divalent Carbon(0)" *Angew. Chem. Int. Ed.* **2006**, *45*, 8038–8042.

[88] R. Tonner, G. Frenking, "$C(NHC)_2$: Divalent Carbon(0) Compounds with N-Heterocyclic Carbene Ligands—Theoretical Evidence for a Class of Molecules with Promising Chemical Properties" *Angew. Chem. Int. Ed.* **2007**, *46*, 8695–8698.

[89] R. Tonner, G. Frenking, "Divalent Carbon(0) Chemistry, Part 1: Parent Compounds" *Chem. – Eur. J.* **2008**, *14*, 3260–3272.

[90] C. A. Dyker, V. Lavallo, B. Donnadieu, G. Bertrand, "Synthesis of an Extremely Bent Acyclic Allene (A 'Carbodicarbene'): A Strong Donor Ligand" *Angew. Chem. Int. Ed.* **2008**, *47*, 3206–3209.

[91] S. Klein, R. Tonner, G. Frenking, "Carbodicarbenes and Related Divalent Carbon(0) Compounds" *Chem. – Eur. J.* **2010**, *16*, 10160–10170.

[92] S. Klein, G. Frenking, "Carbodiylides $C(ECp^*)_2$ (E=B–Tl): Another Class of Theoretically Predicted Divalent Carbon(0) Compounds" *Angew. Chem. Int. Ed.* **2010**, *49*, 7106–7110.

[93] O. Kaufhold, F. E. Hahn, "Carbodicarbenes: Divalent Carbon(0) Compounds" *Angew. Chem. Int. Ed.* **2008**, *47*, 4057–4061.

[94] A. K. Phukan, A. K. Guha, "Stabilization of cyclic and acyclic carbon(0) compounds by differential coordination of heterocyclic carbenes: a theoretical assessment" *Dalton Trans.* **2012**, *41*, 8973.

[95] N. Takagi, T. Shimizu, G. Frenking, "Divalent E(0) Compounds (E=Si–Sn)" *Chem. – Eur. J.* **2009**, *15*, 8593–8604.

[96] P. K. Majhi, T. Sasamori, "Tetrylones: An Intriguing Class of Monoatomic Zero-valent Group 14 Compounds" *Chem. – Eur. J.* **2018**, *24*, 9441–9455.

[97] S. Yao, Y. Xiong, A. Saddington, M. Driess, "Entering new chemical space with isolable complexes of single, zero-valent silicon and germanium atoms" *Chem. Commun.* **2021**, *57*, 10139–10153.

[98] S. Ishida, T. Iwamoto, C. Kabuto, M. Kira, "A stable silicon-based allene analogue with a formally sp-hybridized silicon atom" *Nature* **2003**, *421*, 725–727.

[99] N. Takagi, T. Shimizu, G. Frenking, "Divalent Silicon(0) Compounds" *Chem. – Eur. J.* **2009**, *15*, 3448–3456.

[100] Y. Xiong, S. Yao, S. Inoue, J. D. Epping, M. Driess, "A Cyclic Silylone ('Siladicarbene') with an Electron-Rich Silicon(0) Atom" *Angew. Chem. Int. Ed.* **2013**, *52*, 7147–7150.

[101] K. C. Mondal, H. W. Roesky, M. C. Schwarzer, G. Frenking, B. Niepötter, H. Wolf, R. Herbst-Irmer, D. Stalke, "A Stable Singlet Biradicaloid Siladicarbene: $(L:)_2Si$" *Angew. Chem. Int. Ed.* **2013**, *52*, 2963–2967.

[102] S. Roy, K. C. Mondal, L. Krause, P. Stollberg, R. Herbst-Irmer, D. Stalke, J. Meyer, A. C. Stückl, B. Maity, D. Koley, S. K. Vasa, S. Q. Xiang, R. Linser, H. W. Roesky, "Electron-Induced Conversion of Silylones to Six-Membered Cyclic Silylenes" *J. Am. Chem. Soc.* **2014**, *136*, 16776–16779.

[103] T. Sugahara, T. Sasamori, N. Tokitoh, "Highly Bent 1,3-Digerma-2-silaallene" *Angew. Chem. Int. Ed.* **2017**, *56*, 9920–9923.

[104] Y. Wang, M. Karni, S. Yao, A. Kaushansky, Y. Apeloig, M. Driess, "Synthesis of an Isolable Bis(silylene)-Stabilized Silylone and Its Reactivity Toward Small Gaseous Molecules" *J. Am. Chem. Soc.* **2019**, *141*, 12916–12927.

[105] J. Keuter, A. Hepp, C. Mück-Lichtenfeld, F. Lips, "Facile Access to an NHC-Coordinated Silicon Ring Compound with a Si=N Group and a Two-Coordinate Silicon Atom" *Angew. Chem. Int. Ed.* **2019**, *58*, 4395–4399.

[106] S. Yao, A. Kostenko, Y. Xiong, A. Ruzicka, M. Driess, "Redox Noninnocent Monoatomic Silicon(0) Complex ('Silylone'): Its One-Electron-Reduction Induces an Intramolecular One-Electron-Oxidation of Silicon(0) to Silicon(I)" *J. Am. Chem. Soc.* **2020**, *142*, 12608–12612.

[107] T. Koike, T. Nukazawa, T. Iwamoto, "Conformationally Switchable Silylone: Electron Redistribution Accompanied by Ligand Reorientation around a Monatomic Silicon" *J. Am. Chem. Soc.* **2021**, *143*, 14332–14341.

[108] Y. Li, Y.-C. Chan, Y. Li, I. Purushothaman, S. De, P. Parameswaran, C.-W. So, "Synthesis of a Bent 2-Silaallene with a Perturbed Electronic Structure from a Cyclic Alkyl(amino) Carbene-Diiodosilylene" *Inorg. Chem.* **2016**, *55*, 9091–9098.

[109] L. C. Siemes, J. Keuter, A. Hepp, F. Lips, "Reactions of a Silicon-Based Cyclic Silylone with Chalcogens" *Inorg. Chem.* **2019**, *58*, 13142–13149.

[110] A. Burchert, S. Yao, R. Müller, C. Schattenberg, Y. Xiong, M. Kaupp, M. Driess, "An Isolable Silicon Dicarbonate Complex from Carbon Dioxide Activation with a Silylone" *Angew. Chem. Int. Ed.* **2017**, *56*, 1894–1897.

[111] S. Kumar, *Dissertation*, "Low-Valent Heavier Tetrel Compounds Supported by N-heterocyclic Carbenes: A Comprehensive Experimental and Theoretical Perusal" **2025**, DOI 10.48565/BONNDOC-689.

[112] Y. Xiong, S. Yao, G. Tan, S. Inoue, M. Driess, "A Cyclic Germadicarbene ('Germylone') from Germyliumylidene" *J. Am. Chem. Soc.* **2013**, *135*, 5004–5007.

[113] Y. Li, K. C. Mondal, H. W. Roesky, H. Zhu, P. Stollberg, R. Herbst-Irmer, D. Stalke, D. M. Andrada, "Acyclic Germylones: Congeners of Allenes with a Central Germanium Atom" *J. Am. Chem. Soc.* **2013**, *135*, 12422–12428.

[114] B. Su, R. Ganguly, Y. Li, R. Kinjo, "Isolation of an Imino-N-heterocyclic Carbene/Germanium(0) Adduct: A Mesoionic Germylene Equivalent" *Angew. Chem. Int. Ed.* **2014**, *53*, 13106–13109.

[115] T. Chu, L. Belding, A. van der Est, T. Dudding, I. Korobkov, G. I. Nikonov, "A Coordination Compound of Ge^0 Stabilized by a Diiminopyridine Ligand" *Angew. Chem. Int. Ed.* **2014**, *53*, 2711–2715.

[116] S. Yao, A. Kostenko, Y. Xiong, C. Lorent, A. Ruzicka, M. Driess, "Changing the Reactivity of Zero- and Mono-Valent Germanium with a Redox Non-Innocent Bis(silylenyl)carborane Ligand" *Angew. Chem. Int. Ed.* **2021**, *60*, 14864–14868.

[117] M. T. Nguyen, D. Gusev, A. Dmitrienko, B. M. Gabidullin, D. Spasyuk, M. Pilkington, G. I. Nikonov, "Ge(0) Compound Stabilized by a Diimino-Carbene Ligand: Synthesis and Ambiphilic Reactivity" *J. Am. Chem. Soc.* **2020**, *142*, 5852–5861.

[118] N. Wiberg, H.-W. Lerner, S.-K. Vasisht, S. Wagner, K. Karaghiosoff, H. Nöth, W. Ponikwar, "Tetrasupersilyl-tristannaallene and -tristannacyclopropene (^{t}Bu$_3$Si)$_4$Sn$_3$ – Isomers with the Shortest Sn=Sn Double Bonds to Date" *Eur. J. Inorg. Chem.* **1999**, *1999*, 1211–1218.

[119] J. Flock, A. Suljanovic, A. Torvisco, W. Schoefberger, B. Gerke, R. Pöttgen, R. C. Fischer, M. Flock, "The Role of 2,6-Diaminopyridine Ligands in the Isolation of an Unprecedented, Low-Valent Tin Complex" *Chem. – Eur. J.* **2013**, *19*, 15504–15517.

[120] J. Xu, C. Dai, S. Yao, J. Zhu, M. Driess, "A Genuine Stannylone with a Monoatomic Two-Coordinate Tin(0) Atom Supported by a Bis(silylene) Ligand" *Angew. Chem. Int. Ed.* **2022**, *61*, e202114073.

[121] J. Xu, S. Pan, S. Yao, G. Frenking, M. Driess, "The Heaviest Bottleable Metallylone: Synthesis of a Monatomic, Zero-Valent Lead Complex ('Plumbylone')" *Angew. Chem. Int. Ed.* **2022**, *61*, e202209442.

[122] B. Lei, F. Cao, M. Chen, X. Wang, Z. Mo, "Bisgermylene-Stabilized Stannylone: Catalytic Reduction of Nitrous Oxide and Nitro Compounds via Element-Ligand Cooperativity" *J. Am. Chem. Soc.* **2024**, *146*, 17817–17826.

[123] G. Maier, H. P. Reisenauer, H. Egenolf, J. Glatthaar, "Reaction of Silicon Atoms with Hydrogen Cyanide: Generation and Matrix-Spectroscopic Identification of CHNSi and CNSi Isomers" *Eur. J. Org. Chem.* **1998**, *1998*, 1307–1311.

[124] M. E. Sanz, M. C. McCarthy, P. Thaddeus, "Laboratory Detection of HS[CLC]i[/CLC]CN and HS[CLC]i[/CLC]NC" *Astrophys. J.* **2002**, *577*, L71–L74.

[125] M. C. McCARTHY, C. A. Gottlieb, P. Thaddeus, "Silicon molecules in space and in the laboratory" *Mol. Phys.* **2003**, *101*, 697–704.

[126] C. J. Evans, M. R. Dover, "Spectroscopic Investigation of the Electronic $\tilde{A}^1$ A″–$\tilde{X}^1$ A′ Transition of HSiNC" *J. Phys. Chem. A* **2009**, *113*, 8533–8539.

[127] J. R. Flores, I. Pérez-Juste, L. Carballeira, "A theoretical study of the SiCNH isomers" *Chem. Phys.* **2005**, *313*, 1–15.

[128] Q. Wang, Y. Ding, C. Sun, "Potential energy surface study of [H, Si, C, N] and its ions" *Chem. Phys.* **2006**, *323*, 413–428.

[129] S. Thorwirth, M. E. Harding, "Coupled-cluster calculations of C_2H_2Si and CNHSi structural isomers" *J. Chem. Phys.* **2009**, *130*, 214303.

[130] S. Karwasara, L. R. Maurer, B. Peerless, G. Schnakenburg, U. Das, A. C. Filippou, "(NHC)Si═C═N–R: A Two-Coordinated Si^0 -Isocyanide Compound as Si(NHC) Transfer Reagent" *J. Am. Chem. Soc.* **2021**, *143*, 14780–14794.

[131] Michael. Meot-Ner, Zeev. Karpas, C. A. Deakyne, "Ion chemistry of cyanides and isocyanides. 1. The carbon lone pair as proton acceptor: proton affinities of isocyanides. Alkyl cation nitrogen, oxygen, and carbon lone pair donors" *J. Am. Chem. Soc.* **1986**, *108*, 3913–3919.

[132] M. Liu, I. Yang, B. Buckley, J. K. Lee, "Proton Affinities of Phosphines versus N-Heterocyclic Carbenes" *Org. Lett.* **2010**, *12*, 4764–4767.

[133] N. Takeda, T. Kajiwara, H. Suzuki, R. Okazaki, N. Tokitoh, "Synthesis and Properties of the First Stable Silylene–Isocyanide Complexes" *Chem. – Eur. J.* **2003**, *9*, 3530–3543.

[134] T. Abe, T. Iwamoto, C. Kabuto, M. Kira, "Synthesis, Structure, and Bonding of Stable Dialkylsilaketenimines" *J. Am. Chem. Soc.* **2006**, *128*, 4228–4229.

[135] K. Takeuchi, M. Ichinohe, A. Sekiguchi, "A New Disilene with π-Accepting Groups from the Reaction of Disilyne RSi≡SiR (R = $Si^iPr[CH(SiMe_3)_2]$) with Isocyanides" *J. Am. Chem. Soc.* **2012**, *134*, 2954–2957.

[136] C. Ganesamoorthy, J. Schoening, C. Wölper, L. Song, P. R. Schreiner, S. Schulz, "A silicon–carbonyl complex stable at room temperature" *Nat. Chem.* **2020**, *12*, 608–614.

[137] D. Reiter, R. Holzner, A. Porzelt, P. Frisch, S. Inoue, "Silylated silicon–carbonyl complexes as mimics of ubiquitous transition-metal carbonyls" *Nat. Chem.* **2020**, *12*, 1131–1135.

[138] L. Zhu, J. Zhang, H. Yang, C. Cui, "Synthesis of Silaketenimine Anion and Its Coupling with Isocyanide" *J. Am. Chem. Soc.* **2019**, *141*, 19600–19604.

[139] Y. Wang, A. Kostenko, T. J. Hadlington, M.-P. Luecke, S. Yao, M. Driess, "Silicon-Mediated Selective Homo- and Heterocoupling of Carbon Monoxide" *J. Am. Chem. Soc.* **2019**, *141*, 626–634.

[140] A. Mansikkamäki, P. P. Power, H. M. Tuononen, "Computational Analysis of n→π* Back-Bonding in Metallylene–Isocyanide Complexes R_2MCNR' (M = Si, Ge, Sn; R = ^{t}Bu, Ph; R′ = Me, ^{t}Bu, Ph)" *Organometallics* **2013**, *32*, 6690–6700.

[141] H. Ottosson, A. M. Eklöf, "Silenes: Connectors between classical alkenes and nonclassical heavy alkenes" *Coord. Chem. Rev.* **2008**, *252*, 1287–1314.

[142] K. K. Milnes, L. C. Pavelka, K. M. Baines, "Cycloaddition of carbonyl compounds and alkynes to (di)silenes and (di)germenes: reactivity and mechanism" *Chem. Soc. Rev.* **2016**, *45*, 1019–1035.

[143] J. Escudié, H. Ranaivonjatovo, L. Rigon, "Heavy Allenes and Cumulenes ECE' and ECCE' (E = P, As, Si, Ge, Sn; E' = C, N, P, As, O, S)" *Chem. Rev.* **2000**, *100*, 3639–3696.

[144] J. Escudié, H. Ranaivonjatovo, "Group 14 and 15 Heteroallenes ECC and ECE'" *Organometallics* **2007**, *26*, 1542–1559.

[145] M. C. Holthausen, W. Koch, Y. Apeloig, "Theory Predicts Triplet Ground-State Organic Silylenes" *J. Am. Chem. Soc.* **1999**, *121*, 2623–2624.

[146] A. Sekiguchi, T. Tanaka, M. Ichinohe, K. Akiyama, S. Tero-Kubota, "Bis(tri-*tert*-butylsilyl)silylene: Triplet Ground State Silylene" *J. Am. Chem. Soc.* **2003**, *125*, 4962–4963.

[147] A. Sekiguchi, T. Tanaka, M. Ichinohe, K. Akiyama, P. P. Gaspar, "Tri-*tert*-butylsilylsilylenes with Alkali Metal Substituents (^{t}Bu$_3$Si)SiM (M = Li, K): Electronically and Sterically Accessible Triplet Ground States" *J. Am. Chem. Soc.* **2008**, *130*, 426–427.

[148] D. Geiß, M. I. Arz, M. Straßmann, G. Schnakenburg, A. C. Filippou, "Si□P Double Bonds: Experimental and Theoretical Study of an NHC-Stabilized Phosphasilenylidene" *Angew. Chem. Int. Ed.* **2015**, *54*, 2739–2744.

[149] R. J. Van Zee, R. F. Ferrante, W. Weltner, "Si_2, SiH_3, and HSiO molecules: ESR at 4 K" *J. Chem. Phys.* **1985**, *83*, 6181–6187.

[150] Y. Wang, Y. Xie, P. Wei, R. B. King, H. F. Schaefer, P. Von R. Schleyer, G. H. Robinson, "A Stable Silicon(0) Compound with a Si=Si Double Bond" *Science* **2008**, *321*, 1069–1071.

[151] K. C. Mondal, P. P. Samuel, H. W. Roesky, R. R. Aysin, L. A. Leites, S. Neudeck, J. Lübben, B. Dittrich, N. Holzmann, M. Hermann, G. Frenking, "One-Electron-Mediated Rearrangements of 2,3-Disiladicarbene" *J. Am. Chem. Soc.* **2014**, *136*, 8919–8922.

[152] S. Du, H. Jia, H. Rong, H. Song, C. Cui, Z. Mo, "Synthesis and Reactivity of N-Heterocyclic Silylene Stabilized Disilicon(0) Complexes" *Angew. Chem. Int. Ed.* **2022**, *61*, e202115570.

[153] A. Sidiropoulos, C. Jones, A. Stasch, S. Klein, G. Frenking, "N-Heterocyclic Carbene Stabilized Digermanium(0)" *Angew. Chem. Int. Ed.* **2009**, *48*, 9701–9704.

[154] C. Jones, A. Sidiropoulos, N. Holzmann, G. Frenking, A. Stasch, "An N-heterocyclic carbene adduct of diatomic tin, :Sn=Sn:" *Chem. Commun.* **2012**, *48*, 9855.

[155] Y. Li, K. C. Mondal, P. P. Samuel, H. Zhu, C. M. Orben, S. Panneerselvam, B. Dittrich, B. Schwederski, W. Kaim, T. Mondal, D. Koley, H. W. Roesky, "C_4 Cumulene and the Corresponding Air-Stable Radical Cation and Dication" *Angew. Chem. Int. Ed.* **2014**, *53*, 4168–4172.

[156] K. C. Mondal, S. Roy, B. Dittrich, D. M. Andrada, G. Frenking, H. W. Roesky, "A Triatomic Silicon(0) Cluster Stabilized by a Cyclic Alkyl(amino) Carbene" *Angew. Chem. Int. Ed.* **2016**, *55*, 3158–3161.

[157] M. Lein, A. Krapp, G. Frenking, "Why Do the Heavy-Atom Analogues of Acetylene E_2H_2 (E = Si–Pb) Exhibit Unusual Structures?" *J. Am. Chem. Soc.* **2005**, *127*, 6290–6299.

[158] M. M. Gallo, T. P. Hamilton, H. F. Schaefer, "Vinylidene: the final chapter?" *J. Am. Chem. Soc.* **1990**, *112*, 8714–8719.

[159] H. Lee, J. H. Baraban, R. W. Field, J. F. Stanton, "High-Accuracy Estimates for the Vinylidene-Acetylene Isomerization Energy and the Ground State Rotational Constants of :C=CH_2" *J. Phys. Chem. A* **2013**, *117*, 11679–11683.

[160] A. J. Boone, D. H. Magers, J. Leszczynski, "Searches on the potential energy hypersurfaces of $GeCH_2$, $GeSiH_2$, and Ge_2H_2" *Int. J. Quantum Chem.* **1998**, *70*, 925–932.

[161] P. O'Leary, J. R. Thomas, H. F. Schaefer, B. J. Duke, B. O'Leary, "A study of the silagermylyne ($SiGeH_2$) molecule: A new monobridged structure" *Int. J. Quantum Chem.* **1995**, *56*, 593–604.

[162] P. P. Power, "Bonding and Reactivity of Heavier Group 14 Element Alkyne Analogues" *Organometallics* **2007**, *26*, 4362–4372.

[163] H. K. Brody, D. H. Magers, J. Leszczyński, "Ab initio studies of methylenecarbene and isoelectronic species" *Struct. Chem.* **1995**, *6*, 293–300.

[164] S. Nagase, K. Kobayashi, N. Takagi, "Triple bonds between heavier Group 14 elements. A theoretical approach" *J. Organomet. Chem.* **2000**, *611*, 264–271.

[165] M. Bogey, H. Bolvin, C. Demuynck, J. Destombes, "Nonclassical double-bridged structure in silicon-containing molecules: Experimental evidence in Si_2H_2 from its submillimeter-wave spectrum" *Phys. Rev. Lett.* **1991**, *66*, 413–416.

[166] M. Cordonnier, M. Bogey, C. Demuynck, J.-L. Destombes, "Nonclassical structures in silicon-containing molecules: The monobridged isomer of Si_2H_2" *J. Chem. Phys.* **1992**, *97*, 7984–7989.

[167] A. Sekiguchi, "Disilyne with a silicon-silicon triple bond: A new entry to multiple bond chemistry" *Pure Appl. Chem.* **2008**, *80*, 447–457.

[168] J.-J. Maudrich, F. Diab, S. Weiß, M. Widemann, T. Dema, H. Schubert, K. M. Krebs, K. Eichele, L. Wesemann, "Deprotonation of Organogermanium and Organotin Trihydrides" *Inorg. Chem.* **2019**, *58*, 15758–15768.

[169] David Hoffmann, *Dissertation*, "*Novel synthetic routes for multiple bond formation between Si, Ge, and Sn and the d- and p-block elements*", Bonn, **2021**.

[170] R. S. Ghadwal, H. W. Roesky, S. Merkel, J. Henn, D. Stalke, "Lewis Base Stabilized Dichlorosilylene" *Angew. Chem.* **2009**, *121*, 5793–5796.

[171] A. C. Filippou, O. Chernov, G. Schnakenburg, "$SiBr_2$(Idipp): A Stable N-Heterocyclic Carbene Adduct of Dibromosilylene" *Angew. Chem.* **2009**, *121*, 5797–5800.

[172] A. C. Filippou, O. Chernov, B. Blom, K. W. Stumpf, G. Schnakenburg, "Stable N-Heterocyclic Carbene Adducts of Arylchlorosilylenes and Their Germanium Homologues" *Chem. - Eur. J.* **2010**, *16*, 2866–2872.

[173] G. Frenking, M. Hermann, D. M. Andrada, N. Holzmann, "Donor–acceptor bonding in novel low-coordinated compounds of boron and group-14 atoms C–Sn" *Chem. Soc. Rev.* **2016**, *45*, 1129–1144.

[174] M. Soleilhavoup, G. Bertrand, "Cyclic (Alkyl)(Amino)Carbenes (CAACs): Stable Carbenes on the Rise" *Acc. Chem. Res.* **2015**, *48*, 256–266.

[175] M. Melaimi, R. Jazzar, M. Soleilhavoup, G. Bertrand, "Cyclic (Alkyl)(amino)carbenes (CAACs): Recent Developments" *Angew. Chem. Int. Ed.* **2017**, *56*, 10046–10068.

[176] S. Khan, H. W. Roesky, "Carbene-Stabilized Exceptional Silicon Halides" *Chem. – Eur. J.* **2019**, *25*, 1636–1648.

[177] F. Gstrein, *Dissertation*, "*Silicon Compounds in Low Oxidation States Supported by a Cyclic (Alkyl)(Amino)Carbene*", **2023.**

[178] S. Schwarzwald, *Dissertation*, "*NHC-supported Disilavinylidenes and Oxysilylenes: Synthesis, Characterization and Reactivity Studies*", **2023**.

[179] A. Jana, V. Huch, D. Scheschkewitz, "NHC-Stabilized Silagermenylidene: A Heavier Analogue of Vinylidene" *Angew. Chem. Int. Ed.* **2013**, *52*, 12179–12182.

[180] C. Wilhelm, D. Raiser, H. Schubert, C. P. Sindlinger, L. Wesemann, "Phosphine-Stabilized Germasilenylidene: Source for a Silicon-Atom Transfer" *Inorg. Chem.* **2021**, *60*, 9268–9272.

[181] P. Ghana, M. I. Arz, U. Das, G. Schnakenburg, A. C. Filippou, "Si=Si Double Bonds: Synthesis of an NHC-Stabilized Disilavinylidene" *Angew. Chem.* **2015**, *127*, 10118–10123.

[182] R. Kobayashi, S. Ishida, T. Iwamoto, “Synthesis of an NHC-Coordinated Dialkyldisilavinylidene and Its Oxidation Providing a Silicon Analog of an Acetolactone” *Organometallics* **2021**, *40*, 843–847.

[183] S. Kundu, S. Sinhababu, V. Chandrasekhar, H. W. Roesky, “Stable cyclic (alkyl)(amino)carbene (cAAC) radicals with main group substituents” *Chem. Sci.* **2019**, *10*, 4727–4741.

[184] L. Salem, C. Rowland, “The Electronic Properties of Diradicals” *Angew. Chem. Int. Ed. Engl.* **1972**, *11*, 92–111.

[185] T. Stuyver, B. Chen, T. Zeng, P. Geerlings, F. De Proft, R. Hoffmann, “Do Diradicals Behave Like Radicals?” *Chem. Rev.* **2019**, *119*, 11291–11351.

[186] M. Abe, “Diradicals” *Chem. Rev.* **2013**, *113*, 7011–7088.

[187] E. Miliordos, K. Ruedenberg, S. S. Xantheas, “Unusual Inorganic Biradicals: A Theoretical Analysis” *Angew. Chem. Int. Ed.* **2013**, *52*, 5736–5739.

[188] P. Coburger, R. Wolf, H. Grützmacher, “Isomerism and Biradical Character of Tetrapnictide Dianions: A Computational Study” *Eur. J. Inorg. Chem.* **2020**, *2020*, 3580–3586.

[189] Y. Jung, M. Head-Gordon, “How Diradicaloid Is a Stable Diradical?” *ChemPhysChem* **2003**, *4*, 522–525.

[190] J. Michl, V. Bonačić-Koutecký, “Biradicals and biradicaloids: a unified view” *Tetrahedron* **1988**, *44*, 7559–7585.

[191] M. Abe, J. Ye, M. Mishima, “The chemistry of localized singlet 1,3-diradicals (biradicals): from putative intermediates to persistent species and unusual molecules with a π-single bonded character” *Chem. Soc. Rev.* **2012**, *41*, 3808.

[192] K. Fukuda, M. Nakano, “Intramolecular Charge Transfer Effects on the Diradical Character and Second Hyperpolarizabilities of Open-Shell Singlet X−π–X (X = Donor/Acceptor) Systems” *J. Phys. Chem. A* **2014**, *118*, 3463–3471.

[193] J. J. Dressler, M. Teraoka, G. L. Espejo, R. Kishi, S. Takamuku, C. J. Gómez-García, L. N. Zakharov, M. Nakano, J. Casado, M. M. Haley, “Thiophene and its sulfur inhibit indenoindenodibenzothiophene diradicals from low-energy lying thermal triplets” *Nat. Chem.* **2018**, *10*, 1134–1140.

[194] L. Ji, J. Shi, J. Wei, T. Yu, W. Huang, “Air-Stable Organic Radicals: New-Generation Materials for Flexible Electronics?” *Adv. Mater.* **2020**, *32*, 1908015.

[195] A. Schulz, “Group 15 biradicals: synthesis and reactivity of cyclobutane-1,3-diyl and cyclopentane-1,3-diyl analogues” *Dalton Trans.* **2018**, *47*, 12827–12837.

[196] Y. Jung, T. Heine, P. V. R. Schleyer, M. Head-Gordon, "Aromaticity of Four-Membered-Ring 6π-Electron Systems: N_2S_2 and $Li_2C_4H_4$" *J. Am. Chem. Soc.* **2004**, *126*, 3132–3138.

[197] H. Cox, P. B. Hitchcock, M. F. Lappert, L. J. -M. Pierssens, "A 1,3-Diaza-2,4-distannacyclobutanediide: Synthesis, Structure, and Bonding" *Angew. Chem. Int. Ed.* **2004**, *43*, 4500–4504.

[198] C. Cui, M. Brynda, M. M. Olmstead, P. P. Power, "Synthesis and Characterization of the Non-Kekulé, Singlet Biradicaloid Ar'Ge(μ-$NSiMe_3$)$_2$GeAr' (Ar' = 2,6-$Dipp_2$ C_6H_3, Dipp = 2,6-^{i}Pr$_2$C$_6$H$_3$)" *J. Am. Chem. Soc.* **2004**, *126*, 6510–6511.

[199] X. Wang, Y. Peng, M. M. Olmstead, J. C. Fettinger, P. P. Power, "An Unsymmetric Oxo/Imido-Bridged Germanium-Centered Singlet Diradicaloid" *J. Am. Chem. Soc.* **2009**, *131*, 14164–14165.

[200] K. Takeuchi, M. Ichinohe, A. Sekiguchi, "Access to a Stable Si_2N_2 Four-Membered Ring with Non-Kekulé Singlet Biradical Character from a Disilyne" *J. Am. Chem. Soc.* **2011**, *133*, 12478–12481.

[201] T. Sugahara, J.-D. Guo, D. Hashizume, T. Sasamori, N. Tokitoh, "Reversible Isomerizations between 1,4-Digermabenzenes and 1,4-Digerma-Dewar-benzenes: Air-Stable Activators for Small Molecules" *J. Am. Chem. Soc.* **2019**, *141*, 2263–2267.

[202] M. K. Sharma, D. Rottschäfer, T. Glodde, B. Neumann, H. Stammler, R. S. Ghadwal, "An Open-Shell Singlet Sn ^{I} Diradical and H_2 Splitting" *Angew. Chem. Int. Ed.* **2021**, *60*, 6414–6418.

[203] M. K. Sharma, F. Ebeler, T. Glodde, B. Neumann, H.-G. Stammler, R. S. Ghadwal, "Isolation of a Ge(I) Diradicaloid and Dihydrogen Splitting" *J. Am. Chem. Soc.* **2021**, *143*, 121–125.

[204] P. J. Stang, F. Diederich, Eds., *Modern Acetylene Chemistry*, Wiley, **1995**.

[205] Akira. Sekiguchi, S. S. Zigler, Robert. West, Josef. Michl, "A synthon for the silicon-silicon triple bond" *J. Am. Chem. Soc.* **1986**, *108*, 4241–4242.

[206] N. Wiberg, S. K. Vasisht, G. Fischer, P. Mayer, "Disilynes. III [1] A Relatively Stable Disilyne RSi≡SiR (R = SiMe(Si^{t}Bu$_3$)$_2$)" *Z. Für Anorg. Allg. Chem.* **2004**, *630*, 1823–1828.

[207] Y. Ding, Y. Li, J. Zhang, C. Cui, "Synthesis of an N-Heterocylic Boryl-Stabilized Disilyne and Its Application to the Activation of Dihydrogen and C−H Bonds" *Angew. Chem. Int. Ed.* **2022**, *61*, e202205785.

[208] Y. Apeloig, M. Karni, "Triple Bonds to Silicon. Substituent Effects on the Thermodynamic and Kinetic Stabilities of Silynes Relative to Their Isomeric Silylidenes and Silavinylidenes" *Organometallics* **1997**, *16*, 310–312.

[209] D. Danovich, F. Ogliaro, M. Karni, Y. Apeloig, D. L. Cooper, S. Shaik, "Silynes (RC≡SiR′) and Disilynes (RSi≡SiR′): Why Are Less Bonds Worth Energetically More?" *Angew. Chem. Int. Ed.* **2001**, *40*, 4023.

[210] E. Ploshnik, D. Danovich, P. C. Hiberty, S. Shaik, "The Nature of the Idealized Triple Bonds Between Principal Elements and the σ Origins of Trans-Bent Geometries—A Valence Bond Study" *J. Chem. Theory Comput.* **2011**, *7*, 955–968.

[211] A. C. Hopkinson, M. H. Lien, L. G. Csizmadia, "Ab initio calculations on the singlet and triplet energy surfaces for $CSiH_2$" *Chem. Phys. Lett.* **1983**, *95*, 232–234.

[212] R. Stegmann, G. Frenking, "Silaacetylene: A possible target for experimental studies" *J. Comput. Chem.* **1996**, *17*, 781–789.

[213] H.-Y. Liao, M.-D. Su, S.-Y. Chu, "Effects of Substituents on the Thermodynamic and Kinetic Stabilities of HCGeX (X = H, CH_3 , F, and Cl) Isomers. A Theoretical Study" *Inorg. Chem.* **2000**, *39*, 3522–3525.

[214] Y. Li, H. Mu, Z. Liu, Z. Qi, J. Zhou, Z. Dong, "Dicationic 1-Germa and 1-Stannavinylidenes: Synthesis, Structure, and Reactivity" *JACS Au* **2025**, *5*, 1289–1298.

[215] T. Lu, Q. Hao, J. J. Wilke, Y. Yamaguchi, D.-C. Fang, H. F. Schaefer, "Silylidene ($SiCH_2$) and its isomers: Anharmonic rovibrational analyses for silylidene, silaacetylene, and silavinylidene" *J. Mol. Struct.* **2012**, *1009*, 103–110.

[216] J. Sarcevic, T. Heitkemper, P. N. Ruth, L. Naß, M. Kubis, D. Stalke, C. P. Sindlinger, "A donor-supported silavinylidene and silylium ylides: boroles as a flexible platform for versatile Si(II) chemistry" *Chem. Sci.* **2023**, *14*, 5148–5159.

[217] S. Kumar, L. R. Maurer, G. Schnakenburg, U. Das, A. C. Filippou, "NHC-Supported 2-Sila and 2-Germavinylidenes: Synthesis, Dynamics, First Reactivity and Theoretical Studies" *Angew. Chem. Int. Ed.* **2024**, *63*, e202400227.

[218] M. Karni, Y. Apeloig, D. Schröder, W. Zummack, R. Rabezzana, H. Schwarz, "HCSiF and HCSiCl: The First Detection of Molecules with Formal C≡Si Triple Bonds" *Angew. Chem. Int. Ed.* **1999**, *38*, 331–335.

[219] M. Karni, Y. Apeloig, "The quest for a stable silyne, RSi ≡ CR′. The effect of bulky substituents [1]" *Silicon Chem.* **2002**, *1*, 59–65.

[220] M. Mickoleit, K. Schmohl, R. Kempe, H. Oehme, "Reaction of Dichloromethyltris(trimethylsilyl)silane with Organolithium Reagents: Synthesis of an Intramolecularly Donor-Stabilized Silene" *Angew. Chem. Int. Ed.* **2000**, *39*, 1610–1612.

[221] N. Wiberg, G. Wagner, G. Müller, "Isolation and Structure of a Stable Molecule Containing a Silicon-Carbon Double Bond" *Angew. Chem. Int. Ed. Engl.* **1985**, *24*, 229–230.

[222] S. S. Sen, A. Jana, H. W. Roesky, C. Schulzke, "A Remarkable Base-Stabilized Bis(silylene) with a Silicon(I)–Silicon(I) Bond" *Angew. Chem. Int. Ed.* **2009**, *48*, 8536–8538.

[223] D. Gau, T. Kato, N. Saffon-Merceron, A. De Cózar, F. P. Cossío, A. Baceiredo, "Synthesis and Structure of a Base-Stabilized *C* -Phosphino- *Si* -Amino Silyne" *Angew. Chem. Int. Ed.* **2010**, *49*, 6585–6588.

[224] S. Takahashi, R. Nougué, T. Troadec, A. Baceiredo, N. Saffon-Merceron, V. Branchadell, T. Kato, "Base-Stabilized Cationic Silyne with a π-Accepting Phosphonio Substituent" *Inorg. Chem.* **2023**, *62*, 6488–6498.

[225] X.-F. Wang, C. Hu, J. Li, R. Wei, X. Zhang, L. L. Liu, "A crystalline stannyne" *Nat. Chem.* **2024**, *16*, 1673–1679.

[226] P. Palui, *Dissertation*, "Divergent Chemistry of Ditetrelynes (E_2R_2, E = Si, Ge) with Late Transition Metals and Low-valent Silicon Precursors" **2024**, DOI 10.48565/BONNDOC-300.

[227] T. Sasamori, T. Sugahara, T. Agou, J.-D. Guo, S. Nagase, R. Streubel, N. Tokitoh, "Synthesis and Characterization of a 1,2-Digermabenzene" *Organometallics* **2015**, *34*, 2106–2109.

[228] P. Pyykkö, M. Atsumi, "Molecular Single-Bond Covalent Radii for Elements 1–118" *Chem. – Eur. J.* **2009**, *15*, 186–197.

[229] M. L. McCrea-Hendrick, M. Bursch, K. L. Gullett, L. R. Maurer, J. C. Fettinger, S. Grimme, P. P. Power, "Counterintuitive Interligand Angles in the Diaryls E{C_6H_3 -2,6-(C_6H_2-2,4,6-^{i}Pr$_3$)$_2$}$_2$ (E = Ge, Sn, or Pb) and Related Species: The Role of London Dispersion Forces" *Organometallics* **2018**, *37*, 2075–2085.

[230] P. G. Hayes, Z. Xu, C. Beddie, J. M. Keith, M. B. Hall, T. D. Tilley, "The Osmium–Silicon Triple Bond: Synthesis, Characterization, and Reactivity of an Osmium Silylyne Complex" *J. Am. Chem. Soc.* **2013**, *135*, 11780–11783.

[231] A. Doddi, C. Gemel, M. Winter, R. A. Fischer, C. Goedecke, H. S. Rzepa, G. Frenking, "Corrigendum: Low-Valent Ge_2 and Ge_4 Species Trapped by N-Heterocyclic Gallylene" *Angew. Chem. Int. Ed.* **2013**, *52*, 2148–2148.

[232] M. Ma, L. Shen, H. Wang, Y. Zhao, B. Wu, X.-J. Yang, "*N*, *N* ′-Dipp- *o* -phenylene-diamido Dianion: A Versatile Ligand for Main Group Metal–Metal-Bonded Compounds" *Organometallics* **2020**, *39*, 1440–1447.

[233] T. Henneberger, W. Klein, J. V. Dums, T. F. Fässler, "$[(\mu_2\text{-H})(\eta^2\text{-Ge}_4)\text{ZnPh}_2]^{3-}$, an edge-on protonated E_4 cluster establishing the first three-center two-electron Ge–H–Ge bond" *Chem. Commun.* **2018**, *54*, 12381–12384.

[234] D. Nied, W. Klopper, F. Breher, "Pentagerma[1.1.1]propellane: A Combined Experimental and Quantum Chemical Study on the Nature of the Interactions between the Bridgehead Atoms" *Angew. Chem. Int. Ed.* **2009**, *48*, 1411–1416.

[235] A. Jana, V. Huch, M. Repisky, R. J. F. Berger, D. Scheschkewitz, "Dismutational and Global-Minimum Isomers of Heavier 1,4-Dimetallatetrasilabenzenes of Group 14" *Angew. Chem. Int. Ed.* **2014**, *53*, 3514–3518.

[236] E. Hupf, F. Kaiser, P. A. Lummis, M. M. D. Roy, R. McDonald, M. J. Ferguson, F. E. Kühn, E. Rivard, "Linking Low-Coordinate Ge(II) Centers via Bridging Anionic N-Heterocyclic Olefin Ligands" *Inorg. Chem.* **2020**, *59*, 1592–1601.

[237] G. H. Spikes, P. P. Power, "Lewis base induced tuning of the Ge–Ge bond order in a 'digermyne'" *Chem Commun* **2007**, 85–87.

[238] S.-H. Zhang, C.-W. So, "Synthesis and Characterization of an Amidinate-Stabilized Bisgermylene Oxide and Sulfide" *Organometallics* **2011**, *30*, 2059–2062.

[239] T. B. Rauchfuss, "Phosphorus: An Outline of Its Chemistry, Biochemistry and Technology, Fifth Edition, Studies in Inorganic Chemistry" *J. Am. Chem. Soc.* **1996**, *118*, 7871–7871.

[240] M. Caporali, L. Gonsalvi, A. Rossin, M. Peruzzini, "P_4 Activation by Late-Transition Metal Complexes" *Chem. Rev.* **2010**, *110*, 4178–4235.

[241] B. M. Cossairt, N. A. Piro, C. C. Cummins, "Early-Transition-Metal-Mediated Activation and Transformation of White Phosphorus" *Chem. Rev.* **2010**, *110*, 4164–4177.

[242] M. Scheer, G. Balázs, A. Seitz, "P_4 Activation by Main Group Elements and Compounds" *Chem. Rev.* **2010**, *110*, 4236–4256.

[243] S. Khan, S. S. Sen, H. W. Roesky, "Activation of phosphorus by group 14 elements in low oxidation states" *Chem. Commun.* **2012**, *48*, 2169.

[244] O. Back, G. Kuchenbeiser, B. Donnadieu, G. Bertrand, "Nonmetal-Mediated Fragmentation of P_4 : Isolation of P_1 and P_2 Bis(carbene) Adducts" *Angew. Chem. Int. Ed.* **2009**, *48*, 5530–5533.

[245] J. D. Masuda, W. W. Schoeller, B. Donnadieu, G. Bertrand, "NHC-Mediated Aggregation of P_4: Isolation of a P_{12} Cluster" *J. Am. Chem. Soc.* **2007**, *129*, 14180–14181.

[246] F. Dielmann, A. Timoshkin, M. Piesch, G. Balázs, M. Scheer, "The Cobalt *cyclo* -P_4 Sandwich Complex and Its Role in the Formation of Polyphosphorus Compounds" *Angew. Chem. Int. Ed.* **2017**, *56*, 1671–1675.

[247] A. G. Brook, F. Abdesaken, B. Gutekunst, G. Gutekunst, R. K. Kallury, "A solid silaethene: isolation and characterization" *J. Chem. Soc. Chem. Commun.* **1981**, 191.

[248] R. S. Grev in *Adv. Organomet. Chem.*, Elsevier, **1991**, pp. 125–170.

[249] N. Takagi, S. Nagase, "Theoretical Study of an Isolable Compound with a Short Silicon-Silicon Triple Bond, $(^tBu_3Si)_2MeSiSi{\equiv}SiSiMe(Si^tBu_3)_2$" *Eur. J. Inorg. Chem.* **2002**, *2002*, 2775–2778.

[250] R. Kinjo, M. Ichinohe, A. Sekiguchi, N. Takagi, M. Sumimoto, S. Nagase, "Reactivity of a Disilyne RSi≡SiR (R = $Si^iPr[CH(SiMe_3)_2]_2$) toward π-Bonds: Stereospecific Addition and a New Route to an Isolable 1,2-Disilabenzene" *J. Am. Chem. Soc.* **2007**, *129*, 7766–7767.

[251] C. Cui, M. M. Olmstead, J. C. Fettinger, G. H. Spikes, P. P. Power, "Reactions of the Heavier Group 14 Element Alkyne Analogues Ar'EEAr' (Ar' = C_6H_3-2,6(C_6H_3-2,6-Pr^i_2)$_2$; E = Ge, Sn) with Unsaturated Molecules: Probing the Character of the EE Multiple Bonds" *J. Am. Chem. Soc.* **2005**, *127*, 17530–17541.

[252] Y. Peng, X. Wang, J. C. Fettinger, P. P. Power, "Reversible complexation of isocyanides by the distannyne Ar′SnSnAr′ (Ar′ = C_6H_3-2,6(C_6H_3-2,6-$^iPr_2$)$_2$)" *Chem. Commun.* **2010**, *46*, 943.

[253] J. Shen, G. P. A. Yap, K. H. Theopold, "Chromium Mediated Reductive Coupling of Isonitrile Forms Unusual Heterocycles" *J. Am. Chem. Soc.* **2014**, *136*, 3382–3384.

[254] S. J. Urwin, G. S. Nichol, M. J. Cowley, "Aluminium-mediated carbon–carbon coupling of an isonitrile" *Chem. Commun.* **2018**, *54*, 378–380.

[255] M. J. Evans, M. D. Anker, C. L. McMullin, M. P. Coles, "Controlled reductive C–C coupling of isocyanides promoted by an aluminyl anion" *Chem. Sci.* **2023**, *14*, 6278–6288.

[256] K. Nagata, T. Agou, T. Sasamori, N. Tokitoh, "Formation of a Diaminoalkyne Derivative by Dialumane-mediated Homocoupling of *t* -Butyl Isocyanide" *Chem. Lett.* **2015**, *44*, 1610–1612.

[257] H. Braunschweig, M. A. Celik, R. D. Dewhurst, K. Ferkinghoff, A. Hermann, J. O. C. Jimenez-Halla, T. Kramer, K. Radacki, R. Shang, E. Siedler, F. Weißenberger, C. Werner, "Interactions of Isonitriles with Metal–Boron Bonds: Insertions, Coupling, Ring Formation, and Liberation of Monovalent Boron" *Chem. – Eur. J.* **2016**, *22*, 11736–11744.

[258] M. Ma, A. Stasch, C. Jones, "Magnesium(I) Dimers as Reagents for the Reductive Coupling of Isonitriles and Nitriles" *Chem. – Eur. J.* **2012**, *18*, 10669–10676.

[259] H. Zhu, A. Kostenko, J. A. Kelly, S. Inoue, "Substituent exchange between an imino(silyl)silylene and aryl isocyanides" *Chem* **2024**, *10*, 1213–1224.

[260] O. Kühl, "N-heterocyclic germylenes and related compounds" *Coord. Chem. Rev.* **2004**, *248*, 411–427.

[261] K. Gour, S. S. Sen in *Encycl. Inorg. Bioinorg. Chem.* (Ed.: R.A. Scott), Wiley, **2022**, pp. 1–18.

[262] S. S. Sen, A. H. W. Roesky in *Organogermanium Compd.* (Ed.: V.Ya. Lee), Wiley, **2023**, pp. 561–595.

[263] J. Li, M. Hermann, G. Frenking, C. Jones, "The Facile Reduction of Carbon Dioxide to Carbon Monoxide with an Amido-Digermyne" *Angew. Chem.* **2012**, *124*, 8739–8742.

[264] Z. D. Brown, P. Vasko, J. C. Fettinger, H. M. Tuononen, P. P. Power, "A Germanium Isocyanide Complex Featuring (n → π*) Back-Bonding and Its Conversion to a Hydride/Cyanide Product via C–H Bond Activation under Mild Conditions" *J. Am. Chem. Soc.* **2012**, *134*, 4045–4048.

[265] Z. D. Brown, P. Vasko, J. D. Erickson, J. C. Fettinger, H. M. Tuononen, P. P. Power, "Mechanistic Study of Stepwise Methylisocyanide Coupling and C–H Activation Mediated by a Low-Valent Main Group Molecule" *J. Am. Chem. Soc.* **2013**, *135*, 6257–6261.

[266] K. Takeuchi, M. Ichinohe, A. Sekiguchi, "Reactivity of the Disilyne RSi≡SiR (R = $Si^iPr[CH(SiMe_3)_2]_2$) toward Silylcyanide: Two Pathways To Form the Bis-Adduct [$RSiSiR(CNSiMe_3)_2$] with Some Silaketenimine Character and a 1,4-Diaza-2,3-disilabenzene Analogue" *J. Am. Chem. Soc.* **2008**, *130*, 16848–16849.

[267] T. M. V. D. Pinho E Melo, "Allenes as building blocks in heterocyclic chemistry" *Monatshefte Für Chem. - Chem. Mon.* **2011**, *142*, 681–697.

[268] N. Takeda, N. Tokitoh, "A Bulky Silylene Generated under Mild Conditions: Its Application to the Synthesis of Organosilicon Compounds" *Synlett* **2007**, *2007*, 2483–2491.

[269] M. Weidenbruch, B. Brand-Roth, S. Pohl, W. Saak, “A Cyclodimeric Silaketenimine” *Angew. Chem. Int. Ed. Engl.* **1990**, *29*, 90–92.

[270] N. Takeda, H. Suzuki, N. Tokitoh, R. Okazaki, S. Nagase, “Reaction of a Sterically Hindered Silylene with Isocyanides: The First Stable Silylene−Lewis Base Complexes” *J. Am. Chem. Soc.* **1997**, *119*, 1456–1457.

[271] L. Klemmer, A.-L. Thömmes, M. Zimmer, V. Huch, B. Morgenstern, D. Scheschkewitz, “Metathesis of Ge=Ge double bonds” *Nat. Chem.* **2021**, *13*, 373–377.

[272] W.-P. Leung, K.-W. Kan, T. C. W. Mak, “Synthesis of Heavier Group 14 Metal Compounds from 2,6-Lutidylbis(phosphoranosulfide)” *Organometallics* **2010**, *29*, 1890–1896.

[273] B. Cordero, V. Gómez, A. E. Platero-Prats, M. Revés, J. Echeverría, E. Cremades, F. Barragán, S. Alvarez, “Covalent radii revisited” *Dalton Trans.* **2008**, 2832.

[274] G. H. Spikes, J. C. Fettinger, P. P. Power, “Facile Activation of Dihydrogen by an Unsaturated Heavier Main Group Compound” *J. Am. Chem. Soc.* **2005**, *127*, 12232–12233.

[275] K. M. Mackay in *Chem. Org. Germanium Tin Lead Compd.* (Ed.: S. Patai), Wiley, **1995**, pp. 97–194.

[276] P. B. Hitchcock, M. F. Lappert, A. J. Thorne, “Novel two-coordinate germanium(II) arylamides: $Ge(NHAr)_2$, $ArN[Ge(NHAr)]_2(\mu\text{-}NAr)$ and $[Ge(\mu\text{-}NAr)]_2$, and the X-ray structures of 2 and $Sn(NHAr)_2$ (Ar = $C_6H_2{}^tBu_3$-2,4,6)” *J Chem Soc Chem Commun* **1990**, 1587–1589.

[277] A. B. Makar, K. E. McMartin, M. Palese, T. R. Tephly, “Formate assay in body fluids: application in methanol poisoning” *Biochem. Med.* **1975**, *13*, 117–126.

[278] T. Kunz, C. Schrenk, A. Schnepf, “$Ge_{14}Br_8(PEt_3)_4$: A Subhalide Cluster of Germanium” *Angew. Chem. Int. Ed.* **2018**, *57*, 4088–4092.

[279] J. Fischer, J. Baumgartner, C. Marschner, “Silylgermylpotassium Compounds” *Organometallics* **2005**, *24*, 1263–1268.

[280] V. Ya. Lee, M. Ichinohe, A. Sekiguchi, N. Takagi, S. Nagase, “The First Three-Membered Unsaturated Rings Consisting of Different Heavier Group 14 Elements: 1-Disilagermirene with a SiSi Double Bond and Its Isomerization to a 2-Disilagermirene with a SiGe Double Bond” *J. Am. Chem. Soc.* **2000**, *122*, 9034–9035.

[281] C. R. Samanamu, M. L. Amadoruge, C. H. Yoder, J. A. Golen, C. E. Moore, A. L. Rheingold, N. F. Materer, C. S. Weinert, “Syntheses, Structures, and

Electronic Properties of the Branched Oligogermanes $(Ph_3\ Ge)_3\ GeH$ and $(Ph_3\ Ge)_3\ GeX$ (X = Cl, Br, I)" *Organometallics* **2011**, *30*, 1046–1058.

[282] G. Frenking, R. Tonner, S. Klein, N. Takagi, T. Shimizu, A. Krapp, K. K. Pandey, P. Parameswaran, "New bonding modes of carbon and heavier group 14 atoms Si–Pb" *Chem Soc Rev* **2014**, *43*, 5106–5139.

[283] C. A. Dyker, G. Bertrand, "Soluble Allotropes of Main-Group Elements" *Science* **2008**, *321*, 1050–1051.

[284] N. Takagi, G. Frenking, "Divalent Pb(0) compounds" *Theor. Chem. Acc.* **2011**, *129*, 615–623.

[285] T. Iwamoto, H. Masuda, C. Kabuto, M. Kira, "Trigermaallene and 1,3-Digermasilaallene" *Organometallics* **2005**, *24*, 197–199.

[286] A. Schäfer, W. Saak, M. Weidenbruch, "Tetraarylstannagermene: A Molecule with a GeSn Double Bond[1]" *Organometallics* **2003**, *22*, 215–217.

[287] R. Nishino, N. Tokitoh, R. Sasayama, R. Waterman, Y. Mizuhata, "Unusual nuclear exchange within a germanium-containing aromatic ring that results in germanium atom transfer" *Nat. Commun.* **2023**, *14*, 4519.

[288] M. Hölbling, S. L. Masters (Née Hinchley), M. Flock, J. Baumgartner, K. Hassler, H. E. Robertson, D. A. Wann, "Molecular Structures of the Digermanes $Me_2XGeGeXMe_2$ (X = Me, Cl, and H): An Ab Initio Study Combined with Experimental Investigation by Raman Spectroscopy and Gas Electron Diffraction" *Inorg. Chem.* **2008**, *47*, 3023–3033.

[289] R. S. Simons, L. Pu, M. M. Olmstead, P. P. Power, "Synthesis and Characterization of the Monomeric Diaryls $M\{C_6H_3\text{-}2,6\text{-}Mes_2\}_2$ (M = Ge, Sn, or Pb; Mes = $2,4,6\text{-}Me_3C_6H_2$) and Dimeric Aryl−Metal Chlorides $[M(Cl)\{C_6H_3\text{-}2,6\text{-}Mes_2\}]_2$ (M = Ge or Sn)" *Organometallics* **1997**, *16*, 1920–1925.

[290] F. H. Allen, O. Kennard, D. G. Watson, L. Brammer, A. G. Orpen, R. Taylor, "Tables of bond lengths determined by X-ray and neutron diffraction. Part 1. Bond lengths in organic compounds" *J. Chem. Soc. Perkin Trans. 2* **1987**, S1.

[291] P. Tholen, Z. Dong, M. Schmidtmann, L. Albers, T. Müller, "A Neutral η^5-Aminoborole Complex of Germanium(II)" *Angew. Chem. Int. Ed.* **2018**, *57*, 13319–13324.

[292] P. Jutzi, F. Kohl, P. Hofmann, C. Krüger, Y. Tsay, "Bis(pentamethylcyclopentadienyl)germanium und -zinn sowie (Pentamethylcyclopentadienyl)germanium- und -zinn-Kationen: Synthese, Struktur und Bindungsverhältnisse" *Chem. Ber.* **1980**, *113*, 757–769.

[293] F. X. Kohl, R. Dickbreder, P. Jutzi, G. Müller, B. Huber, "Halbsandwich-Cyclopentadienylkomplexe von Germanium, Zinn und Blei mit zusätzlicher Metall-Olefin-Wechselwirkung" *Chem. Ber.* **1989**, *122*, 871–878.

[294] O. T. Beachley, Richard. Blom, M. Rowen. Churchill, Knut. Faegri, J. C. Fettinger, J. C. Pazik, L. Victoriano, "(Pentamethylcyclopentadienyl)indium(I) and -indium(III) compounds. Syntheses, reactivities, and x-ray diffraction and electron diffraction studies of In(C_5Me_5)" *Organometallics* **1989**, *8*, 346–356.

[295] A. Sekiguchi, R. Izumi, V. Ya. Lee, M. Ichinohe, "The First Silastannene >Si=Sn<: A New Doubly-Bonded System of Heavier Group 14 Elements" *J. Am. Chem. Soc.* **2002**, *124*, 14822–14823.

[296] S. Kumar, *Dissertation,* "*Low-Valent Heavier Tetrels Supported by N-heterocyclic Carbenes: A Comprehensive Experimental and Theoretical Perusal*", University Of Bonn, **2025**.

[297] R. F. W. Bader, "VIBRATIONALLY INDUCED PERTURBATIONS IN MOLECULAR ELECTRON DISTRIBUTIONS" *Can. J. Chem.* **1962**, *40*, 1164–1175.

[298] R. G. Pearson, "Symmetry rule for predicting molecular structure and reactivity" *J. Am. Chem. Soc.* **1969**, *91*, 1252–1254.

[299] P. P. Power, "Interaction of Multiple Bonded and Unsaturated Heavier Main Group Compounds with Hydrogen, Ammonia, Olefins, and Related Molecules" *Acc. Chem. Res.* **2011**, *44*, 627–637.

[300] Y. Peng, B. D. Ellis, X. Wang, J. C. Fettinger, P. P. Power, "Reversible Reactions of Ethylene with Distannynes Under Ambient Conditions" *Science* **2009**, *325*, 1668–1670.

[301] R. L. Melen, "Frontiers in molecular p-block chemistry: From structure to reactivity" *Science* **2019**, *363*, 479–484.

[302] C. Bibal, S. Mazières, H. Gornitzka, C. Couret, "A Route to a Germanium-Carbon Triple Bond: First Chemical Evidence for a Germyne" *Angew. Chem. Int. Ed.* **2001**, *40*, 952–954.

[303] P.-C. Wu, M.-D. Su, "Theoretical designs for germaacetylene (RC≡GeR′): a new target for synthesis" *Dalton Trans.* **2011**, *40*, 4253.

[304] P.-C. Wu, M.-D. Su, "Triply Bonded Stannaacetylene (RC≡SnR): Theoretical Designs and Characterization" *Inorg. Chem.* **2011**, *50*, 6814–6822.

[305] P.-C. Wu, M.-D. Su, "A New Target for Synthesis of Triply Bonded Plumbacetylene (RC≡PbR): A Theoretical Design" *Organometallics* **2011**, *30*, 3293–3301.

[306] J. Berthe, J. M. Garcia, E. Ocando, T. Kato, N. Saffon-Merceron, A. De Cózar, F. P. Cossío, A. Baceiredo, "Synthesis and Reactivity of a Phosphine-Stabilized

Monogermanium Analogue of Alkynes" *J. Am. Chem. Soc.* **2011**, *133*, 15930–15933.

[307] W. Setaka, K. Hirai, H. Tomioka, K. Sakamoto, M. Kira, "Stannaacetylene (RSn≡CR') Showing Carbene-like Reaction Mode" *J. Am. Chem. Soc.* **2004**, *126*, 2696–2697.

[308] W. Setaka, K. Hirai, H. Tomioka, K. Sakamoto, M. Kira, "Formation of a stannylstannylene via intramolecular carbene addition of a transient stannaacetylene (RSn≡CR')" *Chem. Commun.* **2008**, 6558.

[309] Alain. Igau, Hansjorg. Grutzmacher, Antoine. Baceiredo, Guy. Bertrand, "Analogous. alpha.,.alpha.'-bis-carbenoid, triply bonded species: synthesis of a stable .lambda.3-phosphino carbene-.lambda.5-phosphaacetylene" *J. Am. Chem. Soc.* **1988**, *110*, 6463–6466.

[310] R. Wei, X.-F. Wang, C. Hu, L. L. Liu, "Synthesis and reactivity of copper carbyne anion complexes" *Nat. Synth.* **2023**, *2*, 357–363.

[311] C. Hu, X.-F. Wang, R. Wei, C. Hu, D. A. Ruiz, X.-Y. Chang, L. L. Liu, "Crystalline monometal-substituted free carbenes" *Chem* **2022**, *8*, 2278–2289.

[312] R. Cohen, B. Rybtchinski, M. Gandelman, H. Rozenberg, J. M. L. Martin, D. Milstein, "Metallacarbenes from Diazoalkanes: An Experimental and Computational Study of the Reaction Mechanism" *J. Am. Chem. Soc.* **2003**, *125*, 6532–6546.

[313] H. Seino, D. Watanabe, T. Ohnishi, C. Arita, Y. Mizobe, "Mo and W Dihalide Complexes with Uncommon Trigonal-Prismatic Geometry Imposed by the Linear Tetraphosphine Ancillary Ligand and Their Reactivities toward Diazoalkanes" *Inorg. Chem.* **2007**, *46*, 4784–4786.

[314] J. Vignolle, X. Cattoën, D. Bourissou, "Stable Noncyclic Singlet Carbenes" *Chem. Rev.* **2009**, *109*, 3333–3384.

[315] D. Bourissou, O. Guerret, F. P. Gabbaï, G. Bertrand, "Stable Carbenes" *Chem. Rev.* **2000**, *100*, 39–92.

[316] G. Alcaraz, U. Wecker, A. Baceiredo, F. Dahan, G. Bertrand, "Synthesis of a 2*H*-Azirine by [1 + 2] Cycloaddition of a Phosphinocarbene with a Nitrile and Its Ring-Expansion to a 1,2λ^5-Azaphosphete" *Angew. Chem. Int. Ed. Engl.* **1995**, *34*, 1246–1248.

[317] H. V. Huynh, "Electronic Properties of N-Heterocyclic Carbenes and Their Experimental Determination" *Chem. Rev.* **2018**, *118*, 9457–9492.

[318] Y. Canac, M. Soleilhavoup, S. Conejero, G. Bertrand, "Stable non-N-heterocyclic carbenes (non-NHC): recent progress" *J. Organomet. Chem.* **2004**, *689*, 3857–3865.

[319] H. Meyer, G. Baum, W. Massa, A. Berndt, "Stable Germaethenes" *Angew. Chem. Int. Ed. Engl.* **1987**, *26*, 798–799.

[320] N. Tokitoh, K. Kishikawa, R. Okazaki, "Synthesis and structure of the first germaketenedithioacetal" *J. Chem. Soc. Chem. Commun.* **1995**, 1425.

[321] G. Cretiu Nemes, H. Ranaivonjatovo, J. Escudié, I. Silaghi-Dumitrescu, L. Silaghi-Dumitrescu, H. Gornitzka, "A Surprisingly Stable 1-(Chlorosilyl)-2-phosphaethenyllithium Compound, $RCl_2SiC(Li)=PMes^*$" *Eur. J. Inorg. Chem.* **2005**, *2005*, 1109–1113.

[322] N. Y. Tashkandi, S. L. McOnie, J. L. Bourque, C. R. W. Reinhold, K. M. Baines, "The Diverse Reactivity of Disilenes Toward Isocyanides" *Angew. Chem. Int. Ed.* **2019**, *58*, 3167–3172.

[323] M. Ishikawa, H. Sugisawa, M. Kumada, T. Higuchi, K. Matsui, K. Hirotsu, J. Iyoda, "Silicon-carbon unsaturated compounds. 15. Synthesis and molecular structure of stable disilacyclopropanes" *Organometallics* **1983**, *2*, 174–175.

[324] S. Patai, Ed., *Diazonium and Diazo Groups: Vol. 1 (1978)*, John Wiley & Sons, Ltd., Chichester, UK, **1978**.

[325] A. Ford, H. Miel, A. Ring, C. N. Slattery, A. R. Maguire, M. A. McKervey, "Modern Organic Synthesis with α-Diazocarbonyl Compounds" *Chem. Rev.* **2015**, *115*, 9981–10080.

[326] G. Maas, "New Syntheses of Diazo Compounds" *Angew. Chem. Int. Ed.* **2009**, *48*, 8186–8195.

[327] M. P. Doyle, M. A. MacKervey, T. Ye, *Modern catalytic methods for organic synthesis with diazo compounds: from cyclopropanes to ylides*, Wiley, New York Weinheim, **1998**.

[328] M. A. Murcko, S. K. Pollack, P. M. Lahti, "An ab initio study of diazoethene, a propadienone isoelectronic with a bent structure" *J. Am. Chem. Soc.* **1988**, *110*, 364–368.

[329] J. C. Brahms, W. P. Dailey, "Difluoropropadienone as a source of difluorovinylidene and difluorodiazoethene" *J. Am. Chem. Soc.* **1990**, *112*, 4046–4047.

[330] J. Breidung, H. Bürger, C. Kötting, R. Kopitzky, W. Sander, M. Senzlober, W. Thiel, H. Willner, "Difluorovinylidene, $F_2C=C:$" *Angew. Chem. Int. Ed. Engl.* **1997**, *36*, 1983–1985.

[331] W. Sander, C. Kötting, "Reactions of Difluorovinylidene—A Super-Electrophilic Carbene" *Chem. - Eur. J.* **1999**, *5*, 24–28.

[332] P. Varava, Z. Dong, R. Scopelliti, F. Fadaei-Tirani, K. Severin, "Isolation and characterization of diazoolefins" *Nat. Chem.* **2021**, *13*, 1055–1060.

[333] P. W. Antoni, C. Golz, J. J. Holstein, D. A. Pantazis, M. M. Hansmann, "Isolation and reactivity of an elusive diazoalkene" *Nat. Chem.* **2021**, *13*, 587–593.

[334] P. W. Antoni, J. Reitz, M. M. Hansmann, "N_2/CO Exchange at a Vinylidene Carbon Center: Stable Alkylidene Ketenes and Alkylidene Thioketenes from 1,2,3-Triazole Derived Diazoalkenes" *J. Am. Chem. Soc.* **2021**, *143*, 12878–12885.

[335] J. Reitz, P. W. Antoni, J. J. Holstein, M. M. Hansmann, "Room-Temperature-Stable Diazoalkenes by Diazo Transfer from Azides: Pyridine-Derived Diazoalkenes" *Angew. Chem. Int. Ed.* **2023**, *62*, e202301486.

[336] Y. Kutin, J. Reitz, P. W. Antoni, A. Savitsky, D. A. Pantazis, M. Kasanmascheff, M. M. Hansmann, "Characterization of a Triplet Vinylidene" *J. Am. Chem. Soc.* **2021**, *143*, 21410–21415.

[337] B. Kooij, Z. Dong, P. Varava, F. Fadaei-Tirani, R. Scopelliti, L. Piveteau, K. Severin, "Vanadium complexes with N-heterocyclic vinylidene ligands" *Chem. Commun.* **2022**, *58*, 4204–4207.

[338] B. Kooij, P. Varava, F. Fadaei-Tirani, R. Scopelliti, D. A. Pantazis, G. P. Van Trieste, D. C. Powers, K. Severin, "Copper Complexes with Diazoolefin Ligands and their Photochemical Conversion into Alkenylidene Complexes" *Angew. Chem. Int. Ed.* **2023**, *62*, e202214899.

[339] P. Pyykkö, M. Atsumi, "Molecular Double-Bond Covalent Radii for Elements Li–E112" *Chem. – Eur. J.* **2009**, *15*, 12770–12779.

[340] M. Mantina, A. C. Chamberlin, R. Valero, C. J. Cramer, D. G. Truhlar, "Consistent van der Waals Radii for the Whole Main Group" *J. Phys. Chem. A* **2009**, *113*, 5806–5812.

[341] T. Henneberger, W. Klein, J. V. Dums, T. F. Fässler, "$[(\mu_2\text{-H})(\eta^2\text{-Ge}_4)\text{ZnPh}_2]^{3-}$, an edge-on protonated E_4 cluster establishing the first three-center two-electron Ge–H–Ge bond" *Chem. Commun.* **2018**, *54*, 12381–12384.

[342] F. Antolini, B. Gehrhus, P. B. Hitchcock, M. F. Lappert, J. C. Slootweg, "Reaction of the silylene $Si[(NCH_2{}^tBu)_2C_6H_4\text{-}1,2]$ with the alkali metal silylamides $M[N(SiMe_3)R]$(M = Li, Na or K; R = $SiMe_3$ or $SiMe_2Ph$)" *Dalton Trans.* **2004**, 3288.

[343] M. M. D. Roy, M. J. Ferguson, R. McDonald, Y. Zhou, E. Rivard, "A vinyl silylsilylene and its activation of strong homo- and heteroatomic bonds" *Chem. Sci.* **2019**, *10*, 6476–6481.

[344] M. M. D. Roy, S. R. Baird, E. Dornsiepen, L. A. Paul, L. Miao, M. J. Ferguson, Y. Zhou, I. Siewert, E. Rivard, "A Stable Homoleptic Divinyl Tetrelene Series" *Chem. – Eur. J.* **2021**, *27*, 8572–8579.

[345] T. Yamaguchi, A. Sekiguchi, M. Driess, "An *N* -Heterocyclic Carbene−Disilyne Complex and Its Reactivity toward $ZnCl_2$" *J. Am. Chem. Soc.* **2010**, *132*, 14061–14063.

[346] D. B. G. Williams, M. Lawton, "Drying of Organic Solvents: Quantitative Evaluation of the Efficiency of Several Desiccants" *J. Org. Chem.* **2010**, *75*, 8351–8354.

[347] R. Inoue, M. Yamaguchi, Y. Murakami, K. Okano, A. Mori, "Revisiting of Benzophenone Ketyl Still: Use of a Sodium Dispersion for the Preparation of Anhydrous Solvents" *ACS Omega* **2018**, *3*, 12703–12706.

[348] J. Geier, H. Rüegger, H. Grützmacher, "Sodium compounds of the benzophenone dianion (diphenyloxidomethanide)" *Dalton Trans* **2006**, 129–136.

[349] T. R. Hoye, B. M. Eklov, T. D. Ryba, M. Voloshin, L. J. Yao, "No-D NMR (No-Deuterium Proton NMR) Spectroscopy: A Simple Yet Powerful Method for Analyzing Reaction and Reagent Solutions" *Org. Lett.* **2004**, *6*, 953–956.

[350] R. K. Harris, E. D. Becker, S. M. Cabral De Menezes, P. Granger, R. E. Hoffman, K. W. Zilm, "Further conventions for NMR shielding and chemical shifts (IUPAC Recommendations 2008)" *Pure Appl. Chem.* **2008**, *80*, 59–84.

[351] I. Noviandri, K. N. Brown, D. S. Fleming, P. T. Gulyas, P. A. Lay, A. F. Masters, L. Phillips, "The Decamethylferrocenium/Decamethylferrocene Redox Couple: A Superior Redox Standard to the Ferrocenium/Ferrocene Redox Couple for Studying Solvent Effects on the Thermodynamics of Electron Transfer" *J. Phys. Chem. B* **1999**, *103*, 6713–6722.

[352] I. Raabe, K. Wagner, K. Guttsche, M. Wang, M. Grätzel, G. Santiso-Quiñones, I. Krossing, "Tetraalkylammonium Salts of Weakly Coordinating Aluminates: Ionic Liquids, Materials for Electrochemical Applications and Useful Compounds for Anion Investigation" *Chem. – Eur. J.* **2009**, *15*, 1966–1976.

[353] M. P. Stewart, L. M. Paradee, I. Raabe, N. Trapp, J. S. Slattery, I. Krossing, W. E. Geiger, "Anodic oxidation of organometallic sandwich complexes using $[Al(OC(CF_3)_3)_4]^-$ or $[AsF_6]^-$ as the supporting electrolyte anion" *J. Fluor. Chem.* **2010**, *131*, 1091–1095.

[354] J. Heinze, "Cyclic Voltammetry—'Electrochemical Spectroscopy'. New Analytical Methods(25)" *Angew. Chem. Int. Ed. Engl.* **1984**, *23*, 831–847.

[355] N. Elgrishi, K. J. Rountree, B. D. McCarthy, E. S. Rountree, T. T. Eisenhart, J. L. Dempsey, "A Practical Beginner's Guide to Cyclic Voltammetry" *J. Chem. Educ.* **2018**, *95*, 197–206.

[356] J. Kouvetakis, A. Haaland, D. J. Shorokhov, H. V. Volden, G. V. Girichev, V. I. Sokolov, P. Matsunaga, "Novel Methods for CVD of Ge_4C and $(Ge_4C)_xSi_y$ Diamond-like Semiconductor Heterostructures: Synthetic Pathways and Structures of Trigermyl-$(GeH_3)_3CH$ and Tetragermyl-$(GeH_3)_4$ C Methanes" *J. Am. Chem. Soc.* **1998**, *120*, 6738–6744.

[357] M. Tashiro, T. Yamato, "Studies on selective preparation of aromatic compounds. Part 16. A convenient preparation of 1,2-di- and 1,2,3-tri-substituted benzenes using the t-butyl. Function as a positional protective group" *J. Chem. Soc. Perkin 1* **1979**, 176.

[358] K. Nagata, T. Agou, N. Tokitoh, "Syntheses and Structures of Terminal Arylalumylene Complexes" *Angew. Chem. Int. Ed.* **2014**, *53*, 3881–3884.

[359] T. Agou, N. Hayakawa, T. Sasamori, T. Matsuo, D. Hashizume, N. Tokitoh, "Reactions of Diaryldibromodisilenes with N-Heterocyclic Carbenes: Formation of Formal Bis-NHC Adducts of Silyliumylidene Cations" *Chem. – Eur. J.* **2014**, *20*, 9246–9249.

[360] K. Fredenhagen, G. Cadenbach, "Die Bindung von Kalium durch Kohlenstoff" *Z. Für Anorg. Allg. Chem.* **1926**, *158*, 249–263.

[361] W. Rüdorff, E. Schulze, "Über Alkaligraphitverbindungen" *Z. Für Anorg. Allg. Chem.* **1954**, *277*, 156–171.

[362] S. R. Bahr, P. Boudjouk, "Trityl tetrakis[3,5-bis(trifluoromethyl)phenyl]borate: a new hydride abstraction reagent" *J. Org. Chem.* **1992**, *57*, 5545–5547.

[363] N. A. Yakelis, R. G. Bergman, "Safe Preparation and Purification of Sodium Tetrakis[(3,5-trifluoromethyl)phenyl]borate (NaBArF): Reliable and Sensitive Analysis of Water in Solutions of Fluorinated Tetraarylborates" *Organometallics* **2005**, *24*, 3579–3581.

[364] J. E. Borger, M. S. Bakker, A. W. Ehlers, M. Lutz, J. Chris Slootweg, K. Lammertsma, "Functionalization of P_4 in the coordination sphere of coinage metal cations" *Chem. Commun.* **2016**, *52*, 3284–3287.

[365] Herrmann, Salzer, Eds., *Synthetic Methods of Organometallic and Inorganic Chemistry: Volume 1: Literature, Laboratory Techniques, and Common Starting Materials*, Georg Thieme Verlag, Stuttgart, **1996**.

[366] H. F. Klein, H. H. Karsch, "Tris(trimethylphosphine)cobalt(I) halides. Preparation and properties" *Inorg. Chem.* **1975**, *14*, 473–477.

[367] Y. Nagata, Y.-Z. Ke, M. Suginome, "Facile Preparation of Poly(quinoxaline-2,3-diyl)s *via* Aromatizing Polymerization of 1,2-Diisocyanobenzenes Using Phosphine Complexes of Nickel(II) Salts" *Chem. Lett.* **2015**, *44*, 53–55.

[368] N. Kuhn, T. Kratz, “Synthesis of Imidazol-2-ylidenes by Reduction of Imidazole-2(3*H*)-thiones” *Synthesis* **1993**, *1993*, 561–562.

[369] M. L. Luetkens, A. P. Sattelberger, H. H. Murray, J. D. Basil, J. P. Fackler, R. A. Jones, D. E. Heaton in *Inorg. Synth.* (Ed.: H.D. Kaesz), Wiley, **1989**, pp. 7–12.

[370] P. Patil, M. Ahmadian-Moghaddam, A. Dömling, “Isocyanide 2.0” *Green Chem.* **2020**, *22*, 6902–6911.